

BRANNER EARTH SCIENCES LIBRARY
THE STANFORD UNIVERSITY LIBRARIES
STANFORD, CALIFORNIA 94305


21 November 1983

Norma Meeks
Publications Office
New Mexico Bureau of Mines & Mineral Resources
Socorro, NM 87801

Dear Ms. Meeks:

After some circuitous routing of your letter of 10 October 1983, there seems to be only an unsatisfactory outcome. All Stanford copies of the manuscript of the title, "Precambrian granitic rocks of the Dixon-Peñasco area, northern New Mexico: a study in contrasts", have the same page omission as your copy. Even the copy in the files of his thesis advisor is missing page 197. If there is a complete copy in existence, only the author would seem to know. But, no current address is known by his former academic department here, nor by any of his former contacts on campus.

Sincerely yours,


John A. Baltierra
Operations Manager
Branner Library



PRECAMBRIAN GRANITIC ROCKS OF THE
DIXON-PENASCO AREA, NORTHERN
NEW MEXICO: A STUDY IN CONTRASTS

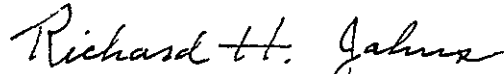
By
Philip E. Long
December 1976

PRECAMBRIAN GRANITIC ROCKS OF THE DIXON-PENASCO AREA,
NORTHERN NEW MEXICO: A STUDY IN CONTRASTS

A DISSERTATION
SUBMITTED TO THE DEPARTMENT OF GEOLOGY
AND THE COMMITTEE ON GRADUATE STUDIES
OF STANFORD UNIVERSITY
IN PARTIAL FULFILLMENT OF THE REQUIREMENTS
FOR THE DEGREE OF
DOCTOR OF PHILOSOPHY

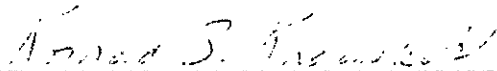
By
Philip E. Long
December 1976

I certify that I have read this thesis and that in my opinion it is fully adequate, in scope and quality, as a dissertation for the degree of Doctor of Philosophy.



Richard H. Jahns
(Principal Adviser)

I certify that I have read this thesis and that in my opinion it is fully adequate, in scope and quality, as a dissertation for the degree of Doctor of Philosophy.



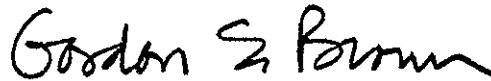
Konrad B. Krauskopf

I certify that I have read this thesis and that in my opinion it is fully adequate, in scope and quality, as a dissertation for the degree of Doctor of Philosophy.



Robert R. Compton

I certify that I have read this thesis and that in my opinion it is fully adequate, in scope and quality, as a dissertation for the degree of Doctor of Philosophy.



Gordon E. Brown

Approved for the University Committee
on Graduate Studies:

Dean of Graduate Studies

ABSTRACT

Precambrian granitic rocks are extensively exposed in the area between Dixon and Peñasco, northern New Mexico, where they form major parts of a complex terrane that includes older metasedimentary and meta-volcanic rocks. At least four distinct episodes of magmatism over a time span of about 300 m.y. resulted in the emplacement of granitic rocks at successively greater depths.

The oldest of these granitic rocks is the Cerro Alto Metadacite, which is fine grained and slightly porphyritic. It may have been in part extruded and in part intruded at very shallow depths. The next younger rock is the Puntiaquedo Granite Porphyry, which is characterized by distinct phenocrysts of K-feldspar, quartz, and plagioclase. It occurs as an epizonal pluton with sharply defined walls, a thin border zone, and marginal aplite dikes. It is intruded by the Rana Quartz Monzonite (1673 m.y.), which forms an epizonal pluton with a discontinuous border zone and an equigranular interior with local aplite dikes. Felsite dikes in the surrounding country rock are probably associated with the border zone of the Rana Quartz Monzonite. The youngest of the major granitic rocks is the Peñasco Quartz Monzonite (1470 ± 20 m.y.), which represents a mesozonal pluton with rare aplite dikes. It is distinctly more mafic than the older rocks, and locally it contains megacrysts of K-feldspar.

Pegmatite bodies crosscut all the plutons and hence are at least in part younger than the major granitic rocks. These pegmatites may well represent more than one generation of magmatism but they probably

are not genetically related to the exposed granitic plutons. Postdating all of the igneous events was a period of epidote veining accompanied by local reddening of feldspars in the plutonites. Radiometric ages suggest that this episode took place about 1200 m.y. ago.

Interpretation of field and petrographic data in terms of Buddington's 1959 classification of granites in North America suggests that the major plutons were emplaced at increasingly greater depths with each successive episode of magmatism. Estimates of depth of intrusion, based on Buddington's criteria, are 0 to 2 km (upper epizone) for the Cerro Alto Metadacite, 2 to 4 km (epizone) for the Puntiaquido Granite Porphyry, 3 to 6 km (lower epizone) for the Rana Quartz Monzonite, 8 to 3 km (mesozone) for the Peñasco Quartz Monzonite, and 9 to 14 km for the pegmatites.

The petrochemistry of these rocks is consistent with an igneous origin, but some of the border-zone rocks and some of the felsite dikes have compositions that reflect considerable postmagmatic alteration.

Details of barium distribution in the Puntiaquido Granite Porphyry, the Rana Quartz Monzonite, and the Peñasco Quartz Monzonite indicate that the K-feldspar megacrysts crystallized from a melt rather than from a water-rich fluid phase. The data also indicate that aplites in these rocks probably formed from rest-liquids associated with each of the granitic bodies, and that each of the aplites crystallized largely as the result of a pressure quench.

A preliminary experimental and theoretical study of the distribution of barium during crystallization of granitic rocks demonstrates that the distribution coefficient of barium between K-feldspar and silicate liquid depends on both temperature and bulk composition of the system.

A relatively simple analysis of the crystallization of granitic rocks indicates that some assumptions commonly made in the calculation of trace-element distribution behavior are inappropriate. Most notable among these assumptions are the neglect of the effect of multiple phases crystallizing simultaneously, neglect of variation in the order of appearance of phases crystallizing, and neglect of temperature-induced changes in distribution coefficients.

A study of the origin and development of late-stage features in the granitic rocks prompts the following conclusions: (1) the bulk of the gross textural features in these rocks formed while a silicate melt was present; (2) the features, both microscopic and megascopic, that are not ascribable to igneous processes were formed mainly during subsequent metamorphic and alteration events; (3) even features that are most likely deuteritic in origin, such as perthitic intergrowths, have been modified by later events.

ACKNOWLEDGEMENTS

I am especially indebted to R. H. Jahns for suggesting this project and for being my advisor during my tenure as a graduate student. His interest and concern during all phases of this research are deeply appreciated. W. C. Luth taught me to view the geologic literature critically and we collaborated on the interpretation of barium zoning in K-feldspar megacrysts. R. R. Compton, K. B. Krauskopf, and G. E. Brown read the rough draft and offered helpful comments and criticisms.

The field work was supported by the New Mexico Bureau of Mines and Mineral Resources under the direction of D. H. Baker, Jr., and by Stanford University School of Earth Sciences. The support of both of these institutions is gratefully acknowledged. The late M. E. Willard of the New Mexico Bureau of Mines and Mineral Resources helped with logistical problems and provided helpful suggestions during the initial stages of the mapping. D. E. Dunn of the University of North Carolina made the facilities of the Fort Burgwin Research Center (Southern Methodist University) available to me during the summer of 1971. He also provided guidance in interpreting the structural features of the metamorphic rocks. Thanks are also due to D. Weaver, formerly of Penasco, for his hospitality and assistance. A. Montgomery helped me to recognize and distinguish the granitic units and extended his warm hospitality on several occasions. The consideration and hospitality of the C. E. Spaths, formerly of Santa Fe, and the D. Hughs of Pojoaque during two summers of field work are greatly appreciated.

K. L. Williams and C. M. Taylor taught me the techniques of microprobe analysis and C. M. Taylor kept the microprobe in operating condition in spite of obstacles. P. M. Fenn, S. E. Swanson, and M. T. Naney provided a great deal of assistance with the experimental work, and their contribution is gratefully acknowledged. T. C. Yao and R. Woldseth of the Kevex Corporation assisted with the XRF analyses and made the necessary equipment available. G. D. Long made the pressed-powder pellets for the XRF analyses. Discussions with C. Carroon, B. E. Taylor, E. E. Foord, and others helped to develop and sift out my ideas on the genesis of the Dixon-Peñasco area. Special thanks is due L. T. Silver of California Institute of Technology for allowing me to quote an unpublished age-date on the Peñasco Quartz Monzonite and for helpful suggestions during a brief visit to the field area in August 1973.

Financial support was provided by a Geological Society of America Research Grant and by the Shell Fund of Stanford University, School of Earth Sciences. Much of this study was completed while the writer held a National Science Foundation Graduate Fellowship. The experimental work was supported by a National Science Foundation Grant to W. C. Luth and R. H. Jahns (GA-1684).

L. M. Echevarria and R. Farnell drafted many of the figures. S. Farnell typed an early draft of the thesis and A. Berry did a superb job of typing and proofing the final draft.

Mary, my wife, supported me in every way during my career as a graduate student. She worked when she would rather have been a mother and she endured California longer than she had anticipated. Then in 1976 she gave birth to our daughter, Anna. Together they patiently helped

and encouraged me while I finished writing. To both of them I am eternally grateful.

TABLE OF CONTENTS

	Page
ABSTRACT	iii
ACKNOWLEDGEMENTS	vi
LIST OF FIGURES	xiii
LIST OF PLATES	xxii
LIST OF TABLES	xxiii
 I. INTRODUCTION	 1
Purpose and Scope of the Study	1
Field Area Chosen for Study	6
Methods of Study	8
General Features of the Dixon-Peñasco Area	9
Previous and Current Geological Investigations of the Area	11
 II. GENERAL GEOLOGY	 13
Regional Setting	13
Precambrian Metasedimentary and Metavolcanic Rocks	13
Precambrian Granitic Rocks	18
General Statement	18
Cerro Alto Metadacite	19
Puntiagudo Granit Porphyry	20
Rana Quartz Monzonite	20
Peñasco Quartz Monzonite	22
Pegmatites	22
Alteration of the Granitic Rocks	24
Cenozoic Sedimentary Deposits	25
General Statement	25
Picuris Tuff	26
Tesuque Formation	27
Younger Terrace Gravels	30
Brown Sand-Soil Deposits	30
Holocene Stream Deposits	32
 III. METASEDIMENTARY AND METAVOLCANIC ROCKS	 34
Ortega Group	34
Pilar Phyllite	34
Lithology	35
Structural Features	36

	Page
Piedra Lumbre Formation	37
General Statement	37
Distribution	39
Lithology	40
Structural Features	44
Vadito Group	46
General Statement	46
Marquenas Quartzite	47
Distribution	47
Lithology	47
Structural Features	53
Unnamed Schist Unit	54
Distribution	54
Lithology	55
Banded Bluish-Gray Schist	55
Phyllitic Schist	59
Amphibolite Dikes and Sills	66
Vadito Schist Southeast of the Main	
Amphibolite Belt	66
Structural Features	70
Amphibolite Unit	74
Lithologies	75
Metadacite and Metafelsite Dikes and Sills	78
Lithology	79
Structural Features	84
Foliated Granodioritic Rocks of Uncertain Age	85
Distribution	85
Lithology	85
Structural Features	87
Metamorphism	87
General Statement	87
Previous Work on the Metamorphism	88
Estimates of the General Metamorphic Grade and	
Paragenetic Sequences of the Vadito Group Rocks	92
IV. GRANITIC ROCKS	102
Cerro Alto Metadacite	102
Distribution and Occurrence	102
Contact Relationships	102
Petrography	103
Modal Composition	105
Structural Features	105
Metamorphism	109
Summary	110
Puntiagudo Granite Porphyry	110
Distribution and Occurrence	110
Contact Relationships	111
Petrography	113
Modal Composition	117

	Page
Structural and Textural Features	117
Metamorphism and Alteration	121
Summary	123
Rana Quartz Monzonite	123
Distribution and Occurrence	123
Contact Relationships	124
Petrography	126
Border Zone	126
Foliated Facies	130
Unfoliated Phase	134
Aplites	138
Modal Composition	139
Structural and Textural Features	148
Metamorphism and Alteration	150
Summary	161
Peñasco Quartz Monzonite	162
Distribution and Occurrence	162
Contact Relationships	162
Petrography	165
Modal Composition	169
Structural and Textural Features	173
Alteration	177
Summary	177
Pegmatites	178
Quartz Pods and Veins	189
General Occurrence and Petrography	189
Age Relations	193
Structural Features	193
Summary of Relative Ages of Granites, Pegmatites, Metamorphism, and Alteration	193
 V. SPECIAL STUDIES OF THE GRANITIC ROCKS	 198
Introductory Statement	198
Petrochemistry	198
Major Element Data	198
Trace Elements	224
Composition of Feldspars from the Granitic Rocks	235
Structural State of Feldspars	246
Late-Stage and Metamorphic Reactions in the Granitic Rocks	248
General Statement	248
Reactions Involving Mafic Phases	250
The Muscovite--K-feldspar Reaction	256
Reactions Producing Myrmekite	261
Genetic Implications of Barium Zoning in Microcline Megacrysts	264
Introduction	264
Puntiagudo Granite Porphyry	271
Peñasco Quartz Monzonite	274

	Page
Barium Distribution--Description of Features	275
Methods and Techniques of Analysis	275
General Barium Zoning	290
Data on Barium Distribution Between K-feldspar and Silicate Melt or a Water-Rich Fluid Phase	300
Preliminary Experimental Data on Barium Distri- bution Between Silicate Liquid and Or-rich Alkali Feldspar	304
Some Aspects of Crystal Growth and Trace-Element Distribution Theory as Related to Barium Zoning . . .	340
Interpretation of the Barium Zoning in the Light of Constraints Imposed by Experimental Data and Crystal Growth Theory	350
Conclusions	352
Barium Distribution in the Rana Quartz Monzonite: Implications for the Formation of Aplite	354
Geochronology	357
VI. GENETIC INTERPRETATIONS OF THE GRANITIC ROCKS	363
General Statement	363
Estimates of Depth of Intrusion Based on Buddington's (1959) Classification of Granitic Plutons	363
Preliminary Crystallization and P-T Estimates	370
Late-Stage Crystallization versus Metamorphism and Alteration	386
VII. SUMMARY AND CONCLUSIONS	393
EPILOGUE	395
REFERENCES	396
APPENDICES	404
I. Petrogenetic descriptions of selected samples of granitic rocks from the Dixon-Peñasco area	405
II. Modal analyses	438
III. Whole-rock analyses for major and minor elements plus barium, rubidium, strontium, and zirconium by energy dispersive X-ray fluorescence	448
IV. Quantitative electron microprobe analyses of feldspars from the Dixon-Peñasco area and of synthetic glasses and feldspars from experimental runs	493
V. Estimates of the structural state of feldspars from the the granitic rocks of the Dixon-Peñasco area	529
VI. Derivation of equations 2, 5, and 6	531

LIST OF FIGURES

Figure	Page
1. Location map	7
2. Physiographic setting of the study area	10
3. Generalized geologic map of the Dixon-Peñasco area . . .	14
4. Generalized stratigraphic section of the Vadito Group and upper Ortega Group rocks	16
5. Detailed stratigraphic section of Ortega and Vadito rocks	17
6. A typical exposure of Tesuque Formation	28
7. A gentle fold in Tesuque Formation	28
8. A typical exposure of brown sand-soil deposit	31
9. Comparison of Pilar Phyllite terminologies	38
10. Detailed stratigraphic section of the Piedra Lumbre Formation	41
11. An outcrop of the second subunit in the Piedra Lumbre Formation	42
12. Stratigraphic section through the Marquenas Quartzite	48
13. An outcrop of Marquenas Conglomerate	49
14. Detailed stratigraphic section of part of the Marquenas Quartzite	52
15. Detailed sections of the unnamed schist unit	56
16. Geologic map of Camp Harding knobs	62
17. An outcrop of knotty schist within the unnamed schist unit	63
18. Possible section of the upper part of Vadito schist . .	67
19. Hypothetical cross section assuming a lack of granitic rocks	71

Figure	Page
20. Outcrops of metavolcanic conglomerate	76
21. Photomicrograph of quartz-epidote intergrowth in the Cerro Alto Metadacite	81
22. Serrated quartz subgrain boundaries in a felsite dike .	82
23. Sketch of a possible fault cutting the main amphibolite belt north of Embudo Creek	86
24. Nielsen's (1972) summary of metamorphism and deformation in the Ortego Group rocks	90
25. Upper stability limit of grossularite + quartz at low P_{CO_2}	94
26. Possible narrowing of stability field of cordierite with increasing pressure	97
27. P-T diagram for aluminosilicates and muscovite-- K-feldspar reaction	98
28. Possible P-T path during metamorphism	99
29. Possible T-time and P-time paths during metamorphism . .	101
30. Cerro Alto Metadacite dike crosscutting a conglomerate bed	104
31. Stained slabs of Cerro Alto Metadacite	104
32. Photomicrographs of Cerro Alto Metadacite	106
33. Plots of modal data for Cerro Alto Metadacite and felsite dikes	107
34. Contact of Puntiaugudo Granite Porphyry with Vadito schist	112
35. Stained slabs of the Puntiaugudo Granite Porphyry	114
36. Photomicrographs of Puntiaugudo Granite Porphyry	116
37. Plot of modal data for the Puntiaugudo Granite Porphyry	118
38. Outcrops of Puntiaugudo Granite Porphyry showing strong deformation	119
39. Contact of Rana Quartz Monzonite with upper Vadito schist	125

Figure	Page
40. Stained slabs of Rana Quartz Monzonite	127
41. Photomicrograph of Rana Quartz Monzonite from border zone	127
42. Allanite core of an epidote grain, border zone of Rana Quartz Monzonite	129
43. Rounded quartz phenocrysts, border zone of Rana Quartz Monzonite	129
44. Typical example of foliated Rana Quartz Monzonite . . .	132
45. Photomicrographs of Rana Quartz Monzonite	136
46. Sketch of Rana Quartz Monzonite aplite dike	137
47. Stained slab showing the two phases of the dike in figure 46	140
48. Plot of modal data from the Rana Quartz Monzonite . . .	141
49. Plot of modal data from the Rana Quartz Monzonite . . .	142
50. Plot of modal data from the Rana Quartz Monzonite . . .	143
51. Plot of modal data from the Rana Quartz Monzonite . . .	144
52. Plot of modes for Rana Quartz Monzonite, from a traverse across the border zone	146
53a. Folding of foliation in Rana Quartz Monzonite	149
53b. Semiductile shear zone in Rana Quartz Monzonite	149
54. Series of stained slabs showing increasing deformation in the Rana Quartz Monzonite	151
55. Photomicrographs of the samples shown in figure 54 . . .	153
56. Photomicrograph of magnetite-hematite in the Rana Quartz Monzonite	159
57. Stained slab showing epidote veining of Rana Quartz Monzonite	159
58. Contact of the Peñasco Quartz Monzonite with the Vadito amphibolite unit	164
59. Chevron folding in Vadito schist(?) near contact with the Peñasco Quartz Monzonite	164

Figure	Page
60. Stained slabs of Peñasco Quartz Monzonite	166
61. Photomicrograph of zoned allanite with a partial epidote rim, Peñasco Quartz Monzonite sample PL71-5a	166
62. Photomicrograph of magnetite with associated hematite, Peñasco Quartz Monzonite	168
63. Photomicrograph of plagioclase alteration in the Peñasco Quartz Monzonite	168
64. Plot of modal data from the Peñasco Quartz Monzonite . .	170
65. Plot of average modes for the granitic rocks	171
66a. Histogram of modal muscovite for the Puntigudo Granite Porphyry, the Rana Quartz Monzonite, and the Peñasco Quartz Monzonite	172
66b. Histogram of modal biotite for the Puntigudo Granite Porphyry, the Rana Quartz Monzonite, and the Peñasco Quartz Monzonite	172
67. Plot of modal plagioclase/K-feldspar vs. modal biotite and modal plagioclase vs. modal biotite	174
68. Slight foliation of biotite in the Peñasco Quartz Monzonite	176
69. Subparallel alignment of K-feldspar megacrysts in the Peñasco Quartz Monzonite	176
70a. Typical examples of simple pegmatite bodies cutting Peñasco Quartz Monzonite	180
70b. Typical examples of simple pegmatite bodies cutting quartz vein in Rana Quartz Monzonite	180
71a. Pegmatite bodies showing limited internal zoning. Note small quartz core	182
71b. Pegmatite bodies showing limited internal zoning. Note directional orientation of blocky K-feldspar as well as that of quartz and muscovite	182
72a. The Peñasco pegmatite. A general view of aplite portion	184
72b. The Peñasco pegmatite. Detail of lower part of aplite portion	184

Figure	Page
73a. Poorly zoned quartz-albite pegmatite	186
73b. Quartz-albite pegmatite with quartz core	186
74. Age relation between simple and somewhat zoned bodies of pegmatite	187
75. Tourmaline-quartz vein in the Vadito schist	191
76. Tourmaline in the Rana Quartz Monzonite	192
77. Diagram of a quartz vein offset along an F_2 shear zone	194
78. Diagram summarizing relative ages of deformation, metamorphism, and magmatism	196
79. Na_2O - K_2O - CaO triangular diagram for felsite, Cerro Alto Metadacite, and pegmatites	201
80. (Na_2O+K_2O) -Fe as Fe_2O_3 -MgO triangular diagram for felsite, Cerro Alto Metadacite, and pegmatites	202
81. ALK-Al-CFM triangular diagram for felsite, Cerro Alto Metadacite, and pegmatites	203
82. Ab-Or-Q triangular diagram for felsite, Cerro Alto Metadacite, and pegmatites	204
83. Ab-An-Or triangular diagram for felsite, Cerro Alto Metadacite, and pegmatites	205
84. Na_2O - K_2O - CaO triangular diagram for Puntiaquedo Granite Porphyry	206
85. (Na_2O+K_2O) -Fe as Fe_2O_3 -MgO triangular diagram for Puntiaquedo Granite Porphyry	207
86. ALK-Al-CFM triangular diagram for Puntiaquedo Granite Porphyry	208
87. Ab-Or-Q triangular diagram for Puntiaquedo Granite Porphyry	209
88. Ab-An-Or triangular diagram for Puntiaquedo Granite Porphyry	210
89. Na_2O - K_2O - CaO triangular diagram for Rana Quartz Monzonite	211

Figure	Page
90. (Na ₂ O+K ₂ O)-Fe as Fe ₂ O ₃ -MgO triangular diagram for Rana Quartz Monzonite	212
91. ALK-Al-CFM triangular diagram for Rana Quartz Monzonite	213
92. Ab-Or-Q triangular diagram for Rana Quartz Monzonite	214
93. Ab-An-Or triangular diagram for Rana Quartz Monzonite	215
94. Na ₂ O-K ₂ O-CaO triangular diagram for Peñasco Quartz Monzonite	216
95. (Na ₂ O+K ₂ O)-Fe as Fe ₂ O ₃ -MgO triangular diagram for Peñasco Quartz Monzonite	217
96. ALK-Al-CFM triangular diagram for Peñasco Quartz Monzonite	218
97. Ab-Or-Q triangular diagram for Peñasco Quartz Monzonite	219
98. Ab-An-Or triangular diagram for Peñasco Quartz Monzonite	220
99. A plot of Sr against Ba for the granitic rocks	225
100. A plot of Rb against Ba for the granitic rocks	226
101. A plot of Rb against Sr for the granitic rocks	227
102. A plot of Zr against Sr for the granitic rocks	228
103. A plot of Rb/Ba against Rb/Sr for the granitic rocks . .	229
104. A plot of Rb/Sr against D.I. for the granitic rocks . .	230
105. A plot of Rb/Sr against total Fe as Fe ₂ O ₃ for the granitic rocks	231
106. Microprobe analyses of feldspars plotted on Ab-An-Or and Ab-Or-Cn diagrams	237
107. Results of a microprobe traverse of a plagioclase feldspar from the Puntiaquedo Granite Porphyry	241
108. Results of a microprobe traverse of a plagioclase feldspar from the Rana Quartz Monzonite	242

Figure	Page
109. Photomicrograph showing limited plagioclase zoning in highly deformed Rana Quartz Monzonite	243
110. Results of a microprobe traverse of a plagioclase feldspar in Peñasco Quartz Monzonite	245
111. An content of albitic rims in the Rana Quartz Monzonite	247
112. Structural state of feldspars from the granitic rocks as determined by the three-peak method	249
113. Sphene rims on opaque grains in the Rana Quartz Monzonite	251
114. Textures of hematite-magnetite intergrowths in the Rana Quartz Monzonite and the Peñasco Quartz Monzonite .	253
115. Stability of muscovite as a function of temperature and fluid composition	259
116. Typical myrmekite texture in Peñasco Quartz Monzonite .	262
117. Photomicrograph of myrmekite with accompanying microprobe traverses for barium in the Peñasco Quartz Monzonite	265
118. X-ray scanning photos of myrmekite from the Rana Quartz Monzonite	267
119. Stained slab, Puntigudo Granite Porphyry	273
120. Close-up of Puntigudo Granite Porphyry megacryst . . .	273
122. Stained slabs, Peñasco Quartz Monzonite	276
123. Line drawing of Peñasco Quartz Monzonite megacryst . . .	277
124. Electron microprobe scanning photographs of a plagioclase inclusion from the Peñasco Quartz Monzonite	291
125. Plots of analyses on Ab-Or-An and Ab-Or-Cn triangular diagrams	292
126. A portion of a continuous traverse for barium in a megacryst from the Peñasco Quartz Monzonite	295
127. General barium variation across a megacryst from the Peñasco Quartz Monzonite	296

Figure	Page
128. Correlation of barium traverses for megacrysts from a single hand specimen of Peñasco Quartz Monzonite . . .	297
129. Correlation of barium traverses for megacrysts from a single hand specimen of Puntiaquedo Granite Porphyry	298
130. Anhydrous bulk composition of starting materials for experimental runs plotted on Ab-Or-Q and Ab-Or-An triangular diagrams	306
131. X-ray scanning photos of synthetic alkali feldspars from run #1	315
132. Phase assemblage diagram for samples R-1 and R-1 + 10 weight percent Or ₁₀₀	317
133. Photomicrograph showing textures of charges with low water content from run #2	318
134. Electron microprobe scanning photographs of zoned, hopper-shaped crystals of alkali feldspar from run #2 .	319
135. Photomicrograph of elongate alkali feldspar crystals from run #3	321
136. Sections perpendicular to the long axis of hollow crystals of zoned alkali feldspar from run #3	323
137. Microprobe traverse for barium across crystal shown in figure 136a	337
138. An Arrhenius plot for $K_D^{Ba}(Kf/l)$ for composition R-1 + 10 weight percent Or ₁₀₀	338
139. Diagram showing depletion or enrichment of solute at a growing crystal interface	341
140. A general plot of $\partial C_S^i / \partial x$ versus $\partial C_L^i / \partial x$	346
141. Barium zoning for a microcline crystal from aplite in the Rana Quartz Monzonite	356
142. Reinterpretation of Fullagar and Shiver's (1973) Rb-Sr age data	360
143. Magmatic, metamorphic, and deformational events in terms of radiometric ages now known	361

Figure		Page
144.	Schematic representation of the emplacement zones of Buddington (1959)	364
145.	Summary of characteristics of the granitic rocks of the Dixon-Peñasco area	366
146.	Plot of age vs. estimated depth of intrusion for the granitic rocks of the Dixon-Peñasco area	367
147.	Summary of the crystallization behavior of the principal granitic rocks of the Dixon-Peñasco area . . .	375
148.	Averages of the chemical data plotted on Ab-Or-Q and Ab-Or-An triangular diagrams	377
149.	Presnall and Bateman's (1973) interpretations of the vapor saturated phase relations in the primary granite system	379
150.	Temperature vs. weight percent H ₂ O at 8 kbar for R-1 of Whitney (1975)	381
151.	P-T and P-X projections for synthetic granite R-1 of Whitney (1975)	382
152.	Stability curve for epidote and the minimum melting curve for granite	385

LIST OF PLATES

Plate

I.	Geologic map of the Dixon-Peñasco area, New Mexico (scale 1:24,000)	in pocket
Ia.	Explanation	"
II.	Geologic map of the Dixon-Peñasco area, New Mexico (scale 1:12,000)	"
III.	Cross section	"
IV.	Distribution of pegmatites, aplites, and alteration in the Dixon-Peñasco area, New Mexico	"

LIST OF TABLES

Table	Page
1. Structural elements of the Ortega Group observed by Nielsen (1972)	45
2. A traverse of a portion of the Marquenas Quartzite . . .	50
3. Electron microprobe analyses of microcline megacrysts from the Puntiaquedo Granite Porphyry and the Peñasco Quartz Monzonite	280
4. Electron microprobe analyses of plagioclase inclusions in microcline megacrysts from the Puntiaquedo Granite Porphyry and the Peñasco Quartz Monzonite and Ba-rich K-feldspar inclusions in megacrysts from the Peñasco Quartz Monzonite	285
5. Conditions and general rules of experimental runs . . .	308
6. Electron microprobe analyses of products of experimental runs and measured K_D^{Ba} values	324
7. List of mathematical symbols	342

I. INTRODUCTION

Purpose and Scope of the Study

One of the fundamental problems in granite petrology has been the difficulty in distinguishing among the products of primary magmatic crystallization, late-stage magmatic processes, and subsolidus metamorphic processes. It has long been supposed that late-stage magmatic processes have a significant effect on primary minerals in granitic rocks, but no criteria have been established for distinguishing the effects of such magmatic processes from those of metamorphic processes. Yet the distinction is fundamental. In the case of the late-stage processes, they are inherent in the crystallization of the magma itself whereas the metamorphic processes result from subsequent events that may or may not be related to the original rock. The basic aim of this investigation has been to establish criteria on which such a distinction might be based.

J. J. Sederholm (1916) was one of the first petrologists to recognize the possible importance of late-stage magmatic effects, and he proposed to call such changes "deuteric." In so doing he made an ad hoc, conceptual distinction between the late-stage and the metamorphic processes. A few years later, R. J. Colony (1923) used the term "aqueo-igneous matters" for end-stage consolidation products which he thought must have been of "low viscosity, great penetrating power, considerable chemical activity, and enriched in volatile gases." The rocks he observed suggested to him that these late-stage products

were rich in silica and alkalies--especially soda--and that they reacted with early formed minerals as, for example, in the albitization of potassium feldspar, uralitization of pyroxene, and serpentinization of hornblende. Colony considered the ultimate late-stage effect to be the formation of micropegmatites, which in his mind represented consolidation of the "concentrates" themselves. Colony's approach was rather qualitative and he did not specifically consider the possible effects of metamorphism, but his work provided valuable insight into some possible late-stage processes in granitic rocks.

Since the time of Sederholm and Colony, numerous and often conflicting ideas have been developed in the context of this problem. For example, "potash metasomatism," which supposedly is a *postmagmatic* process that results in the formation of potassium feldspar porphyroblasts and/or potassium feldspar overgrowths on plagioclase crystals, has been proposed by some investigators (e.g., Eskola, 1956; Robertson, 1959; Leggo, 1966; Nemec, 1967; Dickson, 1968). On the other hand, similar features have been interpreted as products of strictly magmatic crystallization (e.g., Hibbard, 1965; Kerrick, 1969; Nemec, 1975). Contrasting theories also have been advanced to explain perthitic textures. Thus Augustithis (1964), Schermerhorn (1961), and others have supported the idea that perthite results from the "injection" of albitic material or from some other kind of "albitization" by material from external sources, whereas Gates (1953), Tuttle and Bowen (1958), and others have developed the more widely accepted exsolution hypothesis for the formation of most perthites. Such subsolidus behavior might be involved in the formation of intergranular albite and some rapakivi textures as well.

Granophyre, myrmekite, and graphic granite also have been regarded as somehow related to late stages of magmatic crystallization (for a discussion, see Barker, 1970). Various hypotheses have been suggested for the genesis of myrmekite, ranging from exsolution (e.g., Phillips, 1964, 1972) to injection (e.g., Augustithis, 1962).

Pegmatites are likewise thought by most petrologists to represent a late stage of magmatic differentiation, during which relatively large-scale segregation can occur. A viable model for the crystallization of pegmatites (especially zoned bodies) has been developed by Jahns (1953, 1955, 1956) and Jahns and Burnham (1969), in which interactions between silicate melt and a coexisting water-rich fluid phase are emphasized. This model accounts for transfer of certain constituents to different parts of a crystallizing body. It has seemed reasonable that such a model also could be applied to the behavior of water-saturated rest-magma and an accompanying aqueous fluid at near-solidus temperatures in any natural granitic system.

To judge from the published record, development of the late-stage features mentioned above rarely is considered in terms of an overall crystallization sequence, either for a single rock or for a series of comagmatic intrusive rocks. Magmatic and "hydrothermal" processes commonly are discussed without the elucidation of their relationships or possible intervening developments, and "late-stage" tends to be adopted as a catchall expression with few attempts to define sequential relationships or relative significance of various processes that might operate at subsolidus temperatures. The possible complexity of the problem seems even greater when one recognizes that the effects of late-stage magmatic processes on primary igneous features may be mimicked,

at least to some extent, by low- to medium-grade metamorphism. As the physical conditions of such metamorphism approach those of late-stage igneous processes, the products may well be indistinguishable, but there will presumably be specific differences possibly due to consistent variations in the physical conditions. Moreover, differences in the kinetics of reactions in deuteric and metamorphic regimes may be caused in part by differences in the amount of water present. Such differences in kinetics of reactions may be expressed by varying mineral assemblages and different extents of alteration. Anisotropic stress in the metamorphic environment produces characteristic textures that can be used to distinguish some occurrences of metamorphosed granitic rocks, but such deformation might also occur simultaneously with late-stage magmatic alteration. And metamorphism conceivably could occur without significant deformation. In any case, it clearly would be useful to establish criteria upon which a more definite distinction could be based.

Toward that end, this study was planned in order to characterize and evaluate igneous and metamorphic processes in a specific occurrence of Precambrian granitic rocks in northern New Mexico, with particular emphasis on the origin of controversial textural features such as perthite, myrmekite, and microcline megacrysts. In addition, the following specific questions pertinent to understanding the effects of these processes in granitic rocks were asked at the outset:

- (1) What is the distribution of major and minor elements, especially Ca, K, Na, Ba, Rb, and Sr, on both map and microscopic scales, and to what extent is the distribution uniquely controlled by late-stage processes?

(2) What are the variations in structural state of the feldspars for the various intrusive phases of the granitic complex, and can these variations be ascribed to a "normal" thermal decline?

(3) What temperatures and pressures are indicated by late-stage phase relations, and are these consistent with Buddington's (1959) classification of zone of emplacement for granitic plutons or are pressures significantly reduced by the time late-stage processes become active?

(4) Do microscopic analogs of complex or simple pegmatites occur interstitially in any of the granitic rocks?

(5) Can the pegmatites and aplites of the study area be considered "late magmatic differentiates" of the granite, and if so, can a reasonable model for their collection and emplacement be developed? Tuttle and Bowen (1958), in Geological Society of America Memoir 74, considered the textural features discussed above to be post- or late-magmatic in origin, but they noted that not all of the inferred changes are well understood:

. . . many changes have taken place in: (1) the compositions of the minerals, (2) the polymorphic forms of the minerals, and (3) the textural relations among the minerals or the granites, syenites, and the nepheline syenites between the time of final magmatic crystallization and observation under the petrographic microscope. A few of these changes have been described here, but many more complex reactions undoubtedly remain to be discovered (p. 142).

It has been the aim of this study to understand, in a specific suite of granitic rocks, the changes that have taken place in composition, in polymorphic forms, and in textural relations--attempting to delineate some of the more complex reactions that may occur after primary crystallization of the magma.

Field Area Chosen for Study

A granitic terrane collectively termed the Embudo granite by Montgomery (1953) was chosen for the present study. It is located in north-central New Mexico about 20 airline miles south of Taos (fig. 1), and it occupies parts of the 7.5' Peñasco and Trampas quadrangles of the U. S. Geological Survey. This area was initially brought to my attention by Richard H. Jahns, who had a first-hand knowledge of its geology. Its selection was based on the presence of numerous pegmatites and on reports of late-stage petrographic features such as clear microcline grains in clean-cut patches and veinlets, and grains with fringes of untwinned oligoclase (Montgomery, 1953), which suggest the importance of late- or postmagmatic processes in this terrane.

Montgomery (1953) regarded the "Embudo granite" as a series of granitic rock bodies among which he recognized some differences, but he considered them to be genetically related and perhaps to have been intruded over a "protracted period of geological time." He also viewed the pegmatites as younger genetic associates of the granitic rocks. This would appear to be an ideal setting for study of late-stage crystallization in granitic rocks. In the present study, however, detailed field mapping soon revealed that the geological situation is much more complicated than had been thought earlier. Intrusive contacts among the various granitic units, penetrative deformation of some of these units but not of others, and crosscutting relationships between pegmatite and quartz veins in the granitic rocks suggested that an overall genetic relationship might be more apparent than real. Further, a reinterpretation of Rb-Sr dating by Fullager and Shiver

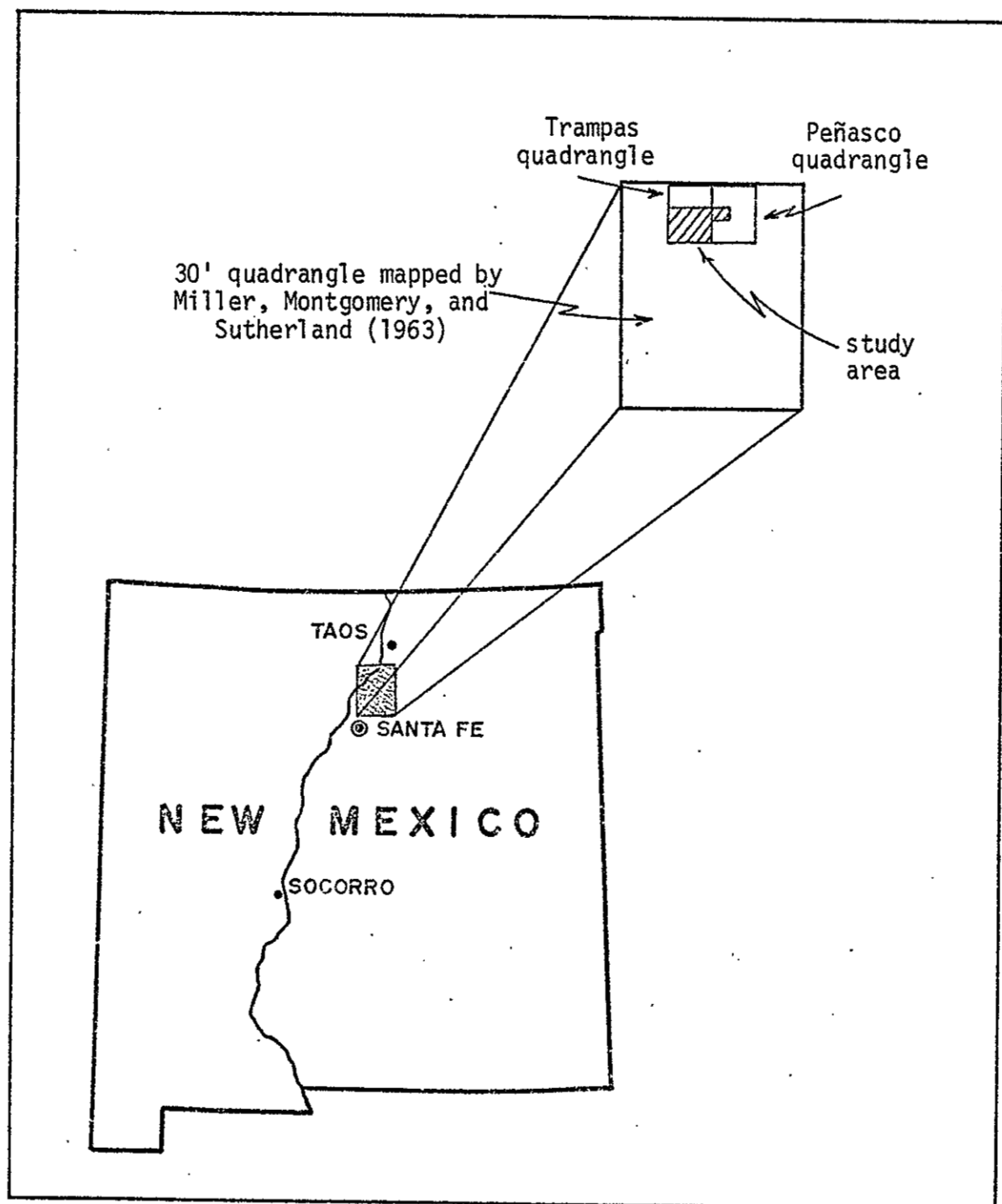


Figure 1. Map of New Mexico showing the location of the Peñasco and Trampas 7.5' quadrangles, and the 30' quadrangle mapped by Miller, Montgomery, and Sutherland (1963).

(1973) indicated that there may have been a time gap of as much as 300 m.y. between some of the intrusive episodes.

Such information clearly strained the original conception of the "Embudo granite" and in some ways made it a less attractive setting for the intended study, in that a greater complexity of metamorphic and igneous history might well obscure important relationships. On the other hand, the obvious expressions of metamorphic deformation in some of the rocks but not in others could well provide a direct basis for comparison of metamorphic and deuteritic effects. An apparent lack of evidence for a genetic relationship between the pegmatites and any of the exposed granitic rocks was disconcerting, yet the presence of aplite bodies apparently in genetic association with each of the granitic units suggested a significant role for late-stage fluids. Thus the study did not exactly follow preplanned lines, but it yielded unexpected and useful information in closely related areas of igneous petrology.

Methods of Study

The basic work in this investigation has been detailed geological mapping and sampling of the Precambrian granitic rocks and the metamorphic rocks they intrude in an area of 45 sq mi between the towns of Dixon and Peñasco in northern New Mexico. The majority of the mapping was done at a scale of 1:12,000 using the Trampas and Peñasco 7.5' quadrangles (U. S. Geological Survey) as a base. The field work was done during the summer months of 1971 and 1972, and for a brief period during the summer of 1973. More than 300 samples were collected, and selected samples were studied using the following techniques:

(1) standard petrographic examination, including modal analysis, of more than 250 standard and polished thin sections; (2) X-ray powder diffractometry of alkali feldspars; (3) chemical analysis of bulk-rock samples for Si, Al, K, Ca, Na, Mg, Mn, Fe, Ti, Rb, Sr, Zr, and Ba by nondispersive X-ray fluorescence; (4) electron microprobe analysis of selected minerals in the granitic rocks for various elements. In addition, an experimental study was done in which the distribution coefficient of barium between alkali feldspar and a synthetic granitic melt was determined as a function of temperature. The purpose of the experimental study was to help explain barium zoning observed in microcline megacrysts from some of the natural granitic rocks.

General Features of the Dixon-Peñasco Area

The study area is a Precambrian terrane in north-central New Mexico, lying between the rural towns of Dixon and Peñasco and about 20 airline miles south of Taos. It forms the southern margin of the Picuris Range, a mass that extends westward as a triangular prong from the Sangre de Cristo Range. Both the Dixon-Peñasco area and the Picuris Range are bounded on the west by the Rio Grande rift valley, and to the south and east the Precambrian rocks south of the range are covered by Cenozoic sediments of the Chamisal-Peñasco re-entrant. Figure 2 shows the location of the study area and its relationship to the major physiographic provinces of northern New Mexico.

The elevation of the area ranges from 7807 to 6020 ft, generally decreasing from east to west. Some prominent hills are present in the west half of the area, but in general the topography is subdued relative to the Picuris Range to the north (maximum elevation 10,801 ft) and

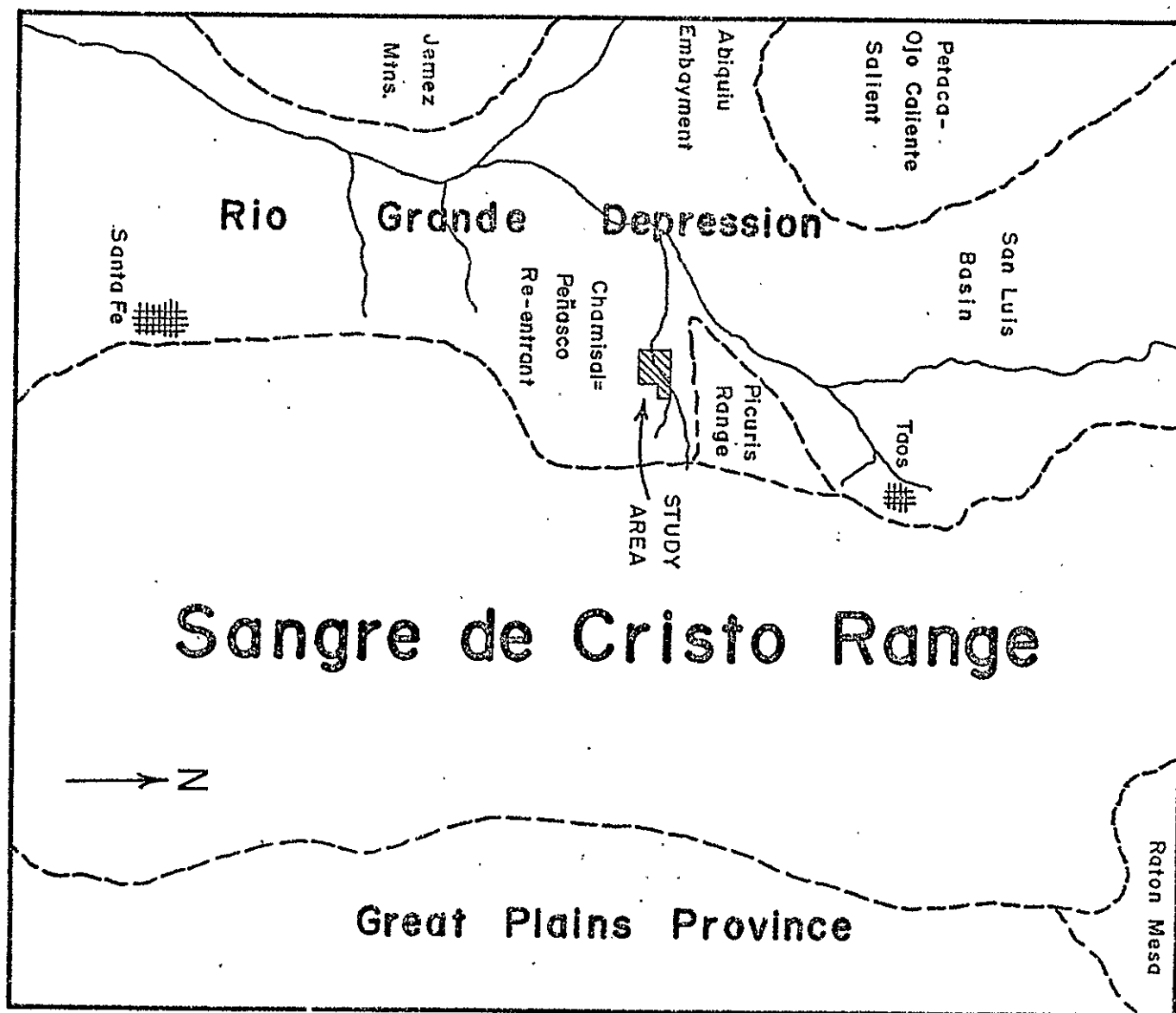


Figure 2. Physiographic setting of the study area.

the Sangre de Cristo Range to the east and southeast (maximum elevation 13,102 ft). Much of the area has been dissected by Embudo Creek and its tributaries; hence there is considerable local relief and good exposures, particularly along the steep, high walls of Embudo Canyon and along the crests of several high ridges of resistant granite.

Embudo Creek drains into the Rio Grande and is the main perennial stream of the area. Several perennial tributaries such as Rio de las Trampas, Rio Pueblo, and Rio Santa Barbara contribute to its flow, but much of the surface drainage in the area is ephemeral.

The climate is semiarid with an average annual precipitation of about 10 in. In the summer months afternoon thunderstorms are common, especially during July and August. This climate supports a typical juniper-piñon woodland to Great Basin sagebrush assemblage of vegetation at the lower altitudes and relatively open pine forests in the higher eastern and southern parts of the area.

The area is rural, and small-scale agriculture is the primary activity of the local inhabitants. Settlement and cultivation are restricted to the valley bottoms, most of which are irrigated. Access to the area is obtained via State Highways 75 and 76, and thence over numerous graded but unpaved roads. Even the most remote parts of the area generally can be reached or closely approached in a light truck or four-wheel-drive vehicle.

Previous and Current Geological Investigations of the Area

The first geologic investigation of the area was made by Just (1937), who mapped it at a scale of 1:62,500 as part of a reconnaissance study of the mineral deposits of Rio Arriba and Taos Counties. Later

Montgomery (1953) mapped the Picuris Range at a scale of 1:48,000 as part of a Ph.D. dissertation. Neither of these workers was able to concentrate much attention on the granitic rocks. Miller, Montgomery, and Sutherland (1963) extended Montgomery's earlier mapping southward and completed coverage of a 30' quadrangle, but they made no attempt to formally subdivide the granitic terrane.

Aldrich and others (1958) reported some Rb-Sr and K-Ar ages for minerals from the Harding pegmatite, but no other dates for rocks in the area were recorded until Fullager and Shiver (1973) suggested a uniform Rb-Sr age for the "Embudo granite." Since then K-Ar mineral ages of pegmatite and granite samples from the area have been estimated by Gresens (1975).

Nielson (1972) and Nielson and Dunn (1974) have outlined the structure, stratigraphy, deformation, and metamorphism of rocks in the Picuris Range. The results of their studies are important for the correlation of metamorphic events in the country rocks with metamorphism in the granitic rocks.

In connection with geochemical studies, Gresens and Stensrud (1974a, b) examined the Precambrian stratigraphy of the Dixon-Peñasco area and attempted to correlate it with that of the Las Tablas-La Madera area to the northwest. They reinterpreted some of the age relations among the metamorphic rocks, but results of the present study do not confirm their conclusions.

II. GENERAL GEOLOGY

Regional Setting

The Dixon-Peñasco area is part of an extensive Precambrian terrane that also forms much of the southern Sangre de Cristo Range. The igneous and metamorphic rocks of this range are in fault or depositional contact with Cenozoic sedimentary deposits, and along its eastern margin with Carboniferous marine sedimentary rocks. In the Dixon-Peñasco area, only Cenozoic sediments and Precambrian metamorphic and igneous rocks are present. Where they are in contact, the Cenozoic sediments appear to rest depositionally upon the older rocks, as shown on the generalized geologic map of the area (fig. 3). Only the Precambrian rocks have been given detailed attention in this study.

Precambrian Metasedimentary and Metavolcanic Rocks

The metamorphic rocks of the Dixon-Peñasco area can be divided into two main units: (1) an older assemblage, the Ortega Group, consisting of metaquartzite, schist, and phyllite; and (2) a younger assemblage, the Vadito Formation, consisting of metaquartzites, metaconglomerate, schist, and amphibolite. These two units are given group status because of their internal complexity, the presence within them of mappable formations, and the geologic significance of the formations within each group. Specifically, the Ortega Group includes the Ortega Quartzite, the Rinconada Schist, the Pilar Phyllite, and the Piedra Lumbre Formation. The Vadito Group has been divided into

a lower metasedimentary unit comprising conglomerate, quartzite, and schist members, and an upper amphibolite unit that consists of interlayered mafic flows, metavolcanic conglomerates, and mafic meta-sediments with minor discontinuous beds of recrystallized chert.

Cross-bedding in the metasedimentary sequence near the base of the Vadito Group indicates that the Ortega Group is stratigraphically lower and hence older. This is the same age relation that Montgomery (1953) established earlier, primarily from structural relationships. Recent speculation that the age relations should be inverted (Gresens and Stensrud, 1974a, b) is not in accord with the evidence provided by the observations of cross-bedding. Figure 4 shows a general stratigraphic section of the Vadito Group and the portion of the Ortega Group that crops out in the map area of figure 3 and plate I. Figure 5 is a specific detailed stratigraphic section, the location of which is shown in figure 3. Southeast of the area represented by figure 5, stratigraphic relationships within the Vadito Group are complicated by isoclinal folding and a belt of amphibolite.

The amphibolite is the youngest stratigraphic unit, but its relationship to the quartzite and schist exposed to its southeast is not yet fully understood. The quartzite and schist may be coeval equivalents of the schists north of the amphibolite belt, or they may be the upward extensions of a thick schist sequence that is unconformably overlain by the amphibolite. In either case the exposed amphibolite appears to occupy the central parts of synforms and is the youngest Precambrian stratigraphic unit exposed in the area.

The complexity of the Vadito Group rocks is increased by the presence of amphibolite dikes, mainly in the schist north and northwest

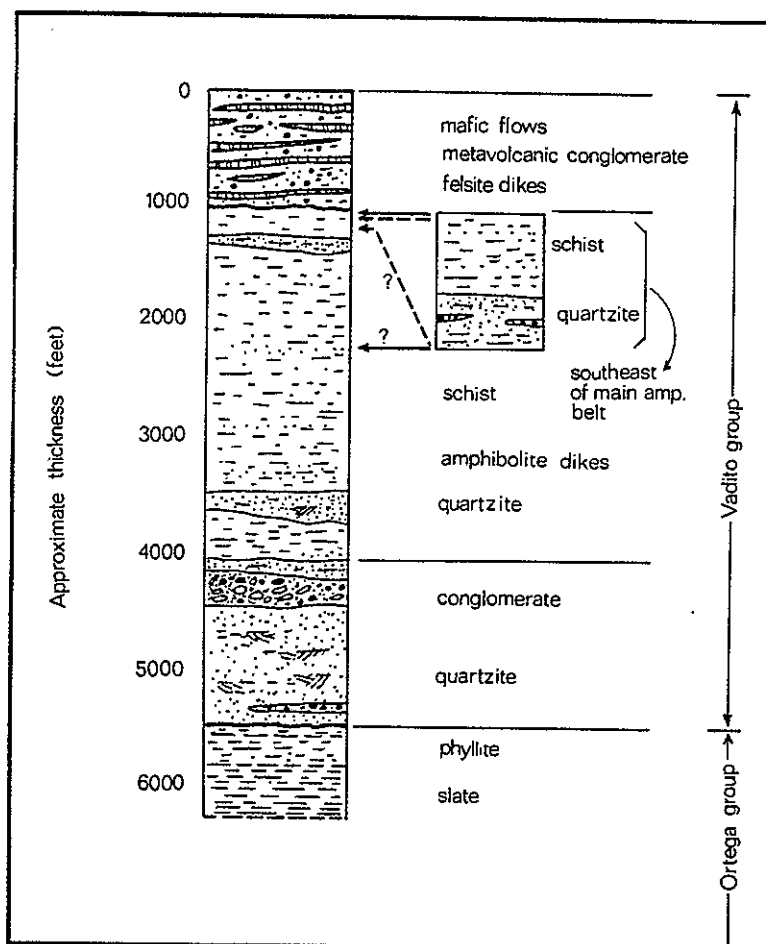


Figure 4. Generalized stratigraphic section of the Vadito Group rocks, showing stratigraphic relationships between the main Vadito sequence and the schists and quartzites southeast of the main amphibolite belt.

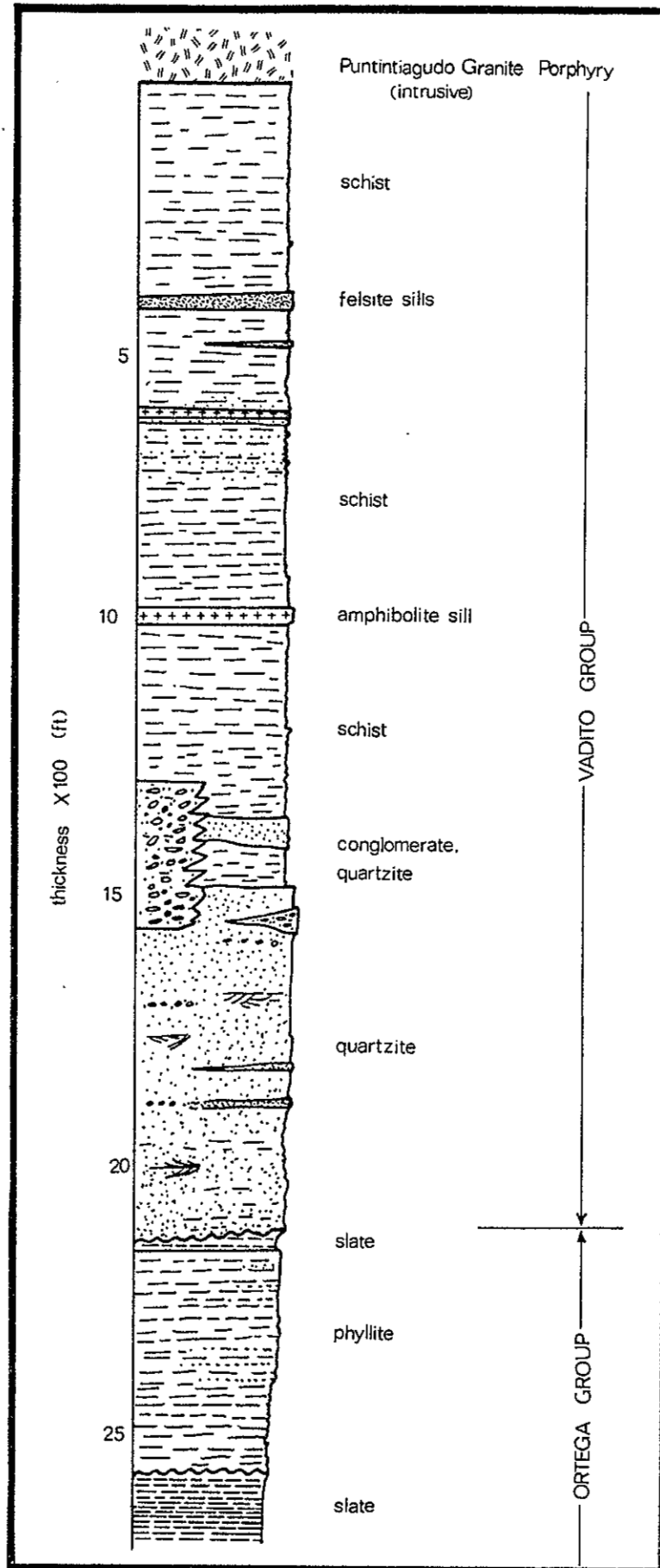


Figure 5. Detailed stratigraphic section showing the contact between Ortega and Vadito rocks.

of the main amphibolite unit, and felsite dikes that occur primarily within the amphibolite unit. The amphibolite dikes probably were emplaced at about the time when rocks of the main amphibolite unit were accumulating as extrusives on the then-existing surface. The felsite dikes were emplaced later on, and probably in several episodes; they may have marked the onset of granitic magmatism, although some may have been related to one of the younger granite intrusions.

Precambrian Granitic Rocks

General Statement

The granitic rocks of the area, as shown in figure 3, comprise four major intrusive units and numerous smaller bodies of pegmatite. The sequence of granitic magmatism began with emplacement of a metadacite stock (Cerro Alto Metadacite), along with widespread sills and dikes of similar lithology. This was followed by emplacement of a more coarse-grained and foliated complex of granite to quartz monzonite porphyry (Puntiagudo Granite Porphyry) with distinctive phenocrysts of microcline and quartz. This rock in turn was apparently intruded by a large body of foliated biotite quartz monzonite (Rana Quartz Monzonite). The last major episode resulted in intrusion of a sphene-bearing biotite quartz monzonite to granodiorite (Peñasco Quartz Monzonite). All of these units were postdated by pegmatites, most of which appear to be distinctly younger than the last granitic intrusion, but which themselves probably represent more than one generation of magmatism.

Cerro Alto Metadacite

The metadacite, oldest of the granitic units in the area, is a dark- to medium-gray, fine-grained, slightly foliated rock containing scattered small (<2 mm) phenocrysts of quartz and plagioclase. The groundmass consists principally of quartz, plagioclase, and K-feldspar with flecks of biotite, muscovite, and magnetite. The rock occurs primarily as a stocklike body shown approximately at the center of figure 3. The westerly margin of the body is in discordant intrusive contact with Vadito metamorphic rocks. Along the easterly margin, however, the relationships are less clear. Here the rock is marked by slabby jointing that resembles bedding or flow banding, and it is more conformably related to the country rocks.

Many isolated sills of metadacite are present in the main amphibolite unit. They are similar in shape and size to the felsite sills but invariably predate them. In a few places there are lithologic gradations between the metadacite sills and the more leucocratic felsite sills.

The metadacite is cut by the other granitic rocks and also occurs as inclusions within them. The inclusions, though not abundant, are so widespread that it is reasonable to assume a once extensive distribution of the metadacite prior to intrusion of the younger granitic rocks. It should be noted that the Cerro Alto Metadacite constitutes part of what Montgomery (Miller and others, 1963) mapped as "Vadito Conglomerate-felsite" (Vcf). The remainder of Vcf in this area comprises schist, fine-grained quartzites, and minor conglomeratic rocks.

Puntiagudo Granite Porphyry

The Puntiagudo Granite Porphyry has a fabric distinguished by subequant and subhedral, Carlsbad-twinned phenocrysts of microcline (1 cm in maximum dimension) and rounded phenocrysts of quartz set in a fine- to medium-grained matrix of plagioclase, K-feldspar, biotite, and muscovite. Modally the rock is a quartz monzonite, locally grading to granodiorite. It occurs as a massive body of irregular shape that is in very sharp, discordant contact with the Vadito rocks. It is featured by a thin border zone (0 to 20 m) of finer grained rhyolitic rock that appears to reflect marginal chilling. Dikes of fine-grained rhyolite also are present, mainly in marginal parts of the body. Aside from the border zone and the dikes, the unit consists of mineralogically homogeneous rocks. Marked textural variations, however, are expressed by differences in abundance of phenocrysts and differing degrees of rock deformation. Foliation is evident in most places, and generally parallels the northeast to east regional trend of structural features in the Precambrian terrane.

Rana Quartz Monzonite

The Rana Quartz Monzonite is dominant among the granitic rocks exposed in the area. Available field evidence such as probable inclusions of Puntiagudo Granite Porphyry suggests that it is younger than the Puntiagudo Granite Porphyry, but the paucity of contact between the two units and the uncertainty of the evidence make it difficult to definitely establish the age relationship. Most of the Rana is a medium-grained foliated biotite quartz monzonite to granodiorite. The biotite grains

have been partly shredded and recrystallized, and they are commonly transected by larger fresh grains of muscovite. The plagioclase has been partly granulated and extensively altered to sericite, epidote, and clinozoisite. The degree of deformation increases somewhat to the south so that the rock in some of the southernmost outcrops shown in figure 3 is strongly lineated. In addition to a prevailing foliation that follows the regional structural trend, closely spaced fractures (\approx N. 50° W.) and narrow ductile shears that trend northeast are present in some places. Thus the Rana Quartz Monzonite appears to reflect at least two and probably three events of regional deformation; this is consistent with the regional deformations inferred by Nielson and Dunn (1974) from Ortega Group rocks to the north.

In addition to the main mass of foliated rocks, the quartz monzonite body is marked by a discontinuous border zone of fine-grained leucocratic muscovite granite that contains oblate phenocrysts of quartz and, locally, phenocrysts of microcline, and by a mass of unfoliated biotite quartz monzonite that is modally similar to the foliated quartz monzonite but lacks biotite alignment and extensive granulation of plagioclase. Both these subunits are in gradational contact with the main mass of foliated biotite quartz monzonite.

The Rana Quartz Monzonite in general shows strong discordance with the rocks it intrudes, although apophyses of border zone rocks commonly are concordant and appear much like the isolated felsite dikes in the amphibolite. This suggests that at least some of these discrete felsite dikes may be directly related to the intrusion of the Rana Quartz Monzonite. Textural, compositional, and structural variations

among the dikes, however, indicate that more than one generation may well be represented.

Peñasco Quartz Monzonite

The youngest major granitic unit is the Peñasco Quartz Monzonite, which is in intrusive contact with the Rana Quartz Monzonite, as shown in the southeast part of figure 3. Like the Rana, it is a biotite quartz monzonite to granodiorite, but it contains more biotite, is featured by wedgelike crystals of sphene, and, in some places, contains less quartz and more plagioclase. Further, the Peñasco rocks lack the strongly pervasive foliation so prevalent in the earlier granitic rocks and, in some areas, they contain abundant tabular megacrysts of Carlsbad-twinned microcline as much as 9 cm in maximum dimension.

The intrusive body of Peñasco rocks is generally conformable with the amphibolite country rocks, particularly in the area just north of Embudo Creek (eastern part of fig. 3). It lacks a distinctive border zone, contains mafic inclusions that are most abundant near its margins, and shows minor migmatization along its contacts. Local chevron folding in the amphibolite near the intrusive contact suggests that forceful injection was important in the emplacement of the quartz monzonite.

Pegmatites

Bodies of pegmatite cut all of the granitic rocks in the area; hence at least some of them are younger than the youngest granitic intrusion. They can be characterized according to five groups:

- (1) simple pegmatites in bodies of relatively small size, containing

microcline, quartz, albite, and muscovite with minor green beryl; these constitute the most abundant type; (2) faintly to well-zoned bodies of generally larger size with various amounts of exotic mineralization; the Harding pegmatites belong in this category; (3) small, zoned bodies of pegmatite containing only albite, quartz, and muscovite; (4) pegmatite-aplite pairs occurring as small dikes, primarily in one locality near Peñasco; and (5) tourmaline-bearing pegmatite in medium-sized, slightly zoned dikes consisting mainly of K-feldspar, plagioclase, quartz, and tourmaline; observed in only one locality 1.5 mi north of Peñasco. In addition, pink to white aplite dikes, which apparently are unrelated to any pegmatites, occur in both the Rana and Peñasco Quartz Monzonites. Quartz veins and pods typically occur in all the Precambrian rocks of the area.

The diverse types of pegmatite suggest that more than one age of pegmatite formation is represented in the area. Further, the pegmatites are consistently younger than the aplite dikes and quartz veins. These aplites may well represent the rest-liquid fractions of the granitic rocks that enclose them, as they are restricted to these rocks and are in part gradational with them. If this is the case, it suggests that the pegmatites, which are younger, may have originated not as rest-liquids of the granitic rocks they cut, but perhaps as rest-liquids of an intrusive body not exposed at the present surface. That the pegmatites cut quartz veins indicates that they are younger than a period of post- or late-magmatic hydrothermal activity, further pointing toward a separate magmatic event for them. Two other field observations also support this notion. First, the pegmatites do not have a consistent spatial relationship to any of the exposed granitic rocks. They are

distributed sporadically throughout the area, possibly increasing slightly in abundance southward along with increasing deformation in the Rana Quartz Monzonite. Second, the granites do not show the kind of compositional variation with time that would lead ultimately to pegmatite formation. Instead, the youngest granitic unit is one of the most mafic plutonites and thus appears least likely to have given rise to pegmatites. Available radiometric ages, although open to some question, indicate that the Harding pegmatite is as much as 100 m.y. younger than the youngest granite. This casts doubt upon any proposed genetic relationship between the pegmatites of the Harding type and the granitic rocks exposed in the area.

Alteration of the Granitic Rocks

Three main types of alteration have been observed in the area: (1) alteration along shear zones, resulting in a quartz-muscovite assemblage; (2) alteration resulting in reddening of feldspars and ultimately in deposition of vein epidote. This kind of alteration occurs in random patches in the Puntiaquedo Granite Porphyry and in the Rana Quartz Monzonite; (3) alteration resulting in deposition of tourmaline and tourmaline-quartz veins. Age relationships among these contrasting types of alteration are uncertain, but it is likely that the quartz-muscovite alteration preceded the other two. It is clear that the epidote alteration occurred after the latest shearing event and the formation of quartz veins and pegmatites.

The epidote alteration is the most widespread, and except for control by joints at some localities, it appears to have been little influenced by structural features. Nor is it spatially correlated

with pegmatite bodies. The available evidence implies that this type of alteration may have been the result of a thermal event occurring after the time of pegmatite emplacement. No significant megascopic alteration has been observed in the Peñasco Quartz Monzonite, but there is some alteration of plagioclase on a microscopic scale. The tourmaline alteration is very common in some localities, especially in the Vadito metasediments, and it also occurs in the Rana Quartz Monzonite. It probably occurred at nearly the same time as the rare tourmaline-bearing pegmatites. These pegmatites cut the Peñasco Quartz Monzonite; hence the tourmaline alteration probably is younger than that rock.

Cenozoic Sedimentary Deposits

General Statement

The only younger rocks in the Dixon-Peñasco area are Cenozoic sedimentary deposits. They consist of poorly sorted to conglomeratic tuffaceous beds (Picuris Tuff) that grade upward into, or interfinger with, a thick sequence of coarse, poorly sorted fluvial sediments (the Tesuque Formation). These buff-colored units are mid-Tertiary in age and are unconformably overlain by Quaternary deposits of boulder gravel (Ancha Formation) and by younger Quaternary alluvium that predates the modern stream deposits. In addition, a mantle of fine brown to tan silt and silty material with rare pebbles and pebble layers is present locally. This material may be equivalent to the Espanola Formation (Galusha and Blick, 1971). It tends to fill topographic depressions and locally reaches a thickness of 15 ft. Currently it is being gullied by ephemeral streams. The youngest deposits in the

area are the Holocene alluvium of the minor flood plains and stream beds. These deposits are particularly well developed where streams cut through the Tesuque Formation.

Picuris Tuff

The Picuris Tuff appears to occur locally near, or at the base of, the Tesuque Formation. It is recognized primarily by its greater degree of induration relative to the Tesuque, and to a lesser extent by its tuffaceous character. It has been observed only in minor occurrences beneath the southeastern and eastern outcrops of Tesuque Formation (pl. I). Just to the east of the area mapped, occurrences of conglomerate were noted to consist of locally derived clasts of biotite quartz monzonite. Strata of similar lithology were interpreted by Montgomery (1953) as a basal unit in the Picuris Tuff. The type locality of Picuris Tuff occurs 2 mi north of Peñasco where it is easily identified, but the relationship between the outcrops of the type locality and the outcrops in the map area is not clear. Unfortunately, this also means that the stratigraphic relationship between the Tesuque Formation and the type Picuris Tuff is obscure. The Picuris Tuff is physically near the base of the Tesuque Formation; however, it is not certain that it is definitely older than the bulk of the Tesuque Formation, as it occurs over a wide area and was deposited on a surface with as much as 1000 ft of relief. It is not known, then, whether there is an unconformity between the two units, whether they are interbedded and thus in part coeval, or whether there is a facies change between them.

Tesuque Formation

The type section of the Tesuque Formation, just north of Santa Fe, was defined by Baldwin (1956) as the middle unit of the Santa Fe Group (see also Galusha and Blick, 1971). The unit presumably extends north to the Dixon-Peñasco area, where it is mainly in depositional contact on the Precambrian rocks. Its thickness in this area is on the order of 1000 ft, but it thins rapidly where it laps up onto the crystalline rocks. Contacts between the Tesuque Formation and the older rocks generally are poorly exposed, but they appear to be irregular in plan view and variable in dip. The lithology of the underlying or adjacent Precambrian rocks is strongly reflected in the clasts of the Tesuque near the contacts. The local steepness of such contacts is consistent with the observation that the Tesuque was deposited on a surface of considerable relief, and there can be little doubt that the Precambrian rocks were at least locally a significant source of coarse detritus during Tesuque time.

The Tesuque Formation comprises variegated beds of sand, silt, gravel, conglomerate, breccia, and volcanic ash. It is generally buff colored and is consistently ill sorted. Wide variations in degree of induration of alternating beds are reflected by ribbed cliffs at some localities. A typical exposure is shown in figure 6. The stratigraphy of the Tesuque Formation is poorly known. No attempt was made to correlate beds in the formation, but it seems clear that discontinuous beds are the rule, and Miller (Miller and others, 1963) reported that few beds can be traced for distances of 1 to 2 mi. Stratification generally dips south-southwestward at angles of 1° to



Figure 6. A typical exposure of Tesuque Formation, 0.75 mi north of La Cuestecita.

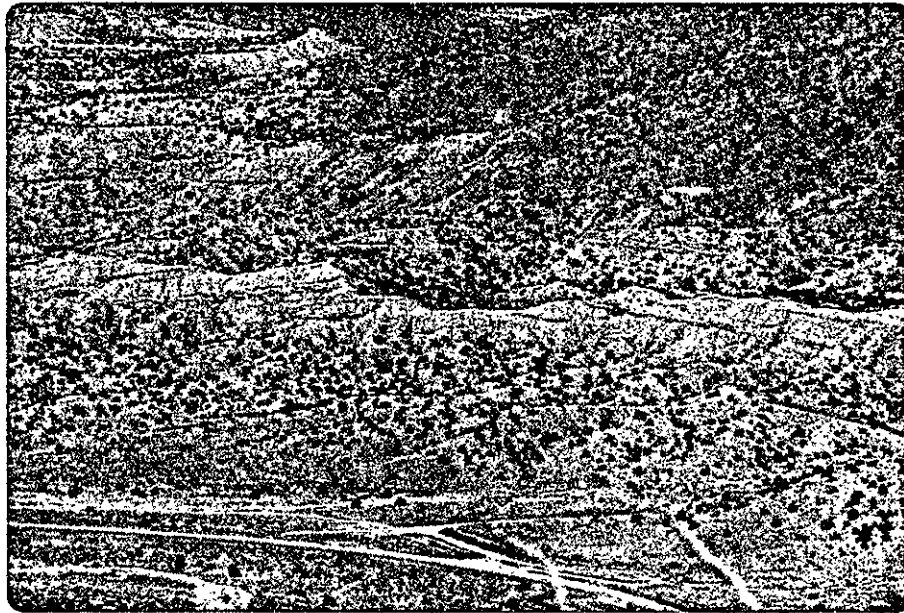


Figure 7. A gentle fold in Tesuque Formation, approximately 0.5 mi north of Apodaca, New Mexico.

10°, but at one locality near the western edge of the map area a broad, gently plunging anticline can be observed (fig. 7). No faults were seen to cut the Tesuque Formation in the map area, but air photo lineations in the basement terrane appear to extend into areas of the Tesuque Formation as definable morphologic features such as stream valleys and gullies. The structural features thus show that late Tertiary tectonic movements in the area have either folded or fractured the Tesuque Formation as the underlying basement blocks were jostled.

The age of the Tesuque Formation is uncertain, but vertebrate faunas found near Pojoaque and Espanola suggest a Miocene-Pliocene age (Frick, 1937; Simpson, 1953). Presumably the strata outcrops in the Dixon-Peñasco area are of a similar age. Work currently in progress by Kim Manley of the U. S. Geological Survey, Denver, should provide more definitive information about the Tesuque Formation.

The name Ancha Formation has previously been applied to gravel deposits overlying the Tesuque Formation, and Miller and others (1963) considered it to be the upper member of the Santa Fe Group. Manley (1974) more appropriately chose to consider it post-Santa Fe and pointed out that it may be misleading to give all such gravel deposits the formational name Ancha. Following this suggestion, the thick gravel deposits that lie to the southwest of the main outcrops of Precambrian rocks are here referred to informally as the gravel deposits of Cejita Mesa. These deposits are on the order of 200 ft thick and consist largely of sand and gravel. Quartzite is the dominant lithology among the clasts.

Younger Terrace Gravels

Gravels whose elevation and geomorphic expression show that they are younger than the gravels of Cejita Mesa are here referred to informally as the younger terrace gravels. They are lithologically similar to the Cejita Mesa gravels and probably were derived from them either as lag deposits or as products of a more active fluvial reworking. In either case these younger deposits seem to represent temporary base levels in the erosional history of the area.

Some deposits mapped as younger terrace gravels, notably those just east and northeast of Cerro Puntigudo and those north of Trampas (pl. I), may in fact be direct correlations of the Cejita Mesa gravels. They are considerably thinner than the typical Cejita Mesa deposits, but could be erosional remnants. The correlation is difficult to prove or disprove, owing to geographic separation and the inherent complexity of such gravel deposits. Manley (1974), for example, has postulated "shifts in drainage direction with time" and "considerable post Santa Fe Group topographic relief."

Brown Sand-Soil Deposits

The brown sand-soil deposits occur locally on the upland surfaces of the eastern and northern parts of the area. They mantle terrace gravels in some localities, but their relationship to the younger terrace gravels (e.g., south and southwest of Cerro Puntigudo) is uncertain, although there is a conspicuous absence of the brown sand-soil deposits in the more dissected areas. Figure 8 shows a typical exposure of the material, which on all slopes is gullied by recent stream erosion.



Figure 8. A typical exposure of brown sand-soil deposit, about 1 mi northwest of Cerro Alto.

Its origin is uncertain, but it may be equivalent to, or reworked from the Espanola Formation which is primarily a wind-blown sand (Galusha and Blick, 1971). Its occurrence and lithology suggest that it may have a large eolian component. In some localities, it is difficult to distinguish from Holocene alluvium, since both can occupy stream bottoms, but it is a significant map unit because it commonly obscures the Precambrian rocks in areas where Holocene alluvium is not present.

Holocene Stream Deposits

Erosion and deposition by currently active streams in the Dixon-Peñasco area has produced significant Holocene alluvial deposits. The largest occurrences are along Embudo Creek downstream from Cañoncito and along Cañada de Ojo Sarco and Las Trampas tract. In some areas, especially along Las Trampas tract, Cañada de Ojo Sarco, and near Chamisa, what has been mapped as Holocene stream deposits (based largely on morphology) may actually be brown sand-soil deposits or at least products from the reworking of such deposits.

The occurrence of Holocene stream deposits along the Río de Las Trampas, especially at Vallecito and Las Trampas tract, is curious in that they form large hollows (up to 0.5 mi long) between exposures of Precambrian rocks. This apparently is due to the relatively soft, unconsolidated character of the underlying Tesuque Formation. The asymmetry of ridges between Río de Las Trampas and the Cañada de Ojo Sarco, and between Cañada de Ojo Sarco and Cañada de Oso, suggests lateral migration of these streams with time. The cause of such migration is not apparent, but it is interesting that these are the same

streams that tend to line up as extensions of air photo lineations in the exposed Precambrian terrane. Again, their position and possibly their migration may have been controlled in part by joints in the Tesuque Formation that could have been caused by a slight jostling of the Precambrian basement in this area. Such adjustments probably were related to uplift of the Picuris Range and Sangre de Cristo Range along marginal faults of the Rio Grande rift.

III. METASEDIMENTARY AND METAVOLCANIC ROCKS

Ortega Group

Rocks of the Ortega Group crop out mainly in the Picuris Range, where the older units of the group, the Ortega Quartzite and the Rinconada Schist, are found. The younger units of the group, the Pilar Phyllite and the Piedra Lumbre Formation, crop out in the northwest corner of the map area (pl. I). The Ortega Quartzite and the Rinconada Schist do not occur in the map area, but they have been discussed in detail by Montgomery (1953), Miller and others (1963), Nielsen (1972), Nielsen and Dunn (1974), and Holdaway (1975). The work of Nielsen and Dunn has corroborated Montgomery's initial suggestion that the Pilar Phyllite and the Piedra Lumbre Formation are the uppermost units of the Ortega Group but are older than nearby rocks of the Vadito Group. Except for some differences in assigned nomenclature, the results of my field work are in essential agreement with those of Nielsen and Dunn (1974).

Pilar Phyllite

The Pilar Phyllite was named as a member of the Ortega Formation by Montgomery (1953) on the basis of extensive outcrops of phyllitic slate south and west of Pilar, New Mexico. These rocks occur only in the extreme northwest corner of the map area (pl. I), but they are part of a belt of Pilar Phyllite that extends off the map area and forms a portion of the southern limb of a westward-plunging anticline

(Miller and others, 1963, pl. I). The general lithology of the Pilar Phyllite has been described by Montgomery (1953), and the description that follows here is limited to the rocks occurring in the small area of exposure shown on plate I.

Lithology

The Pilar Phyllite is dark gray except on cleavage surfaces, which have a slight sheen that gives the rock a medium-gray to medium-light-gray appearance. The well-developed slaty cleavage also gives most outcrops a rubbly to slabby appearance. The general lithology is intermediate between phyllite and slate, and Just (1937) originally referred to the formation as the Hondo Slate. Montgomery (1953) noted that the name Hondo had prior usage and substituted Pilar; he also preferred a designation as phyllite.

The rock is extremely fine grained except for muscovite flakes visible with a hand lens on cleavage surfaces, quartz-muscovite veins (1 mm thickness) that parallel the cleavages, and minute porphyroblasts (0.4 mm) that occur along some layers in the matrix. Some of the quartz veinlets cut across the cleavage. The veinlets also typically contain small lenticular cavities and locally are stained by iron oxides. The spacing and continuity of these veinlets differ considerably from outcrop to outcrop, which may account for the characteristic variability in coarseness of rubble derived from the rock.

The following description of thin sections from the Pilar rocks is quoted directly from Montgomery (1953, p. 20):

Thin sections show a very fine-grained mineral aggregate, in which dark, streaky patches of carbonaceous material are very prominent. Crossed nicols show elongate quartz grains,

0.01 to 0.02 mm. long and murky from carbonaceous inclusions, strung out irregularly in sub-parallel orientation. Interspersed with them are muscovite flakes 0.05 by 0.01 mm. in size. The quartz commonly makes up 50% to 75% of the rock; the muscovite 15% to 30%. The muscovite plates are not generally matted together, but some form very thin, continuous trains. Darker parts of the rock, relatively rich in carbonaceous matter, in some places cross the foliation as distinct bedding layers.

Larger quartz grains, as much as 0.25 to 0.5 mm. in size, occupy lenticular areas or criss-crossing veinlets 0.1 to 0.25 mm. wide. The grains rarely are flattened perpendicular to the veinlet walls. Some veinlets offset other veinlets where they cross, and some are complexly folded on a minute scale. Most sections show a scattering of lenticular porphyroblasts 0.1 to 0.5 mm. in size that consist of yellowish or dark-brownish limonitic material. Some of these augen are wisplike, and a few are bent into pinwheel shapes. Some porphyroblasts show traces of biotite stained dark by iron oxides, and others have a distinct outline, generally rounded, squarish, or diamond-shaped. A few stubby-prismatic shapes stand across the foliation. These crude relic porphyroblasts constitute as much as 5% of the rock in most places.

Structural Features

In the small area of Pilar Phyllite that was examined, the attitude of the slaty cleavage ranges from about N. 66° W. strike, 58° S. dip to about N. 75° E. strike, 75° S. dip. Small-scale isoclinal and chevron folds (wavelength 1 to 2 m) occur locally and crenulations with axial plane traces trending N. 75° E. and plunging N. 75° W. at 42° S. are developed on cleavage planes. The variability in attitude of the cleavage suggests that large-scale folding may be present within the Pilar at this locality. The observable small-scale folding and crenulations also suggest that the rocks may have been deformed rather incompletely relative to nearby quartzite units. Local well-developed vertical joint sets strike N. 77° E.

Piedra Lumbre Formation

General Statement

Piedra Lumbre is a new formational designation here applied to an eastward-tapering belt of rocks that lie stratigraphically and physically between the Pilar Phyllite and rocks of the Vadito Group. The name derives from Cañada de Piedra Lumbre, which transverses excellent exposures of an apparently complete section of the formation. Montgomery (1953) mapped these rocks as a muscovite-quartz-biotite-garnet phyllite unit of the Rinconada Schist Member of the Ortega Formation. Nielsen (1972), however, recognized that the rocks of the Piedra Lumbre Formation are lithologically and stratigraphically distinct from the upper part of the Rinconada Schist, noting in particular that they contain less garnet. Unfortunately, he referred to this unit as the muscovite-biotite phyllite member of the Pilar Formation. This requires an unnecessary redefinition of earlier nomenclature, in that Montgomery's (1953) Pilar Phyllite (member status) did not include the Piedra Lumbre Formation. Thus the most straightforward revision of the nomenclature is to rename the rocks that Montgomery erroneously thought were part of the Rinconada Schist. A comparison of Piedra Lumbre terminologies is given in figure 9.

Regardless of terminology, the work of Nielsen (1972) and Nielsen and Dunn (1974) has made the stratigraphic relationships clear. The Pilar Phyllite is directly and conformably overlain by a sequence of mainly phyllitic rocks, the Piedra Lumbre Formation, which separates the Pilar rocks from the overlying Vadito Group rocks stratigraphically but not everywhere physically. This contact between the Pilar Phyllite

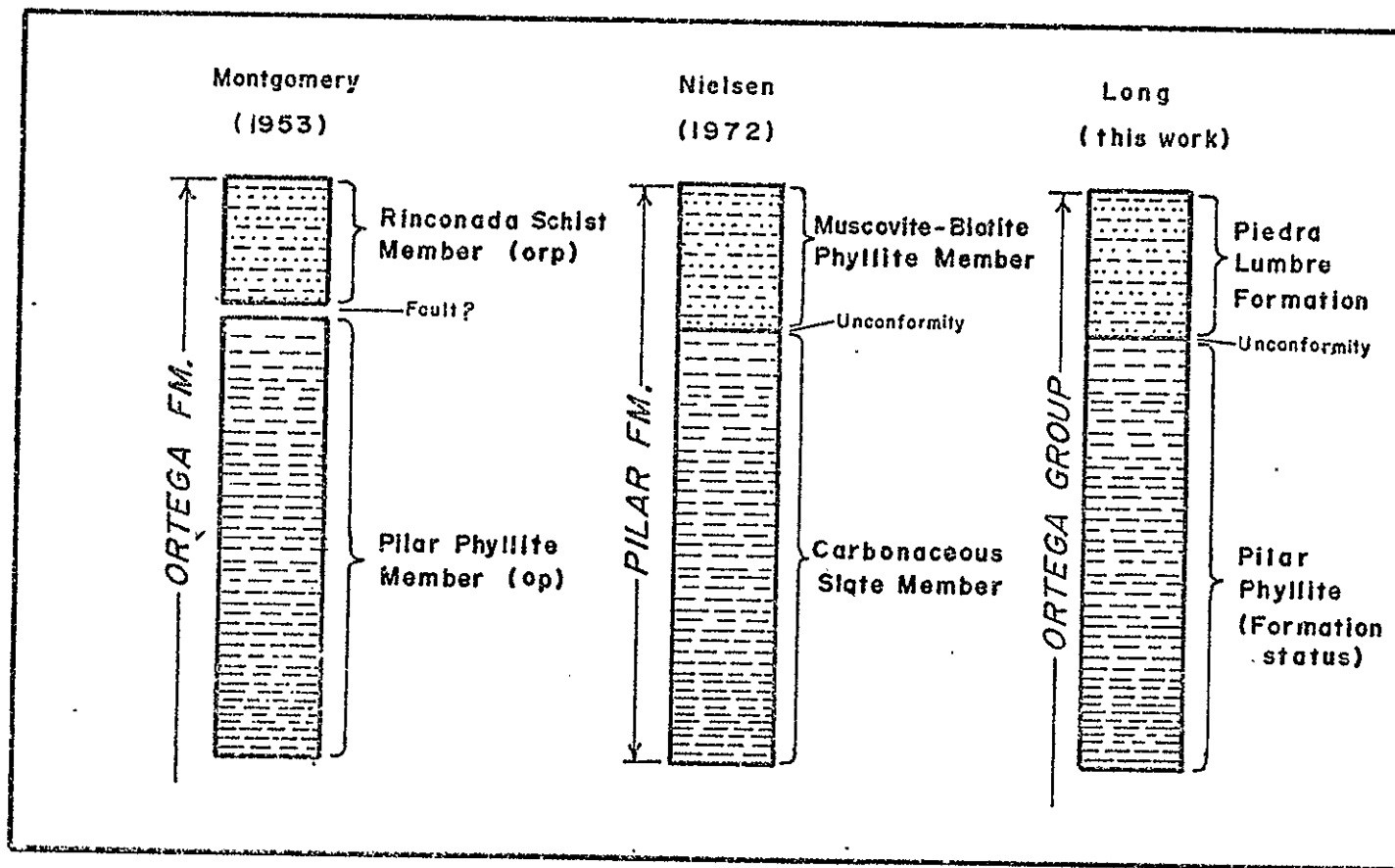


Figure 9. Comparison of Pilar Phyllite terminologies.

and the Piedra Lumbre Formation is in one sense gradational, as some of their lithologies are similar, but it can be accurately mapped. The contact between the Piedra Lumbre Formation and the overlying Vadito Group rocks is sharp. Stratigraphic and structural relationships immediately east of the map area (Nielsen, 1972, pl. I) indicate that the contact is either an unconformity or a fault. Nielsen (1972) and Nielsen and Dunn (1974) mapped this contact in two localities and concluded that it is an unconformity. Detailed examination of this contact in the SE¼ sec. 24 revealed no evidence of a fault, even though the lithology of the upper part of the Piedra Lumbre Formation is such that any fault should have created a significant zone of disruption. In the absence of positive evidence for a fault in a situation where such evidence might be expected, the Vadito Group rocks are here considered to unconformably overlie the Piedra Lumbre Formation in accordance with the interpretation made by Nielsen (1972).

Distribution.

The Piedra Lumbre Formation is exposed only in the northeast corner of the map area. About 4 mi north-northwest of this area, extensive outcrops along Rito Cieneguilla and the uppermost reaches of Hondo Canyon have been mapped by members of the University of North Carolina field camp. Results of that mapping, as compiled by Nielsen (1972), show the expected stratigraphic relationships. Furthermore, Montgomery's (1953) description of certain calcareous beds in the Cieneguilla exposures matches perfectly the calcareous beds observed in the exposures along Cañada de Piedra Lumbre. Thus, there seems little doubt as to the equivalence of the rocks in these two areas of exposure.

Lithology

The formation as mapped along Cañada de Piedra Lumbre actually consists of distinctive subunits which can be readily mapped at a scale of 1:12,000. A detailed stratigraphic section is shown in figure 10. The lowermost subunit is about 120 ft thick and consists of quartz-muscovite-biotite-garnet-staurolite phyllitic schist. It has a characteristic light-gray sheen on crenulated cleavage surfaces and is specked with 1 mm polyhedra of garnet, 2 mm tablets of biotite, and widely scattered 3 to 5 mm anhedral crystals of staurolite. Small pods of quartz (<5 cm) and iron stains are common. In the area of the detailed section, the rock becomes somewhat finer grained, with smaller porphyroblasts, and it becomes less crenulated upward in the section.

The lowermost subunit is overlain by a sequence of closely interbedded schist and quartzite, a typical sample of which is shown in figure 11. The schist layers are light gray, phyllitic, and consist of quartz, muscovite, and biotite with minor garnet. The quartzite is medium dark bluish gray, fine grained, and contains biotite. The thickness of the quartzite beds ranges from 1 cm to 1 m. The schist is generally subordinate except toward the top of the sequence, where bedding becomes generally finer and the rock has a higher percentage of schist. Thus the uppermost 25 ft of section is primarily black phyllitic schist with white banding. The quartzite beds in the lower part of the subunit have small-scale cut-and-fill features, and some 2 to 15 cm beds of calcareous material are present. On a weathered surface, these calcareous beds are distinctively light yellowish gray, pale yellowish gray, or pale yellowish brown and contain randomly

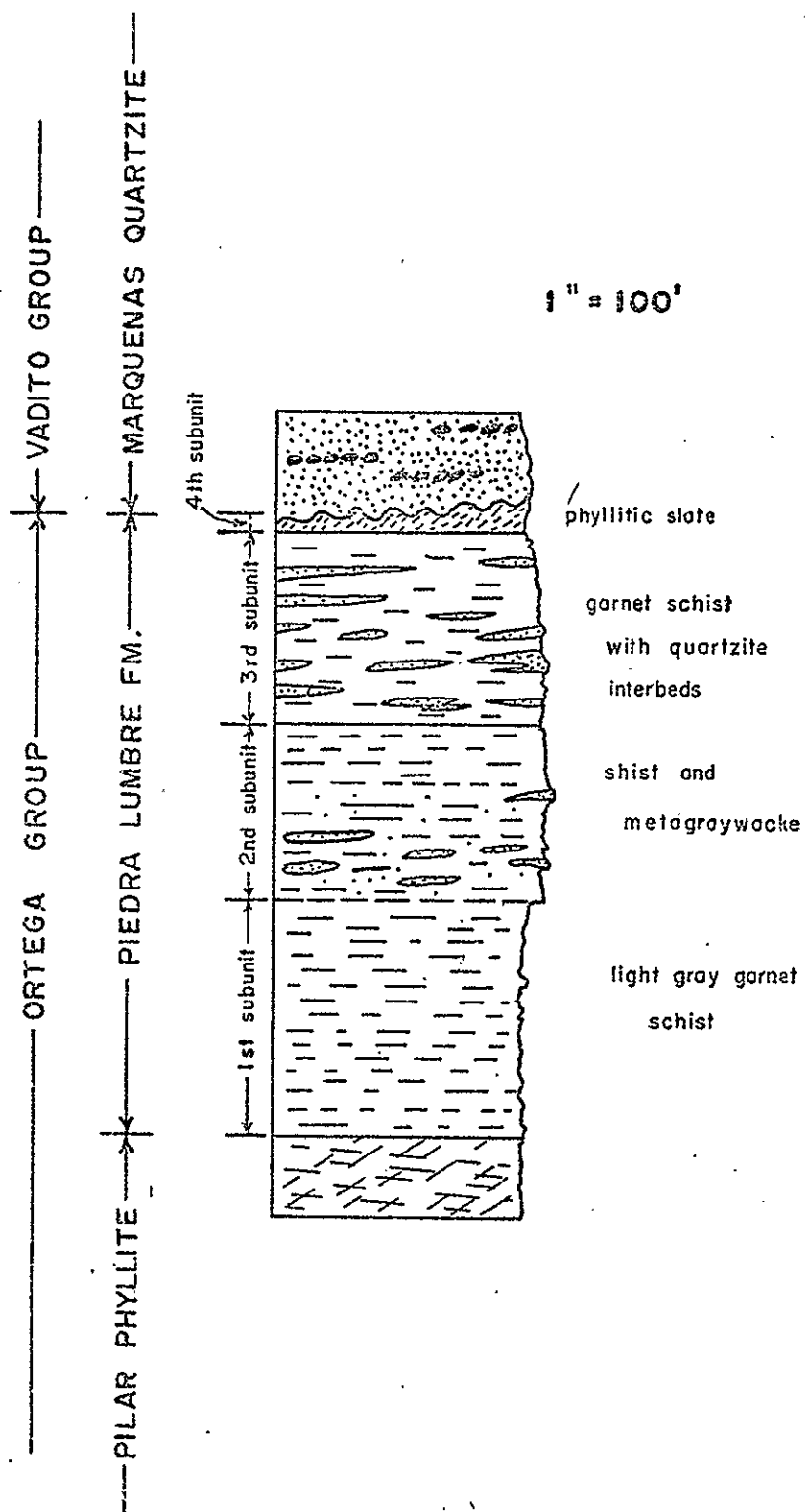


Figure 10. Detailed stratigraphic section of the Piedra Lumbre Formation.

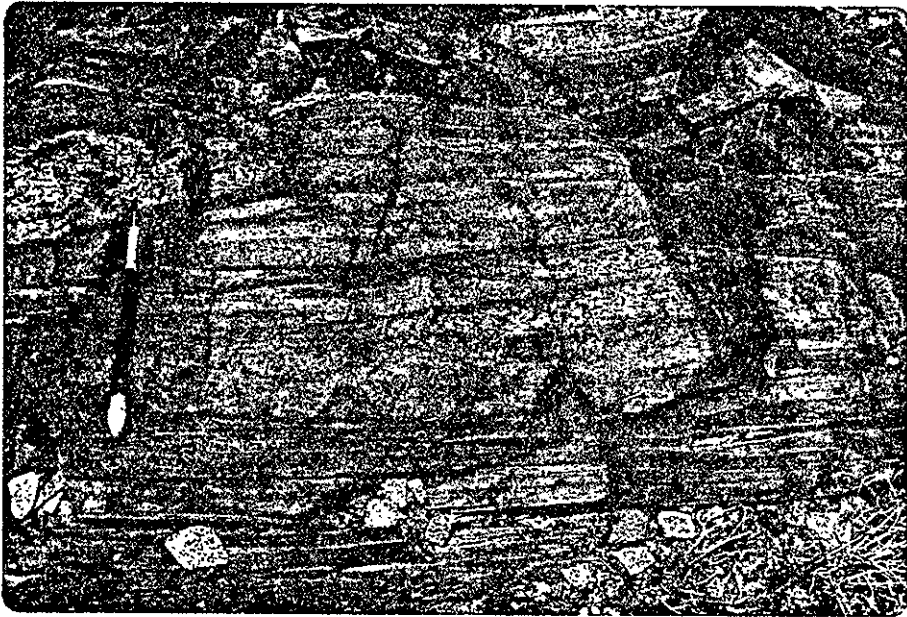


Figure 11. An outcrop of the second subunit in the Piedra Lumbre Formation. Light-colored beds are calc-silicate layers. Located 0.5 mi north-northwest of Cerro Puntigudo.

oriented elipsoidal cavities (≈ 4 mm long) that represent weathered-out crystals of hornblende. In thin sections of fresh material these beds are seen to contain hornblende and garnet porphyroblasts set in a matrix of very fine-grained (0.05 mm) anhedral calcite and quartz. Both the hornblende and garnet are sievelike in appearance, owing to numerous inclusions of quartz. The hornblende, pleochroic in shades of green, light green, and pale yellow, probably is an actinolite. Sphene and ilmenite are accessory minerals. Similar calcareous beds were described by Montgomery (1953) as occurring to the north in rocks that he identified with the Rinconada schist. These rocks since have been mapped by Nielsen (1972) as lying stratigraphically between the Pilar Phyllite and the Vadito Group rocks.

Overlying the subunit of interbedded schist and quartzite is a subunit consisting of light-gray to gray garnet schist with discontinuous lenses of quartzite. It is about 100 ft thick where the section was measured, but its thickness is not uniform. A thinning to less than 25 ft was observed at one point.

The uppermost subunit of the Piedra Lumbre Formation is a 15 to 30 ft thickness of phyllitic slate that is virtually indistinguishable from the Pilar Phyllite. That it is not in fact a faulted-in slice of Pilar seems evident from its occurrence as a thin layer that is conformable with the underlying subunits of Piedra Lumbre Formation. This uppermost subunit was reported by Nielsen (1972), even though a section of Piedra Lumbre Formation along the Rio Cienequilla to the north is complete in the sense of including lower Vadito Group rocks. It is therefore assumed that in spite of a lesser thickness, 320 ft as contrasted with 600 ft for the Cienequilla section, the section

described here may well be even more complete because it apparently includes the youngest units of the Piedra Lumbre Formation.

Structural Features

The subunits of the Piedra Lumbre Formation have well-developed bedding-plane schistosity (fig. 11). This is especially well demonstrated in the subunit with interbedded quartzite and schist, where the bedding planes are easily distinguished from the schistosity. Irregular crenulations with a typical wavelength of 0.7 cm and an amplitude of 0.2 cm are common, especially in the lowermost subunit which tends to become less crenulated toward its top. The mesoscopic structural elements, which include bedding, schistosity parallel to bedding, crenulations, and a less well-developed schistosity not parallel to bedding, have been recognized and systematized by Nielsen (1972) and Nielsen and Dunn (1974). Their terminology is given in table 1 and is here used, insofar as it is applicable, in discussions of deformational features in all the rocks of the area.

Commonly all of the planar elements could be recognized in a single outcrop of Piedra Lumbre Formation, although S_2 in particular can be difficult to recognize. L_1 was never observed, whereas L_2 could be seen as biotite alignment on some cleavage surfaces, particularly in the lowermost subunit. In some beds L_2 alignment is conspicuously absent, suggesting some variability in the timing of growth of biotite and/or in the local intensity of deformation forming L_2 . L_3 is observed only in rocks that show well-developed crenulations. The fact that the crenulations themselves are rarely observed in the interlayered quartzite schist or in the phyllitic slate, but are very

Table 1

Structural Elements of the Ortega Group Observed by
Nielsen (1972). Terminology after
Turner and Weiss (1968).

Planar features:

S_0	Bedding
S_1	Schistosity parallel to S_0
S_2	Schistosity that cuts S_1
S_3	Crenulation cleavage (cuts S_2 , S_1 , and S_0)
S_4^*	Semiductile shear zones (cut S_2 and S_3 in granitic rocks)

Linear features:

L_1	$S_1 \wedge S_0$
L_2	$S_2 \wedge S_1$ and $S_2 \wedge S_0$
L_3	$S_3 \wedge S_1$ and $S_3 \wedge S_0$
L_4	$S_3 \wedge S_2$

Folds:

F_1	$\beta S_1 // S_0$
F_2	$\beta S_2 \wedge S_1$
F_3	$\beta S_3 \wedge S_1$ and $\beta S_3 \wedge S_2$
F_4	$\beta S_4 \wedge S_2$ and $\beta S_4 \wedge S_3$ (?)

*Directly observed only in the granitic rocks.

common in the phyllitic schist suggests that their development is strongly dependent on lithology. L_4 is observed only rarely, as it is dependent on a good expression of S_2 . It is a crinkle lineation that appears very similar to crinkle lineations in the S_1 surface. Mesoscopic folds were more difficult positively to identify relative to Nielsen's (1972) classification, and in general there are few mesoscopic folds in the Piedra Lumbre Formation. Folds observed in the adjacent Pilar Phyllite are probably F_2 , but no other mesoscopic folds were observed near the Piedra Lumbre outcrops.

Vadito Group

General Statement

The Vadito Group comprises three formational units: the Marquenas Quartzite, an unnamed schist unit, and an unnamed amphibolite unit. The quartzite unit and the schist and amphibolite units combined previously were given status as members of the Vadito Formation in Montgomery's (1953) terminology. The units are lithologically disparate, however, and are so readily mapped that it has seemed advisable to accord them formational status. The original formational name was applied by Montgomery (1953) from the village of Vadito, which is 2 mi south of outcrops of amphibolite and schist that lie about 3 mi east of the present map area.

Marquenas Quartzite

Distribution

The Marquenas Quartzite is named for Cerro de las Marquenas which is just north of sec. 30 (off the map area) and is underlain by this unit. These rocks occur as an east-trending belt that extends east and north beyond the map area. Quartzite beds do occur in the overlying schist unit, but with only one possible exception these quartzites appear to be stratigraphically part of the schist sequence and have been mapped as such. Thus the Marquenas Quartzite is defined as those quartzites and conglomerates that lie stratigraphically above the rocks of the Ortega Group but below the first occurrence of the unnamed schist unit.

Lithology

More than 80 percent of the Marquenas Quartzite is quartzite, and the remainder is coarse stretched-pebble conglomerate that generally has a muscovite quartzite matrix. Figure 12 shows a typical section of this unit. Lenses and beds of conglomerate are widely distributed in the section, but the most significant occurrence is near the top of the unit. A typical exposure of the conglomerate is shown in figure 13. The pebbles are on the average about half the size of a flattened fist. Montgomery (1953) traversed a section of the conglomerate and quartzite and recorded average sizes of cobbles; the results are reproduced here in table 2. He also noted that the cobbles are crudely ellipsoidal in shape as the result of flattening in the plane of foliation, and he estimated the average ratio of axial lengths to be

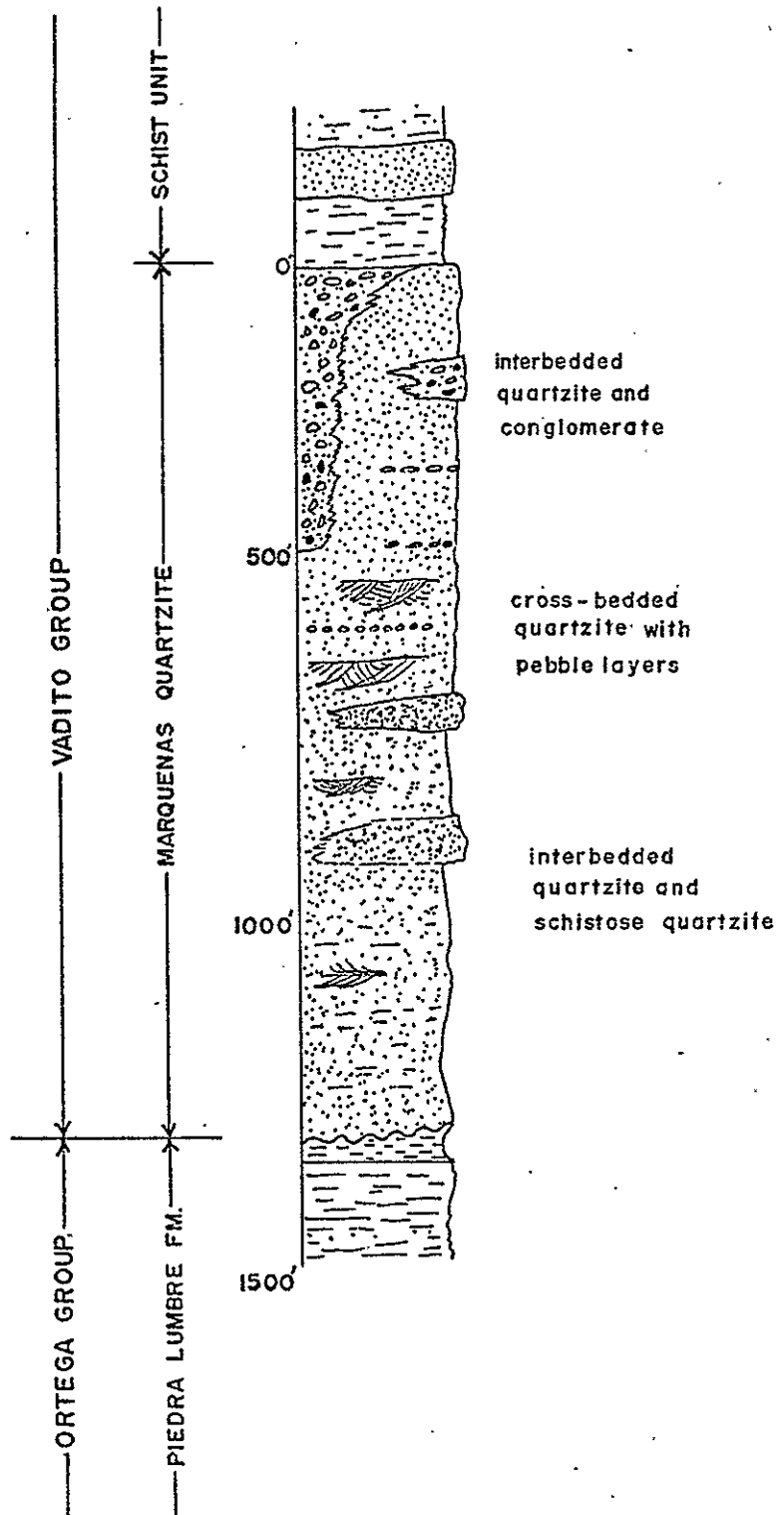


Figure 12. Stratigraphic section through the Marquenas Quartzite.

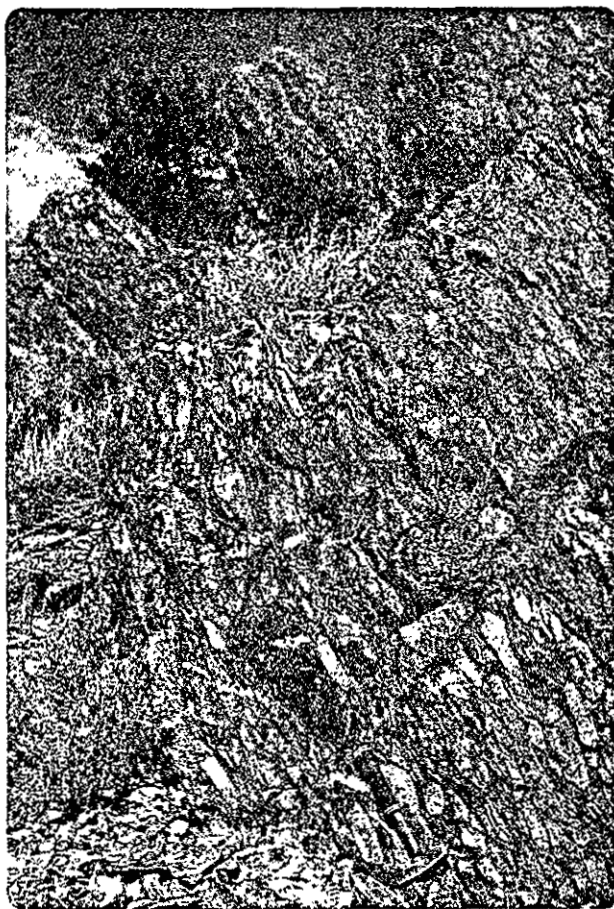


Figure 13. An outcrop of Marquenas Quartzite, about 0.5 mi northwest of Cerro Puntigudo.

Table 2

A Traverse of a Portion of the Marquenas Quartzite
(from Montgomery, 1953), Showing Typical Lithologic
Variation as its Base is Approached

<u>Lithology</u>	Distance traversed in feet
Coarse conglomerate (cobbles averaging 3 to 10 cm in size)	300
Pebbly conglomerate (pebbles averaging 3 to 5 cm in size)	200
Fine-grained quartzite (gray white, gritty, with rare pebbles, containing microscopic thinly disseminated flakes of muscovite and a few black iron oxide bands up to 0.5 cm wide)	500
Pebbly conglomerate (pebbles averaging 3 to 5 cm in size)	200
Coarse conglomerate (cobbles averaging 6 to 8 cm in size)	200
Pebbly conglomerate and fine-grained micaceous quartzite	100-200

1:2:3. The ratio commonly is as great as 1:2:6 in some localities, and the maximum is 1:8:16.

The cobbles typically are very light-gray cloudy quartzite with dark-gray inclusions, but some are more vitreous and darker in appearance. Some of the cobbles, about 10 percent of them according to Montgomery, consist of other rock types, in general softer than the quartzite. Many of these have been nearly obliterated by deformation, appearing as extremely thin smears and patches that consist of a white muscovite plus quartz with scattered porphyroblasts of biotite (1 to 3 mm) that have been largely chloritized. The original lithology of these deformed clasts is difficult to determine, but some sort of felsite is a reasonable inference.

The matrix of the rock consists of fine-grained quartz and muscovite (0.05 to 0.3 mm), ilmenite, biotite, magnetite, hematite, zircon, and tourmaline. The texture is very complicated in detail, apparently due in part to the effects of "jostling" between adjacent quartzite pebbles, resulting in irregular pebble shapes. Streaks of dark minerals are intimately admixed with muscovite and quartz, and randomly oriented porphyroblasts of biotite speckle the contorted pattern. The matrix generally accounts for less than 30 percent of the rock except where the conglomerate grades into quartzite.

The quartzites themselves differ in texture and bedding, but they are ordinarily fine to medium grained, light gray to medium dark gray, and cross-bedded. They contain muscovite, biotite, and magnetite as accessory minerals. Pebble layers or lenses are not uncommon and generally the quartzites grade into the conglomerate beds. The details of the stratigraphic sequence are shown in figures 12 and 14. Individual

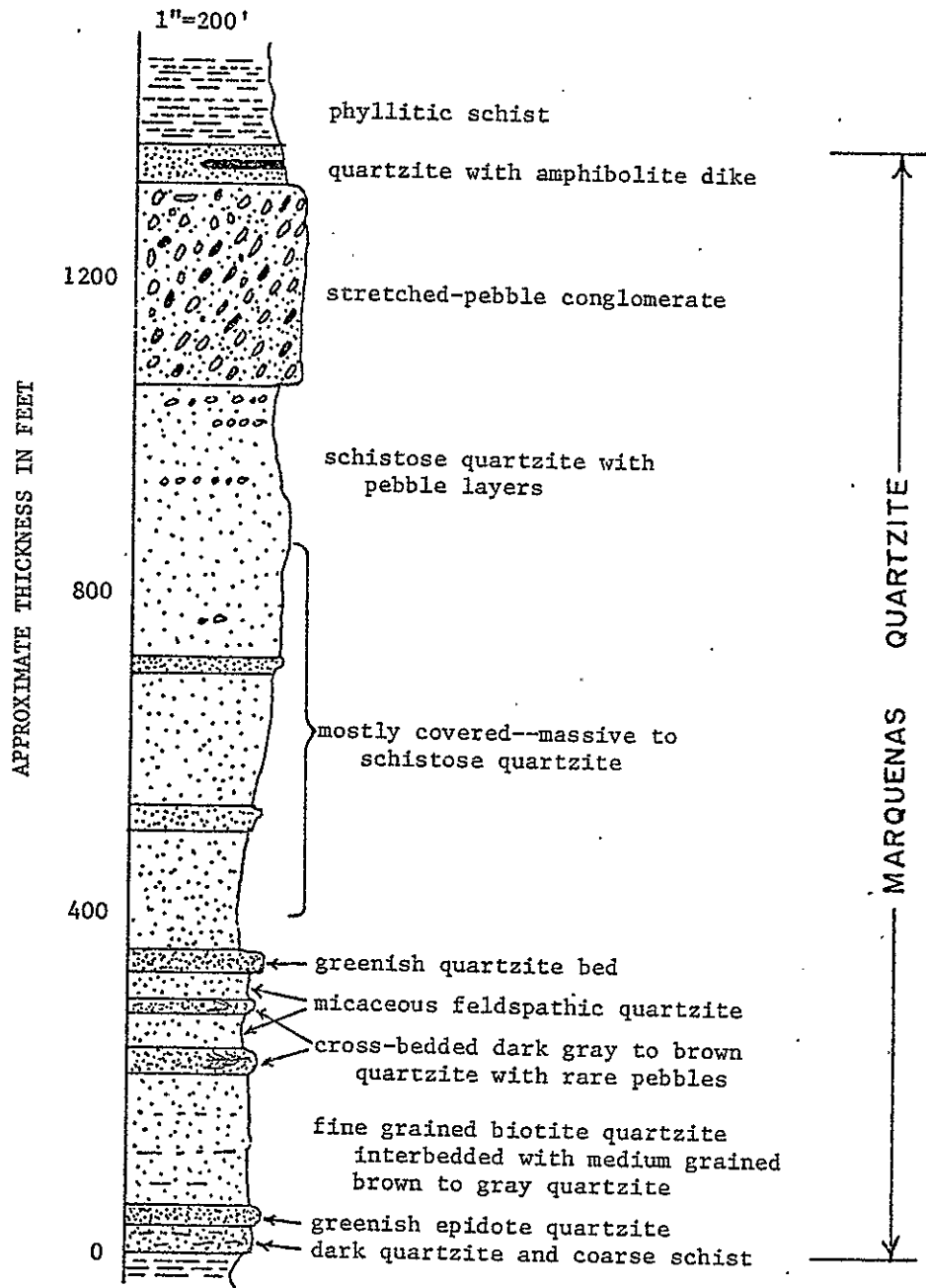


Figure 14. Detailed stratigraphic section of part of the Marquenas Quartzite.

beds, particularly the thinner ones, do not appear to be continuous enough to allow detailed correlation of one section of quartzite with another. Cross-bedding in the quartzite is particularly useful in providing a consistent indication of the "up" stratigraphic direction. This is important because it definitely determines that the Vadito Group stratigraphically overlies the Ortega Group. This is in direct conflict with speculative suggestions (Gresens and Stensrud, 1974a, b) that the Vadito Group may be the oldest rocks in the area. Not only is there no direct evidence for such a notion, but both my observations and those of Nielsen (1972) show conclusively that Montgomery (1953) was correct in considering the Vadito rocks to be younger than the Ortega rocks.

Structural Features

The bedding planes, (S_0) and S_1 or S_2 , are the dominant structural features of the quartzite-conglomerate sequence. The bedding is particularly well developed in the quartzites but they tend not to show a strong S_1 or S_2 foliation except in the more schistose layers. The conglomerates show S_2 by the flattening and stretching of the pebbles. In addition, there are marked changes in thickness in the main conglomerate bed, particularly in the northern part of sec. 30, north of Cerro de las Arboles. This change may be due to original differences in bedding thickness, but in view of the general degree of deformation in the area, it may well be the result of a large-scale stretching and thinning of the bedding. This possibility obscures the stratigraphic relationships in the north part of sec. 30, but nevertheless the fact that the phyllitic schist which overlies the Marquesas Quartzite

is in contact with both a major conglomerate bed *and* quartzite, suggests the possibility of an unconformity at the top of the Marquenas Quartzite. Similar evidence may exist in the northwest corner of sec. 25, but again structural complexity makes it impossible to positively distinguish between infolding of beds, actual interbedding, or the relationships of an unconformity. It does seem, though, that a slight angular unconformity may exist at the top of the Marquenas Quartzite.

Minor faults offset bedding the Marquenas Quartzite. These faults are subparallel and nearly vertical, with trends that are within 10° or 15° of due north. They appear to be rather short, perhaps an eighth of a mile in maximum length, and their occurrence is limited to the northwest parts of secs. 25 and 30.

Unnamed Schist Unit

Distribution

The unnamed schist unit of the Vadito Group--hereafter referred to informally as the Vadito schist--is present over a rather large aggregate fraction of the map area, cropping out in parts of secs. 25, 26, 27, 28, 29, 30, 32, 33, and 34. It can be defined as those schists, phyllitic schists, quartzites, and conglomerates that occur stratigraphically above the contiguous outcrops of the Marquenas Quartzite. The stratigraphy of the Vadito schist, however, is complicated by intense isoclinal folding and lithologic variability, including amphibolite and felsite dikes and the main amphibolite belt. Basically, the problem involves estimating the true thickness of the unit and specifying the stratigraphic position of the schists that are physically

separated from the main schist belt. These problems will be discussed further, following lithologic description of the unit.

Lithology

The Vadito schist that lies to the north and west of the main amphibolite belt is made up of four major rock types: phyllitic schist with rare cordierite knots, quartzites with minor conglomerates, felsites, and amphibolites. South and east of the amphibolite belt, the schists tend to be more quartzose and less phyllitic, and have andalusite rather than cordierite as the main constituent of knotty layers. Dikes and sills of amphibolite are largely absent. Even though the stratigraphic succession is not everywhere clear, it is possible to describe all the lithologies that occur, and to construct detailed sections where the stratigraphy is rather straightforward (fig. 15).

Banded Bluish-Gray Schist

Bluish-gray schist commonly occurs as a thin bed (100 to 200 ft) near the base of the Vadito schist (secs. 25 and 30). This schist is partly interbedded or infolded with the Marquenas Quartzite and shows a remarkable banding expressed by alternation of discontinuous fine-grained dark layers and coarse-grained lighter layers 0.2 to 0.8 cm thick. The banding appears to be the result of intense deformation and granulation along certain planes in the rock. The rock is in general fine grained, but it contains porphyroblasts of garnet (1 to 2 mm) and augen-shaped quartz masses up to 2 cm in length. In polished thin section, the rock is seen to consist of alternating discontinuous layers and pods of 1 mm polygonated quartz grains, light-green chlorite sheaves, and finer grained zones of finely comminuted quartz with minor

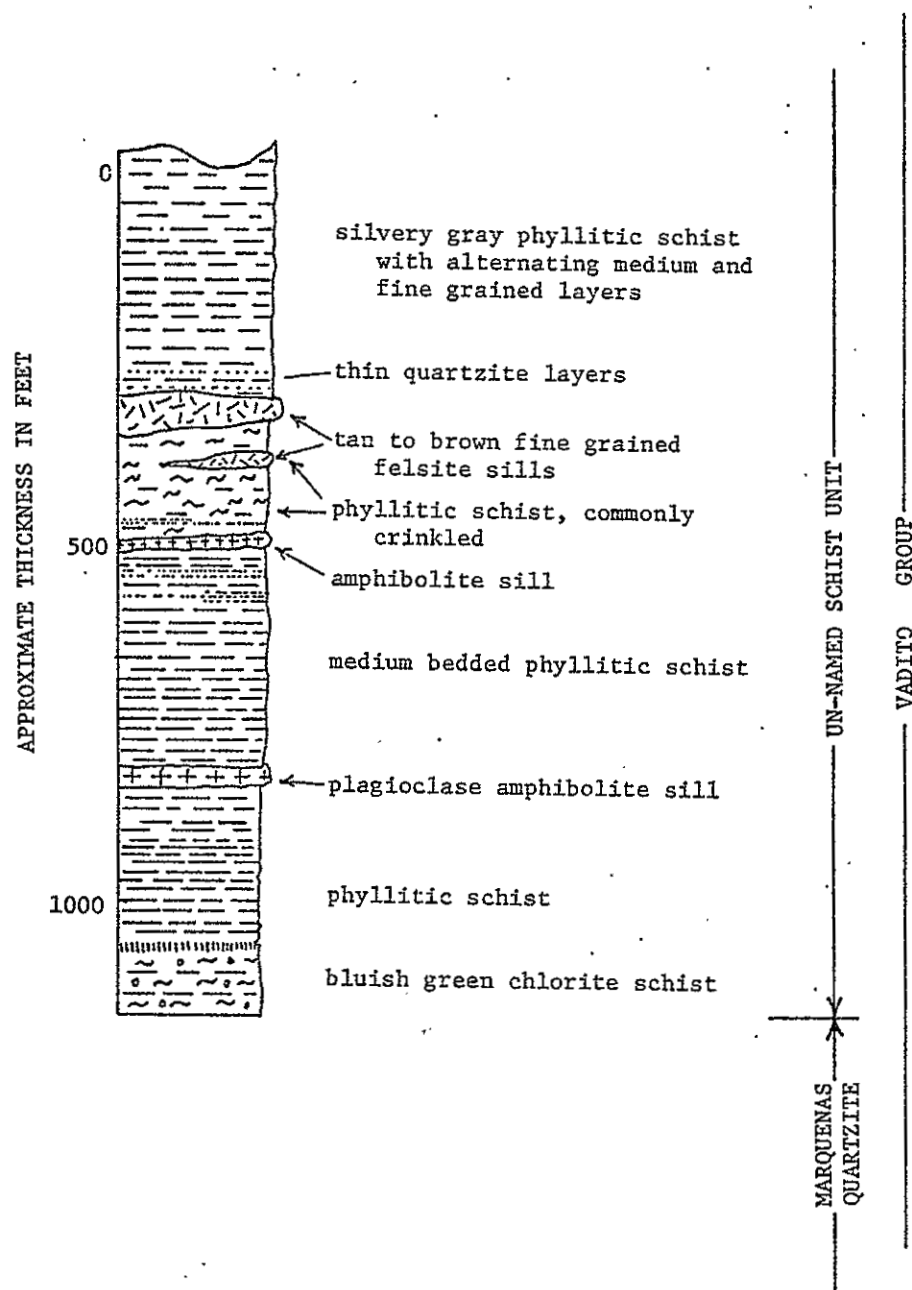


Figure 15a. Detailed section of lower part of the unnamed schist unit.
 Sec. 25, 0.25 mi north of Cerro de los Arboles.

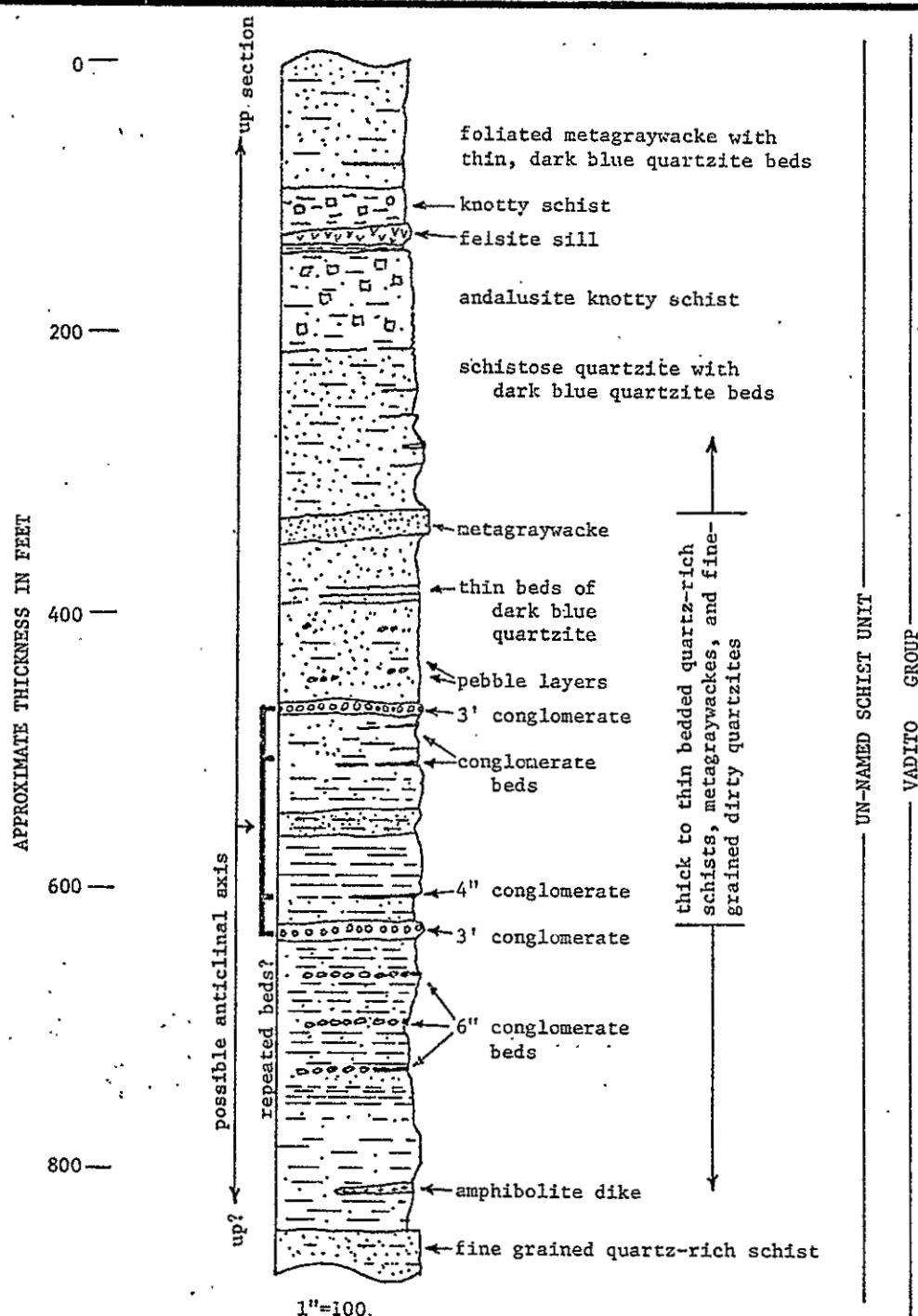


Figure 15b. Detailed section of Vadito Schist between main amphibolite belt and Embudo Creek. Secs. 29 and 32, 0.3 mi west of Cerro Alto.

feldspar which is interlaced with muscovite and chlorite as subparallel undulating stringers. Within the coarser grained portions, 0.5 mm, randomly oriented chlorite sheaves are interstitial to the polygonated quartz grains. Along the margins of the coarse-grained portions are layers of well-oriented muscovite and chlorite, as well as 1 mm grains of ilmenite with widmannstätten patterns of hematite exsolution lamellae. These large ilmenite grains are also scattered throughout the rock, but seem to be preferentially associated with the coarser grained parts. The finer grained parts of the rock contain, in addition to quartz, chlorite, and muscovite, grains of garnet (0.8 mm) with quartz inclusions near their centers, irregular staurolite grains of similar size, and somewhat larger but rare grains of epidote. In addition there is also a small percentage of feldspar, probably albitic plagioclase. The most finely comminuted layers are dusted with tiny grains of hematite containing irregular inclusions of ilmenite. These opaque grains apparently account for the darker color of the finest grained bands. From the texture of the rock, it appears that quartz, muscovite, chlorite, ilmenite, hematite, and possibly garnet and epidote were coexisting phases during the last period of readjustment of the rock's mineral assemblage. Staurolite and plagioclase may be relict phases from an earlier and somewhat higher state of metamorphism.

Stratigraphically above the bluish-gray banded schist lies a thick sequence of silvery-gray schist that extends from either the bluish-gray banded schist or the Marquesas Quartzite to the main amphibolite belt. The sequence includes quartz-muscovite phyllite and phyllitic schist, quartz-muscovite-biotite schist, a variety of andalusite- or cordierite-bearing knotty schists, and interbeds of more quartzose schists or

quartzite with rare conglomerates. There is a slight tendency for the rocks to become more schistose and less phyllitic and to contain more quartzose layers in the more southerly and easterly outcrops of the unit, i.e. upward in the stratigraphic section. The exact stratigraphic sequence of beds becomes uncertain as one moves upward in the section toward the main amphibolite belt. This probably is due in part to the presence of tight isoclinal folding. However, marker beds of knotty schist indicate that in spite of folding, the sequence is essentially intact. That is, the upper or lower contacts of the unit largely appear to be sedimentary rather than fault contacts. Unfortunately there are no continuous marker beds that would permit the tracing of folds in the middle of the sequence.

Phyllitic Schist

The rocks immediately above the bluish-gray schist are silver-gray phyllitic schists that consist primarily of fine- to medium-grained quartz, muscovite, chlorite, staurolite, garnet, and an opaque mineral. Quartz occurs as 0.2 to 0.05 mm polygonal grains that are interwoven with well-oriented plates of muscovite and chlorite plates that are similar in size. This fabric is studded with anhedral porphyroblasts (0.3 mm) of pinkish-brown staurolite, and scattered throughout the rock are abundant 0.05 to 0.25 mm opaque grains, probably of ilmenite with hematite. Rarely there are 1 mm layers of chlorite and muscovite that are a distinct green color and which are somewhat coarser grained than the bulk of the rock. These layers commonly cut the dominant foliation at a low angle and may represent primary bedding.

In terms of grain size and texture there are all gradations between the phyllitic schist just described and a coarser grained, more quartzose schist that generally occurs higher in the section. A typical sample is a dull light-gray rock that is speckled with black biotite grains (0.3 to 0.8 mm) and bright muscovite platelets of a similar size. In thin section the rock is seen to have an average grain size of 0.15 to 0.05 mm and to contain quartz, muscovite, biotite, opaque grains, probably ilmenite(?), chlorite, staurolite, and garnet. Zircon and apatite are accessory minerals. The quartz, forming about 50 percent of the rock, occurs as typical polygonal grains. In contrast, oriented plates of green-brown biotite and water-clear muscovite give a planar fabric to the rock. About 10 percent of the biotite is chloritized, and in some places chlorite occurs as separate grains. The rare zircon grains appear to be detrital. This rock appears different in composition from the more phyllitic schist, but the most obvious differences are textural, this lithology having a coarser grain size, a higher quartz content, and less of a planar fabric.

These relatively quartz-rich schists commonly contain thin (2 to 15 cm) interbeds of meta-arenite or quartzite, which are widely spaced and are characterized by a grain size of 1 to 0.5 mm, being either a dull light to medium gray or vitreous dark gray to black. They are very impure quartzites containing feldspar, garnet, opaques, muscovite, and apatite. They have a distinct planar fabric, but schistosity is generally poorly developed owing to the low percentage of platy minerals.

In addition to the thin quartzite beds interlayered with schist, coarser grained quartzites occur as thicker lenticular bodies ranging from 0.12 to 1 mi in maximum dimension. These quartzites are similar

to those of the Marquenas Quartzite except that they tend to be slightly coarser, less vitreous, and more argillaceous. Also, conglomerate beds within these quartzites contain a variety of clast lithologies with an abundance of felsite clasts. The quartzite typically is dull light brown or buff to vitreous dark gray, and consists of discrete rounded quartz grains (0.5 to 1 mm) and interstitial blebs of altered feldspar. Concentration of opaque minerals in thin (2 mm) layers is common. This layering does not everywhere represent bedding and it is rarely parallel to the dominant foliation. The more vitreous quartzite contains less altered feldspar and muscovite and tends to be darker in color. The internal structure of these quartzite masses can be complex, as can be seen from figure 16 which is a detailed map of one such mass near the Harding mine. The significance of this structure is discussed in the section on structural features.

A variety of knotty schists, which in some places have rather spectacular textures, also features the Vadito schist. Figure 17 shows the appearance of some of these rocks in outcrop. The knots or porphyroblasts are either cordierite or andalusite, and in most occurrences they are severely altered. These knotty schists could, in many areas, be mapped as separate units. One bed in particular serves as an excellent marker horizon that lies stratigraphically just northwest of the main amphibolite unit (pl. II). This rock has a matrix that is a typical quartz-muscovite-biotite (staurolite) phyllitic schist but it contains large (5 to 10 cm) porphyroblasts of dark bluish-gray cordierite. These cordierite knots appear unaltered in hand specimen and are either rounded subequant ellipsoidal masses or are shaped like stubby cigars with hexagonal outlines. Rarely, the knots occur as irregular

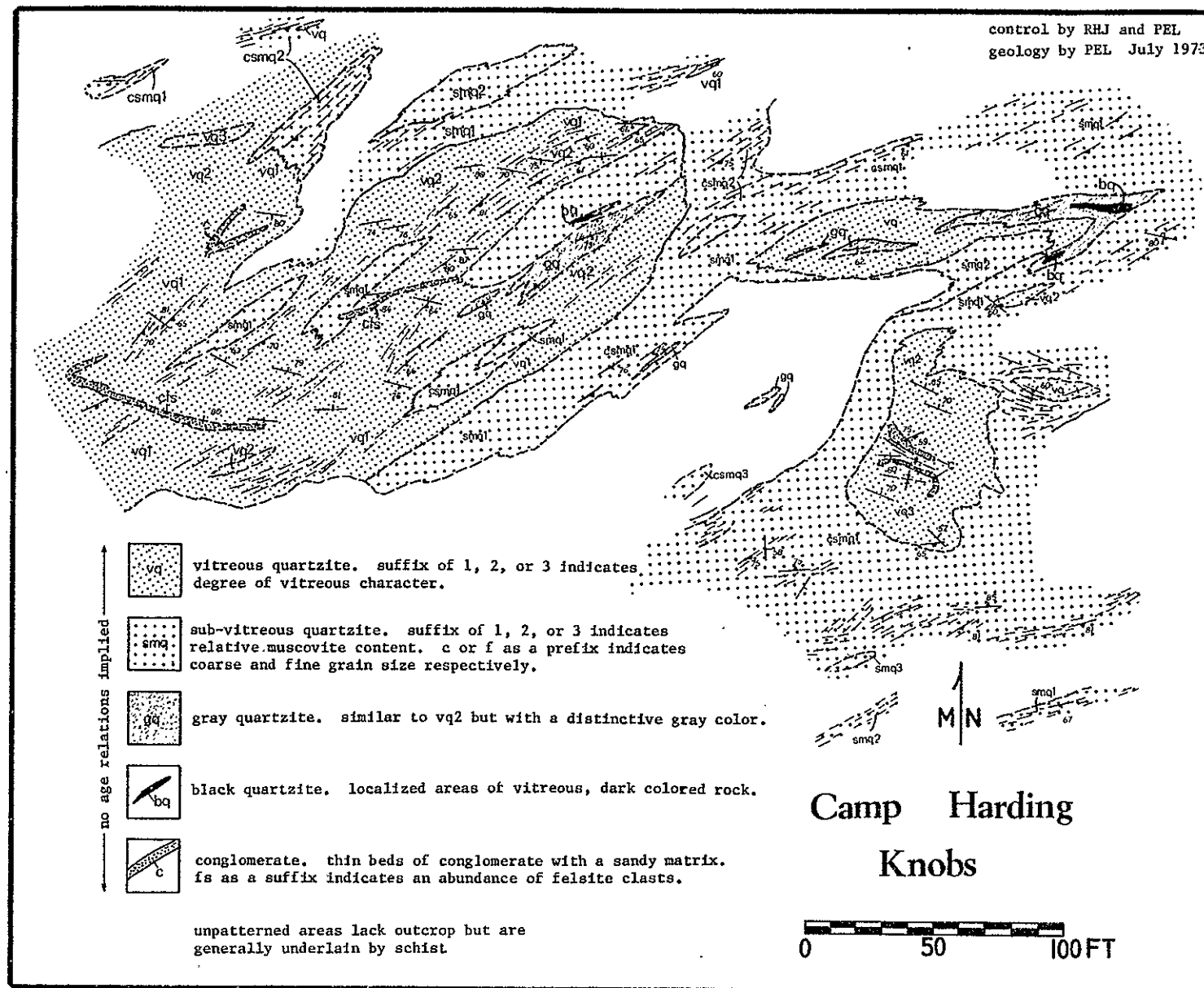


Figure 16. Geologic map of Camp Harding knobs.



Figure 17. An outcrop of knotty schist where the knots are especially large and have been converted to chlorite and muscovite. 0.5 mi northeast of Cerro de las Arboles.

tapering masses up to 15 x 8 cm. Rocks with these fresh-appearing cordierite porphyroblasts generally contain relatively large (2 to 3 mm) biotite porphyroblasts, which are especially prominent in the finer grained, more phyllitic schists. Thin-section examination shows that the cordierite porphyroblasts are riddled with tiny inclusions of quartz, muscovite, garnet, and andalusite. In addition there are larger inclusions of biotite (1 to 2 mm). All of these minerals are also found in the matrix which is well foliated, rich in muscovite, and is featured by discontinuous 1 mm sized trains of polygonal quartz grains interlacing the fabric. Andalusite occurs as 0.7 mm augen-shaped crystals that are commonly surrounded by a thin rind of a rusty-colored unidentified material. The biotite porphyroblasts are various shades of pale brown to straw yellow and are either partly chloritized or appear to be considerably muscovitized. They occur in all orientations and appear to have been rotated during deformation. Scattered, large muscovite flakes are typically associated with the biotite porphyroblasts. Garnet occurs as very small (0.1 mm) euhedra that show a moderate to very heavy concentration of inclusions at their cores. Rare small grains of apatite and zircon apparently are detrital. The opaque mineral in this rock type is largely magnetite, with a very minor amount of intergrown or included ilmenite. Some specimens of this type lack andalusite and show larger biotite porphyroblasts that are less muscovitized. Some of the biotite and cordierite porphyroblasts have been strongly deformed.

Most of the cordierite porphyroblasts have a halo of concentrated and preferentially oriented fine- to medium-grained muscovite. Some porphyroblasts show different extinction angles in different zones

of the crystal, especially in a narrow zone around the outside of the crystal. Part of the extinction pattern probably is due to crude pseudo-hexagonal cyclic twinning, but the marginal zone may instead represent a late-stage addition of cordierite to the porphyroblast. As noted by Montgomery (1953), some of the cordierite crystals show layering on a fine scale (0.02 to 0.04 mm). The lack of concordance between these layers and layers in the matrix suggests possible rotation of the porphyroblasts.

In addition to the cordierite porphyroblasts there are relict andalusite porphyroblasts that have been largely replaced by muscovite. These pseudomorphs commonly have small cores of andalusite and a cross-shaped pattern of carbonaceous inclusions, indicating that they were once andalusite porphyroblasts.

In contrast to the occurrence just described, most of the knotty schists lack unaltered cordierite porphyroblasts. Instead, the knots are poorly defined flattened ovoid masses consisting of muscovite, chlorite, and quartz. In some places they contain a core of cordierite or andalusite. The minerals within the knots, especially the chlorite, tend to be randomly oriented, but those outside the knots show the typical strong foliation of the schist. Chlorite occurs in the knots as 1 mm tabular to sheaflike crystals that are intergrown with generally smaller muscovite plates and quartz grains. The matrix of the rock, ranging from schistose to phyllitic, consists of foliated quartz and muscovite with biotite porphyroblasts (2 mm) that show some chloritization. The opaque mineral is magnetite with included blebs and stringers of ilmenite.

Amphibolite Dikes and Sills

The Vadito schist lying north and east of the main amphibolite belt contains numerous amphibolite dikes and sills. These bodies are mostly of intrusive origin as they crosscut bedding in places. Some of the bodies may be flows, but there is no definite evidence to this effect. Most of them are large enough to map at a scale of 1:12,000 and are shown, in part schematically, on plate II. Amphibolite dikes also occur in the Marquenas Quartzite but they are not as common there.

For the most part, these rocks are fine- to medium-grained plagioclase amphibolites, but there is considerable variability from one dike to the next in texture and, to a lesser degree, in mineralogy. Coarse-grained samples collected from dikes that crop out in the far northwest corner of the map area show fibrous radiating crystals of black amphibole (1 to 5 mm) with interstitial light-gray plagioclase. In thin section the featherlike hornblende crystals project into interstitial aggregates of granular plagioclase (An_{33} to An_{21}) that also contain sphene, epidote, and rarely quartz. Small ilmenite grains contain blebs of exsolved magnetite. These grains are commonly rimmed with sphene. Other lithologies have textures in which the hornblende is finer grained and less acicular. Biotite accompanies hornblende in some dikes.

Vadito Schist Southeast of the Main Amphibolite Belt

Schists southeast of the main amphibolite belt are similar in many respects to those just described but since they are physically separated and there are some lithologic differences, they are described separately. Figure 15b and figure 18 show stratigraphic sections of

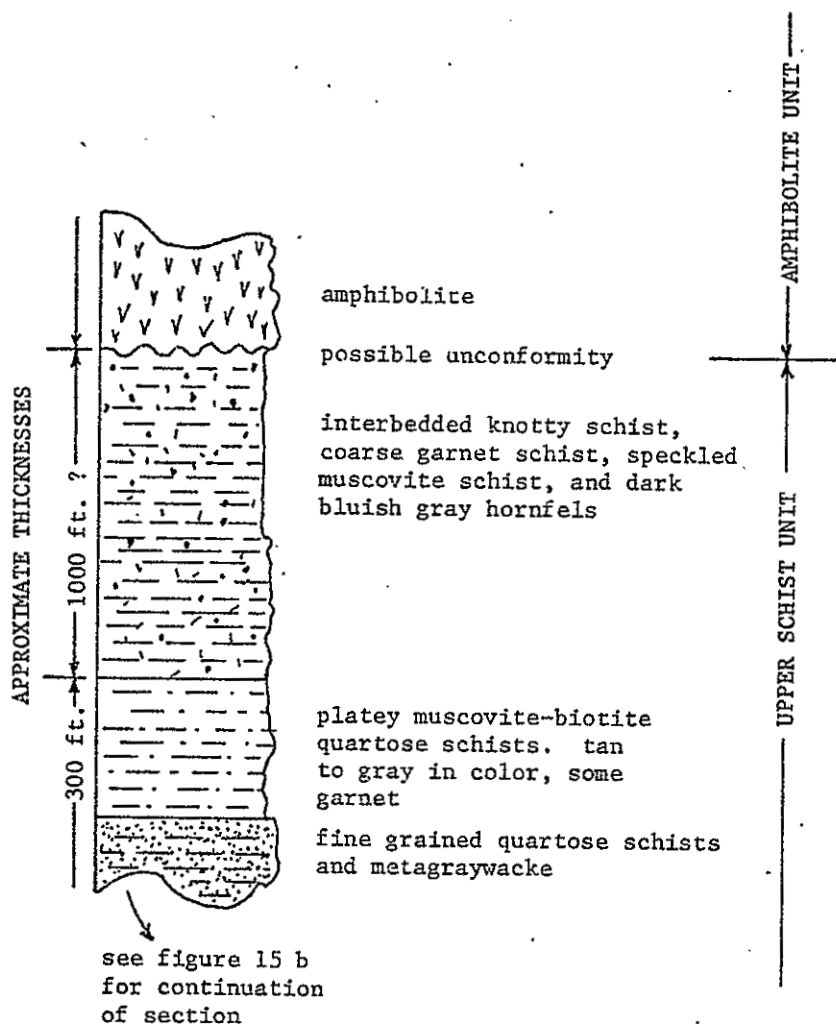


Figure 18. Possible section of upper part of Vadito schist southeast of the main amphibolite belt, 0.3 mi west of Cerro Alto.

these rocks. Lithologies in these rocks are similar to those schists lying to the northwest of the main amphibolite belt, but these rocks are in general more quartz-rich and less phyllitic. The section shown in figure 15b also contains several pebbly conglomerate beds that have no exact equivalent to the northwest. There are numerous occurrences of knotty schists in this area, but none appears to be lithologically identical to the knotty schist that lies immediately north of the main amphibolite belt. This lack of exact lithologic correlation permits several stratigraphic and structural interpretations that are discussed in the section on structural features.

A typical knotty schist from the area southeast of the main amphibolite belt appears much like those to the northwest in that garnet and biotite porphyroblasts are included both in a phyllitic matrix and in the knots. The knots, however, are andalusite rather than cordierite. These subrounded knots are medium gray and are 2 cm in maximum diameter. In thin section part of the matrix, primarily the quartz grains, appears to extend through the knots. The garnet crystals are 1 mm in size and show a moderate concentration of inclusions toward their centers. Blocky, 3 mm biotite plates show slight evidence of deformation and rotation into the plane of foliation. Rarely there are 3 mm euhedra of hematite. All of these porphyroblasts are enclosed in a typical schistose matrix with subparallel trains of lathlike muscovite plates (0.1 mm), separated by equant polygonal quartz grains (0.2 mm). Scattered grains of ilmenite are present, and are locally concentrated in some layers.

Immediately adjacent to the south side of the main amphibolite belt is knotty schist that is locally similar in appearance to the one

occurring to the immediate north of the amphibolite belt. The knots are about the same size as many to the north (5 cm) and have a similar shape and color, but again they are andalusite rather than cordierite.

Two other different lithologies found in this area are beds of quartz-rich gritty metasediments that tend to lack a strong foliation because of a lack of platy minerals, and beds of pebbly conglomerate. The quartz-rich sediments show all gradations between "dirty" fine-grained light gray-brown quartzite to near-massive beds of light-to medium-gray granulose garnet schist and phyllitic schists as already described. Some beds have an abundance of reddish garnet. An excellent description of thin sections from these rocks is here quoted from Montgomery (1953, p. 29).

The quartz-biotite granulite is commonly a fine-grained, sandy, crudely-foliated rock showing irregular, silvery-white, micaceous surfaces on which tiny black flakes of biotite stand out sharply. With less muscovite the rock becomes a biotite-specked quartzose gneiss or quartzite. With more muscovite it grades into the quartz-muscovite phyllite already described. As seen in thin section, quartz grains 0.04 to 0.25 mm. in size make up at least 50% of the rock. They are angular and highly irregular in shape. Sodic feldspar constitutes 20% to 30% of the rock, and occurs as interstitial murky-brown patches 0.2 mm. in size; these are crowded with kaolin and iron-oxide dust but show very little sericite. Muscovite plates 0.1 by 0.05 to 0.2 by 0.1 mm. in size and partly of stubby habit amount to 10% of the rock; they are well oriented in parallelism, but cross the feldspathic patches and are not interstitial to the quartz grains. Scattered irregular patches of biotite, 0.25 to 0.5 mm. in size, are haphazard in their orientation. Some of the fresh ones have a brownish-black color, with a tinge of olive-green, but most are partly altered to pale grass-green chlorite. Some biotite crystals show alteration to streaky iron-oxide and wisps of leucoxene. Abundant platy grains of ilmenite, 0.1 by 0.04 mm. in size, are well orientated in parallelism and are associated mainly with the feldspar and biotite. A few small grains of apatite, zircon, and granular sphene are present.

Structural Features

The dominant structural feature in the Vadito schist is the pervasive regional foliation or schistosity which varies in orientation from about east-west in the northeast part of the area to about 60° E. near the main amphibolite belt. Isoclinal folding is the dominant style of deformation, as evidenced mainly by the outcrop patterns of some amphibolite dikes but also by the style of small-scale folding in some thick quartzite beds. In the northeast part of the area, it is possible to observe most of the planar structural elements and many of the linear elements postulated by Nielsen (1972) and Nielsen and Dunn (1974), but to the southeast, as structures and lithologies become less well defined, it becomes increasingly difficult to relate Nielsen's structural elements to those observed in outcrop. However, it does seem that the dominant orientation of beds in the schist unit corresponds to S_1 , while S_2 is expressed as the dominant foliation in the schist. S_3 could rarely be identified. The best evidence for the existence of F_4 appeared to be linear elements and crinkle lineations thought to correspond to L_2 and L_3 respectively.

It was possible, by detailed mapping of a quartzite mass near the Harding mine (fig. 16), to observe parts of megascopic folds involving conglomerate beds. This fold pattern is not related to the dominant foliation, but its orientation suggests that it is related to either F_2 or F_4 . Alternatively, it may be related to shearing or faulting that resulted in the marked thinning of the main amphibolite belt in secs. 28 and 29. This supposed fault or shear zone is not obvious in outcrop, but may well extend westward into the schist itself, as suggested in a sketch map of the area (fig. 19).

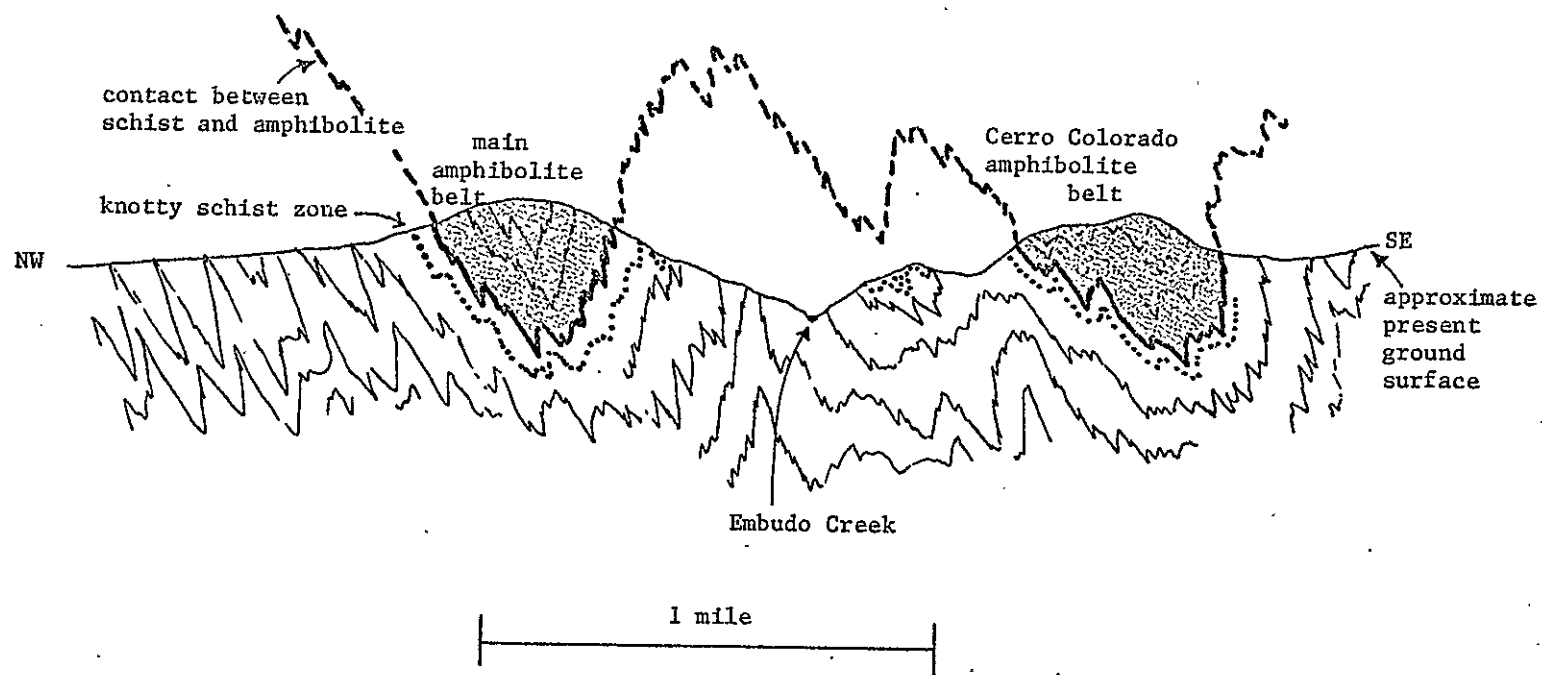


Figure 19. Sketch of hypothetical cross section assuming no granitic rocks were intruded.
The line of cross section runs northwest to southeast from sec. 29 to sec. 4.

In the area south of the main amphibolite belt and just southwest of Cerro Alto, there is some evidence for the existence of a large anticline. A crude repetition of bedding can be recognized in the section transversing the supposed structure (fig. 15b), and foliation clearly crosscuts bedding on the hillside above the location of the section line and at a point about where the axis of the anticline should be. Unfortunately, it is difficult to confirm this possibility as the exposures are limited by the close proximity of intrusive bodies.

Other, later structural features are minor tear-faults and sub-parallel lineaments observed on air photos. These features, shown on plate II, probably are related to Tertiary block faulting that uplifted the Picuris and Sangre de Cristo Ranges.

As previously stated, a significant structural and stratigraphic problem in the Vadito schist is the relationship between the schists north and south of the main amphibolite belt. Three main possibilities exist: (1) The schists to the south are coeval with the upper part of the schists to the north, but there is a sedimentary facies change, north to south, to explain the lithologic differences; (2) The schists to the south are equivalent to the lower part of the schists to the north, possibly even including the Marquenas Quartzite. This would require an unconformity above the schist and considerable structural complexity prior to emplacement of the main amphibolite unit; (3) The schists to the south are younger than the amphibolites and represent a continuation of sedimentation similar to that of the schist north of the amphibolite, after cessation of the volcanism and sedimentation that resulted in the amphibolite. Overall the evidence favors the

first possibility, primarily because of lack of evidence supporting the other two possibilities.

The second possibility is unlikely because of the lithological differences between the quartzites and conglomerates on either side of the main amphibolite belt. This could be attributed to a sedimentary facies difference but that would obviate the need for an unconformity and case 2 becomes case 1. However, the most compelling evidence that there is no profound unconformity involved is the apparent stratigraphic parallelism between the schist-amphibolite contact on the north side of the main amphibolite belt and the very distinctive bed of relatively unaltered cordierite knotty schist. The distance between this contact and the cordierite-bearing bed is nearly constant, as can be seen on plate II. Thus, any significant angular conformity between the two units would have to be oriented in such a fashion as not to be apparent in the section observed at the present surface. This would be highly fortuitous.

Evidence that the schist south of the main amphibolite belt does not overlie the amphibolite is that (1) there probably is an anticline in the schist southeast of Cerro Alto, and (2) the exposure pattern of the amphibolite suggests that it may die out with depth. Both of these observations suggest that the amphibolite occupies the cores of synclines and hence is the youngest Precambrian stratigraphic unit in the area. Unfortunately, neither of these two observations is particularly conclusive, so it should be emphasized that possibility 1 is only tentatively correct. Additional detailed mapping might provide a more definite solution to the problem. The cross section (pl. III) and figure 19 are constructed assuming possibility 1 to be true.

Figure 19 is a hypothetical cross section showing relationships as they might have appeared if no granitic rocks had been intruded.

Amphibolite Unit

The amphibolite unit is a complex metavolcanic and metasedimentary sequence that consists of about two-thirds metavolcanic conglomerates and metavolcaniclastic rocks, and about one-third mafic flows, i.e. metabasalts and meta-andesites. Near its base it is commonly interbedded or infolded with biotite schist, and farther up in the section there is an abundance of thin (0.2 to 2 m) vitreous black metacherts or metaquartzites. Intrusive into the section are metadacite and metafelsite dikes.

In general, the amphibolite unit occurs in two belts, the main one extending from sec. 31 northeast through sec. 27 and into the Picuris Pueblo. A second, smaller belt lies southeast of the main amphibolite belt and on the northwest side of Cerro Colorado. This smaller belt is lithologically very similar to the main belt and is probably a remnant of a once continuous extension of the main belt that formed the southern limb of a large anticline or the northern limb of an adjacent syncline.

It was nearly impossible to map different rock types in the amphibolite unit except the metacherts, metadacites, and metafelsites. This was due to a combination of poor exposure and the complex interbedding and deformation of the mafic flows and the metasediments. Thus no attempt has been made to show the flows and metasediments as separate units on plates I and II.

Lithologies

The metasedimentary rocks and metavolcanic conglomerates constitute about two-thirds of the amphibolite unit. There are all gradations between very coarse metavolcanic conglomerates and breccias with boulder-sized clasts to schistose amphibolitic or biotitic rocks that are fine to medium grained. The coarse clastic rocks seem to constitute most of the metasedimentary types but this impression may be largely a function of exposure. Figure 20 shows photographs of outcrops of typical metavolcanic conglomerate. As can be seen from this figure, the rock contains a wide range of clast types including quartzite, plagiogranite, gabbro, and basalt. The fragments are angular to sub-rounded and are very poorly sorted. This rock type has a well-developed foliation that is evidenced by flattening and shearing of the softer clasts. In thin section, the matrix between the clasts (about 25 to 45 percent of the rock) is seen to consist of 0.4 mm and smaller prisms of blue-green hornblende, many with perfect diamond-shaped cross sections, interspersed with lesser amounts of equant polygonal grains of quartz and plagioclase (0.1 to 0.25 mm). Accessory minerals are epidote, sphene, and an alteration product of sphene, probably anatase. The clasts, except for the quartz-rich ones, generally consist of the same phases but in various proportions and textures. There also are patchy areas (0.5 mm) of inclusion-riddled microcline in some clasts, and some have a fringe of concentrated slightly coarser hornblende. The optical properties of the hornblende are constant whether it occurs in the matrix or in clasts.

The metavolcanic flow rocks are typically very fine grained and dark gray to black, with a saccharoidal texture. Some are faintly



(a)



(b)

Figure 20. Outcrops of metavolcanic conglomerate in the main amphibolite unit about 0.5 mi southeast of Cerro de los Arboles.

dark greenish and display fine felted needles of hornblende which can have a slight preferred orientation to form a weak foliation. Still other rocks contain relict phenocrysts of plagioclase or epidote-filled relict vesicles. In thin section these rocks consist primarily of blue-green to straw-yellow idiomorphic hornblende (0.2 mm) in a kind of jack-straw network, the interstices of which are occupied by plagioclase (An_{33} to An_{21}) (0.2 to 0.15 mm) and the common accessory minerals sphene and epidote. The sphene occurs as clumps of 0.03 mm oblate granules and the epidote as irregular 0.05 mm grains. In some sections the hornblende shows a strong preferred orientation and is arranged in crude layers or trains, with altered plagioclase occupying intervening layers. In addition, some samples contain minor biotite and quartz.

The para-amphibolites which are not conglomeratic commonly contain considerable biotite and quartz, and in some areas grade into quartz-biotite-garnet-epidote schist. In other samples the rock takes on a migmatitic character with crude mineralogic layering being thoroughly contorted. These rocks have garnet as a common constituent locally, and epidote is commonly pseudomorphous after hornblende. Very rare pods of coarse bladed amphibole, massive garnet, and epidote appear to be local expressions of skarn-type mineralization. In still other rare beds are thin alternating layers of quartz and hematite, with or without epidote, and light-green hornblende with garnet. These beds apparently are a very small-scale banded iron formation.

Thin beds of metachert or metaquartzite have been mapped as separate units on plate II. They are almost pure quartz and have a vitreous to subvitreous dark-gray to black color with some lighter colored zones. Texture and grain size differ from one exposure to

another, but most samples have a compact interlocking granular texture and a grain size averaging about 0.5 mm. Thin section examination confirms, in particular, the interlocking nature of the grains which commonly have 120° deg triple junctions with other grains and show no evidence of rounding or original sedimentary grain structure. Also present are rare veinlets of secondary reddish-brown garnet and scattered tiny blebs of magnetite. These magnetite grains are concentrated in the finer grained, less recrystallized parts of the rock and apparently account for the darker color of these parts.

Whether these rocks are metaquartzites or metacherts is not positively known. Bedding features clearly indicate that they are sedimentary, but recrystallization has obliterated any evidence of original clastic grains of quartz if indeed the material was once quartzite. Lacking such evidence, and recognizing that all clastic quartzites in the area are not so recrystallized, it is suggested that these rocks may be metamorphosed cherts that formed in association with the volcanic activity that created the bulk of the amphibolite belt, a possibility first pointed out to the writer by L. T. Silver of California Institute of Technology.

Metadacite and Metafelsite Dikes and Sills

Numerous dikes and sills, generally granitic in composition, occur in both the Vadito schist and the main amphibolite belt, but they are particularly concentrated in the central part of the amphibolite belt (pl. II). These rocks characteristically occur as tapering, tabular, and partly irregular bodies that range in thickness from less than a meter to several tens of meters or more.

Lithology

The metadacite dikes are in part gradational with lighter colored dikes here referred to as felsite dikes informally. For the most part, though, the metadacite dikes are a distinct rock type which is very similar to the large metadacite body underlying Cerro Alto. Hence the lithologic description of these dikes is included in a later section on the Cerro Alto Metadacite. Some of the felsite dikes may be related to other bodies and a few apparently are appendages of the Rana Quartz Monzonite pluton. In general, such relationships are difficult to prove because of differences in textures of the felsites, and in part because most of them have no well-defined spatial arrangement relative to any one of the major granitic intrusive bodies.

Rocks that have been mapped as felsites have two features in common: (1) all are more or less light colored, although some contain biotite streaks or inclusions, and (2) they are all fine to medium grained and many of them contain small quartz and/or feldspar phenocrysts. The color of these rocks ranges from a light pinkish white to a medium grayish brown, which makes it possible to divide the felsites into three broad groups: (1) those that are light pinkish white to light gray brown, (2) those that are medium gray and are streaked with opaque minerals or biotite, and (3) those that are medium grayish brown and very fine grained. On plate II, the felsites are not subdivided into three categories, because of difficulties in making direct comparison of hand specimens from each dike. It should also be noted that the categories may not have much genetic significance.

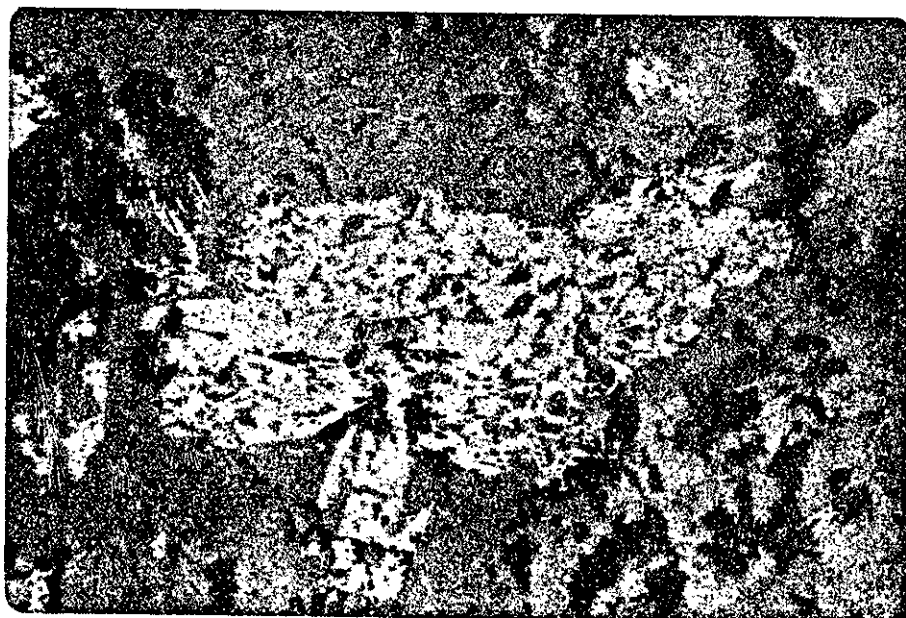
The light pinkish-white to light gray-brown felsites occur primarily, but not exclusively, within the middle parts of the main amphibolite

belt. These rocks typically are very fine grained but in places have phenocrysts of quartz. They very commonly show mineral alignment, crude foliation, or other evidence of severe deformation. One common feature is the presence of thin (0.5 mm) planes of slight concentration of dark minerals, biotite and magnetite, that have apparently random orientations. In part, these appear to be associated with penetrative deformation and in part with later fracturing of the rock. In thin section, a typical sample has distinctly anhedral, 0.15 mm quartz grains which conform to the rounded shape of the quartz that is interspersed with smaller grains of altered plagioclase. Relict plagioclase phenocrysts (2 mm) are fairly common, commonly showing a polygonated subgrain structure and being altered and replaced by large (1 to 2 mm) poikilitic muscovite flakes. Epidote as discrete grains and as tiny granules is scattered through these rocks, as are 0.1 mm flakes of muscovite. The epidote granule areas, as seen in reflected light, are actually symplectic intergrowths of epidote and quartz (fig. 21). In some samples, the discrete crystals of epidote have small cores of allanite. Muscovite and epidote appear to be the main alteration products of the plagioclase. Biotite, largely altered to chlorite, and opaque grains of magnetite occur primarily along the fracture planes previously noted. Also present are tiny subhedral to anhedral crystals of zircon. K-feldspar is present but is difficult to identify owing to small grain size and apparent lack of M-twinning. Tiny crystals of bluish tourmaline also occur rarely.

Other samples of this type have phenocrysts of plagioclase zoned An_{22} to An_{15} , some with distinct rims of An_5 . Microcline and quartz also occur as phenocrysts, ranging in size from 1 to 5 mm, and they are



(a)



(b)

0.1 mm

Figure 21. Photomicrographs of quartz-epidote intergrowth from type 1 felsite (PL72-157). A. transmitted light, crossed nicols. B. reflected light.

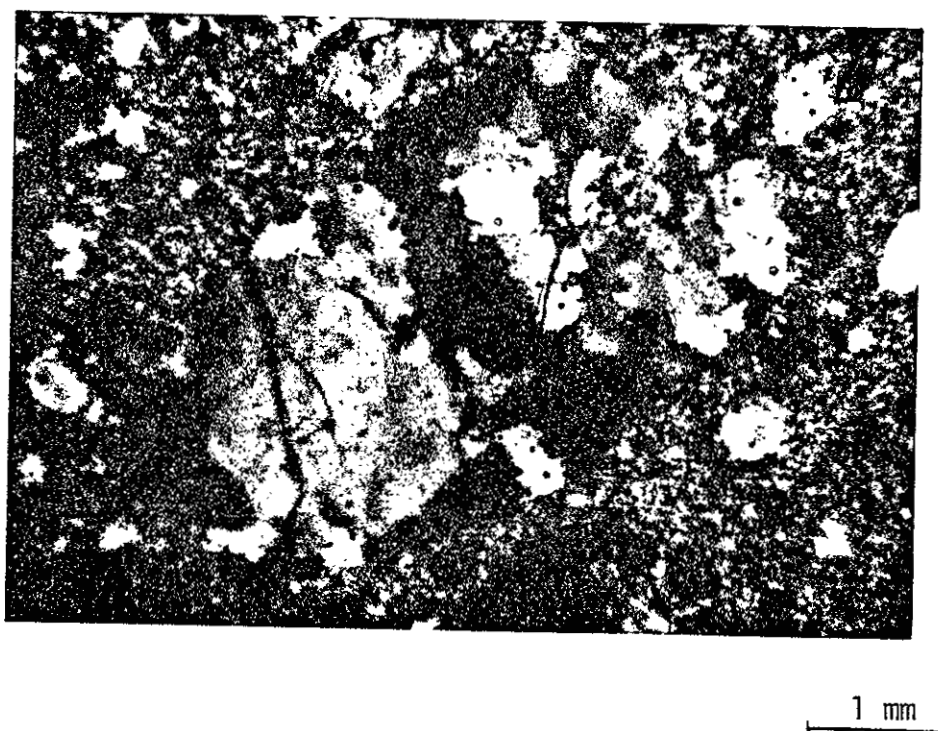


Figure 22. Serrated quartz subgrain boundaries in type 1 felsite (PL72-157).

set in a very fine-grained groundmass (<0.6 mm) similar to that just described. The quartz phenocrysts show strong polygonation and consist of subgrains that have a peculiar serrated texture along grain-to-grain contacts (fig. 22). Anhedral sphene occurs with biotite in some sections.

Still other type 1 felsites appear to be pervasively altered and contain muscovite rather than biotite. This muscovite is strongly oriented and is slightly concentrated in domains or layers, giving the rock a marked schistosity. In spite of this alteration, zircon crystals and allanite crystals rimmed by epidote appear as in the unaltered felsites.

The dikes of medium-gray felsite with dark streaks (Group 2) are commonly porphyritic and have substantially more biotite and/or magnetite than those of Group 1. Fractured quartz augen (5 to 7 mm) are common, and in thin section are seen to consist of numerous subgrains having 120° triple junctions with some subgrains but interlacing, serrated contacts with others. Severely sericitized and deformed plagioclase phenocrysts are also common, and the alignment and structure of biotite and muscovite impart a strong foliation to the rock in thin section and have a shredded appearance. Biotite appears to be much replaced by muscovite, rarely by biotite. Magnetite with ilmenite lamellae, apatite, epidote, and zircon are the common accessories. One large dike in the lower part of sec. 29 has petrographic characteristics of both Group 1 and 2, in that it has considerable biotite and is medium to dark gray in color. It also has diamond-shaped epidote crystals with brownish allanite cores and magnetite partly altered to hematite, features found mostly in Group 1 felsites and the

border zone of the Rana Quartz Monzonite pluton. This suggests that this large Group 2 dike may have a common origin with the Group 1 felsites.

Group 3 felsites are characterized by a brownish-gray to gray color and are very fine grained. In thin section and in a textural sense, however, they appear to be a scaled-down version of Group 1 felsites. Partly connected polygonal quartz grains are interspersed with grains of altered plagioclase, and microcline, greenish-brown biotite, clear muscovite, magnetite, and epidote are scattered throughout the rock. The biotite occurs as well-oriented 1 mm plates whereas the muscovite plates are randomly oriented, slightly larger than the biotite, and commonly poikilitic. The magnetite optically appears to be titaniferous and is altered along margins and cleavage planes to hematite. Epidote occurs as tiny diamond-shaped euhedra with cores of brownish allanite. These petrographic features suggest that Group 3 felsites may be genetically related to those of Group 1, but that they crystallized under different conditions.

Structural Features

The dominant structural feature of the amphibolite unit is its reflection of the pervasive regional foliation (S_1 and/or S_2). This foliation can be readily seen in most hand specimens and is expressed in part by the orientation of tabular bodies within the amphibolite unit such as metachert beds and felsite sills. The orientation of felsite bodies, particularly in secs. 26, 27, and 33, also suggests another phase of folding probably equivalent to Nielsen's (1972) F_3 which produced similar fold styles and orientations to the north.

A possible fault, as discussed previously, is shown in figure 23, and air photo lineaments that cut the amphibolite are shown on plate II. Some of the lineaments appear to be subparallel with a northwest-trending set of near-vertical joints that are locally well developed in the amphibolite.

Foliated Granodioritic Rocks of Uncertain Age

Distribution

A small, irregular body of diorite to quartz-diorite composition occurs about 1 mi west of Trampas (southeast corner of pl. I). This body is structurally and mineralogically complex. To the north it is intruded by the Rana Quartz Monzonite but to the south it is bordered by schist that is tentatively correlated with the Vadito schist to the north. The dioritic rocks themselves probably are related to the Cerro Alto Metadacite, but this cannot be demonstrated directly; they may represent a separate, distinct phase of magmatism.

Lithology

The dioritic rocks are marked by substantial differences in texture, principally as a reflection of variations in deformation and degree of injection or invasion by the nearby Rana Quartz Monzonite. A typical rock, though, has an overall medium dark-gray color and a crude to well-developed foliation resulting from either mineral segregation (gneissic banding) or parallelism of platy minerals or both. The average grain size ranges from about 1 to 2.5 mm. In thin section the rocks show an allotriomorphic granular texture that is disrupted only

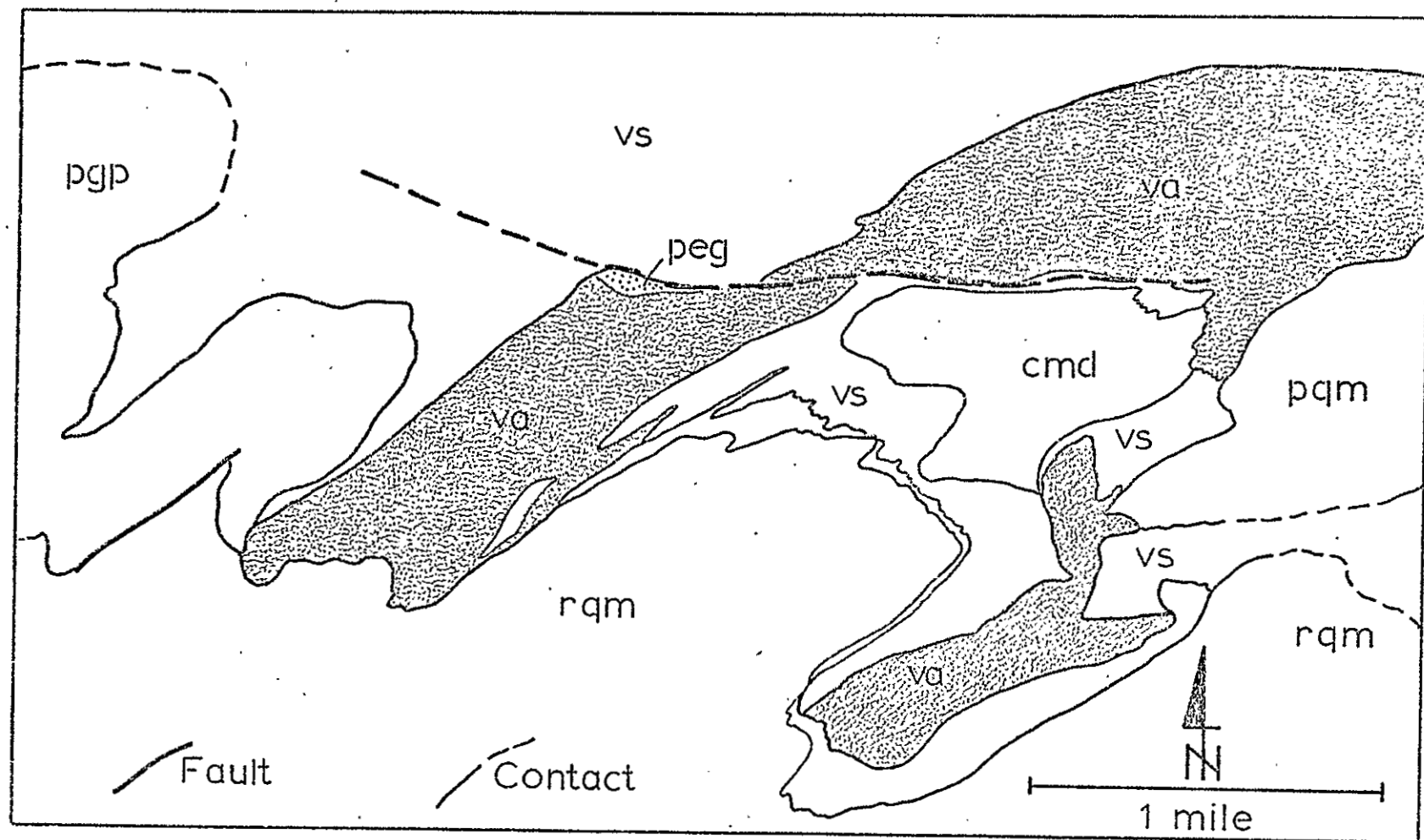


Figure 23. Sketch of a possible fault cutting the main amphibolite belt.

slightly by the orientation of biotite and hornblende laths. The biotite is a brown-yellow variety whereas the hornblende has a typical blue-green, green, straw-yellow pleochroism. The quartz has a slightly larger grain size than the other minerals, has a pronounced lobate texture, and shows undulatory extinction. Plagioclase is zoned from about An_{50} to An_{30} in a continuous normal fashion, with minor continuous reversed zones. Narrow discrete rims of about An_5 to An_{10} are common. Microcline shows typical M-twinning and has hairlike exsolution lamellae of albite. The common accessory minerals are epidote, magnetite, allanite, apatite, sphene, and zircon. There are also rare occurrences of myrmekite.

Structural Features

The main structural feature of this small, isolated body is the strong foliation which ranges from N. 15° E. to N. 15° W. and has low east or west dip. A strong lineation that plunges gently to the south is present in many exposures. The structure of the contact with the Rana Quartz Monzonite has a generally low dip although in most areas the contact is either poorly exposed or is an injection zone that has been modified by the intense deformation that produced the foliation. In general, the body appears to be a part of a screen of country rock between two younger granite intrusive bodies.

Metamorphism

General Statement

The metamorphism of the Vadito and upper Ortega rocks can be considered in terms of: (1) the sequence of pressure-temperature

regimes that resulted in the observed mineral assemblages, and (2) the deformational events that resulted in the folding and development of schistosity and foliation in the rocks. These two aspects appear to have been in part independent of each other, making it possible to outline an internally consistent sequence of pressure-temperature regimes and deformation events. The fact that the older granitic units had already been emplaced at the time of some of the deformational events means that in principle it is possible to relate the sequence of intrusive events to the sequence of deformational events. The deformational events in turn can be related by textural relationships to the metamorphism of the Vadito and upper Ortega rocks. These relationships provide the opportunity to check any hypotheses about possible changes in depth of intrusion of the granites by establishing independently the sequence of regional metamorphic events in the surrounding country rocks and relating it, via deformational features, to the intrusive sequence. This is the principal aim of the following discussion.

Previous Work on the Metamorphism

Montgomery (1953), in attempting the first systematic appraisal of metamorphic events in the area, inferred a phase of dynamothermal regional metamorphism of "medium grade to high grade." This, he concluded, was followed by "widespread hydrothermal metamorphism related to granitic intrusion." In the Ortega Group rocks in particular, Montgomery recognized sillimanite, kyanite, and staurolite zones of progressive metamorphism. He considered these zones to be in part related to depth in the stratigraphic pile, and thus his isograds

generally are parallel to bedding. He noted, however, that some of the sillimanite "apparently is of hydrothermal origin." The Vadito Group rocks were mapped as representing the staurolite zone and a "middle grade of metamorphism." "Hydrothermal metamorphism" was supposed to have followed closely on the heels of the main metamorphic event and was thought to have involved hydrothermal fluids from the granitic rocks. In the Ortega Quartzite this resulted, according to Montgomery, in formation of tourmaline-quartz veins and segregations of coarse-grained sillimanite, kyanite, and staurolite in quartz veins. Montgomery further distinguished a period of "retrograde metamorphism" that supposedly was evidenced by seritization of plagioclase, alteration of cordierite to sericite-chlorite, and local formation of abundant epidote in the amphibolite.

Neilsen (1972) and Nielsen and Dunn (1974) attempted to relate a sequence of deformational events with metamorphism by examining the mineral paragenesis relative to deformational features as observed in thin section. Figure 24 is taken from their work (Nielsen, 1972) and gives a synopsis of their conclusions. It is greatly oversimplified for two reasons. First, the intensity of inferred deformation is nonspecific relative to particular grade of metamorphism (P-T regimes), and second, their acceptance of Montgomery's (1953) and Fullagar and Shiver's notions of a single Embudo granite severely limits interpretations of the timing of magmatism relative to metamorphism. Their work nonetheless is valuable because it defines a working model for the deformational history, a model that implies clear recognition of the long-term polybaric and polythermal history of the area as well as its polyphase deformation. They did not attempt to map isograds, and

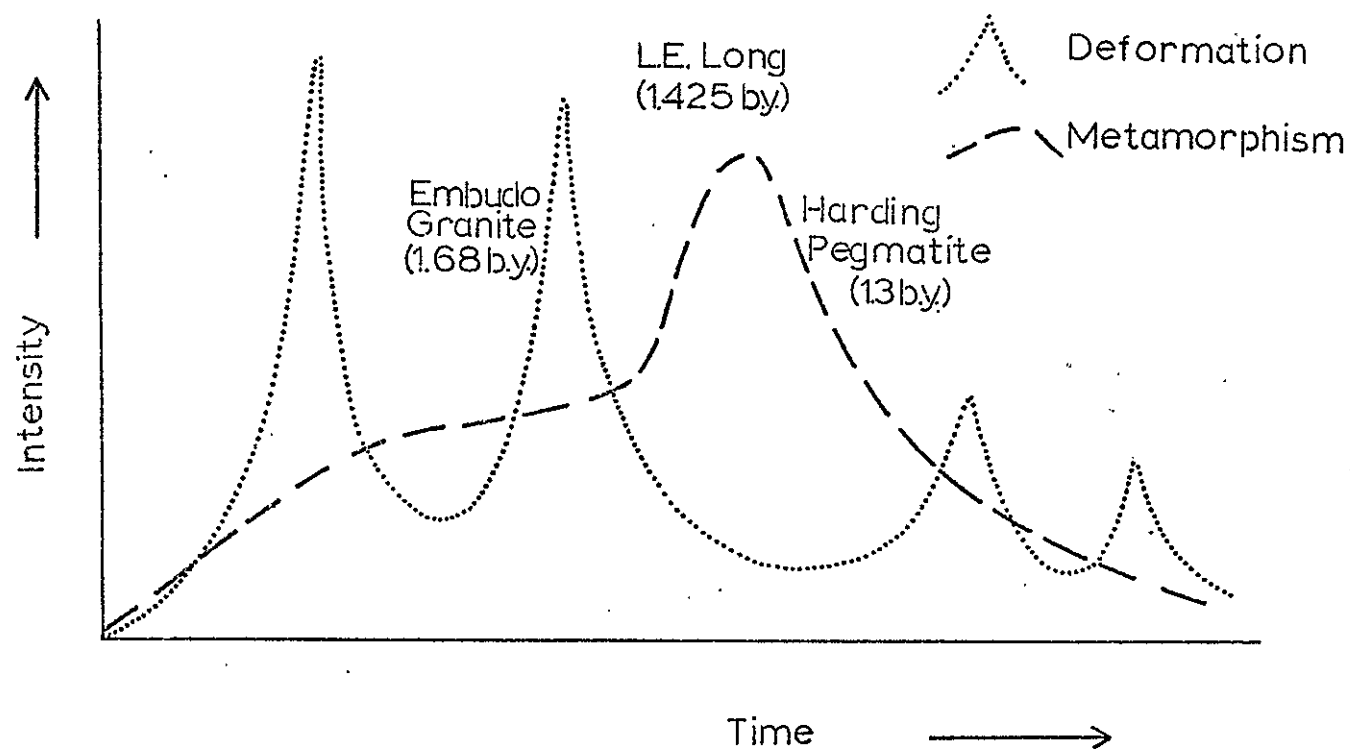


Figure 24. Nielsen's (1972) summary of metamorphism and deformation in the Ortega Group rocks.

apparently they considered the whole terrane to have attained the same metamorphic grade during the main metamorphic event. Montgomery's metamorphic zones might thus be explained in terms of differences in bulk composition and degree of retrogression.

Holdaway (1975) estimated a temperature of 527°C and a pressure of 3.7 kbar for metamorphism of the Rinconada Schist and the Ortega Quartzite. The pressure estimate was based on the Al-silicate triple point of Holdaway (1971) and on the textural interpretation of Al-silicate paragenesis in these rocks, which according to Holdaway are either kyanite-andalusite-sillimanite or kyanite-sillimanite, with kyanite the most common and sillimanite the least common. The temperature estimate was based on the pressure of 3.7 kbar, and the reactions $4 \text{ Ctd} + 5 \text{ Al-Sil} = 2 \text{ Staur} + 1 \text{ Qz} + 3 \text{ H}_2\text{O}$ and $23 \text{ Ctd} + 8 \text{ Qz} = 4 \text{ Staur} + 5 \text{ Alm} + 21 \text{ H}_2\text{O}$. Experimental determinations of these reactions, with consideration of the effect of fluid compositions, prompted Holdaway to conclude that, in spite of the apparent staurolite isograd between them, the two units probably were metamorphosed at the same temperature (527°C). This analysis suggests that Montgomery's isograds have little significance in terms of fossil thermal or pressure gradients. However, it does assume an effectively constant pressure for the lithologic system and presumably refers only to the maximum temperature of the major metamorphic event. In other words, it is an estimate valid for one point in geologic time, whereas what is of interest here is an estimate of the actual P-T path of these metamorphic rocks. Holdaway (1975) gives no textural data, but if his estimate refers in fact to the main metamorphic event of Nielsen (1972) (fig. 24), then it provides one possible point on the P-T path.

Estimates of the General Metamorphic Grade and Paragenetic
Sequences of the Vadito Group Rocks

Four main rock types in the upper Ortega Group and Vadito Group rocks provide a range of metamorphic assemblages upon which to base an assessment of the highest metamorphic grade of the terrane. They are amphibolite, pelitic schists, calcareous hornfels, and quartzite. The quartzites have not been examined in detail because of their relatively simple and nondiagnostic mineral assemblage. The other rocks, however, are all useful in estimating metamorphism, and textural information from certain cordierite-bearing beds within the schists is particularly valuable in placing an upper limit on the pressure at which retrograde metamorphism took place.

Montgomery noted that the plagioclase in the amphibolites is typically andesine, and that the hornblende appears to be aluminous according to its optical properties. It was on this basis that these rocks were considered to be "middle grade." The complete assemblage for the dikes of coarse-grained amphibolite is hornblende + andesine + sphene + ilmenite (with magnetite blebs and stringers included) + epidote + quartz. The textural occurrence of the epidote suggests that it may have developed in part as a retrograde mineral and in part as a prograde mineral. In either case, the maximum grade may be amphibolite facies (Turner, 1968). The assemblage in relatively homogeneous mafic flows from the main amphibolite belt is similar: hornblende + plagioclase (An_{21-33}) + sphene + epidote. It is uncertain whether the sphene and epidote are prograde or retrograde. In some of the metabasalts, clouding of feldspars occurs, and this may be related to retrogression following the development of epidote. Alteration of sphene is also common locally.

Again amphibolite grade is suggested. The metavolcanic conglomerates also contain quartz and, rarely, microcline, whereas still other amphibolites, some of which have a magmatic parentage, contain in addition to hornblende and plagioclase, biotite, ilmenite, garnet, and typically larger crystals of epidote. All of these assemblages are compatible with a maximum grade of amphibolite facies, followed by some retrogression.

The metamorphosed calcareous rocks in the Piedra Lumbre Formation contain the assemblage calcite + quartz + garnet + actinolite \pm sphene \pm ilmenite, and textural evidence indicates that the actinolite was formed prior to the garnet. This assemblage may well have resulted from an original impure dolomite by an initial reaction of the type dolomite + quartz + $H_2O \rightleftharpoons$ Tr (actinolite in this case) + calcite + CO_2 . If dolomite was consumed, then this would result in the paragenesis Q + Tr (Ac) + Cc. This may have been followed by a reaction such as zoisite + calcite \rightleftharpoons grossularite + anorthite + CO_2 . In order for the first reaction to have taken place at reasonable temperatures (475° to $530^{\circ}C$) relative to the grade of the basic assemblages, the pressure probably was in the range of 1 to 2 kbar (Winkler, 1974; Slaughter and others, 1975). The second reaction may have taken place at higher pressures, and certainly at somewhat higher temperatures than the first. The stability of the garnet at low P_{CO_2} , which is consistent with its occurrence in thin beds, is limited by the reaction grossular + quartz + wollastonite + anorthite. Data for this reaction (Newton, 1966; Storre, 1970) and Holdaway's (1971) aluminosilicate triple point suggest that the garnet could not have been stable beyond the region shown in figure 25.

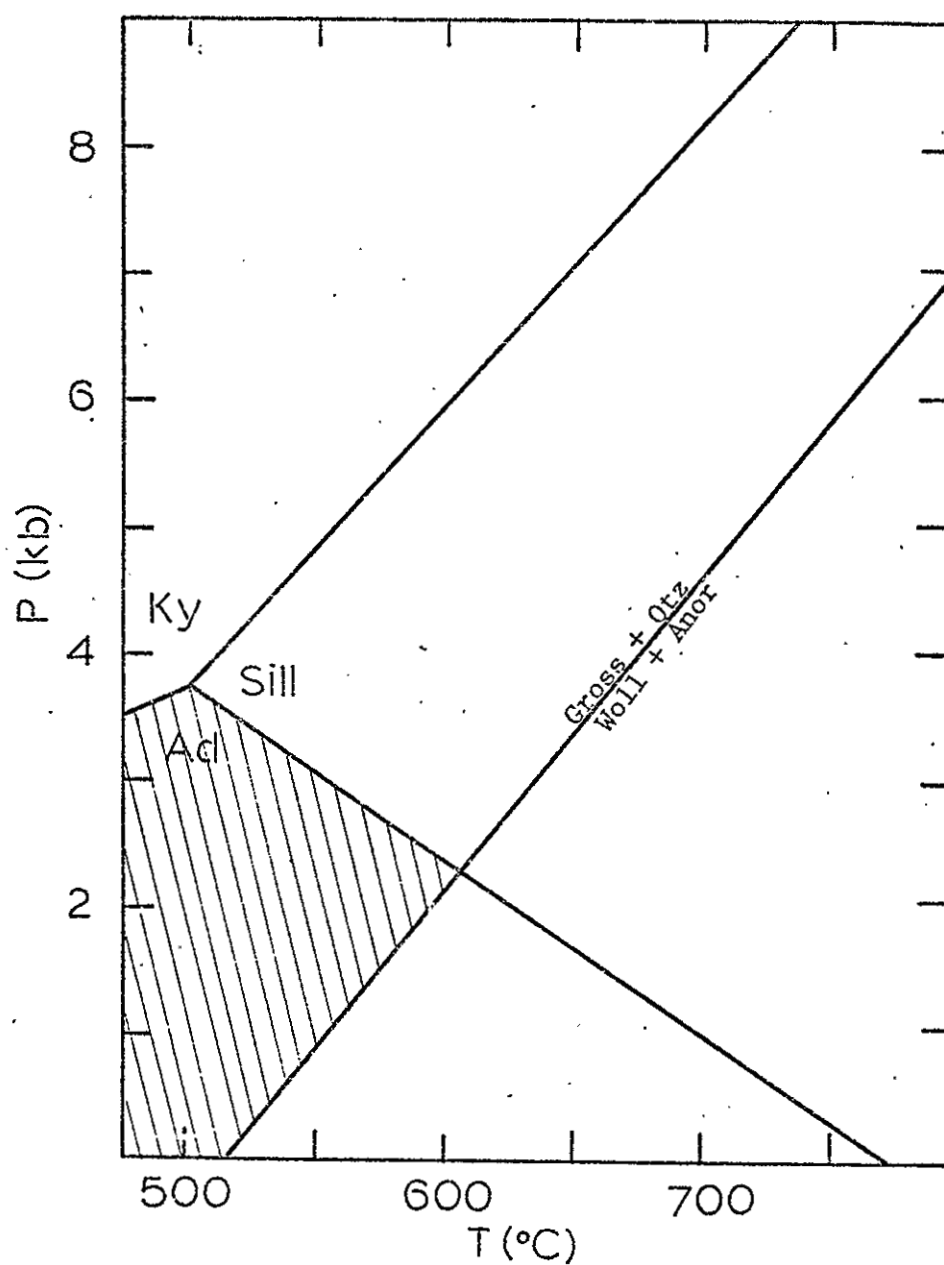


Figure 25. Upper stability limit of grossularite + quartz at low P_{CO_2} and the aluminosilicate triple point combined to limit the P-T regime of the calcareous layers in the Piedra Lumbre Formation. Data from Holdaway (1971) and Storre (1970).

The random orientation of the actinolite grains suggests that they grew after the F_2 phase of deformation, a notion in agreement with Nielsen's (1972) assertion that prograde metamorphism peaked after the two major folding events. The slope of the grossularite + quartz reaction in figure 25 indicates that if equilibrium was maintained during any subsequent retrogression pressure could not have dropped without some decrease in temperature or the grossular would not have remained stable.

The mineral assemblages in the pelitic rocks have a variety of textures which for the most part are difficult to interpret relative to a definite pressure and temperature of formation. The strong control of composition of the original sediments on paragenesis and texture is obvious even from a casual examination in the field. All of the assemblages, however, include quartz, muscovite, and biotite, and where an Al_2SiO_5 polymorph is present it is invariably andalusite. Specific assemblages are:

- I. quartz + muscovite + chlorite + ilmenite + (hematite)
+ almandine garnet + (staurolite) + (plagioclase)
- II. quartz + muscovite + chlorite + garnet + staurolite
+ opaque (ilmenite?)
- III. quartz + muscovite + biotite + opaque (ilmenite?) + chlorite
+ (staurolite) + (garnet) + (zircon) + (apatite)
- IV. quartz + feldspar + garnet + opaques + muscovite + (apatite)
- V. quartz + muscovite + biotite + cordierite + andalusite
- VI. quartz + muscovite + biotite + cummingtonite(?).

These assemblages are typical of either the amphibolite facies (lower) of Turner (1968) or an epidote-amphibolite facies. That andalusite is the only Al_2SiO_5 polymorph in these rocks limits the pressure under which

metamorphism(s) could have occurred to 3.7 kbar (Holdaway, 1972).

This is consistent with the occurrence of cordierite in these rocks as shown by figure 26, which also indicates that even if andalusite persisted metastably, the narrowing of cordierite stability against the granite minimum melting curve still limits the pressure of metamorphism to about 8 kbar.

The textures of some of the cordierite schist are especially interesting. Unaltered cordierite porphyroblasts enclose smaller porphyroblastic and unoriented biotite crystals. In addition, relict chiastolite crystals have been altered to muscovite. The sequence of mineral formation then is: biotite \rightarrow cordierite + andalusite \rightarrow muscovite; or biotite \rightarrow andalusite \rightarrow cordierite + late muscovite. The timing relative to deformation is: $F_1 \rightarrow F_2 \rightarrow$ biotite \rightarrow andalusite + cordierite $\rightarrow F_3 \rightarrow$ late muscovite $\rightarrow F_4(?)$. The particular importance of this sequence is that alteration of the andalusite to muscovite must have taken place during a late metamorphic event as the result of a reaction of the type $K\text{-feldspar} + \text{aluminosilicate} \rightleftharpoons \text{muscovite} + \text{quartz} + 4 \text{H}_2\text{O}$. The combination of the andalusite-sillimanite transition and the univariant equilibria for the above reaction (Evans, 1965; Kerrick, 1972) provides an upper limit on pressure during at least the start of retrogression as shown in figure 27. This assumes that residual andalusite in the cores of the altered chiastolite crystals indicates that P-T conditions were not far from the univariant curve at the time of replacement. Textural relationships suggest that the reaction occurred largely after the F_3 deformation.

Combining the data from all of the above assemblages, we can now suggest a possible P-T path like that shown in figure 28. The sequence

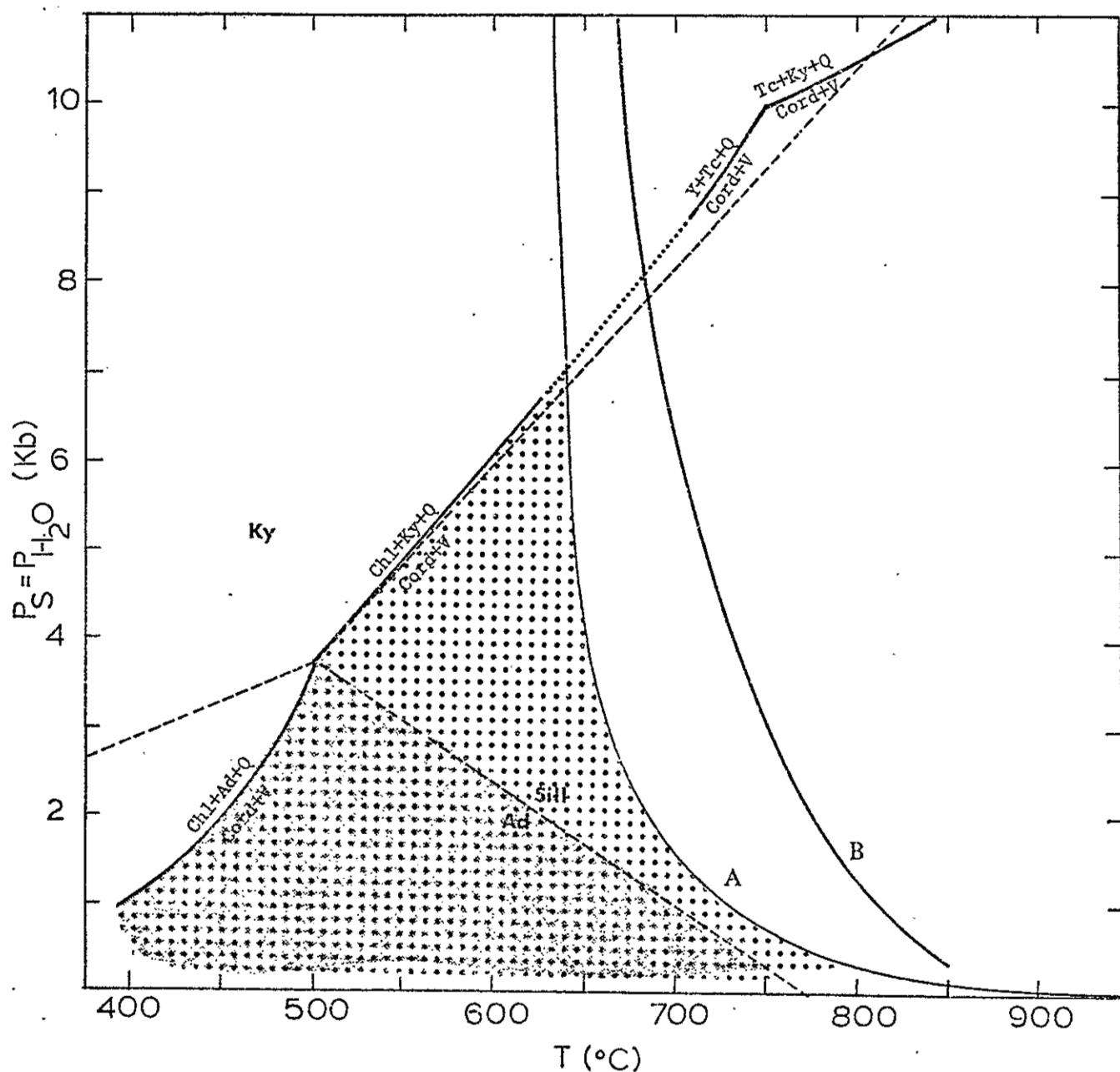


Figure 26. Stability of cordierite (modified from Seifert and Schreyer (1970) to be compatible with Holdaway's (1971) aluminosilicate triple point). *A* is minimum melting curve of granite; *B* is melting of sanidine-quartz-water (Luth and others, 1964). Combination with aluminosilicate stability (Holdaway, 1971) restricts metamorphism of the Vadito Schist cordierite layers to the stippled and shaded area. If aluminosilicate stability is not considered then the minimum melting curve of granite restricts conditions of metamorphism to the stippled area.

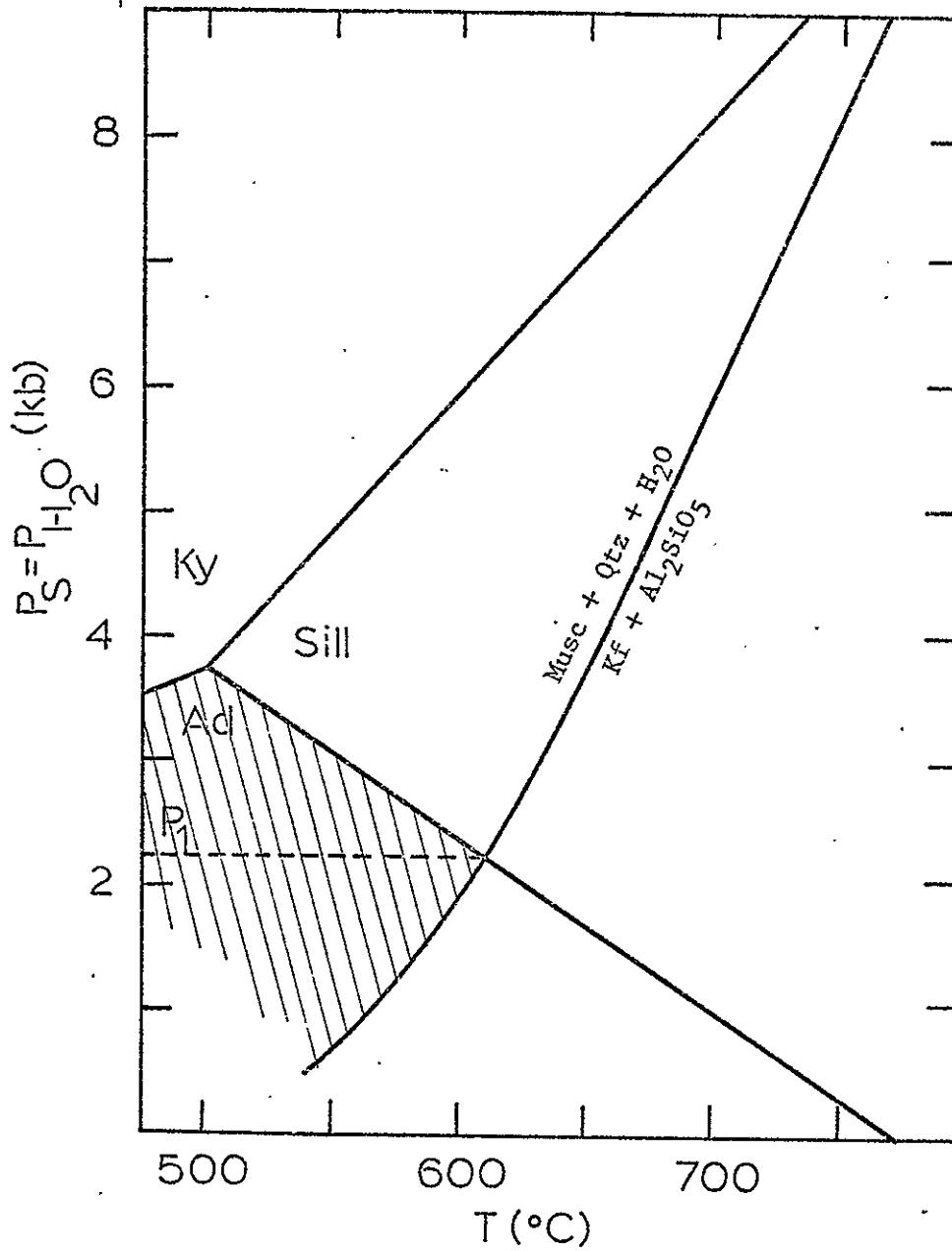


Figure 27. Possible restriction on pressure (P_1) at time of alteration of chiasolite to muscovite if the reaction actually took place along the reaction curve. In any case the P-T regime is again restricted by the stability of andalusite.

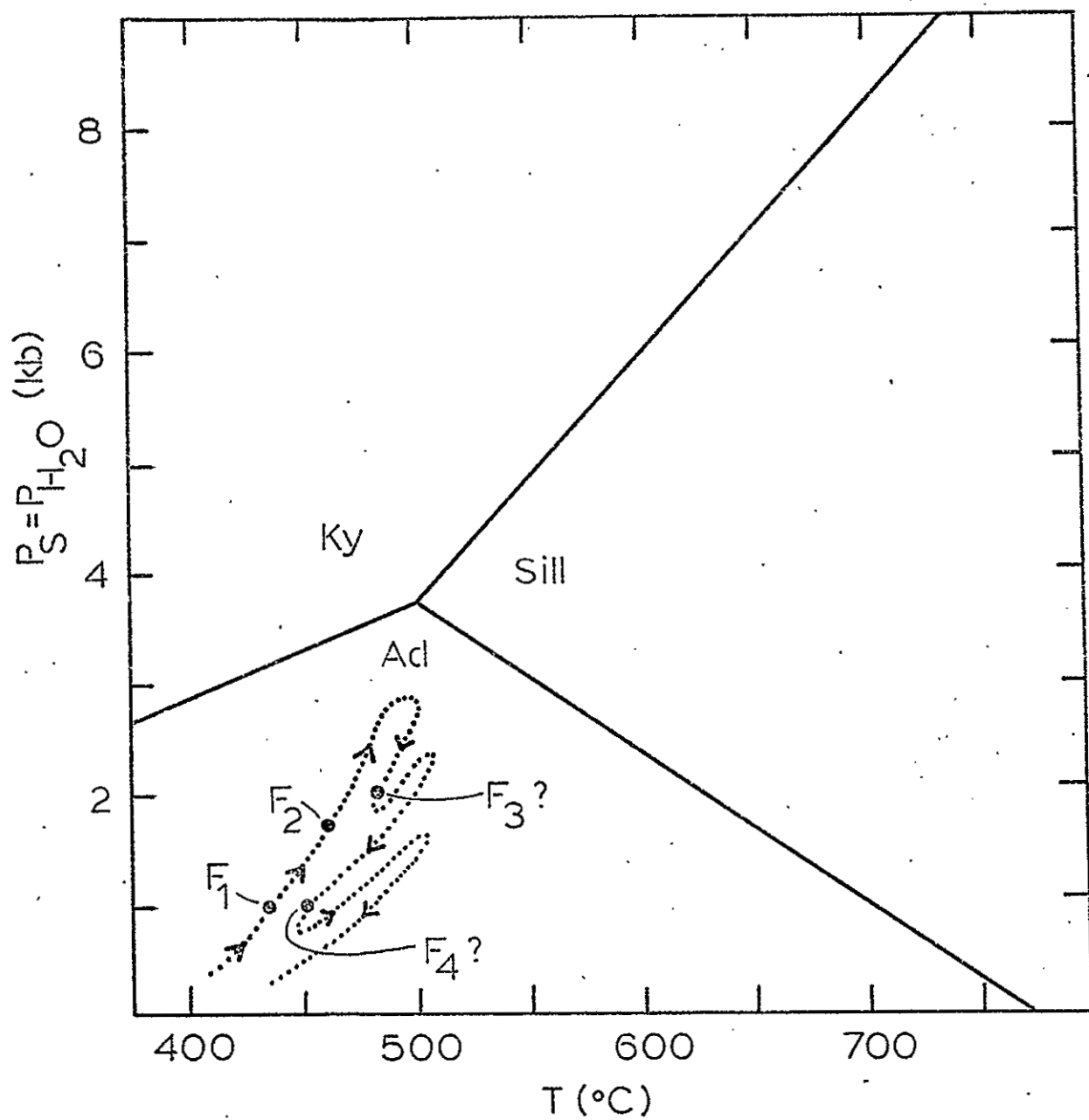


Figure 28. Possible P-T path during metamorphism. The P-T path during the retrogressive stages is highly conjectural and the paths may have actually overlapped one another.

of mineralization in the calcareous beds suggests an initial steep rise in pressure. The presence of epidote in some of the amphibolites may be prograde and again suggests fairly high pressures during initial metamorphism. Maximum pressure is apparently limited by the aluminosilicate triple point although some excursion into the sillimanite field may have occurred. The alteration of the andalusite suggests a lower pressure late in the metamorphic sequence. This late metamorphic alteration may have occurred at a higher temperature, as figure 28 shows, but it is difficult to prove because the introduction of fluids may well have been an important factor in the development of the alteration. Finally, it is possible to suggest the relative timing of the P-T path by noting the deformation events on the curve and by reducing it to P-time and T-time plots as shown in figure 29. This information is particularly useful when combined with data on the age, deformation, and probable depth of intrusion of the granitic rocks.

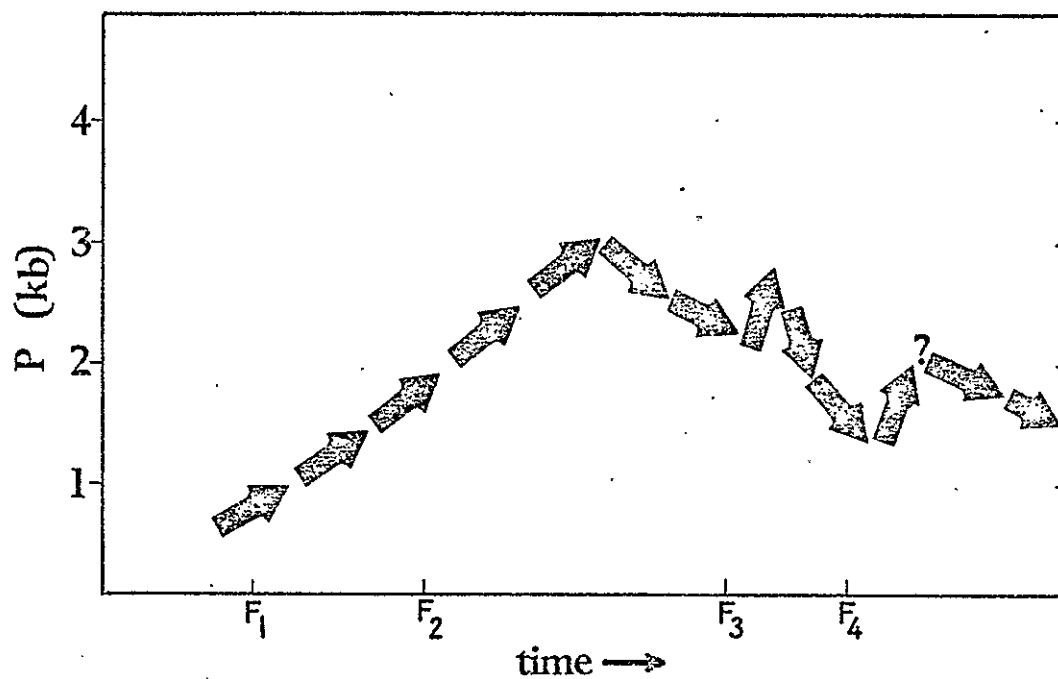


Figure 29a. Possible P-time path during metamorphism.

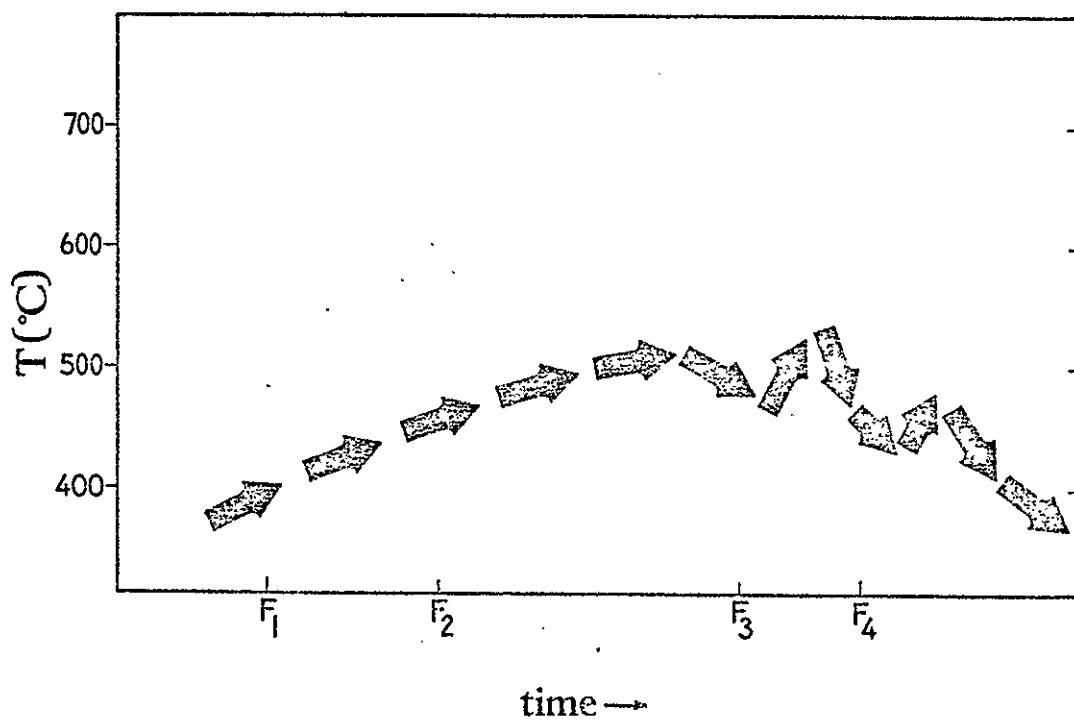


Figure 29b. Possible T-time path during metamorphism.

IV. GRANITIC ROCKS

Cerro Alto Metadacite

Distribution and Occurrence

The Cerro Alto Metadacite crops out mainly in secs. 28 and 33 as a small (0.3 sq mi), stocklike body, but it also occurs as isolated dikes and sills especially in the main amphibolite belt. Its fine-grained character sometimes makes it difficult to distinguish in the field from some of the quartz-rich schists and metagraywackes south of the main amphibolite belt. As a result Montgomery (1953) included this rock type in a unit called "Vadito Felsite-Conglomerate." Here it is recognized as a distinct, and at least partly intrusive unit that is named for Cerro Alto (SW $\frac{1}{4}$ sec. 28). Its widespread occurrence as dikes and as inclusions in younger granitic rocks suggests that its original extent may have been much greater than indicated by present exposures. In general, this rock type is fairly homogeneous except for mild textural variations, especially in dike occurrences. Felsite dikes and large (1 to 1000 mm) inclusions or dikes of amphibolite are found within the main body of metadacite. The amphibolites are of uncertain age and origin.

Contact Relationships

The main body of the Cerro Alto Metadacite generally has sharp contacts with the country rocks, particularly along its western margin

where definite crosscutting relationships with the schists are observed. Near this contact, metadacite dikes also crosscut the sedimentary structures (fig. 30). Most other parts of the margin of the main body are less clear cut. Exposures are not everywhere good, but the general shape of the contact, especially along the eastern margin, suggests a much more conformable character. This may be the result of postintrusion regional deformation, or it may stem from emplacement of the rock as an extrusive or nearly extrusive body, thus making it partly interlayered with surrounding stratified rocks. There is compelling evidence to support both possibilities, and it appears that the present shape of the body arises from a combination of an irregular initial shape of a partly extrusive body and postintrusion deformation resulting in further misshapen character. The north margin of the body may actually be an extension of a shear zone or a fault that apparently offsets the main amphibolite belt (see section on structural features of the Vadito schist and fig. 23). The southern and part of the western margins, on the other hand, appear to follow general fold structures in the surrounding Vadito schist.

Petrography

The Cerro Alto Metadacite is a nondescript gray rock that consists largely of fine-grained quartz, plagioclase, microcline, biotite, and muscovite. Epidote, allanite, sphene, magnetite, and zircon are the common accessory minerals. Hand specimens are shown in figure 31. A typical sample is medium dark gray on fresh surfaces and brownish gray on weathered surfaces. Overall, the rock has an allotriomorphic granular to porphyritic texture with relict oblate phenocrysts of

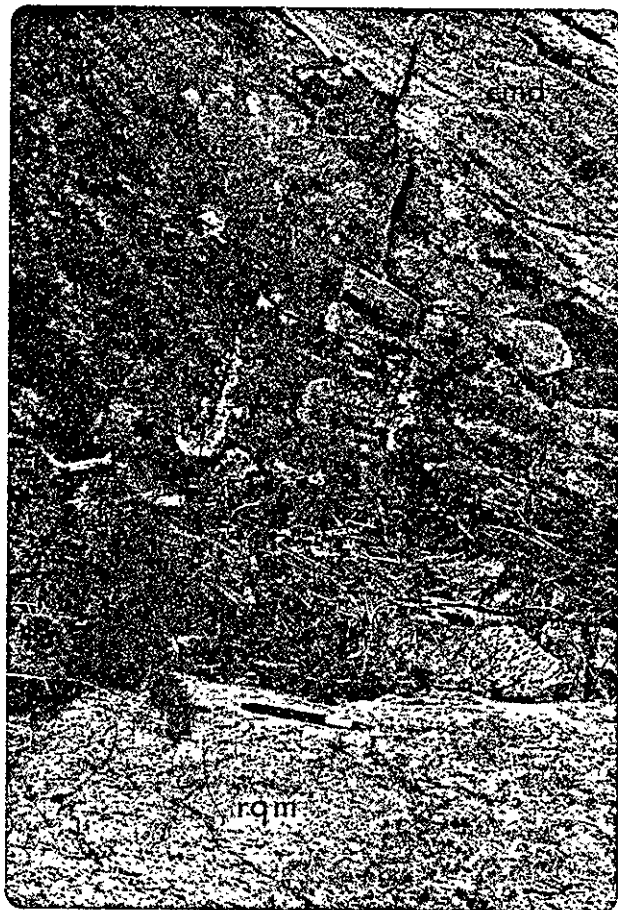
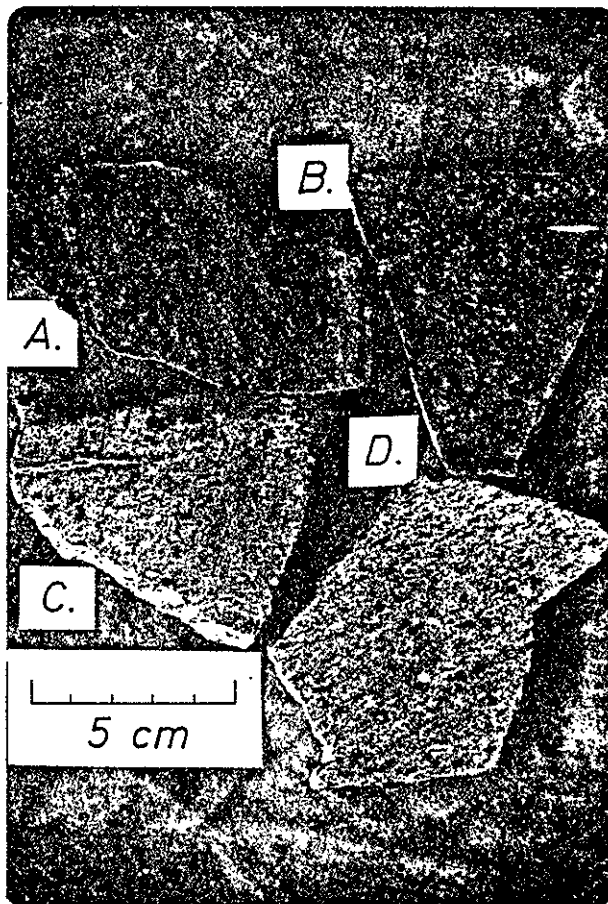


Figure 30. Cerro Alto Metadacite dike crosscutting a conglomerate bed. 1/3 mi southwest of Cerro Alto.

Figure 31. Stained slabs of Cerro Alto Metadacite. K-feldspar is stained yellow. A. PL72-135; B. PL72-133; C. PL72-214; D. PL72-198.



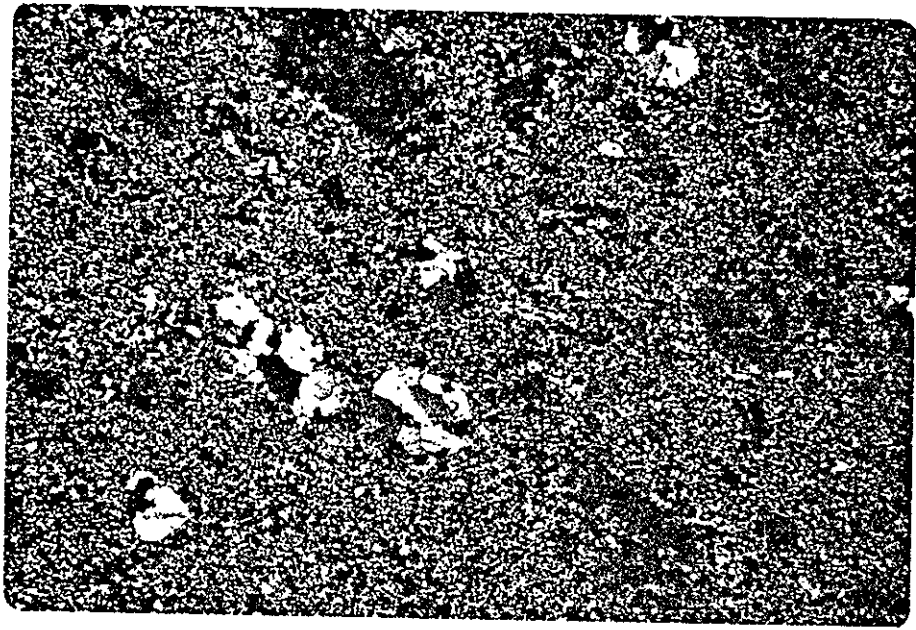
quartz and/or plagioclase up to 4 mm long set in a groundmass (0.15 mm average grain size) of quartz, plagioclase, microcline, and biotite plus accessory minerals. The quartz and plagioclase phenocrysts consist of 1 to 0.5 mm subgrains. Muscovite occurs both as single plates like the biotite and as poikilitic grains commonly with optical continuity maintained over distances of 2 mm. The groundmass typically has a very granular appearance, with numerous 120° triple junctions between mineral grains. Biotite occurs both as single subparallel grains and as glomeroporphyritic masses with associated epidote, allanite, magnetite, and sphene. Epidote grains commonly have a core of brownish allanite. Typical photomicrographs of thin sections are shown in figure 32.

Modal Composition

Modal data for the Cerro Alto Metadacite are given in Appendix II and are plotted as crosses on a plagioclase-K-feldspar-quartz triangular diagram in figure 33. The open hexagons represent felsite dikes, and the single metadacite sample that has more than 50 percent quartz occurs as a dike. These data demonstrate the generally silicic, but still plagioclase-rich nature of the metadacite. The modal similarity of the one sample of a metadacite dike and the felsite dikes may reflect similar alteration histories for both types of dikes rather than a primary magmatic association.

Structural Features

A significant foliation is usually visible in hand specimen and in thin section, but in casual examination of outcrops it is easily overlooked, because the rock is so fine grained. This foliation strikes



(a)

5 mm



(b)

0.5 mm

Figure 32. Photomicrographs of Cerro Alto Metadacite; crossed nicols, PL72-133.

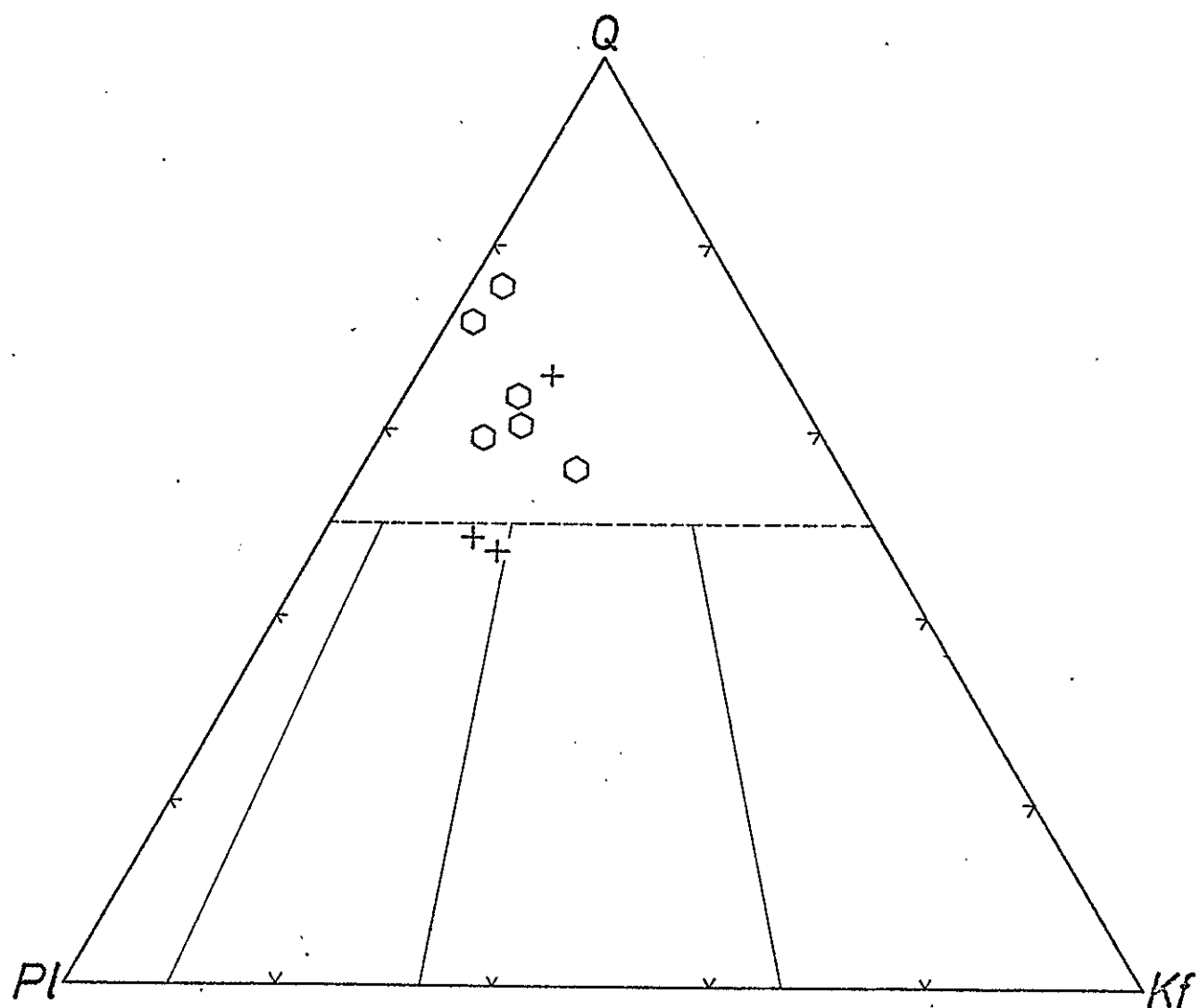


Figure 33a. Plots of modal data for Cerro Alto Metadacite (crosses) and felsite dikes (open hexagons).

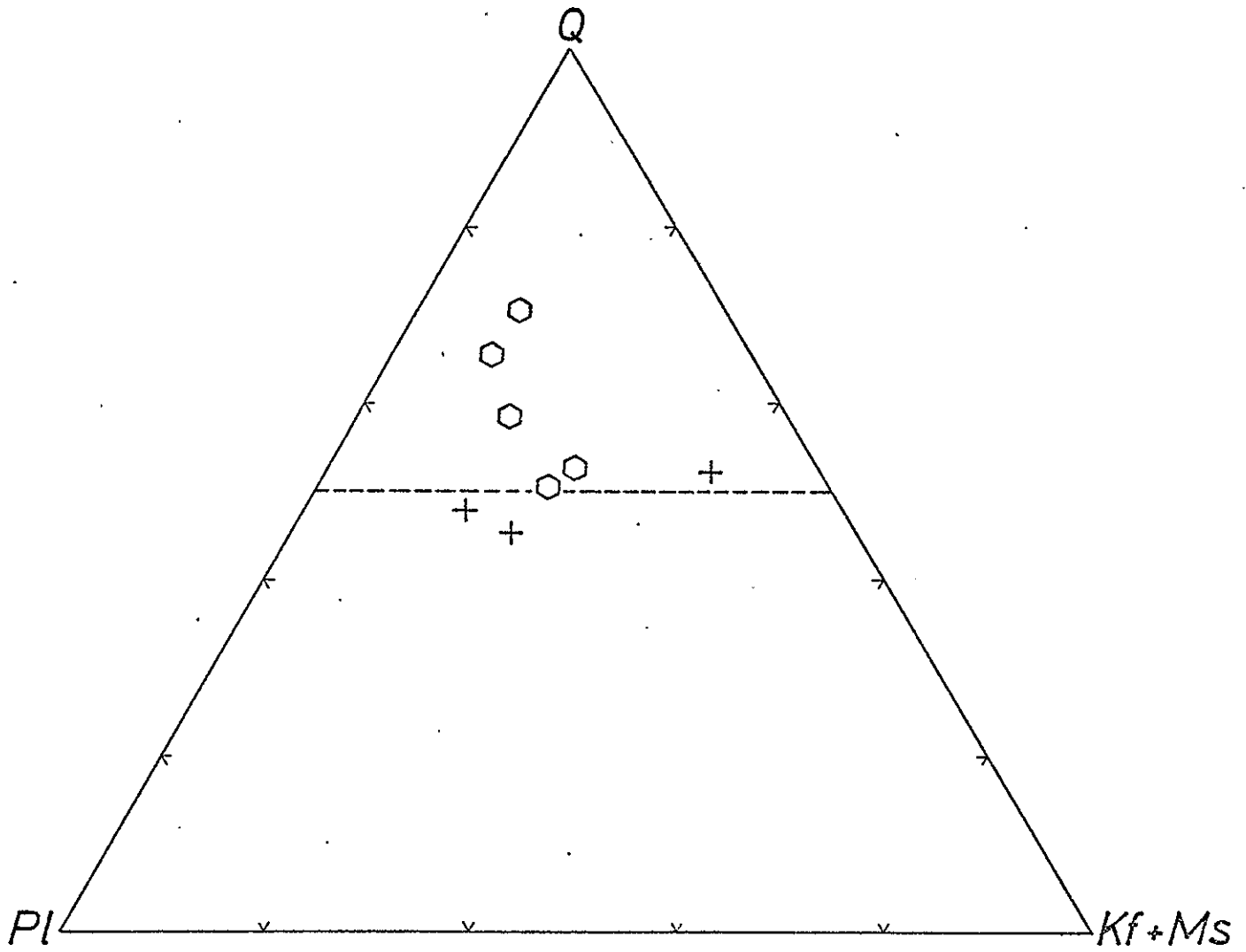


Figure 33b. Plots of modal data for Cerro Alto Metadacite (crosses) and felsite dikes (open hexagons).

N. 50° - 60° E. with local strikes of due east and has steep southeast dip. Thus it generally follows the regional trend and is presumably the result of F_2 . Rarely a distinct lineation is present striking north-south and plunging 55° S. In one locality a joint set was noted with a N. 77° E. strike and a 65° N. dip. As previously stated, the general outcrop pattern of the main Cerro Alto Metadacite body suggests some larger scale folding, and it is possible that the deviations from the general N. 60° E. foliation trend south of Embudo Creek and at the extreme eastern margin are due to the broader, more open folding and warping associated with the F_3 deformation period of Nielsen (1972).

Metamorphism

Timing of the deformation events F_1 and F_2 relative to the main metamorphic event indicates that the Cerro Alto Metadacite was metamorphosed along with the surrounding amphibolites and pelitic schists. However, the original igneous phases of the metadacite apparently were relatively insensitive to the prograde metamorphism in the area. The most substantial readjustment seems to have been a "retrogressive" type analogous to the reaction: aluminosilicate + K-feldspar \rightleftharpoons muscovite + quartz + H_2O . In the dacite, however, the plagioclase must have acted as the peraluminous source instead of Al_2SiO_5 . This type of reaction accounts for much of the muscovite, probably for the severe alteration, and possibly for the local mechanical instability of the plagioclase phenocrysts. The reaction also would tend to reduce the modal amounts of microcline and calcic plagioclase while increasing quartz, perhaps accounting for the high quartz content of the altered

dike rocks in particular. That the destruction of calcic plagioclase would release calcium may account for at least some of the epidote--especially that which is texturally associated with muscovite and/or altered plagioclase. These reactions are discussed in more detail in a later section, as they apparently were important in the histories of the younger granitic rocks as well. Some of the sphene may be metamorphic in origin but its lack of association with the magnetite grains suggests that it did not form from exsolution of titanium from the magnetite.

Summary

The Cerro Alto Metadacite is the remnant of what probably was once a much more extensive subvolcanic complex. The main body of the metadacite is at least partly intrusive and has sharp discordant contacts with the country rock. This fact plus the texture of the rock suggests that it was emplaced at very shallow depths. At the time of intrusion and chilling quartz and plagioclase, and probably biotite, epidote-allanite, and zircon coexisted with a silicate liquid. Subsequently, the rock was deformed and metamorphosed at least once prior to the largely postdeformational retrogressive development of muscovite, epidote, and possibly sphene.

Puntiagudo Granite Porphyry (Quartz Monzonite)

Distribution and Occurrence

The Puntiagudo Granite Porphyry occurs as a large lobate body in the northwest and central parts of the map area. Its total exposed

area is about 1.5 sq mi. As one of the more resistant rock types, it forms prominent ridges and hills that include Cerro Puntiaugudo and Cerro de Los Arboles. To the south and west it is covered by Tertiary sedimentary rocks whereas to the north and east it either intrudes Vadito schist or is intruded by the Rana Quartz Monzonite (pls. I and II). Near Trampas there are limited and mostly isolated exposures of rocks that are in part similar to those in the main body of Puntiaugudo Granite Porphyry. These exposures have been tentatively mapped as equivalent to the Puntiaugudo Granite Porphyry although it is recognized that they may represent a separate pluton.

Contact Relationships

The Puntiaugudo Granite Porphyry generally has sharp contacts with the country rock it intrudes (fig. 34). The shape of the contact is irregularly lobate and in one area a large tapered tongue of schist nearly 0.5 mi long projects into the main body. In addition, parts of the margin show thin dikes which are apophyses of the main mass.

The contact is clearly discordant, but its general shape and the variability of dip near Cerro de Los Arboles suggest that the intrusion may be in part phacolithic or, alternatively, that its shape is largely a result of postintrusion deformation. If the latter were the case, however, one would expect the body to have generally more conformable contacts. So while the Puntiaugudo Granite Porphyry has obviously undergone considerable deformation, such deformation does not appear to have been mainly responsible for the present shape of the body. Its basic shape is primarily the result of the nature of the intrusion, but it has been modified and perhaps accentuated by subsequent deformation.



Figure 34. Contact of marginal sill of Puntigado Granite Porphyry with Vadito schist. The main contact is in the top portion of the photo. 0.25 mi north of Cerro Puntigado.

The modifying effects of deformation are particularly important for the contact between the Puntigudo Granite Porphyry and the Rana Quartz Monzonite, which is a shear zone along much of its length (pl. II).

Petrography

The Puntigudo Granite Porphyry was mapped as a single unit, but it has a narrow, discontinuous border zone (0 to 30 m). Typically associated with this border zone are fine-grained slightly porphyritic dikes that commonly occur within the body. The main mass of the body has no obvious internal contacts, but is characterized by variations in degree of deformation and by differing amounts and proportions of microcline, quartz, and plagioclase phenocrysts.

A consistent feature of this rock is its porphyritic character (fig. 35). Finer grained border zone rocks and fine-grained dike rocks are not as obviously porphyritic but do contain small phenocrysts. In a typical sample, which might be called a porphyritic biotite quartz monzonite, subequant, nearly euhedral 1 cm grayish-orange-pink microcline grains are set in a fine-grained matrix along with 4 to 6 mm oblate anhedral quartz grains. The matrix consists of 0.07 mm quartz, plagioclase, and microcline. Biotite occurs in the groundmass as 1 to 2 mm clots of partly shredded and bent 0.5 mm grains or as scattered single flakes. Muscovite is either associated with biotite as fresh, randomly oriented 1 mm plates or it appears to partly replace deformed and polygonized grains of plagioclase. These granulated portions of the rock appear to be relict plagioclase phenocrysts. Locally plagioclase phenocrysts are preserved as partially included grains in

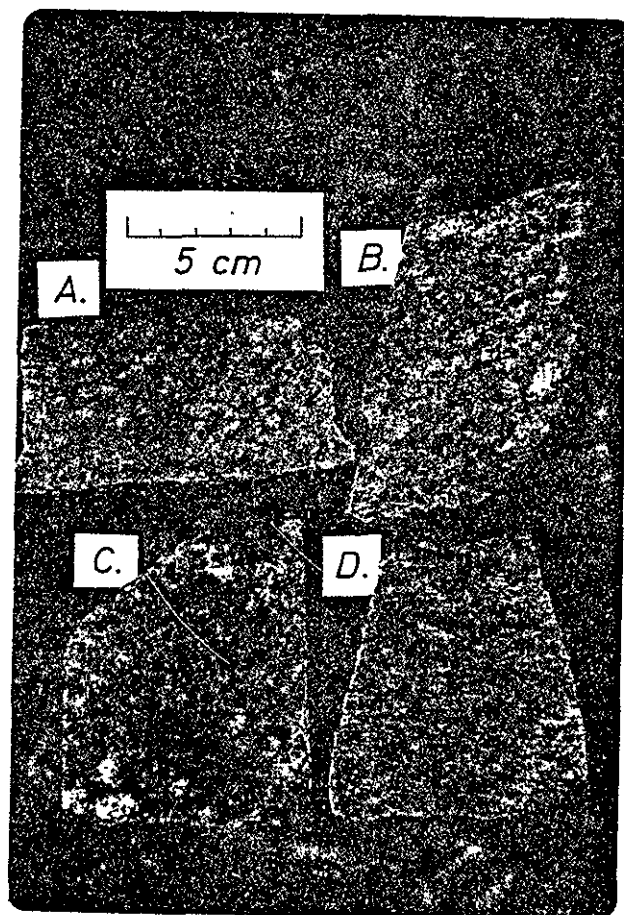


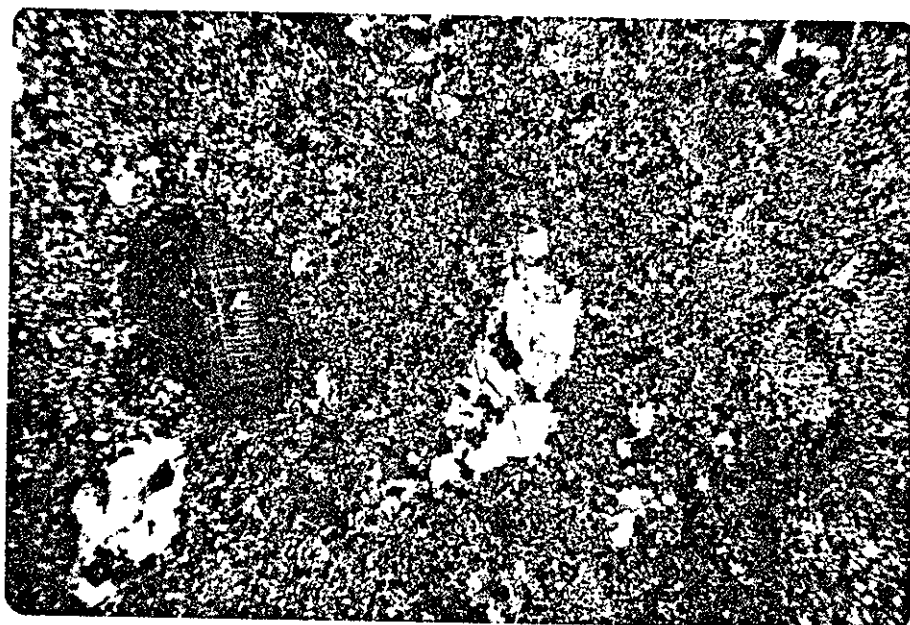
Figure 35. Stained slabs of the Puntigudo Granite Porphyry. Note the differences in grain size and the wide range of deformational textures in this unit. K-feldspar is stained yellow. A. PL72-126; B. PL72-100; C. PL72-124; D. PL71-44.

the microcline megacrysts. Accessory minerals are granules and stubby crystals of epidote which replace plagioclase, elongate, zoned 1 mm crystals of allanite, granules of sphene and zircon associated with biotite, and octahedra of magnetite partly altered to hematite. In some places chlorite replaces biotite. Some of these petrographic features are shown in figure 36.

The border zone of the Puntiaquido Granite Porphyry is more leucocratic than the main mass, and it commonly has a coarse sugary texture and an orange-pink color. Quartz is more abundant as phenocrysts than are plagioclase and microcline. The matrix contains less biotite than does that of the main mass but its mineralogy is otherwise similar. Its texture is markedly different, however, showing peculiar interlobate serrated plagioclase grains that appear to cement the grains of microcline and quartz together.

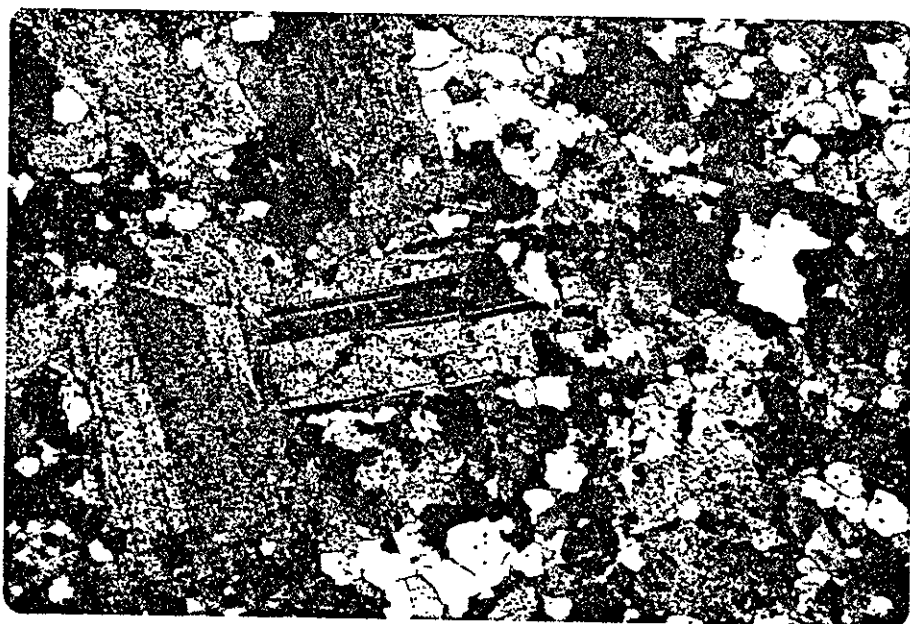
The porphyritic aplite dikes have a very fine-grained groundmass (0.1 mm) which has an overall yellowish-brown color. Phenocrysts are quartz (1 to 3 mm), microcline (0.5 to 1 mm), and plagioclase (0.5 to 2 mm). There are also rare clots of biotite. The cores of plagioclase microphenocrysts are invariably replaced by muscovite, and they commonly have low-An rims that show little or no alteration. The matrix consists of interlobate grains of quartz, microcline, and plagioclase with irregular flakes (0.3 mm) of muscovite scattered throughout. These rocks have a definite foliation, but the fine grain size makes it difficult to see.

In one area there appeared to be two generations of fine-grained dikes, an older one with numerous small phenocrysts and a younger one which lacked obvious phenocrysts and which intruded the older one. The



(a)

1 cm



(b)

1 mm

Figure 36. Photomicrographs of Puntagudo Granite Porphyry samples.
A. PL71-68; B. PL71-44.

younger dikes have a distinct trace-element chemistry as well, and are discussed further in that context in a later section.

Modal Composition

Modes from seven samples of Puntiaugudo Granite Porphyry show a variation from quartz monzonite to granodiorite (fig. 37; Appendix II). Two samples of porphyritic aplites, however, have considerably higher plagioclase contents than do the samples of the main unit. This suggests that the general fractionation trend in the Puntiaugudo Granite Porphyry may have been toward higher plagioclase and quartz, behavior that would be consistent with the large microcline crystals forming as a primary, early crystallized phase. The "horizontal" trend on the modal plot, though, suggests that quartz and plagioclase may also have participated in the supposed fractionation, with quartz being more efficiently separated than plagioclase.

Structural and Textural Features

The main structural feature of the Puntiaugudo Granite Porphyry is its pervasive foliation. It has a trend which is generally about due east ($\approx 20^\circ$) with a steep south dip. A few outcrops show a lineation that plunges about 20° E. in the plane of the foliation. In addition, some outcrops show a well-developed pattern of near-vertical closely spaced fractures that are oriented about N. 25° - 20° W. Differences in the intensity of deformation, though, are curious. Figure 38 shows examples of extreme deformation whereas figure 36a shows, in thin section, an example of very little deformation. Note that in figure 38 the rock has a gneissic appearance with microcline grains being augen shaped

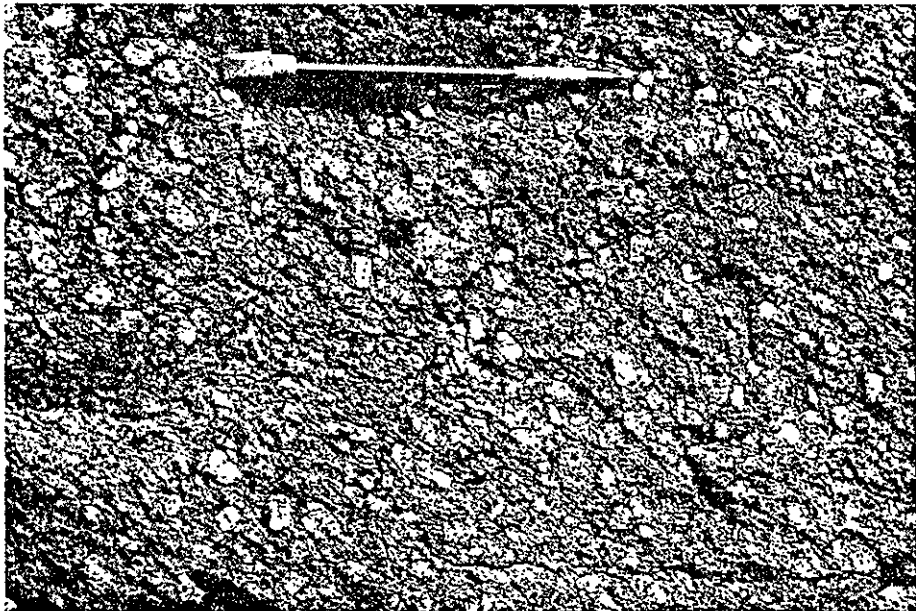


Figure 38. Outcrops of Puntigudo Granite Porphyry showing strong deformation. Notice flattening of gray quartz grains. Located on the southeast shoulder of Cerro Puntigudo.

and quartz having a flaser texture. The groundmass and plagioclase grains were obliterated during granulation while biotite appears to have been recrystallized. In the well-preserved sample (fig. 36a) the deformation is nearly imperceptible in hand specimen or thin section. There is little problem in distinguishing relict plagioclase phenocrysts from the groundmass and in general, except for alteration, the texture has not been strongly modified by any of the regional deformations.

The variability of the orientation of the foliation, the presence of lineation, and the occurrence of a closely spaced fracture pattern all suggest polyphase deformation. Further, these features can be reconciled with the data of Nielsen (1972) who indicated that the "Embudo" granite was post- F_1 , but simply stated that this was based on "field relations." If we accept this, then F_2 produced the main foliation and F_3 produced the lineations and the closely spaced fracture pattern. The quasi-ductile shear zones of F_4 are only rarely observed in the Puntagudo Granite Porphyry. Thus it is necessary for a single phase of deformation, F_3 , to have produced the closely spaced fracture pattern, the lineation, and the general disruption or folding of the F_2 foliation. If the maximum compressive stresses of F_3 were oriented east-west as proposed by Nielsen (1972), then it is possible that initial slippage along east-west foliation planes could have produced the lineation while further deformation may have disrupted the orientation of F_2 foliation in widely spaced outcrops. The closely spaced fractures are oriented about normal to the proposed east-west F_3 stresses and may have been generated as decompressive features similar to sheet fractures, or they may represent a kind of incipient foliation. Any alternative

explanations of the deformation sequence either would have to involve F_1 in the initial deformation or would require an additional phase of deformation that was not recognized by Nielsen and that would have occurred between F_2 and F_3 . There is no independent evidence to suggest either of these two latter possibilities.

Metamorphism and Alteration

If the proposed deformational sequence just discussed is correct, then the Puntiaquido Granite Porphyry must have been metamorphosed simultaneously with the Vadito Group rocks. Modification of the original igneous, or possibly deuteritic, phase assemblage does not, in general, seem to have occurred in a way that can be positively attributed to prograde metamorphism. The two main features that might be attributed to metamorphism are the alteration of the cores of plagioclase grains to muscovite and epidote and the sporadic development of epidote alteration over fairly large areas. This alteration is characterized by a distinct reddening of the feldspars and by local development of epidote veining. Unfortunately, neither of these features is unique to metamorphism, and both could have formed as the result of deuteritic processes. Yet there are substantial arguments that they did not. The epidote veining in particular seems to have completely escaped any deformation, and large muscovite grains in the unaltered Puntiaquido Granite Porphyry generally lack any evidence of deformation. Furthermore, the spatial distribution of the epidote alteration bears no systematic relationship to the Puntiaquido Granite Porphyry itself, such as occurring only along its margins, and in fact affects the next younger granite, the Rana Quartz Monzonite as well. Finally, some epidote veining is definitely

later than pegmatites that occur in the Rana Quartz Monzonite and, as shown farther on, all the pegmatites probably are substantially younger than either the Rana Quartz Monzonite or the Puntiaquito Granite Porphyry. It must be pointed out, however, that the alteration probably was complex. This is pointed up by the rare occurrence of muscovite-quartz alteration of Puntiaquito Granite Porphyry along narrow discontinuous shear zones (N. 50° E.) and by the occurrence of a variety of cross-cutting alterations and epidote veining in the Rana Quartz Monzonite. It is here suggested that the alteration is primarily the result of metamorphism, in particular a "retrograde" phase of metamorphism when fluids apparently were available for the alteration process. It should be stressed, however, that the alteration seems largely to have enhanced features that might well have been initiated in a deuteritic process. Whether or not alteration actually was begun during late-stage crystallization would depend on the details of the cooling history of the body and such factors as water content and permeability of the rock. It should be clear, though, that there will in some sense be a continuum between deuteritic and metamorphic processes in that every cooling granite body probably passes through a P-T regime appropriate for alteration. The question is, are the kinetics of the alteration process rapid enough relative to the cooling rate of the body in order to actually effect any alteration? In the case where no evidence is available for the timing of a subsequent metamorphic event, it may be very difficult to distinguish products of the two processes. Fortunately, in this instance the evidence indicates that much of the epidote veining and associated alteration must have been due to a postmagmatic metamorphic event or events.

Summary

The Puntiaquito Granite Porphyry probably was intruded as a crystal-liquid mush in which microcline, quartz, and plagioclase coexisted and were apparently crystallized simultaneously. Intrusion of the body resulted in formation of the discontinuous chilled margin which may have been part of an early formed melt and development of the strongly porphyritic texture that occurs in much of the body. The aplitic rocks associated with the margins of the body represent residual liquids separated from the Puntiaquito Granite Porphyry at various stages of crystallization.

Three periods of deformation (F_2 , F_3 , and F_4) followed primary intrusion and crystallization of the body. Although prograde metamorphism must have been experienced by the Puntiaquito Granite Porphyry, the most obvious effects were caused by fluids accompanying regional retrogressive metamorphism, an event that occurred during the waning stages of the F_3 phase of deformation or shortly thereafter.

Rana Quartz Monzonite

Distribution and Occurrence

The Rana Quartz Monzonite, named for Cerro de la Rana, occurs in the central and south-central parts of the map area (pl. I). It has a total exposed area of about 4.5 sq mi and is divided into three subunits: the border zone (0.25 sq mi exposure), a foliated facies (3 to 4 sq mi exposure), and an unfoliated facies (about 0.75 sq mi exposure). Aplite dikes occur sporadically throughout the foliated and unfoliated phases. The border-zone rocks occur discontinuously

along the contact of the foliated facies with the country rock and have a gradational contact with the foliated facies. The unfoliated facies occurs as a single block in secs. 1 and 6 and parts of secs. 36 and 33. It has a gradational relationship with the foliated facies.

Contact Relationships

The Rana Quartz Monzonite has sharp and, in general, strongly discordant contacts with the Vadito Group rocks. In detail this contact is very jagged, and numerous sills and dikes protrude out from the border zone into the Vadito schist. Close examination of contacts, however, shows that they are not as sharp as in the case of the Puntiaquedo Granite Porphyry. Figure 39 shows the slightly more diffuse nature of a typical Rana Quartz Monzonite contact.

The Rana Quartz Monzonite also is in contact with the Puntiaquedo Granite Porphyry. This boundary is difficult to interpret in terms of relative age because over most of its short length it is actually a broad shear zone (F_4 type deformation), and where it is not a shear zone it is occupied by a large mass of aplitic or rhyolitic material. Careful observation in the vicinity of the contact, though, suggests that the Rana Quartz Monzonite intruded the Puntiaquedo Granite Porphyry and included diffuse blocks of that unit in itself. Though this evidence is not definite, the Rana Quartz Monzonite is tentatively assigned as younger than the Puntiaquedo Granite Porphyry.

The Rana Quartz Monzonite also intrudes dioritic rocks along a conformable contact in the south portion of plate I, but the very limited exposure of this contact as well as the deformation that has taken place in this area, make it difficult to interpret. The Rana



Figure 39. Contact of Rana Quartz Monzonite with upper Vadito schist (here a metagraywacke). Note the slightly less than sharp character of the contact. 0.3 mi southwest of Cerro Alto.

Quartz Monzonite itself is definitely intruded by the Penasco Quartz Monzonite, as discussed farther on.

Petrography

Border Zone

Rocks of the Rana Quartz Monzonite are of three basic types: (1) fine-grained, but generally porphyritic leucocratic granitic rock, (2) altered versions of (1) that are now quartz-muscovite schists, and (3) a moderately coarse-grained muscovite granite and quartz monzonite. The border-zone rocks are defined as those that occur along the margins of the Rana Quartz Monzonite but which are distinctly more leucocratic than the main mass of Rana Quartz Monzonite. The principal difficulty in mapping and interpreting these rocks is that they are gradational with the main mass of foliated Rana Quartz Monzonite. Further, the three types of border-zone rocks tend to have gradational boundaries among themselves. In general, though, types 1 and 2 occur largely in section 32 and in the west half of sec. 33 whereas type 3 occurs mainly on the south side of Cerro Colorado where the border zone is thickest.

Type 1 lithologies are best preserved where the border zone projects out into the country rock as tongues or dikes. A typical example (fig. 40a) consists largely of a fine-grained matrix of quartz, muscovite, plagioclase, and microcline in which ovoid, 8 mm phenocrysts of quartz are embedded. This matrix also contains clots of muscovite, rare octahedra of magnetite, and rare grains of schorl. A thin-section view of a typical sample is shown in figure 41. Note the interlocking allotriomorphic granular texture of the groundmass and the serrated

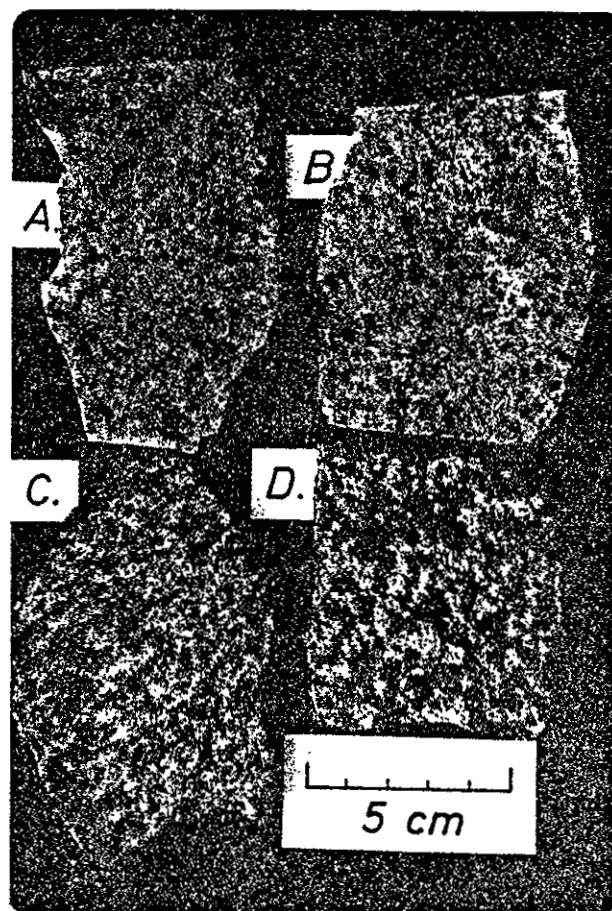


Figure 40. Stained slabs of various Rana Quartz Monzonite.

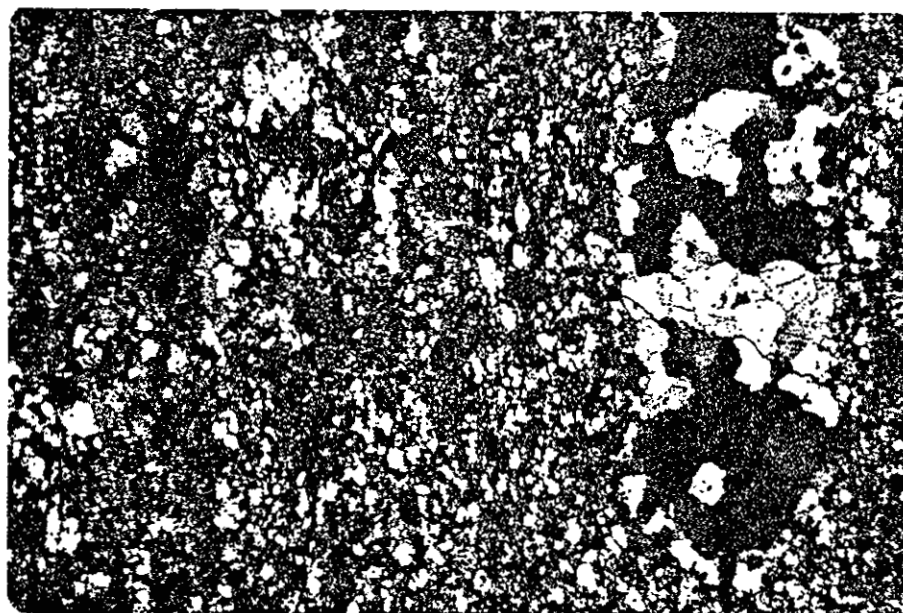
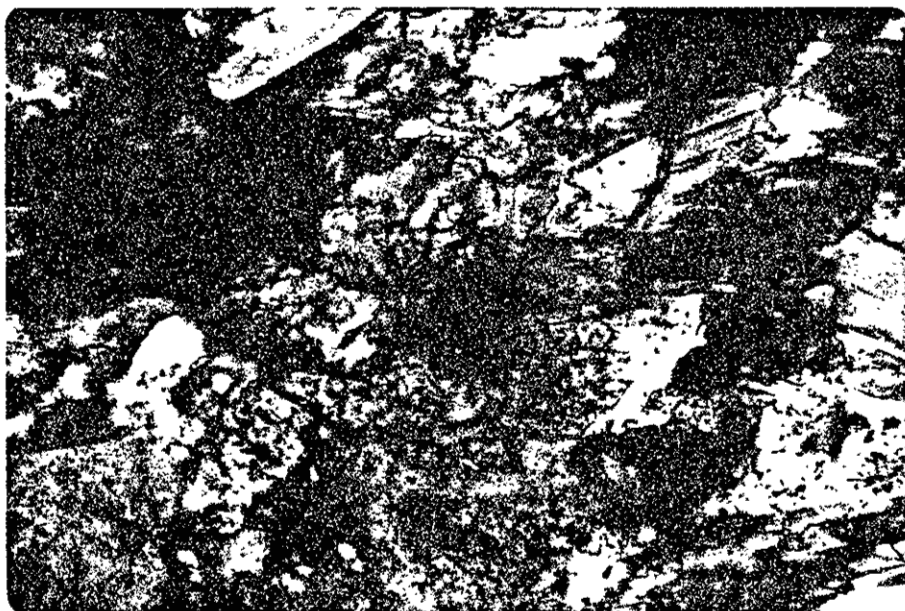


Figure 41. Photomicrograph of Rana Quartz Monzonite from border zone (PL73-267). Notice the oblate polygonated quartz phenocryst.

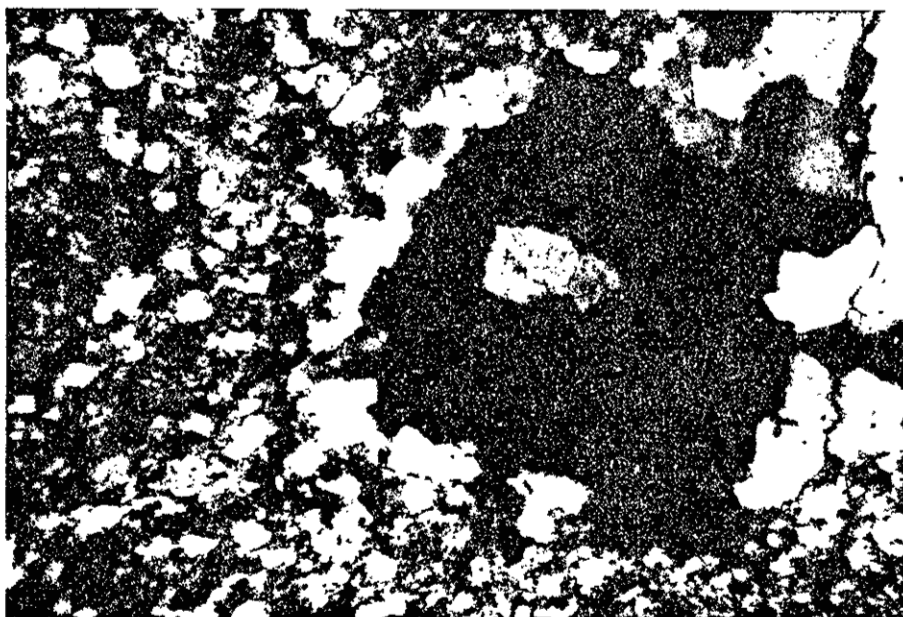
edges of neighboring quartz subgrains within the quartz phenocrysts. Muscovite occurs as pods or clots within the matrix and as individual flakes scattered through it. Accessory minerals are allanite, epidote, zircon, and hematite (after magnetite). It is of particular interest that the allanite occurs as tiny (0.1 mm) cores of epidote grains (fig. 42).

More altered border-zone rocks occur within the border zone itself and range from porphyritic muscovite quartz monzonite to quartz-muscovite schists. A typical sample has oblate rounded quartz grains (<10 mm) and flattened muscovite clots set in a fine-grained matrix of feldspar, muscovite, and quartz. These rocks have a substantial foliation defined by flattening of the quartz phenocrysts and by a subparallel orientation of the muscovite. The quartz grains are clearly relict phenocrysts which typically consist of subgrains that have serrated contacts with one another. They also have light-bluish-gray cores that are rimmed with a thin layer of transparent quartz grains as shown in figure 43. Careful examination of the light-bluish-gray cores shows that there are slight zonal changes in color, and under high magnification the bluish zones are seen to contain a large number of minute rutile needles which are lacking in the clear quartz grains of the rim. This feature is common in the border-zone rocks and also occurs in the main mass of Rana Quartz Monzonite, although the quartz grains there are matched in size by the other minerals. Accessory minerals are epidote, allanite, schorl, biotite, and magnetite. Alteration to hematite has taken place along cleavage planes or around the margins of the grains. As in all Rana rocks, epidote forms thick overgrowths on tiny equant allanite grains.



0.1 mm

Figure 42. Photomicrograph showing allanite core of an epidote grain.
Rana Quartz Monzonite border zone; sample PL73-267.



1 mm

Figure 43. Rounded quartz phenocryst with internal zoning. Rana Quartz
Monzonite border zone, detail of figure 42; PL73-267.

Border-zone rocks of the other major type (type 3) are richer in microcline than those just described. These rocks have an overall grayish-orange-pink color with obvious translucent medium-gray quartz phenocrysts (1 to 3 mm). Less obvious are subhedral microcline phenocrysts (2 to 5 mm) which, along with the quartz grains, are set in a finer grained (<1 mm) matrix of plagioclase, quartz, muscovite, and microcline. Accessory minerals are magnetite-hematite, biotite, garnet, epidote, and zircon. This type of border zone generally is less foliated and somewhat coarser than types 1 and 2, and it also contains myrmekite, a textural feature that is lacking in other border-zone rocks.

The border-zone rocks are rather strongly deformed, and they are characterized by marked differences in grain size and degree of alteration and/or deformation. The alteration and deformation make interpretation of the early magmatic history difficult, but it appears that some of the border zone formed in more than one stage with possible multiple injection of magma. This may account for some of the marked differences in grain size.

Foliated Facies

As previously stated, the border zone grades into the foliated facies. The contact between the two units was placed where biotite began to appear as readily visible, discrete clots in the rock. This generally coincided with the coarsening of the groundmass, i.e. with the loss of a porphyritic texture. There are different degrees of foliation within the foliated phase, ranging from moderately foliated biotite quartz monzonite to gneissic biotite quartz monzonite. The general tendency is for the deformation to increase in intensity from

the northwest to the southeast part of the body, with the least deformation occurring near the unfoliated facies (pl. I) and the greatest deformation occurring near the contact with the Peñasco Quartz Monzonite about 1.25 mi north-northwest of Trampas.

A moderately foliated rock commonly shows a crude but distinctly planar alignment of biotite clots and some granulation of feldspars, especially plagioclase. There also is some orientation of oblate aggregates of quartz grains which are flattened as well as slightly elongated. A typical example of the fabric of this lithology is shown in figure 44. It is an equigranular network of aggregates of quartz grains (<12 mm), granulose aggregates of plagioclase (5 to 9 mm), and anhedral, broken-appearing grains of microcline (<7 mm). Biotite and magnetite commonly occur together in clots that tend to form groups over 3 to 4 cm areas. Quartz shows a very marked undulatory extinction. The microcline occurs as fairly large grains which generally are associated with aggregates of smaller grains (0.4 mm). The microcline commonly contains "flame" and/or "film" microperthite and inclusions or patches of albitic plagioclase and quartz. M-twinning is ubiquitous in the microcline and some larger grains also have a single Carlsbad twin plane. Plagioclase occurs as altered aggregates of 0.5 to 0.1 mm grains, with composition An_{27} to An_{22} . Little primary zoning is apparent in thin section, and all of the plagioclase grains are dusted with epidote and muscovite. The only unaltered plagioclase occurs in perthite and as rims on altered grains that are adjacent to microcline. Myrmekite occurs consistently as wartlike projections into microcline, where it is in contact with adjacent plagioclase grains. Accessory muscovite, magnetite-hematite, sphene, allanite, epidote,

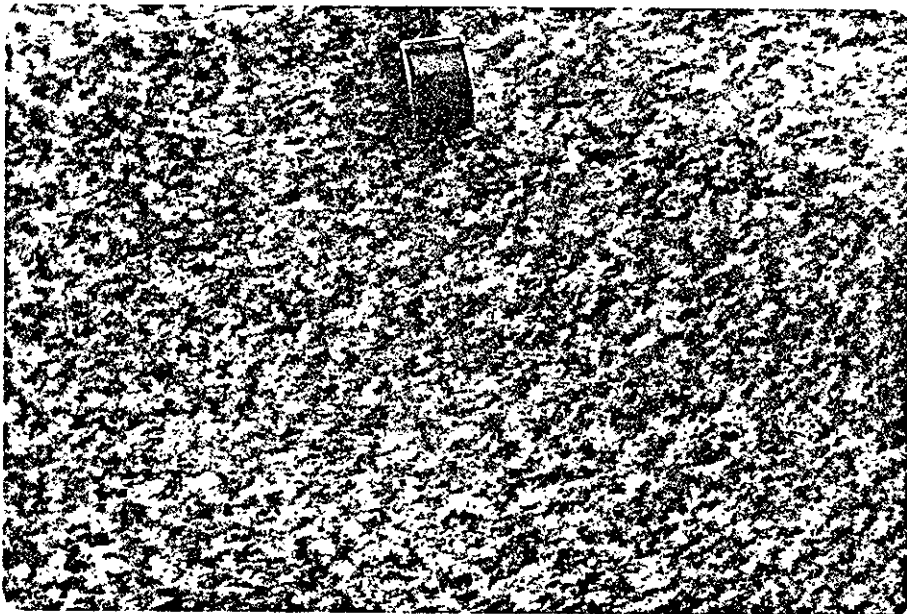


Figure 44. Typical example of foliated Rana Quartz Monzonite. 0.75 mi south of Cerro de la Cruz.

zircon, and apatite are associated with biotite (see Appendix I for a detailed description of the accessory minerals--sample PL72-193).

The most foliated types of Rana Quartz Monzonite are gneissic biotite quartz monzonites which have a strong foliation expressed by preferred orientation of undulatory biotite layers which are separated by irregular lenses and layers of granulose quartz and feldspar. In thin section, the rock has a foliated and seriate allotriomorphic granular texture, with microcline and quartz being the largest in grain size and plagioclase being distinctly smaller and more granulose or polygonized. The microcline occurs as anhedral grains (<5 mm) showing crosshatch twinning and rarely a crude Carlsbad twinning. Some of the crosshatch twinning is clearly deformed. The quartz occurs as allotriomorphic grains shaped like pieces of jigsaw puzzle. These grains have a cracked appearance, and their largest dimension (<1 mm) commonly is parallel to the foliation plane. The plagioclase grains (<0.5 mm) are anhedral, show uniform normal continuous zoning from An_{30} to An_{25} , and commonly are altered. Biotite forms pods and trains of anastomosing strongly oriented flakes (1 mm) most of which have a fresh appearance, whereas others appear shredded. Accessory minerals associated with biotite are muscovite as crisp, clear flakes replacing biotite, magnetite-hematite grains as irregular octahedra, sphene as anhedral 0.5 mm granules associated with the magnetite, epidote as thick rims on tiny allanite grains, apatite as clear, anhedral stubby grains, and zircon as euhedral to anhedral prisms with tube-shaped fluid inclusions. Muscovite and epidote also occur as fine-grained alteration products of plagioclase.

Unfoliated Phase

The unfoliated phase has a very gradational contact with the foliated phase of the Rana Quartz Monzonite. An average sample of the unfoliated phase has a typical granitic texture with interlocking grains of rounded quartz (<10 mm), tabular to rounded grains of light-gray plagioclase (<6 mm), and anhedral grains of pink to light-gray microcline (<9 mm). Aggregates of biotite and magnetite-hematite (<1 to 7 mm) are scattered throughout this rock. Quartz occurs as aggregates of 1 to 2 mm subgrains showing some undulatory extinction. In some samples the quartz grains have cores of light-bluish-gray color similar to those of the border-zone rocks. The largest single grains are anhedral microcline (<7 mm) with both Carlsbad and M-twinning. These grains commonly are perthitic and contain round quartz blebs (or pods) and patchy areas of albite as well as rounded albite inclusions. Blebs of albite between adjacent grains of microcline are very common. Plagioclase grains are subhedral (<7 mm) but commonly project into the distinctly anhedral and interstitial microcline. They show slightly undulatory normal zoning from An_{33} to An_{15} and in many places, particularly adjacent to microcline, they have discrete unaltered rims of albite (An_8 to An_4). The other parts of the plagioclase grains are commonly altered to muscovite and fine-grained epidote, especially in their more calcic cores. Large plates of green-brown biotite (<2 mm) and biotite with magnetite (+ hematite) occupy areas that appear interstitial in the fabric of the rock and are adjacent to or included in quartz grains. Sphene, allanite, zircon, apatite, and epidote are associated with the biotite and magnetite.

Muscovite occurs either as fine-grained stubby flakes (<0.5 mm) in plagioclase or as large (2 mm) fresh flakes transecting or infiltrating

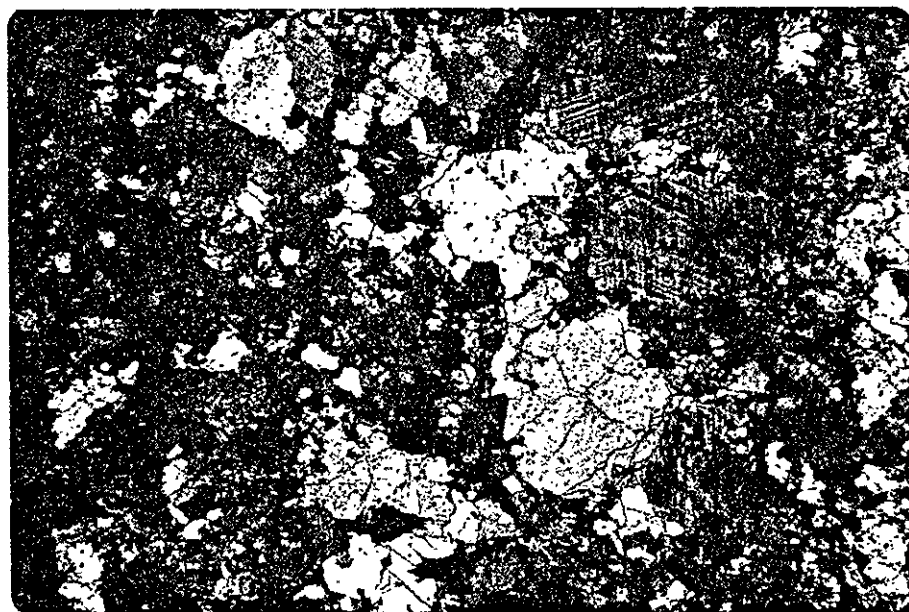
into biotite. The magnetite-hematite grains (<3 mm) are subhedral to anhedral and nearly equant. They are mostly magnetite, and the hematite occurs along margins or cleavage fractures as spindly branches projecting into the magnetite interiors of the grains. It also occurs as irregular trails of discrete blebs within the interiors of magnetite grains. Sphene commonly rims the magnetite grains and also forms tiny granules throughout the rock. Epidote occurs as individual grains associated with biotite, as thick rims (0.4 mm) around tiny allanite grains, and as small granules (0.05 mm) in altered plagioclase. The allanite is rimmed by epidote or is otherwise associated with it, and occurs as zoned equant to slightly elongate crystals (0.3 mm). Apatite is usually found with biotite, either included in it or sandwiched between it and another mineral. The crystals of apatite are squatty, sausage-shaped single grains (0.5 mm). Zircon grains have a similar habit but they tend to be more elongate and more idiomorphic, characteristically containing one or more tubelike inclusions. A minor amount of chlorite occurs as an alteration product of biotite. Myrmekite, with its cauliflower or wartlike intrusion into microcline, is common where plagioclase grains are in contact with microcline grains. In one instance myrmekite appeared to transect albite lamellae in microcline. Figure 45 shows typical petrographic features of the Rana rocks.

In thin section the rock gives the impression of being a framework of fresh quartz and microcline that is collapsed around the altered plagioclase grains. There is, however, only the slightest hint of foliation. The mutually perpendicular closely spaced fractures, visible in polished slabs, and the slight granulation seen in thin section indicate that the rock has undergone some deformation.



(a)

5 mm



(b)

5 mm

Figure 45. Photomicrographs of Rana Quartz Monzonite. A. Unfoliated facies (PL71-14); B. Foliated facies (PL72-190).

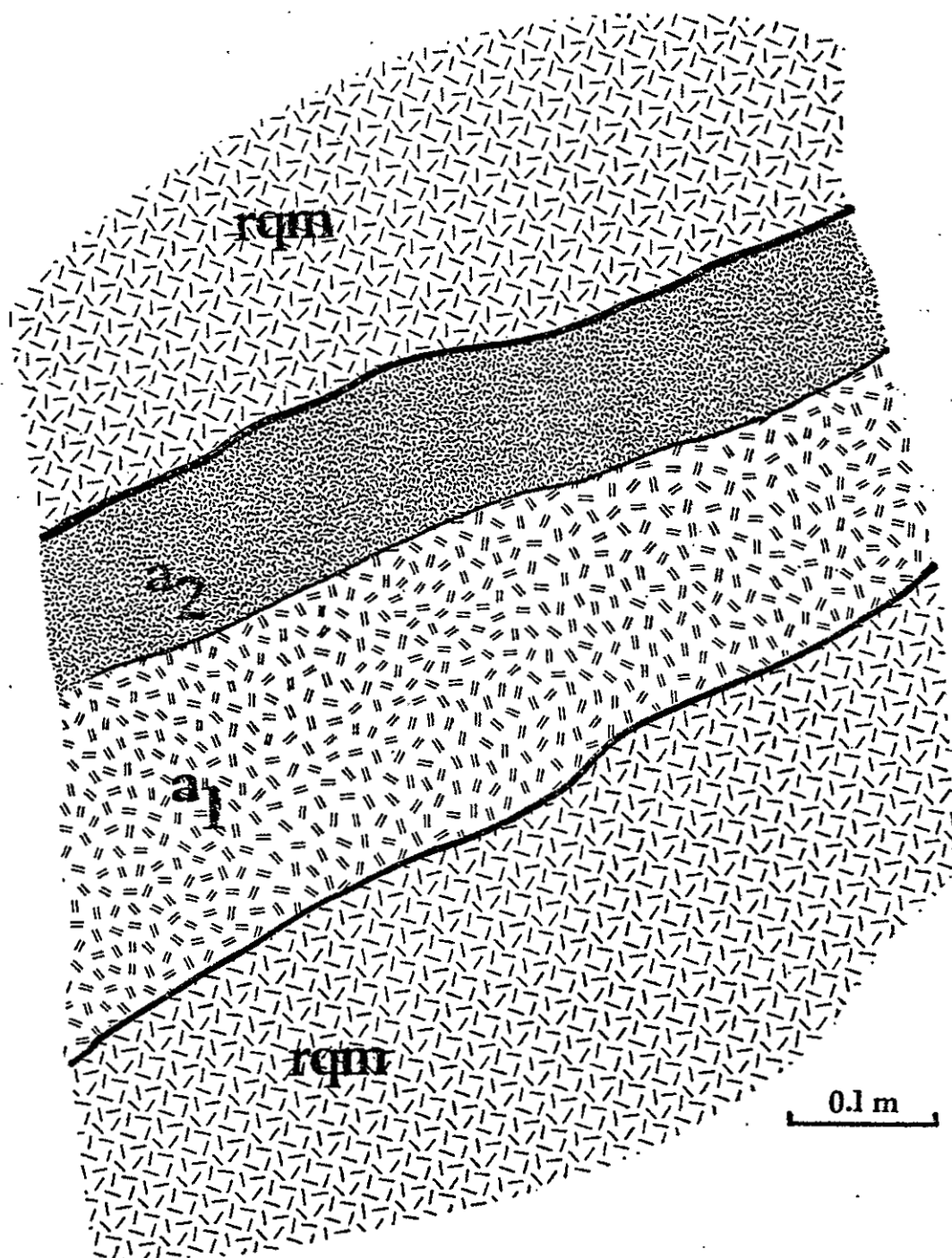


Figure 46. Sketch of Rana Quartz Monzonite aplite dike with coarse and fine facies. 0.5 mi southwest of Cerro del Abrevadero.

Aplites

Aplites in the Rana Quartz Monzonite are common and occur as irregular dikes 3 to 30 cm thick. They are ordinarily white or pink and in some places contain small amounts of biotite and/or are somewhat porphyritic. They are older than pegmatites that occur in the Rana Quartz Monzonite, as demonstrated by consistent crosscutting relationships. Furthermore, aplites associated with the Rana Quartz Monzonite itself are not found in any surrounding rocks.

A typical pink or pale-red aplite has a fine-grained sugary texture (average grain size 0.5 to 0.6 mm) that is subequigranular. The microcline is slightly larger in average grain size than the quartz or plagioclase. The quartz has a lobate, partly inequigranular texture and shows undulatory extinction. Plagioclase is primarily intergranular and is dusted with muscovite, epidote, and possibly kaolinite(?). Muscovite also is scattered throughout the rock as small interstitial grains. Some dikes contain dendritic schorl and most have minor hematite and granular epidote.

One occurrence of particular petrogenetic interest is a porphyritic biotite aplite dike which contains two distinct rock types. One is a coarser, more porphyritic and biotite-rich aplite, the other finer grained with less biotite and a more nearly equigranular texture. These two types of rock each occupy about half of the dike at one point (fig. 46). The finer grained rock is more abundant. The general character and mineralogy of these two rock types suggest that they are cogenetic fractions of a late-stage differentiate of the Rana Quartz Monzonite and hence might provide opportunity to trace the chemical

and mineralogical directions of fractionation. Textures of the two rocks are compared in figure 47. Complete descriptions of both portions are given in Appendix I, modes in Appendix II, and chemical analyses in Appendix III. The modal and chemical data are discussed farther on, but here it is worth noting some of the salient textural features of the two rock types. First, the coarse facies shows a moderate foliation (N. 50° E.) defined by a slight flattening of biotite clots and by an alignment of relict phenocrysts (fig. 47). The fine-grained portion may also be foliated but if it is, it is very much less visible in hand specimen. Second, in the coarse facies, textural features such as alteration of plagioclase, albite overgrowths on plagioclase, and the mafic associations of biotite, zircon, and other accessory minerals occur in a manner analogous to that of the host Rana Quartz Monzonite. Plagioclase, quartz, microcline, and biotite appear to have coexisted with a silicate liquid phase at an early point in the rock's crystallization. Finally, in the finer facies, textural relations are similar to those of the coarser facies except for the marked decrease in grain size. Although the proportions of phenocrysts are different, plagioclase, quartz, microcline, and possibly biotite again appear to have coexisted with a silicate liquid phase early in the crystallization sequence. Some minor quartz veining appears to have occurred after crystallization was essentially complete.

Modal Composition

The modal compositions of Rana Quartz Monzonite rocks are given in Appendix II and plotted in figures 48 through 51. The bulk of the Rana Quartz Monzonite samples cluster around the arbitrary dividing line

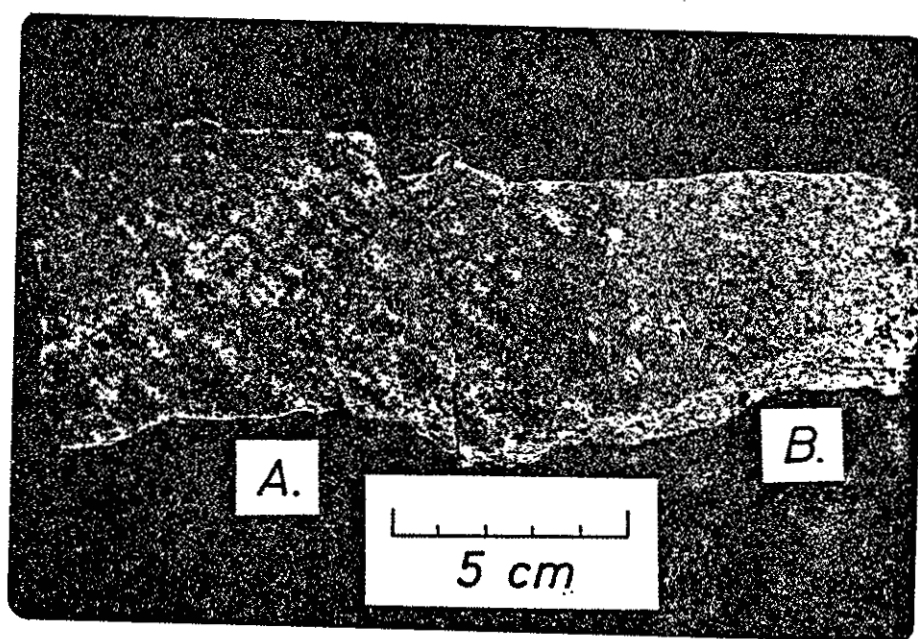


Figure 47. Stained slab showing the two facies (A and B) of the dike in figure 46. K-feldspar is stained yellow.

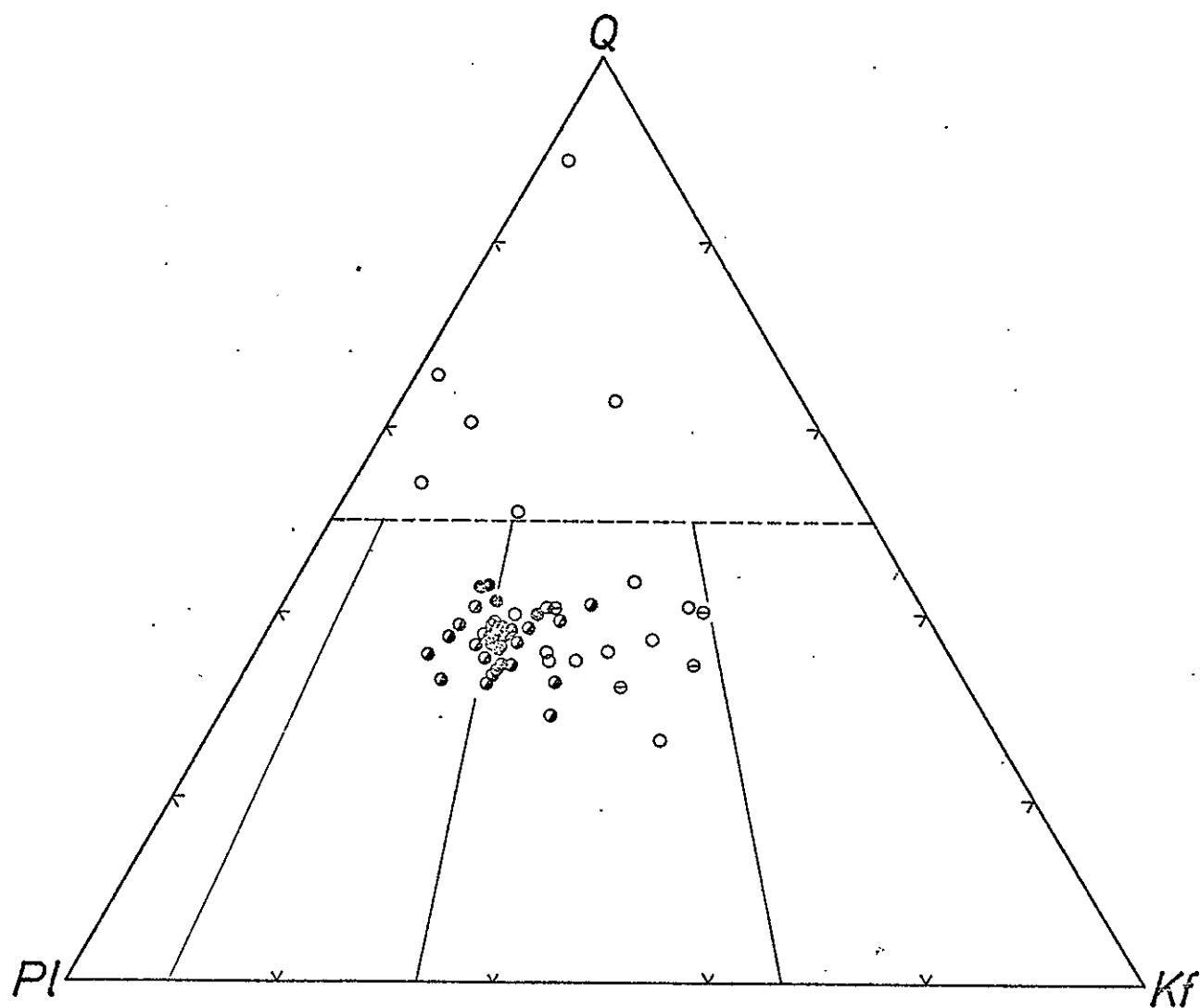


Figure 48. Plot of modal data from the Rana Quartz Monzonite. Solid circles are unfoliated facies, half solid circles are foliated facies, open circles are border zone, bar circles are aplites.

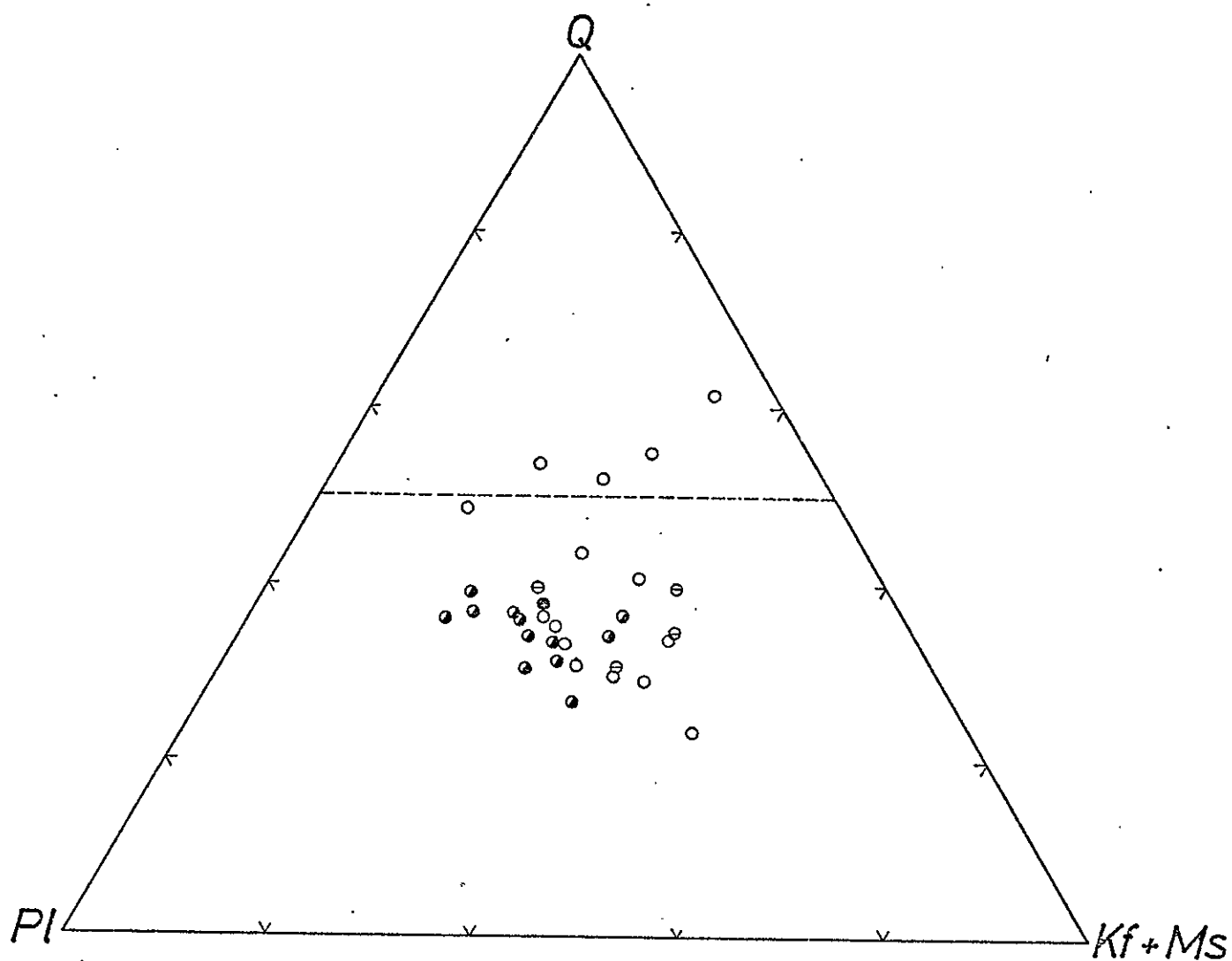


Figure 49. Plot of modal data from the Rana Quartz Monzonite. Symbols same as figure 48.

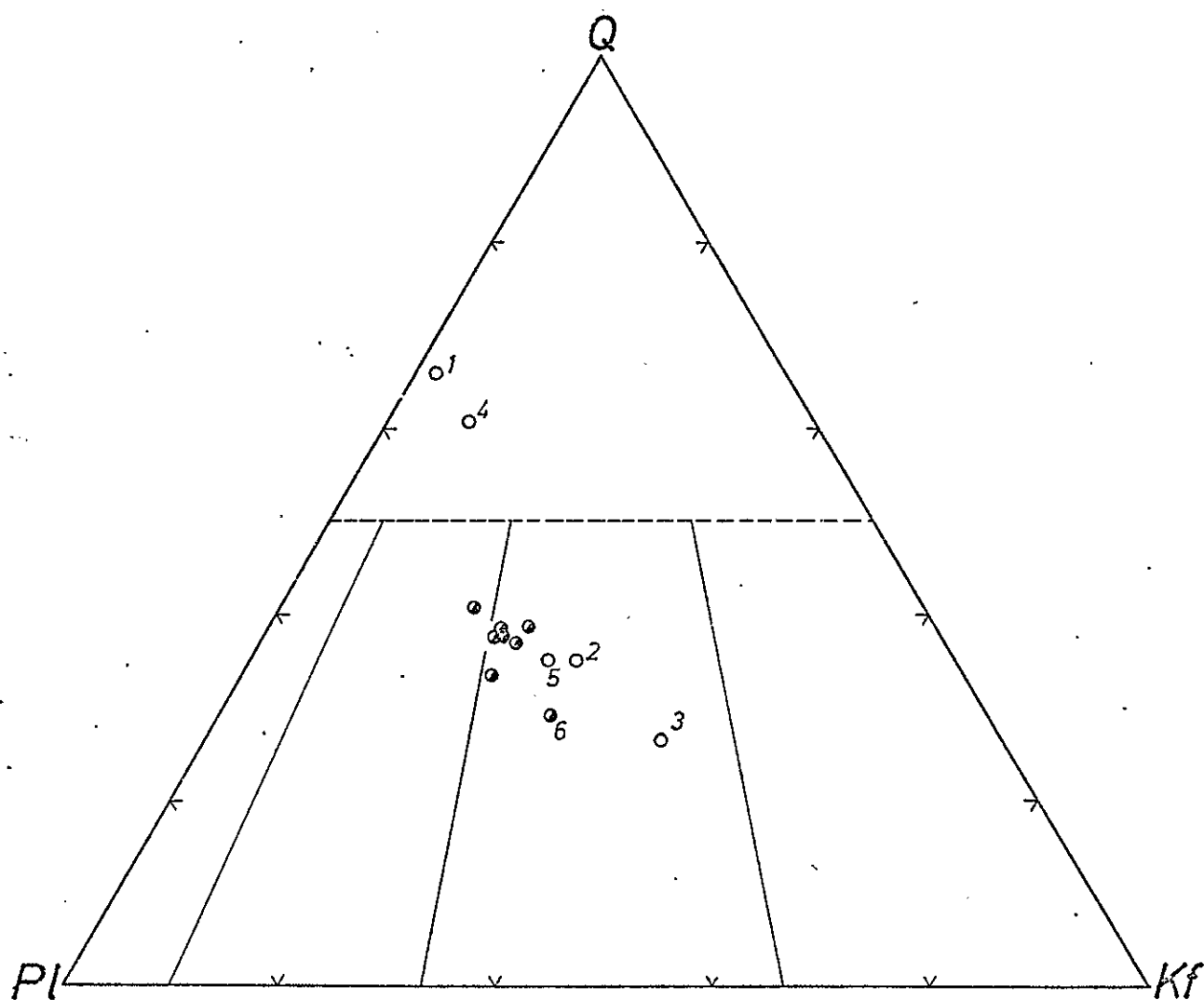


Figure 50. Plot of modal data from the border zone of the Rana Quartz Monzonite. Numbers refer to proximity to contact in a sample traverse (see fig. 52). Symbols as in figure 48.

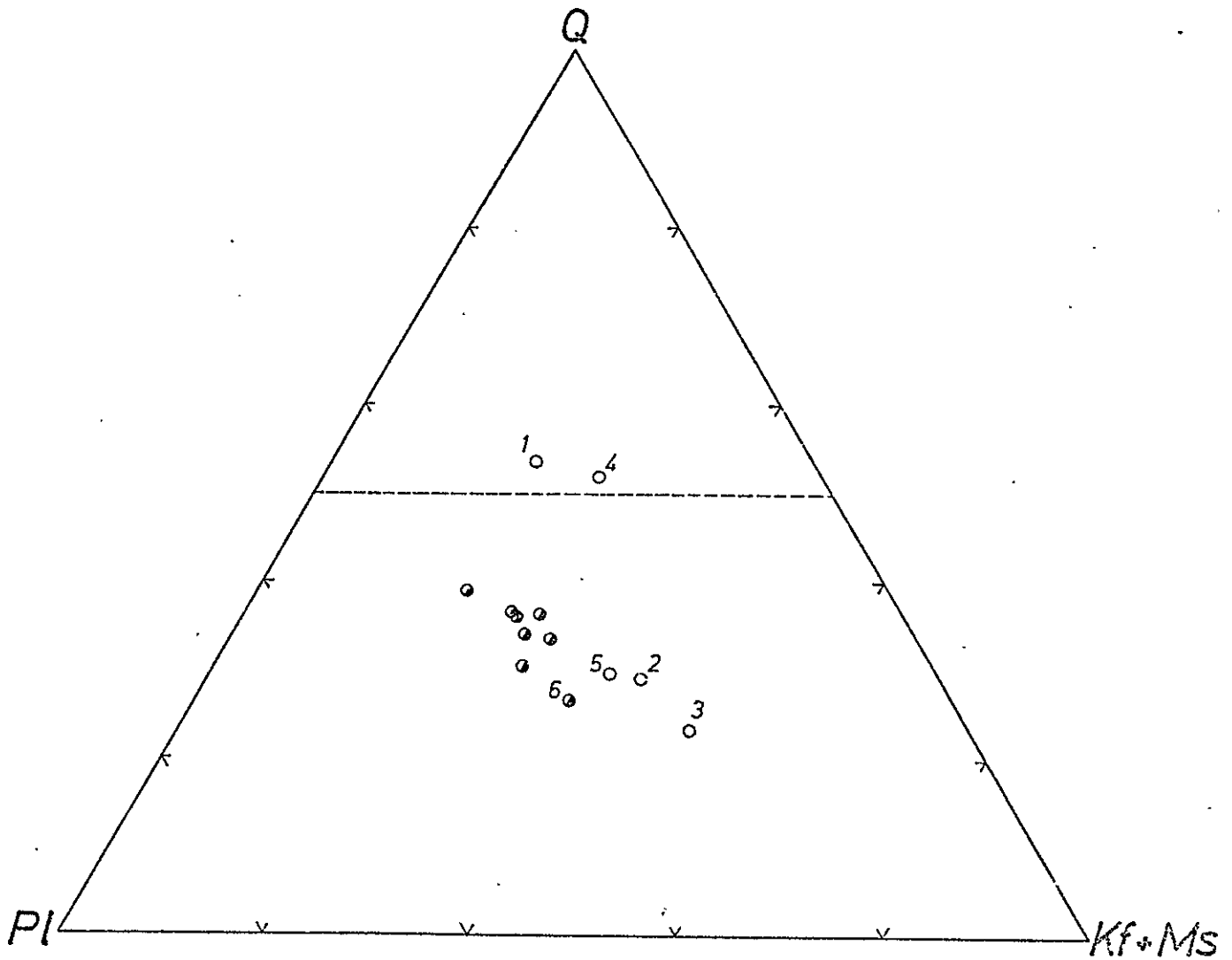


Figure 51. Plot of modal data from the border zone of the Rana Quartz Monzonite. Numbers refer to proximity to contact in a sample traverse. (see fig. 52). Symbols as in figure 48.

between granodiorite and quartz monzonite. These data suggest that while there may be some local compositional changes within the main body, it is largely of a rather constant mineralogical composition. The border-zone rocks and the aplite dikes, however, show considerable variations in mode as plotted on the quartz-plagioclase-K-feldspar triangular diagram. The border-zone rocks especially show a wide variation in quartz-feldspar ratios, a feature that is due at least in part to alteration of some of the border-zone rocks to quartz-muscovite schist. With this in mind, quartz, plagioclase, and K-feldspar *plus* muscovite were plotted in figures 49 and 51. This plot reveals that for the main foliated facies there is a slight suggestion that muscovite may be a significant alteration product in some samples causing a slight shift away from the main cluster. Some of the border-zone rocks show a tendency toward higher quartz and muscovite, while the others tend toward high K-feldspar and muscovite. These tendencies suggest that two kinds of processes may have occurred in the border-zone rocks: (1) an early process, possibly magmatic differentiation, resulting in enrichment of some rocks in K-feldspar and others in plagioclase + quartz; and (2) a later alteration process giving rise to much of the muscovite in these rocks, particularly in the quartz-muscovite schists.

To test this idea, a sample traverse was made across the border zone in sec. 32, where a significant amount of alteration can be observed. The cross section along which the traverse was made is shown in figure 52, along with the plotted modal percentages of biotite and muscovite. These data demonstrate the existence of a marginal, mineralogically distinct border zone followed by a gradational change inward to typical foliated Rana Quartz Monzonite. Triangular plots of just

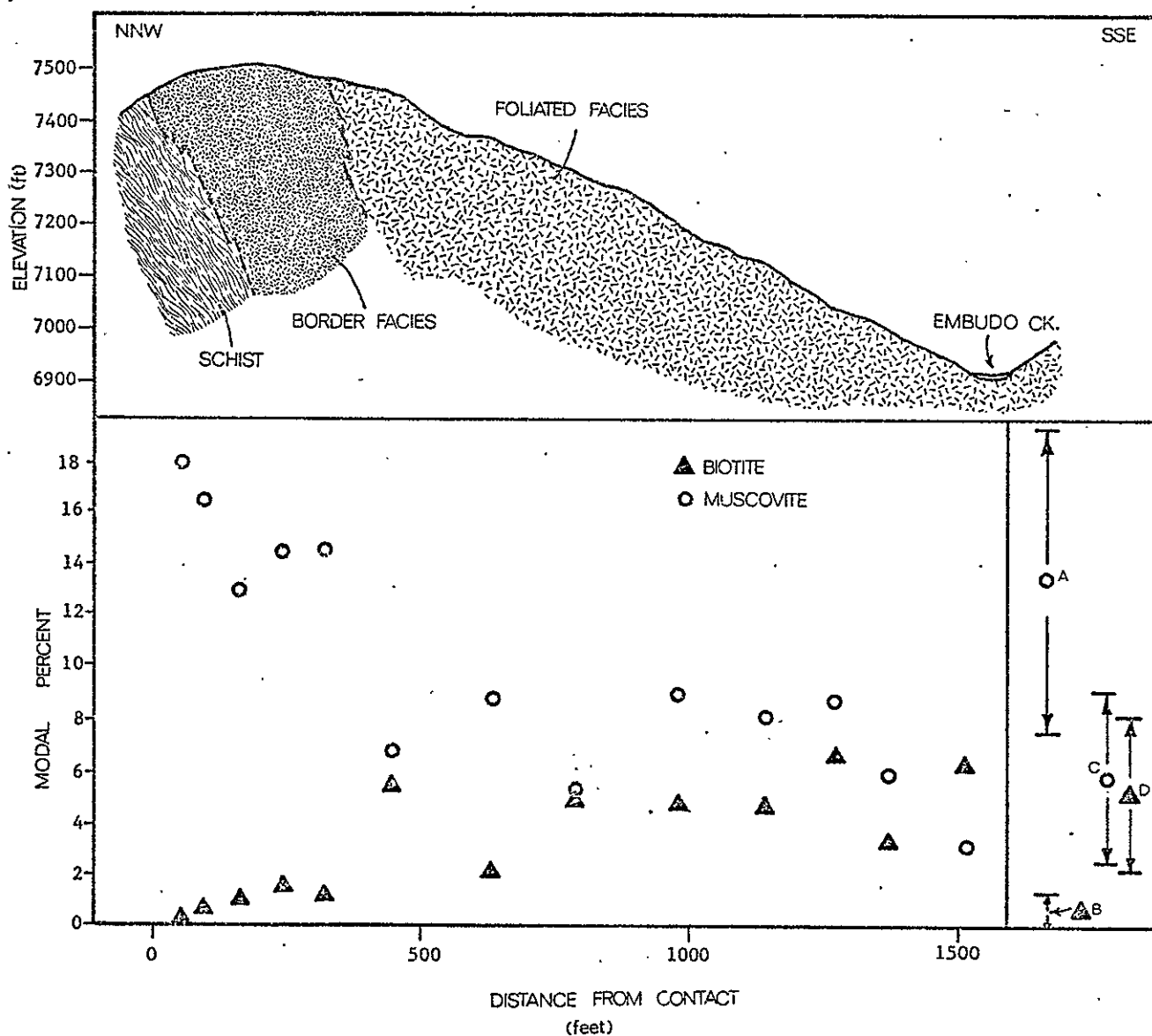


Figure 52. Plot of modes for biotite and muscovite from a sample traverse across the Rana Quartz Monzonite. The traverse is located 0.5 mi southwest of Cerro Alto.

the traverse samples (figs. 50 and 51) show that the two "trends" or rock types are not clearly separated in space. This points up the general complexity of the border zone and suggests that the alteration may have been superimposed on what was already a structurally and mineralogically complex set of rock types. One possible explanation is that the initial pulse of magma, which differentiated as the result of fractionation of quartz and plagioclase, gave rise to a series of injections and reinjections of liquids of different compositions which were quickly cooled and crystallized. Alteration, which took place preferentially along shear zones, may also have preferentially altered the more plagioclase-rich rocks. It is uncertain exactly why the border-zone rocks are so leucocratic or to what extent their compositions were changed by the quartz-muscovite alteration. These general problems, as well as the possible details of the differentiation and alteration processes are addressed in the light of petrochemical data in a later section.

In general, the modal compositions of the aplites show that they are more enriched in K-feldspar than the average Rana Quartz Monzonite. The percentage of quartz varies from one aplitite to another, but consideration of the fine and coarse aplitite pair previously described suggests that there may have been a slight tendency toward enrichment in quartz in the finer grained portion of the dike (fig. 48). Thus there is an overall trend toward enrichment in K-feldspar, but this is accompanied by first a slight depletion and then a slight increase in quartz. A possible explanation of this is slight fractionation caused by extraction of plagioclase and quartz from residual liquids. A resulting increase in K-feldspar crystallization may then account for

the slight increase in quartz in the most fractionated aplites. This interpretation is consistent with the texture and implied crystallization sequence in the Rana Quartz Monzonite itself, and with textures in the coarser grained aplites. It is a question that is tested in terms of chemical data in a later section.

Structural and Textural Features

The bulk of the Rana Quartz Monzonite is featured by a distinct foliation defined by orientation of biotite clots and by flattening and/or granulation of quartz and feldspar. This foliation is largely missing in the unfoliated facies, but fracture patterns and foliation in some aplites within the unfoliated facies indicate that it existed at the time of the main deformation but for some reason it escaped strong penetrative deformation. The main foliation, which apparently corresponds to F_2 , has itself been folded (fig. 53a) and in some areas there is a distinct lineation that appears to represent the intersection of two planar features. Both of these features can be attributed to F_3 . Local closely spaced fractures may also have been caused by F_3 . The last major deformation in the area, F_4 , is evidenced in the Rana Quartz Monzonite by numerous quasi-ductile shear zones that are vertical and trend $N. 28^{\circ}-61^{\circ} E.$ (fig. 53b). Joint sets commonly trend north to $N. 20^{\circ} W.$ and have opposing dips of 90° to 20° , but odd orientations that do not seem to fit any obvious pattern also occur. Lineaments that appear clearly on air photos are shown on plates I and II. Their orientation is typically either northwest (dominant) or northeast. Their origin is uncertain, but they may be related either to the F_4 shear zones or to the joint structures.

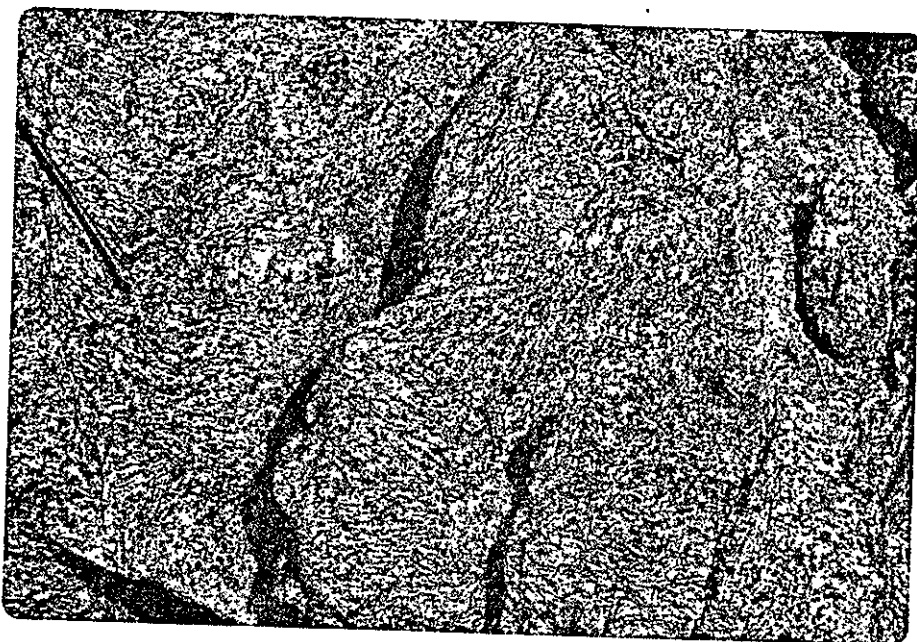


Figure 53a. Folding of foliation in Rana Quartz Monzonite.

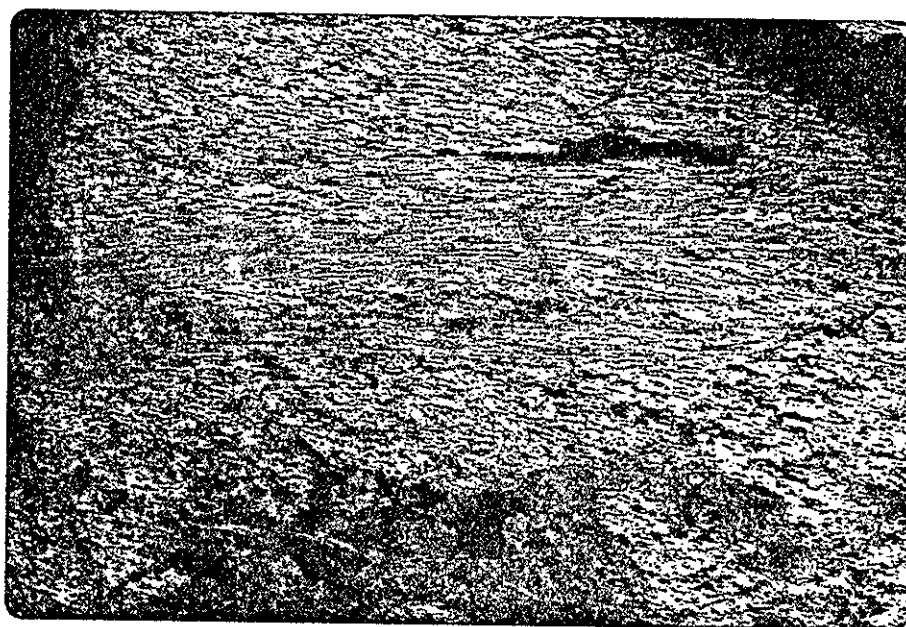


Figure 53b. Semiductile shear zone in Rana Quartz Monzonite.

A general trend in the Rana Quartz Monzonite is an increase in the severity of deformation from northwest to southeast in the study area. In the south and southeasternmost exposures a lineation becomes the dominant structure. Any foliation present in these exposures has either the typical northeast to east-northeast orientation or it has a north-northwest to northwest orientation, the latter probably being caused by F_3 . The lineation typically has a plunge and azimuth that one would expect from the intersection of S_2 and S_3 (i.e. L_3), but where S_3 is not sufficiently well developed to form a distinct planar feature and yet thoroughly disrupts S_2 , a lineation is produced but no well-defined foliation remains.

Metamorphism and Alteration

The Rana Quartz Monzonite provides an opportunity to observe the progressive deformation and possibly the progressive metamorphism of a granitic rock body. The central questions that arose during field and petrographic examination were: Was the increase in deformation accompanied by an increase in temperature or average pressure to the southeast, or was differential stress alone greater there than it was to the northwest? If there was a thermal gradient involved, were there mineralogic adjustments to the gradients? Even if there were no thermal gradients, what were the major textural adjustments to the increased deformation and how did these affect "late-stage" features?

The gross textural features are best shown by the series of stained slabs in figure 54. Note that with increased deformation there is a general reduction in grain size, with quartz and microcline being the most resistant to this grain-size reduction. Biotite clots first are

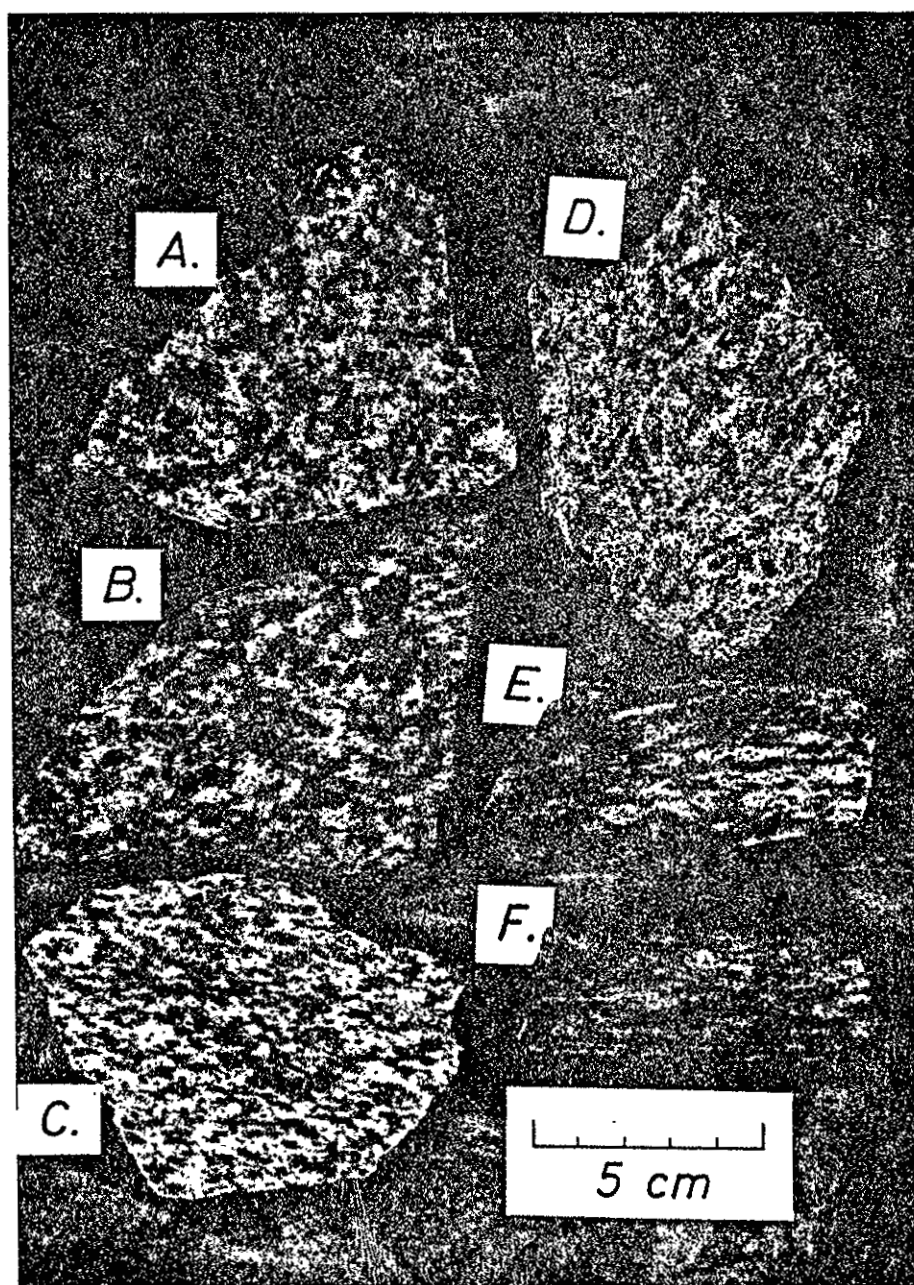
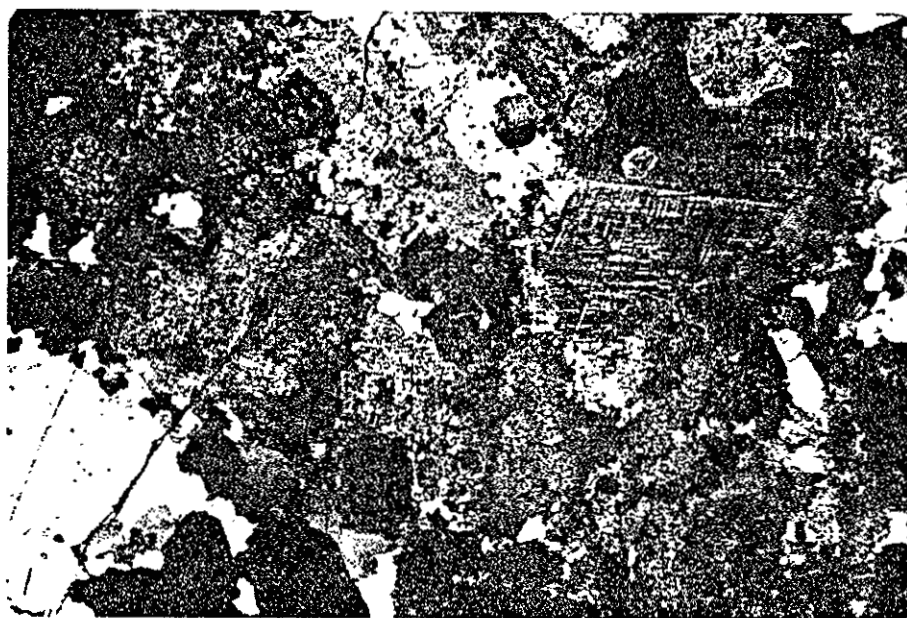
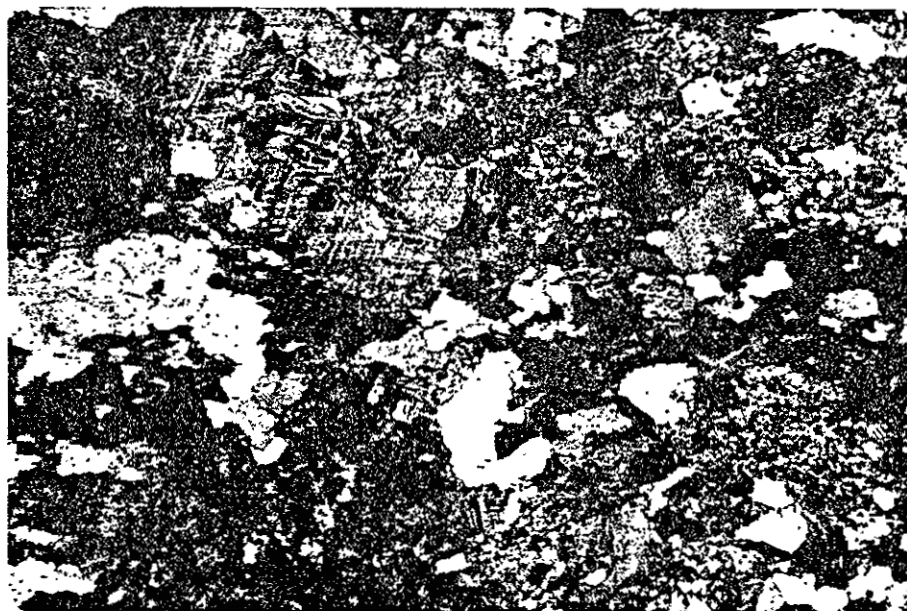


Figure 54. A series of stained slabs (A through F) showing increasing deformation from northwest to southeast in the Rana Quartz Monzonite. Microcline is stained yellow. A. Unfoliated facies, PL71-14; B. Foliated facies, PL72-193; C. Foliated facies, PL72-174; D. Foliated facies, PL72-224; E. Foliated facies, PL72-73; F. Foliated facies, PL72-74.

increasingly flattened and oriented in the foliation plane and then become increasingly smaller in grain size and more recrystallized until they occur in the wispy planes and as isolated, peppery flakes. Plagioclase in particular becomes very fine grained and granulose with the increased deformation. A more detailed view is afforded by the thin sections shown in figure 55. If we assume that all the samples began with gross textures similar to the unfoliated facies (fig. 55a), we see that the two least foliated samples of the foliated facies (figs. 55b, c) show polygonized plagioclase that is clearly the result of recrystallization of the original undisturbed plagioclase grains. They are characteristically altered throughout by very fine muscovite and epidote. This is in contrast with the fairly coarse muscovite and epidote that are concentrated in the more anorthite-rich cores of the unpolygonized grains, suggesting that the alteration may already have occurred at the time of deformation and that the alteration products themselves have been recrystallized and dispersed. Still more deformed rocks (fig. 55d) show a slight increase in plagioclase grain size but still retain the polygonal grain shape. They are notably less altered, however, with alteration that is present being patchy or in some instances partly controlled by orientation of albite twin lamellae. These plagioclase grains also have a crackled appearance that is shown especially well in figure 55d. The most deformed rocks (figs. 55e, f) again show a smaller grain size, possibly the result of greater deformation without appropriate conditions for recrystallization to increased grain size. Alteration in these samples, however, is patchy and less extensive than in some of the slightly less deformed rocks.



(a)



(b)

5 mm

Figure 55. Photomicrographs of samples A-F shown in figure 54. Notice decreasing grain size, increasing polygonation and increasing dispersion of biotite going from A to F.



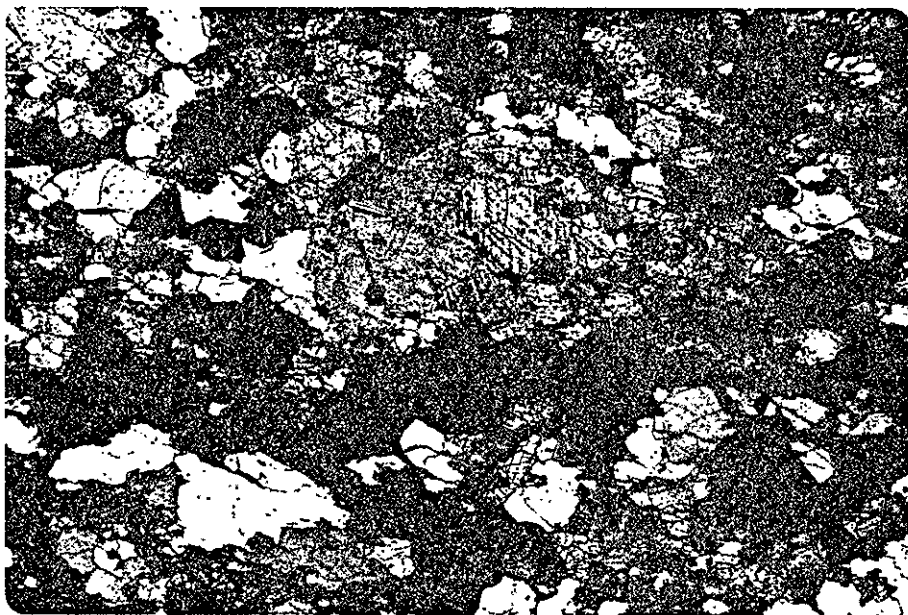
(c)



(d)

5 mm

Figure 55.



(e)



(f)

5 mm

Figure 55.

Some of the larger grains of recrystallized plagioclase have a slight normal continuous zoning, but most appear to be unzoned.

Quartz shows some undulatory extinction in all samples but it is more pronounced in the samples that show light to moderate foliation. The two most foliated samples have considerably less undulatory extinction than the other samples. There is, however, a general tendency for the size of quartz-grain aggregates to decrease with increasing deformation. Yet the size of the subgrains themselves is only slightly larger in undeformed samples than it is in the most deformed ones. Further, in rocks where deformation is great enough that biotite is significantly dispersed, the quartz becomes noticeably clearer than in less deformed samples.

Microcline is apparently unaffected in the undeformed rocks but rapidly shows increased polygonization around the margins of grains with increasing deformation. In spite of this, the largest single grains in any sample are invariably microclines that appear to have withstood the deformation except for granulation and rounding off of their edges and corners. The amount of microcline that has not been polygonized decreases with increasing deformation. Certain textural features associated with microcline persist or are even enhanced with deformation. For example, perthitic lamellae are commonly more obvious in microcline subgrains than in intact crystals. Also myrmekite generally is finer grained in the more deformed rocks, but it is not obvious that it has actually withstood deformation, because it may have formed after or during the waning stages of deformation. Albitic rims on recrystallized grains of plagioclase that abut against microcline also are common in the more deformed rocks, as well as in those with no foliation.

This suggests that the deformation that resulted in polygonization must have occurred at temperatures high enough to give rise to the rims of albite by exsolution from K-feldspars at lower temperatures. It is even possible that higher temperatures which would have increased the albite content of K-feldspar were reached *after* the main deformation. Subsequent cooling could have then resulted in the albite rims. In any case, the textures seem to preclude the interpretation of the rims as relicts from primary cooling and late-stage crystallization of the original quartz monzonite.

As previously stated, biotite becomes increasingly shredded, recrystallized, and redistributed with increasing deformation, the grain sizes reduced from about 3.0 to 1.0 mm or less. Some muscovite flakes appear to replace biotite, and others occur as large semipoikilitic plates which replace plagioclase grains. These muscovite grains appear less deformed than the biotite and in some places actually transect the biotite foliation. This raises the possibility that muscovite alteration of biotite and plagioclase may have postdated deformation or perhaps may have occurred during the waning stages of deformation. This is at variance with the notion already suggested that alteration of plagioclase to coarse-grained muscovite was disrupted by polygonization of the plagioclase. Instead, recrystallization of the plagioclase may have destroyed zoning so that the cores of the plagioclase were not particularly susceptible to alteration, hence the even- and fine-grained nature of the muscovite alteration in the moderately deformed rocks. Still another possibility is that alteration, particularly of plagioclase, took place at more than one time, i.e. before and after

deformation. This is not parsimonious, however, and further evidence is needed to support the idea.

The assemblage of minerals associated with the biotite is remarkable in that many textural features in the undeformed rocks persist in even the most deformed rocks. For example, sphene commonly rims opaque grains, epidote is found as thick rims on tiny brownish allanite crystals, and apatite occurs as cigar-shaped rounded prisms in both the deformed and undeformed rocks. Also hematite and magnetite are commonly found intergrown (fig. 56), regardless of the degree of deformation. One conclusion that might be drawn from this observation is that the phase assemblage associated with biotite was stable through the deformation process and that granulation was not strong enough significantly to disrupt the details of the textures. Another possibility is that some of these textural features may represent reactions that have occurred after deformation as metamorphic reactions. Evidence for or against either of these ideas in part relates to later magmatic events and the reactions involved, as discussed in a later section.

Megascopic alteration of the Rana Quartz Monzonite probably occurred in several episodes, but the main type is a distinct reddening of the feldspars which in the most severely altered areas is accompanied by irregular epidote veining. A typical sample of epidote-veined material is shown in figure 57. It is noteworthy that the epidote veining is not deformed or foliated, and cuts a pegmatite in the foliated Rana Quartz Monzonite. These observations indicate that the epidote alteration is younger than the pegmatites and the youngest penetrative deformational event. In thin section the reddening associated with the epidote veining is seen to correlate with an increased alteration



0.5 mm

Figure 56. Photomicrograph of hematite altering and/or exsolving from magnetite. Rana Quartz Monzonite, sample PL71-14b.

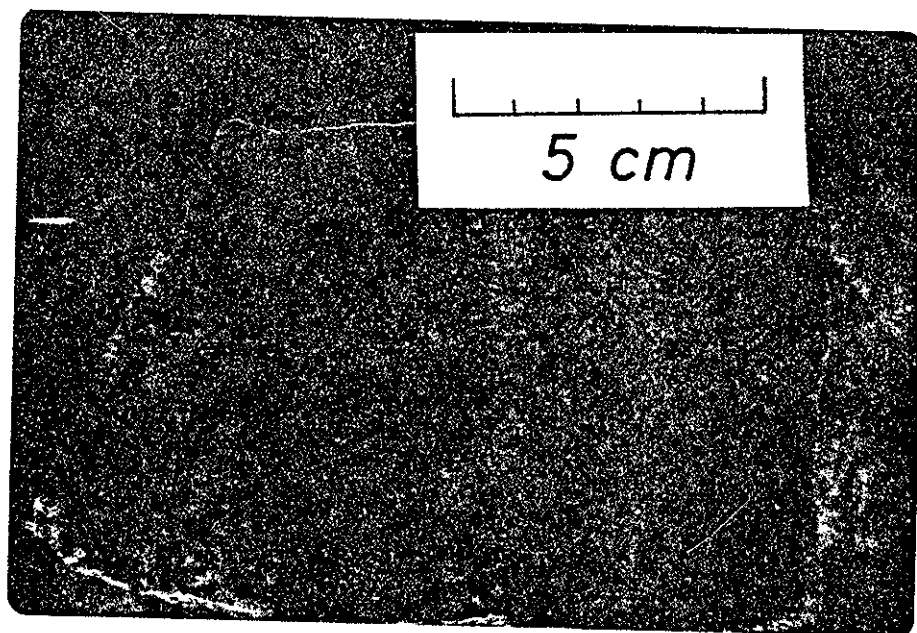


Figure 57. Stained slab showing epidote veining of Rana Quartz Monzonite.

or clouding of the feldspars, especially plagioclase, by mostly very fine-grained epidote and muscovite. This reddening of plagioclase also is commonly accompanied by an increased chloritization of biotite.

The occurrence of the alteration is locally controlled by joint planes, but in general there is no obvious structural or spatial control. Instead it has a patchy irregular distribution that appears to be independent of the distribution of any other rock in the area. This feature, together with the relative age relationship already mentioned, indicates that the alteration represents an event that was late in the history of the area and was not related to any evident igneous events.

Other types of alteration and veining in the area include epidote veins that are accompanied by minor bleaching of feldspars, thin, tabular zones of bleaching that occur in the unfoliated Rana Quartz Monzonite, open-space veins of amethyst and hematite, and alteration accompanied by the formation of rosettes of schorl and by quartz-schorl veins. Age relationships among these types of alteration are uncertain, but it is known that epidote alteration postdates F_4 shearing, whereas quartz veins predate it. Also, it is likely that the schorl rosettes, the quartz-schorl alteration veins, and the rare schorl-bearing pegmatites are all genetically related. One possible origin of the boron in the tourmaline is from the metasediments (Montgomery, 1953). It is well known that boron is released from 1 \underline{M} disordered illite when transformed to 2 \underline{M} muscovite during the early stages of metamorphism (Perry, 1972; Weaver and others, 1971; Perry and Hower, 1970; Muffler and White, 1969). The boron then may have resided in interstitial fluids in the sedimentary rock until conditions permitted transportation of the boron in solution and later, deposition of the boron as tourmaline.

The exact conditions under which this might have occurred are not known, but Muffler and White (1969) indicate that the illite-muscovite transition takes place below 210°C in the Salton Sea geothermal field, and the occurrence of greenschist facies apparently marks the complete redistribution of boron because muscovite is almost all in the 2 M polymorph in this facies (Erd, 1977).

The origin of the other types of alteration are even less certain. The open-fracture-filling amethyst veins, though, are very well preserved, suggesting that they were formed after the last deformation and after sufficient uplift had occurred to allow the formation of open fractures.

Summary

The Rana Quartz Monzonite was intruded under conditions that gave rise to a distinct but discontinuous fine-grained leucocratic border zone with a main interior facies that originally was a typical sub-equigranular biotite quartz monzonite. The crystallization sequence in this unit was quartz, plagioclase, biotite(?), and K-feldspar. Late-stage differentiation produced aplites and possibly some quartz veins. Subsequent to the intrusion and crystallization, the body was subjected to at least three phases of deformation that in parts of the body produced a foliation which increases to the southeast. Subsequently, sporadic alteration by water-rich fluids reddened and altered feldspars and deposited epidote veins locally.

Peñasco Quartz Monzonite (Granodiorite)

Distribution and Occurrence

The Peñasco Quartz Monzonite occurs in the eastern part of the map area (pl. I). It intrudes the main amphibolite unit which lies along the northern margin of the pluton. Along its western margin, only partially exposed, it intrudes either the Vadito schist or Rana Quartz Monzonite. Its southern and eastern contacts are not exposed. To the east and northeast of the map area, Peñasco Quartz Monzonite also occurs in generally relatively small, isolated outcrops.

The Peñasco Quartz Monzonite lacks any distinctive border zone, and the degree of exposure generally prevents detailed mapping of internal zoning. Nonetheless the body can be divided into porphyritic and equigranular facies. The bulk of the body has a subequigranular texture but there are sporadic occurrences of a strongly porphyritic rock that contains large microcline megacrysts. These occurrences have gradational relationships with the equigranular facies, a fact which, along with relatively poor exposures, made mapping internal contacts between facies impractical. Thus the occurrences of the porphyritic facies are simply noted by a symbol on plate II.

Contact Relationships

Unlike either the Puntagudo Granite Porphyry or the Rana Quartz Monzonite, the Peñasco Quartz Monzonite has a generally concordant contact with the Vadito amphibolite unit along its northern margin. The few apophyses that invade the amphibolite from the main body characteristically have rounded, irregular shapes that contrast markedly

with the ragged margin of the Rana Quartz Monzonite. Where Peñasco Quartz Monzonite intrudes the Rana rocks, it transects the Rana foliation along a contact with features that suggest some combination of forceful injection and partial digestion of the Rana rocks. Large, partly rounded and digested blocks of Rana Quartz Monzonite are included in the Peñasco Quartz Monzonite near the irregular contact. The saw-tooth nature of the contacts suggests that the Rana rocks have been prised apart.

The contact of the unit is also characterized by minor amounts of migmatization, and it is much less sharp than the contacts of the older rocks. This is shown particularly well in figure 58, where it is clear that there is considerable interaction between the country rock and the invading Peñasco Quartz Monzonite. Figure 59 shows an example of folding in the country rock near the contact. This folding may simply be an expression of F_3 deformation or it may be a very local effect of the intrusion of the Peñasco Quartz Monzonite. If it is folding due to intrusion then it suggests that one mode of emplacement was forceful injection. Physical incorporation and partial digestion of the country rock also may have been important, because the marginal parts of the pluton, especially along its northern contact, contain numerous discoidal mafic inclusions. In addition, the rock is slightly more mafic in that zone. These features were interpreted by Montgomery (1953) as indicating that the Peñasco Quartz Monzonite magma had assimilated amphibolitic country-rock material. This idea is difficult to prove or disprove, but the abundance of inclusions suggests that it is at least partially correct. Certainly a great deal more mafic material has been incorporated in the Peñasco Quartz Monzonite than in the older granitic units.

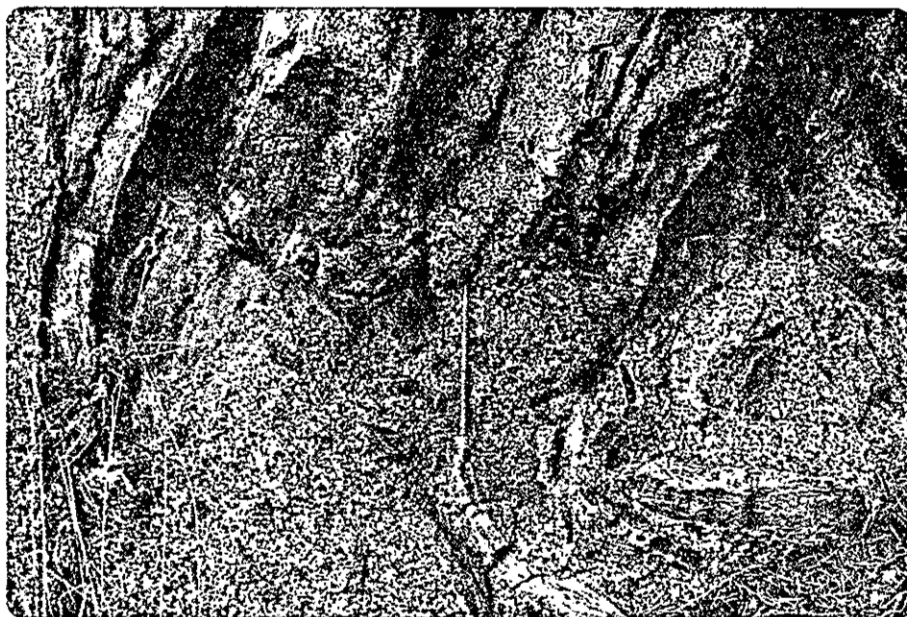


Figure 58. Contact of the Peñasco Quartz Monzonite with the Vadito amphibolite unit. Note the incipient migmatization along the contact. About 1.2 mi east of Cerro Alto.



Figure 59. Chevron folding in Vadito Schist(?) near contact with the Peñasco Quartz Monzonite. About 1.5 mi east of Cerro Alto.

Petrography

When examined in detail the Peñasco Quartz Monzonite shows considerable differences in texture and composition. Some of the variations are illustrated by the stained slabs in figure 60. Even though the textures and proportions of minerals obviously change from sample to sample, the types of minerals present do not. All the samples are biotite granodiorites to quartz monzonites with biotite or very rarely hornblende as the mafic mineral and muscovite, allanite, epidote, sphene, magnetite (+ hematite), apatite, and zircon as accessory minerals. Microcline is invariably blocky but is not commonly euhedral except where it occurs as megacrysts. Plagioclase grains, on the other hand, are typically subhedral to euhedral and show continuous normal undulatory zoning. In some instances the plagioclase has clear rims of albite, particularly where a plagioclase grain is in contact with a microcline grain. Quartz is typically transparent and medium gray, and it occurs as aggregates of anhedral grains. Biotite occurs as aggregates of tapered flakes that are pleochroic in shades of green to light yellow green. The accessory minerals are associated with the biotite. One of the most persistent and characteristic features of the Peñasco Quartz Monzonite is the presence of 1 mm sized euhedral wedges of sphene. These are readily visible in hand specimen even where they are altered to anatase. These sphene wedges and the generally higher biotite content of the Peñasco Quartz Monzonite make it possible readily to distinguish it from the Rana Quartz Monzonite. The occurrences of the other accessory minerals are described in detail in Appendix I, but two points can be emphasized here: (1) Allanite and epidote commonly

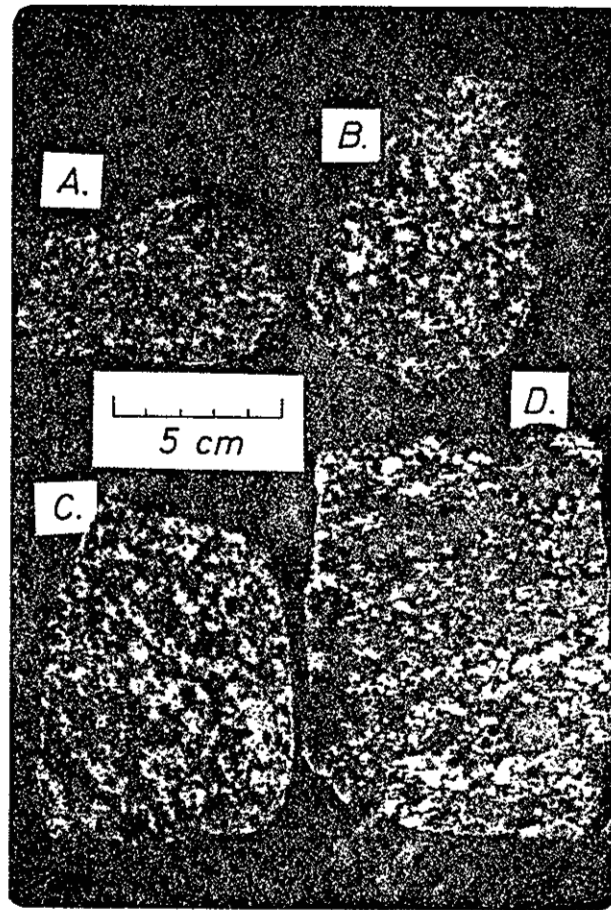


Figure 60. Stained slabs of Peñasco Quartz Monzonite. K-feldspar is stained yellow.

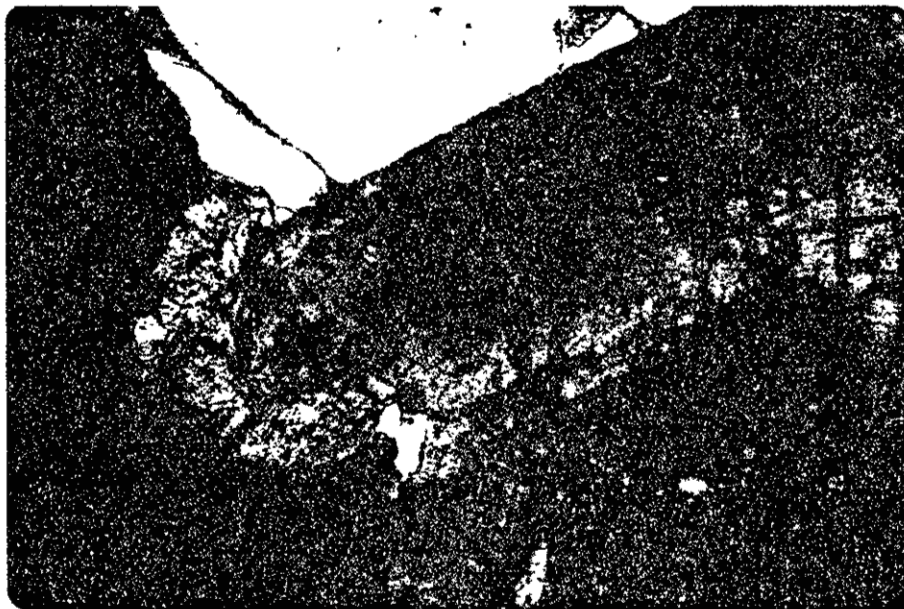


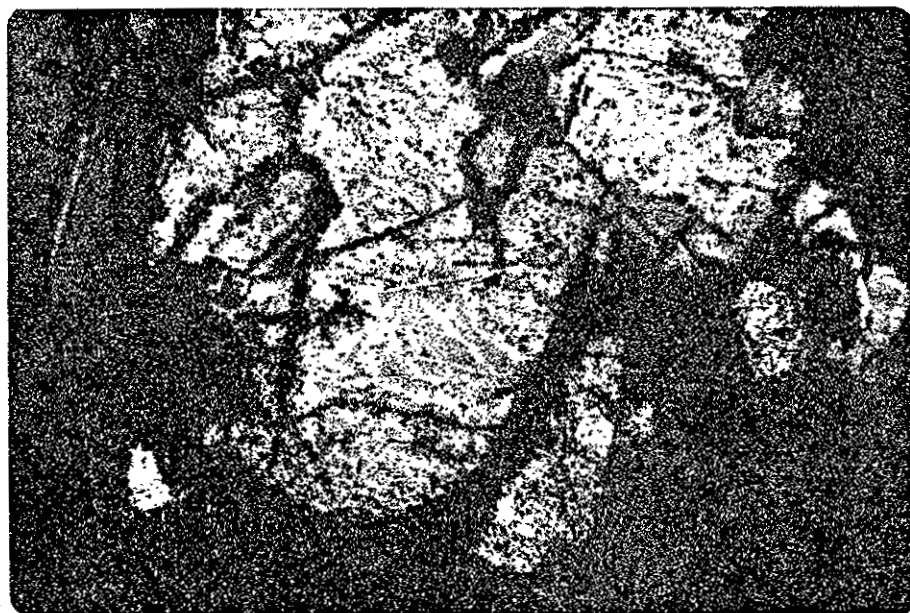
Figure 61. Photomicrograph of zoned allanite with a partial epidote rim. Peñasco Quartz Monzonite sample PL71-5a.

are associated in this unit as in the Rana unit, but here the allanite also occurs as 1 mm sausage-shaped crystals that commonly have little or no epidote rim and that are strongly color zoned in shades of brown and red (fig. 61). (2) The magnetite-hematite association is similar to that of the Rana Quartz Monzonite, as shown in figure 62.

In many samples there is some suggestion of slight deformation in that some biotite grains are kinked, quartz and feldspar grains are fractured, and some plagioclase albite twin lamellae are bent. In addition granulation or polygonization of plagioclase and some microcline may occur, particularly around the margins of the moderate-sized grains. Megacrysts commonly show a subparallel alignment, but nowhere in the unit was there a strong preferred orientation of biotite similar to that found in the Rana Quartz Monzonite.

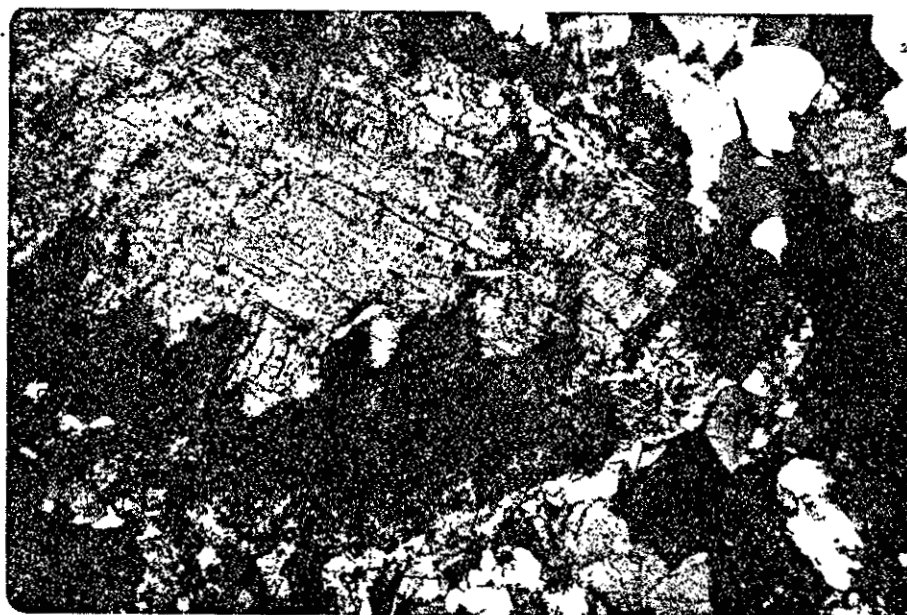
Myrmekite and albite rims on plagioclase are common. Myrmekite occurs as wartlike projections into microcline at points where the microcline is in contact with plagioclase. Slight alteration of plagioclase by very fine-grained muscovite and epidote is common but by no means ubiquitous and its occurrence does not seem to be strongly controlled by the anorthite content of the altered grains (fig. 63).

The Peñasco Quartz Monzonite, like the older granite units in the area, is cut by both pegmatites and aplites. The aplites are consistently older than the pegmatites and appear to be restricted to the Peñasco unit itself. In at least one locality, however, there are crosscutting relationships between aplites. The older aplite is darker and clearly more mafic than the younger one and is apparently genetically related to the Peñasco Quartz Monzonite. The younger, more leucocratic aplite presumably is associated with nearby pegmatite-aplite dikes.



0.1 mm

Figure 62. Photomicrograph of magnetite (white) with associated hematite (light brown), Peñasco Quartz Monzonite.



2 mm

Figure 63. Photomicrograph of plagioclase alteration in the Peñasco Quartz Monzonite. Notice irregular distribution. Sample PL71-35.

Evidence for this is that the younger dike locally contains garnet that is similar to garnet occurring in the pegmatite-aplite. Also, its general texture and leucocratic character suggest a genetic relationship to the pegmatite-aplite. Aplites that occur in the Peñasco Quartz Monzonite commonly contain biotite, which in itself sets them apart from those associated with the pegmatites or most of the older granitic units. The generally mafic character of these aplites is consistent with their having been derived from the Peñasco Quartz Monzonite as it is the most mafic of the granitic rocks in the area.

Modal Composition

The Peñasco Quartz Monzonite is characterized by a wide range in modal composition, particularly with respect to plagioclase-K-feldspar ratios as shown in figure 64, which demonstrates that the body actually consists of rocks ranging from quartz diorite to quartz monzonite. The quartz to feldspar ratio, however, has a narrowly defined range suggesting that it is roughly independent of the relative proportions of K-feldspar and plagioclase. Figure 65 shows that on the average the Peñasco Quartz Monzonite contains less quartz than any of the other granitic rocks. Figure 66 demonstrates that this unit has muscovite in lower amounts than much of either the Puntigudo Granite Porphyry or the Rana Quartz Monzonite. Even more distinctive, however, is the biotite content which except for two samples is in excess of 12 volume percent while the highest observed in the other granitic rocks is about 11 volume percent. Figure 66 shows the lack of correlation between biotite content and plagioclase/K-feldspar ratios. Finally, it is of interest that the aplites in the Peñasco Quartz Monzonite (fig. 64)

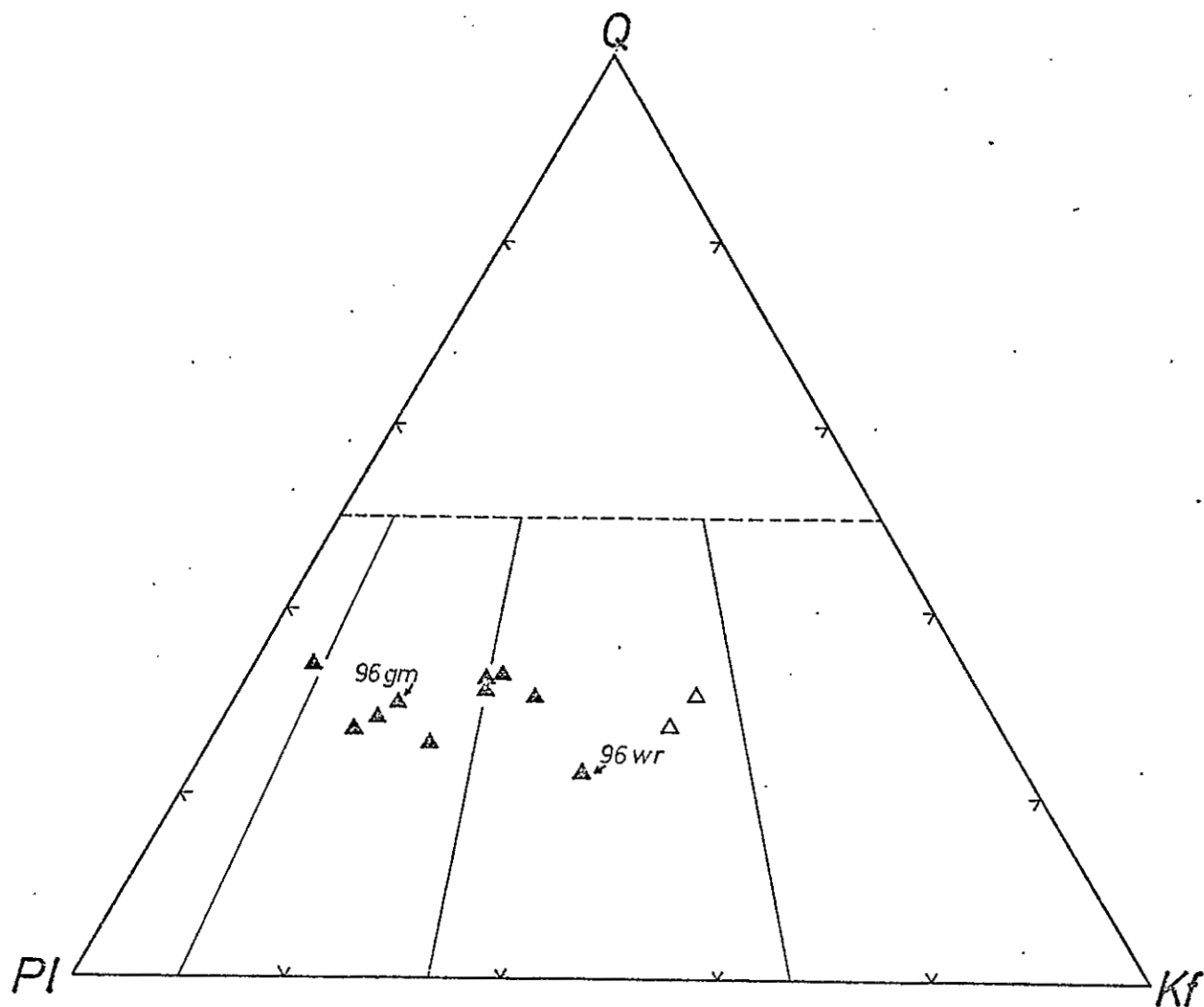


Figure 64. Plot of modal data from the Penasco Quartz Monzonite. Solid triangles are from the main mass. 96 gm is the groundmass of sample PL72-96 while 96 wr is the whole rock. Open circles are aplites.

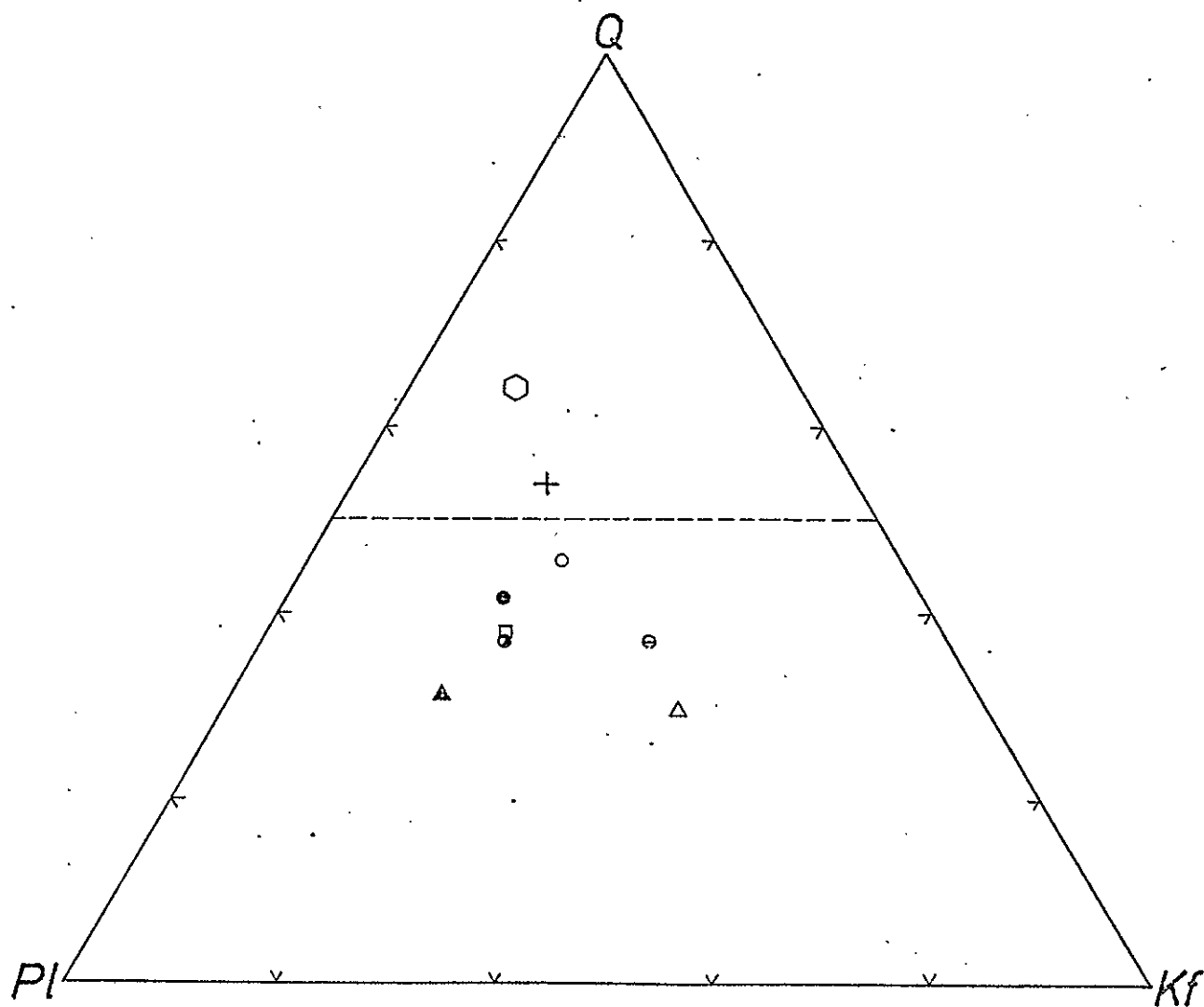


Figure 65. Plot of average modes for the granitic rocks. Symbols as in previous mode plots.

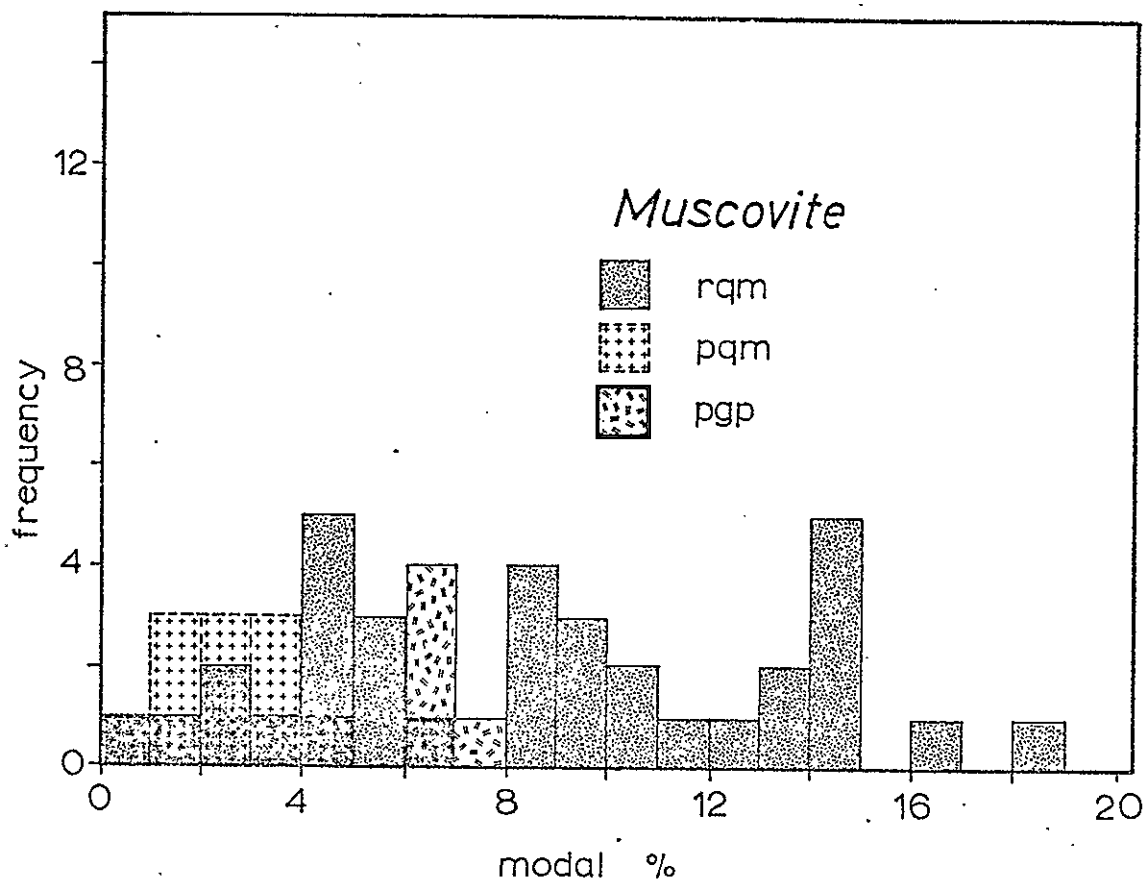


Figure 66a. Histogram of modal muscovite for the Puntigudo Granite Porphyry, the Rana Quartz Monzonite, and the Peñasco Quartz Monzonite.

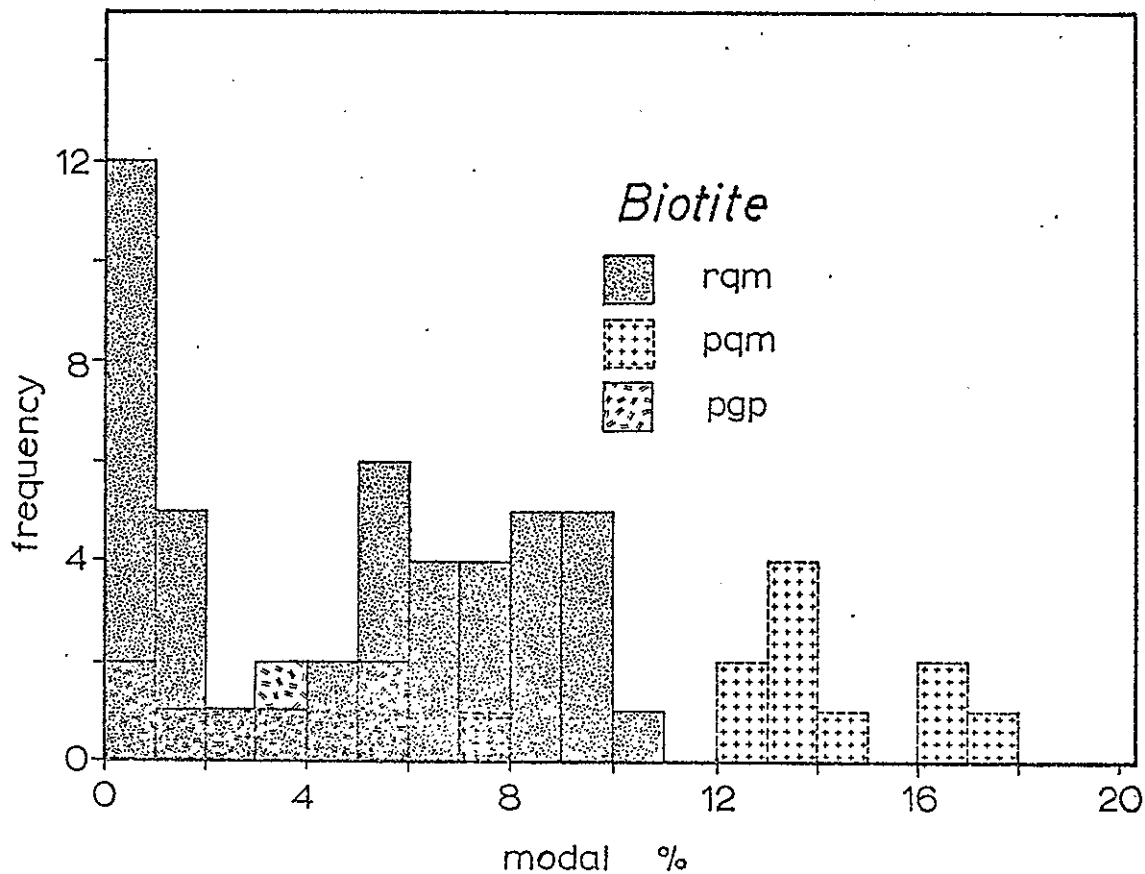


Figure 66b. Histogram of modal biotite for the Puntigudo Granite Porphyry, the Rana Quartz Monzonite, and the Peñasco Quartz Monzonite.

are one endpoint of a "trend" toward lower plagioclase/K-feldspar ratios. These data taken together suggest that the compositional variation in the body may be attributed to fractional crystallization of plagioclase and biotite, leaving residual melts relatively more enriched in components forming K-feldspar. Alternatively, some of the compositional variation may reflect digestion of mafic wall-rock material. This could have an effect similar to that of fractional crystallization, although if this were the case a tendency for the more mafic (and thus more contaminated) rocks to show a depletion in quartz might be expected. Instead, the most mafic sample of Peñasco Quartz Monzonite is enriched in quartz relative to the others, suggesting that assimilation does not explain the compositional variation here observed. The question is not resolvable solely on the basis of modal data, and it is further discussed in the section of petrochemistry.

Structural and Textural Features

Structural and textural features in the Peñasco Quartz Monzonite are of three main types: (1) joint sets, (2) very slight penetrative foliation, and (3) alignment of tabular K-feldspar megacrysts. The alignment and/or deformation of mafic xenoliths constitutes a possible fourth structural feature. Also one prominent lineament was observed on air photos.

Joint sets in the Peñasco Quartz Monzonite have a wide range of orientations, but they commonly strike either northwest to north-northwest or within 25° of east-west. Their dips commonly show that the joint sets are conjugate. The general strike directions of the joints

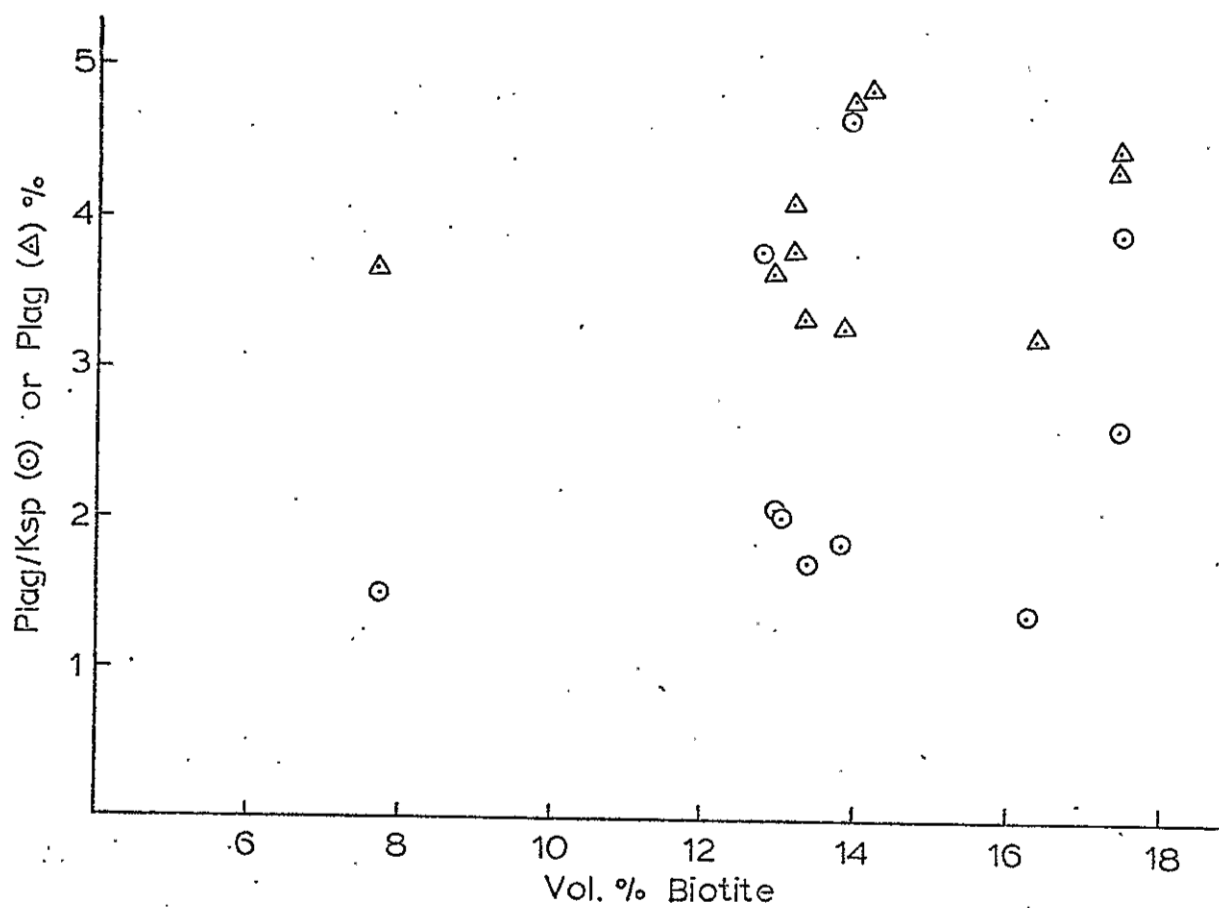


Figure 67. Plot of modal plagioclase/K-feldspar vs. modal biotite (circles) and modal plagioclase vs. modal biotite (triangles).

are similar to those in the older granitic units, but lower dips are more common in those in the Peñasco Quartz Monzonite. This suggests that the Peñasco Quartz Monzonite either responded differently to similar stress or that slightly different stresses gave rise to the joint sets in the older granitic bodies.

The slight foliation in the Peñasco Quartz Monzonite, often not readily noticed in outcrop, is typified by a slight alignment of biotite clots and tabular minerals (fig. 68). Fractures in larger grains of plagioclase commonly parallel the general direction of the foliation. In the majority of outcrops it is impossible confidently to determine a specific foliation plane, and hence relatively few measurements were taken. From the sparse outcrops that do show a measurable foliation it appears that the strike ranges from northeast to east-west and the dip from 27° to 78° S. It also appears that the attitude of the foliation near the contact tends to conform to the orientation of the contact.

Alignment of tabular K-feldspar megacrysts is nearly ubiquitous, and a typical example is shown in figure 69. This orientation appears to have been caused by laminar flow in the magma while it was still a crystal-liquid mixture. Evidence for this is alignment parallel to the walls of apophyses of Peñasco Quartz Monzonite and a lack of systematic orientation of the megacrysts that would be expected if they had been oriented by regional stress during growth. The flow orientation of the megacrysts, together with the general conformity to the walls of the weak foliation of rocks without megacrysts, suggests that much of the foliation in the Peñasco Quartz Monzonite was produced by flow

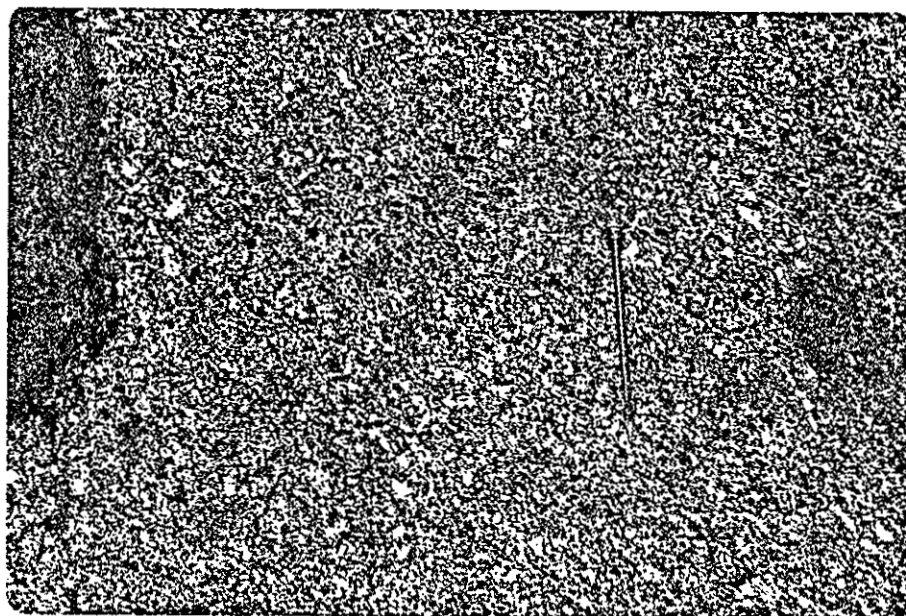


Figure 68. Slight foliation of biotite visible in an outcrop of the Peñasco Quartz Monzonite. About 1 mi east of Cerro Alto.



Figure 69. Subparallel alignment of K-feldspar megacrysts in the Peñasco Quartz Monzonite. About 1.2 mi north of Trampas.

in the magma while it was being emplaced. Any regional stresses that may have been partly responsible for the deformation were definitely weaker than those that produced the dominant foliation of earlier granitic bodies.

Alteration

Megascopic alteration involving epidote veining and reddening of feldspars is largely absent from the Peñasco Quartz Monzonite. Only in a few localities was minor reddening observed along joint surfaces. Microscopically, plagioclase is commonly altered to muscovite and epidote, but the degree of alteration is much less than in the Rana Quartz Monzonite. Also its occurrence within grains appears to have been only partly controlled by the anorthite content of the plagioclase. Some plagioclase grains show little or no alteration while others in the same rock have a patchy dusting of muscovite and epidote and still others show fairly severe alteration. In any case, it is certain that the Peñasco Quartz Monzonite has not been subjected to the same amount of microscopic or megascopic alteration as have the older granitic rocks.

Summary

The Peñasco Quartz Monzonite was intruded partly by forceful injection and partly by incorporation and perhaps digestion of country rocks. Conditions were such that no border zone was formed, and minor migmatization occurred along the contacts with the country rocks. The variation in modal composition of this unit can be explained by fractionation of plagioclase and quartz from magma, although it is recognized

that assimilation may have played a role as well. The sequence of crystallization is not completely known but plagioclase and biotite were generally the early phases followed shortly by K-feldspar and quartz. Most of the associated aplites appear to be genetically related to the main body and probably formed from residual liquids.

This unit shows very little of the obvious alteration and deformation of the older granitic rocks, although there is microscopic evidence for limited alteration of the plagioclase.

Pegmatites

The pegmatites of the Dixon-Peñasco area are of particular interest because among them is one of the most unusual occurrences in the world, the Harding pegmatite. It is one of the largest known concentrations of tantalum, lithium, and beryllium, and it is a spectacularly coarse-grained, zoned pegmatite body. The Harding is, however, only one of almost innumerable pegmatites in the area and no attempt is made here to describe it in detail (see Jahns and Ewing, 1976, for the most comprehensive description available). Instead it is discussed in a general way as an example of one of five broad categories of pegmatites that occur in the area.

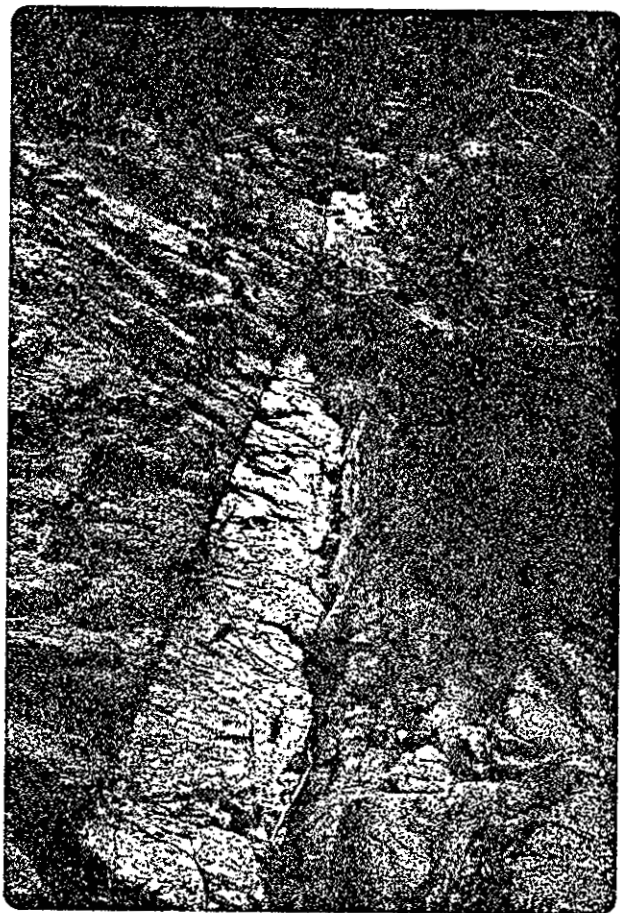
The general distribution of pegmatites in the area is shown on plate IV, and pegmatites are also shown in some detail on plate II. It can be readily seen that there is no consistent spatial relationship between the pegmatites and any of the major granitic bodies. Instead, the pegmatite bodies appear to have a semirandom distribution over the area, and are slightly concentrated in its southern and southeastern parts. The bodies occur typically as dikes or pods that differ markedly

in size ranging from 2 cm to 15 m in thickness. The detailed shapes of the dikes in three dimensions are difficult to determine, but in section they commonly show rolls and other changes in orientation. In some places they branch and they typically thin toward their terminations although their actual terminations are rarely exposed.

Most of the dikes apparently are not connected to any larger igneous body at depth, and no evidence for such a connection has been observed in the area despite considerable topographic relief along parts of Embudo Creek. The variations in exposed lengths suggests that the dikes may be very irregular in a view perpendicular to their large dimensions. In addition to branching, some larger dikes show bulges that give them the shape of a two-tailed flattened tadpole.

In terms of internal zoning and mineralogic composition, the pegmatite bodies can be classified as (1) simple pegmatites of small to moderate size and consisting primarily of coarse quartz, K-feldspar, and albitic plagioclase, (2) complex pegmatites that contain rare minerals and show at least some degree of internal zoning, (3) pegmatite-aplite pairs with complex internal zoning but no rare minerals, (4) rare tourmaline-bearing pegmatites without distinct internal zoning and of relatively simple mineralogy, and (5) albite-quartz-muscovite pegmatites which in some instances are internally zoned but which consistently lack unusual minerals.

The simple pegmatites are by far the most abundant in the area. Photographs of typical occurrences are shown in figure 70. The bodies, unzoned or only crudely zoned, consist of blocky to sugary K-feldspar (microcline), masses of anhedral quartz, sugary albite, and irregular books of greenish muscovite. Some dikes contain minor hematite as



(a)

Figure 70. Typical examples of simple pegmatites, (a) cutting Peñasco Quartz Monzonite, about 1.25 mi west of Rio Lucio, (b) cutting a quartz vein in Rana Quartz Monzonite, about 0.5 mi south of Cerro de Los Arboles.



(b)

stains, bright-yellowish bismutite, and very rare euhedral crystals of green beryl. Although most of these pegmatites are unzoned, some show features of crude segregation (fig. 71). In general, the thicker pegmatites seem to show more internal segregation but thickness does not, however, seem to correlate with the content of rare minerals. Indeed, the thin, terminal parts of the Harding pegmatite appear to be of the "simple" type which further suggests a possible link between at least some of the simple pegmatites and some of the complex ones.

The distinction, then, between the simple and complex pegmatites is not everywhere simple or clear. Still, it is useful to place in a separate category those pegmatite bodies that show marked internal zoning and contain significant amounts of rare minerals. In the Dixon-Peñasco area this type of pegmatite is exemplified by the Harding occurrence (Jahns and Ewing, 1976). The main body is about 30 m thick and 300 m in apparent length. It is characterized by strong internal zoning defined by changes in both texture and mineralogic composition. Particularly spectacular is a zone containing lath-shaped spodumene crystals up to about 5 m in length with an interstitial matrix that is mostly quartz but also includes lepidolite, muscovite, beryl, microcline, apatite, and microlite. In all there are four major zones in the dike including a border rind, a zone of massive quartz, the spodumene zone mentioned above, and a core of lithium- and tantalum-rich pegmatite (Jahns and Ewing, 1976). In addition, irregular masses of sugary, porous albite with minor K-feldspar appear mainly in footwall parts of the dike.

The Harding is a highly unusual occurrence, not only in this area but also on a worldwide basis. Other pegmatites in the area that might



(a)

Figure 71. Examples of pegmatites which are simple in mineralogy but which show limited zoning.

(a) Note small quartz core, about 0.5 mi north of Cerro del Abrevadero; (b) note directional orientation of blocky K-feldspar as well as that of quartz and muscovite, northwest shoulder of Cerro del Abrevadero.



(b)

be considered as complex because of their marked internal zoning generally lack lepidolite or spodumene, but some of them contain garnet and/or tantalum-niobium minerals. The Harding and two other smaller pegmatites in the area may well be the only *bona fide* complex pegmatites in the area with the others which are internally zoned being considered variants of the simple type.

The third category of pegmatite in the area, pegmatite-aplite pairs, has only one known occurrence and that is at the west end of downtown Peñasco. This pegmatite, a part of what is known as "the Peñasco outcrop," is similar in overall texture and zoning to pegmatite-aplite pairs in San Diego County, California (Foord, 1976; Jahns, 1954). The occurrence consists of at least two dikes 30 to 60 cm thick, each having basically a two-ply structure with moderately coarse-grained uniform pegmatite in the upper part of the dike and fine-grained layered aplite in the lower part. The layering in the aplite is defined by slight changes in grain size and by definite bands of garnet (fig. 72). The only K-feldspar crystals in the aplite portion are tapered downward toward the footwall contact; they appear to have grown upward more or less simultaneously with crystallization of the aplite. This pegmatite has been singled out as a particular type largely because its zoning is so markedly different from the more symmetric zoning found in other zoned bodies in the area. Despite its gross similarity to many pegmatites in San Diego County, California, it differs from them in that it lacks "pockets," i.e. gem-producing, crystal-lined cavities.

The fourth type, tourmaline-bearing pegmatite, has been observed in only two localities, but these occurrences are noteworthy because otherwise the pegmatites and granitic rocks in northern New Mexico are



(a)



(b)

Figure 72. The Peñasco pegmatite. (a) General view of the aplite portion showing garnet banding; (b) detail of slightly tapered K-feldspar crystals near the footwall.

low in boron. Indeed, tourmaline has not been observed in the Harding pegmatite, nor in most of the other complex pegmatites in northern New Mexico. The tourmaline pegmatites, however, contain abundant crystals of black schorl up to 2.5 cm in diameter in a pegmatite matrix that consists largely of albite, quartz, and lesser amounts of K-feldspar. Zoning in these pegmatites is not conspicuous, but they contain some medium- to coarse-grained aggregates of schorl and quartz with minor feldspar.

The fifth type of pegmatite, consisting of quartz, muscovite, and albite, is reasonably common and tends to occur as small dikes in which albite forms bladed radiating masses that project inward toward a quartz core (fig. 73a), or in which albite, quartz, and muscovite occur together in a medium-grained, unzoned, or crudely zoned massive aggregate (fig. 73b).

The above characterization of pegmatites in the Dixon-Peñasco area does not necessarily describe boundaries between genetically separate episodes of pegmatite emplacement, but it does point out the overall complexity of the pegmatites and suggests that there was more than one age of pegmatite formation in the area. Owing to their mode of occurrence, however, it is difficult to establish relative ages between the various types of pegmatites, and no one has yet attempted a systematic age-dating program on them. Still, certain field observations bear on the problem. First of all, pegmatites consistently transect the granitic rocks and their dominant foliation. Aplites that are not associated with pegmatites are restricted in distribution to the granitic bodies with which they are associated. In one instance a pegmatite with a core of aplite is cut by a pegmatite without aplite (fig. 74). Epidote



(a)



(b)

Figure 73. Quartz-albite pegmatites. (a) Zoned with a quartz core, about 1 mi north-northwest of Cerro de los Arboles; (b) near massive quartz-albite-muscovite pegmatite, about 0.3 mi south of Cerro Alto.

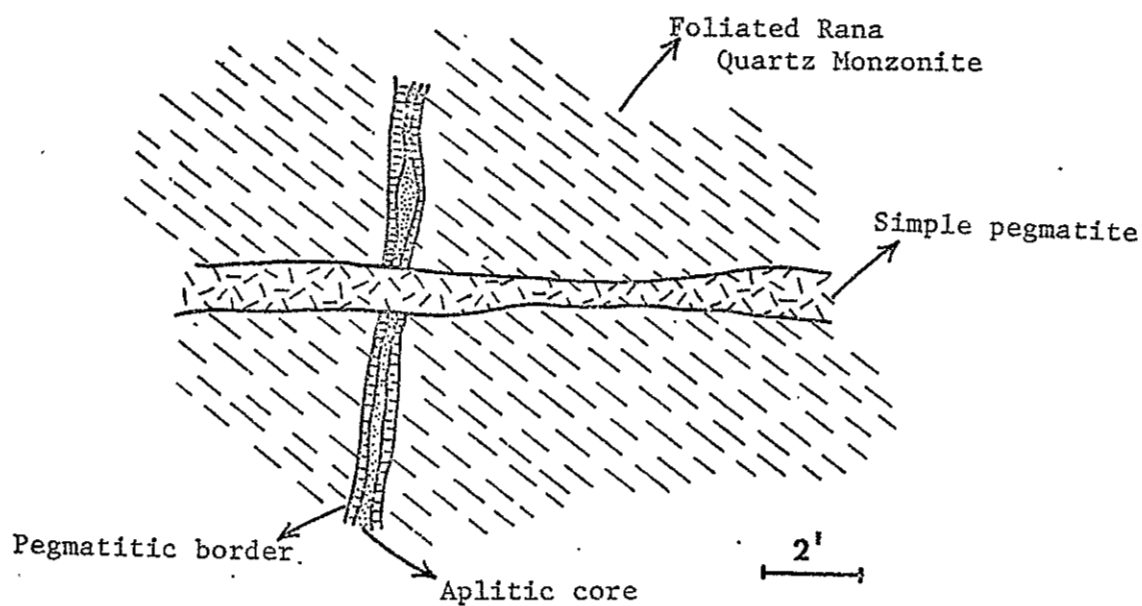


Figure 74. Simple pegmatite body cutting one which shows symmetrical zoning similar to figure 71a. About 0.8 mi south of Vallecito.

alteration and veining has, in one locality, transected a typical simple pegmatite, whereas at another locality a simple pegmatite was observed to cut a quartz vein in the foliated portion of the Rana Quartz Monzonite. Finally, all pegmatites in the area show little or no effects of regional deformation.

These observations suggest that (1) the pegmatites are at least in part younger than the youngest granite, (2) they are at least in part younger than late-stage features such as quartz veins in the Rana Quartz Monzonite, (3) there are at least two ages or generations of pegmatites, (4) the pegmatites are not associated with aplites that appear to be genetically related to the granites, and (5) at least the simple pegmatites are older than the epidote alteration. It also is suggested that the early pegmatites may have tended toward association with aplite (e.g. fig. 74) and also may have tended to be zoned, whereas later ones may have been predominantly the simple types. This is highly conjectural, however, and it is difficult to determine where the tourmaline or quartz-albite-muscovite pegmatites belong in the sequence of pegmatite emplacement.

There can be little doubt that pegmatite emplacement was a complicated and probably protracted process which for the most part took place after intrusion and crystallization of the youngest granitic unit, the Peñasco Quartz Monzonite. How long after is a question addressed in a later section on geochronology, but it is interesting to note here that the Peñasco Quartz Monzonite is the most mafic of all the granitic units, even in its most leucocratic facies. It does not seem to be sufficiently differentiated, at least in surface exposures, to have been a likely progenitor for the very leucocratic and obviously

highly differentiated pegmatites of the area. On the other hand, 9 mi to the southwest of the map area near Cordova, New Mexico, there are exposures of a leucocratic muscovite granite with intimately associated pegmatites and this seems to be a much more likely relationship with the pegmatites in the Dixon-Peñasco area. All this suggests that there may be no genetic link between the pegmatites and the Peñasco Quartz Monzonite, and indeed there may well have been a considerable time span between them. Radiometric dating of the pegmatites and of the muscovite granite near Cordova, New Mexico, would help in resolving the pegmatite problem.

Quartz Pods and Veins

General Occurrence and Petrography

Pods and veins of massive quartz, with or without accessory minerals such as magnetite, hematite, chalcocite(?), bornite, chrysocolla, and azurite or malachite, are common in the Dixon-Peñasco area. On plate IV the larger masses are shown as dotted lines or stippled areas. These features do not appear to be related to pegmatites, and some are clearly transected by pegmatite bodies, but it is by no means certain that all quartz masses in the area are older than the pegmatites. Indeed, the quartz masses probably represent more than one age of hydrothermal activity.

The bulk of the quartz occurs as barren, irregular, pod-shaped masses ranging from 5 cm in thickness to 200 x 10 m in exposed dimensions. Some of the bodies are more dike-like in form and as much as 0.5 m thick. Some show copper mineralization, and most of these have

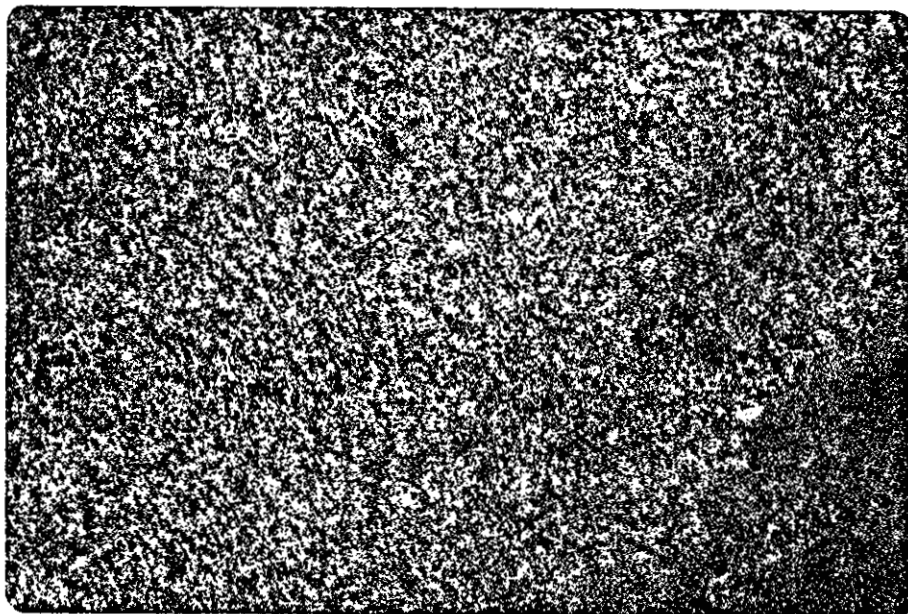
been prospected. In some places, notably near the top of Cerro Alto, shafts as deep as 10 m have been sunk. In these occurrences, the quartz is iron stained and contains small pods and stringers of hematite and/or chrysocolla with malachite or azurite. Some veins, apparently the less altered or weathered ones, contain visible chalcopryrite, bornite(?), and chalcocite. Copper mineralization, chrysocolla and malachite(?), presumably associated with that of the quartz veins, also has been observed locally in the schists of the Vadito Group, and in one place in an epidote-altered part of the Rana foliated biotite quartz monzonite. Minor amounts of similar mineralization also have been observed in the Harding pegmatite (Jahns and Ewing, 1976).

Thin quartz veins also are associated with black tourmaline, particularly in schists of the Vadito Group (fig. 75). Locally the Rana Quartz Monzonite shows both isolated rosettes of black tourmaline and, rarely, small bleach zones with concentrations of black tourmaline (fig. 76). As previously suggested, the boron could have been derived from the metasediments themselves, and this is consistent with the behavior of boron during diagenesis and metamorphism (see section on alteration of the Rana Quartz Monzonite). It is further suggested here that the rare tourmaline pegmatites may have also been derived from the metasediments at depth, by a partial melting process and which would have given rise to a boron-rich silicate melt. Conceivably, the quartz-tourmaline veins and the tourmaline-bearing pegmatites may have formed during the same episode of metamorphism and/or partial melting.

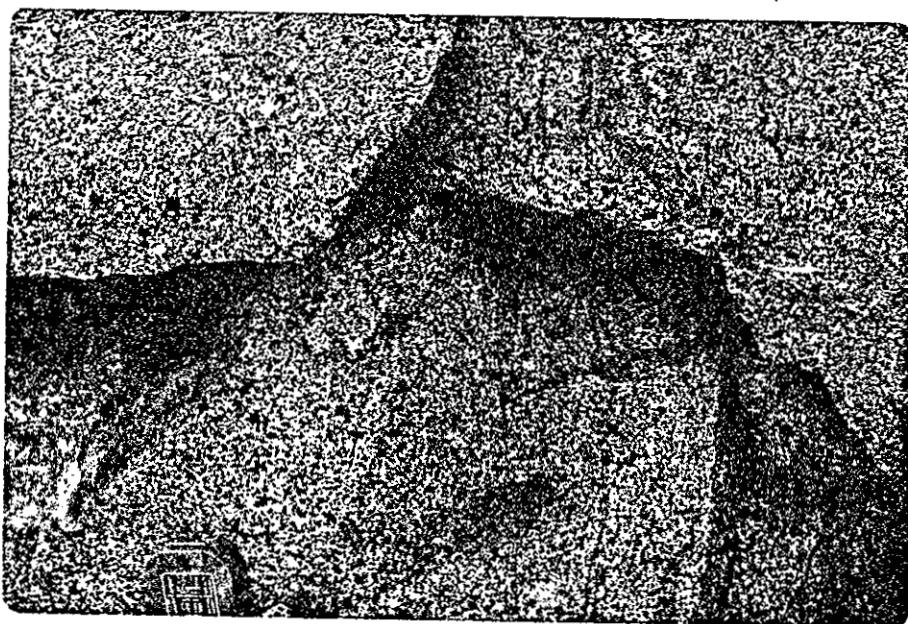
One example of an amethyst-bearing quartz vein was observed in the Rana Quartz Monzonite. It is about 5 cm in maximum width and is traceable as an echelon segments for about 30 m. The vein comprises symmetrical



Figure 75. A tourmaline-quartz vein in Vadito schist. 0.3 mi southwest of Cerro Alto.



(a)



(b)

Figure 76. Tourmaline in Rana Quartz Monzonite. (a) Single rosettes (0.5 mi northeast of Cerro del Abrevadero); (b) rosettes in a bleached zone (0.5 mi north of Cerro del Abrevadero).

halves which on the outside margins consist of very fine-grained quartz and feldspar. The rind gives away inward to dog-tooth amethyst (1 cm maximum size) and small, botryoidal crystals groups of hematite(?). This is the only observed occurrence in which a quartz vein could be classed as an open-space filling.

Age Relations

It is generally difficult to establish the age of any particular occurrence of a quartz pod, but some crosscutting relationships with pegmatites (see previous section and fig. 70) indicate a quartz vein to be older than a simple pegmatite. On the other hand, the Harding pegmatite appears to have been affected by copper mineralization associated with quartz veins, suggesting that some of them may have formed after at least one of the pegmatite episodes.

Structural Features

For the most part the quartz bodies, though commonly broken and fractured, do not appear to have been subjected to penetrative deformations typical of F_2 and F_3 . Indeed, in most localities they clearly transect the dominant foliation, F_2 , and in one area an F_4 quasi-ductile shear zone offsets a small quartz vein as shown in figure 77. This particular outcrop further demonstrates that the epidote alteration postdates not only the quartz veins and F_4 , but also the jointing.

Summary of Relative Ages of Granites, Pegmatites, and Alteration

Based on the preceding field and petrographic observations, it is possible to suggest a scenario of geologic events that occurred in the

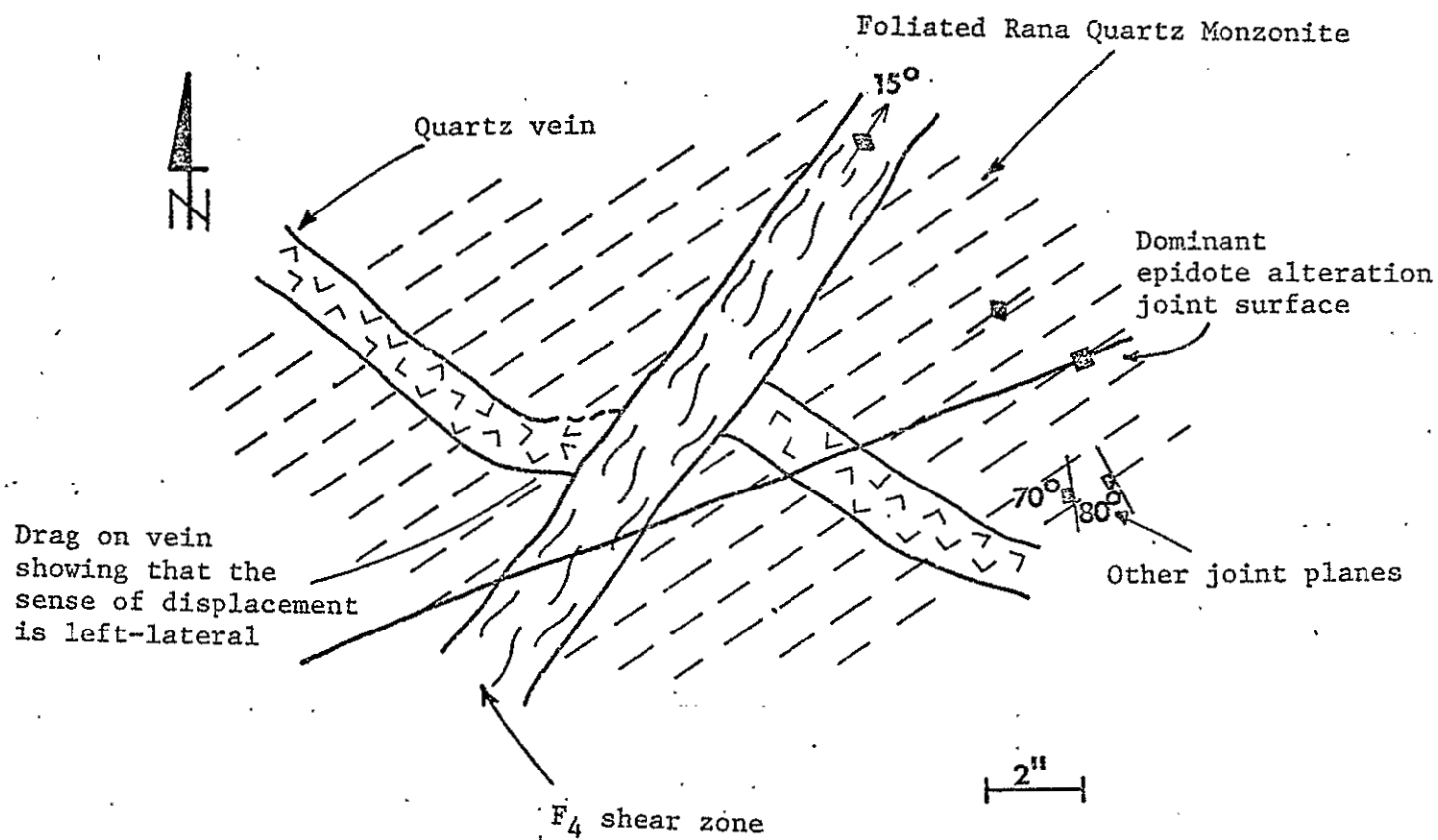


Figure 77. Diagram of a quartz vein offset along an F_4 shear zone.
0.8 mi south of Cerro de los Árboles.

Dixon-Peñasco area. After deposition of the Ortega Group, the Vadito Group was deposited ending with a period of andesitic to basaltic volcanism that probably was accompanied by shallow burial of the underlying sedimentary rocks. There followed a period of large-scale folding (F_2) and then widespread intrusion and/or extrusion of magma now partially represented by the Cerro Alto Metadacite. The Puntiaquedo Granite Porphyry subsequently was emplaced, and in turn it was intruded by the Rana Quartz Monzonite. Metamorphism of the country rocks probably increased after intrusion of the Rana Quartz Monzonite, and at some point thereafter deformation episode F_2 produced the dominant foliation in the previously intruded granitic rocks and in much of the country-rock terrane. Metamorphism continued to increase in intensity until some point in time prior to the F_3 deformation. Some quartz pods and veins probably were developed by hydrothermal solutions at this time (shortly after F_3), and it is possible that some pegmatites were formed as well. The Peñasco Quartz Monzonite apparently was intruded after or during the waning stages of F_3 , but it is uncertain whether it was intruded before or after F_4 . In any case, pegmatites probably were emplaced in several episodes after F_4 , but at least in part prior to the widespread development of epidote alteration. Some of the quartz veins probably were formed after the pegmatites in an environment of waning metamorphism.

These events are summarized in a diagram (fig. 78) similar to that of figure 24 but which includes the intrusive and alteration events. The age relations shown are only relative, and radiometric geochronology is discussed in a later section. Furthermore, there are uncertainties in some of the age relations such as that between the Rana Quartz

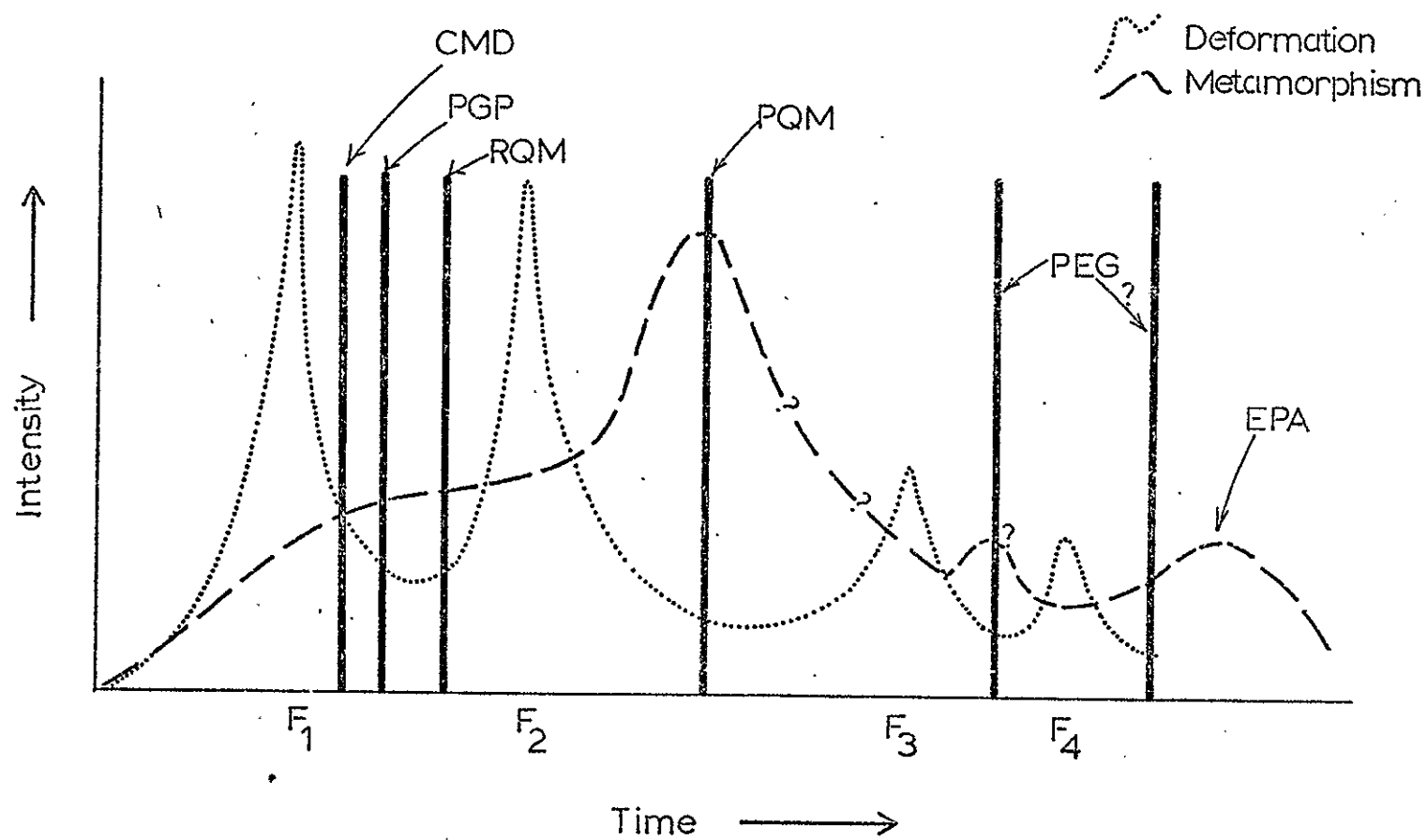


Figure 78. Diagram summarizing relative ages of deformation, metamorphism and magmatism in the Dixon-Peñasco area.

V. SPECIAL STUDIES OF THE GRANITIC ROCKS

Introductory Statement

The specific questions posed in the introduction clearly could not all be answered by field and petrographic analyses, particularly in view of the unexpected complexity of the field area. As a result, several special studies of the granitic rocks were undertaken: (1) a petrochemical investigation of the granites, (2) determination of composition of feldspars with the electron microprobe, (3) determination of the structural state of feldspars, (4) a study of specific late-stage and metamorphic reactions in the granites, (5) a study of barium zoning in K-feldspar megacrysts from the granitic rocks, including determination of the distribution coefficient for barium between K-feldspar and a granitic melt, and (6) a review and reinterpretation of the radiometric geochronology of the area.

Petrochemistry

Major Element Data

Chemical analyses of 68 samples of the granitic rocks, including felsites and aplites from the granitic terrane, are reported in Appendix III. The analyses are for major elements plus barium, rubidium, strontium, and zirconium. The purposes were mainly (1) to generally characterize the granitic rocks, (2) to determine the extent of differentiation within each granitic unit, (3) to determine trace-element

distribution in these rocks, specifically to see if trace-element behavior could be attributed to differentiation, to late-stage effects, or to metamorphism, (4) to distinguish possible origins for the border-zone rocks of the Rana Quartz Monzonite and the Puntiaquito Granite Porphyry, (5) to determine if the isolated southeasternmost outcrops of Puntiaquito Granite Porphyry are in fact chemically similar to the main body of Puntiaquito Granite Porphyry, and (6) to characterize the felsite dikes chemically in an attempt to ascertain whether they are more closely associated with the Cerro Alto Metadacite, the Puntiaquito Granite Porphyry, or the Rana Quartz Monzonite.

Figures 79 to 98 depict the major-element chemistry of the granitic rocks on five commonly used triangular diagrams. Considering these for each of the major units, it becomes clear that all show differentiation to varying degrees. The Cerro Alto Metadacite, for example, shows a wide range of compositions compared to the fairly tight clustering for the Puntiaquito Granite Porphyry and Rana Quartz Monzonite. In general, the Cerro Alto Metadacite has a compositional range that overlaps those of the other units. It seems reasonable that fractionation between a silicate liquid and plagioclase and quartz could have produced the observed distribution, i.e. it does not seem necessary to call on alteration subsequent to initial crystallization. In contrast, the felsites are characterized by wide scatter in their major-element chemistry and by a lack of specific trends. Only the border-zone rocks of the Rana Quartz Monzonite show a similar tendency for scattering, and even they are not as variable as the felsites. Yet the general composition of the felsites, particularly as plotted in figure 79, suggests that at least some of them are genetically

Symbols Used

Figures 79 to 105

- + Cerro Alto Metadacite
- Puntigudo Granite Porphyry (main body)
- ▣ Puntigudo Granite Porphyry (altered)
- Puntigudo Granite Porphyry (border zone)
- ▤ Puntigudo Granite Porphyry (marginal aplite)
- ⬡ Felsite
- Rana Quartz Monzonite (unfoliated)
- ◐ Rana Quartz Monzonite (foliated)
- Rana Quartz Monzonite (border zone)
- ⊕ Rana Quartz Monzonite (altered)
- ⊖ Rana Quartz Monzonite (aplite)
- ▲ Peñasco Quartz Monzonite
- △ Peñasco Quartz Monzonite (aplite)
- ◇ Pegmatite

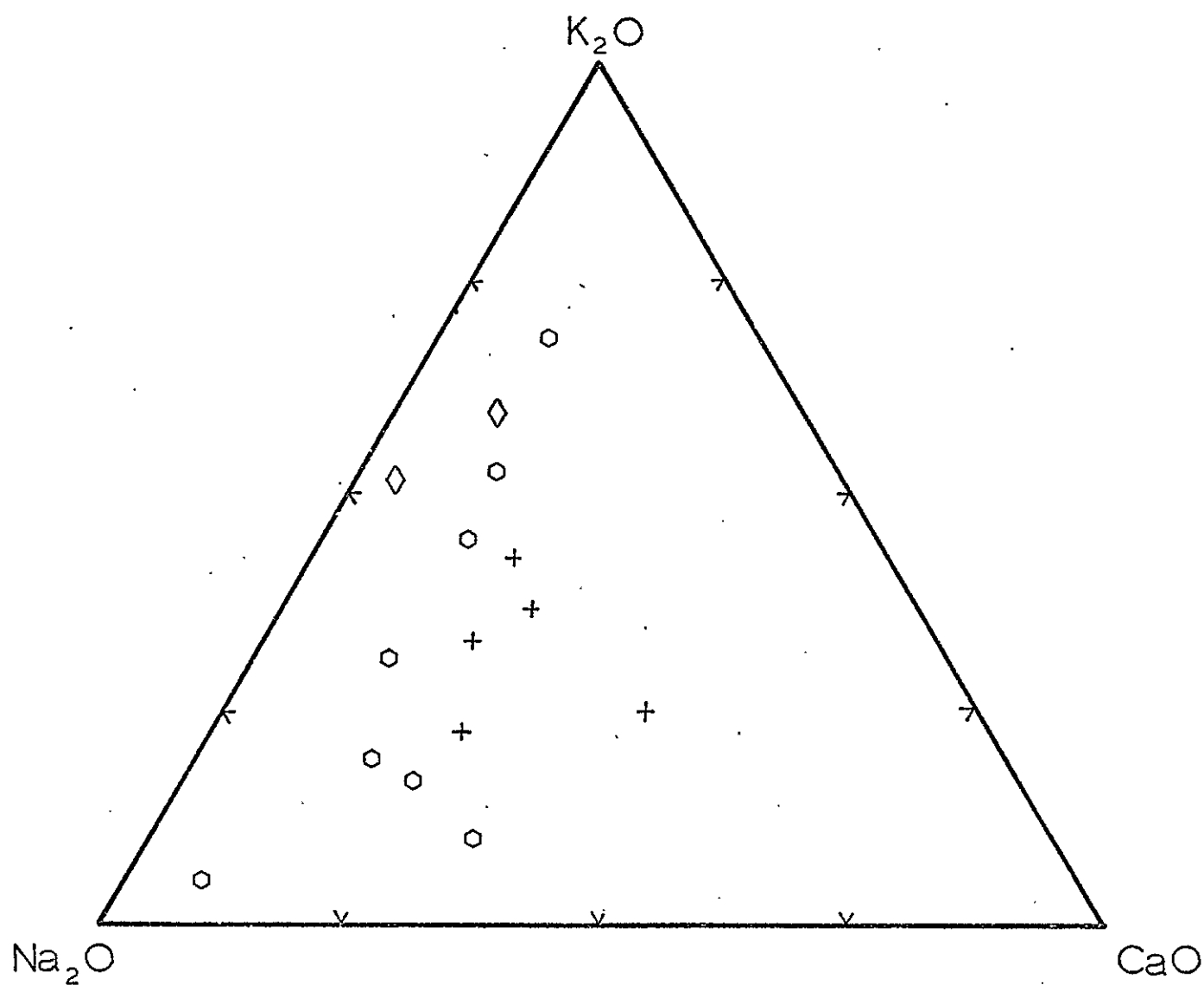


Figure 79. Na_2O - K_2O - CaO triangular diagram for felsite, Cerro Alto Metadacite, and pegmatites.

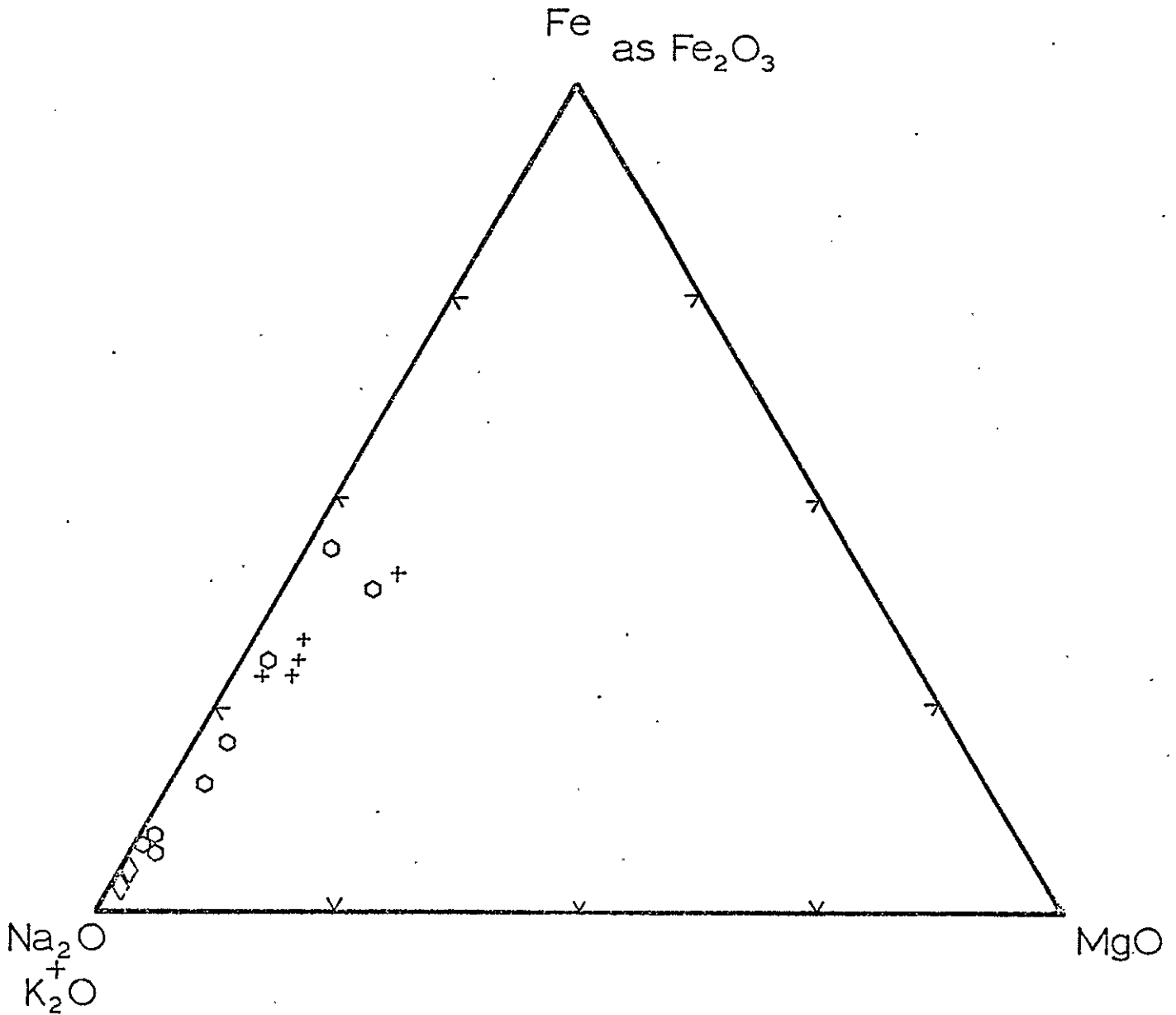


Figure 80. $(\text{Na}_2\text{O} + \text{K}_2\text{O})$ -Fe as Fe_2O_3 -MgO triangular diagram for felsite, Cerro Alto Metadacite, and pegmatites.

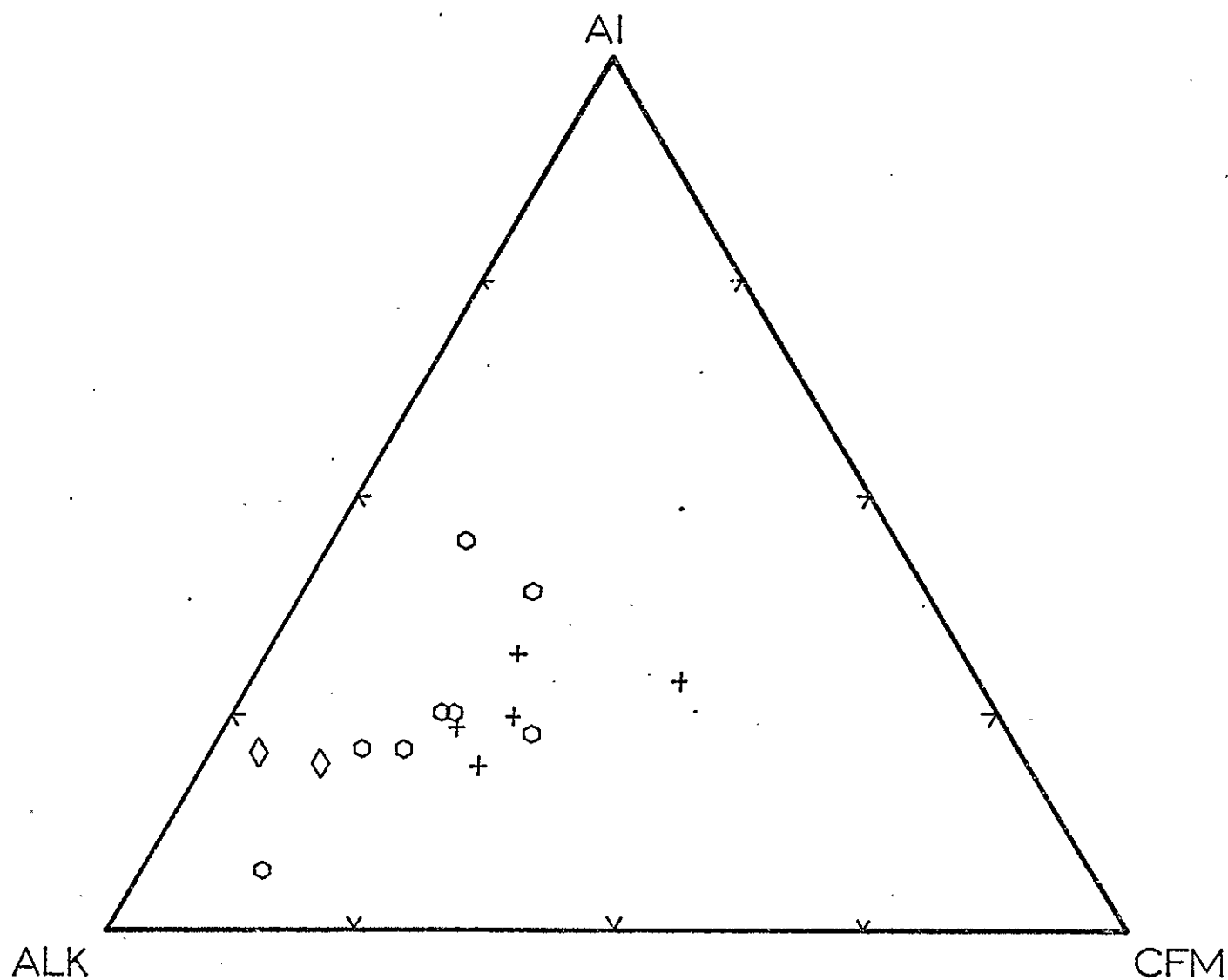


Figure 81. ALK-Al-CFM triangular diagram for felsite, Cerro Alto Metadacite, and pegmatites.

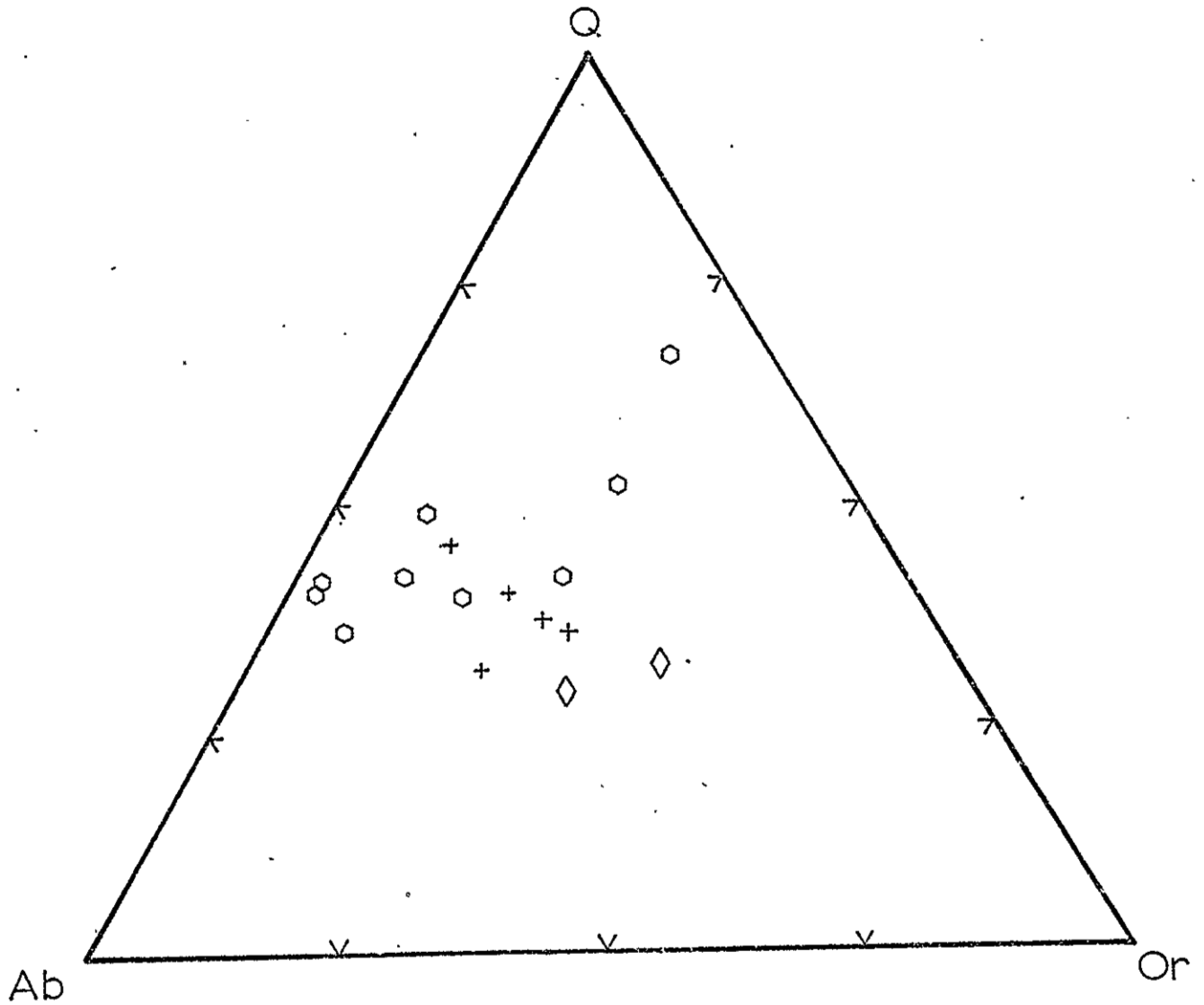


Figure 82. Ab-Or-Q triangular diagram for felsite, Cerro Alto Metadacite, and pegmatites.

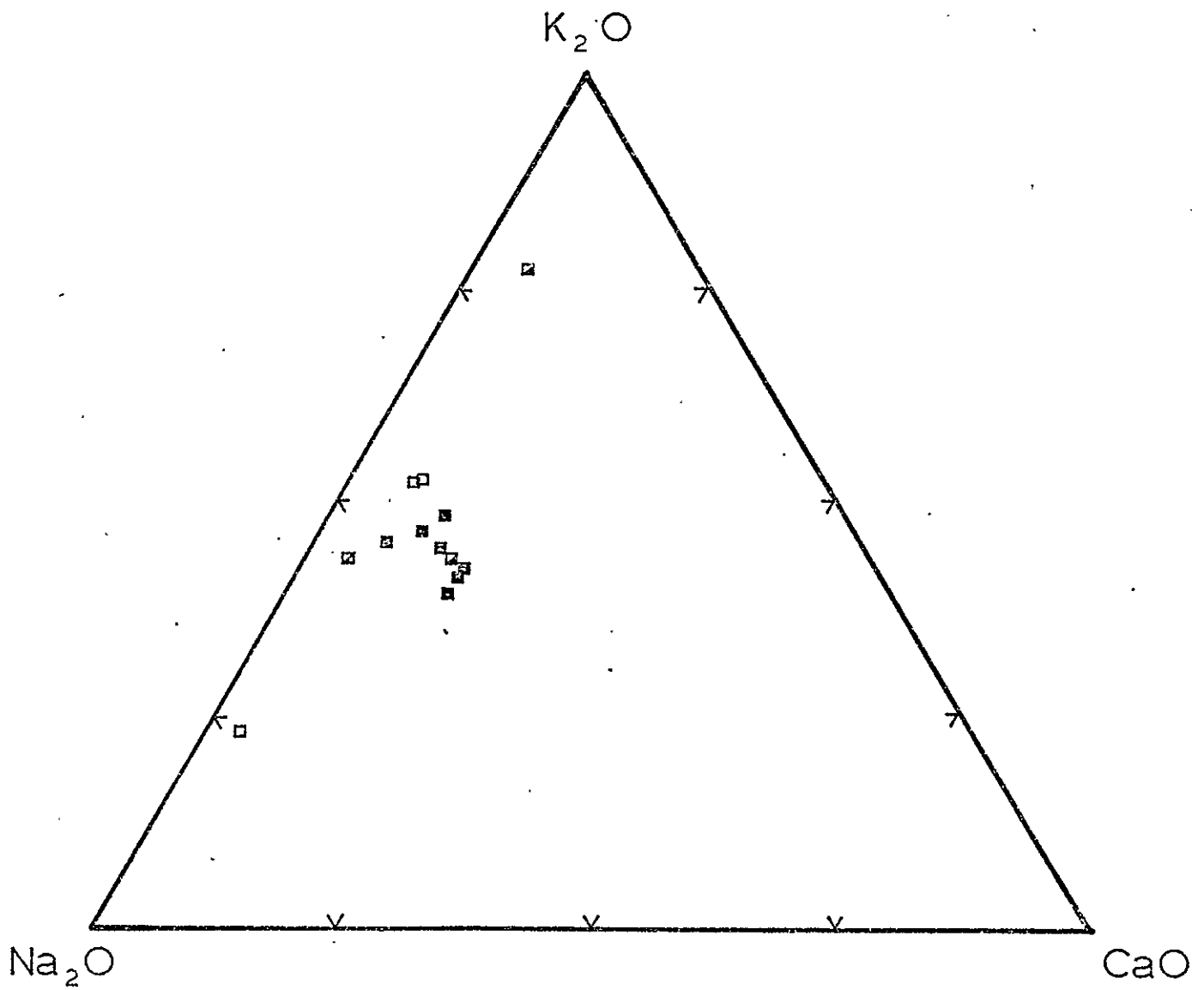


Figure 84. Na_2O - K_2O - CaO triangular diagram for Puntigudo Granite Porphyry.

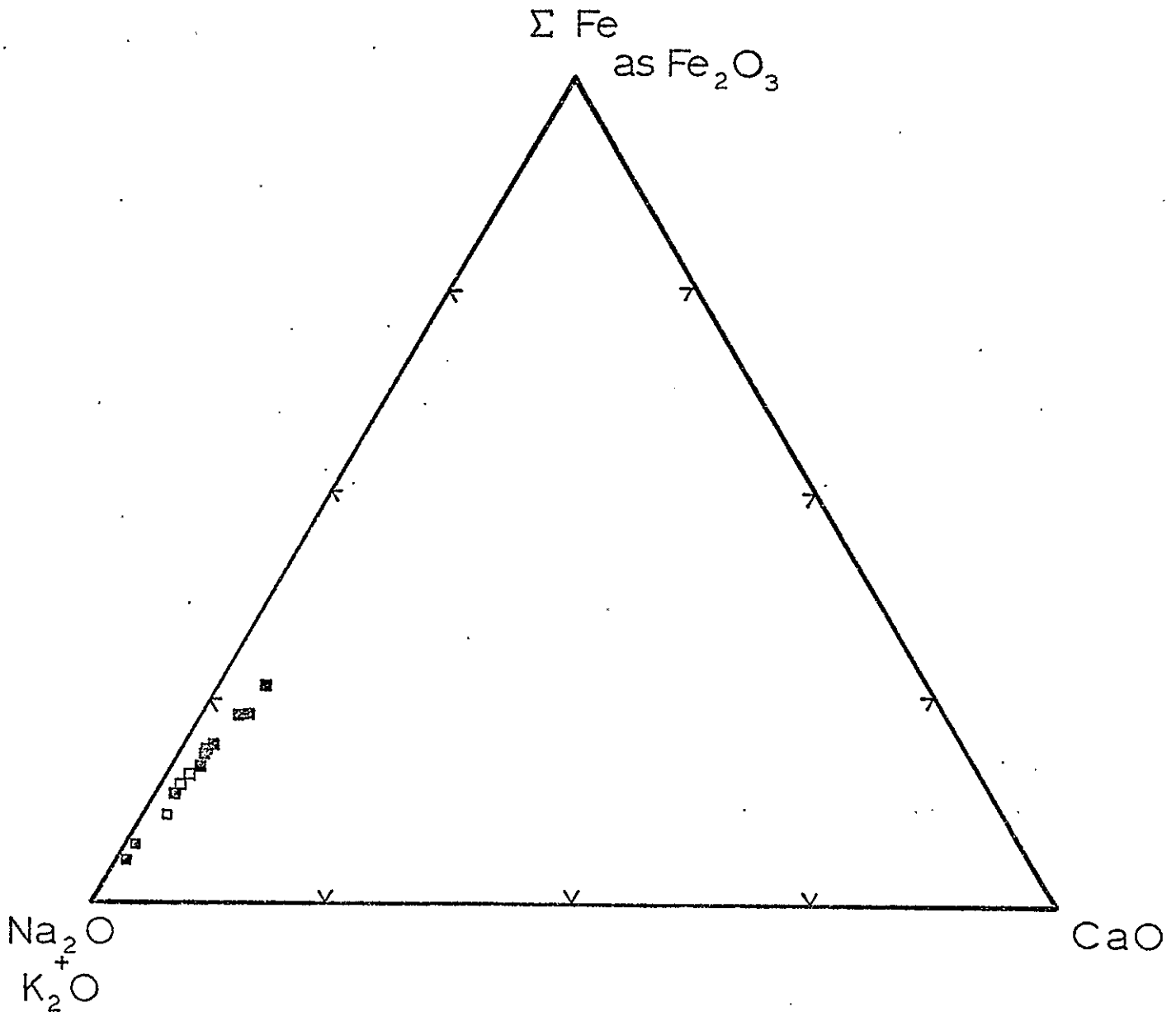


Figure 85. $(\text{Na}_2\text{O}+\text{K}_2\text{O})$ -Fe as Fe_2O_3 -MgO triangular diagram for Puntigudo Granite Porphyry.

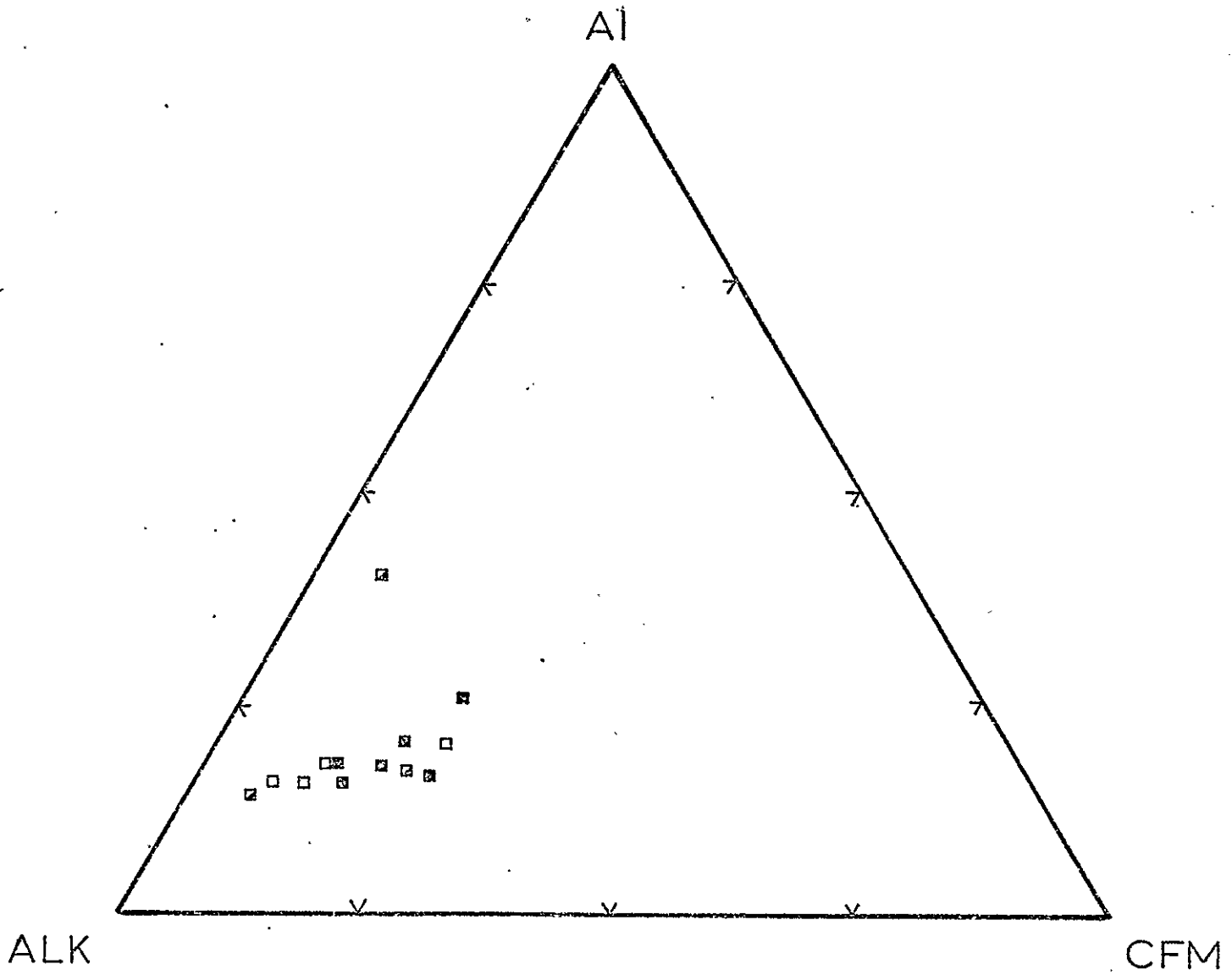


Figure 86. ALK-AI-CFM triangular diagram for Puntigado Granite Porphyry.

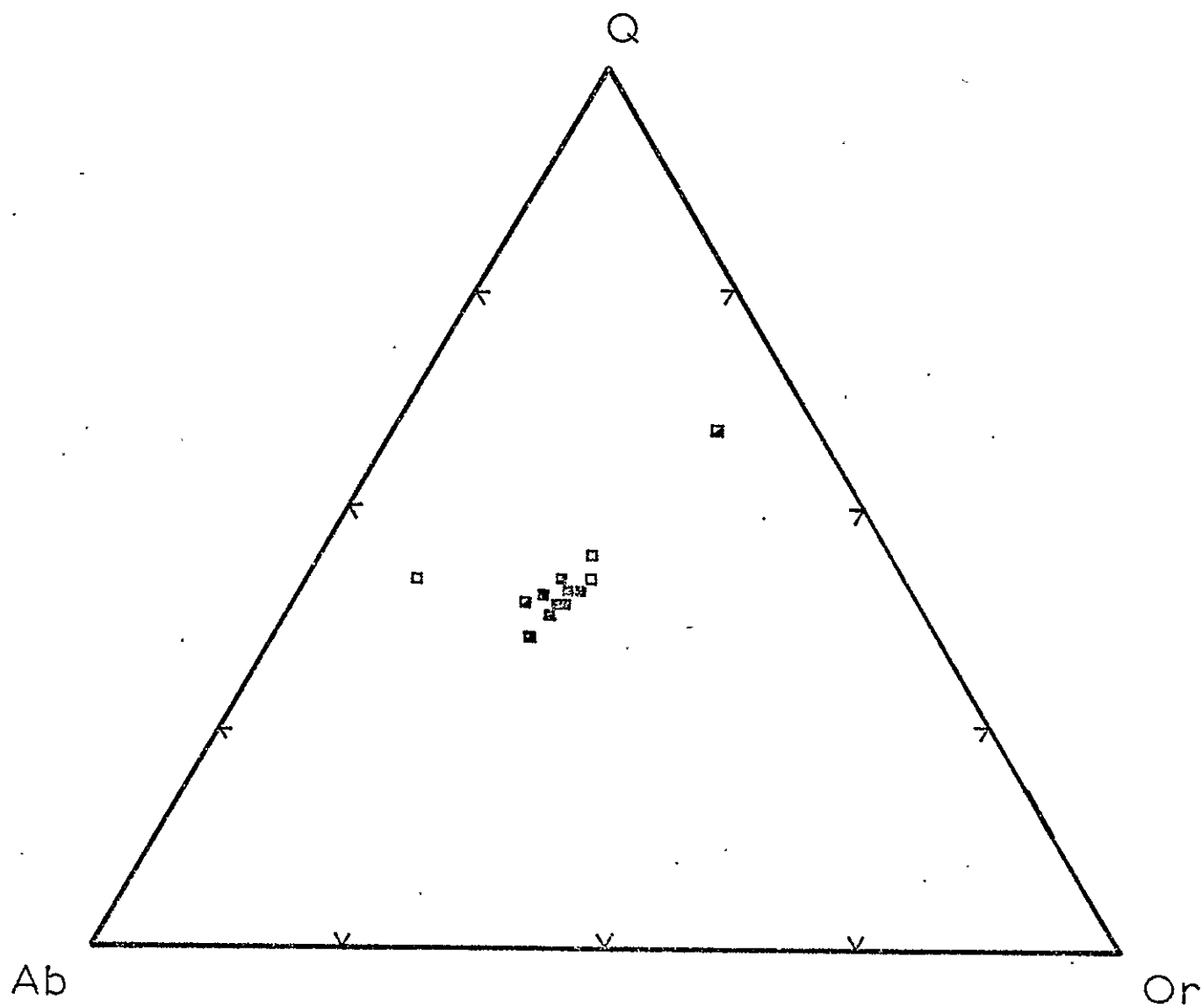


Figure 87. Ab-Or-Q triangular diagram for Puntigudo Granite Porphyry.

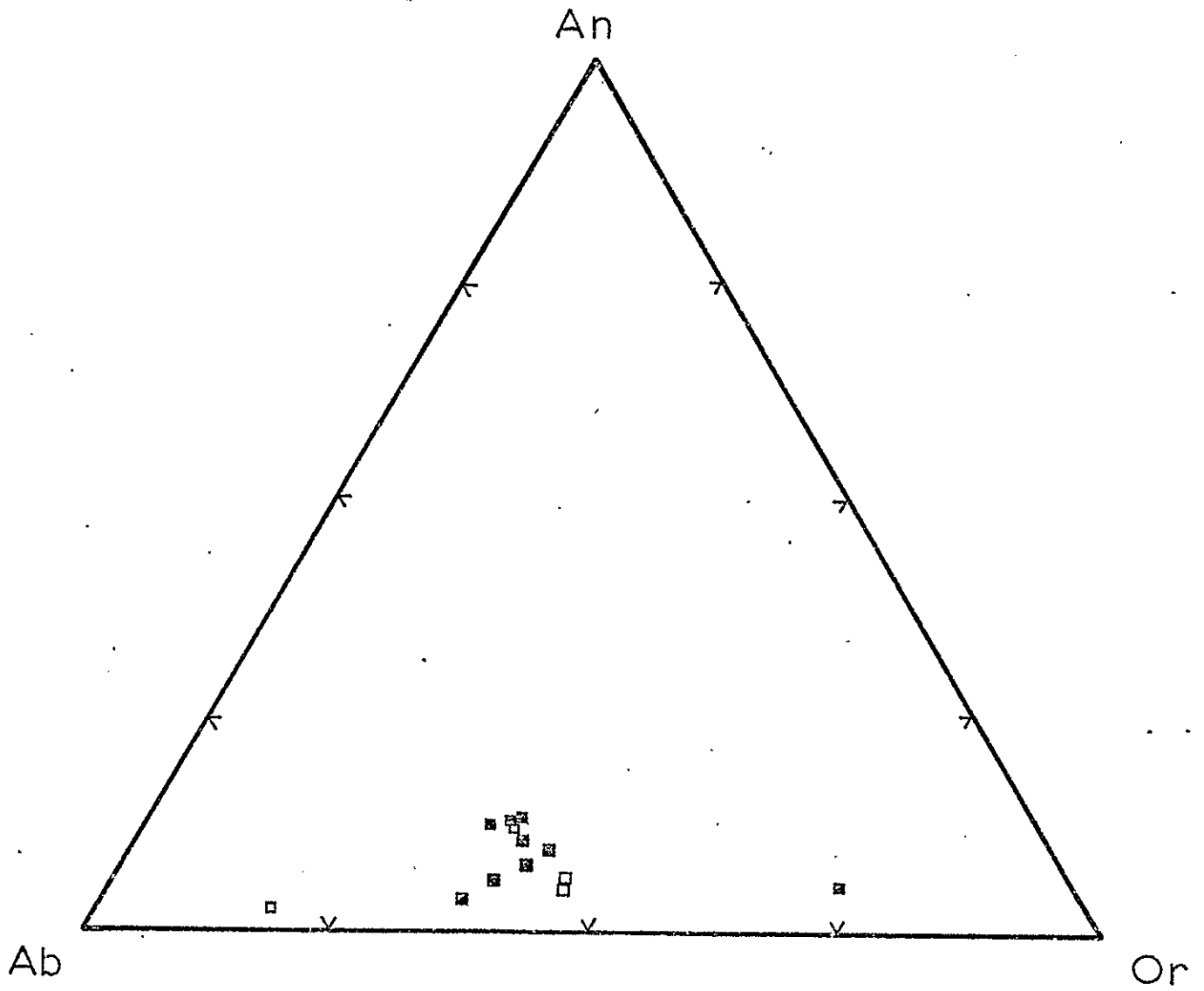


Figure 88. Ab-An-Or triangular diagram for Puntigado Granite Porphyry.

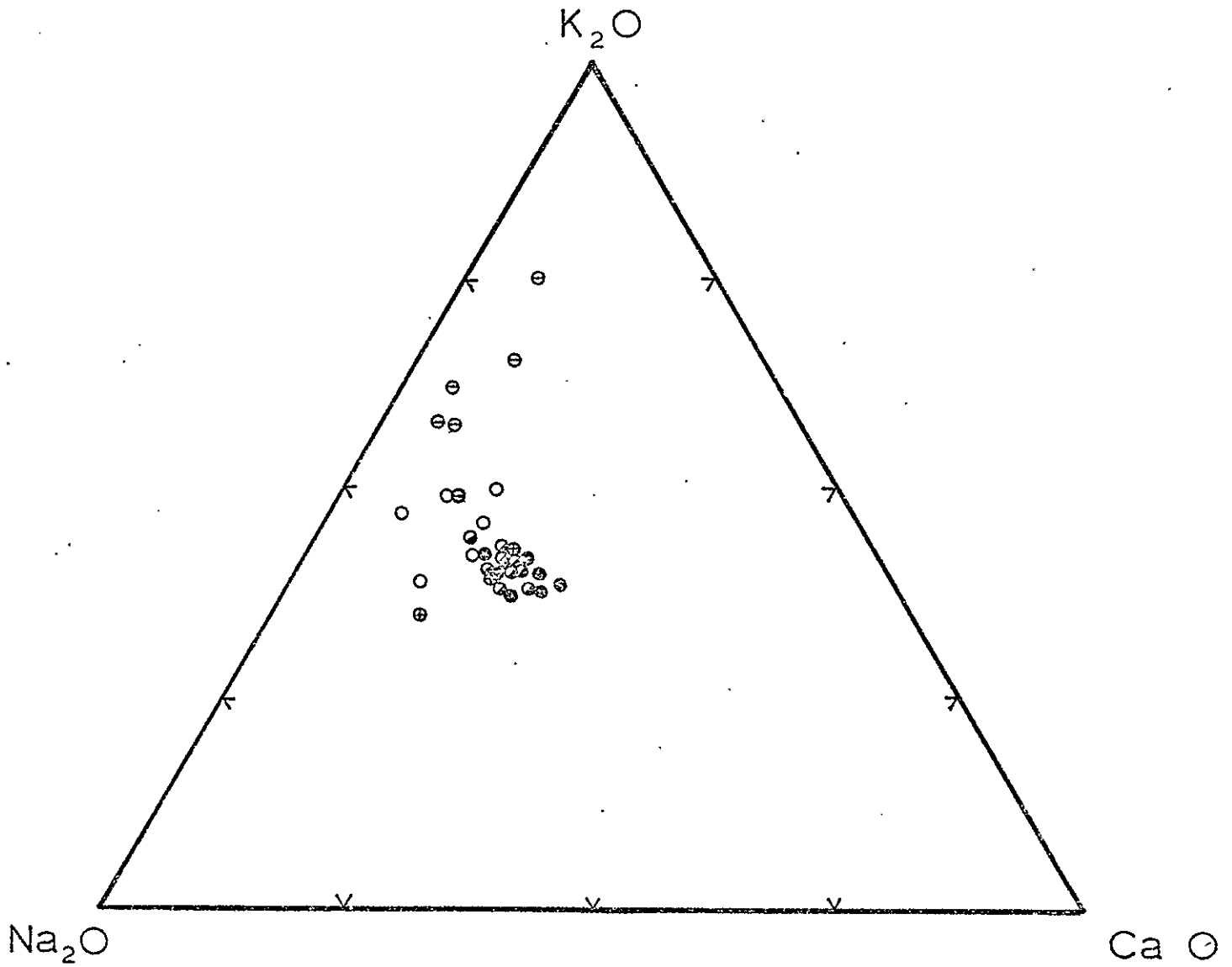


Figure 89. Na_2O - K_2O - CaO triangular diagram for Rana Quartz Monzonite.

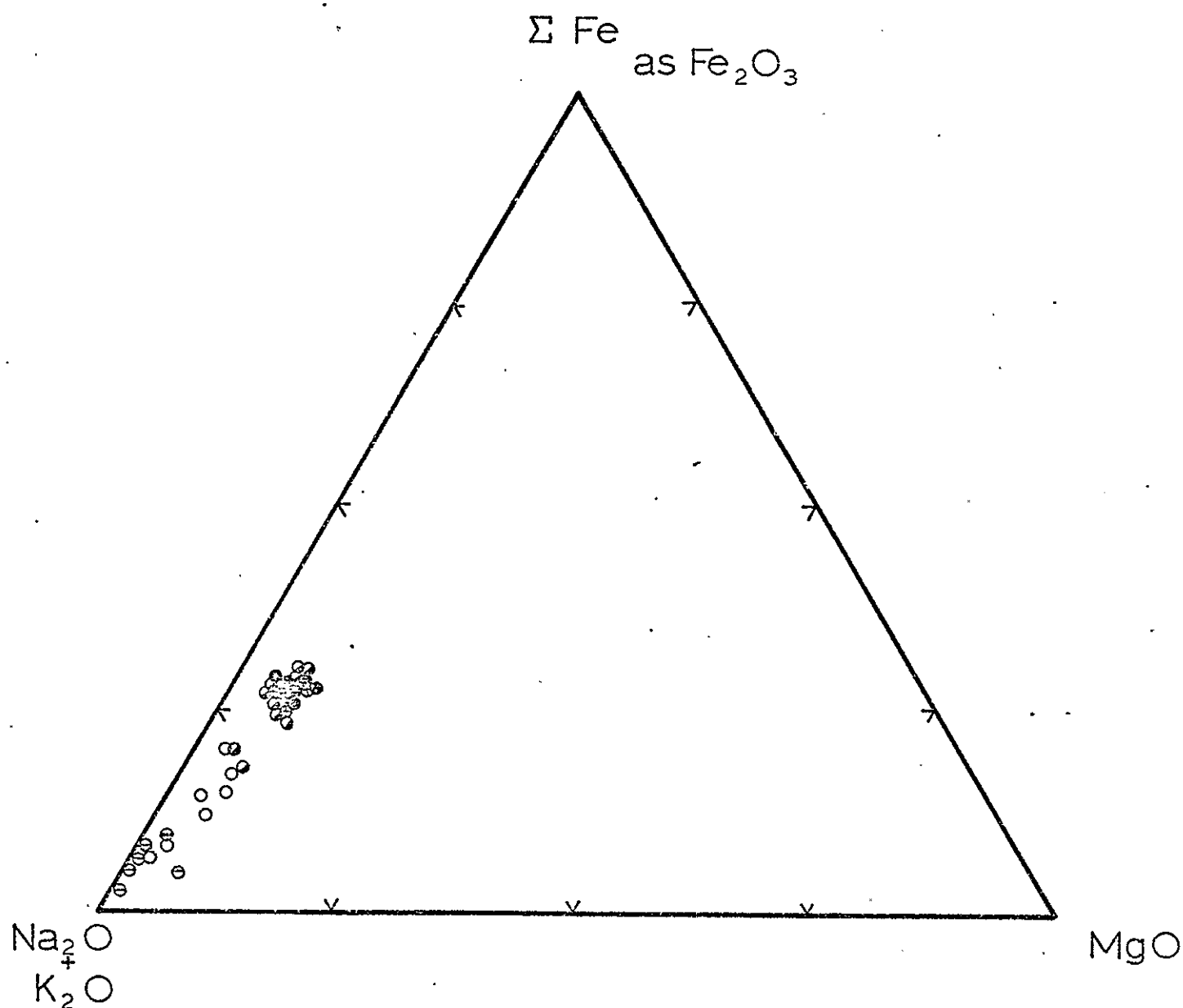


Figure 90. $(\text{Na}_2\text{O} + \text{K}_2\text{O})$ -Fe as Fe_2O_3 -MgO triangular diagram for Rana Quartz Monzonite.

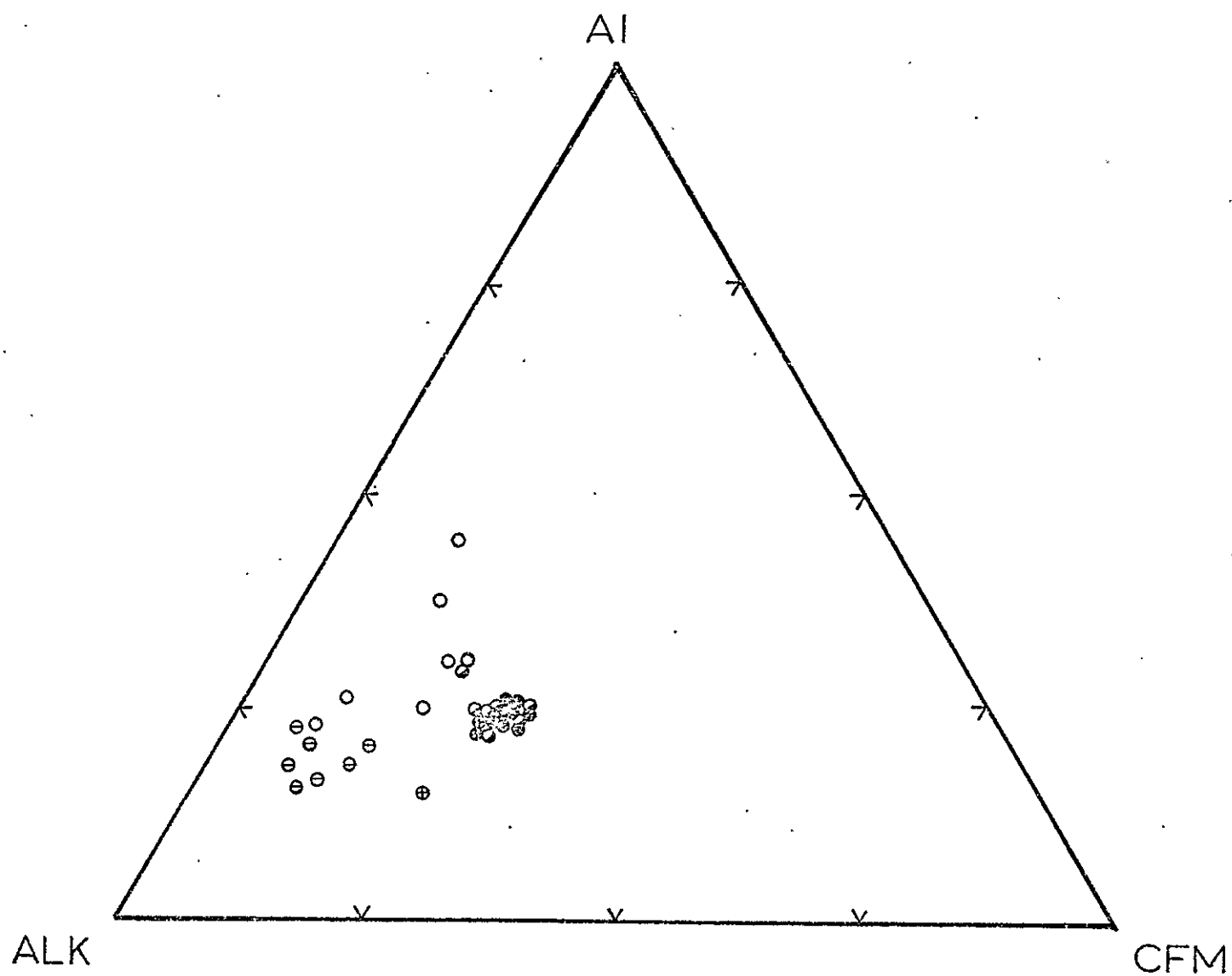


Figure 91. ALK-Al-CFM triangular diagram for Rana Quartz Monzonite.

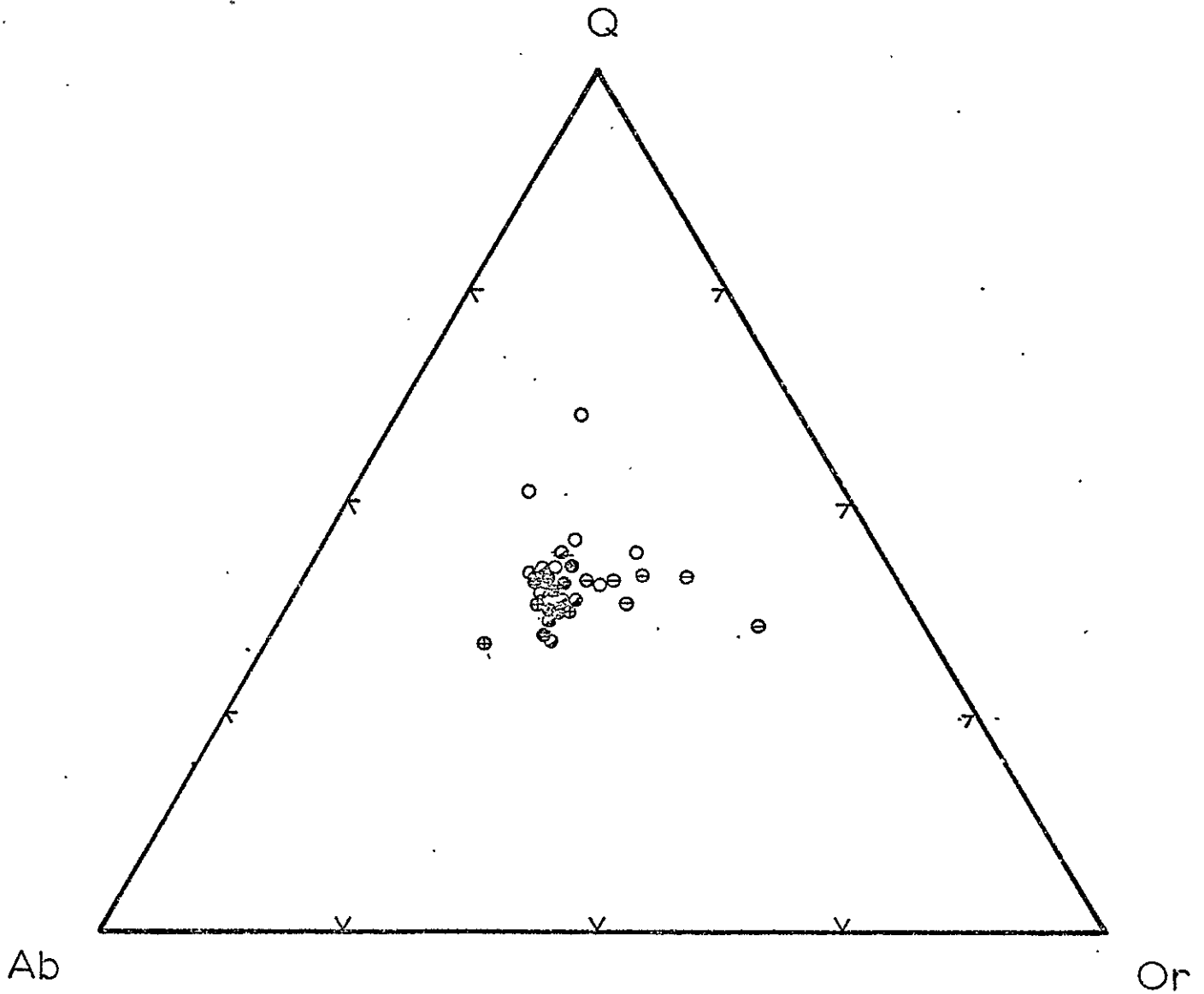


Figure 92. Ab-Or-Q triangular diagram for Rana Quartz Monzonite.

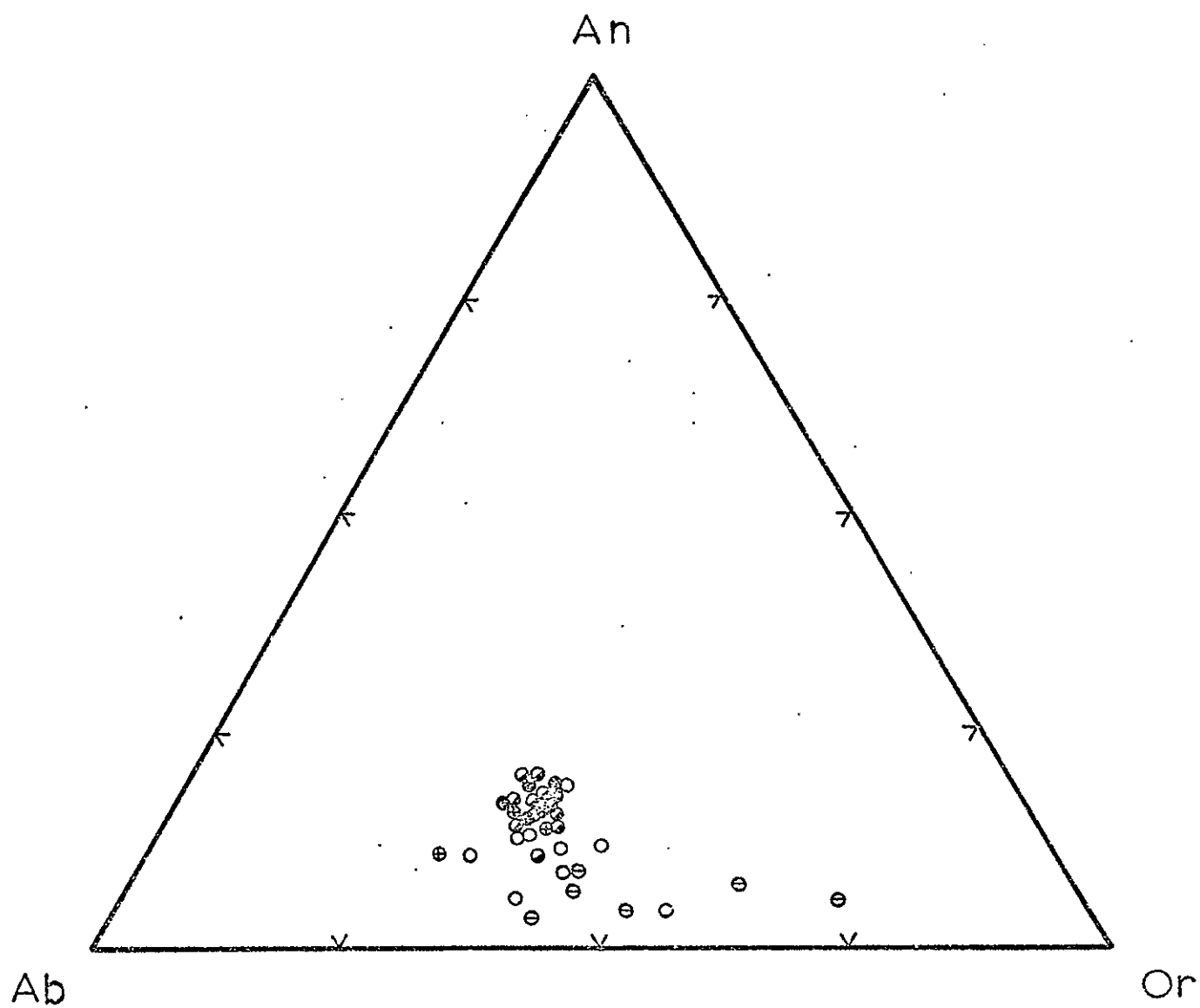


Figure 93. Ab-An-Or triangular diagram for Rana Quartz Monzonite.

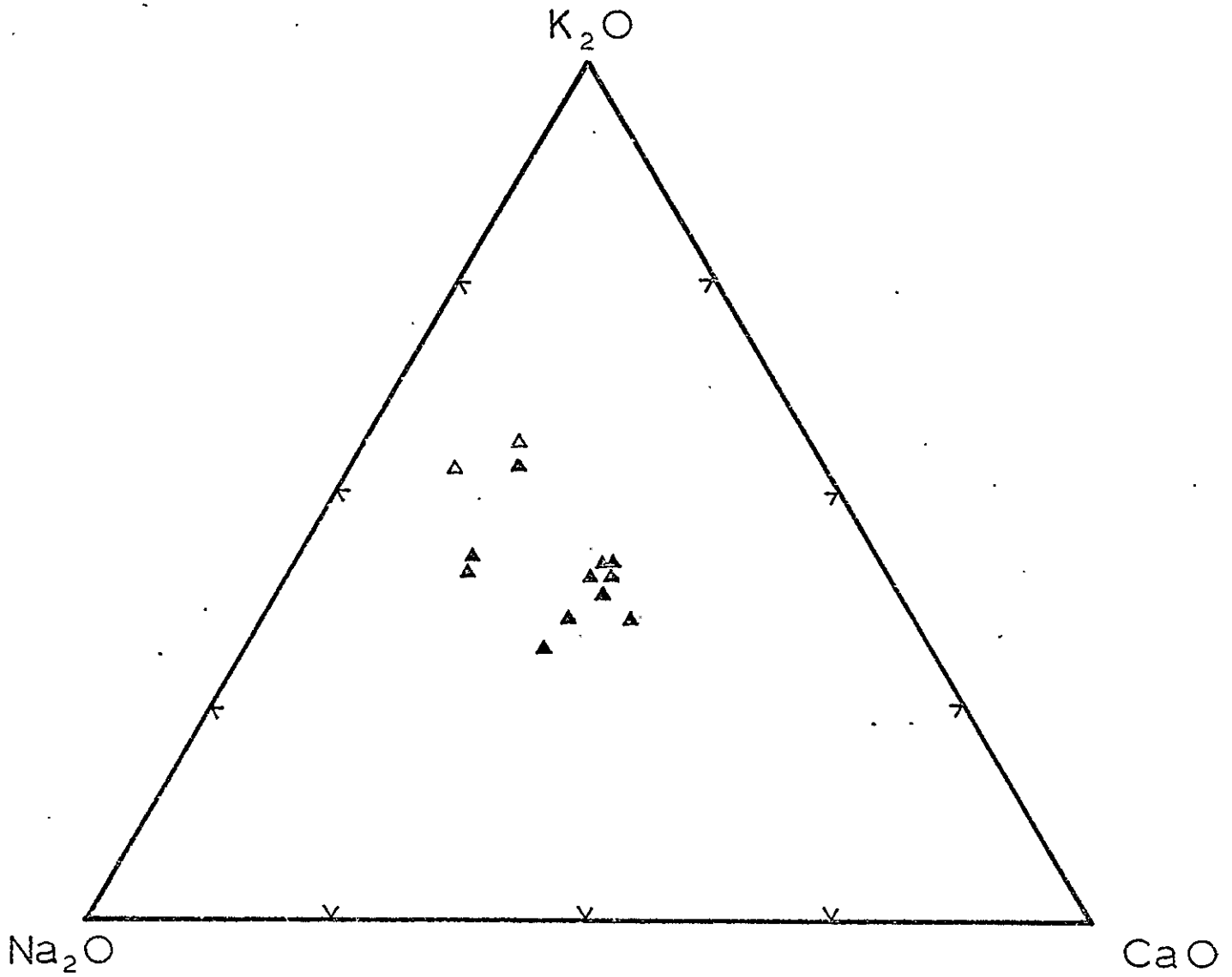


Figure 94. Na₂O-K₂O-CaO triangular diagram for Peñasco Quartz Monzonite.

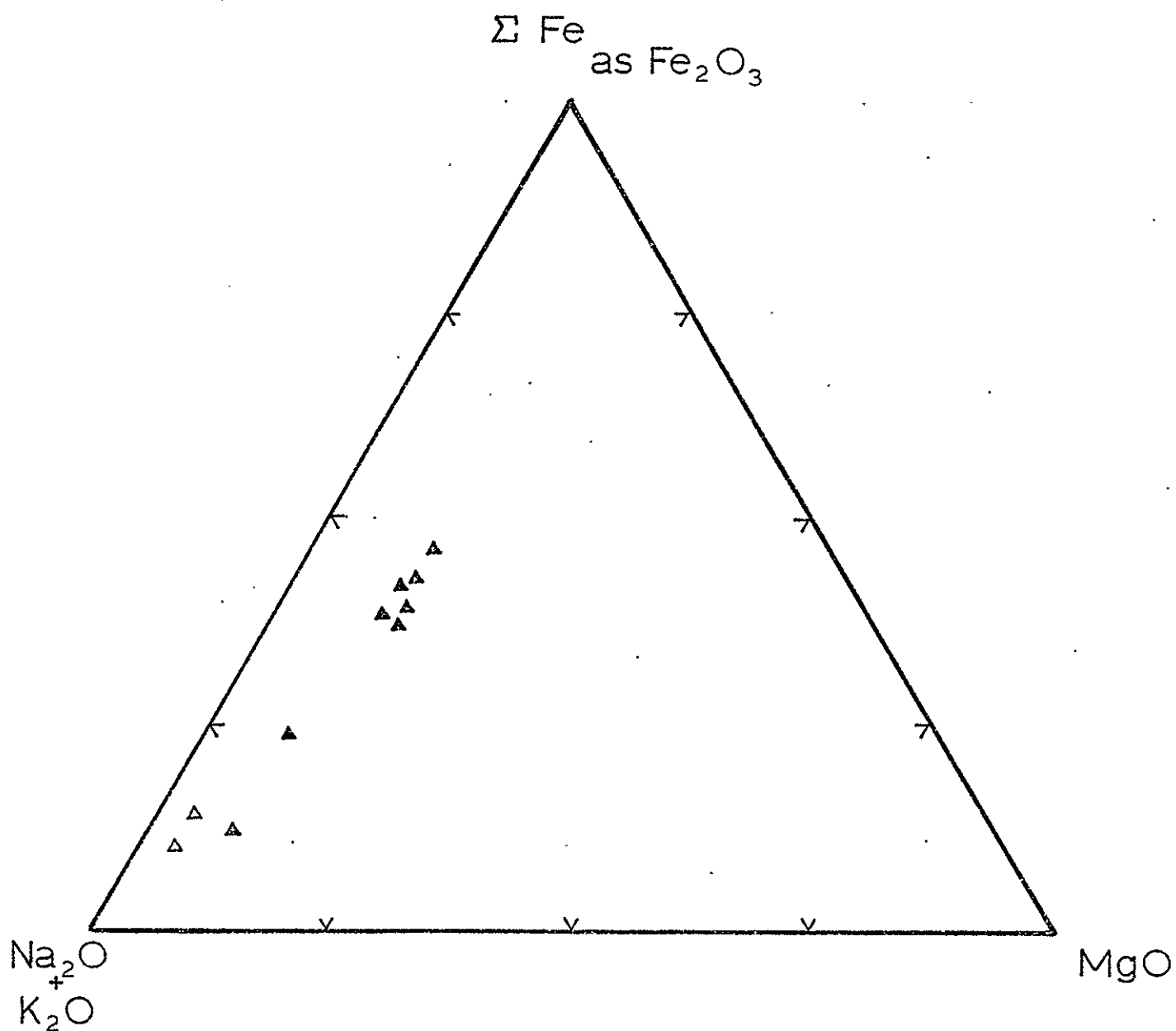


Figure 95. $(\text{Na}_2\text{O} + \text{K}_2\text{O})$ -Fe as Fe_2O_3 -MgO triangular diagram for Peñasco Quartz Monzonite.

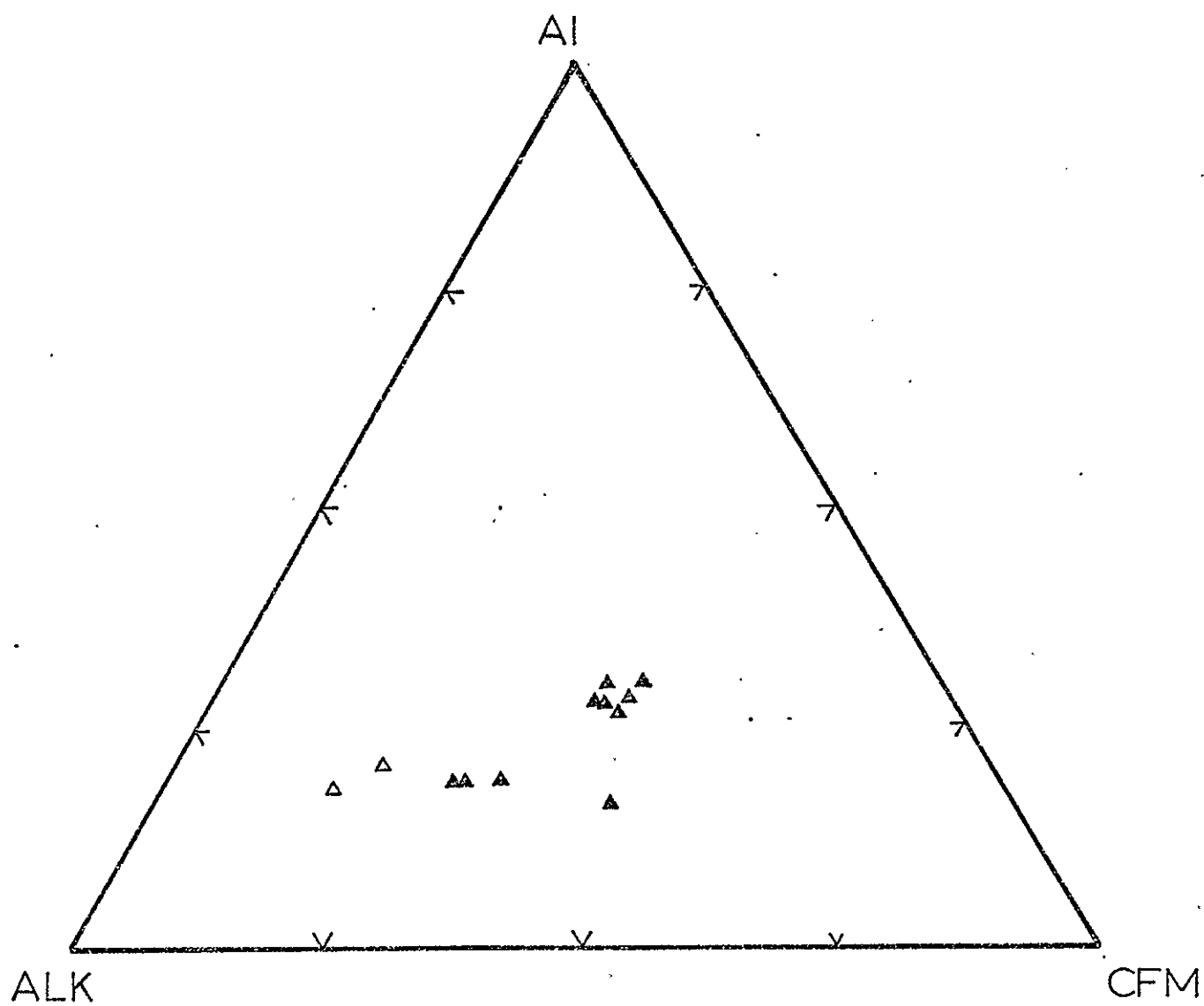


Figure 96. ALK-Al-CFM triangular diagram for Peñasco Quartz Monzonite.

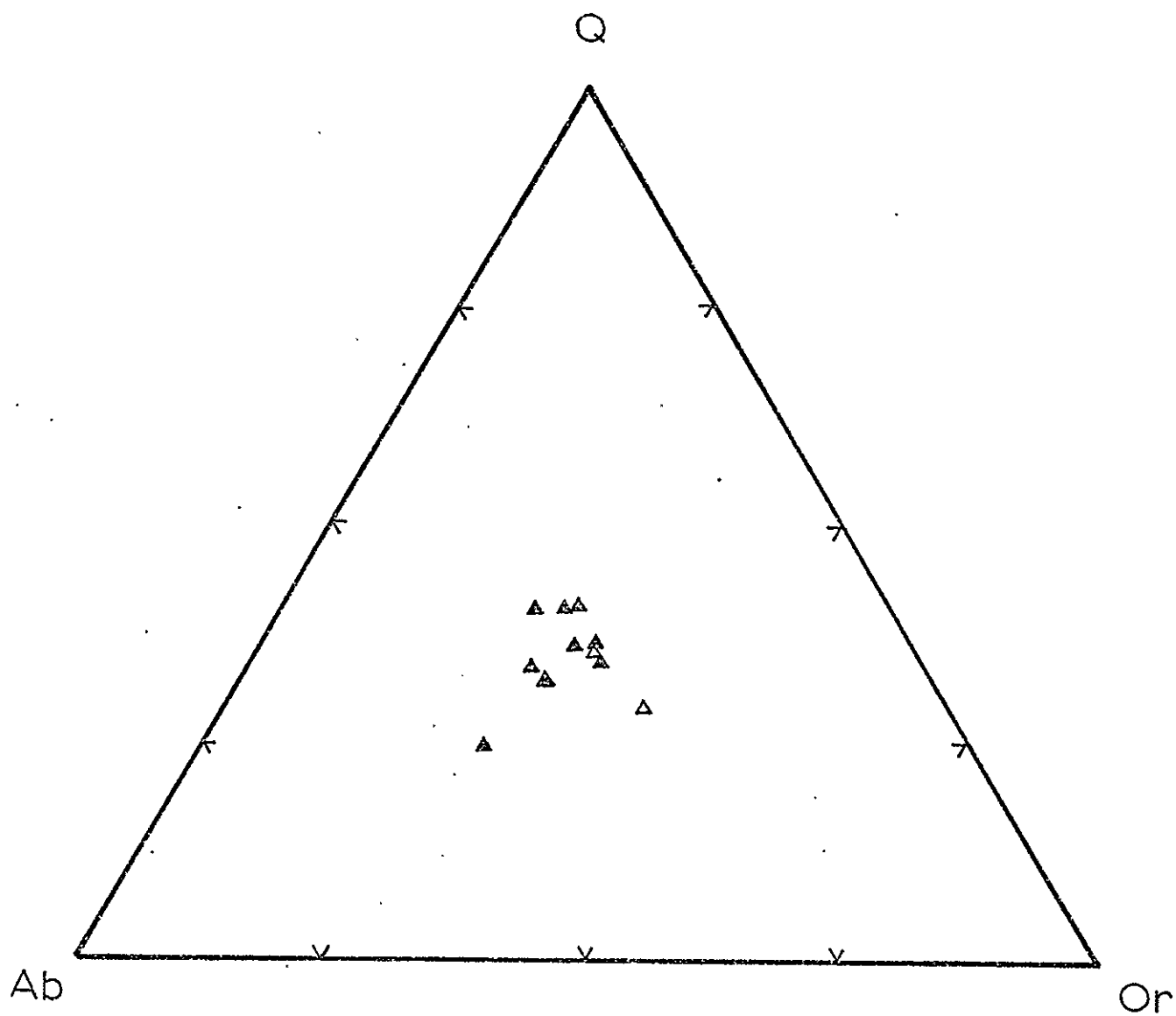


Figure 97. Ab-Or-Q triangular diagram for Peñasco Quartz Monzonite.

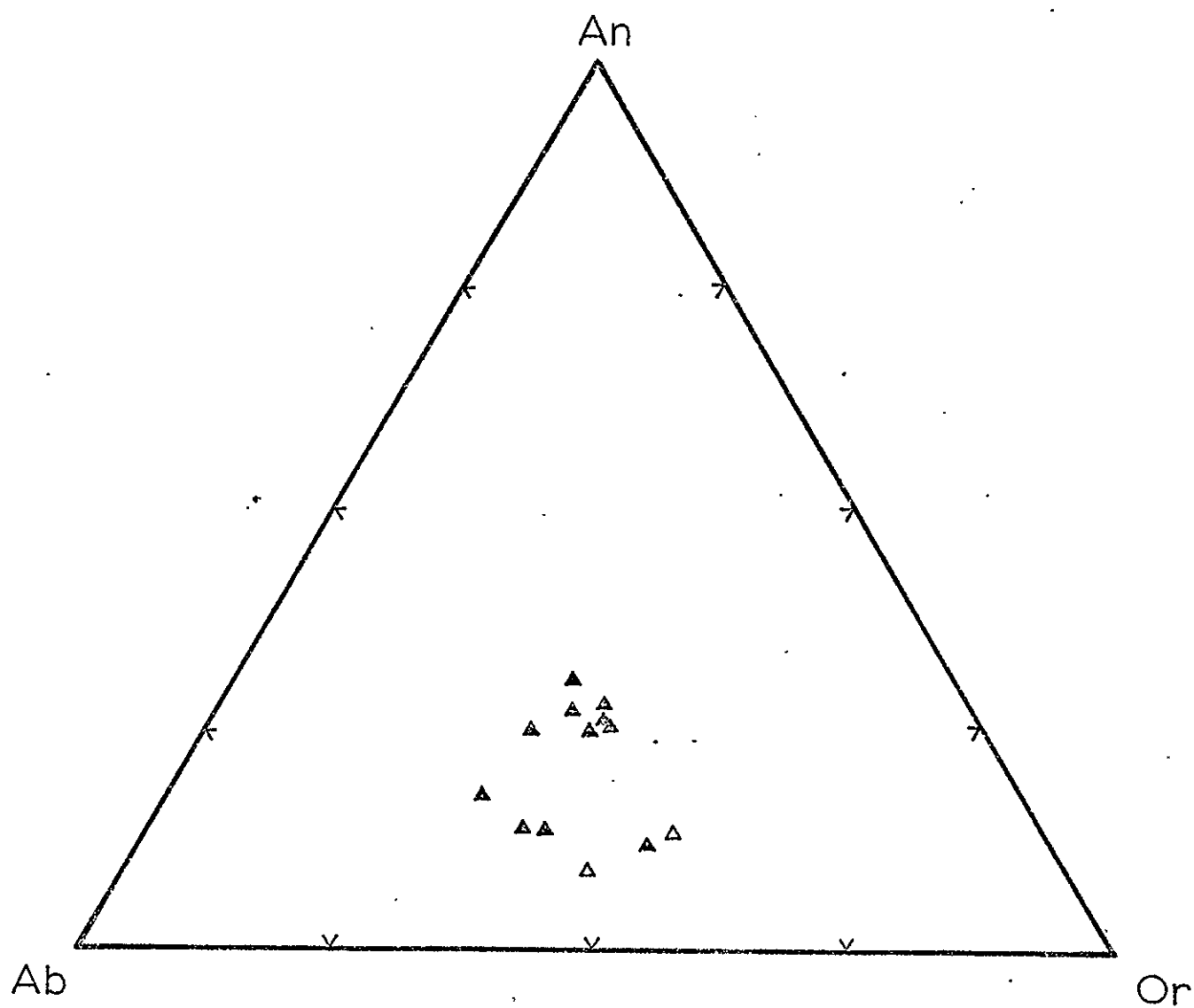


Figure 98. Ab-An-Or triangular diagram for Peñasco Quartz Monzonite.

related. Others may be more closely akin to the Puntiaquedo Granite Porphyry or even the Cerro Alto Metadacite. In short, the major elements do not demand that the felsites be genetically related to the Rana Quartz Monzonite, but a combination of differentiation from early Rana Quartz Monzonite magmas and later metamorphic alteration might well account for the data on bulk composition.

The Puntiaquedo Granite Porphyry shows much more systematic behavior (figs. 84 to 88), with the samples (with few exceptions) defining elongate trends or clusters on the triangular diagrams. These trends partly overlap with those of the Rana Quartz Monzonite but are generally distinct from those of the Peñasco Quartz Monzonite. Of particular interest is the similarity of the two samples from the isolated southern outcrops of Puntiaquedo Granite Porphyry to those of the main mass. On the $AlK-Al-CFM$ and $(Na_2O+K_2O)-Fe_2O_3-MgO$ plots (figs. 85 and 86) they tend to be extremes of a trend, but this is consistent with their being one fraction of an original melt system at depth. The data on bulk chemistry also show that one sample of Puntiaquedo Granite Porphyry, severely altered to a muscovite-quartz-K-feldspar assemblage, has been slightly shifted away from the main grouping toward higher Al_2O_3 and higher normative anorthite, quartz, and albite. Other samples that do not plot with the main grouping are either aplitic rocks or border facies, and these show either an enrichment of K_2O and SiO_2 , or an enrichment of Na_2O and SiO_2 . Either behavior can be explained by the fractionation of plagioclase ^{or} K-feldspar. For example, some of the border-zone facies are enriched in Na_2O and SiO_2 , which could be due either to early accretion of plagioclase and quartz along the margins of the intrusion, or to accumulation of those minerals in the

part of the magma chamber that was intruded first. Residual liquids from such a melt would likely be more K_2O enriched, and such is the case for sample PL73-234 (aplite) which can be ascribed to residual liquids from a more plagioclase-rich sample. Figure 85 shows the definite fractionation with respect to Fe relative to Ca and $Na_2O + K_2O$. This can be attributed in part to fractionation of biotite, but in order to explain the general lack of iron in the border facies of the rocks one must appeal to early crystal accretion along the margins, which may be unlikely in view of its fine grain size, or to a low iron composition of the original melt possibly caused by previous fractionation or low degrees of initial partial melting at depth.

The major-element data for Rana Quartz Monzonite, with the exception of its border zone and its aplites, cluster tightly around mean values and they show the least differentiation of all the granitic units. Still some slight trends are noticeable; e.g. a slight decrease in normative anorthite and a slight increase in quartz relative to mean values is noticeable in some analyses. Two of the three samples of epidote-altered Rana Quartz Monzonite appear unaffected in bulk chemistry, whereas the third may have been shifted slightly toward greater normative albite than the average Rana Quartz Monzonite. The border-zone samples, though, show considerable scatter without any single trend except on the $(Na_2O+K_2O)-Fe_2O_3-MgO$ diagram where they clearly depleted in iron relative to alkalis. The alkali-Al CFM diagram suggests that there may be two trends, one toward alkali enrichment and the other toward aluminum enrichment. When examined in detail the samples with aluminum enrichment prove to be the most muscovitized and deformed of the analyzed samples. These same samples show slight

to great increases in normative quartz over all other Rana samples. They are not the most iron-poor relative to alkalies, a fact which is partly explained by their increased aluminum. These data can be explained if the border zone is assumed to have formed from an initial melt that was generally leucocratic but ranged in iron content toward the composition of the bulk of the Rana Quartz Monzonite. After emplacement and local fractionation this initial melt probably crystallized by rapid cooling and/or pressure relief, and it then was superseded gradually by the main mass of Rana Quartz Monzonite. As the main mass was intruded, it also altered portions of the border zone along shear zones and other permeable places, removing some of the alkalies and possibly some of the mafic constituents. An alternative hypothesis would be that the border zone is a quenched version of the Rana Quartz Monzonite and that alteration alone produced alkali enrichment in some areas and a complementary aluminum enrichment in others, with mobile mafic constituents being partially removed. This is attractive except for the difficulty in disposing of the mafic constituents. Still another possibility is that the border zone was more leucocratic initially and the alkali-aluminum compositional changes were caused by alteration. The major-element data alone are apparently insufficient to distinguish the above possibilities.

The major-element chemistry of the Rana Quartz Monzonite aplites shows a marked trend toward increased K_2O and decreased CaO , accompanied by a slight decrease in normative quartz relative to $Ab + Or$. The AFM diagram, though, shows the aplites as being definitely poorer in Fe_2O_3 relative to alkalies than the main Rana rocks. This suggests that the aplites represent distinct late-stage fractionation as opposed

to continuous formation during crystallization of the main mass. The general trends observed are consistent with a dominant early crystallization of plagioclase, quartz, and biotite.

The Peñasco Quartz Monzonite rocks are compositionally distinct from the other granitic rocks in the area, as is clear from figures 94 to 98. Although the number of analyzed samples of this unit is small, the data suggest trends toward increasing alkalies (initially sodium then potassium) and decreasing iron, magnesium, and calcium accompanied by slight decreases in normative quartz. These trends would be consistent with early fractionation of anorthite-rich plagioclase and biotite, and possibly hornblende. The increased potassium in the aplite samples would suggest that they could have formed from residual liquids formed from rocks crystallizing along these trends. These data do not, however, give any particular suggestion as to the possible importance of contamination relative to fractionation in these rocks.

Trace Elements

The trace-element data for the samples discussed above are plotted in figures 99 to 105. These plots show that each of the granitic rock types has a distinct or nearly distinct trace-element chemistry, which is consistent with their representing separate episodes of magmatism. The Rana Quartz Monzonite and the Puntiaquedo Granite Porphyry are most similar in their trace-element concentrations, as shown by the slight overlap in their plotted ranges (figs. 99 to 105). This may allow a genetic relationship between the two rock units, but strong textural differences and some distinctions in details of trace-element fractionation suggest otherwise. For example, a plot of Rb/Sr versus differentia-

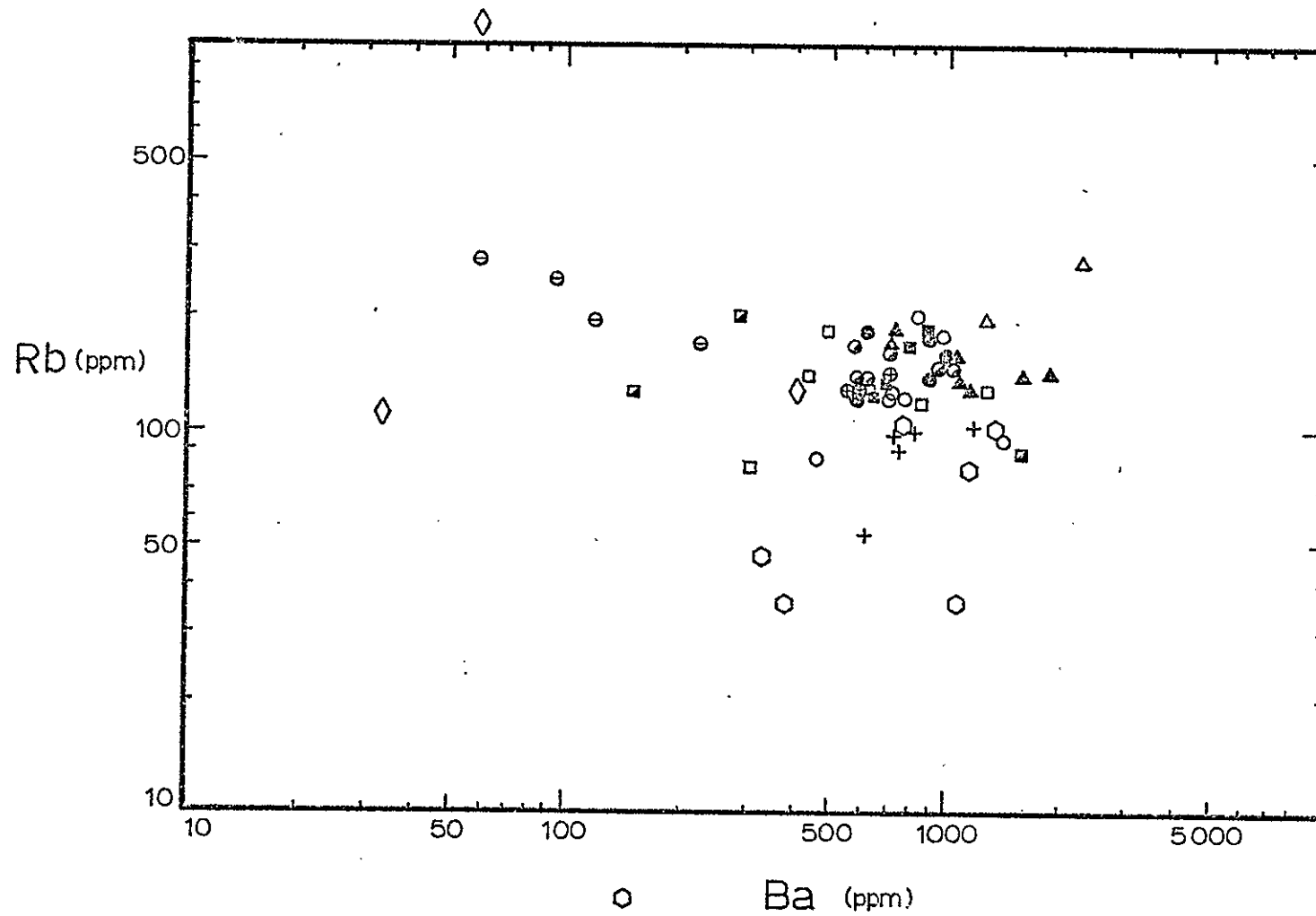


Figure 99. A plot of Sr against Ba for the granitic rocks. Symbols used in figures 99 to 105 are given on page .

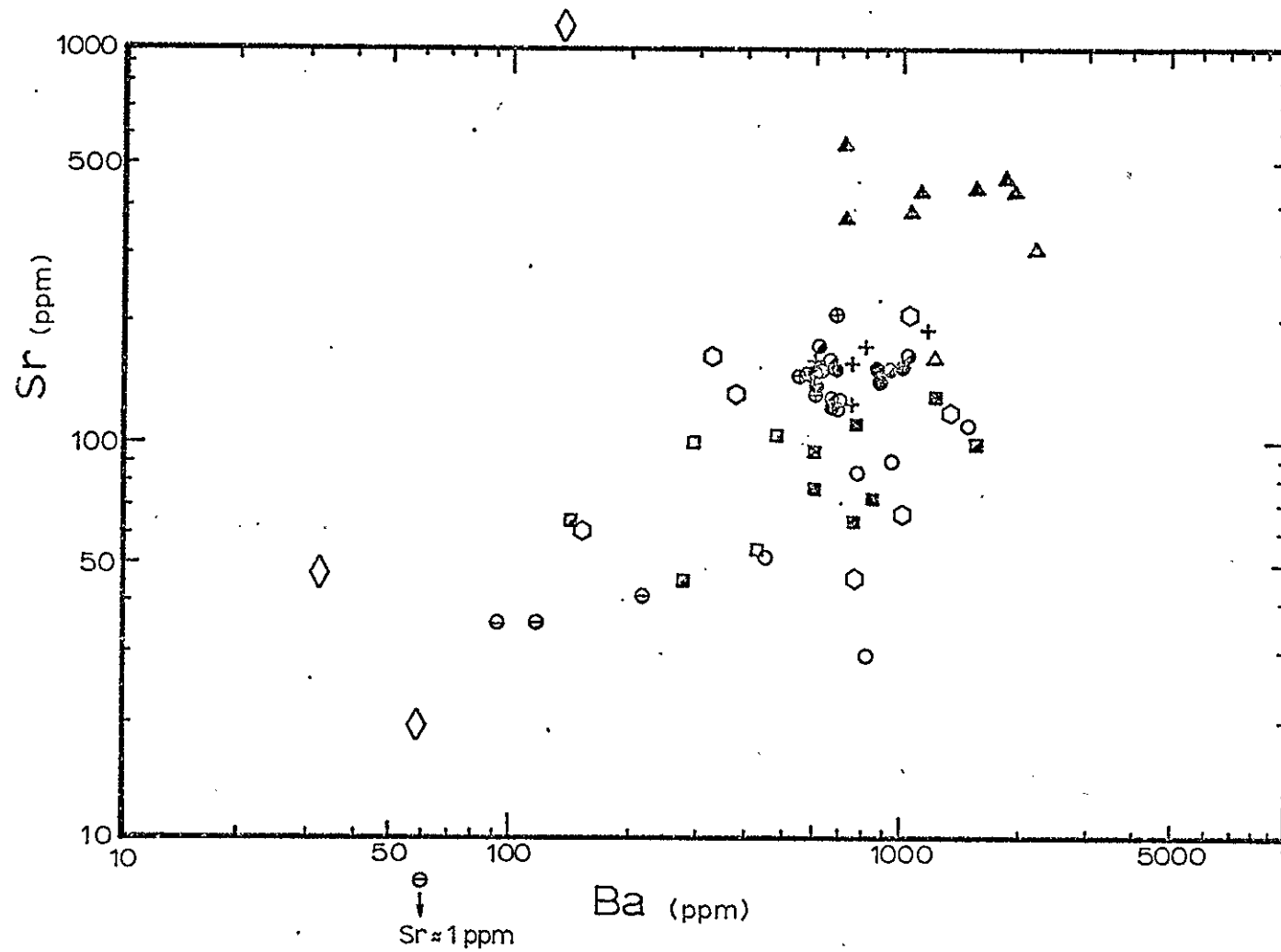


Figure 100. A plot of Rb against Ba for the granitic rocks.

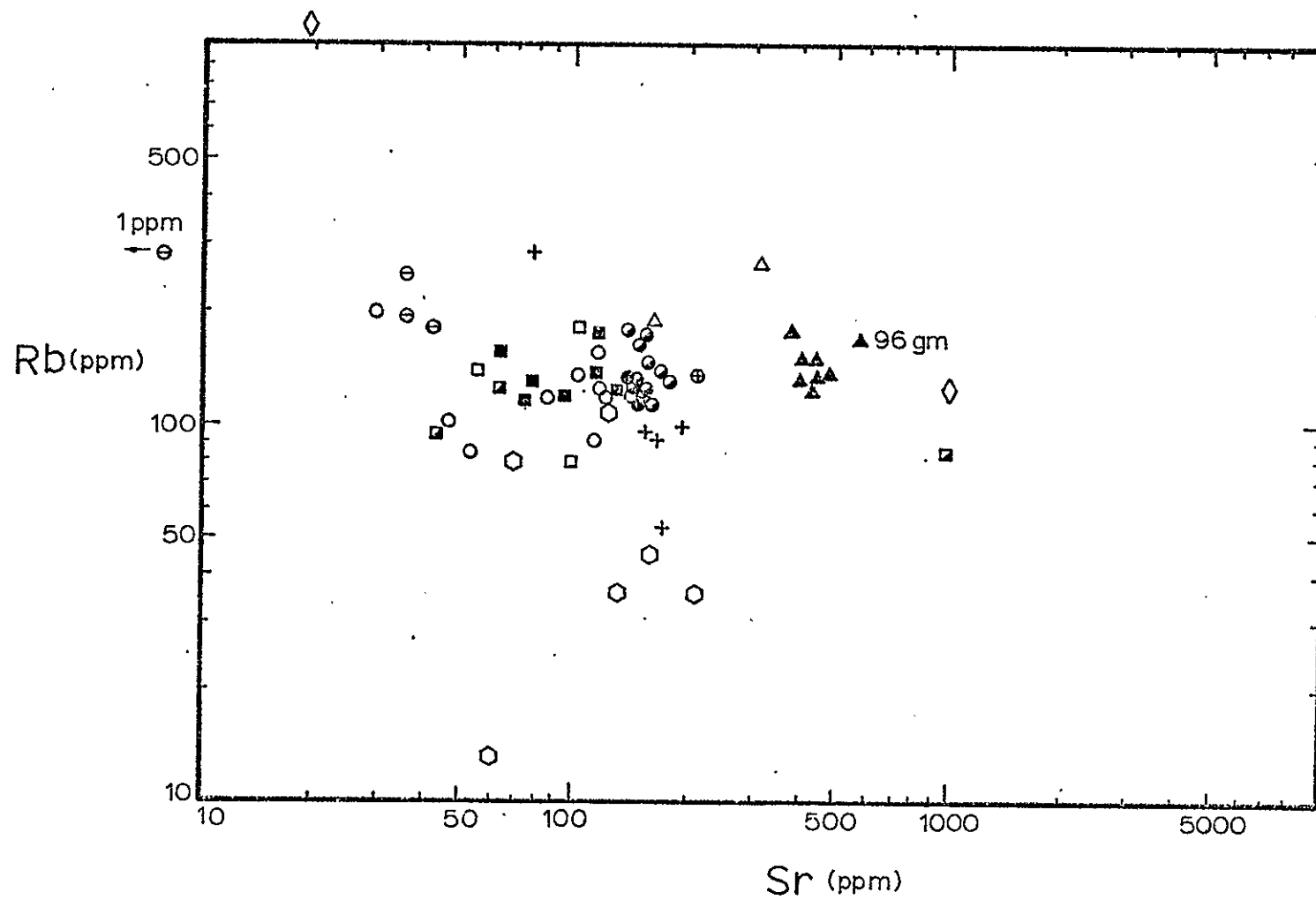


Figure 101. A plot of Rb against Sr for the granitic rocks.

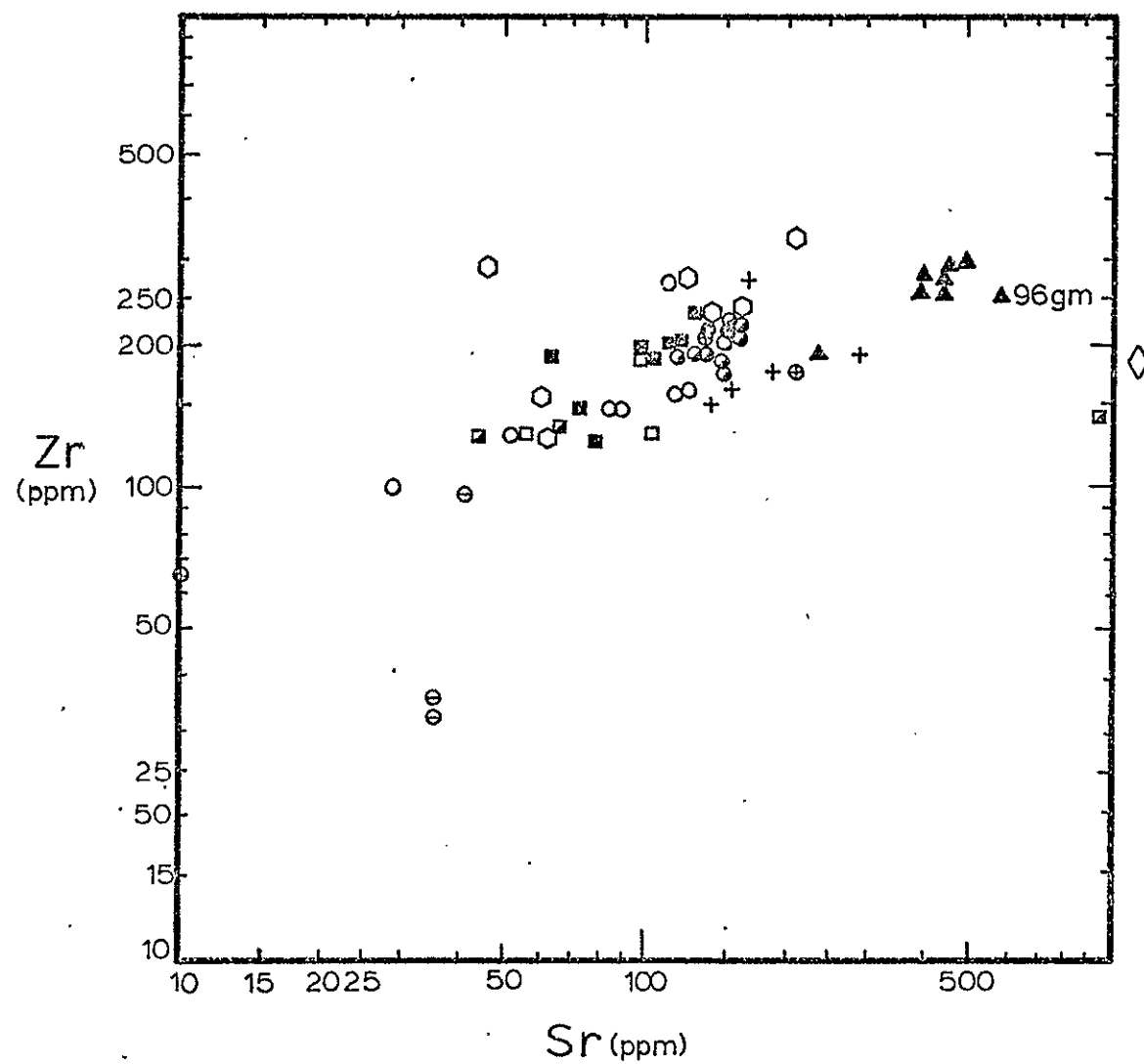


Figure 102. A plot of Zr against Sr for the granitic rocks.

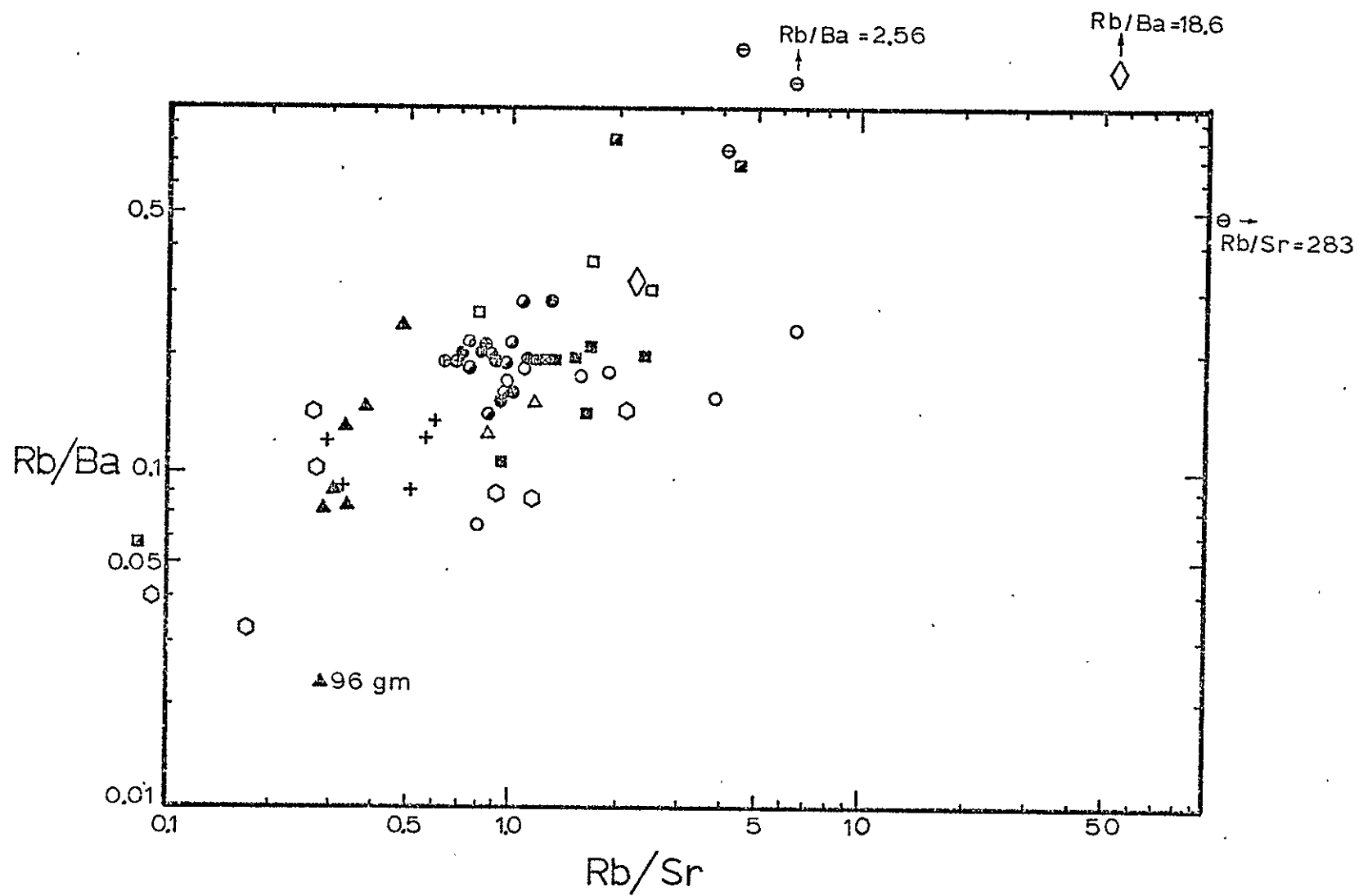


Figure 103. A plot of Rb/Ba against Rb/Sr for the granitic rocks.

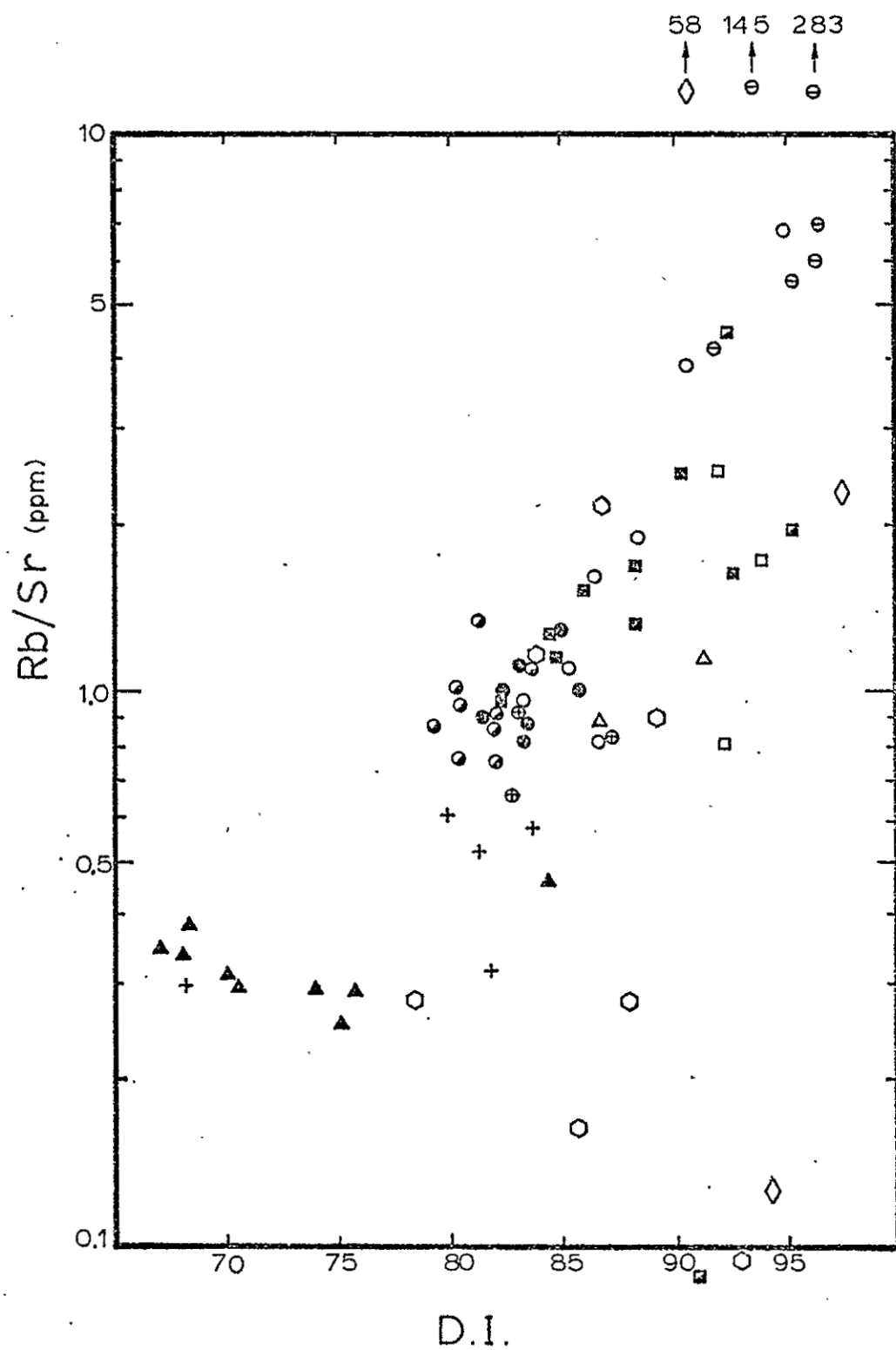


Figure 104. A plot of Rb/Sr against D.I. (differentiation index) for the granitic rocks.

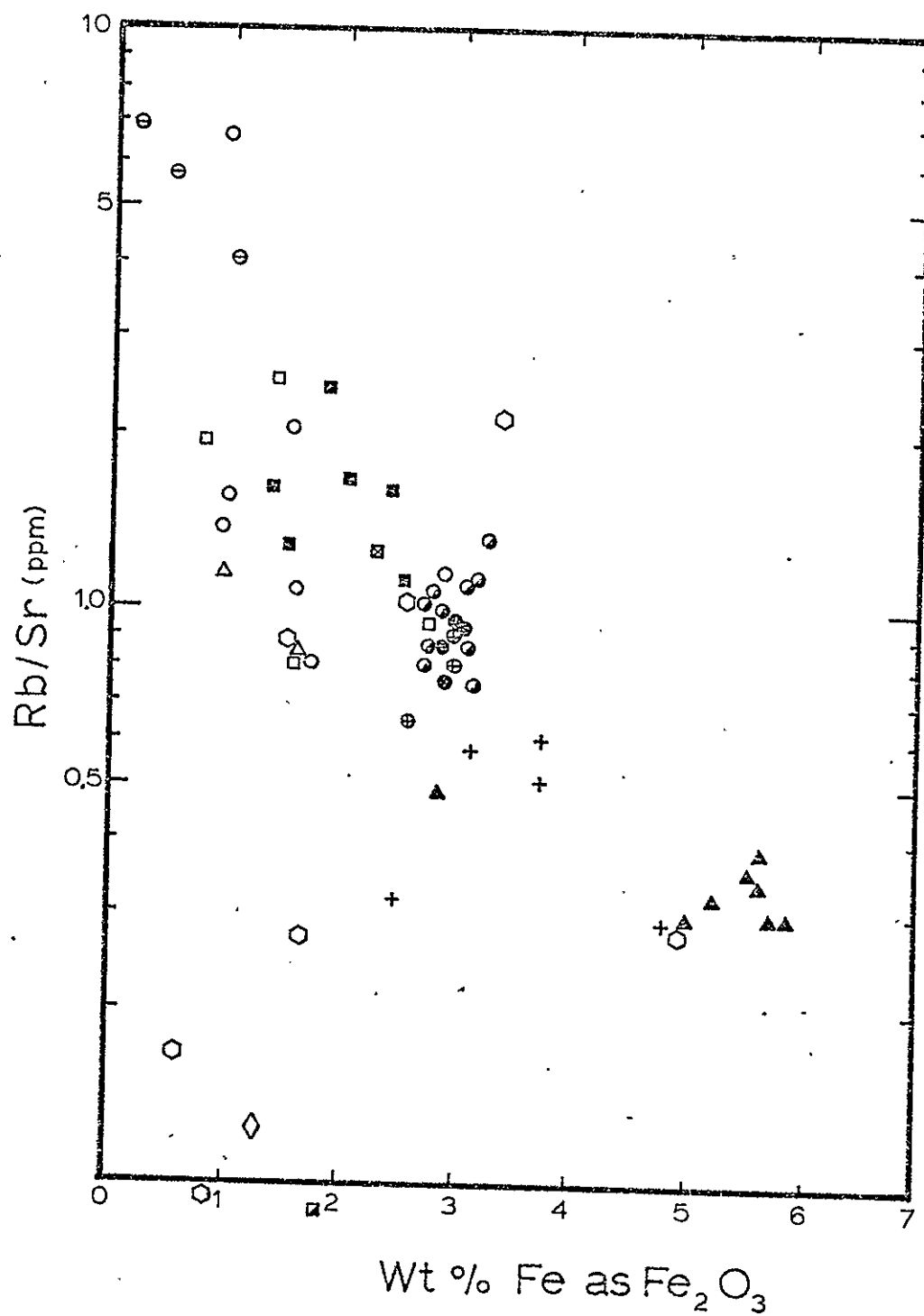


Figure 105. A plot of Rb/Sr against total Fe as Fe_2O_3 for the granitic rocks.

tion index (D.I.) (fig. 104) shows that Puntiaquedo Granite Porphyry samples tend to have higher Rb/Sr and higher D.I. than the Rana Quartz Monzonite, but that their aplites do not attain as high a Rb/Sr ratio as do those of the Rana Quartz Monzonite.

The felsites and the Cerro Alto Metadacite samples show the kind of wide scatter that typifies their major-element chemistry, yet there is some indication that, given more data, the Cerro Alto Metadacite could be distinguished from the other units on the basis of its trace-element chemistry. The scatter for the felsites on figure 104 is extreme, and this has been used by Ragland and Butler (1972) as an indication of alteration or a nonmagmatic origin for the granitic rocks. This appears to be valid for the felsite dikes, as it is consistent with their field occurrence and petrography. It is interesting to note, however, that the trace elements of the altered samples of the Puntiaquedo Granite Porphyry and the Rana Quartz Monzonite are not strongly affected by the alteration. This indicates that the felsites may have experienced a much different and perhaps much more severe alteration than the epidote-altered samples. Another possible explanation is that there are too few samples of the felsites to reveal the expected fractionation trend or that the type of fractionation was different from that expected by Ragland and Butler (1972).

Fullager and Shiver's interpretation of their data as plotted in a diagram similar to figure 104 is clearly in error because the Peñasco Quartz Monzonite, according to their idea, should have differentiated to give rise to the other plutonic units. Instead it is actually the youngest, albeit the most mafic, granitic unit in the area. Examined in detail, the Peñasco Quartz Monzonite shows an interesting trend in

which Rb/Sr decreases slightly with increasing differentiation and then increases dramatically with the most differentiated granitic sample and the two aplite samples. It is significant that the aplite that is least differentiated is associated with the less differentiated rocks of the main mass and has the lower Rb/Sr of the two aplites. The most differentiated aplite is associated with the most differentiated (and highest Rb/Sr) of the Peñasco Quartz Monzonite samples and has the higher Rb/Sr of the two aplites. This supports the idea that the aplites originated as accumulated rest-liquids, especially since progressive enrichment in Rb relative to Sr is expected if plagioclase is the dominant early phase as is the case for the bulk of the Penasco Quartz Monzonite. Similar arguments can be marshalled from plots such as Ba versus Sr and Rb versus Ba. In total these data indicate that the aplites from all of the granitic units were formed by very late-stage magmatic differentiation of their host granites. Their trace-element distributions, though, were controlled by the total crystallization sequence of host granites and trace-element contents of their enclosed aplites.

The origin of the border zones of the Rana Quartz Monzonite and Puntiaquido Granite Porphyry is not clearly spelled out by the trace-element data. Figure 104 does, however, suggest a somewhat systematic trend for the Rana border zone, and the trace elements in the Puntiaquido border samples can be explained by strong fractionation of alkali feldspar (e.g. sample PL73-235). Oddly enough, the most altered parts of the Rana border zone are not the ones which show the greatest shift in D.I. versus Rb/Sr. This further supports the notion of crystal-liquid fractionation, but it does not distinguish a mode of origin involving

differentiation from one involving an early melt of different initial composition.

In summary, it can be stated that the trace- and major-element data are consistent with field observations and that they shed considerable light on some of the problems mentioned earlier. First, most of the granitic rocks have chemical compositions that are fairly typical for intermediate granites. They are differentiated to various degrees and along at least partially distinct paths, the bulk of the Rana Quartz Monzonite showing the least differentiation and the Peñasco Quartz Monzonite, the Cerro Alto Metadacite, and the Puntiaquedo Granite Porphyry showing considerably more differentiation. Except in the felsites, most of the trace-element data can be attributed to crystal-liquid differentiation. While such an interpretation is not necessarily unique, the chemical data, especially when examined in the light of field relations, do not bespeak any other interpretation. This fact, in addition to the large body of supportive field and petrographic evidence, means that a granitization model has a very low probability of being correct for these rocks. The origin of the border-zone rocks of the Puntiaquedo Granite Porphyry and the Rana Quartz Monzonite is still uncertain, even with the chemical data, but a fundamentally magmatic origin is indicated with superimposed alteration particularly in the case of the Rana Quartz Monzonite. The most favored interpretation of these data is that the initial melts of both intrusive episodes were more leucocratic than the later ones, and that they were quenched to form the fine-grained porphyritic texture that typifies these rocks. Some differentiation may have occurred in situ by crystal fractionation prior to quenching. Superimposed alteration may have produced additional

chemical variation, particularly by redistribution of alkalis via a vapor phase, and the alteration certainly was responsible for much of the widespread development of muscovite in the border-zone rocks. The southern isolated outcrops of the Puntigudo Granite Porphyry are chemically compatible with the main mass in that they may well represent part of a differentiation series. They also are similar to the Rana Quartz Monzonite, so that their classification as Puntigudo Granite Porphyry must still rest on petrographic grounds. The felsites remain enigmatic as well, but the chemical data do suggest severe alteration and a wide range of compositions that probably are not well explained by magmatic differentiation alone. Field relations show that some of the felsite dikes must be part of the Rana Quartz Monzonite, and the chemical data are not entirely inconsistent with this. By the same token they are not inconsistent with the earlier conclusion that the felsites may be of more than one genetic type. In short, a petrologic indicator that is "alteration-resistant" is needed to determine the parentage of the felsite dikes.

Composition of Feldspars from the Granitic Rocks

Feldspars from selected samples of the Puntigudo Granite Porphyry, the Rana Quartz Monzonite, and the Peñasco Quartz Monzonite were analyzed for Ca, Na, K, Ba, Al, and Si by the electron microprobe. The purpose of these analyses was to characterize the overall compositions of the feldspars and to determine the nature and extent of zoning of the plagioclases and zoning of the K-feldspar megacrysts with respect to barium. The barium zoning is reported in a later section. Further, specific efforts were directed to analyzing altered parts of plagioclase

grains and albitic rims of plagioclase grains from samples of Rana Quartz Monzonite which showed various amounts of deformation. The idea in analyzing altered feldspars was to establish the composition of plagioclase coexisting with the alteration products muscovite and epidote, and thus to help in establishing the nature of the alteration process. In examining albitic rims as a function of deformation in the Rana Quartz Monzonite, it was hoped that systematic changes in the An content of the rims might be found which could be interpreted as indicating the presence of a thermal gradient accompanying the progressively greater deformation. If no systematic changes were found the possibility of a thermal gradient would still exist, as re-equilibration of the feldspars may have occurred or the rims themselves may have formed at a later time.

The probe data are reported in tabulated form in Appendix IV, and are plotted on triangular diagrams (Ab-Or-An and Ab-Or-Cn) in figures 106 and 107. Plagioclase from the Puntagudo Granite Porphyry shows only very slight zoning (An_5 to An_1) in intact crystals, and probe traverses across polygonized grain aggregates show no detectable zoning. Plagioclases from the Rana Quartz Monzonite, on the other hand, are zoned as is shown by the probe traverse diagrammed in figure 108. Extinction patterns in the Rana plagioclases show that the zoning pattern here is fairly typical of those from the undeformed to moderately deformed Rana rocks. These plagioclases have a range in An content from about An_{32} to An_{12} , with distinct but discontinuous rims of An_9 to An_1 . The most deformed Rana rocks have zoning patterns, as shown in figure 109, which have a smaller range (An_{30} to An_{23}) and which only rarely show any reverse zoning. Plagioclases from the Peñasco Quartz

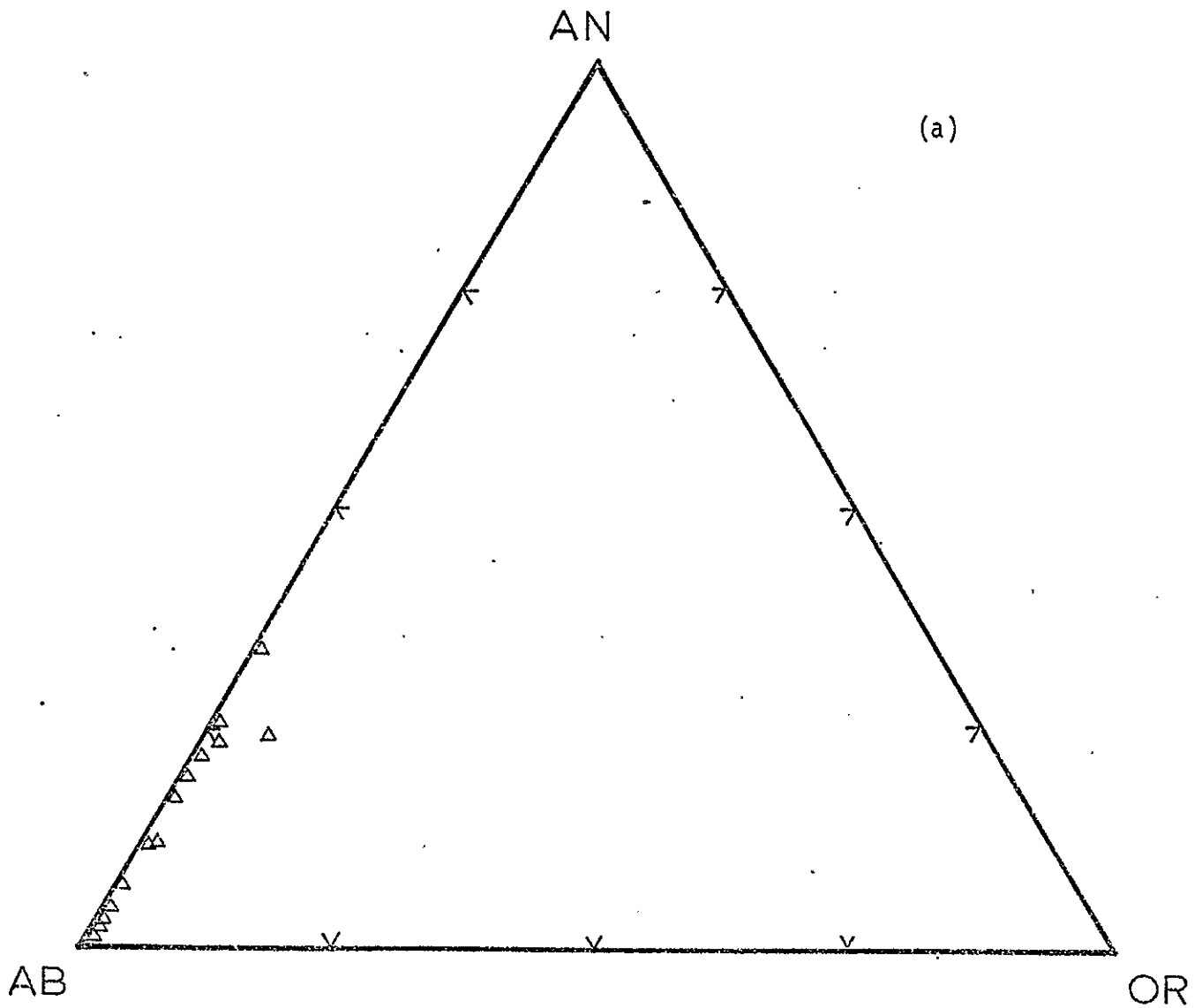


Figure 106. Microprobe analyses of feldspars plotted on (a) Ab-An-Or and (b) Ab-Or-Cn diagrams. Squares are Puntigudo Granite Porphyry, circles are Rana Quartz Monzonite and triangles are Peñasco Quartz Monzonite.

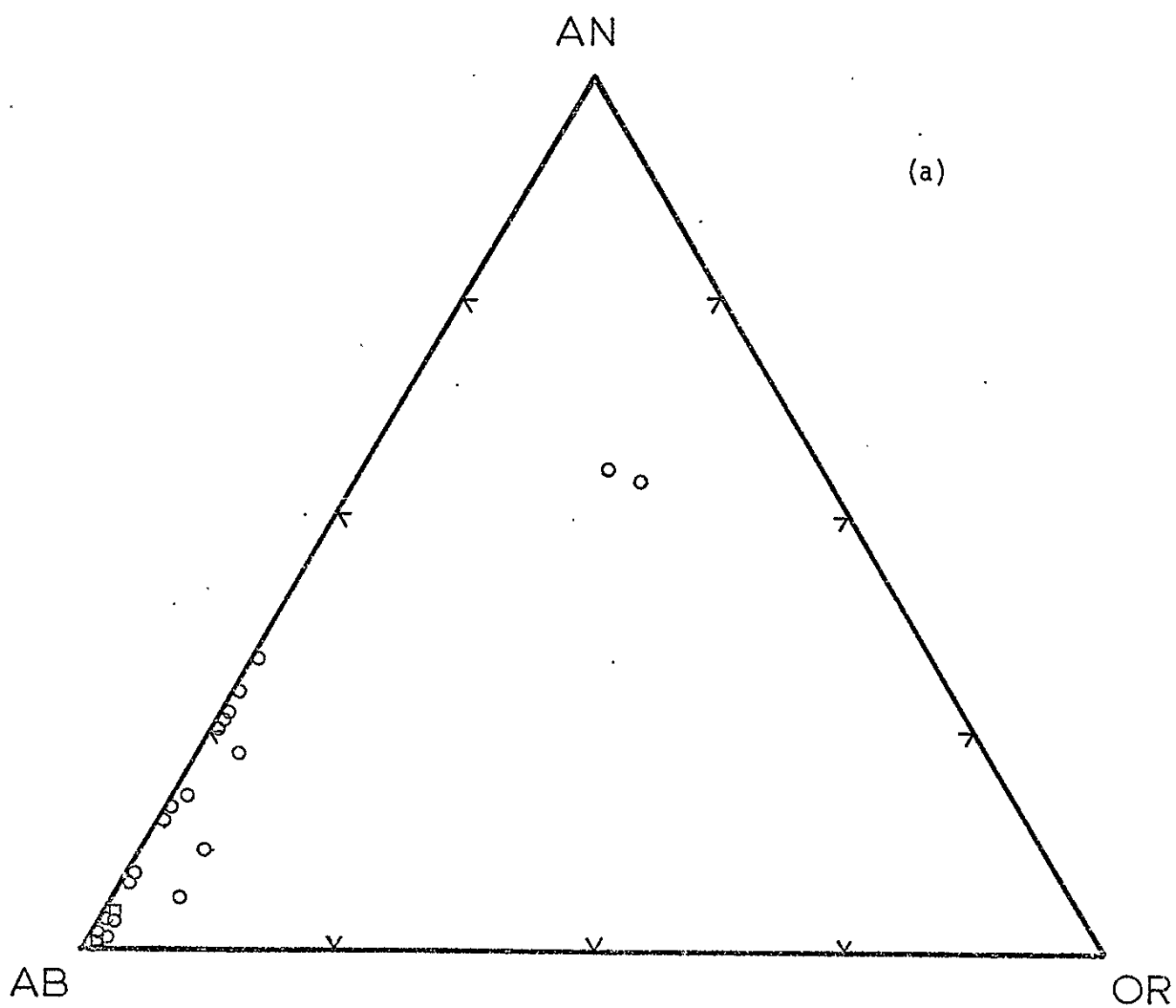


Figure 106.

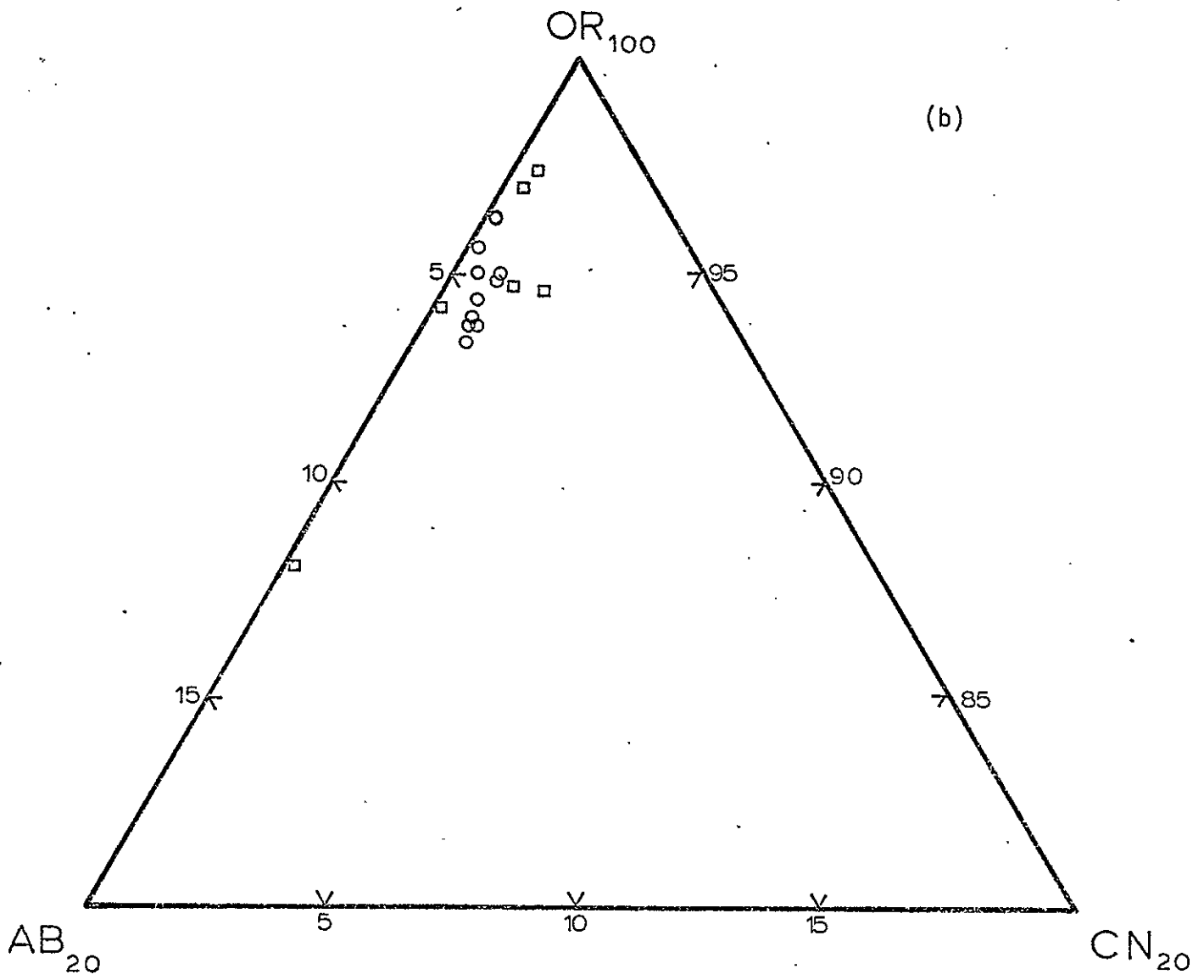


Figure 106.

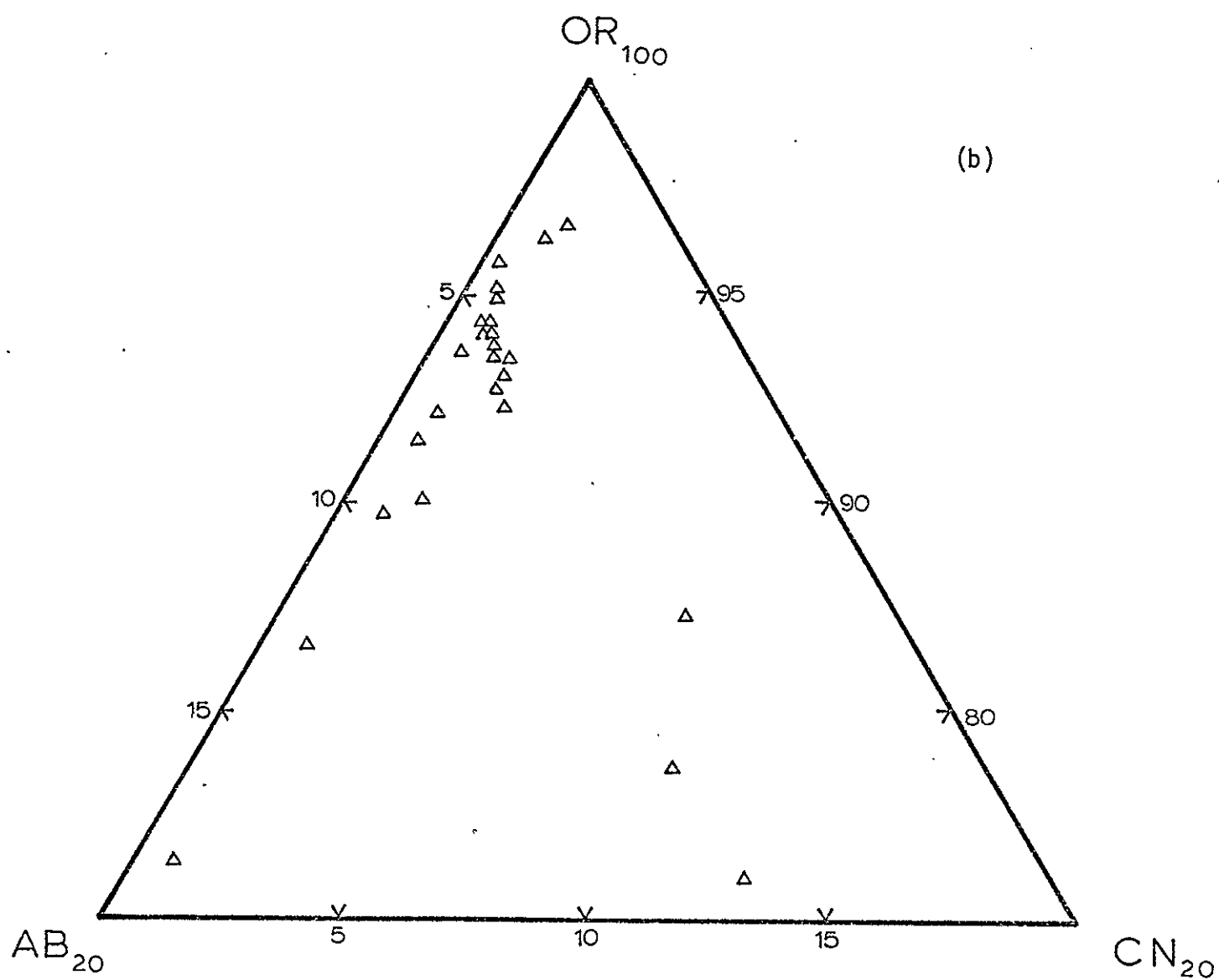


Figure 106.

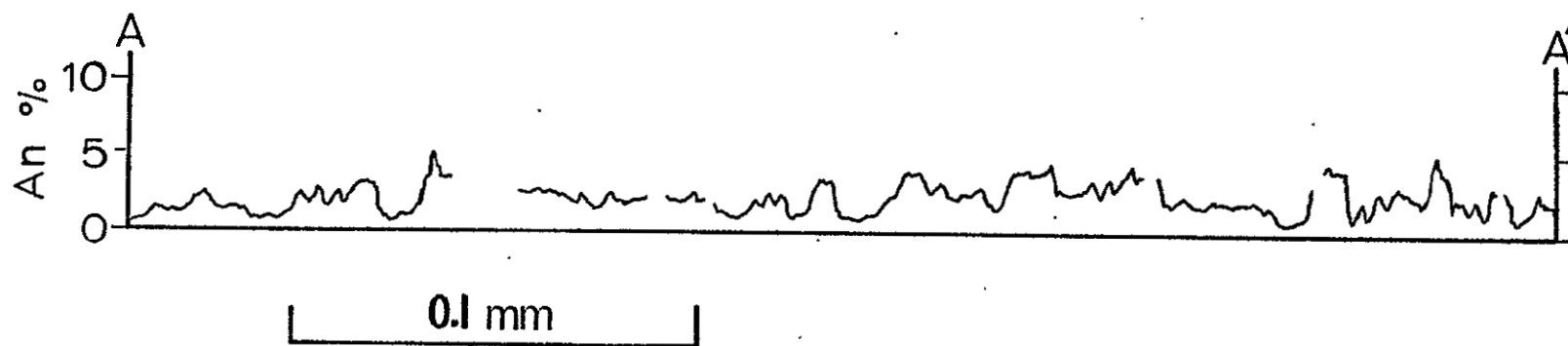
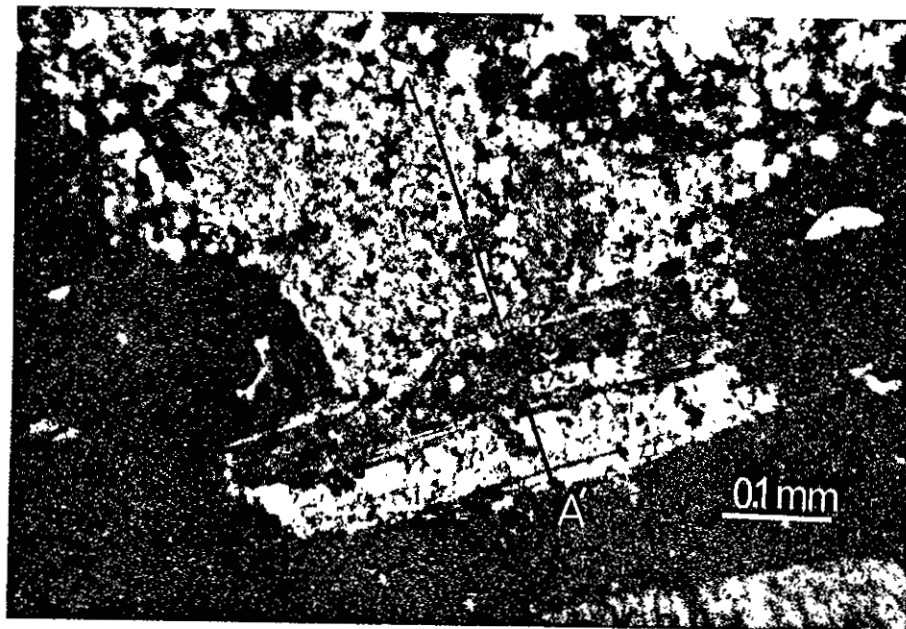


Figure 107. Results of a microprobe traverse of a plagioclase feldspar from the Puntigudo Granite Porphyry.

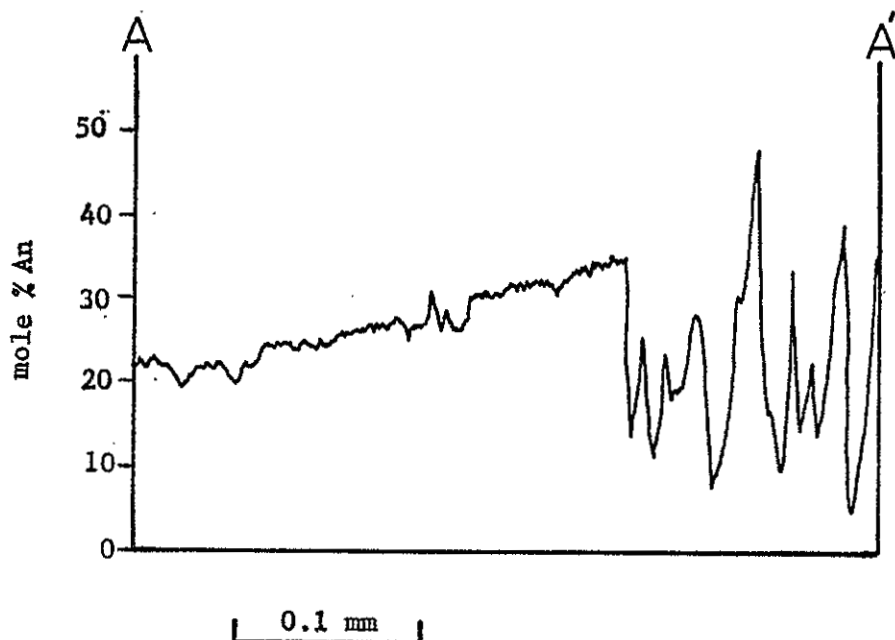
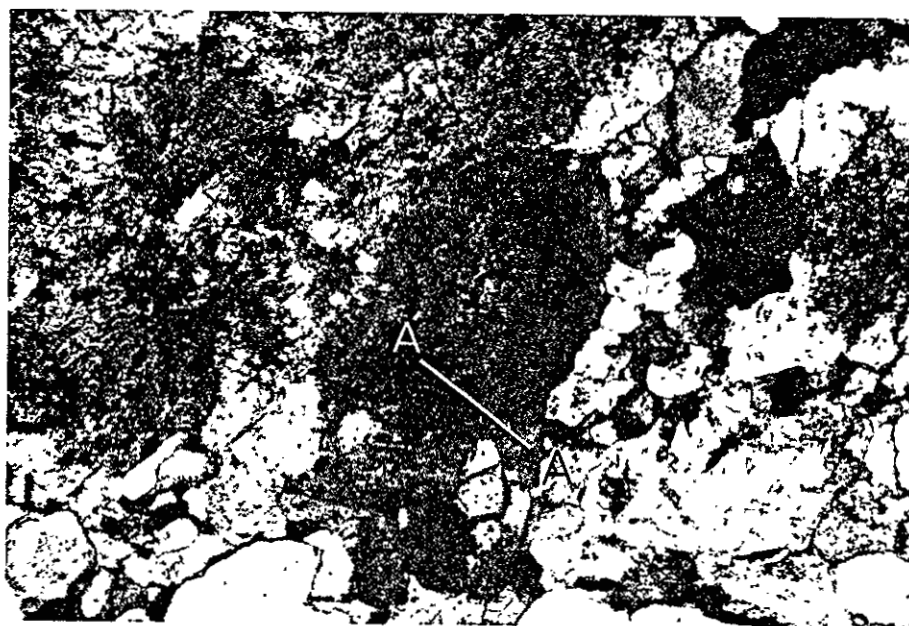


Figure 108. Results of a microprobe traverse of a plagioclase feldspar from the Rana Quartz Monzonite.

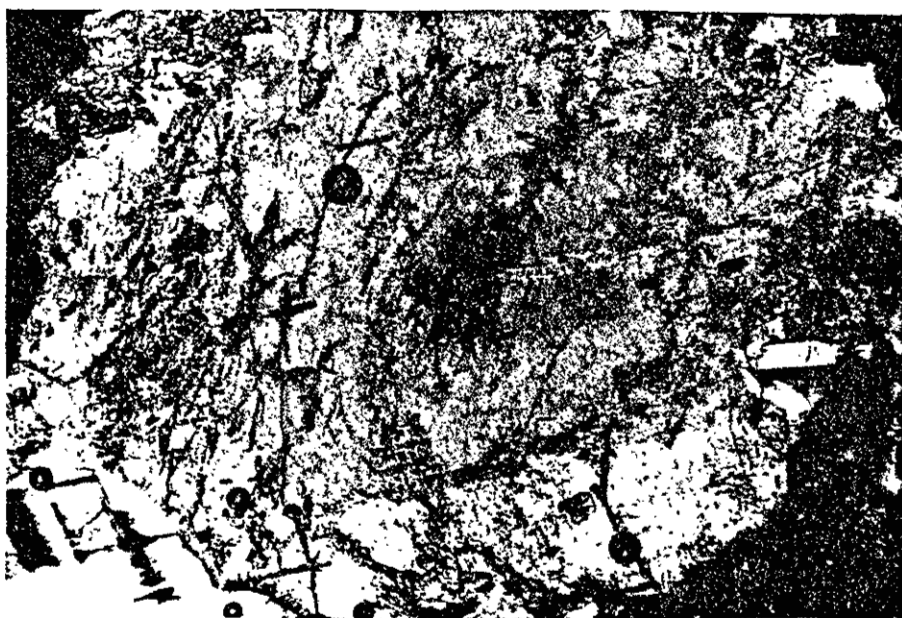


Figure 109. Photomicrograph showing limited plagioclase zoning in highly deformed Rana Quartz Monzonite. Sample PL72-75.

Monzonite are zoned in a fashion similar to that of the Rana plagioclase (fig. 110). These plagioclases commonly contain slightly more An (An_{34} to An_{15}) and some show greater complexity in their zoning. The albitic rims are An_5 to An_2 .

In general, the plagioclase zoning in these rocks is typical of granites. The sole exception is the Puntigudo Granite Porphyry, in which the lack of plagioclase zoning is consistent with its having undergone the severest deformation and metamorphism as the oldest of the three granitic units here considered. There is a strong possibility, however, that the zoning in the Rana and Peñasco plagioclases is not in its original state. This is certainly true for the more deformed Rana rocks whose plagioclase zoning appears more like that found in metamorphic rocks than that of a typical granite. In the unfoliated Rana facies the plagioclase zoning may have been sharper, perhaps oscillatory, but it is now subdued because of diffusion that has occurred since initial crystallization. Thus the plagioclase zoning may still reflect the general original zoning trends, even though some of the details may have been lost.

The megacrysts from the Peñasco Quartz Monzonite and the Puntigudo Granite Porphyry are zoned with respect to barium, but the anhedral microcline grains of the Rana Quartz Monzonite are not. The barium zoning is discussed in detail farther on. Figure 106 is included here, however, as part of a general description of the microcline compositions. The bulk of the samples is about Or_{93-96} and has as much as 2.5 mol percent celsian. Analyses showing less than Or_{93} probably result from overlap problems with the electron beam falling partly on a lamella or inclusion of plagioclase.

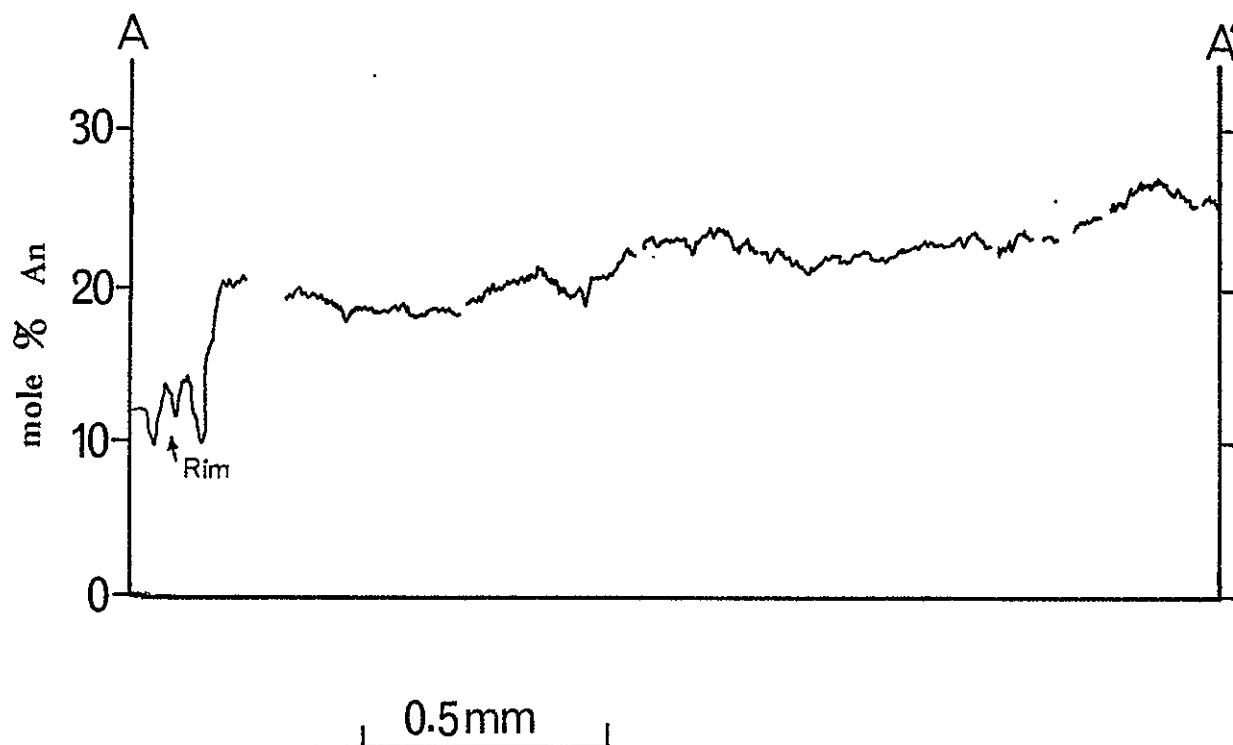


Figure 110. Results of a microprobe traverse of a plagioclase feldspar in the Peñasco Quartz Monzonite.

Similar overlap problems occurred in attempting analyses of the altered cores of plagioclases. Apparently the presence of tiny grains of muscovite and epidote leads to analyses such as those shown in figure 106, which are impossible compositions for a single feldspar. As a result further work will be needed in order to determine the composition of plagioclase feldspar coexisting with alteration products.

The compositions of albite rims from the Rana samples are shown in figure 111. There appears to be no systematic relationship between degree of deformation and rim composition, suggesting that no thermal gradients affected the albite rims or that their composition was determined by other factors such as re-equilibration or fluid composition. Bulk composition apparently is not a factor as albite rims on plagioclase from one of the more mafic samples of the Peñasco Quartz Monzonite have as low an An content as those in any of the Rana rocks. Instead, the rim compositions may be very sensitive to local fluid composition determined in part by the details of plagioclase alteration. One might expect, for example, that rims with the highest An content would occur in rocks that show the greatest alteration and thus perhaps the greatest release of calcium into interstitial fluids. This is an area where further research, particularly detailed probe work on compositions of alteration products and albite rims, would be especially fruitful.

Structural State of Feldspars

An attempt was made to look for systematic differences in the structural state of feldspars from the granitic rocks in the hope of discovering evidence for thermal gradients and/or different cooling histories for different parts of the plutonic bodies. The technique

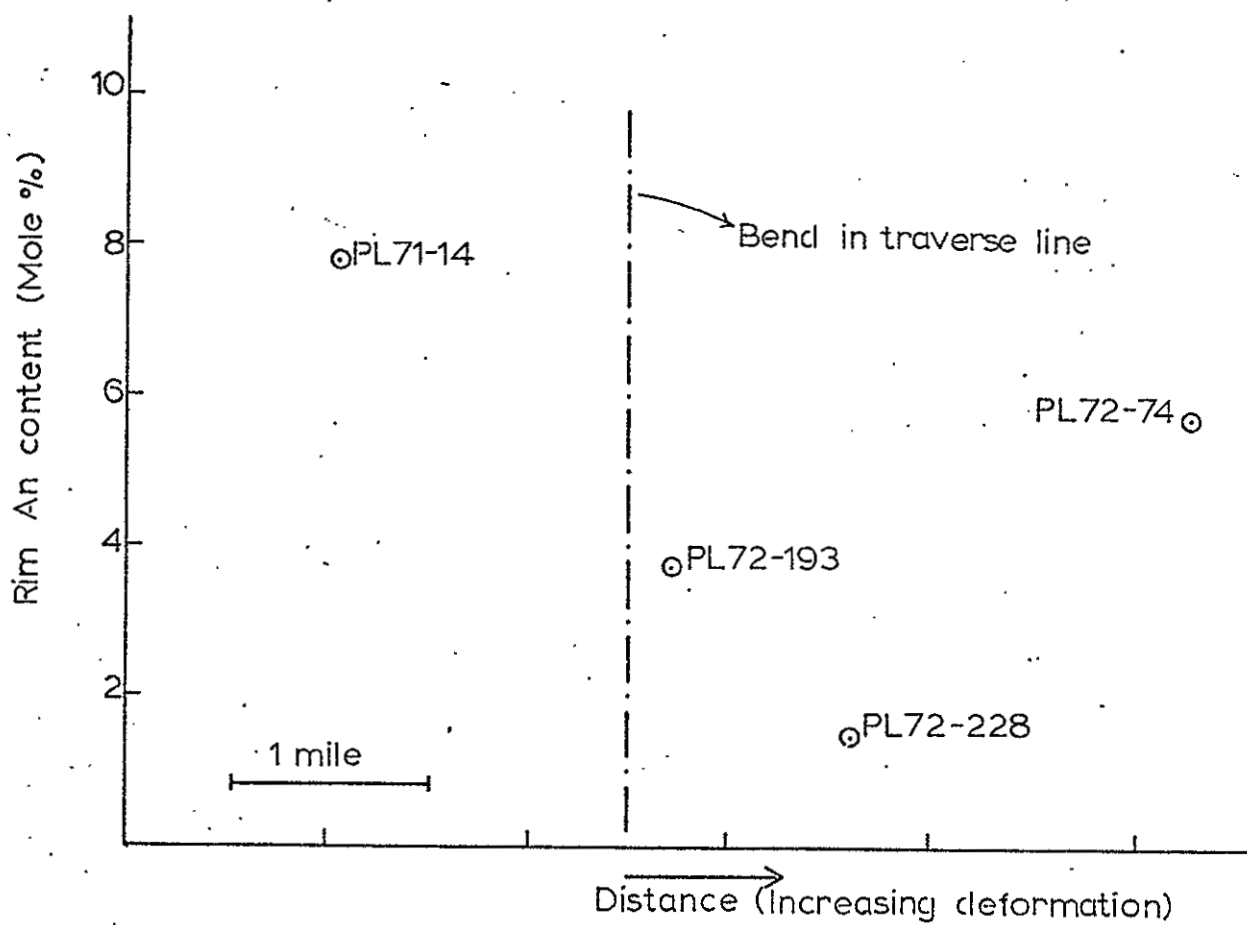


Figure 111. Plot of An content of albitic rims vs. distance in the Rana Quartz Monzonite. The traverse is plotted so that deformation in Rana Quartz Monzonite increases from left to right.

used was that of Wright (1968), and the results are given in Appendix V. They are plotted in figure 112. The data are largely inconclusive, i.e. there appears to be no systematic trend in structural state, either from one body to the next or from one area of a given body to another even where adjacent to a younger pluton. Instead the data points cluster around maximum microcline, suggesting that the K-feldspar in the area is maximum microcline or nearly so, with some scatter attributable to random error in the data (Appendix V). The few albites that were X-rayed appear to be low albite, with large random errors present. These data are consistent with a pervasive low-temperature thermal event as one of the last major Precambrian events expressed in these rocks. Because of this thermal overprinting effect, further conventional studies of the structural state of feldspars from this area probably will not produce much information on original history of the rocks. Detailed studies of single crystals, however, may yield information relative to deformation or perhaps growth conditions of hydrothermally altered feldspars, but in general the structural-state view of thermal history seems to have been obscured by the most recent thermal event. This conclusion is not entirely unexpected for such an area, and it is consistent with field and petrographic relations already discussed.

Late-Stage and Metamorphic Reactions in the Granitic Rocks

General Statement

There is textural evidence for at least three major types of late-stage and/or metamorphic reactions in the granitic rocks: (1) reactions

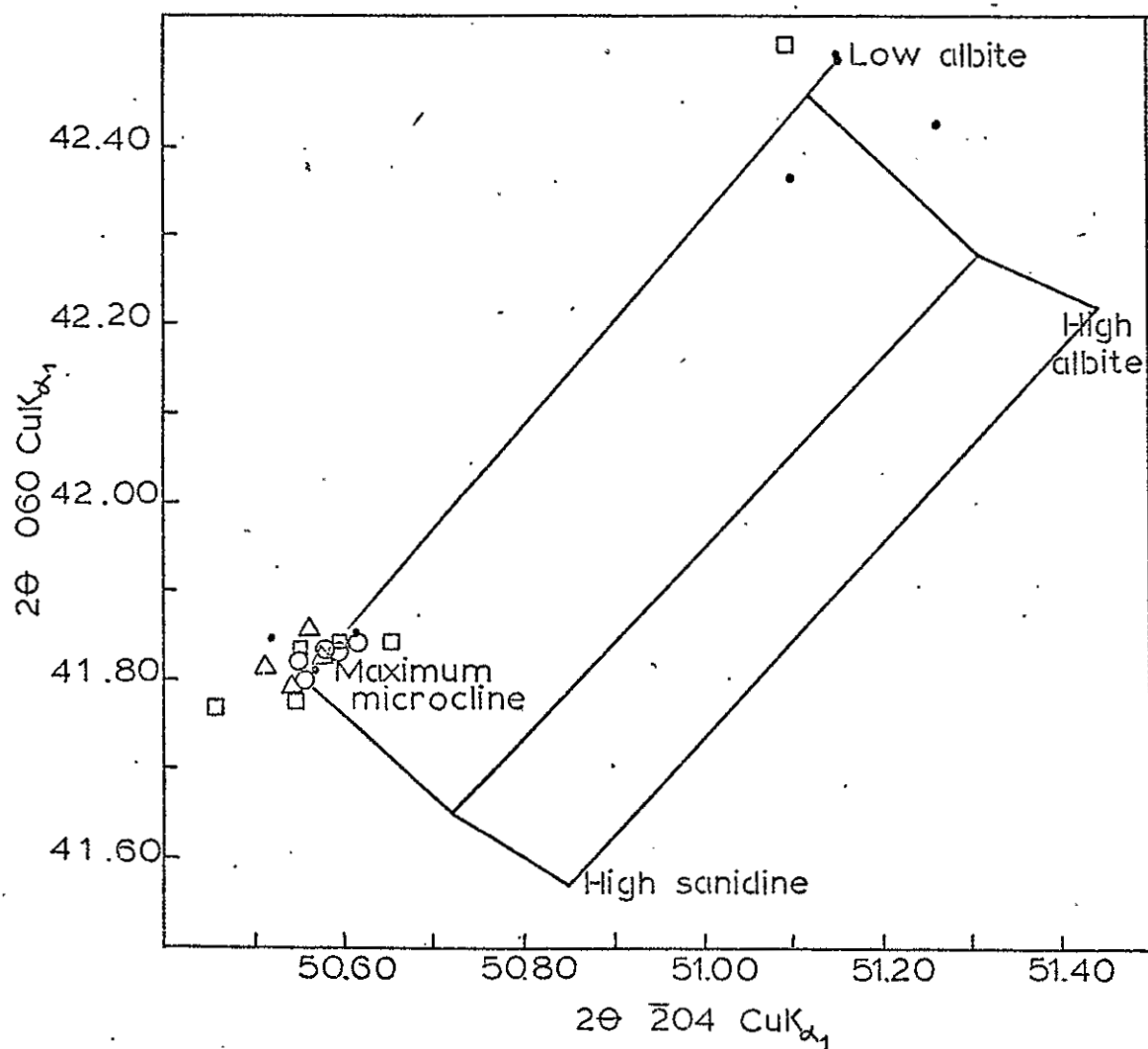


Figure 112. $2\theta\ 060$ plotted against $2\theta\ \bar{2}04$ to indicate structural state of feldspars from the granitic rocks. Squares are Puntigudo Granite Porphyry; solid circles, pegmatite; open circles, Rana Quartz Monzonite; and triangles, Peñasco Quartz Monzonite.

involving mafic phases and epidote or sphene, (2) reactions of the type $K\text{-feldspar} + \text{aluminosilicate} + \text{water} \rightleftharpoons \text{muscovite} + \text{quartz}$, and (3) reactions producing myrmekite. In a given rock these reactions are not necessarily independent of one another but they are here discussed separately. This particular special study by no means provides a final answer as to the origin of the features here considered, but it does set forth their occurrence in terms of possible reactions. This may serve as basic groundwork for future experimental or chemographic analysis as possible ultimate solutions to the problems.

Reactions Involving Mafic Phases

Petrographic data from the four major granitic units, especially the Rana Quartz Monzonite, suggest that biotite and associated minerals such as epidote, muscovite, hematite-magnetite, and sphene have participated in complex interactions among themselves and with the major minerals, particularly plagioclase. The pertinent petrographic relationships are: (1) occurrence of rims of sphene around magnetite grains that are partially oxidized to hematite (fig. 113), (2) occurrence of epidote as rims on allanite, and occurrence of epidote partly replacing biotite, and (3) muscovite crosscutting and apparently replacing biotite. In addition is the ubiquitous partial replacement of plagioclase by muscovite and epidote-clinozoisite, especially in the more calcic cores of plagioclase grains.

A possible reaction that might account for the sphene rims would involve the breakdown of calcic plagioclase to provide Ca ions:



(a)

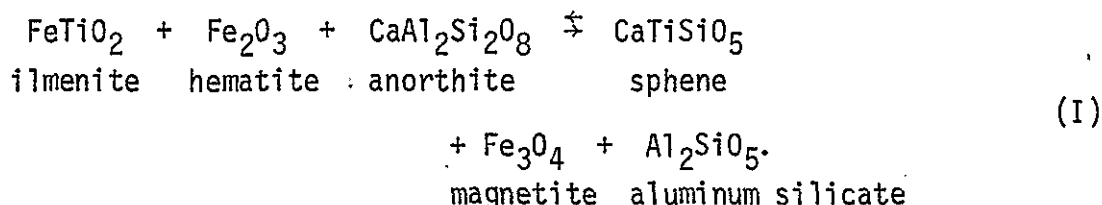
0.2 mm



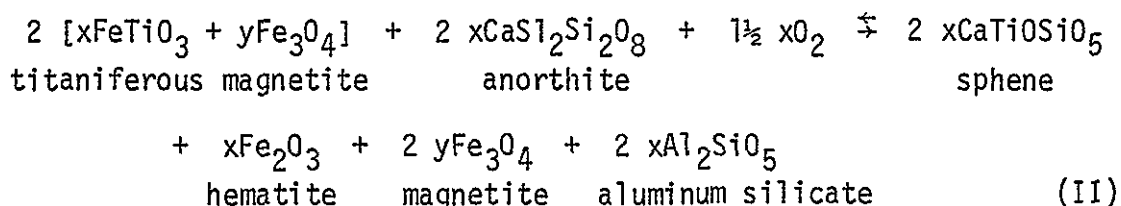
(b)

0.1 mm

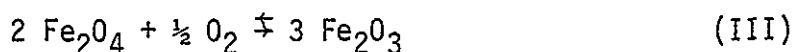
Figure 113. Sphenes rims (medium gray) on a magnetite grain (light gray), Rana Quartz Monzonite. (a) Sample PL71-14; (b) sample PL72-229.



Magnetite, however, is the dominant host phase for the hematite, so what is required is a reaction that produces hematite and sphene from titaniferous magnetite. As an example:



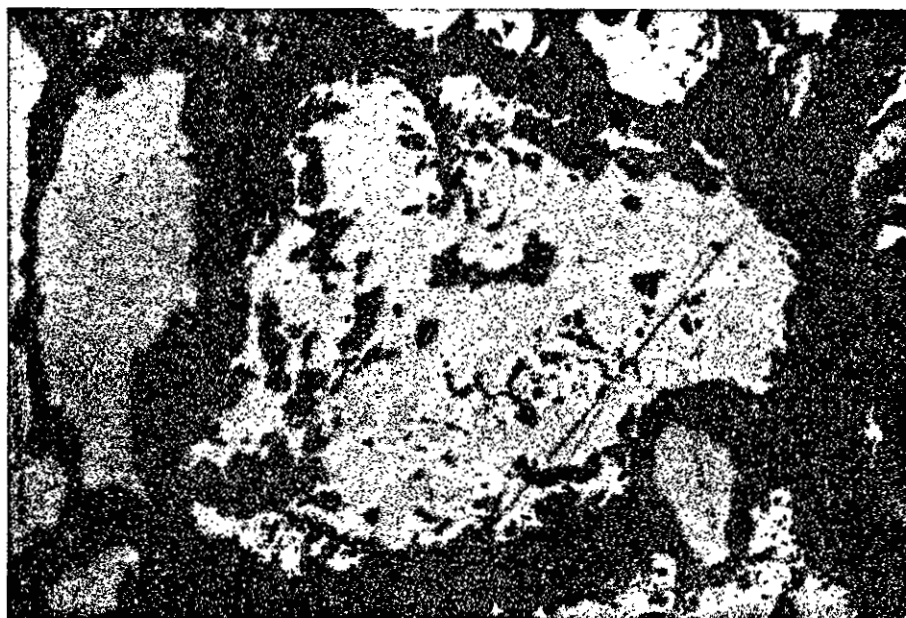
where $x + y = 1$ and $y \gg x$. This indicates that a somewhat oxidizing environment would be required. In fact, if some approach to equilibrium were attained, the oxygen fugacity of the system presumably on a scale of a large portion of the pluton mass but at minimum on a hand-specimen scale at a given pressure and temperature is defined by the equilibrium:



i.e. the hematite-magnetite buffer.

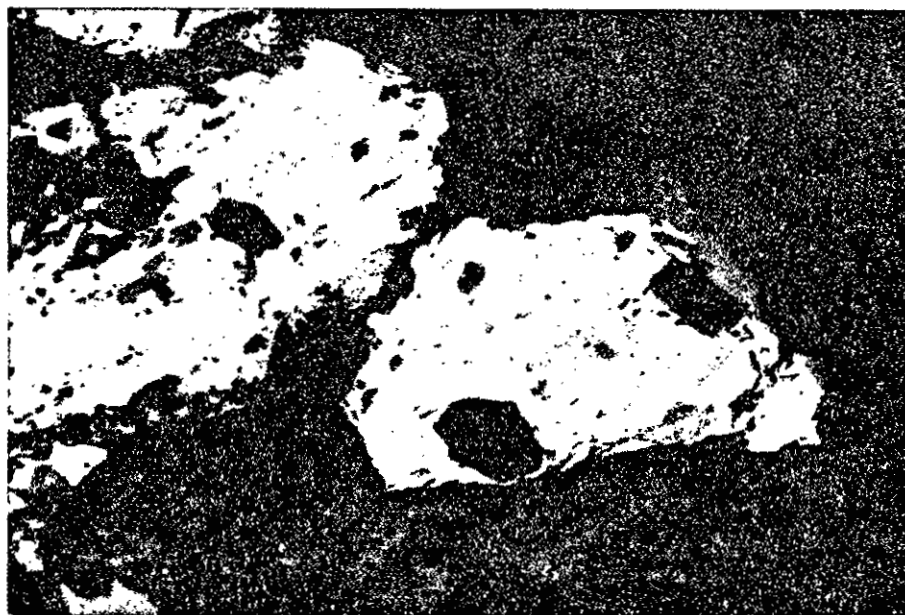
The occurrence of hematite in and around magnetite in at least two different morphologies (fig. 114) is here interpreted to mean that at two different times, but perhaps under different physical conditions, the system was on the hematite-magnetite buffer. Although the timing is not clear, this matches in a general way with the polymetamorphic history as interpreted from field and petrographic evidence.

Reaction II is obviously idealized as it requires the presence of anorthite and aluminum silicate, neither of which occurs as a discrete phase in any of the granitic rocks. They do occur as components in



(a)

0.1 mm



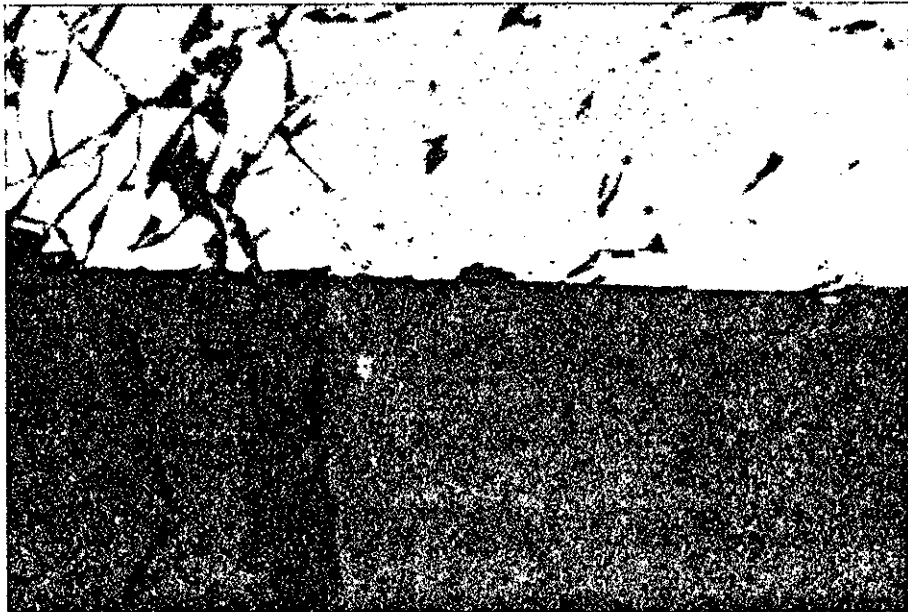
(b)

0.1 mm

Figure 114. Textures of hematite-magnetite intergrowths. (a) Rana Quartz Monzonite, PL71-14e; (b) foliated Rana Quartz Monzonite, PL72-73; (c) Peñasco Quartz Monzonite, PL72-92; (d) Peñasco Quartz Monzonite, PL71-5.



(c)

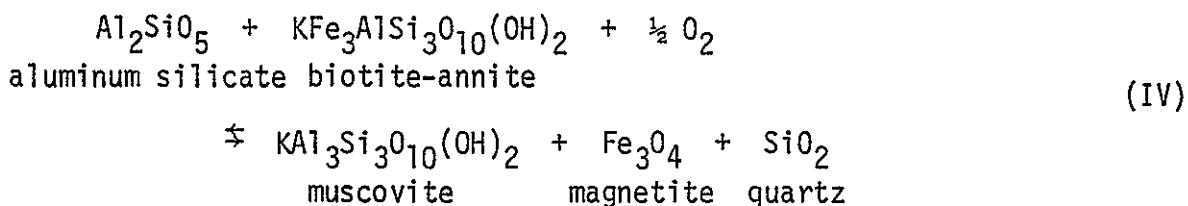


(d)

Figure 114.

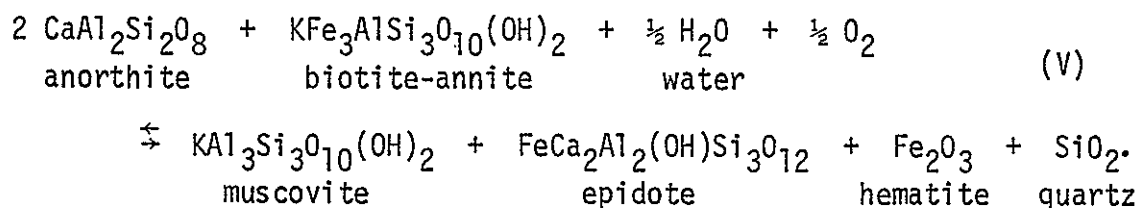
other phases, however, and in this context they will be considered later as part of another reaction.

The "replacement" of biotite by muscovite could be effected by a reaction such as:



This reaction shows the possibility that biotite (annite), when provided with a peraluminous source in an oxidizing environment, reacts to form muscovite. The other products could easily go unnoticed by removal from the primary site of the reaction and precipitation on existing phases. The magnesium component of natural biotite also could participate in the reaction in solid solution with other phases or by production of phlogopite, although none has been observed in these rocks. One possible reason is that the reaction may simply increase the magnesium content of residual biotite. This has not been checked by microprobe analyses, but it may be a fruitful area for future research.

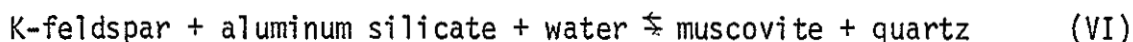
Epidote rims on allanite may be primary magmatic features or they may be the result of postmagmatic reaction between allanite and other minerals. If they are magmatic features, the reaction would be silicate liquid \rightarrow epidote + other minerals, or silicate liquid + allanite \rightarrow epidote + other minerals. The allanite does not usually appear to be resorbed; the first reaction is the more likely. On the other hand, if the reaction is postmagmatic it may involve the breakdown of biotite:



Again the participation of anorthite component (or at least Ca^{++}) is required in this reaction. The altered character of plagioclase cores suggests that calcium may have been available from plagioclase breakdown, thus driving reactions II and V and providing a peraluminous source for reaction IV and for the muscovite-K-feldspar reaction discussed below. Thus the reactions can be related in a consistent manner which includes the production of epidote by late-stage reactions. This does not prove, however, that the epidote is not magmatic, and the wide stability range of epidote (Holdaway, 1972) precludes any firm distinction at the present. Future work might be focused on the details of compositional variation of epidotes in a wide variety of granitic rocks. For example, if epidote were consistently to reflect the iron content of the host granite, one might argue a magmatic origin, but if iron contents were widely scattered and independent of iron content of the host it might suggest a postmagmatic origin in which the epidotes were not in complete chemical communication with their surroundings. Similarly, more than one generation of epidote, as might be evidenced by iron content, could suggest the effect of a metamorphic event as opposed to a late-stage postmagmatic origin.

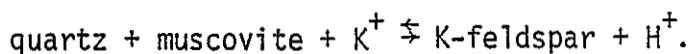
The Muscovite-K-Feldspar Reaction

The second type of reaction participates in the overall equilibrium in the rocks by taking up the Al_2SiO_5 from the breakdown of the more anorthite-rich plagioclase.



In fact, this may be the primary reaction involved, with the others responding to resultant changes in fluid composition. The aluminum silicate components may well be the least mobile, and as a consequence the aluminum-rich products of the reaction are localized in the calcic plagioclase. The occurrence of quartz blebs in K-feldspar may also result from this reaction in that potassium and aluminum ions migrate to the reaction site in the plagioclase leaving excess SiO_2 in the residual K-feldspar. This feature is most prominent in severely altered rocks, and in most of the granitic rocks the partial breakdown of K-feldspar is not obvious.

This reaction is also pertinent to the development of altered parts of the border zone of the Rana Quartz Monzonite and rare altered shear zones of the Puntagudo Granite Porphyry. The final product of this type of alteration is a quartz-muscovite schist with quartz grain structure largely inherited from the original rock. Gresens (1971) and Gresens and Stensrud (1974a) report this type of alteration in meta-rhyolites from northern New Mexico and attribute it to reaction VI described as an hydrolysis reaction as experimentally determined by Hemley and Jones (1964) and Shade (1968):



This reaction is responsible for the so-called hydrogen metasomatism of Hemley and Jones (1964) and Gresens (1971) and indicates that acid leaching of granitic compositions would result in removal of soluble components leaving the quartz-muscovite residue. Such rocks then would lose Na, Ca, Fe, and Mg. Depending on the K^+/H^+ ratio, they also could lose K if the solutions were so acid that muscovite is not stable.

This was not the case in the border zone of the Rana Quartz Monzonite, as it is only in certain localized areas which apparently are shear zones that the alteration is most severe, and in these areas aluminum silicates are not observed. Thus the metasomatism took place under the conditions shown in figure 115 and was superimposed on an already inhomogeneous border zone (see previous section on petrochemistry). This alteration probably occurred at the time of intrusion of the largely undifferentiated main mass of the Rana Quartz Monzonite, as a result of circulation of fluids given off by the crystallizing granitic body. Considering that there is no evidence that the Rana Quartz Monzonite was particularly "wet" as a magma, the solutions may well have had to collect in favorable areas such as the upper marginal surfaces of the main body before they could be effective in altering the rocks. Alternatively, the main Rana mass may have acted primarily as a heat engine, setting up circulation of waters derived mainly from the country rock. In either case, the alteration of the border-zone rocks has been superimposed, i.e. it does not appear to be inherent in the crystallization of the border zone itself. It is also incorrect to attribute it to a metamorphic event per se. Instead it might be called the exodeuteric alteration of the Rana Quartz Monzonite. Despite the fact that a similar reaction probably was responsible for both the alteration of the border zone and the internal, less obvious alteration of the Rana Quartz Monzonite plagioclase, it appears that the two features may have formed at different times. The lack of preferred orientation of muscovite associated with the alteration of plagioclase may well mean that the alteration took place during one or more low-grade thermal events after emplacement of the Rana Quartz Monzonite.

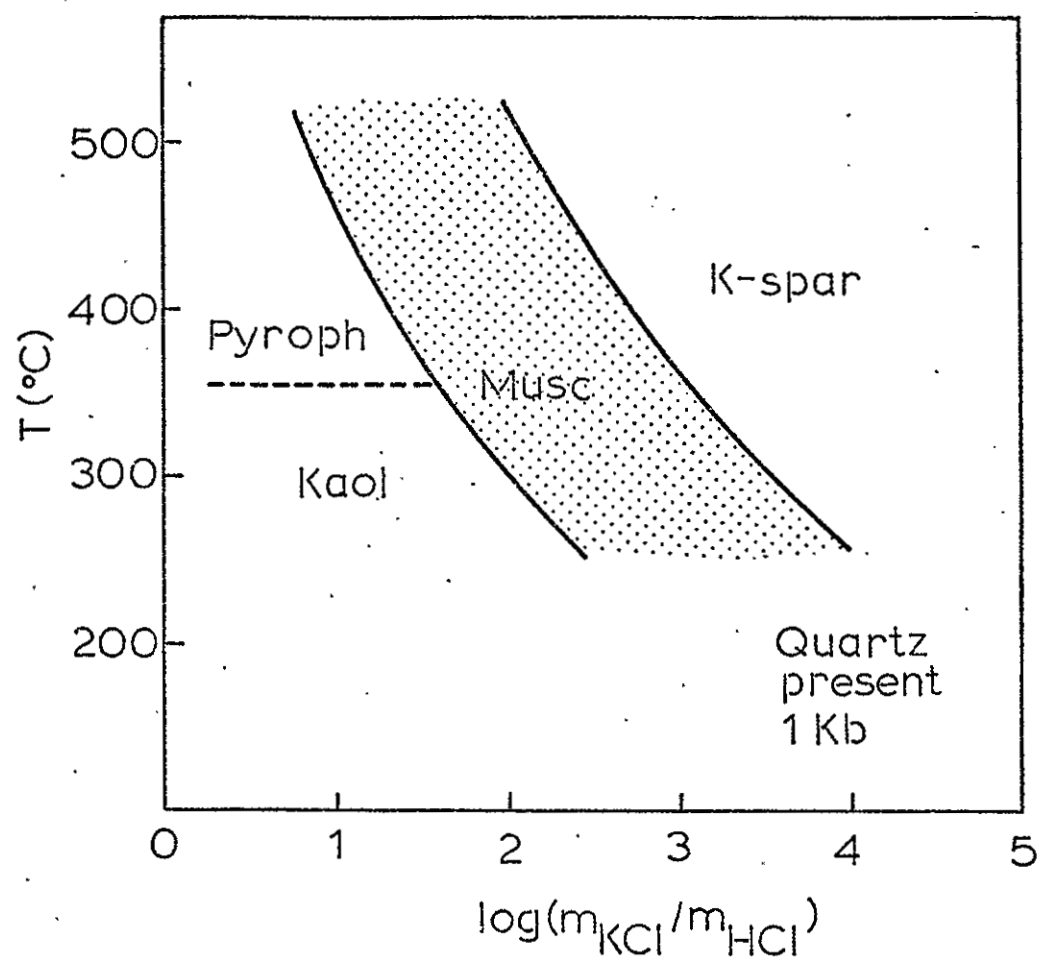


Figure 115a. Stability of muscovite at 1 kbar as a function of temperature and $M_{\text{KCl}}/M_{\text{HCl}}$ as determined by Hemley and Jones (1964).

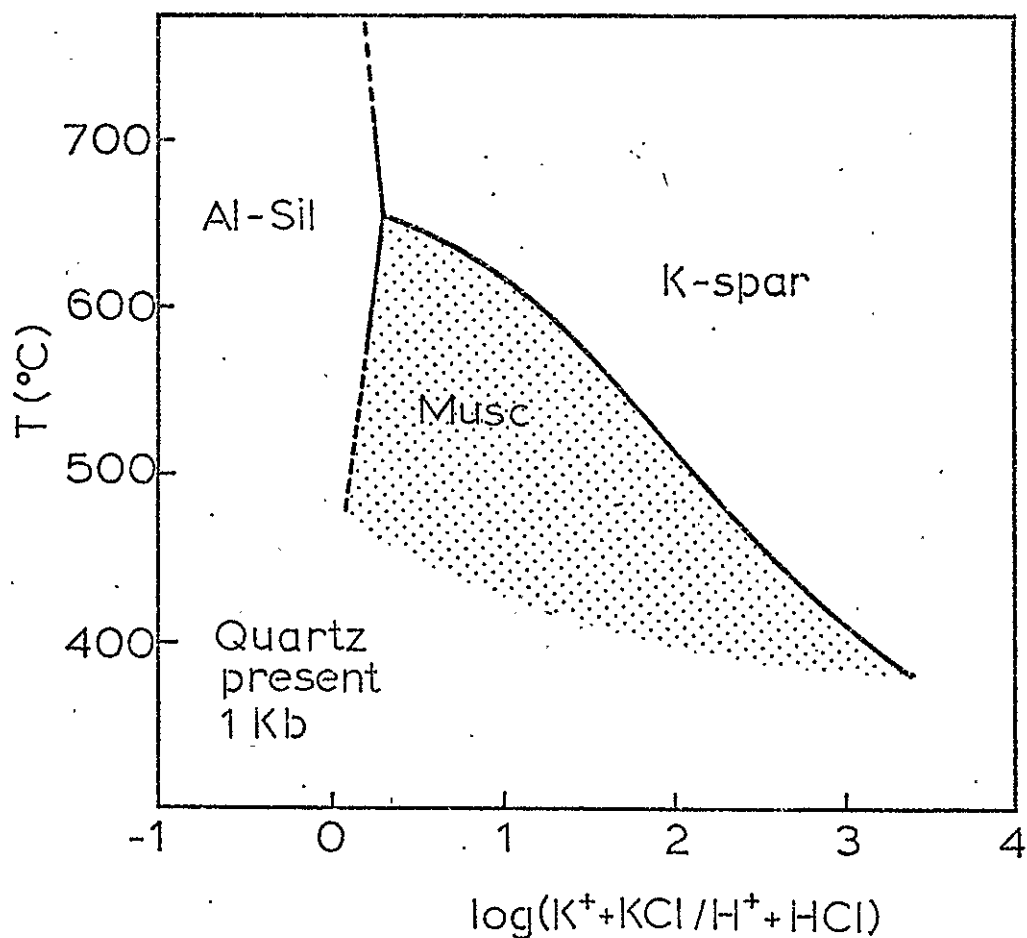
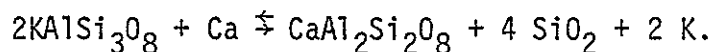
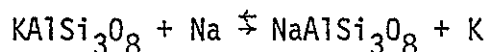


Figure 115b. Stability of muscovite at 1 kbar as a function of temperature and $(\text{K}^+ + \text{KCl})/(\text{H}^+ + \text{HCl})$ as determined by Shade (1968).

Reactions Producing Myrmekite

Myrmekite has attracted the attention of numerous investigators for nearly a century. The occurrences of myrmekite in the Dixon-Peñasco area are typical of those described in the literature in that it most commonly forms wartlike intrusions into K-feldspar at a point where K-feldspar and plagioclase touch (fig. 116). Myrmekite is most common in the more deformed rocks of the Rana Quartz Monzonite, where it tends to be finer grained than elsewhere, and is least common in the Puntiaquedo Granite Porphyry. Exceptions to the wart shape occur in all the granitic units, and some myrmekitic intergrowths occupy an entire side of a K-feldspar grain. In one occurrence in the Rana Quartz Monzonite, myrmekite appeared to truncate perthite lamellae in the adjacent microcline. (See Appendix I for further description of myrmekite as it occurs in various samples.)

The ideas for explaining these phenomena have been reviewed in some detail recently by Smith (1974) and Phillips (1974), and no attempt will be made to repeat that review here. Though details of theories vary from one author to another and a number of improbable explanations have been proposed, the basic controversy is still the same as it was in the first decade of this century: Is myrmekite formed by a process of replacement or by a process of exsolution? The replacement hypothesis was first advanced by Becke (1908) according to the reactions:



Schwantke (1909), on the other hand, suggested the exsolution model whereby $\text{CaAl}_2\text{Si}_6\text{O}_{16}$ was supposed to be contained in solid solution

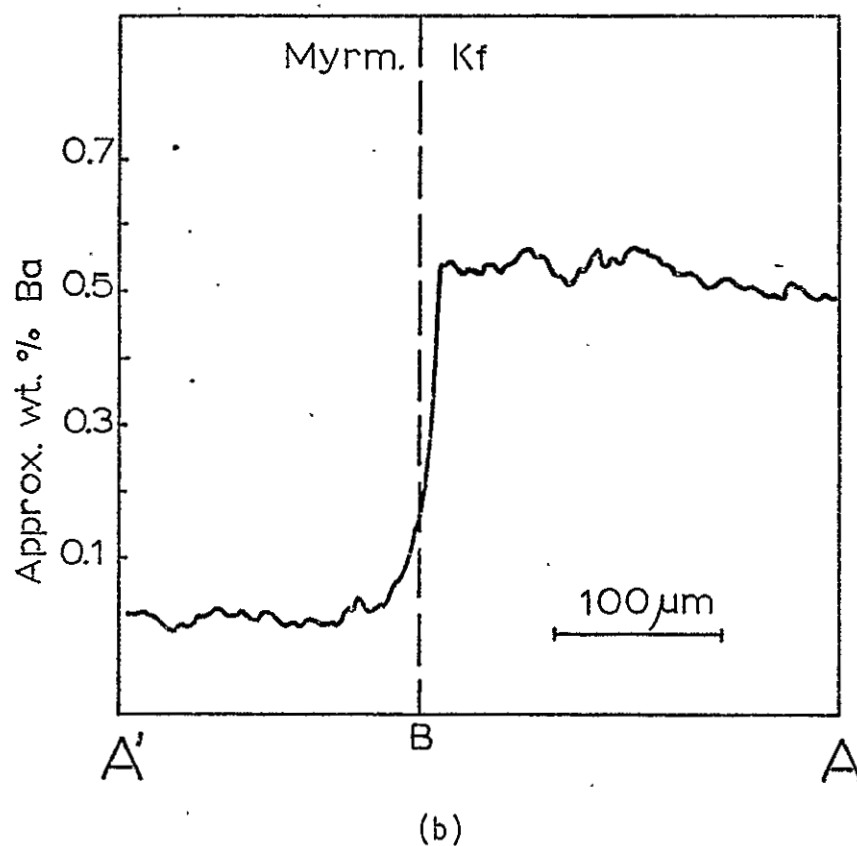
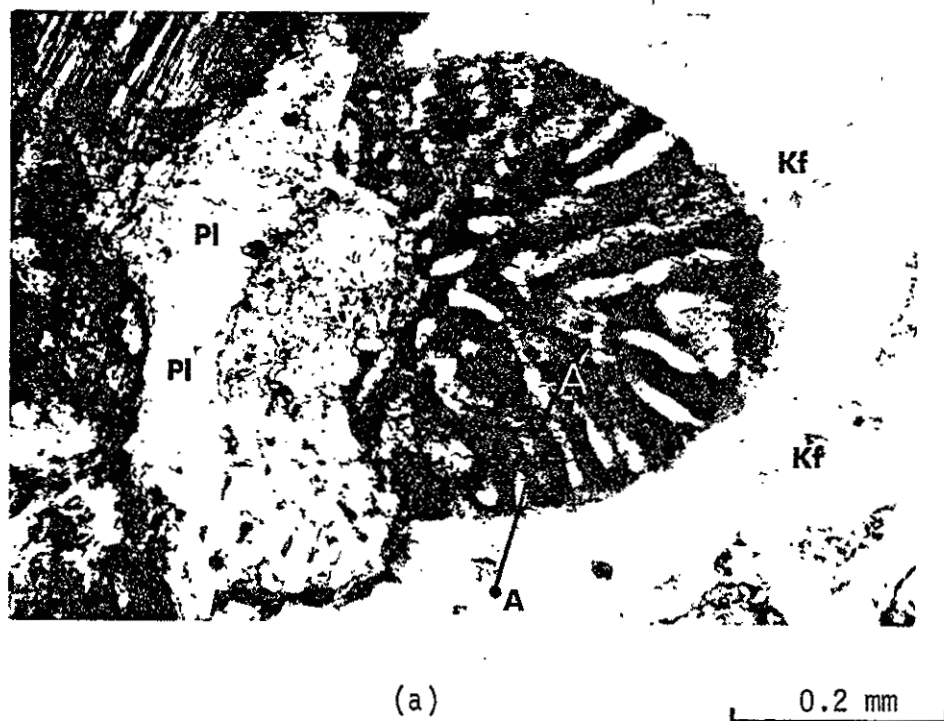
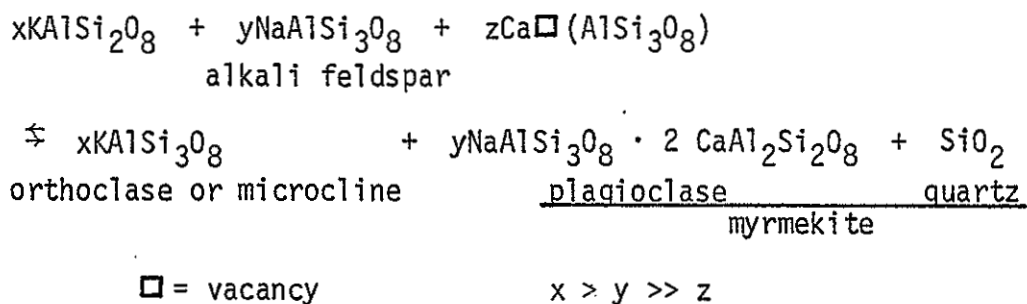


Figure 116. (a) Typical myrmekite texture. Peñasco Quartz Monzonite sample PL72-96b. (b) Results of a microprobe traverse for Ba from A to A'.

and gave rise to plagioclase and quartz at lower temperatures. This has been expressed by Phillips and others (1972) in the form:



As Smith (1974) and others before him have pointed out, both of these mechanisms produce quartz in the same ratio to An content of the plagioclase, so that determining the mole percent of quartz in myrmekite will not provide a distinction between the two mechanisms. Similarly, the textural features common in myrmekites could well have formed by either mechanism. The behavior of barium in relation to myrmekite formation had not been investigated, however, and this seemed to have possibilities because the barium distribution might well be different for a replacement versus an exsolution origin. For example, if an exsolution mechanism were responsible it might be expected that barium would be concentrated in the microcline adjacent to the myrmekite, either as solid solution or as discrete barium-rich phases (see section on barium zoning in K-feldspar megacrysts). Conversely, if a replacement mode involving a fluid phase were operative, the solution-redeposition processes would mean that excess barium could be removed in solution and the myrmekite would merely impinge on the pre-existing barium content of the K-feldspar.

In order to test this, the barium distribution adjacent to myrmekite was examined by traverses for barium with the electron microprobe

and by X-ray scanning images for barium. The results are shown in figure 117 and 118.

These figures show no strong barium gradients approaching the myrmekite and no high barium phases directly along the contact between the myrmekite and the K-feldspar. This supports the replacement hypothesis or at least indicates that actual growth of the myrmekite takes place by a solution-redeposition process, such that if exsolution in the K-feldspar is involved it communicates with the myrmekite itself via a fluid phase capable of removing barium. The replacement origin is consistent with the breakdown of plagioclase, which as previously discussed can release calcium and sodium to interstitial fluids (Barker, 1970). All myrmekites do not necessarily have the same origin (Smith, 1974), but the evidence presented here favors the replacement mode. Additional data on barium distribution from a variety of myrmekite occurrences eventually may resolve the problem.

Genetic Implications of Barium Zoning in Microcline Megacrysts

Introduction

The origin of potassium feldspar megacrysts in granitic rocks has been a long-standing problem in petrology. Interpretations of their origin fall largely into two groups: (1) the megacrysts are porphyroblasts, having grown after the bulk of the rock solidified (Dickson, 1958; Emmermann, 1968, 1969; Mehnert, 1968), or (2) the megacrysts are phenocrysts crystallized directly from a melt as a primary phase (Kerrick, 1969; Nemec, 1975). Unfortunately, most of the petrographic criteria that have been employed to distinguish these two possibilities are



(a)

Figure 117. Photomicrograph of myrmekite (Peñasco Quartz Monzonite, PL72-96i) with accompanying microprobe traverses for barium.

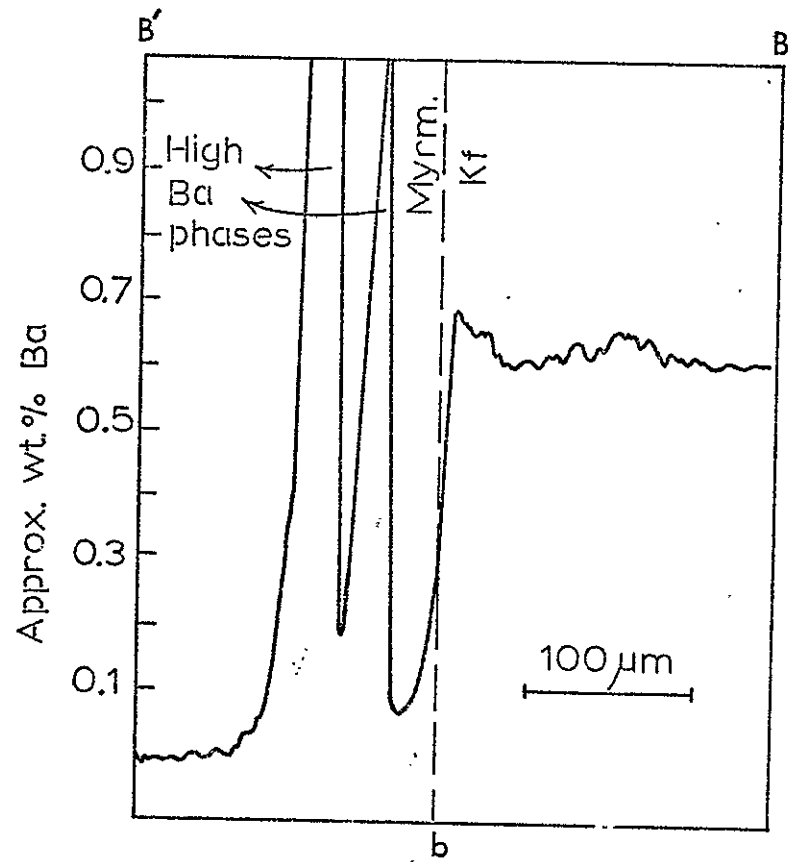
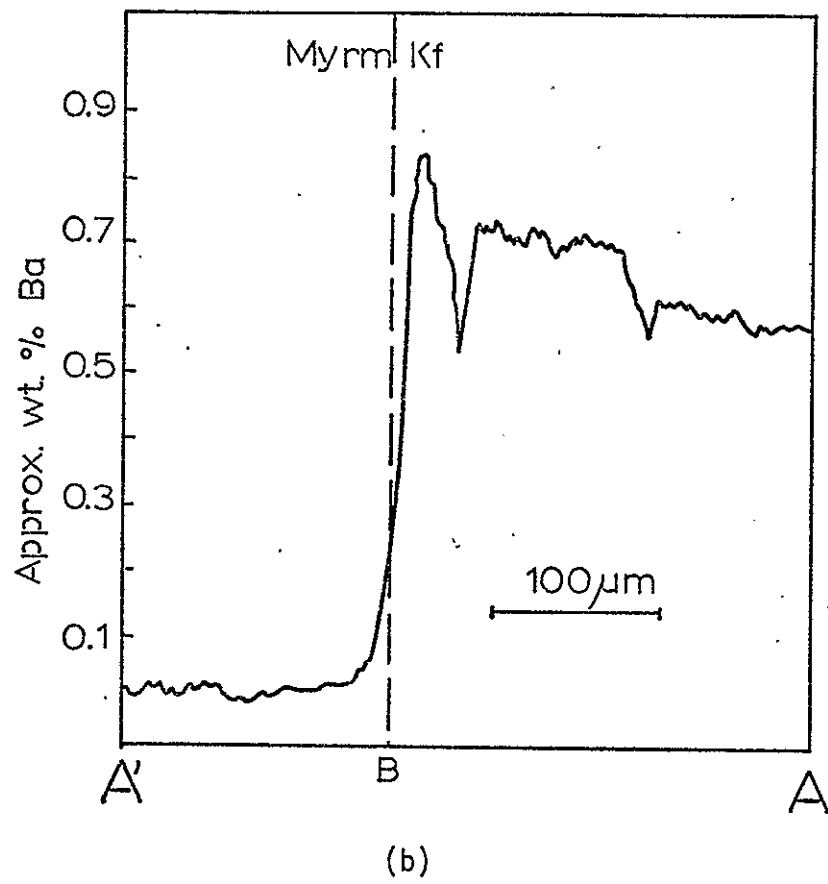


Figure 117.

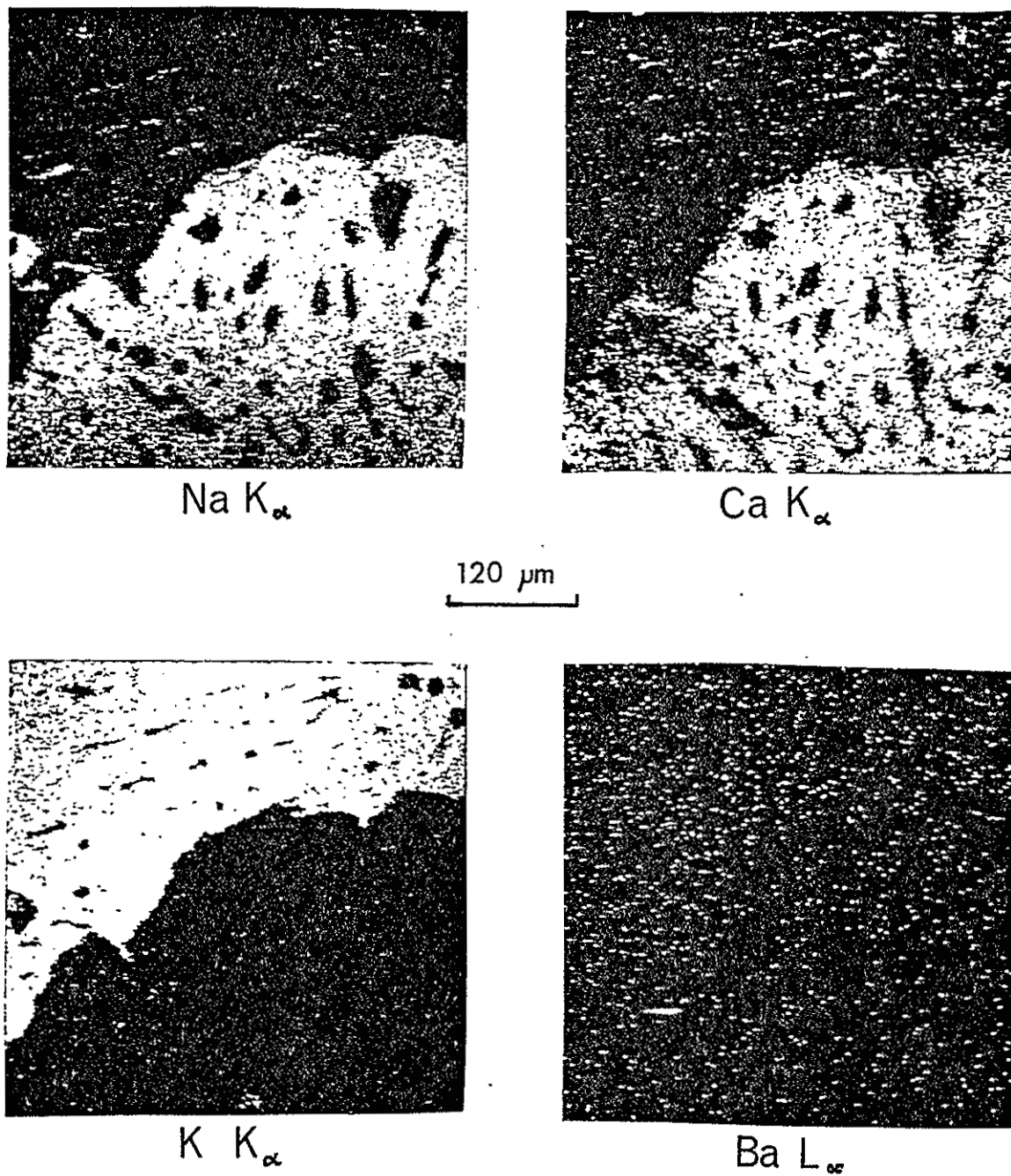


Figure 118. X-ray scanning photos of myrmekite from the Rana Quartz Monzonite.

inconclusive. For example, it has been argued that the presence of megacrysts in the country rock adjacent to a granitic intrusive body is evidence that the megacrysts in the granite itself did not grow from a melt. Such observations, however, are only permissive as they do not demand that the megacrysts in the granite be porphyroblasts. Indeed, an alternative explanation might be that the megacrysts in the country rock grew from a vapor phase that coexisted with a crystallizing magma. On the other hand, the subparallel orientation of tabular megacrysts has been cited as evidence of a magmatic origin, the alignment supposedly being due to flow in the magma. Alternative explanations are possible here also. For example, the alignment could be ascribed to subsolidus growth of the megacrysts while the granite was being deformed. Other field and petrographic criteria have similar uncertainties.

The stability range of K-feldspar is not particularly informative either, as K-feldspar is found in a variety of geologic environments and phase-equilibria studies only confirm this apparent large range of stability conditions. For example, Whitney (1972) has shown that for a typical synthetic granite composition, under conditions of high water content (6 weight percent H_2O or greater) and high pressure (8 kbar), an Or-rich alkali feldspar can be expected as the primary liquidus phase. At lower pressures and lower water contents, however, plagioclase is the primary liquidus phase and K-feldspar is the solidus phase. In more potassium-rich granitic compositions K-feldspar may be a liquidus phase under most reasonable conditions of temperature, pressure, and water content. K-feldspar also is stable under hydrothermal conditions, as evidenced by its occurrence in druses, pegmatite pockets, and hydrothermal vein deposits.

Since neither field, petrographic, nor experimental data seem to give a definitive answer for the origin of the megacrysts, some investigators have examined the chemistry of such megacrysts with particular emphasis on the distribution of barium. Dickson (1958) studied megacrysts from the Papoose Flat pluton in the Inyo Mountains of California by staining for barium. He observed numerous sharp, concentric zones of unequal thickness, each commonly characterized by a gradual depletion in barium concentration followed by a sharp increase which marked the start of the next zone. Dickson obtained no quantitative data, however, so the overall changes in barium content across the megacrysts are not known. His interpretation of the data, which included observation of the megacrysts in the country rocks adjacent to the pluton, was that the megacrysts were subsolidus, representing a fairly high temperature (700°C) and late-stage autometasomatism of the pluton. He accounts for the barium zoning by changes in the barium content of the fluid from which the megacrysts supposedly grew.

Kerrick (1969) examined megacrysts from a quartz monzonite in the central Sierra Nevada, California, by making microprobe analyses for barium at 400 μm intervals on a line through the center of several of the megacrysts. There was considerable variation in barium along the traverses, but with a slight tendency for barium to be highest at their centers. The most interesting observation, however, was that the groundmass K-feldspars had consistently less barium than did the megacrysts. Kerrick interpreted this to indicate that the megacrysts must have grown prior to the groundmass K-feldspars. His reasoning was that the early formed megacrysts would have depleted the remaining melt in barium, thus leading to lower barium groundmass feldspar.

In contrast, Emmermann (1968, 1969) studied the megacrysts of the Aplital Granite in the southern Black Forest, Germany, by examining their bulk chemistry. He discovered that the megacrysts had higher barium than the groundmass K-feldspars but interpreted this to mean that (1) there were two separate generations of feldspars and (2) the megacrysts formed as porphyroblasts from an interstitial fluid phase that gave rise to the high barium content. Emmermann reports that a microprobe traverse for barium showed no zoning for these megacrysts.

A different approach was taken by Nemec (1975), who obtained barium analyses for megacrysts from the southeastern part of the Bohemian Massif and was able to document "normal zoning" of barium by finding a strong correlation between bulk barium concentration and size of the megacrysts. He interpreted this relationship as indicating a magmatic origin for the megacrysts.

Some of the most recent data on barium zoning in megacrysts has been provided by Kuryvial (1976), who used a technique similar to that of Kerrick (1969) for analyzing barium in megacrysts from the central Wasatch Range, Utah (Little Cottonwood stock). His results were similar to Kerrick's, in that there was considerable scatter in the data from one point to another (500 μm steps) and a general tendency for normal zoning, i.e. a decrease in barium toward the edges of the megacrysts. Furthermore, the groundmass K-feldspar is substantially poorer in barium in this case as well (0.3 to 1.3 weight percent). Kuryvial appears to have assumed from the outset that the megacrysts were, in fact, early formed phenocrysts and implies that his data confirm his assumptions.

In this study, megacrysts from the Puntigudo Granite Porphyry and the Peñasco Quartz Monzonite were analyzed for barium by continuous microprobe traverses from center to edge. This was done as part of this thesis because it became important to distinguish between an igneous or metasomatic origin for these megacrysts in order to evaluate relative importance of these processes in the Dixon-Peñasco area. In addition, the study of the barium zoning became an end in itself when it became clear that there was a paucity of data on the subject and that the available data had not been interpreted with much sophistication. That is, any two investigators seem to be able to interpret similar data in very different ways. This may be partly from not clearly stating assumptions and partly because of not considering data in the light of constraints imposed by experimental data or crystal growth theory. Thus the purposes of this study were to provide additional information on barium distribution in a particular megacryst occurrence, to provide some preliminary data on the experimental determination of the distribution of barium in synthetic granites, and finally to interpret both kinds of data in the light of crystal growth theory. The immediate goal is to decide whether the megacrysts in the Dixon-Peñasco area are magmatic or metasomatic, but similar consideration of megacrysts in occurrences around the world ultimately should allow us to decide, in a general way, the origin of K-feldspar megacrysts in granitic rocks.

Puntigudo Granite Porphyry

The Puntigudo Granite Porphyry, actually a quartz monzonite, contains moderate-sized, subequant, Carlsbad- and M-twinning megacrysts

of microcline. In addition to the megacrysts of microcline, less obvious oblate and polygonized quartz grain aggregates appear to be relict phenocrysts of quartz. Furthermore, elongate clots of thoroughly polygonized plagioclase are distinguished from the matrix only by a slightly larger grain size and, in some instances, by a greater amount of secondary muscovite. These clots are probably relict plagioclase phenocrysts that have been destroyed by a combination of chemical breakdown and mechanical granulation. Evidence that euhedral grains of plagioclase once existed in this rock is provided by rare grains in the matrix that have not been so thoroughly granulated and by large intact grains of plagioclase within some of the microcline megacrysts. Some of these textural features of the Puntiaquedo Granite Porphyry are illustrated in figure 119.

Figure 120 shows a detailed view of typical microcline megacrysts from the Puntiaquedo Granite Porphyry. The slightly asymmetrical shape of the two halves of the Carlsbad twin and the irregularity of the twin plane are common features of the megacrysts. The presence of the Carlsbad twinning and the very existence of the M-twinning (Ribbe, 1975) indicate that the K-feldspar originally crystallized with monoclinic symmetry. While this does not distinguish between a magmatic or post-magmatic origin for the megacrysts, it does seem to preclude direct growth at temperatures below the monoclinic-triclinic inversion.

The large plagioclase inclusion in the megacryst in figure 120 is fairly typical. Rarely are such individuals completely included, and some are simply adjacent to a megacryst. Smaller inclusions, however, are very common, and they show a slight suggestion of a concentric arrangement around the centers of the megacrysts. Veinlets of albite

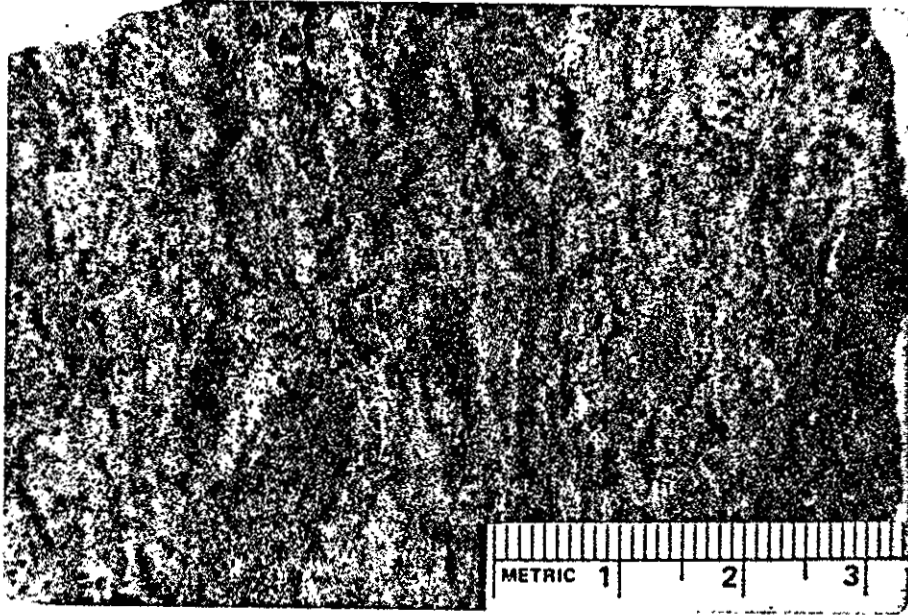
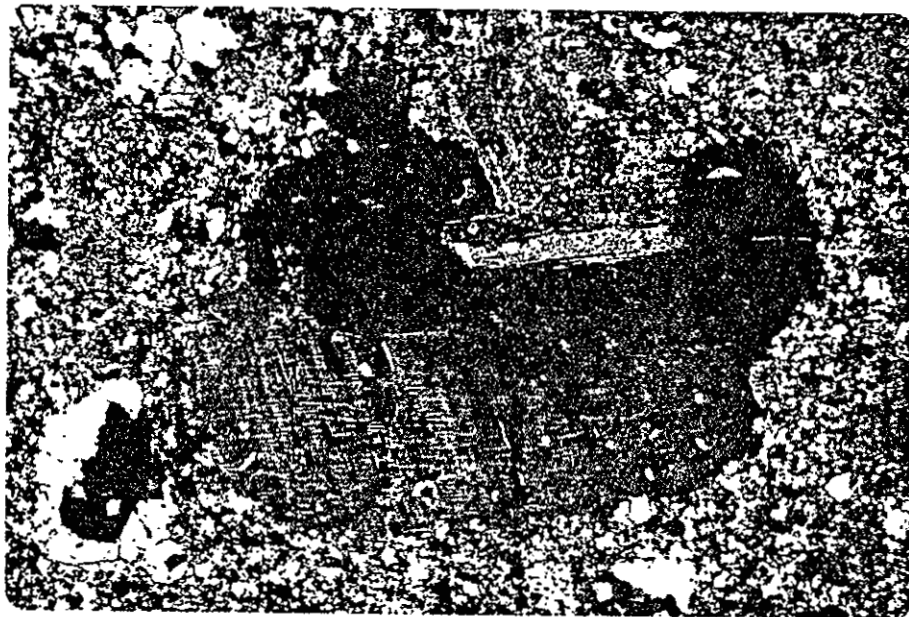


Figure 119. Stained slab, Puntigudo Granite Porphyry.



5 mm

Figure 120. Close-up of Puntigudo Granite Porphyry megacryst.

are not uncommon. The megacrysts appear resistant to deformation, but in some severely deformed rocks they are granulated around their margins.

Overall, the petrographic evidence that the microcline megacrysts in the Punttiagudo Granite Porphyry are phenocrysts seems rather compelling. Yet such textural evidence, as any skeptic would point out, does not provide substantial proof that the megacrysts did not grow in a postmagmatic environment. In the case of the Peñasco Quartz Monzonite, the textural evidence is even less clearcut, and the need for additional criteria becomes obvious.

Peñasco Quartz Monzonite

In contrast to the Punttiagudo Granite Porphyry, the Peñasco Quartz Monzonite is largely concordant with the country rock and shows minor migmatization along its contacts. It is a sphene-bearing biotite quartz monzonite to granodiorite that shows fairly strong compositional variations, but which lacks a distinctive border zone or a strong orientation of platy minerals. The concentration of megacrysts varies markedly in the body from 0 to about 30 percent. No sharp, internal contacts have been observed, but the greatest concentrations of megacrysts seem to bear no obvious relationship to the margins of the body.

Where the Peñasco Quartz Monzonite does contain megacrysts they are fairly large (<9 cm), tabular crystals set in a medium-grained matrix of plagioclase, quartz, microcline, biotite, and sphene, with numerous accessory minerals such as epidote, muscovite, zircon, and allanite. The plagioclase grains are euhedral to subhedral and typically show undulatory normal zoning. The quartz grains, on the other hand, are distinctly anhedral and show undulatory extinction. Biotite is

commonly associated with quartz and occurs as clots or groups of grains that include the assemblage of mafic accessory minerals.

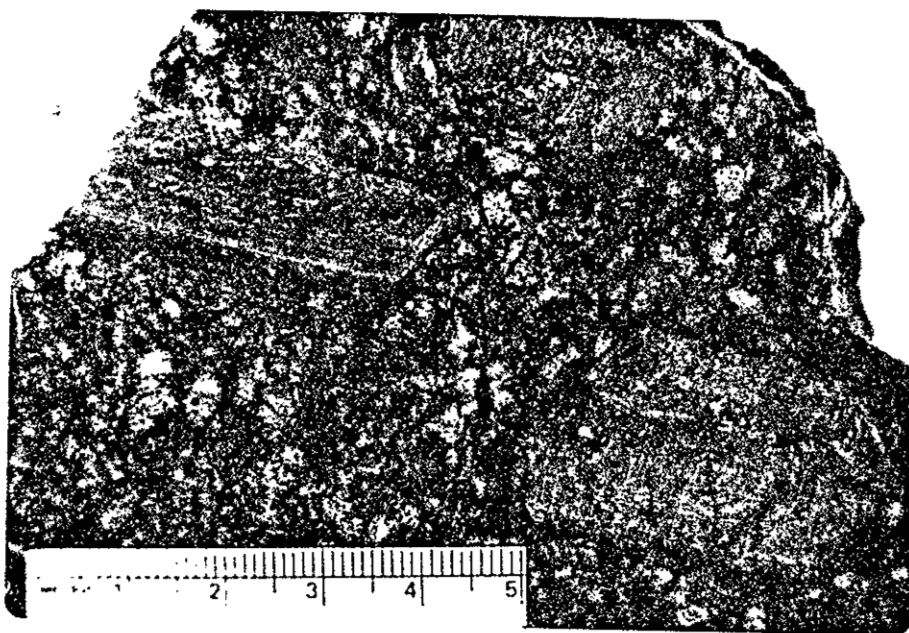
The megacrysts themselves (fig. 122) generally show a simple Carlsbad interpenetration twin plane and consist primarily of microperthitic M-twinning microcline with plagioclase inclusions, and rare albite veinlets. The inclusions are about 0.5 mm in length, roughly tabular in shape, and show a definite pattern of concentric arrangement which appears to indicate ghost crystal faces (fig. 123). That is, they mark the position of crystal growth faces at successive stages in the development of megacrysts. The concentricity of these crystal growth faces allows the determination of the exact center, presumably also the nucleation point, of the megacryst. The inclusions are generally zoned, with a more anorthite-rich core that is itself normally zoned, and this core is rimmed by a discrete zone of albite-oligoclase composition. The more An-rich portion is commonly altered to very fine-grained epidote and muscovite.

Barium Distribution--Description of Features

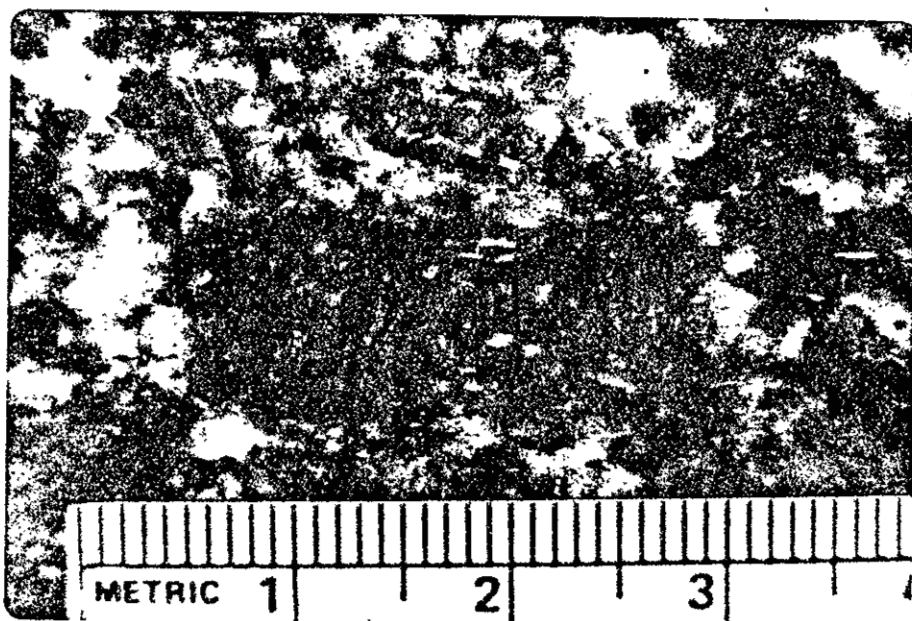
Methods and Techniques of Analysis

The variation of barium evidenced in Kerrick's (1969) spot microprobe analyses suggests the need for a different technique in analyzing megacrysts. This, plus generally high amounts of barium in megacrysts, indicated the possible value of continuous microprobe traverses. The initial results proved extremely interesting and provided very nearly quantitative results in a relatively short time.

The analytical conditions were 10 μ m beam diameter, 20 kV accelerating potential, 0.5 μ A sample current on an ARL EMX microprobe. The



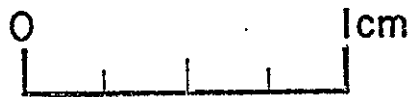
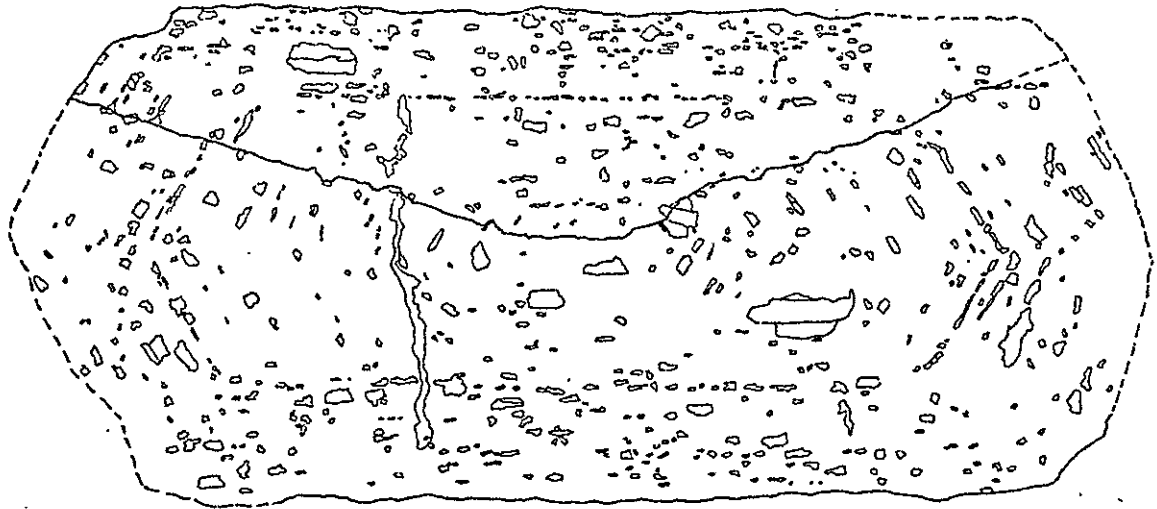
(a)



(b)

Figure 122. Stained slabs, Peñasco Quartz Monzonite. (a) PL72-96;
(b) PL71-5.

PL 72-96c



PL73-68ls

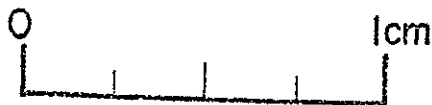
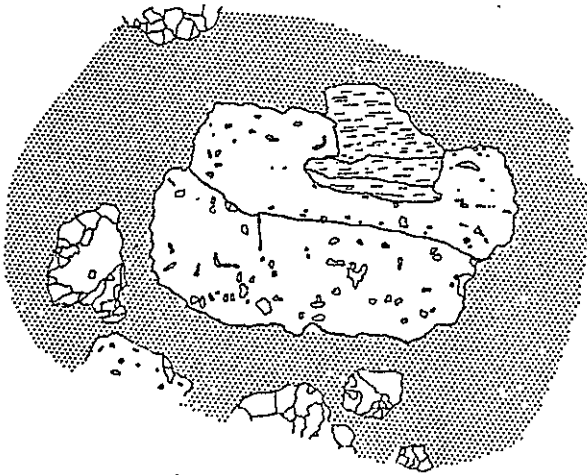


Figure 123. Line drawings of (above) Peñasco Quartz Monzonite megacryst, and (below) Puntigudo Granite Porphyry megacryst.

sample was translated at a rate of 100 $\mu\text{m}/\text{min}$. Most of the traverses were designed to parallel the shortest dimension of the crystal, parallel to the *b* crystallographic axis in the original monoclinic symmetry, but traverses in other directions were also made in order to demonstrate that the barium zoning was concentric and that there was no significant sector zoning. About 50 traverses were made on megacrysts from both the Peñasco Quartz Monzonite and the Puntiaquedo Granite Porphyry. In addition, numerous individual points were analyzed quantitatively under similar analytical conditions, except that the beam diameter was reduced to about 2 μm and sample current to 0.1 to 0.03 μA depending on susceptibility of the sample to damage by the electron beam. Finally, X-ray scanning photographs and secondary electron photographs were taken in order to verify the distribution pattern of certain barium feldspar phases. Limited use also was made of cathodeluminescence properties of feldspars as observed in a luminescope (TM) (Smith and Stenstrom, 1965), in order to obtain certain textural and chemical information not available from the microprobe analyses.

In general, the traverse technique proved to be invaluable. In fact it was impractical to attempt quantitative analyses of the megacrysts without first doing a continuous traverse, due to heterogeneity on a 5 to 10 μm scale.

In addition to barium, sodium and either potassium or calcium also were monitored so that barium levels could be correlated with position in the megacrysts and with major phases present. The traverses thus produced two kinds of information: (1) the number and kinds of phases present within the megacrysts, and (2) the general variation of barium as a function of position relative to the center of the megacrysts.

The traverses show that there are four phases present in all of the megacrysts. They are maximum microcline (Or_{96}), plagioclase solid solution (An_7 to An_{12}), "albite" (An_5 to An_2), and a barium-rich phase ($Or_{31}Cn_{13}Ab_6$). Cathodeluminescence suggests that the "albite" is actually two phases, one rimming plagioclase inclusions and the other occurring as perthite lamellae. Microcline is the dominant phase, acting as host to all of the others. It has a barium concentration that ranges from about 3000 to 8000 ppm. Other cations, however, are rather constant. The Or content is about 96 mol percent, Ab is approximately 3 mol percent, and Ca is less than or equal to 50 ppm. Table 3 gives representative analyses of megacryst microcline from both the Puntiaquado Granite Porphyry and the Peñasco Quartz Monzonite.

The plagioclase inclusions consist of two parts, cores or central zones that show a continuous but spatially erratic variation in An content from An_{12} to An_7 , and rims that show a more restricted An content of An_4 to An_2 . Barium content of these phases is much lower than in the microcline, less than the detection limit of about 50 ppm. Table 4 gives typical compositions of the plagioclase inclusions.

Perthitic lamellae in the microcline are albitic in composition (An_2), but their exact An content is uncertain because of difficulty in analyzing such narrow features. Cathodeluminescence, however, indicates that they have a composition distinct from that of the albite rims on the plagioclase inclusions. This is probably due in part to a lower An content (Smith and Stenstrom, 1965). Barium concentration is again low, probably less than 50 ppm.

Finally, barium-rich phases occur as tiny discrete grains commonly associated with the plagioclase inclusions. They contain up to 6 weight

Table 3

Electron Microprobe Analyses of Microcline Megacrysts
from the Puntigudo Granite Porphyry and
the Peñasco Quartz Monzonite

Puntiagudo Granite Porphyry

68 Ksp1		68 Ksp2		68 Ksp3		68 Ksp4	
<u>Oxide</u>	<u>Wt. %</u>	<u>Oxide</u>	<u>Wt. %</u>	<u>Oxide</u>	<u>Wt. %</u>	<u>Oxide</u>	<u>Wt. %</u>
Na ₂ O	0.44	Na ₂ O	0.37	Na ₂ O	0.23	Na ₂ O	0.28
K ₂ O	15.95	K ₂ O	15.91	K ₂ O	16.43	K ₂ O	16.43
CaO	0.00	CaO	0.00	CaO	0.00	CaO	0.00
BaO	0.67	BaO	1.09	BaO	0.25	BaO	0.18
Al ₂ O ₃	18.52	Al ₂ O ₃	18.57	Al ₂ O ₃	18.34	Al ₂ O ₃	18.09
SiO ₂	63.62	SiO ₂	63.65	SiO ₂	64.25	SiO ₂	64.17
Total	99.20	Total	99.59	Total	99.51	Total	99.15
Ba	6030 ppm	Ba	9720 ppm	Ba	2230 ppm	Ba	1640 ppm
	<u>Mol %</u>		<u>Mol %</u>		<u>Mol %</u>		<u>Mol %</u>
Ab	3.94	Ab	3.33	Ab	2.11	Ab	2.50
Or	94.83	Or	94.69	Or	97.44	Or	97.17
An	0.00	An	0.00	An	0.00	An	0.00
Cn	1.23	Cn	1.98	Cn	0.45	Cn	0.33

Peñasco Quartz Monzonite

92 Ksp1		92 Ksp2		960 Ksp1-07		960 Ksp1-08	
Oxide	Wt. %	Oxide	Wt. %	Oxide	Wt. %	Oxide	Wt. %
Na ₂ O	0.61	Na ₂ O	0.54	Na ₂ O	0.54	Na ₂ O	0.49
K ₂ O	15.43	K ₂ O	15.67	K ₂ O	15.97	K ₂ O	16.11
CaO	0.00	CaO	0.01	CaO	0.00	CaO	0.00
BaO	1.16	BaO	0.90	BaO	0.44	BaO	0.51
Al ₂ O ₃	18.59	Al ₂ O ₃	18.59	Al ₂ O ₃	18.15	Al ₂ O ₃	19.19
SiO ₂	64.18	SiO ₂	64.29	SiO ₂	65.38	SiO ₂	65.62
Total	99.98	Total	99.99	Total	100.48	Total	101.92
Ba	10430 ppm	Ba	8080 ppm	Ba	3960 ppm	Ba	4530 ppm
Mol %		Mol %		Mol %		Mol %	
Ab	5.53	Ab	4.86	Ab	4.86	Ab	4.40
Or	92.32	Or	93.45	Or	94.34	Or	94.69
An	0.01	An	0.03	An	0.00	An	0.00
Cn	2.14	Cn	1.65	Cn	0.80	Cn	0.91

960 Ksp1-09		960 Ksp1-10		960 Ksp2-05		960 Ksp2-06	
<u>Oxide</u>	<u>Wt. %</u>	<u>Oxide</u>	<u>Wt. %</u>	<u>Oxide</u>	<u>Wt. %</u>	<u>Oxide</u>	<u>Wt. %</u>
Na ₂ O	0.84	Na ₂ O	0.54	Na ₂ O	0.57	Na ₂ O	0.64
K ₂ O	15.30	K ₂ O	15.87	K ₂ O	15.89	K ₂ O	15.85
CaO	0.00	CaO	0.00	CaO	0.00	CaO	0.00
BaO	0.45	BaO	0.60	BaO	0.40	BaO	0.35
Al ₂ O ₃	18.15	Al ₂ O ₃	18.90	Al ₂ O ₃	18.82	Al ₂ O ₃	19.39
SiO ₂	65.35	SiO ₂	64.76	SiO ₂	64.76	SiO ₂	65.20
Total	100.10	Total	100.68	Total	100.44	Total	101.42
Ba	4030 ppm	Ba	5350 ppm	Ba	3540 ppm	Ba	3130 ppm
	Mol %		Mol %		Mol %		Mol %
Ab	7.68	Ab	4.87	Ab	5.15	Ab	5.72
Or	91.49	Or	94.04	Or	94.13	Or	93.64
An	0.00	An	0.00	An	0.00	An	0.00
Cn	0.83	Cn	1.09	Cn	0.72	Cn	0.63

960 Ksp2-08	
<u>Oxide</u>	<u>Wt. %</u>
Na ₂ O	0.74
K ₂ O	14.93
CaO	0.01
BaO	0.46
Al ₂ O ₃	19.19
SiO ₂	64.45
Total	99.78
Ba	4110 ppm
	<u>Mol %</u>
Ab	6.94
Or	92.15
An	0.04
Cn	0.87

960 Ksp2-10	
<u>Oxide</u>	<u>Wt. %</u>
Na ₂ O	1.93
K ₂ O	13.41
CaO	0.01
BaO	0.46
Al ₂ O ₃	19.10
SiO ₂	65.46
Total	100.36
Ba	4110 ppm
	<u>Mol %</u>
Ab	17.79
Or	81.31
An	0.04
Cn	0.85

960 Ksp3-02	
<u>Oxide</u>	<u>Wt. %</u>
Na ₂ O	0.30
K ₂ O	16.37
CaO	0.00
BaO	0.55
Al ₂ O ₃	18.83
SiO ₂	65.02
Total	101.07
Ba	4910 ppm
	<u>Mol %</u>
Ab	2.67
Or	96.34
An	0.00
Cn	0.99

Table 4

Electron Microprobe Analyses of Plagioclase Inclusions
in Microcline Megacrysts from the Puntagudo Granite
Porphyry and the Peñasco Quartz Monzonite and
Ba-rich K-feldspar Inclusions in Megacrysts
from the Peñasco Quartz Monzonite

Plagioclase Inclusion, Puntigado Granite Porphyry

68 Plg1		68 Plg2		68 Plg2.1	
<u>Oxide</u>	<u>Wt. %</u>	<u>Oxide</u>	<u>Wt. %</u>	<u>Oxide</u>	<u>Wt. %</u>
Na ₂ O	11.83	Na ₂ O	11.43	Na ₂ O	11.45
K ₂ O	0.03	K ₂ O	0.12	K ₂ O	0.12
CaO	0.17	CaO	0.81	CaO	0.81
BaO	0.00	BaO	0.01	BaO	0.01
Al ₂ O ₃	19.41	Al ₂ O ₃	20.48	Al ₂ O ₃	19.53
SiO ₂	68.54	SiO ₂	67.65	SiO ₂	68.42
Total	99.98	Total	100.50	Total	100.33
Ba	30 ppm	Ba	80 ppm	Ba	80 ppm
Mol %		Mol %		Mol %	
Ab	99.01	Ab	95.62	Ab	95.62
Or	0.19	Or	0.63	Or	0.63
An	0.79	An	3.73	An	3.73
Cn	0.01	Cn	0.02	Cn	0.02

Plagioclase Inclusions, Peñasco Quartz Monzonite

96B Plg1		96B Plg2		96C Plg1		96C Plg2	
Oxide	Wt. %	Oxide	Wt. %	Oxide	Wt. %	Oxide	Wt. %
Na ₂ O	9.47	Na ₂ O	8.68	Na ₂ O	10.13	Na ₂ O	11.15
K ₂ O	0.13	K ₂ O	0.27	K ₂ O	0.12	K ₂ O	0.12
CaO	3.49	CaO	4.71	CaO	1.29	CaO	0.46
BaO	0.01	BaO	0.04	BaO	0.01	BaO	0.02
Al ₂ O ₃	22.83	Al ₂ O ₃	23.23	Al ₂ O ₃	21.45	Al ₂ O ₃	20.03
SiO ₂	64.95	SiO ₂	64.00	SiO ₂	67.93	SiO ₂	68.59
Total	100.87	Total	100.93	Total	100.92	Total	100.37
Ba	80 ppm	Ba	370 ppm	Ba	70 ppm	Ba	160 ppm
	Mol %		Mol %		Mol %		Mol %
Ab	82.47	Ab	75.65	Ab	92.73	Ab	97.07
Or	0.73	Or	1.56	Or	0.75	Or	0.68
An	16.78	An	22.71	An	6.50	An	2.22
Cn	0.02	Cn	0.07	Cn	0.01	Cn	0.03

96C Plg3		96I Plg1		96I Plg2		96I Plg3	
<u>Oxide</u>	<u>Wt. %</u>	<u>Oxide</u>	<u>Wt. %</u>	<u>Oxide</u>	<u>Wt. %</u>	<u>Oxide</u>	<u>Wt. %</u>
Na ₂ O	11.17	Na ₂ O	10.14	Na ₂ O	10.22	Na ₂ O	11.33
K ₂ O	0.11	K ₂ O	0.16	K ₂ O	0.17	K ₂ O	0.16
CaO	0.91	CaO	2.50	CaO	2.54	CaO	0.52
BaO	0.00	BaO	0.04	BaO	0.03	BaO	0.01
Al ₂ O ₃	20.30	Al ₂ O ₃	22.19	Al ₂ O ₃	22.05	Al ₂ O ₃	22.04
SiO ₂	67.67	SiO ₂	63.95	SiO ₂	64.35	SiO ₂	65.28
Total	100.17	Total	98.98	Total	99.36	Total	99.35
Ba	30 ppm	Ba	330 ppm	Ba	290 ppm	Ba	130 ppm
Mol %		Mol %		Mol %		Mol %	
Ab	95.10	Ab	87.16	Ab	87.05	Ab	96.63
Or	0.61	Or	0.89	Or	0.92	Or	0.88
An	4.28	An	11.88	An	11.96	An	2.47
Cn	0.01	Cn	0.06	Cn	0.06	Cn	0.03

Ba-rich K-feldspar Inclusions, Peñasco Quartz Monzonite

960 Ba1		96I Ba1		96I Ba2	
<u>Oxide</u>	<u>Wt. %</u>	<u>Oxide</u>	<u>Wt. %</u>	<u>Oxide</u>	<u>Wt. %</u>
Na ₂ O	0.47	Na ₂ O	0.63	Na ₂ O	0.63
K ₂ O	14.36	K ₂ O	12.45	K ₂ O	12.40
CaO	0.01	CaO	0.02	CaO	0.01
BaO	4.45	BaO	6.41	BaO	4.76
Al ₂ O ₃	19.98	Al ₂ O ₃	20.87	Al ₂ O ₃	19.18
SiO ₂	61.76	SiO ₂	61.55	SiO ₂	60.68
Total	101.03	Total	101.94	Total	97.66
Ba	39820 ppm	Ba	57440 ppm	Ba	42620 ppm
	<u>Mol %</u>		<u>Mol %</u>		<u>Mol %</u>
Ab	4.39	Ab	6.26	Ab	6.48
Or	87.27	Or	80.85	Or	83.61
An	0.05	An	0.11	An	0.05
Cn	8.30	Cn	12.79	Cn	9.86

percent BaO (13 mol percent celsian) and are a K-rich feldspar. Typical microprobe analyses are given in table 4. The maximum values of barium concentration given may not represent the actual composition of all the grains owing to their very small size relative to the microprobe beam size. Barium-rich phases are present in megacrysts from both rock units but are more common in the Peñasco Quartz Monzonite megacrysts, perhaps because small plagioclase inclusions are more common in those megacrysts.

Figure 124 and 125 summarize the composition of the phases just discussed. Figure 124 is a series of scanning photos showing secondary electron image, Ba, Ca, Na, and K scanning images of a plagioclase inclusion and surrounding microcline. Note in particular the distribution of Ca within the inclusion and the distribution of the high-Ba phases. Figure 125 shows the analyses from tables 3 and 4 plotted on Ab-Or-An and Ab-Or-Cn triangular diagrams. The distinctive compositions of the four main phases is readily apparent, and the significance and probable origin of the plagioclases and the Ba-rich phase are discussed farther on.

General Barium Zoning

Table 3 and figure 125 show that the microcline itself has a variable barium composition, and it is this variation in barium with position in the megacrysts that is particularly well demonstrated by the continuous traverses. A portion of the results of a typical traverse is shown in figure 126. Note that the traverse intersected some grains of high-Ba feldspar and numerous plagioclase inclusions and albite lamellae with low barium concentrations. If these phases are ignored and only

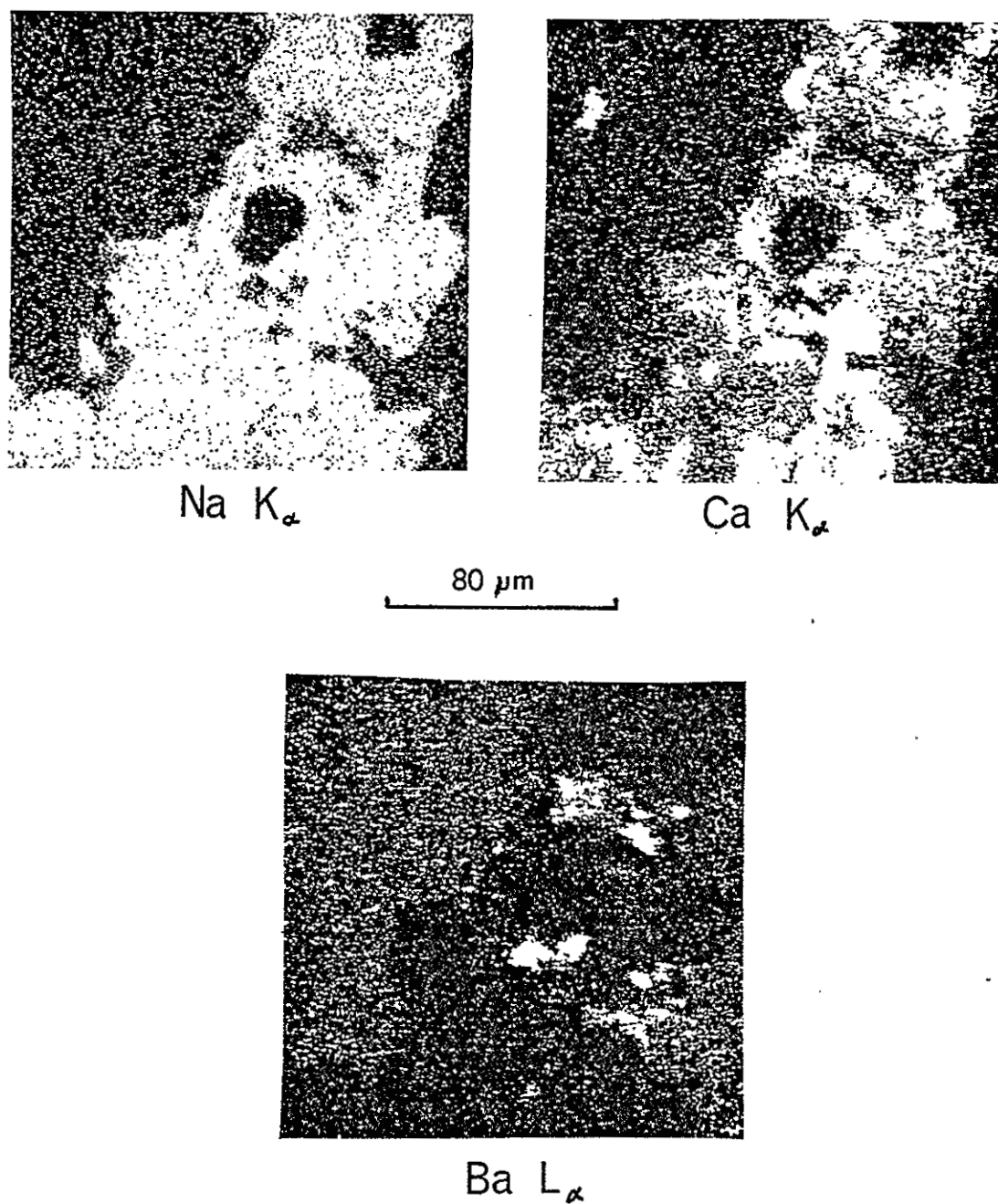


Figure 124. Electron microprobe scanning photographs of a plagioclase inclusion in a megacryst from the Peñasco Quartz Monzonite (PL72-96).

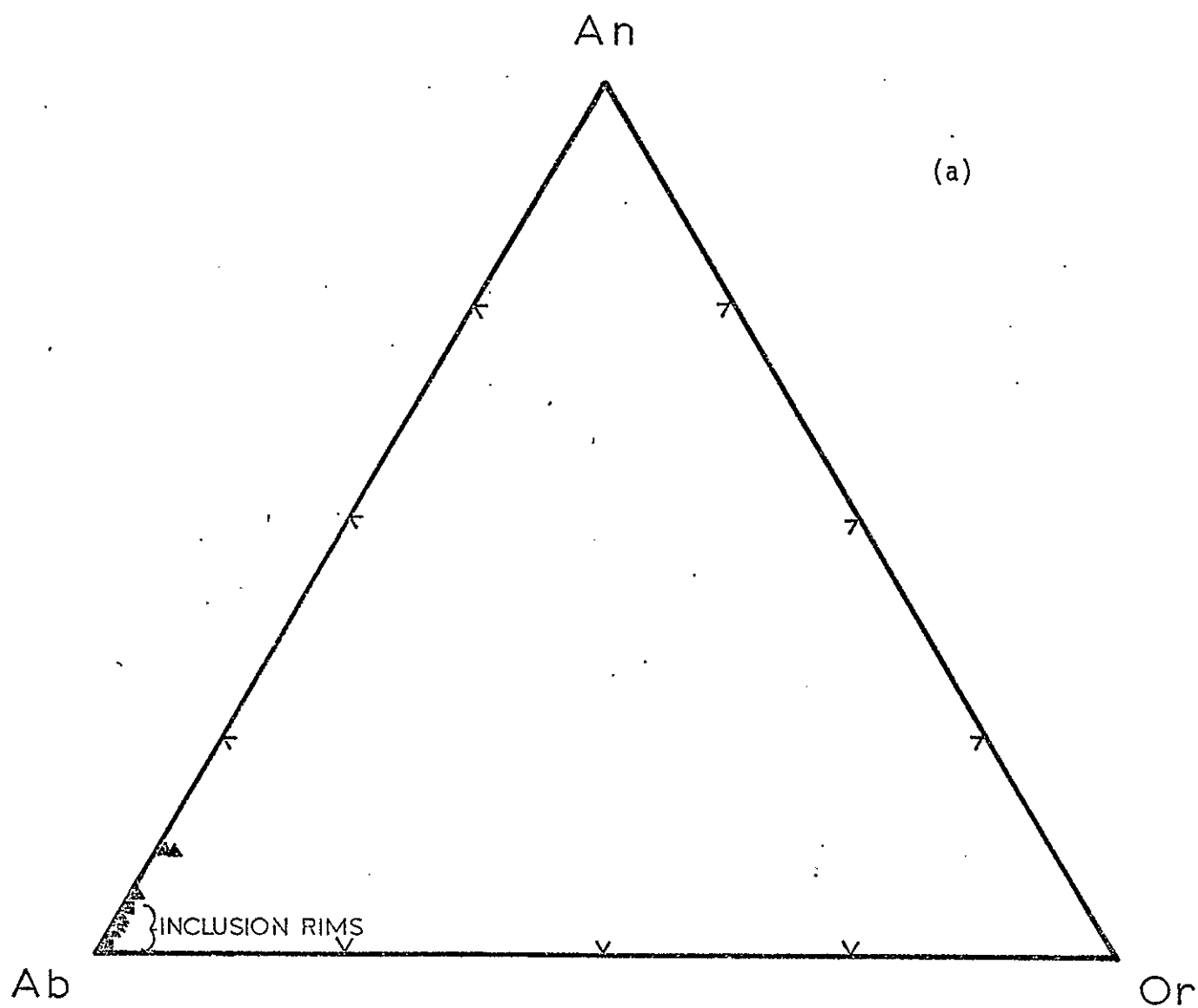


Figure 125. Plots of microprobe analyses of feldspars from the megacrysts on Ab-Or-An (a) and Ab-Or-Cn (b) triangular diagrams.

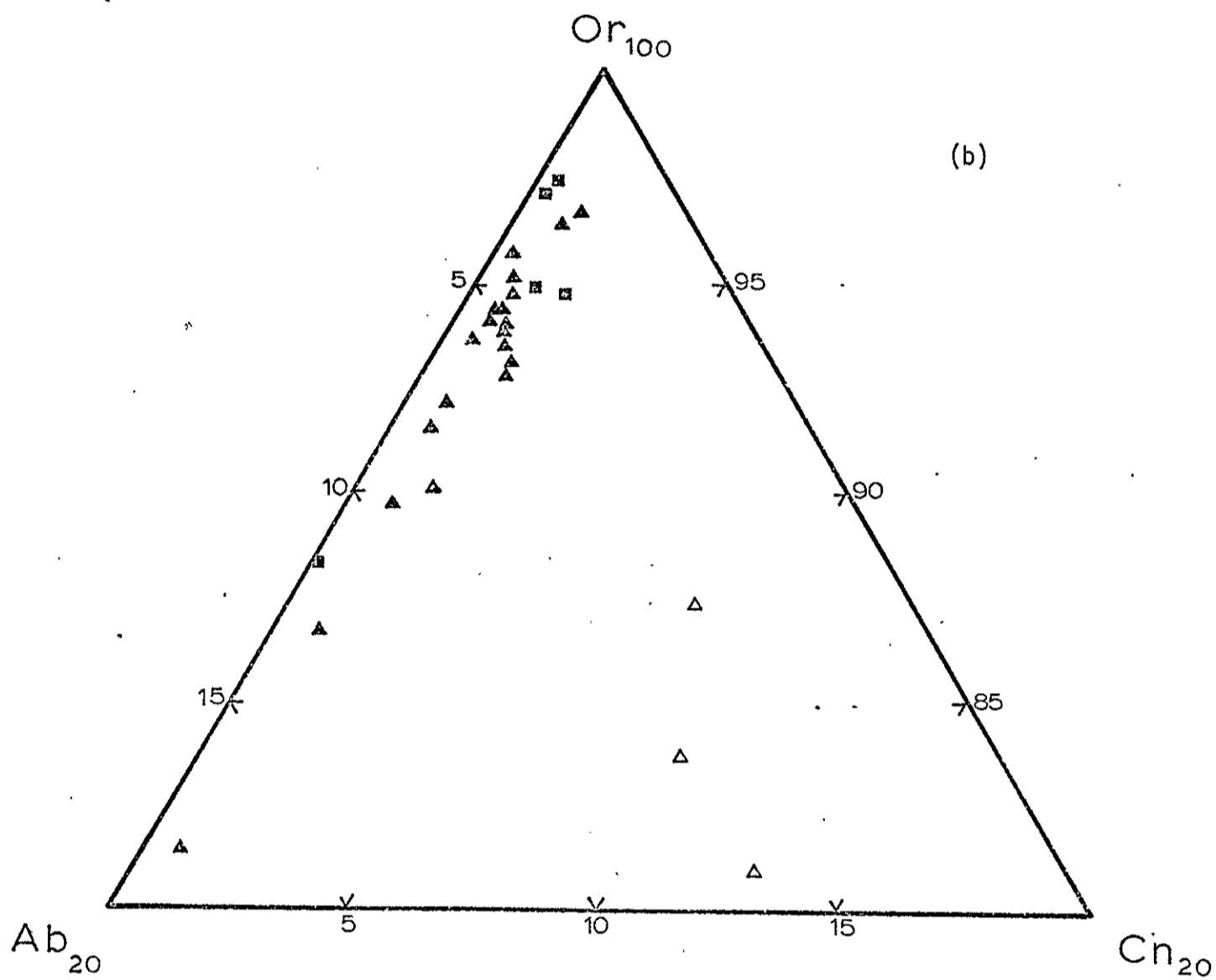


Figure 125.

the general level of barium concentration in the microcline is considered, it is possible to plot the barium zoning across a megacryst. One such plot is shown in figure 127. A series of such plots from megacrysts of varying size from a single hand specimen from the Peñasco Quartz Monzonite is shown in figure 128. In this series of plots each zoning profile can be correlated with the others if one assumes that the smaller megacrysts began growing at an appropriately later time than the larger ones. For example, note that each of the megacrysts, starting at the outer margins, shows a decrease in barium toward the center. If a megacryst is large enough, it then shows an increase in barium toward the center which is then followed by a decrease, until in the largest megacryst, the lowest barium content is actually at its center. The smaller megacrysts do not show this complete zoning pattern because they apparently did not nucleate until the cores of the larger megacrysts had already grown. Thus it is possible to correlate positions in the megacrysts that were simultaneously exposed to the medium from which they grew. Such a correlation is represented by the position letters in figures 128 and 129.

Problems in correlations arise from two sources. One is that it was not always possible to insure that the megacrysts were cut precisely through their centers. The other is that the correlation is based on general gradients in the crystals rather than on exact barium concentrations. Traverse 5 in figure 128, for example, probably did not pass through the center of the megacrysts and as a result much of the center part of the traverse was actually in a single zone or along a growing face instead of perpendicular to it. That the correlation must depend on general gradients and not on precise barium concentration is seen

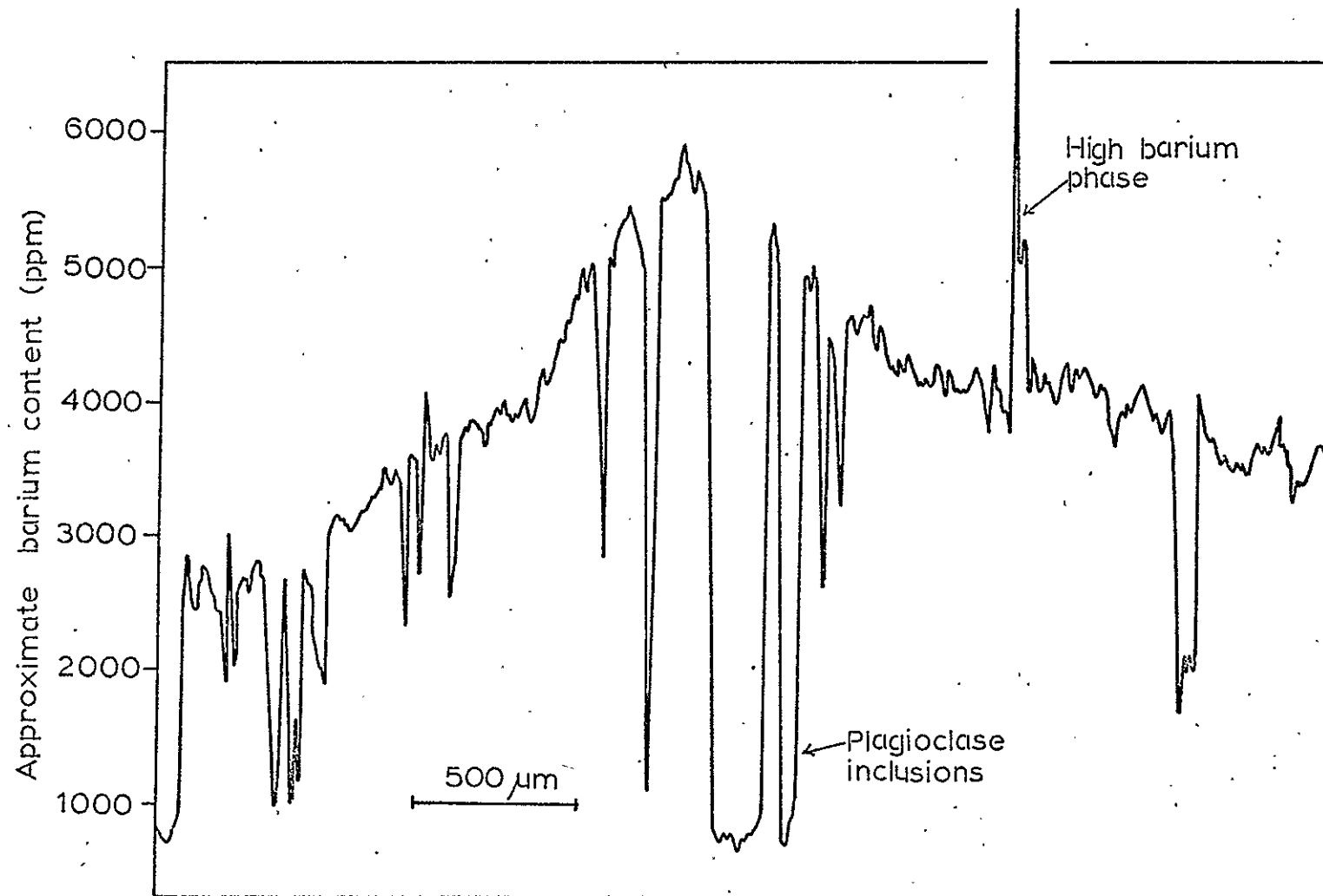


Figure 126. A portion of a continuous traverse for Ba in a megacryst from the Peñasco Quartz Monzonite.

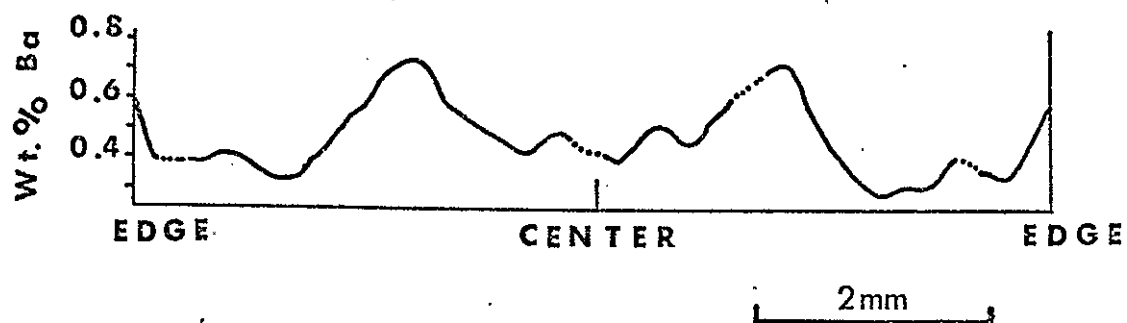


Figure 127. A plot of general barium variation across a megacryst from the Peñasco Quartz Monzonite.

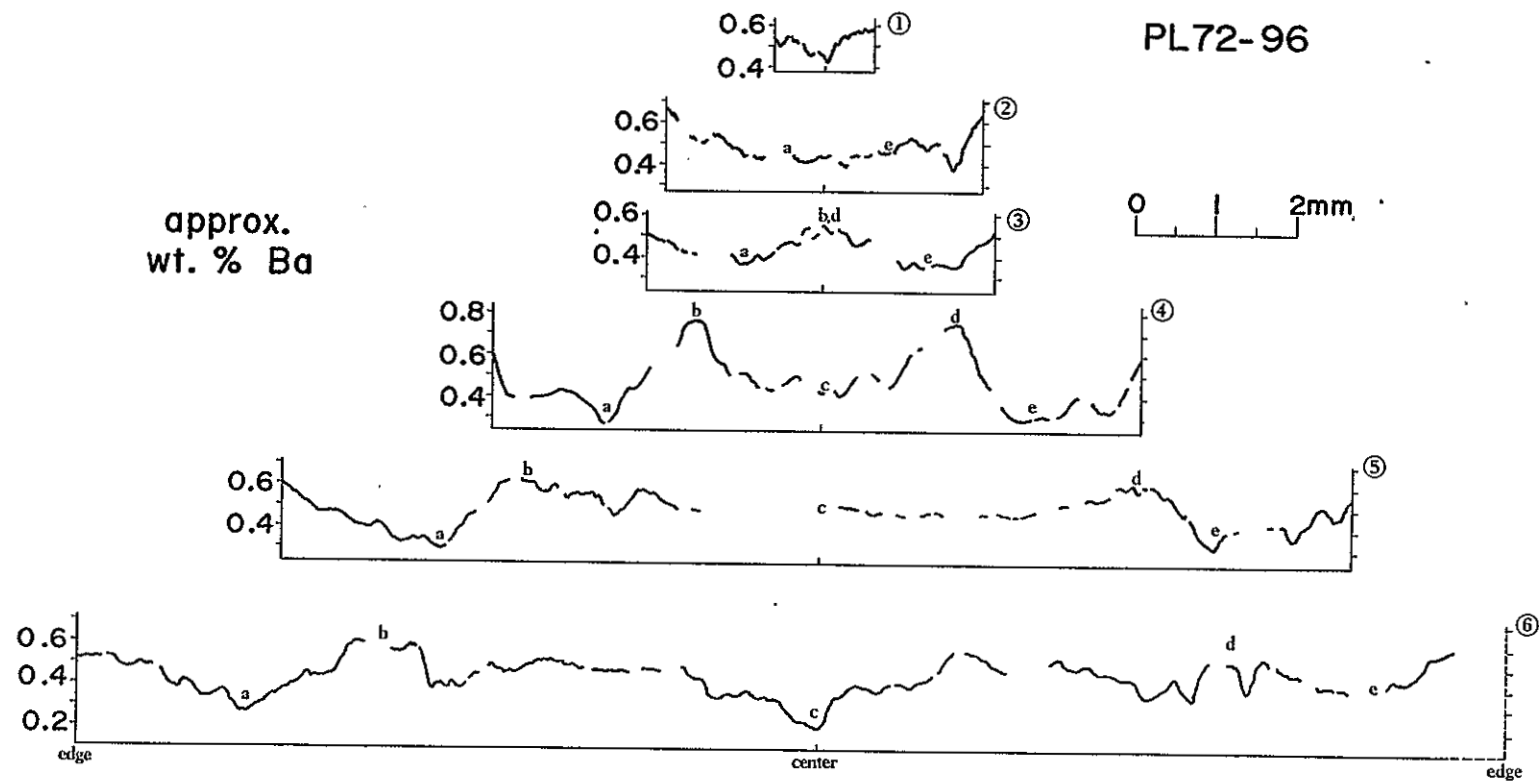


Figure 128. Correlation of Ba traverses for megacrysts from a single hand specimen of Peñasco Quartz Monzonite. See text for explanation.

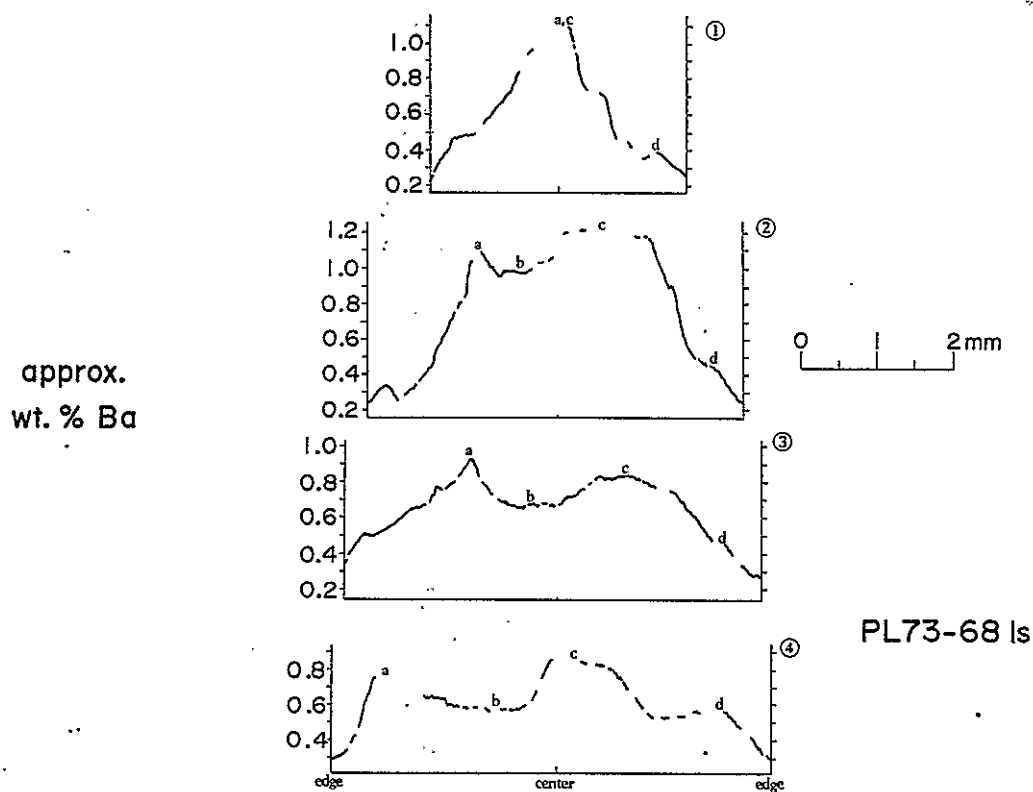


Figure 129. Correlation of Ba traverses for megacrysts from a single hand specimen of Puntigudo Granite Porphyry. See text for explanation.

from the lack of exact correlation of marginal barium concentration compared with the consistent correlation of the gradients near the megacryst margins. Possible reasons for this and for local deviations in gradients are discussed farther on.

Figure 129 is a similar series of traverses for megacrysts from a single hand specimen of Puntiaquedo Granite Porphyry. The general notion of correlation of barium still holds for this sample. There is, however, a marked asymmetry in the distribution which is itself fairly consistent from megacryst to megacryst. If the megacrysts are large enough, one-half will typically show a sharp peak in barium while the other half will show a broad maximum. If both this asymmetry and the size of the megacrysts are taken into account, then it is possible to make a megacryst-to-megacryst correlation in a fashion similar to that for the Peñasco Quartz Monzonite. There are several differences, however. First, there is no increase in barium toward the margins. Instead there is a steady decrease in barium during the later stages of growth. Also, the grain-size distribution in the Puntiaquedo Granite Porphyry is such that there is not a continuous gradation from megacrysts to groundmass grains and the very small matrix microclines consistently have uniform barium concentrations identical with those in the margins of nearby megacrysts.

Overall, there are some gross similarities between megacrysts from the two rock units. The average level of barium concentration, although not constant, is roughly the same. More important, in both cases the concentration gradients go through reversals, starting out positive and then becoming negative. In the case of the Peñasco Quartz Monzonite samples, they return to positive in the final stages of growth. It is these reversals in barium concentration gradients that occur consistently in megacrysts from rocks representing rather different magmatic and

postmagmatic environments, and that provide information pertinent to the origin of the megacrysts. The interpretation of these zoning patterns depends on application of crystal growth theory and the knowledge of certain parameters involved in that theory, most notably the distribution coefficient for barium between alkali feldspar and any supposed growth medium. This growth medium presumably is either a water-rich, low-viscosity fluid phase or a high-viscosity silicate melt, depending on whether the megacrysts are in fact porphyroblasts or phenocrysts. Estimates of the values of the distribution coefficient for each case are considered next.

Data on Barium Distribution Between K-Feldspar and Silicate Melt or a Water-Rich Fluid Phase

There are two approaches to the determination of distribution coefficients for natural systems. The first and most primitive is to use volcanic rocks, to measure phenocryst and groundmass concentrations of a given trace element, and to calculate the distribution coefficient directly. As many investigators have noted, this method has inherent problems and yields only order-of-magnitude approximations. For example, assumptions must be made about equilibrium coexistence of groundmass and phenocrysts, and any zoning present in the phenocrysts generally produces significant error in the results. Further, the distribution coefficient usually is strongly dependent on temperature, which normally is not known for a given volcanic rock. The second approach is to determine distribution coefficients via high-temperature experiments with synthetic rock compositions. This technique is not entirely without problems but it generally provides more useful information.

In this study published data of both types are assessed and the results of some previously unpublished, preliminary experiments in synthetic granitic systems are also reported.

Data on compositions of natural K-feldspar suggest that the interphase distribution coefficient for barium (K_D^{Ba}) is generally greater than 1. This is evidenced by alkali feldspar consistently containing more barium, when it is available in the system, than coexisting minerals (Handbook of Chemistry; Wedepohl, 1969). This seems to be true in igneous rocks regardless of position in paragenetic sequence. In moderately basic rocks, where K-feldspar commonly is a residual phase, barium in K-feldspar is relatively high (e.g. Trzcinski and Kulick, 1972) and the same is true for pegmatites if sufficient barium is available, even though K-feldspar commonly is a primary phase (e.g. Afonina and Shmakin, 1970; Shmakin, 1971). However, the depletion of residual liquids in barium by crystallizing K-feldspar commonly means that there is little barium in pegmatite systems. This was expressed by McIntire (1963) when he noted that barium tends to increase with differentiation in basic rocks but decreases in more felsic ones, this being attributed to the paragenesis of K-feldspar in the crystallization of such rocks. Similarly, in hydrothermal systems barium is concentrated in K-feldspar if there is sufficient barium in the system when K-feldspar is stable. Even though hydrothermal fluids themselves are rarely available for sampling, one can infer that they do not contain more barium than K-feldspar because barium appears not to be concentrated during the late stages of hydrothermal systems.

Attempts to measure K_D^{Ba} for plagioclase directly, using groundmass-phenocryst barium concentrations, have been made by numerous investigators including Berlin and Henderson (1969), Ewart and Taylor (1969), Philpotts and Schnetzler (1970), and Nagasawa and others (1971). Berlin and Henderson (1969) and Philpotts and Schnetzler (1970), however, have published the only data available for K_D^{Ba} K-feldspar, which range from 1.17 to 8.95. This tends to confirm the deduction made above from the generally high barium concentrations in K-feldspar. One attempt (Bethke and others, 1976) has been made to calculate the relative concentration of barium in an aqueous phase of a hydrothermal system, thereby making it possible to estimate the distribution coefficient if barium concentration in K-feldspar is known. Again, the results suggest a K_D^{Ba} greater than 1.

Experimental work on barium distribution has been of three types: (1) determination of K_D^{Ba} between K-feldspar and water-rich fluid (Iiyama, 1968, 1972, 1973), (2) phase equilibria studies in the systems Or-Cn-Q-H₂O and Ab-Cn-H₂O (Gay and Roy, 1968; Rudert, 1972; Mall and Rudert, 1974), and (3) direct measurement of K_D^{Ba} between K-feldspar (as well as other crystalline phases) and silicate liquid (Drake and Weill, 1975; Long, this study).

Iiyama's work has been done mainly at 600°C, 2 kbar, although recently he has begun to examine temperature dependence of barium distribution. His results show a strong partitioning of barium into sanidine ($K_D^{\text{Ba}} = 25$ at 600°C, 2 kbar). Behavior according to Henry's law obtains until concentration of barium in the sanidine exceeds 4920 ppm. Iiyama also has investigated the distribution of barium between a fluid phase and albite, a fluid phase and anorthite (Iiyama, 1972), and between

a fluid phase and two coexisting feldspars. The results of these studies indicate that barium should be more or less equally distributed between a plagioclase of intermediate to albitic composition and an orthoclase-rich alkali feldspar that coexist with a vapor phase.

The first phase equilibria study involving barium in feldspar systems was done by Gay and Roy (1968). They suggested that there is complete crystalline solution between celsian and orthoclase, and that some sort of exsolution takes place in the subsolidus region (Roy, 1967). This work was later extended by Mall and Rudert (1974), who studied the system Or-Cn-Q-H₂O at 1 kbar and concentrated on the Or-Cn join. They report an ascending-type solid solution, with barium concentrated in the solid feldspar phase. An investigation of Ab-Cn-H₂O at 1 kbar (Rudert, 1972) shows a similar situation with barium concentrated in the albite as opposed to the coexisting liquid. Rudert's data also show possible Ab-Cn exsolution taking place starting from 925° to 850°C depending on bulk composition. In ternary and quaternary systems involving Cn, plagioclase may contain only small amounts of Ba, owing to exsolution-type processes or to the effect of bulk composition on K_D^{Ba} plagioclase. This indicates that these studies, though needed as a base of information, involve such restricted compositions that they may not apply directly to natural rock systems. The phase equilibria studies do indicate, however, the general tendency for alkali feldspars to concentrate barium from a coexisting silicate liquid.

Direct experimental measurement of the distribution coefficient in synthetic and natural silicate systems doped with barium and a variety of other trace elements has been made by Drake and Weill (1975). Some preliminary experiments of this type, involving Or-rich alkali

feldspar in a synthetic system with granite composition, have been done in the present study. Here the data of Drake and Weill are pertinent insofar as their distribution coefficients for barium ($K_{D(P1)}^{Ba}$) can be extrapolated to temperatures appropriate to granitic systems. They found that $K_{D(P1)}^{Ba}$ for andesites and basalts is strongly dependent on temperature and is less than 1 above 1060°C. Unfortunately, they did not demonstrate that it is not also partially dependent on bulk composition, a possibility that stems from the wide range of bulk compositions which they used in order to crystallize plagioclase in the 1150° to 1400°C temperature range. The problem of the effects of bulk composition complicates the application of their data to granitic systems, but data from phenocryst-lava pairs for rhyolite strongly suggest that $K_{D(P1)}^{Ba}$ remains less than 1 down to temperatures appropriate for the crystallization of more felsic rocks (Philpotts and Schnetzler, 1970; Ewart and Taylor, 1969; Berlin and Henderson, 1969). This is important because plagioclase with a K_D^{Ba} different from unity, when crystallizing simultaneously from a melt with alkali feldspar megacrysts, will affect barium concentration in the residual silicate liquid.

Preliminary Experimental Data on Barium Distribution Between Silicate Liquid and Or-Rich Alkali Feldspar

In order to gain information on barium distribution that would be directly applicable to the megacryst problem, three high temperature and pressure crystal growth experiments were performed. These experiments were designed to provide a general notion of the magnitude of $K_{D(Kf)}^{Ba}$ and preliminary data on the effects of temperature and bulk composition on $K_{D(Kf)}^{Ba}$. The effect of crystal growth rates and growth

morphology on zoning in synthetic crystals was also of interest. The results show that the distribution coefficient invariably is much greater than 1, ranging from about 6 to as much as about 14 for petrologically relevant bulk compositions. Further, the distribution coefficient appears to be strongly dependent on temperature and also is sensitive to significant changes in bulk composition, particularly the addition or subtraction of major components in the systems involved. Crystallization, at progressively decreasing temperatures, of a single alkali feldspar phase from a granitic melt doped with barium results in progressive depletion of barium in the melt so that, despite an increase in value of the distribution coefficient, the crystals are normally zoned with respect to barium.

The procedures and techniques used in these experiments are those developed recently in the Jahns-Tuttle Laboratory for Experimental Petrology at Stanford. Most of the techniques used are reported in Fenn (1973) and Swanson (1974). The basic approach was to homogenize a synthetic rock-composition gel with added barium and H_2O at a temperature and pressure above its liquidus, and then to drop the temperature either in a single step or in multiple steps for a sufficient length of time for nucleation to occur (2 to 4 days per step). The quenched products, comprising crystals and glass, were then examined under the petrographic microscope and appropriate portions were selected for polishing and microprobe analysis. The conditions and general results of the runs are shown in table 5. The anhydrous bulk compositions, prior to addition of barium, are shown in figure 130.

The first run, designed to test the feasibility of the method, involved two compositions, $Ab_{50}Or_{50} + 2.14$ weight percent Ba (as $BaCO_3$)

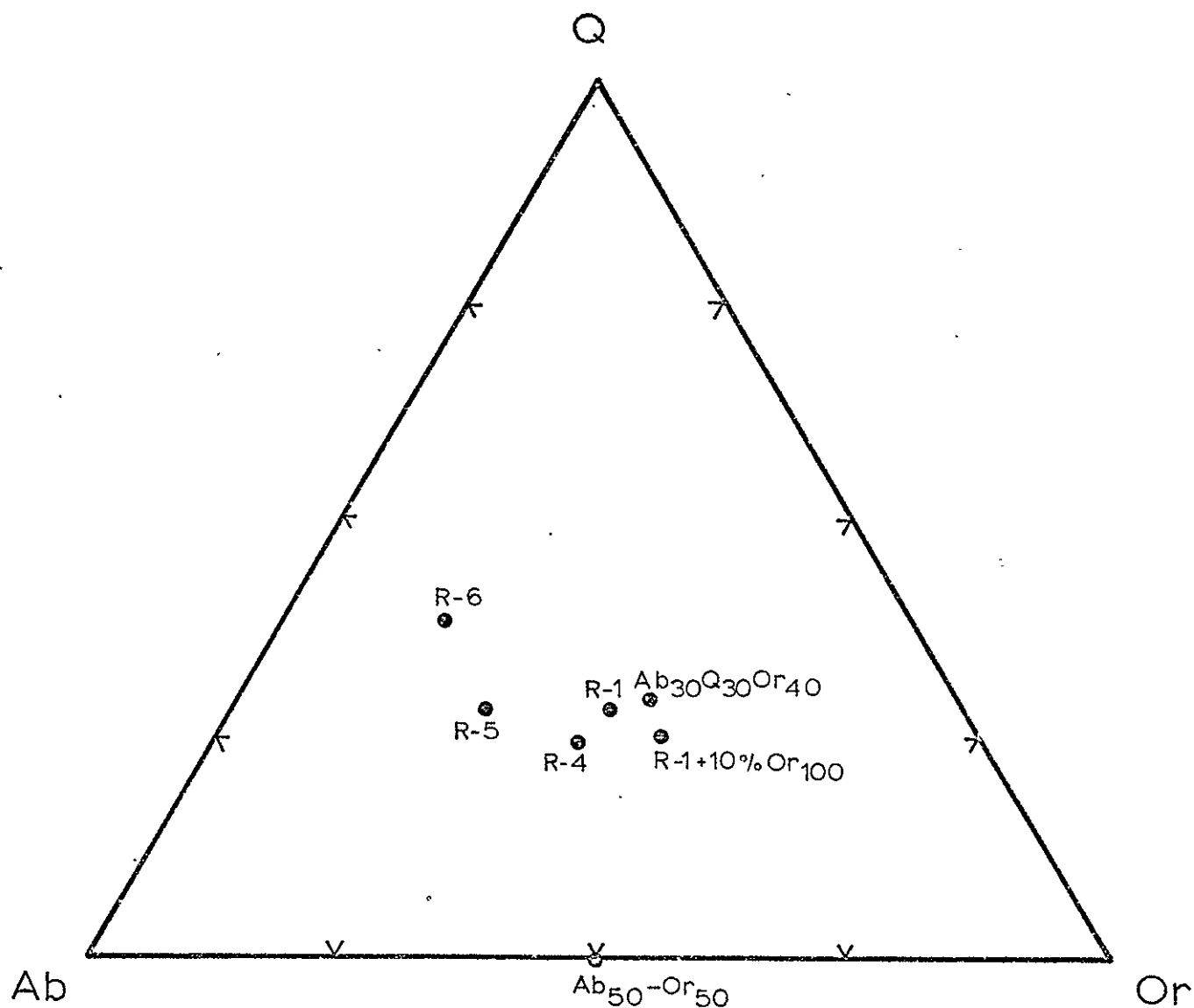


Figure 130a. Anhydrous bulk composition of starting materials for experimental runs plotted on an Ab-Or-Q triangular diagram.

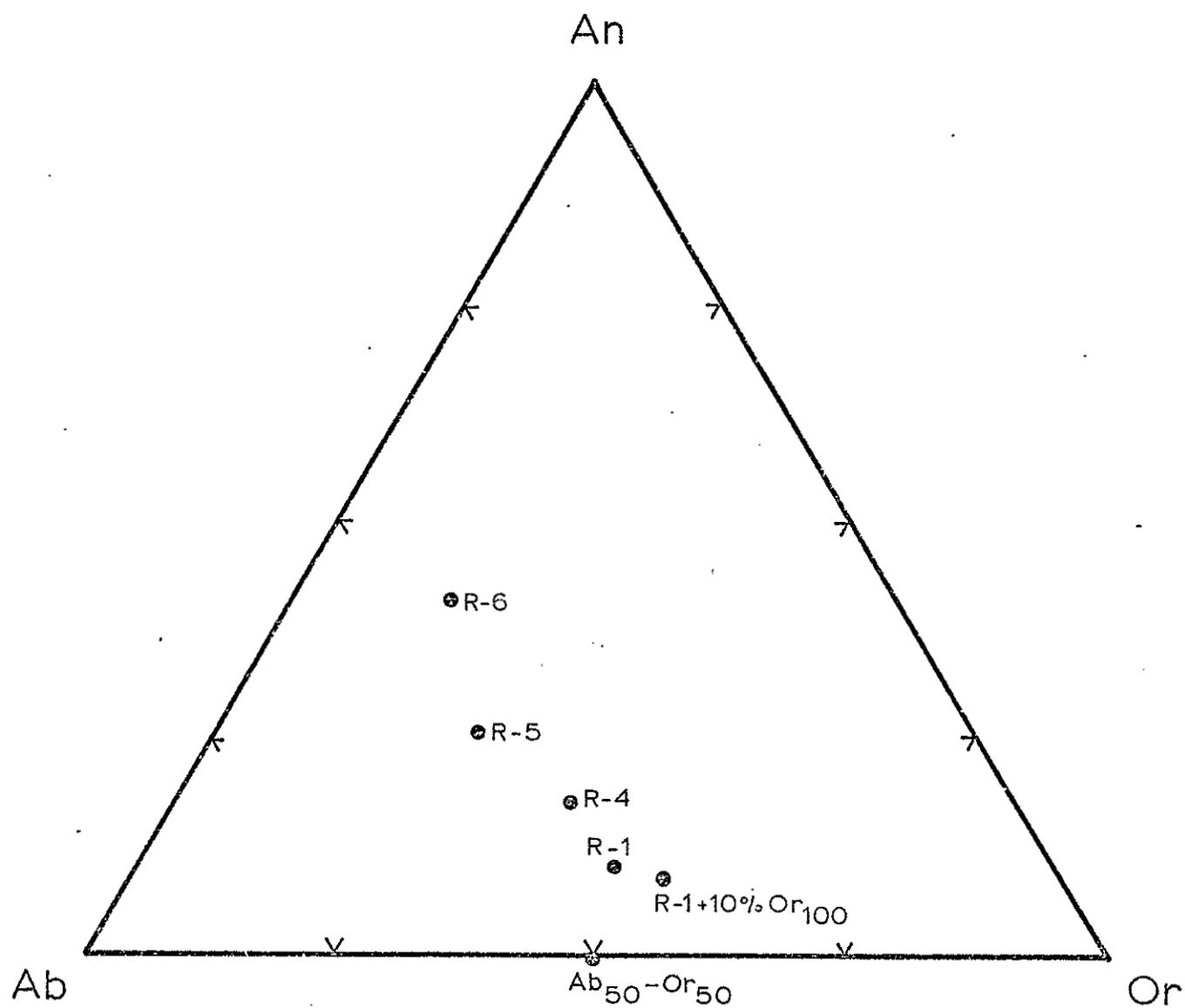


Figure 130b. Anhydrous bulk composition of starting materials for experimental runs plotted on Ab-Or-An triangular diagram.

Table 5
Conditions and General Results of Experimental Runs

Run #1

	<u>Pressure</u>	<u>Temperature</u>	<u>Duration</u>
Homogenization conditions	2.5 kbar	1000°C	115 hrs
Crystallization conditions	2.5	900	48

<u>Charge no.</u>	<u>Bulk composition</u>	<u>Phases present</u>	<u>Textures observed</u>
1	Ab ₃₀ Or ₄₀ Q ₃₀ + Baf + H ₂ O	Af + L + V Undigested gel?	Rosettes of 25-50 μm elongate hollow crystals in vapor saturated glass
2	Anhydrous composition same as #1, H ₂ O = 2.95 wt. %	Af + L + V	Felted mass of 2-3? μm crystals in glass
3	Ab ₅₀ Or ₅₀ + Baf + H ₂ O (Ab _{44.79} Or _{44.79} Cn _{6.54} CO ₂ _{0.77} H ₂ O _{3.41})	Af + L + V	Equant, hollow 5-10 μm crystals in vapor saturated glass
4	Anhydrous composition same as #3, H ₂ O = 3.09 wt. %	Af + L + V	1? μm crystals in vapor saturated glass

Run #2

	<u>Pressure</u>	<u>Temperature</u>	<u>Duration</u>
Homogenization conditions	8 kbar	1150°C	72 hrs
Crystallization conditions	8	1050	48
	8	950	48
	8	850	48
	8	750	48
	8	650	48

<u>Charge no.</u>	<u>Bulk composition</u>	<u>Phases present</u>	<u>Textures observed</u>
10	R1 + Or ₁₀₀ + H ₂ O (Ab _{28.8} Or _{40.6} Q _{23.9} An _{6.7} + 2.89 wt. % H ₂ O)	Af + Pl + Q + L	Zoned spherulites (four growth zones) with the last zone consisting of Af filaments
12	Anhydrous composition same as #10 (+ 4.92 wt. % H ₂ O)	Af + Pl + Q? + L + V	Zoned spherulites (two growth zones) coarsening toward margin
13	Anhydrous composition same as #10 (+ 6.55 wt. % H ₂ O)	Af + Q + Pl + L + V	Rosettes of filamentary Af and plagioclase with intergrown quartz
19	Anhydrous composition same as #10 (+ 3.98 wt. % H ₂ O)	Af + Pl + Q + L + V	Zoned spherulites (two to three zones), last zone consists of intergrown Af + Q

Run #2 (cont'd.)

<u>Charge no.</u>	<u>Bulk composition</u>	<u>Phases present</u>	<u>Textures observed</u>
20	$Rl + Or_{100} + Cn + H_2O$ $(Ab_{29.71}Or_{39.4}Q_{24.6}An_{6.5}Cn_{3.0}$ $+ 2.95 \text{ wt. \% } H_2O)$	Af + Pl + Q + L	Large zoned spherulites
21	Anhydrous composition same as #20 (+ 3.94 wt. % H_2O)	Af + Pl + Q + L + V	Large zoned spherulites
22	Anhydrous composition same as #20 (+ 4.98 wt. % H_2O)	Af + Pl + Q? + V	Rosettes of skeletal Af and Pl; some large Af mantled by Pl
23	Anhydrous composition same as #20 (+ 5.99 wt. % H_2O)	Af + Pl + Q? + V	Rosettes and isolated crystals of Pl and Af

Run #3

	<u>Pressure</u>	<u>Temperature</u>	<u>Duration</u>
Homogenization conditions	8 kbar	1000°C	96 hrs
Crystallization conditions	8	825	96
	8	800	96
	8	775	96
	8	750	96
	8	725	96
	8	700	96

<u>Charge no.</u>	<u>Bulk composition</u>	<u>Phases present</u>	<u>Textures observed</u>
14	R1 + Or ₁₀₀ + H ₂ O (Ab _{28.8} , Or _{40.6} Q _{23.9} An _{6.7} + 7.04 wt. % H ₂ O)	Af + L + V	Zoned elongate crystals in sheaflike aggregates
16	Anhydrous composition same as #14 (+ 8.88 wt. % H ₂ O)	Af + L + V	Zoned, hollow elongate crystals some in aggregates, others as single crystals
24	Ab _{29.7} Or _{39.4} Q _{24.6} An _{6.5} Cn _{3.0} + 7.01 wt. % H ₂ O	Af + Q + L + V	Zoned hollow elongate crystals (up to 4 mm in length); single quartz crystal occurs as an hexagonal plate (0.02 mm)

Run #3 (cont'd.)

<u>Charge no.</u>	<u>Bulk composition</u>	<u>Phases present</u>	<u>Textures observed</u>
25	Anhydrous composition same as #24 (- 8.02 wt. % H ₂ O)	Af + L + V	Zoned hollow elongate crystals (up to 3 mm in length)
27	Anhydrous composition same as #24 (- 9.90 wt. % H ₂ O)	Af + L + V	Single zoned crystal of Af (\approx 1 mm)

and $\text{Ab}_{30}\text{Or}_{40}\text{Q}_{30}$ + 3.05 weight percent Ba (as BaCO_3), both with 3.5 weight percent H_2O . The run was homogenized at 1150°C , 2.5 kbar for 4 days, then the temperature was dropped at constant pressure to 900°C for 2 days, after which the run was quenched to room temperature. The results of the run are shown graphically by electron microprobe X-ray scanning photos in figure 131. For both compositions barium is strongly concentrated in the crystals, but quantitative microprobe analyses (table 4) show that there is a strong difference in K_D^{Ba} for the two compositions (table 5). The excess quartz in the $\text{Ab}_{30}\text{Or}_{40}\text{Q}_{30}$ composition apparently favors barium in the melt more than does the alkali feldspar composition. In these simple systems barium has a K_D much greater than 1 (7.3 to 95), and the addition of silica to the Ab-Or join has a pronounced effect on the distribution coefficient. The crystals resulting from this experiment, however, were not as large as is desirable, because of a large number of nucleation sites caused by incomplete homogenization of barium carbonate. Thus it was clear that for subsequent experiments it would be necessary to make a Ba-feldspar gel for addition, in the desired amounts, to a rock-composition gel. It also was clear that the rock composition should be an Ab-Or-Q-An granite and should yield, under appropriate conditions of pressure and temperature, alkali feldspar as a primary crystallizing phase. Whitney (1972, 1975) studied the phase equilibria of selected quaternary granitic compositions as a function of temperature and water content, and his R-1, a synthetic analogue of Nockold's hornblende biotite granite, yields alkali feldspar as a primary phase at 8 kbar and water contents greater than 6 weight percent. It was decided to use his R-1 sample and to add 10 weight percent Or_{100} in order to extend

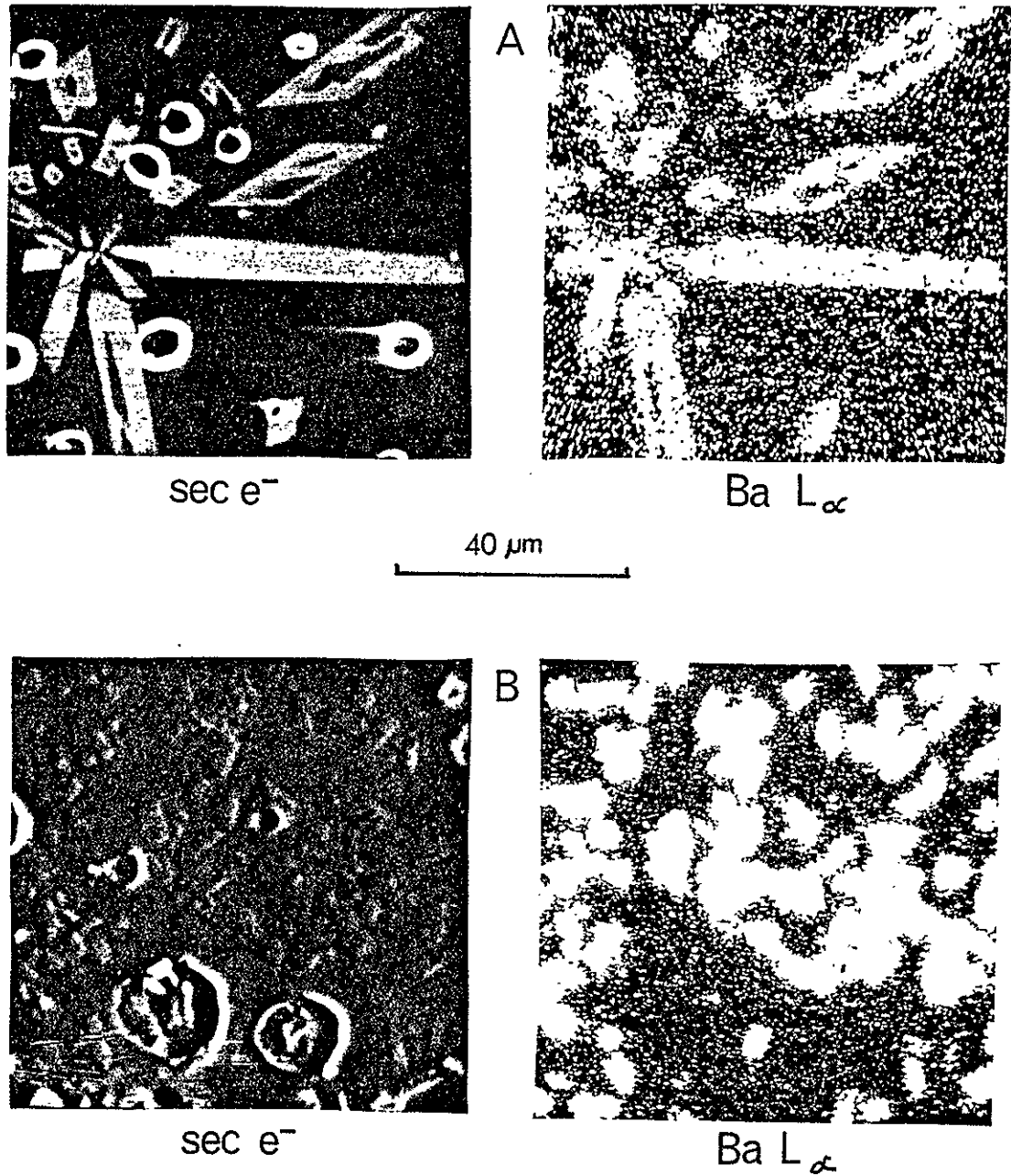


Figure 131. X-ray scanning photos of synthetic alkali feldspars from run #1. (a) $\text{Ab}_{30}\text{Q}_{30}\text{Or}_{40}$; (b) $\text{Ab}_{50}\text{Or}_{50}$.

the phase field of alkali feldspar (fig. 132). The resulting bulk composition is given in table 5. To this was added 3 weight percent of Ba-feldspar gel, equivalent to 1.09 weight percent of barium. The material then was crystallized in two separate staged-growth runs as shown in figure 132. The charges with lower water content (3 to 6 weight percent) were homogenized at 1150°C, 8 kbar and were crystallized in 100°C steps from 1050°C to 650°C. The charges with higher water content were homogenized at 1000°C, 8 kbar and were crystallized in 25°C steps from 825°C to 700°C. In each of the above runs, capsules with and without barium were included in order to check the effects of barium addition on general textures and phase compositions.

Typical textures of the charges with low water content are shown in figure 133. Generally, two to four nucleation sites resulted in 2 to 3 mm spherulitic, filamental rosettes of plagioclase, alkali feldspar, and glass that are mineralogically and chemically zoned. The last crystallization step resulted in growth of hopper-shaped fringes of alkali feldspar on the spherulites. These crystals were of sufficient size for direct measurement of $K_D^{Ba}(Ksp)$ (table 6, fig. 134). The charges with higher water content, however, produced large single crystals of alkali feldspar, some of which are shown in figure 135. Their longest dimension is roughly parallel to the a crystallographic axis, their intermediate dimension about parallel to b, and their shortest dimension about parallel to c. When sectioned perpendicular to their long dimension the crystals are conspicuously sector zoned (fig. 136a). They commonly are hollow, with the hollow portion tapered and elongate parallel to the long dimension of the crystal. Some crystals have the shape of a broad "u" (fig. 136b). The birefringence or degree of brightness

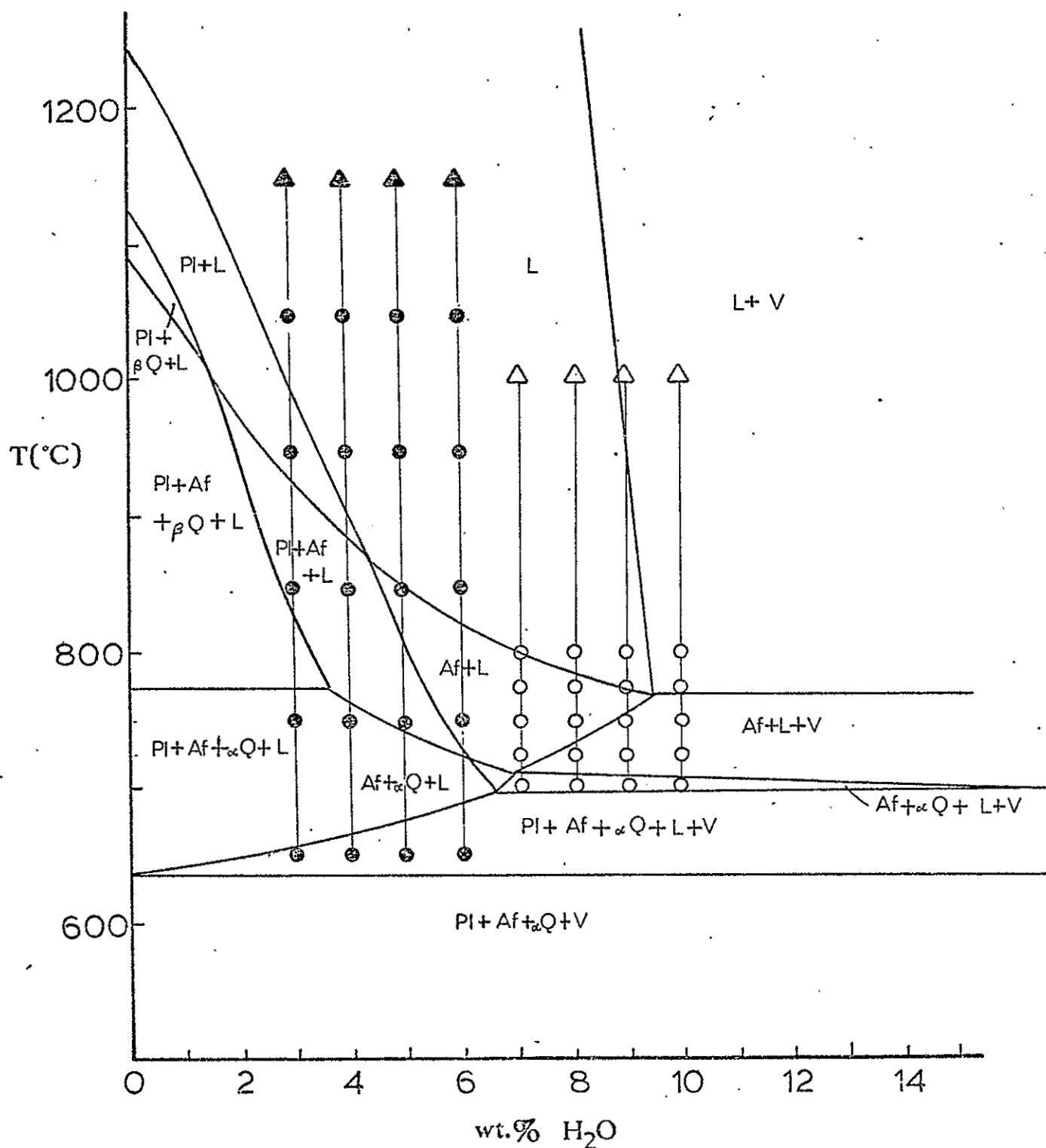


Figure 132. Possible phase assemblage diagram for R-1 + 10 weight percent Or_{100} (modified from Whitney, 1972). The triangles represent homogenization conditions and the circles are crystallization conditions. Solid symbols are for run #2; open symbols for run #3.



2 mm

Figure 133. Photomicrograph showing textures of charges with low water content (run #2).

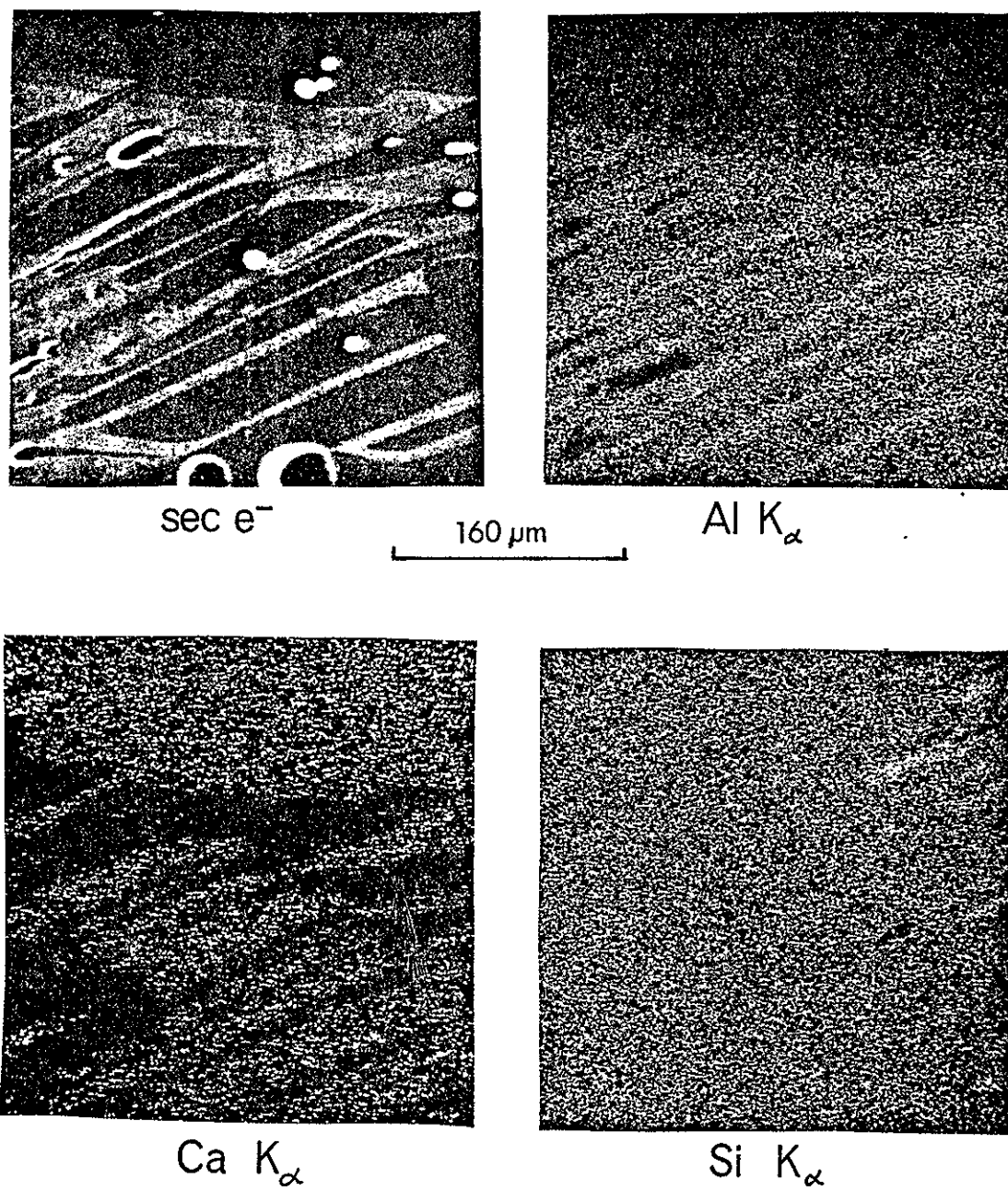
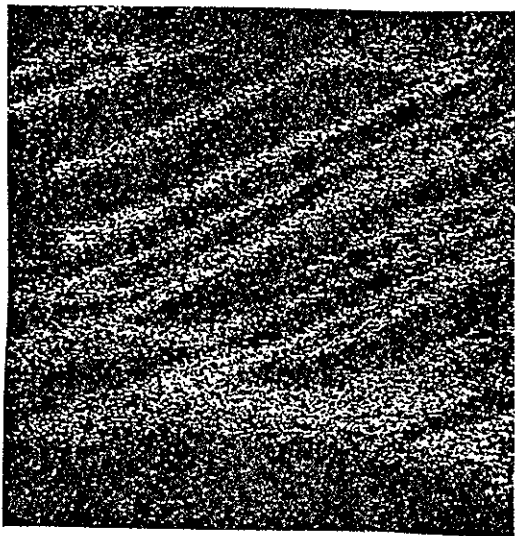


Figure 134. Electron microprobe scanning photographs of zoned, hopper-shaped crystals of alkali feldspar from run #2.

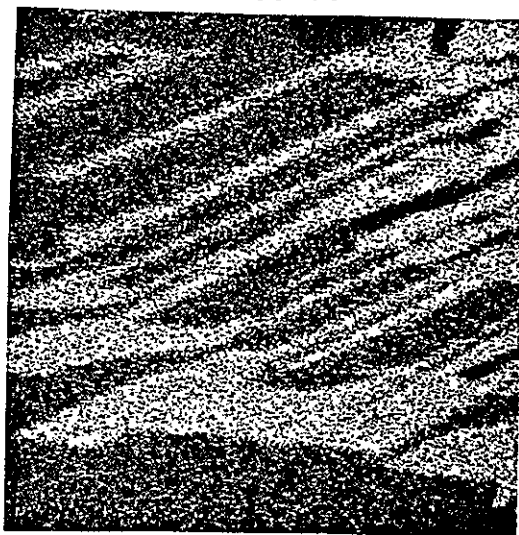
Figure 134.

Ba L_{α}

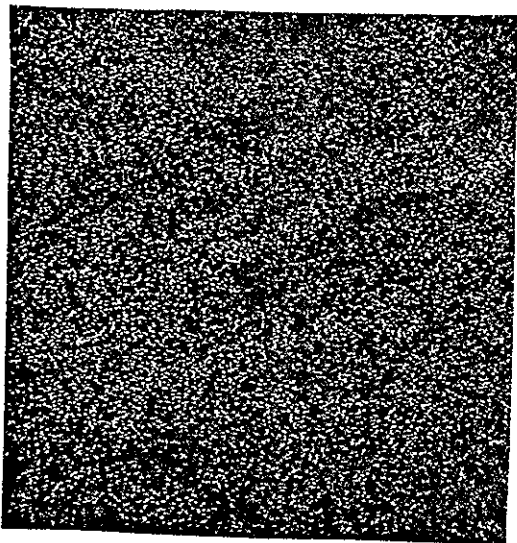


160 μ m

K K_{α}



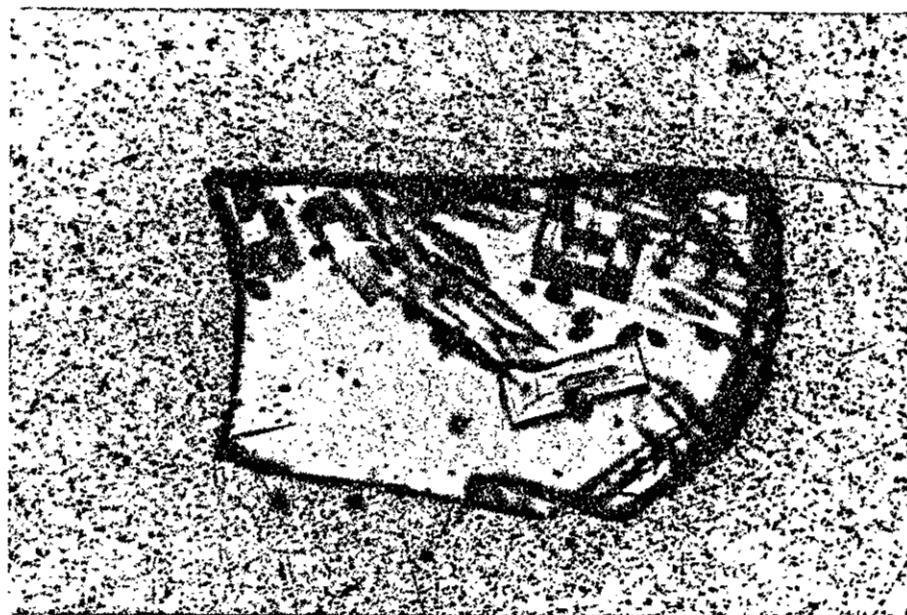
Na K_{α}





(a)

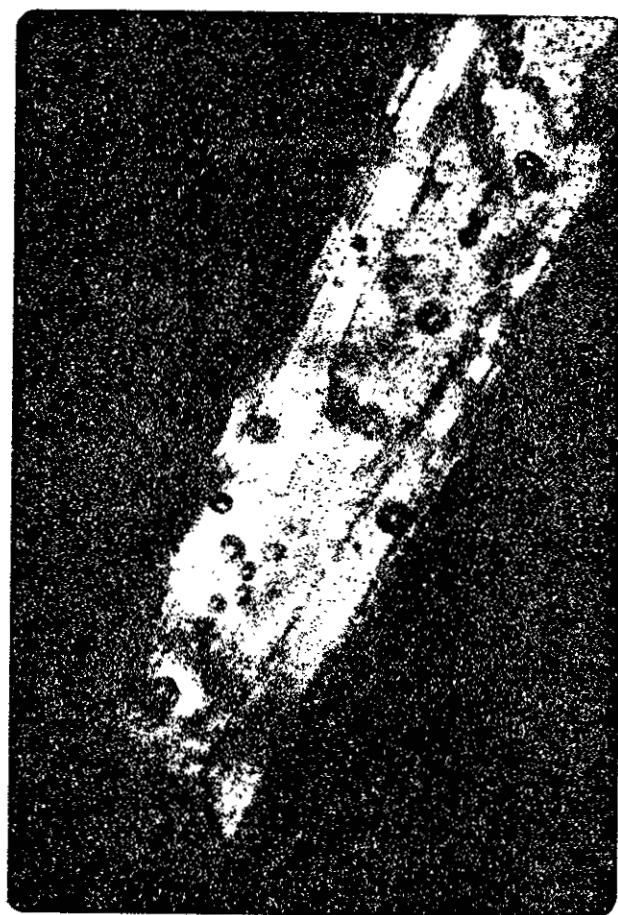
1 mm



(b)

400 μ m

Figure 135. Photomicrograph of elongate alkali feldspar crystals from run #3.



1 mm

Note two-phase vapor bubbles in glass.

Figure 135.

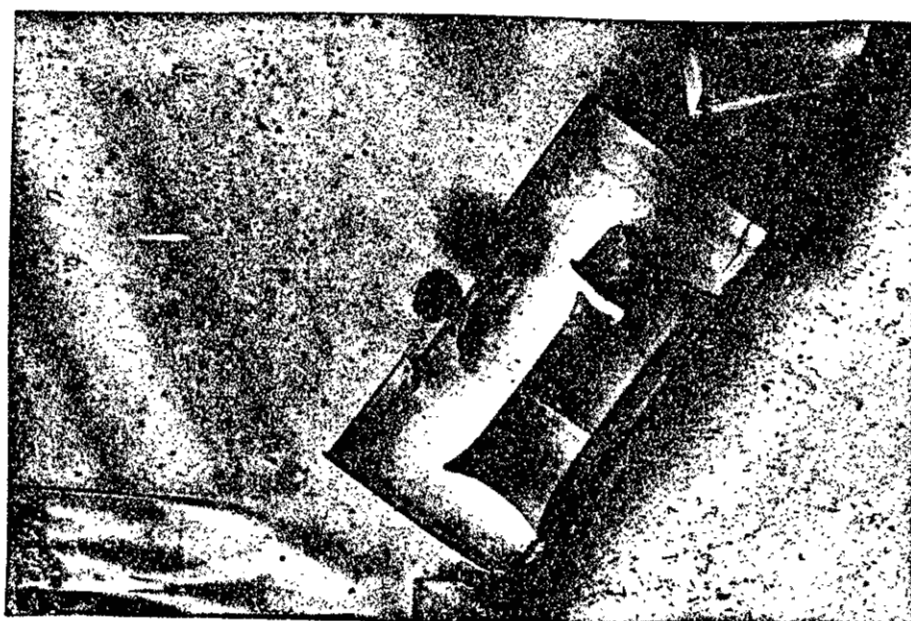
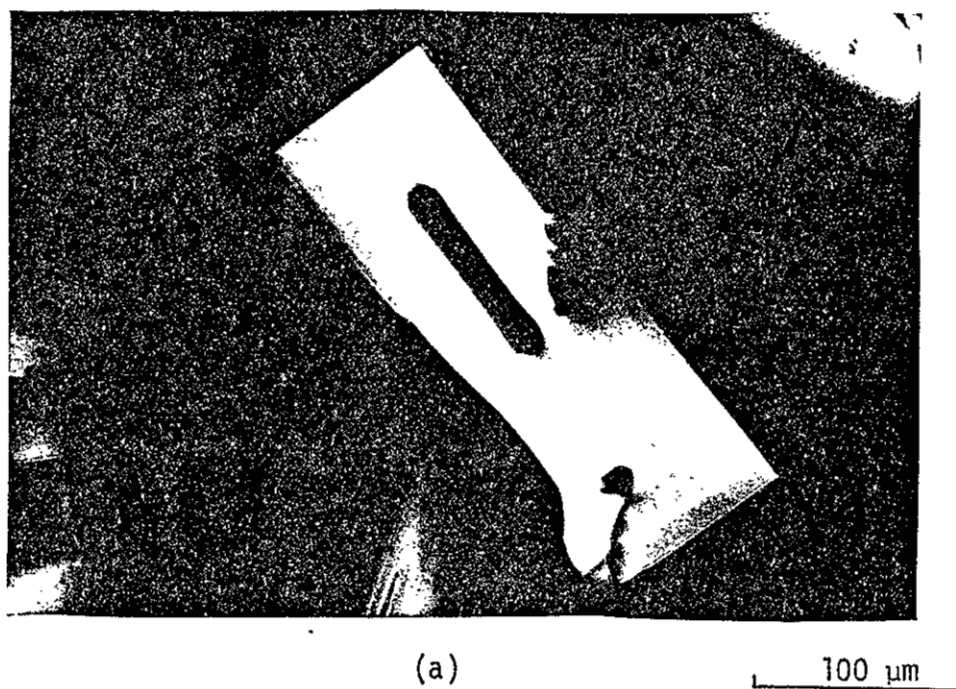


Figure 136. Sections perpendicular to the long axis of hollow crystal of zoned alkali feldspar from run #3.

Table 6
Electron Microprobe Analyses of Products of Experimental
Runs and Measured K_D^{Ba} Values

CHG1 Ksp1.1	
Oxide	Wt. %
Na ₂ O	1.96
K ₂ O	7.90
CaO	0.00
BaO	13.69
Al ₂ O ₃	20.99
SiO ₂	56.84
Total	101.38

Ba 122590 ppm

	Mol %
Ab	19.75
Or	52.36
An	0.02
Cn	27.87

$$K_D^{\text{Ba}} = 7.8$$

CHG1 Ksp1.12	
Oxide	Wt. %
Na ₂ O	1.90
K ₂ O	7.65
CaO	0.00
BaO	14.26
Al ₂ O ₃	22.07
SiO ₂	55.92
Total	101.80

Ba 127700 ppm

	Mol %
Ab	19.37
Or	51.26
An	0.00
Cn	29.37

$$K_D^{\text{Ba}} = 8.2$$

CHG1 G1 1.2	
Oxide	Wt. %
Na ₂ O	1.52
K ₂ O	4.71
CaO	0.01
BaO	1.76
Al ₂ O ₃	12.38
SiO ₂	70.51
Total	90.89

Ba 15740 ppm

	Mol %
Ab	15.10
Or	30.79
Q	54.11

CHG1 G1 1.22	
Oxide	Wt. %
Na ₂ O	1.46
K ₂ O	4.47
CaO	0.01
BaO	1.67
Al ₂ O ₃	11.31
SiO ₂	69.25
Total	88.17

Ba 14970 ppm

	Mol %
Ab	14.81
Or	29.84
Q	55.35

CHG3 Ksp3.1

<u>Oxide</u>	<u>Wt. %</u>
Na ₂ O	2.40
K ₂ O	8.60
CaO	0.00
BaO	9.18
Al ₂ O ₃	20.48
SiO ₂	61.80
Total	102.47

Ba 82260 ppm

Mol %

Ab	24.21
Or	57.06
An	0.00
Cn	18.73

 $K_D^{Ba} = 95$

CHG3 G1 3.2

<u>Oxide</u>	<u>Wt. %</u>
Na ₂ O	1.99
K ₂ O	5.48
CaO	0.00
BaO	0.10
Al ₂ O ₃	16.51
SiO ₂	57.32
Total	81.40

Ba 870 ppm

Mol %

Ab	35.43
Or	64.21

CHG22 G1 1

<u>Oxide</u>	<u>Wt. %</u>
Na ₂ O	0.71
K ₂ O	2.75
CaO	1.64
BaO	0.14
Al ₂ O ₃	10.79
SiO ₂	64.98
Total	81.00

Ba 1250 ppm

CHG22 Ksp2

<u>Oxide</u>	<u>Wt. %</u>
Na ₂ O	2.29
K ₂ O	11.59
CaO	0.39
BaO	1.84
Al ₂ O ₃	16.24
SiO ₂	63.96
Total	96.31

Ba 16460 ppm

Mol %

Ab	21.82
Or	72.61
An	2.04
Cn	3.53

 $K_D^{Ba} = 13.7$

CHG22 Plg3

Oxide	Wt. %
Na ₂ O	8.90
K ₂ O	0.92
CaO	2.40
BaO	0.11
Al ₂ O ₃	18.92
SiO ₂	68.25
Total	99.50

Ba 990 ppm

Mol %

Ab	82.01
Or	5.58
An	12.21
Cn	0.21

$$K_D^{Ba(P1/\ell)} = 0.68$$

CHG22 Ksp4

Oxide	Wt. %
Na ₂ O	2.32
K ₂ O	9.57
CaO	0.25
BaO	2.01
Al ₂ O ₃	15.25
SiO ₂	70.06
Total	99.46

Ba 17980 ppm

Mol %

Ab	25.34
Or	68.74
An	1.49
Cn	4.43

$$K_D^{Ba} = 12.3$$

CHG22 G1 5

Oxide	Wt. %
Na ₂ O	0.56
K ₂ O	2.08
CaO	1.85
BaO	0.16
Al ₂ O ₃	10.60
SiO ₂	62.25
Total	77.50

Ba 1460 ppm

CHG22 Ksp6

Oxide	Wt. %
Na ₂ O	2.06
K ₂ O	9.21
CaO	0.17
BaO	5.81
Al ₂ O ₃	19.87
SiO ₂	62.06
Total	99.17

Ba 52040 ppm

Mol %

Ab	21.92
Or	64.58
An	0.99
Cn	12.51

CHG22 Ksp7	
<u>Oxide</u>	<u>Wt. %</u>
Na ₂ O	2.09
K ₂ O	10.69
CaO	0.30
BaO	2.35
Al ₂ O ₃	18.48
SiO ₂	63.66
Total	97.57

Ba 21040 ppm

	<u>Mol %</u>
Ab	21.37
Or	72.05
An	1.72
Cn	4.86

CHG22 G1 8	
<u>Oxide</u>	<u>Wt. %</u>
Na ₂ O	0.62
K ₂ O	2.17
CaO	1.70
BaO	0.11
Al ₂ O ₃	12.02
SiO ₂	66.23
Total	82.85

Ba 990 ppm

CHG22 Ksp9	
<u>Oxide</u>	<u>Wt. %</u>
Na ₂ O	2.05
K ₂ O	9.12
CaO	0.24
BaO	1.51
Al ₂ O ₃	19.10
SiO ₂	62.54
Total	94.54

Ba 13530 ppm

	<u>Mol %</u>
Ab	24.12
Or	70.72
An	1.56
Cn	3.60

CHG22 G1 10	
<u>Oxide</u>	<u>Wt. %</u>
Na ₂ O	1.26
K ₂ O	3.16
CaO	1.76
BaO	0.46
Al ₂ O ₃	10.51
SiO ₂	65.10
Total	82.26

Ba 4130 ppm

CHG23 Ksp1		CHG23 G1 2		CHG27 G1 1		CHG25 Ksp1	
<u>Oxide</u>	<u>Wt. %</u>	<u>Oxide</u>	<u>Wt. %</u>	<u>Oxide</u>	<u>Wt. %</u>	<u>Oxide</u>	<u>Wt. %</u>
Na ₂ O	2.82	Na ₂ O	3.22	Na ₂ O	2.93	Na ₂ O	1.27
K ₂ O	10.74	K ₂ O	3.32	K ₂ O	5.59	K ₂ O	11.43
CaO	0.18	CaO	2.10	CaO	1.16	CaO	0.04
BaO	2.42	BaO	0.25	BaO	1.12	BaO	4.90
Al ₂ O ₃	14.29	Al ₂ O ₃	12.60	Al ₂ O ₃	14.08	Al ₂ O ₃	12.80
SiO ₂	72.31	SiO ₂	64.97	SiO ₂	63.60	SiO ₂	66.91
Total	102.77	Total	86.45	Total	88.47	Total	97.36
Ba	21660 ppm	Ba	2220 ppm	Ba	10020 ppm	Ba	43930 ppm
Mol %						Mol %	
Ab	26.95					Ab	12.99
Or	67.42					Or	76.70
An	0.97					An	0.21
Cn	4.66					Cn	10.11
$K_D^{Ba} = 9.8$						$K_D^{Ba} = 11.4$	

CHG25 G1 2	
<u>Oxide</u>	<u>Wt. %</u>
Na ₂ O	1.54
K ₂ O	4.28
CaO	1.01
BaO	0.43
Al ₂ O ₃	7.30
SiO ₂	62.26
Total	76.82
Ba	3860 ppm

CHG24 G1 1	
<u>Oxide</u>	<u>Wt. %</u>
Na ₂ O	2.22
K ₂ O	3.66
CaO	1.49
BaO	0.25
Al ₂ O ₃	12.90
SiO ₂	66.70
Total	87.21
Ba	2250 ppm

CHG24 Ksp2	
<u>Oxide</u>	<u>Wt. %</u>
Na ₂ O	2.20
K ₂ O	12.43
CaO	0.22
BaO	3.42
Al ₂ O ₃	18.16
SiO ₂	62.21
Total	98.64
Ba	30610 ppm

CHG16 Ksp1	
<u>Oxide</u>	<u>Wt. %</u>
Na ₂ O	1.68
K ₂ O	11.82
CaO	0.05
BaO	0.00
Al ₂ O ₃	9.41
SiO ₂	81.46
Total	104.41
Ba	10 ppm

	<u>Mol %</u>
Ab	19.63
Or	73.11
An	1.08
Cn	6.17

$$K_D^{Ba} = 13.6$$

	<u>Mol %</u>
Ab	17.69
Or	82.04
An	0.26
Cn	0.00

CHG16 G1 2.1

<u>Oxide</u>	<u>Wt. %</u>
Na ₂ O	3.02
K ₂ O	3.88
CaO	1.56
BaO	0.00
Al ₂ O ₃	12.68
SiO ₂	61.35
Total	82.50

Ba 10 ppm

CHG16 G1 2.2

<u>Oxide</u>	<u>Wt. %</u>
Na ₂ O	3.30
K ₂ O	3.49
CaO	1.55
BaO	0.00
Al ₂ O ₃	12.70
SiO ₂	61.43
Total	82.48

Ba 10 ppm

CHG25 KspZ1

<u>Oxide</u>	<u>Wt. %</u>
Na ₂ O	1.28
K ₂ O	12.32
CaO	0.03
BaO	4.13
Al ₂ O ₃	19.39
SiO ₂	62.53
Total	99.67

Ba 36960 ppm

Mol %

Ab 12.49

Or 79.19

An 0.17

Cn 8.15

K_D^{Ba} = 11.5

CHG25 KspZ2

<u>Oxide</u>	<u>Wt. %</u>
Na ₂ O	1.25
K ₂ O	11.84
CaO	0.05
BaO	5.55
Al ₂ O ₃	19.81
SiO ₂	61.42
Total	99.92

Ba 49700 ppm

Mol %

Ab 12.28

Or 76.47

An 0.25

Cn 11.01

CHG25 KspZ3

<u>Oxide</u>	<u>Wt. %</u>
Na ₂ O	1.27
K ₂ O	11.94
CaO	0.03
BaO	5.35
Al ₂ O ₃	19.89
SiO ₂	61.39
Total	99.88

Ba 47940 ppm

	<u>Mol %</u>
Ab	12.40
Or	76.84
An	0.19
Cn	10.58

CHG25 KspZ4

<u>Oxide</u>	<u>Wt. %</u>
Na ₂ O	1.26
K ₂ O	12.44
CaO	0.03
BaO	4.42
Al ₂ O ₃	19.54
SiO ₂	62.14
Total	99.82

Ba 39560 ppm

	<u>Mol %</u>
Ab	12.15
Or	79.05
An	0.18
Cn	8.62

CHG25 KspZ5

<u>Oxide</u>	<u>Wt. %</u>
Na ₂ O	1.44
K ₂ O	12.51
CaO	0.04
BaO	3.60
Al ₂ O ₃	19.40
SiO ₂	62.80
Total	99.79

Ba 32270 ppm

	<u>Mol %</u>
Ab	13.83
Or	78.97
An	0.21
Cn	6.99

$$K_D^{Ba} = 11.3$$

CHG25 KspZ6

Oxide	Wt. %
Na ₂ O	1.42
K ₂ O	12.30
CaO	0.08
BaO	4.23
Al ₂ O ₃	19.56
SiO ₂	61.79
Total	99.37

Ba 37920 ppm

Mol %

Ab 13.61

Or 77.76

An 0.41

Cn 8.22

 $K_D^{Ba} = 11.8$

CHG25 KspZ7

Oxide	Wt. %
Na ₂ O	1.20
K ₂ O	11.16
CaO	0.05
BaO	7.91
Al ₂ O ₃	20.18
SiO ₂	62.17
Total	102.66

Ba 70800 ppm

Mol %

Ab 11.77

Or 72.26

An 0.25

Cn 15.72

CHG25 G1 Z8

Oxide	Wt. %
Na ₂ O	0.68
K ₂ O	3.54
CaO	1.04
BaO	0.35
Al ₂ O ₃	12.48
SiO ₂	69.97
Total	88.05

Ba 3090 ppm

CHG25 G1 Z8.1

<u>Oxide</u>	<u>Wt. %</u>
Na ₂ O	1.10
K ₂ O	3.95
CaO	1.04
BaO	0.35
Al ₂ O ₃	12.50
SiO ₂	70.02
Total	88.96
Ba	3100 ppm

CHG25 G1 Z9

<u>Oxide</u>	<u>Wt. %</u>
Na ₂ O	2.13
K ₂ O	4.72
CaO	1.15
BaO	0.36
Al ₂ O ₃	12.62
SiO ₂	68.37
Total	89.34
Ba	3220 ppm

CHG25 G1 Z10

<u>Oxide</u>	<u>Wt. %</u>
Na ₂ O	1.40
K ₂ O	4.43
CaO	1.10
BaO	0.32
Al ₂ O ₃	12.39
SiO ₂	69.93
Total	89.56
Ba	2860 ppm

Summary of K_D Values

<u>Charge #</u>	<u>Temperature</u>	<u>Pressure</u>	<u>Wt. % H₂O</u>	<u>Nominal anhydrous bulk composition</u>	<u>K_D^{Ba}</u>
1	900°C	2.5 kbar	3.54	Ab ₃₀ Q ₃₀ Or ₄₀	7.8, 8.2
3	900	2.5	3.41	Ab ₅₀ Or ₅₀	95
22	650	8	4.98	R-1±10% Or	13.7, 12.3 ($K_D^{Ba(P1/l)} = 0.68$)
23	650	8	5.99	R-1±10% Or	9.8
24	700	8	7.01	R-1±10% Or	13.6
25	700	8	8.02	R-1±10% Or	11.5, 11.3, 11.8

of the crystal (fig. 136) correlates well with barium concentration (fig. 137). As expected, barium is concentrated in the crystal relative to the glass, and with progressive crystallization the barium content steadily decreases in each successive zone of the crystal. Quantitative analyses, as given in table 6, make it possible directly to calculate the distribution coefficient for the last zone ($k_D^{\text{Ba}} = 10.5$). By making a mass balance calculation, it is possible to estimate the distribution coefficient for the first, second, and third zones ($k_D^{\text{Ba}} = 6.79, 6.81$, and 9.16 respectively). It thus appears that, as the temperature was dropped from 775° to 700°C , the distribution coefficient increased from 6.8 to 10.5 . This behavior is consistent with trends observed by Drake and Weill (1975). An Arrhenius plot shows this relationship in figure 138. In spite of this increasing distribution coefficient, the depletion of barium in the melt with crystallization was sufficient to result in the observed steady decrease in barium with each successive growth zone.

The morphology and sequence of crystallization also are interesting. From figures 135 and 136 it is clear that these crystals began to form as two subparallel filaments, which grew as the two arcuate high-barium domains flanking the hollow part of the crystal (fig. 136a). These filaments grew most rapidly in a direction normal to the plane of the photograph. Subsequent growth stages, more planar in nature, first thickened the two filaments and then joined them at both ends while continuing to thicken them. As each zone was added, growth at the ends of the filaments presumably continued. In some instances, the ends of the filaments appear to have been joined, sealing off the hollow portion of the crystal from the surrounding glass.

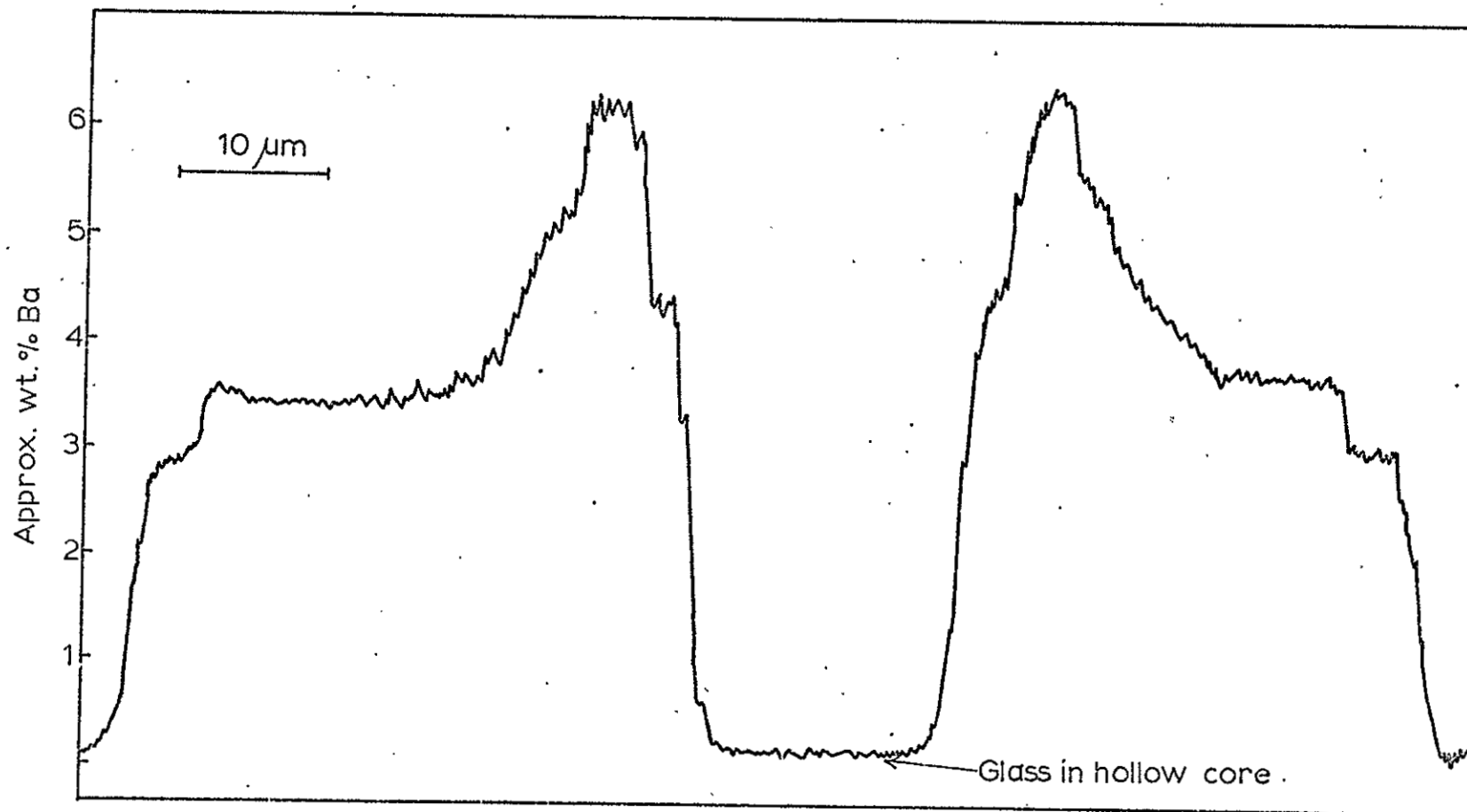


Figure 137. Microprobe traverse for Ba across crystal shown in figure 136a.

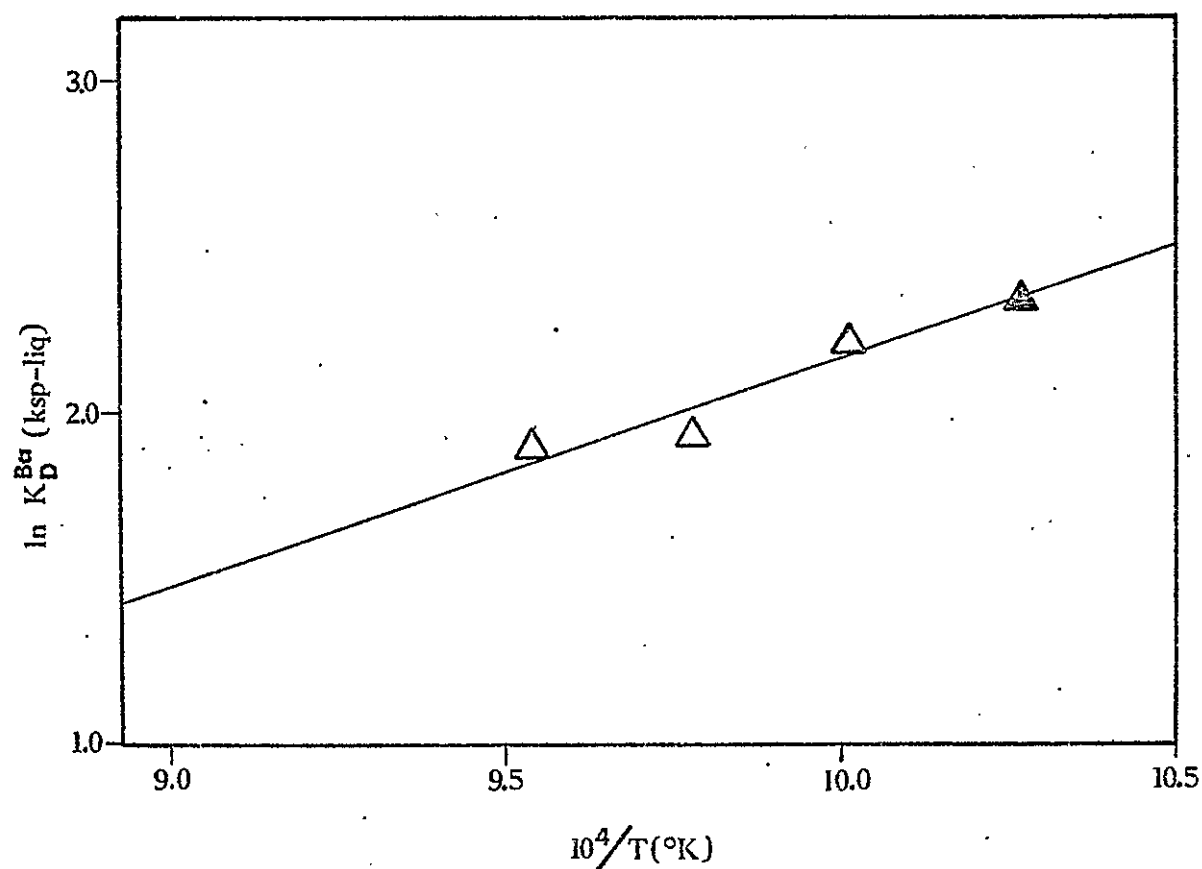


Figure 138. An Arrhenius plot for $K_D^{Ba}(Kf/l)$, composition R-1 + 10 weight percent Or_{100} at 8 percent H_2O and 8 kbar. Solid triangle represents K_D^{Ba} measured directly whereas the open triangles are K_D^{Ba} values calculated from mass balance.

Traverses such as those shown in figure 137 demonstrate that, with the possible exception of the very innermost two zones, the barium content within each zone is nearly constant. Furthermore, there are no detectable gradients for barium in the glass adjacent to the crystal. These two observations suggest that the 4-day growth period allowed for each zone was sufficient for any gradients or diffusion boundary layers in the glass to be erased by diffusion and for any gradients within the latest zone to be annealed out. In some of the zones, however, slight increases in barium in the outer parts of the zone may be an expression of slowing of growth. In any case, it is possible to conclude that diffusion of barium in the glass was sufficiently rapid to erase any steep gradients formed during crystal growth, or to the formation of significant gradients during the growth process itself. In addition, evidence for depletion of barium in the liquid during each stage of growth was apparently erased after growth stopped but before the next temperature step was taken. At the same time, there was no interaction between any outer zone and the next inner zone with which it is in contact. This phenomenon is not well understood but presumably it accounts for the persistence of oscillatory zoning in some igneous plagioclase.

In summary, the experimental data on barium in magmatic systems indicate that (1) the distribution coefficient for barium between alkali feldspar and silicate melt is greater than 1 and tends to increase with decreasing temperature, (2) the distribution coefficient for barium between plagioclase and silicate melt probably is less than 1 for most conditions, but also tends to increase with increasing temperature, (3) the value of the distribution coefficient for barium, and

probably for other elements as well, is dependent on bulk composition as well as on temperature, and (4) the diffusion of barium in silicate liquid and in alkali feldspar is rapid enough that re-equilibration of crystal rims is to be expected during any cessation of growth. This may result in significant differences between zoning patterns in natural feldspar crystals and those predicted by simple crystal growth models.

Some Aspects of Crystal Growth and Trace-Element Distribution Theory as Related to Barium Zoning

The basic ideas of crystal growth phenomena have been developed largely by workers in the field of materials science (e.g. Pfann, 1952; Tillier and others, 1953; Tillier, 1970), and more recently also by petrologists seeking to apply such ideas to natural rock systems (e.g. McIntire, 1963; Albarede and Bottinga, 1972; Fenn, 1973). The problem that concerns us here is a mathematical description of trace-element distribution during the growth process in a closed system. This approach so far has not defined precisely what takes place in a natural system, but it does provide a clear notion of possible physical processes that might well lead to zoning of the sort observed in the megacrysts. Figure 139 describes crudely the kind of phenomenon with which we are dealing. With the exception of the special case where $K_D = 1$, the solute is either rejected and concentrated, or accepted and depleted at the interface of the growing crystal. This process, in addition to solute depletion or concentration in the remaining liquid as a whole, will result in some type of zoning in a growing crystal. The possible types of zoning that might be observed have been discussed by Tillier and others (1953) and by Albarede and Bottinga (1972). The latter investi-

$$K_D = C_S^I / C_L^I$$

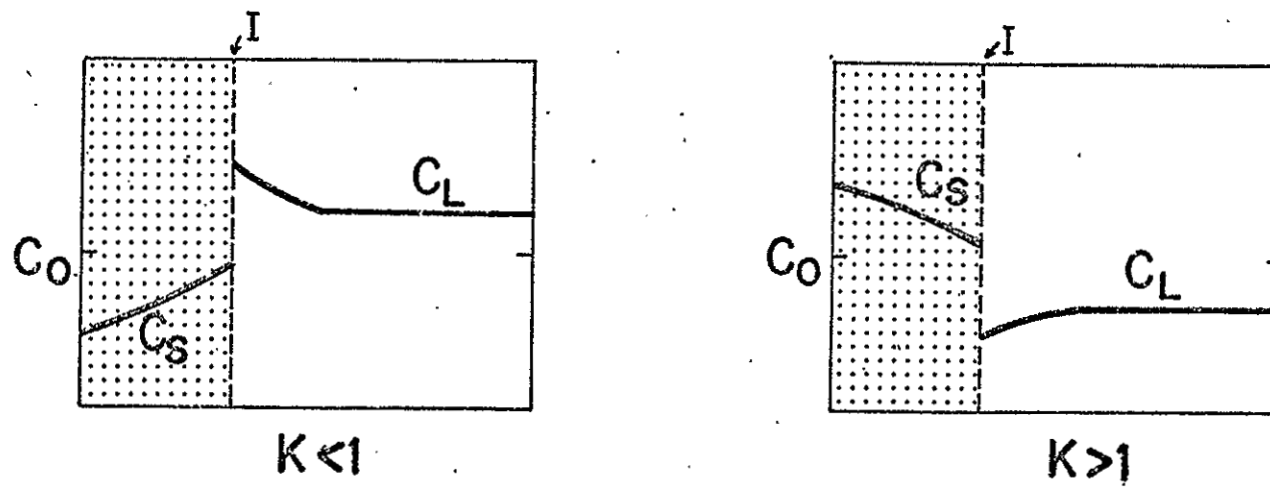


Figure 139. Diagram showing depletion or enrichment of solute at an interface between fluid and a growing crystal.

Table 7

List of Mathematical Symbols

D_l^i, D_s^i	diffusivity of the i th component in the liquid and solid phase respectively
v or $\frac{\partial X_I}{\partial t}$	velocity of the crystal-liquid interface
C_l^i, C_s^i	solute concentration of the i th component in the liquid and solid phase respectively
(x, t)	as subscripts refer, respectively, to the position and time within the coordinate system
K_D	interface distribution coefficient $K_D = \frac{C_s^i(0, t)}{C_l^i(0, t)}$
T	absolute temperature, degrees Kelvin
a, b	linear coefficients describing the temperature dependence of K_D

gators give a particularly informative discussion regarding possible growth models and the assumptions and equations that apply to each. The model is the most complicated and least tractable case they present. This involves a closed system in which diffusion in the solid phase limits solute redistribution (i.e. zoning persists) and the growth rate of the crystal relative to the diffusivity of the solute in the liquid is such that a diffusion boundary layer may significantly affect zoning. The assumptions specified by Albarede and Bottinga for this model are: (1) the crystal-liquid interface is planar, (2) some approach to equilibrium is maintained, at least right at the interface. (3) $K_D = \text{a constant}$, (4) diffusivity of the solute = a constant for a given phase, (5) the system comprises only two phases, a crystalline solid and a liquid, (6) the density of solid phase and the density of liquid phase are constant, and (7) the growth rate is constant. They then point out that the mathematical expression of this case is the solution to the following differential equation:

$$D_l^i \frac{\partial^2 C_l^i}{\partial x^2} + v \frac{\partial C_l^i(x,t)}{\partial x} = \frac{\partial C_l^i(x,t)}{\partial t} \quad (1)$$

(See table VII for a list of symbols.)

The boundary conditions are:

$$D_l \frac{\partial C_l(0,t)}{\partial x} + (1 + K_l)v C_l(0,t) = 0 \quad (2)$$

(mass balance and distribution behavior)

and:

$$-D_l \frac{\partial C_l(x_e,t)}{\partial x} = 0 \quad (3)$$

(gradients in concentration = 0 at edge of system)

and:

$$C_0 = C(x, 0) \quad (4)$$

(initial condition)

These boundary conditions mean that there is in fact no analytical solution, only numerical ones to equation (1). It is possible, however, to rewrite the mass balance equation into a form which is particularly useful in that it clearly relates the parameters of interest even though it does not allow numerical solution for a diffusion profile as does equation (1). It is:

$$\frac{\partial X_I}{\partial t} (C_\ell^i - C_s^i) = D_s^i \left(\frac{\partial C_s^i}{\partial x} \right) - D_\ell^i \left(\frac{\partial C_\ell^i}{\partial x} \right) \quad (5)$$

(See Appendix VI for derivation.)

A relatively simple analysis of this equation demonstrates some pertinent relationships. In particular, it can be shown that for most cases where $(C_\ell - C_s) < 0$ and as long as

$$D_\ell^i \left(\frac{\partial C_\ell^i}{\partial x} \right) > \left| \frac{\partial X_I}{\partial x} (C_\ell - C_s) \right|$$

then $\frac{\partial C_s^i}{\partial x}$ will be positive (Appendix VI).

Thus, a crystal grown with $K_D > 1$ for the i th component under the assumptions previously mentioned should be normally zoned with respect to that component. Numerical solutions to equation (1) (Albarede and Bottinga, 1972) corroborate this notion in that even when a steady state is reached and $\partial C_s^i / \partial x$ becomes zero no reversals in zoning are predicted. Considering that this is not what we observe for barium zoning in the megacrysts, we need to examine the circumstances under which reversals in barium concentration gradients, $\partial C_s^i / \partial x$, might occur and in that light review the assumptions made to see which ones, if any,

might be responsible for failure to predict gradient changes. A graphical representation of equation (5) is shown in figure 140, which makes it obvious that to obtain a reversal in $\partial C^i / \partial x$, it is necessary to cross the ordinate or to shift from region II to region III, from region V to region VI or vice versa. The explicit factors that might cause such a reversal are obvious from equation (5): (1) a change in the distribution coefficient ($C_L^i - C_S^i$); (2) a change in the growth rate, $(\frac{\partial x}{\partial t})$; and (3) an unaccounted change in the liquid composition with respect to a particular component (C_X^i). Each of these possibilities violates, in some way, the assumptions previously stated. It is therefore worthwhile to reconsider the original assumptions.

The first assumption of a planar crystal-liquid interface seems appropriate for the megacrysts, particularly in view of the orientation of tabular plagioclase inclusions along ghost crystal faces. The second assumption of an approach to equilibrium at the growing interface probably obtains in natural granitic systems, considering growth rates likely for minerals in these rocks. A constant K_D , according to assumption three, is demonstrably invalid, and at the very least some account must be taken of K_D as a function of temperature. Assumption four is that the diffusivities are constant. In general, however, they will be a function of temperature and bulk composition of the solid or liquid phase. Still it is clear that the diffusivity of barium in feldspar is sufficiently small that zoning persists in the megacrysts, but changes in it may well exert a significant effect on the zoning, especially at higher temperature early stages of growth. The diffusivity of barium in the liquid probably is much greater than in K-feldspar. The experimental evidence suggests that the ratio of D_S^{Ba} to $\partial X_I / \partial t$ is

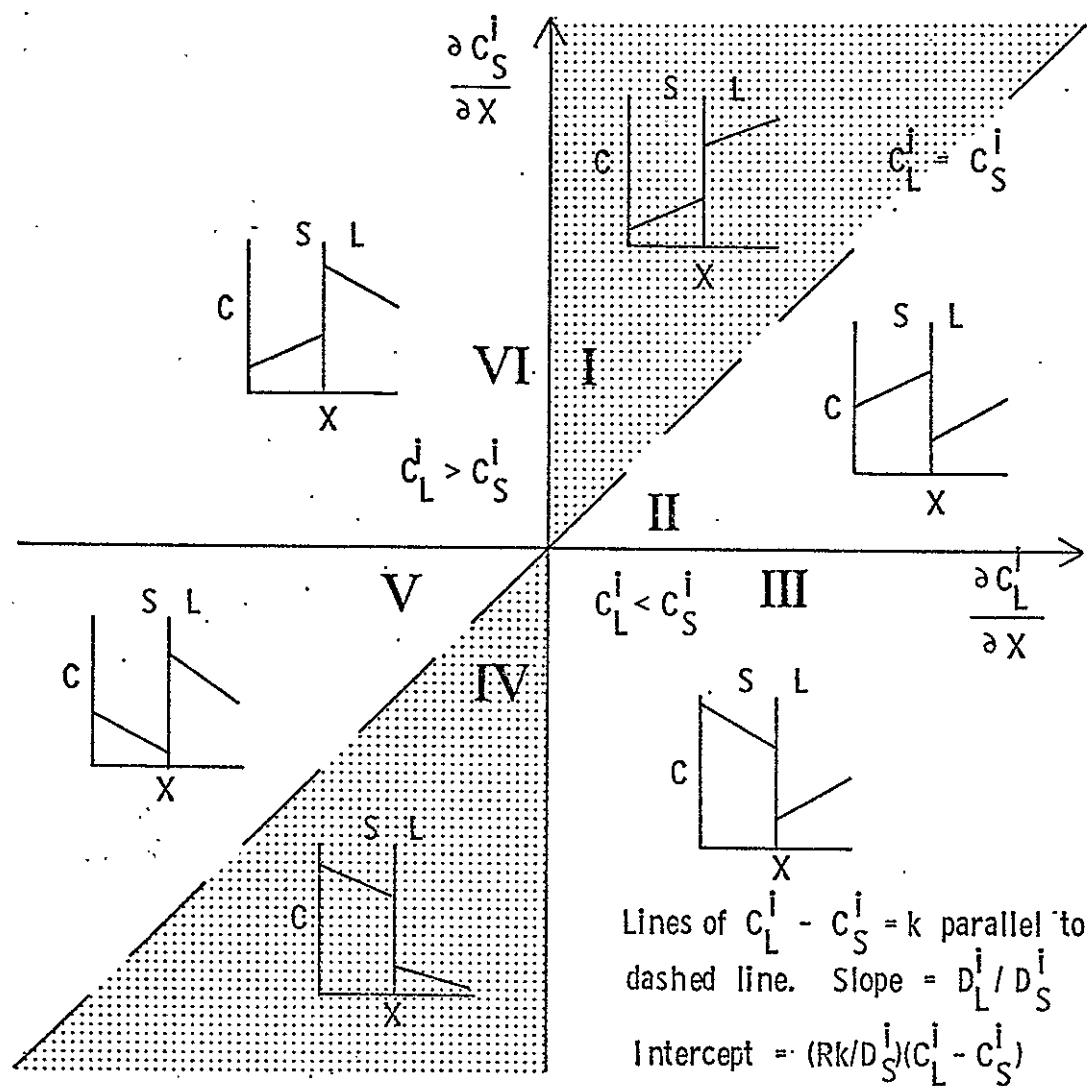


Figure 140. A general plot of $\partial C_S^i / \partial X$ vs. $\partial C_L^i / \partial X$ showing possible configurations of compositional gradients of the solid-liquid interface.

such that the diffusion boundary layer does not play an important role in zoning of the megacrysts. In general, changes in diffusivity may influence the exact form of zoning, but most likely cannot produce reversals in $\partial C_S^i / \partial x$. The fifth assumption, that the system is limited to two phases, is inappropriate for the crystallization of most igneous rocks. The possible effect of crystallization of phases other than the one in which the zoning occurs, must be considered. This is especially true if the phases differ markedly in concentration of the trace element, which obviously is the case for the major phases in granites and many other igneous rocks. Finally, the sixth assumption that density of the liquid equals density of the solid is unrealistic, particularly if any process of igneous differentiation is to take place by crystal settling or floating. It is possible to take account of density changes within phases by proper choice of concentration parameters that allow the density of a given phase to be defined as

$$\rho = \sum_{i=1}^N C^i.$$

The seventh assumption of constant growth velocity probably is not strictly true, but as long as growth velocities are low relative to diffusivities, changes in velocity should have no marked effect on general zoning patterns. Still, changes in growth rate cannot be completely ignored, as they may affect the details of a zoning pattern. Ideally, growth-rate changes should be accounted for in equation (5), but because general zoning patterns are probably not affected no attempt will be made to account for variable growth rate.

The assumption of a constant K_D and the assumption of a two-phase system are particularly troublesome. It is possible to substitute,

based on the experimental data presented here, a functional relationship for $C_S - C_L$ in equation (5) that describes the change of $C_S - C_L$ with temperature:

$$\left(\frac{\partial X_I}{\partial t}\right) C_S^I \left(1 - \left[\left(\frac{10^4}{T}\right)a + b\right]\right) = D_S^i \left(\frac{\partial C_S^i}{\partial x}\right) - D_L^i \left(\frac{\partial C_L^i}{\partial x}\right) \quad (6)$$

(See Appendix for derivation.)

This equation accounts for a changing K_D and theoretically allows for a density change within liquid or solid phases. This equation does not, however, in any way account for the crystallization of more than one phase. It may be more useful to consider the experimental evidence directly, in particular taking note of the fact that despite a K_D change with increasing temperature the crystals still showed distinct normal zoning. Depletion of the liquid in barium evidently was more significant, for the particular bulk composition of the system, than was the shift to larger values of K_D^i . In general, the zoning pattern for such two-phase systems will depend strongly on the amount of the crystalline phase and the exact values for the K_D^i during the crystallization interval. Still, the experimental data suggest that when a single alkali feldspar crystallizes from a granite melt with no accompanying solid phase it tends to be normally zoned in barium. The experimental data of run three do not encompass the possibility of simultaneous crystallization of phases other than alkali feldspar, but it is obvious that the crystallization of significant amounts of plagioclase ($K_D^{Ba} < 1$) and/or quartz ($K_D^{Ba} \rightarrow 0$) concomitantly with Or-rich alkali feldspar (e.g. the megacrysts) will produce marked changes in the liquid composition with respect to barium, which in turn will be reflected by the barium concentration in the alkali feldspar as it

crystallizes. Clearly, the simple application of even a sophisticated version of the mass balance equation (i.e. equation 6) generally has no predictive value in terms of interpreting zoning in the megacrysts or in igneous minerals. It is necessary to account for the changing liquid composition, with respect to any element of interest, as a variable dependent on the total crystallization behavior of the rock, not just on the behavior of one phase. Unfortunately, to trace the liquid composition during crystallization requires knowledge of the proportions of crystalline phases and their compositions at each infinitesimal step of crystallization. Such knowledge is not generally available for quinary granite systems, nor can it ordinarily be inferred in detail from interpretation of rock textures. As a general case, however, subsolvus granites crystallize at least three phases simultaneously (quartz, plagioclase, and K-feldspar) during significant parts of their cooling histories. In theory, by changing the relative timing of crystallization and the relative proportions of phases it would be possible to produce almost any continuous zoning pattern desired. Considering that the proportions and timing of phases crystallizing from a granitic melt are sensitive to such things as pressure, water content, and bulk composition, it would appear that reversals in barium concentration gradients in megacrysts can readily be produced by purely igneous processes.

Thus it is possible that the megacrysts grew from a melt, and that during part of their growth period quartz and/or plagioclase crystallized in sufficient quantity to increase the barium concentration in the liquid. This produced the reversed zoning in the megacrysts. At some point depletion of the liquid in barium by the megacrysts themselves

results in a reversal in $\partial C_S^{\text{Ba}} / \partial x$ and a normal zoning pattern. Changing distribution coefficients and variations in growth rate also are likely to affect the zoning pattern, but growth-rate changes in particular are probably not of primary importance.

Interpretation of the Barium Zoning in the Light of Constraints Imposed by Experimental Data and Crystal Growth Theory

Given the nonunique character of zoning patterns that theoretically can be produced in a crystallizing granite, it would seem that no zoning pattern actually observed in a rock could provide useful information about the origin of megacrysts. Two observations should be emphasized in this regard: (1) despite probable differences in exact conditions of crystallization, megacrysts from both the Peñasco Quartz Monzonite and the Puntigudo Granite Porphyry show reversals in their barium zoning patterns, and (2) the crystallization of quartz and plagioclase provided a mechanism which could consistently produce reverse zoning during part of a megacryst's crystallization. These two points are especially pertinent if one suggests a subsolidus origin for the megacrysts. It is not at all clear why distinctly different megacrysts from very different rocks should display similar zoning patterns if they were formed from an aqueous fluid phase. This would require a relatively consistent change of barium concentration in a fluid phase during megacryst growth, and there is no obvious mechanism for such behavior. Furthermore, locally in the Puntigudo Granite Porphyry there is epidote alteration, and in most of these altered rocks the megacrysts retain their characteristic zoning pattern. In the most severely altered rocks, however, the relict megacrysts have a constant,

relatively high barium content. This suggests that under conditions of severe alteration a fluid phase is capable of homogenizing barium in the megacrysts, which in turn can be interpreted to mean that if the megacrysts had actually grown from a fluid phase they might well have lacked zoning. In short, it can be stated that growth of megacrysts from a granitic melt provides a mechanism that can readily explain the barium zoning observed in megacrysts from both the Puntagudo Granite Porphyry and the Peñasco Quartz Monzonite. No such mechanism appears to be at hand to explain the barium zoning, if megacrysts grew from a water-rich fluid phase.

It remains necessary to consider the origin of the barium-rich phases and of the distribution of calcium in the plagioclase inclusions. These features seem best accounted for as results of subsolidus re-equilibration at temperatures below those of the original crystallization of the megacrysts. With falling temperature, exsolution of Ab from the Or-rich alkali feldspar formed exsolution lamellae within the microcline and epitaxial overgrowths on the plagioclase inclusions. As a result of the overgrowth a certain volume of microcline, having a much higher barium content than the albitic plagioclase, is replaced by the albitic plagioclase. Thus there should be an increase in barium at the moving interface between the two phases. This increase in barium apparently gave sufficient driving force to nucleate and grow the barium-rich phases. At the same time, the plagioclase apparently underwent internal adjustments, probably in response to intersecting the peristerite solvus or solvi, so that the anorthite component was redistributed in the interior of the inclusions. It is interesting to note that the cathode-

luminescence suggests a significant difference in composition between the albitic lamellae and the albitic epitaxial overgrowths. This indicates that there was a lack of equilibrium between these two phases, possibly reflecting a simple lack of chemical communication between them. If this is true, then cation exchange for calcium, as well as for barium, has occurred only on a very local scale.

An alternative explanation for the barium-rich phases would involve their formation in a diffusion boundary layer during primary growth of the plagioclase inclusions. Prior to their incorporation in a megacryst and while they were still growing from the melt a barium-rich diffusion boundary layer would have formed around them. The barium-rich Or phase could have nucleated in such a layer and that would explain their association with the inclusions. If this explanation were correct one would expect barium-rich phases to be everywhere associated with plagioclase in igneous rocks. Such an association is not known to exist and consequently the subsolidus origin for the barium-rich phases is favored.

Conclusions

Barium zoning in the microcline megacrysts from the Peñasco Quartz Monzonite and the Puntagudo Granite Porphyry suggests that they crystallized from a granitic melt, in large part simultaneously with quartz and/or plagioclase. This stems from an interpretation of the possible cause of the zoning based on the behavior of barium relative to the crystallization of an Or-rich alkali feldspar, plagioclase, and quartz. Experimental data demonstrate that (1) the distribution coefficient for barium between alkali feldspar and granitic silicate liquid

is significantly greater than 1 and is dependent on temperature and bulk composition; (2) the distribution coefficient for barium between plagioclase feldspar and granitic silicate liquid is less than 1 and similarly depends on temperature and bulk composition. These two relationships, together with the obvious rejection of barium by quartz, mean that a variety of zoning patterns is possible during crystallization of Or-rich alkali feldspar in granitic systems. On the other hand, this is the most likely mechanism for consistently producing the reversals in barium concentration observed in the megacrysts here studied.

Subsequent to the initial crystallization, subsolidus re-equilibration resulted in formation of perthitic lamellae, growth of epitaxial rims on the plagioclase inclusions, redistribution of calcium within the inclusions, and formation of tiny grains of barium-rich K-feldspar.

In addition, this study points out that assumptions commonly made in the interpretation of trace-element distribution in igneous rocks are in many instances inappropriate. In particular, the assumptions that K_D is a constant and that only two phases, solid and liquid, are involved in the crystallization process are almost always erroneous for igneous rocks.

Before trace-element distributions in granitic rocks can be properly interpreted, a detailed experimental study is required. Ultimately, we need to know the functional dependence of distribution coefficients on temperature, pressure, bulk composition, and growth kinetics for the more important trace elements, especially barium, rubidium, and strontium. When such data are available it may be possible to calculate, for various crystallization sequences, the expected zoning patterns for various trace elements in both plagioclase and K-feldspar. In the

meantime, available data may make it possible to calculate, for simple systems (e.g. Ab-Or-Q-H₂O), the expected barium distribution patterns in K-feldspar. In their simplest form such calculations are relatively straightforward, but they have not been made. The results of such calculations should emphasize the importance of the liquid composition in producing the zoning patterns in the megacrysts studied here.

Finally, more data on barium zoning should be collected for a variety of megacrysts. It does not necessarily follow from this study that all K-feldspar megacrysts in granites are of strictly igneous origin, and it would be useful to examine barium zoning in megacrysts from as many environments as possible, to establish the types of zoning that predominate, and to interpret each type in terms of crystallization history and mode of origin.

Barium Distribution in the Rana Quartz Monzonite:
Implications for the Formation of Aplite

No megacrysts occur in the Rana Quartz Monzonite; hence it was not examined as part of the barium zoning study. However, the recognition of barium zoning in groundmass microcline from the Peñasco Quartz Monzonite made it logical to check the microcline of the Rana Quartz Monzonite for any indication of zoning. This was done and no zoning was found; the barium levels are essentially constant across the grains. Around the margins of some larger grains are small domains of somewhat higher barium content, but these were not concentric nor did they occur consistently and thus do not appear to represent primary zoning. In contrast, the porphyritic microcline grains from the coarse facies of the two-part aplite dike have distinct barium zoning, as shown in

figure 141. In the fine-grained facies of the aplite, the microcline is generally nonporphyritic, is poorer in barium, and shows no zoning. Is there a rational explanation for this seemingly irregular and inconsistent behavior of barium in microcline? The principal difficulty is in explaining why there is no barium zoning in the Rana Quartz Monzonite, whereas there is zoning in similar interstitial grains in the Peñasco Quartz Monzonite. One possible explanation is that the Rana Quartz Monzonite system was vapor saturated during the end stages of crystallization, whereas the Penasco Quartz Monzonite was not, particularly if it had less water initially and much of it was incorporated into biotite. The free vapor phase in the Rana Quartz Monzonite, if it was confined, may have been instrumental in homogenization of barium in the microcline, or perhaps the availability of water during the late stages of crystallization allowed the microcline to homogenize and/or recrystallize as it grew. In any case it is clear that the conditions under which the K-feldspar grew, or to which it was subjected shortly after growth, were different in the Rana Quartz Monzonite from those in the Peñasco Quartz Monzonite or the Puntagudo Granite Porphyry. The contention here is that availability and confinement of a free vapor phase during the late stages of crystallization constituted the critical difference. This has interesting implications for the formation of aplites, because the large microcline grains in the coarse aplite phase are zoned. This would suggest that a free vapor phase was not present, or at least was not confined so as to effect the homogenization of barium in the K-feldspar. This is consistent with the idea that aplites can form as the result of a pressure quench caused by partial escape of a vapor phase. The coarse aplite facies then

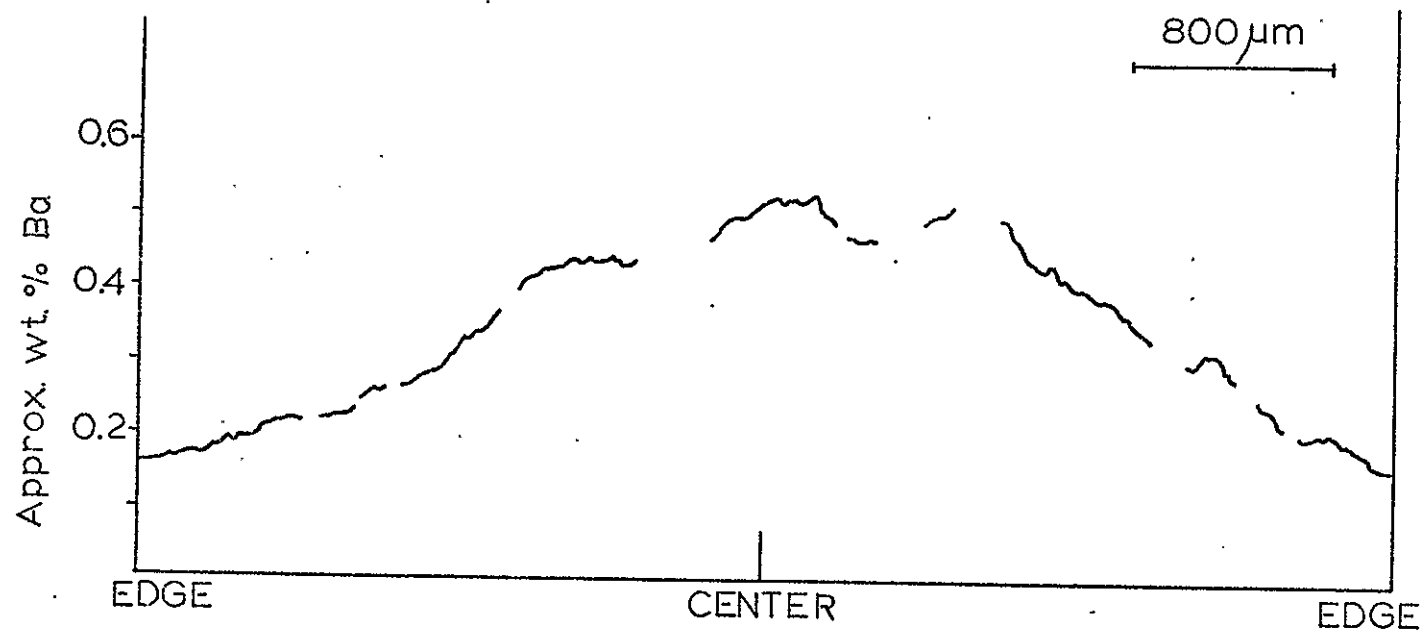


Figure 141. Pattern of barium zoning for large microcline crystal from the coarse facies of a Rana Quartz Monzonite aplite.

would represent accumulated rest-liquids that probably were vapor saturated and which began to yield biotite, quartz, plagioclase, and microcline when pressure was relieved with concomitant partial escape of the vapor phase. The fine-grained aplite facies apparently represents a greater degree of fractionation (see section on petrochemistry) in which the overall barium content of the rest-liquid was lowered and it had less opportunity than the coarse facies to produce large crystals. It too probably was quenched by rapid, partial loss of volatiles, but apparently there was sufficient vapor phase remaining to homogenize microcline formed before and during the quench. Further experimental work to determine the conditions under which barium-zoned feldspar can be homogenized would be valuable in attempting to verify the above hypothesis.

Geochronology

The relative ages of the granitic rocks, as inferred from field relations, are depicted in figure 78. The age sequence is rather definite except for the Puntiaquedo Granite Porphyry and the Rana Quartz Monzonite. It would be even more helpful to know the absolute ages of the granitic rocks, because without that knowledge it is impossible to make the time axis of figure 78 quantitative. Recently, attempts have been made radiometrically to date some of the rocks in the area by both K-Ar and Rb-Sr methods (Fullager and Shiver, 1973; Gresens, 1975), and the results are in some instances at variance with the field relationships. Also available are older age-dates (Rb-Sr and K-Ar) on the Harding pegmatite (Aldrich and others, 1958), unpublished U-Pb (zircon) age-dates on the Peñasco Quartz Monzonite (Leon T. Silver, pers. commun.), and

age-dates of various types from surrounding Precambrian terranes. This study itself has not generated any new radiometric dates. The purpose here is simply to coordinate the age-dates with the field and petrographic relationships, bringing together and in some instances reinterpreting the isotopic data.

The earliest radiometric geochronology was established in the area by Rb-Sr and K-Ar methods on muscovite and lepidolite from the Harding pegmatite (Aldrich and others, 1958), but the Rb-Sr ages they obtained are model Rb-Sr ages and hence are of limited value. Furthermore, the K-Ar ages may not refer to a specific event as they are so susceptible to thermal resetting. Together they range from 1350 to 1260 m.y., with an average of about 1300 m.y. Recasting the data for these dates in terms of an estimated Rb-Sr mineral isochron suggests that the Harding pegmatite may be somewhat older than the 1300 m.y. average, and possibly as old as about 1375 m.y. Modern determinations of Rb-Sr mineral and whole-rock ages on various pegmatites of this area would be extremely useful in light of the fact that the Harding pegmatite represents only one of the several types that are present. More recently, Gresens (1975) has reported a K-Ar age of 1335 m.y. for muscovite from what is presumably a simple pegmatite body. This age is consistent with the above reinterpretation of the data of Aldrich and others (1958), but it is uncertain that it actually refers to the specific time of formation of the pegmatite. That is, 1335 m.y. must be considered a minimum age for the simple pegmatites.

Fullager and Shiver (1973) have dated the "Embudo Granite" by Rb-Sr whole-rock methods, and have assigned to it an age of 1673 ± 41 m.y. The field relations of the rocks that are involved, however, invite

reinterpretation of their data to give about a 1400 m.y. age for the Peñasco Quartz Monzonite, with the age estimate for the Rana Quartz Monzonite remaining at about 1673 m.y. (fig. 142). Such ages, though compatible with geologic and petrologic relationships, must be regarded as rather imprecise because there are so few geologically well-controlled points on each isochron. In addition, Fullager and Shiver (1973) obtained mineral isochrons for these rocks that gave ages from 1208 ± 63 and 1212 ± 23 m.y., and Gresens (1975) reported a K-Ar (biotite) age, from a sample a few miles southeast of Trampas, of 1235 ± 19 m.y. Uncertainties plague the interpretation of these dates, as it is difficult to determine whether isotopic systems were completely reset or not. However, the overlap of the K-Ar and the Rb-Sr ages does suggest that a thermal event may have occurred about 1200 to 1250 m.y. ago. None of the above data have been collected with sufficient knowledge of the field relations nor with much appreciation of the potential complexity of the magmatic history of the area.

In an attempt to remedy the situation, Dr. Leon T. Silver of the California Institute of Technology has systematically collected and has been dating (U-Pb, zircon) samples of the Puntiaquedo Granite Porphyry, the Rana Quartz Monzonite, the Peñasco Quartz Monzonite, and the Harding pegmatite. Unfortunately, the only age-date that has been completed in this series is one for the Peñasco Quartz Monzonite of 1470 ± 20 m.y. (L. T. Silver, pers. commun.). This confirms the general notion of the reinterpretation of Fullager and Shiver's (1973) Rb-Sr data, but it also points up the probable uncertainty of the Rb-Sr data. There is definite need for additional Rb-Sr data before the Rb-Sr age and the U-Pb zircon age can be compared.

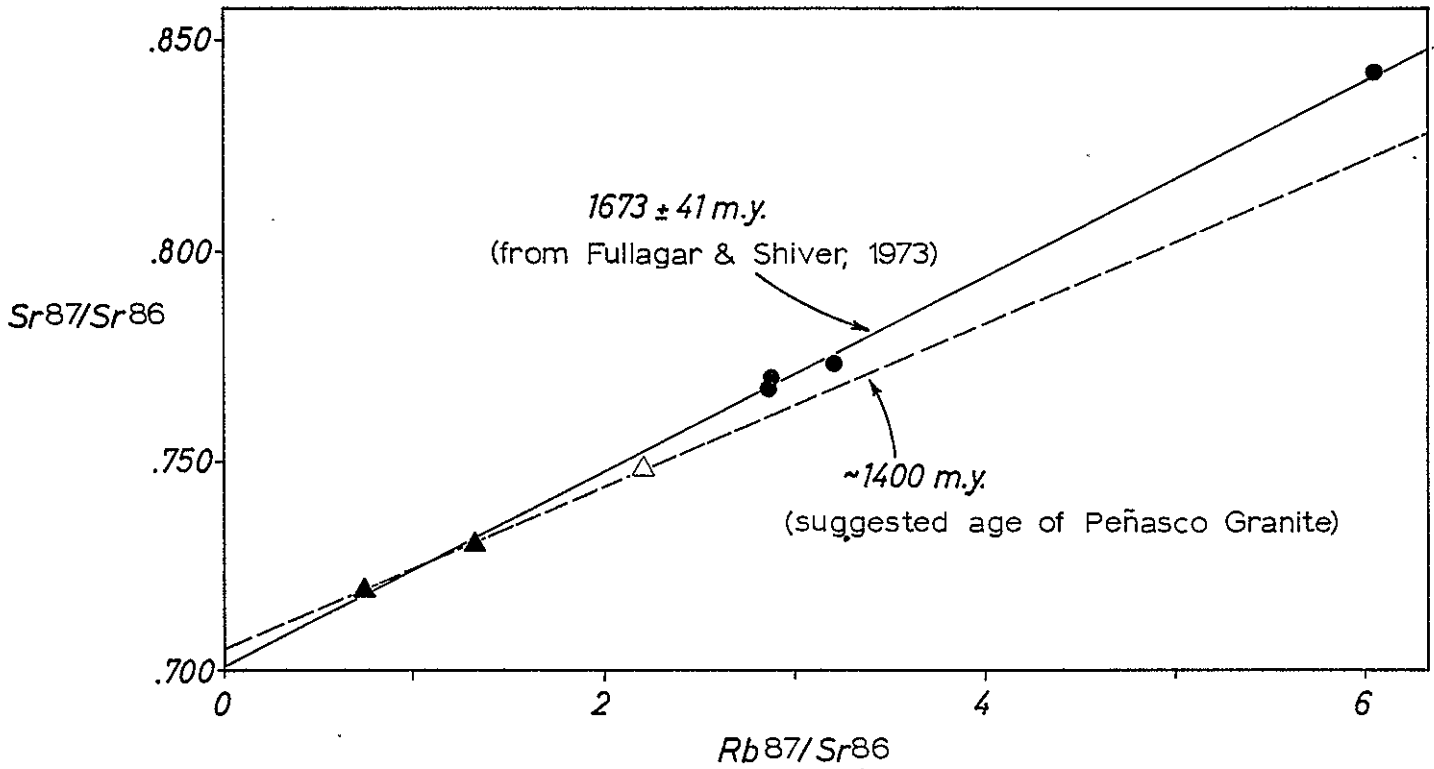


Figure 142. Possible reinterpretation of the Rb-Sr data from Fullagar and Shiver (1973). Closed triangles are Peñasco Quartz Monzonite. The open triangle is an apparently cogenetic granite without Peñasco Quartz Monzonite lithology; it is from an isolated outcrop about 5 mi southeast of the map area. The closed circles are in part Rana Quartz Monzonite and in part granites from outside the map area.

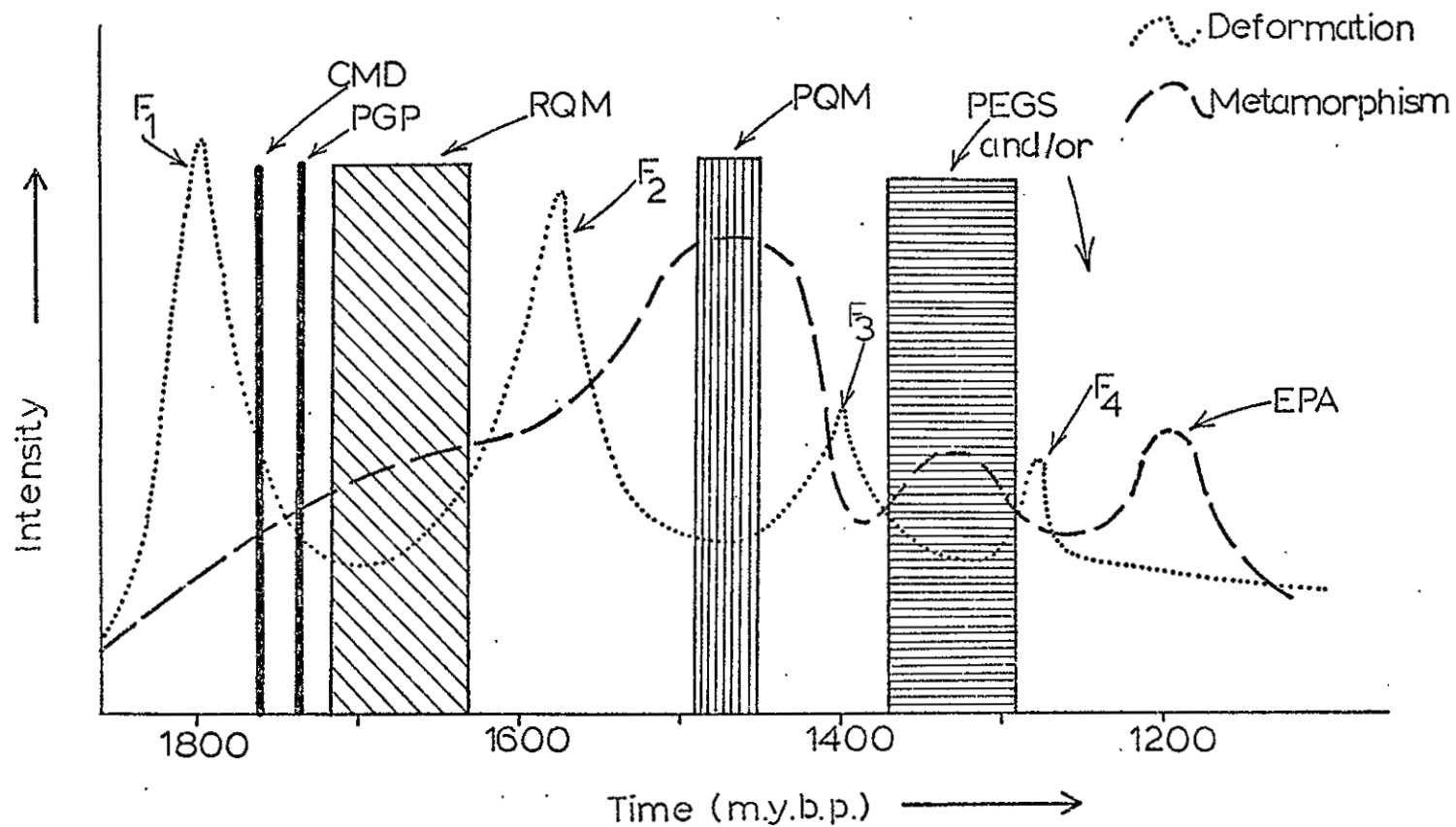


Figure 143. Possible arrangement of magmatic, metamorphic, and deformation events in terms of radiometric ages now known. Width of bars for magmatic events represent possible error in age determination. Cerro Alto Metadacite and Puntigado Granite Porphyry are represented only in terms of relative ages.

In summary, the age-dates in the area make it possible to revise figure 78 to figure 143. The absolute ages of the Cerro Alto Metadacite, the Puntigudo Granite Porphyry, and the felsites are still unknown, but at least it is now clear that the terrane has a complex igneous history over a considerable span of Precambrian time. Furthermore, these ages are represented elsewhere in northern New Mexico (Long, 1972; Brookins, 1974; Gresens, 1975; Brookins, 1975; Maxon, 1976). There can be little question that magmatism has been episodic in the Precambrian terranes of northern New Mexico. Not all of the Precambrian igneous and/or metamorphic events in northern New Mexico are recognized in the Dixon-Peñasco area, but when all the ages are known a surprising number of those events probably will be represented among the rocks in the relatively small area here studied.

VI. GENETIC INTERPRETATIONS OF THE GRANITIC ROCKS

General Statement

The following section is an attempt to bring together the information thus far presented and to interpret it in an internally consistent manner. Many of the interpretations already have been discussed, but we have not yet answered all the questions initially posed. Here we will try to answer those questions in the light of the overall observations. We will start with an interpretation of field and petrographic data based on Buddington's (1959) classification of granitic plutons, and then will consider textural and petrochemical data in the light of phase equilibria studies of synthetic granitic systems in an attempt to make pressure-temperature estimates for development of these rocks. Finally, the sequence of late-stage crystallization, metamorphism, and alteration will be summarized and interpreted, and possible general implications considered.

Estimates of Depth of Intrusion Based on Buddington's (1959) Classification of Granitic Plutons

Buddington (1959) proposed a three-fold classification of granitic plutons--epizonal, mesozonal, and catazonal--and inferred a depth-range of intrusion for each zone as shown in figure 144. He based his classification on the following criteria: (1) The relationship between the country rock and the intrusive body. Discordant bodies are typical of the epizone, and concordant bodies can show either relationship.

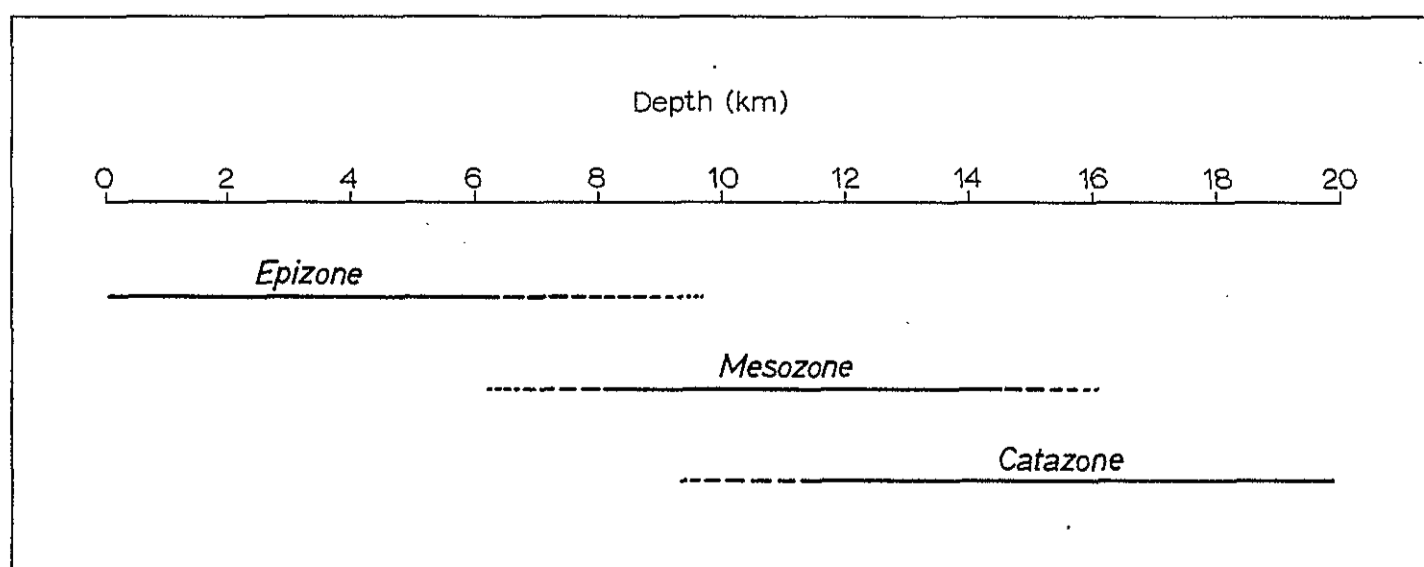


Figure 144. Schematic representation of the pluton emplacement zones of Buddington (1959).

(2) Manner of emplacement. Passive block stoping is predominant in the epizone, and forceful injection is most evident in the catazone. (3) The nature of intrusive contacts. Sharp contacts characterize the epizone, whereas migmatization becomes significant in the mesozone and catazone. (4) The presence or absence of a border zone. Border zones are essentially restricted to plutons of the epizone. (5) The metamorphic grade of the country rock. Very low-grade metamorphism or none is found in areas of epizonal intrusion, lower middle grades appear in the mesozone, and high-grade metamorphism occurs in catazonal regions.

Applying the above criteria to the granites of the Dixon-Peñasco area yields the chart shown in figure 145. It becomes immediately apparent that the estimated depth of intrusion increases with the passing of time, starting at near-surface levels with the Cerro Alto Metadacite and ending with the intrusion of pegmatite at mesozonal or deeper levels. This time-depth relationship is illustrated in figure 146.

The metadacite is thought to be a near-surface, perhaps subvolcanic rock, owing to its fine grain size, fabric, and partially intertonguing relationships with the country rocks. It seems unlikely that such a fine-grained rock could have been formed at depths greater than about 2 km. The Puntiaquido Granite Porphyry also is a shallow-level intrusive body, but its large K-feldspar and quartz phenocrysts, chilled margin, and associated fine-grained dikes suggest that it was intruded at somewhat deeper levels than the Cerro Alto Metadacite. It may or may not have been associated with acidic volcanism at the surface. Its depth of intrusion is estimated at 1 to 4 km. The absolute ages of the Cerro Alto Metadacite and Puntiaquido Granite Porphyry are not known;

DEPTH CRITERIA GRANITIC UNITS ↓	RELATIONSHIP TO COUNTRY ROCK	MANNER OF EMPLACEMENT	NATURE OF CONTACTS	PRESENCE OR ABSENCE OF A BORDER ZONE	METAMORPHIC GRADE OF COUNTRY ROCK	ESTIMATED DEPTH OF INTRUSION
CERRO ALTO METADACITE	discordant-- in part extrusive (?)	uncertain	sharp	entire unit fine grained	uncertain	upper epizone 0-2 km
PUNTIAGUDO GRANITE PORPHYRY	discordant	uncertain	very sharp	narrow one present	uncertain	epizone 2-4 km
RANA QUARTZ MONZONITE	discordant	in part forceful injection	fairly sharp	extensive but discontinuous one present	uncertain	lower epizone 3-6 km
PEÑASCO QUARTZ MONZONITE	mostly concordant	forceful injection	minor migmati- zation along contacts	absent	lower middle grade (epidote- andesine-am- phibolite)	mesozone 8-13 km
PEGMATITES	---	forceful injection (dilation)	sharp in most places	---	lower middle grade(?)	mesozone or deeper (?) 9-14 km

Figure 145. Summary of characteristics of the granitic rocks in the Dixon-Peñasco area.

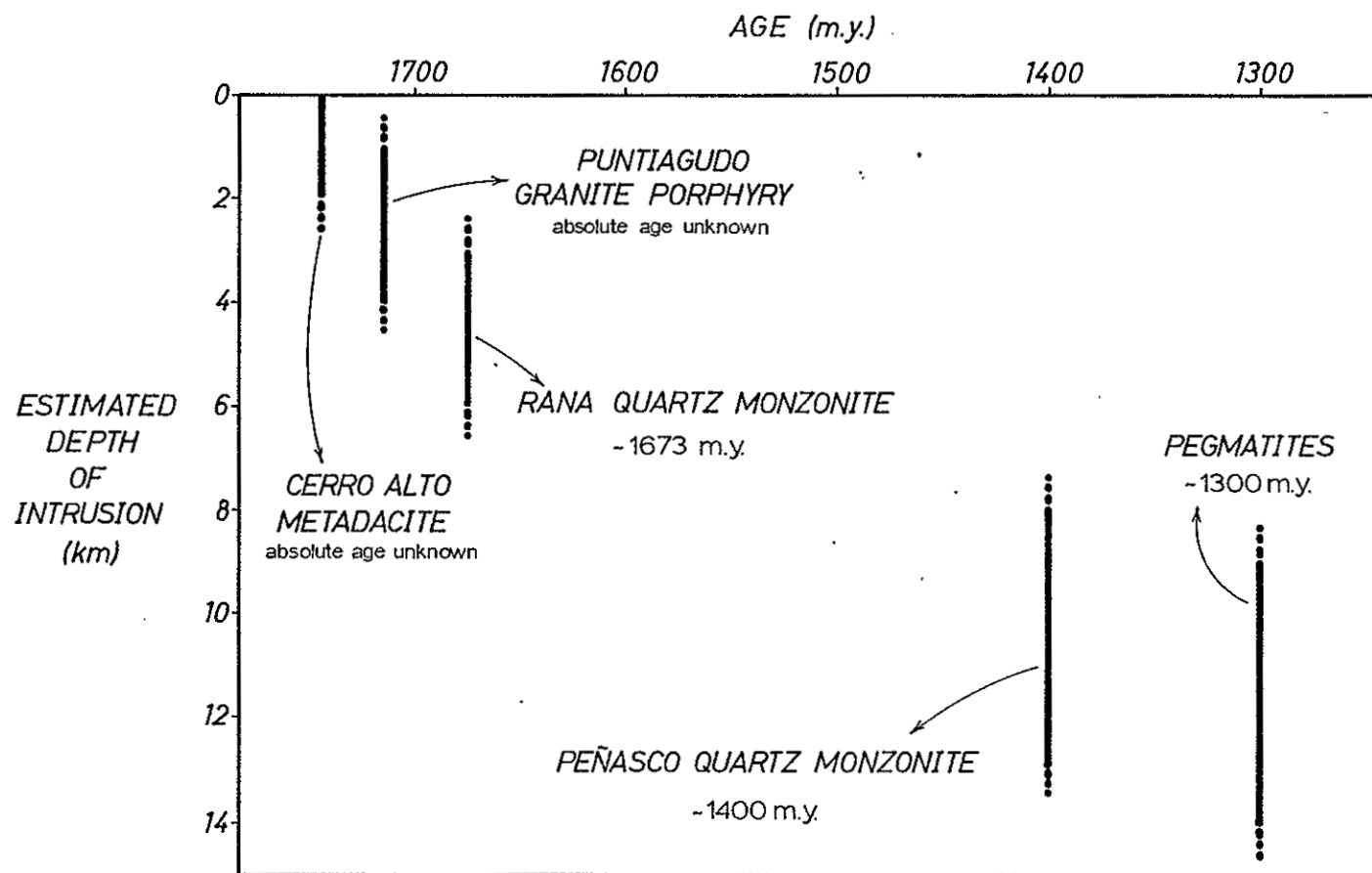


Figure 146. Plot of age vs. estimated depth of intrusion for the granitic rocks. The 1400 m.y. age for the Peñasco Quartz Monzonite is that determined by reinterpretation of Fullagar and Shiver's (1973) Rb-Sr data. A more accurate age for the Peñasco Quartz Monzonite is 1470 ± 20 m.y. by U-Pb in zircons (L. T. Silver, 1976, pers. commun.).

hence their age positions shown in figure 146 are purely schematic. They actually may belong closer to the Rana Quartz Monzonite or farther away from it in time.

The estimated depth of intrusion of the Rana Quartz Monzonite is 3 to 6 km. This is based on the medium to coarse equigranular texture of the nonfoliated facies, which suggests a deeper environment of crystallization than that of the Puntigado Granite Porphyry. However, the presence of an extensive border zone suggests that the intrusion is epizonal, so it is here assigned to the lower epizone. Additional support for this estimate is indicated by the slightly less sharp contacts of this unit, suggesting a depth of intrusion somewhat greater than that of the Puntigado Granite Porphyry.

The Peñasco Quartz Monzonite, on the other hand, has characteristics indicating that it was emplaced in the mesozone. In particular, its minor migmatization along contacts, its generally equigranular texture typical of moderate- to deep-seated plutonic rocks, and the lower middle grade of metamorphism of the adjacent country rocks all point to a mesozonal environment. Its conformable northerly margin and the evidence of forceful intrusion suggest the possibility of a catazonal environment, and its depth of intrusion is thus inferred to have been within the fairly wide range of 8 to 13 km.

Pegmatites present a problem in estimating depth of intrusion, as none of Buddington's criteria can be applied directly. These rocks are relatively rare in the epizone, and most are exposed in Precambrian terranes that probably have been eroded to mesozonal levels or deeper. Those few pegmatites known to have formed at shallow levels are characterized by sanidine and by quartz in bipyramidal crystals, features that

are absent from the pegmatites in the region here studied. On the basis of relatively low-temperature assemblages of essential minerals, lack of cavities or "pockets," and degree of metamorphism of the enclosing rocks, these pegmatites are inferred to have been emplaced at depths of 9 to 14 km. This broad range seems reasonable as the four or five types of pegmatites previously discussed may well have developed at different times and over a wide range of depths.

Field and petrographic evidence from a rather complex Precambrian terrane of relatively limited exposure thus prompts the conclusion that at least five episodes of granitic magmatism are represented here. They resulted in the emplacement of granitic rocks first at shallow depths and then at successively greater ones. Isotopic age data, as interpreted in the light of structural and petrologic relations, suggest that these episodes must have spanned a period of at least 300 m.y. However, the evidence for increasing depth of intrusion is questionable on several grounds, as the final characteristics of an intrusive body must be influenced by a large number of variables such as volatile content, rate of intrusion, volume of magma, temperature differences between magma and wall rock, wall rock type, and pressure on the magma. The interaction of such variables gives rise, in some highly complex way, to what one observes in the field. Even though some of them may be related to depth of intrusion, it is clearly a simplification of a very complex situation to attribute all of the diverse characteristics of the granitic rocks of this area to the single variable of depth. Buddington recognized this in stating that his depth zones are not related entirely to depth but also are "intensity zones" in which depth plays a major role. It is the contention here that depth

of intrusion was, in fact, one of the most important variables in the development of the contrasting types of granitic rocks in the Dixon-Peñasco area. This hypothesis is open to testing by geochronologists through careful dating of the intrusive events, and by geochemists through estimates of the pressure-temperature paths that both the metamorphic rocks and the granitic magmas must have experienced. Regardless of results from such tests, however, the field evidence demonstrates that characteristics of the intrusive activity changed progressively with time, and it is this progressive change that must be explained by any theory of the development of the Precambrian crust in the area.

One immediate test that can be made in this area is to compare the P-T history of the metamorphic rocks (figs. 28 and 29) with the above interpretation. While the time axis still cannot be completely quantified, the timing of increasing depth of intrusion relative to deformation events possibly corresponds to the suggested increase in pressure during metamorphism. At the present time, it is difficult to determine if the prograde increase in pressure is monotonic, nor is it clear what may have taken place between intrusive episodes, but the general agreement between the interpretation of events in the metamorphic rocks and depth of intrusion of the granites does strengthen the notion of overall increase in depth of burial with time.

Primary Crystallization and P-T Estimates (An Interpretation
Based on Textural, Petrochemical, and Phase Equilibria Data)

Some textures of the granitic rocks of the Dixon-Peñasco area ideally can be interpreted in terms of a crystallization sequence,

i.e. an order of appearance of phases during crystallization. Other textures may not be so ideal and only the relationship of one phase relative to others may be known, or it may only be known which phases coexisted with a silicate liquid at the time of intrusion or quenching. These crystallization sequences along with compositional data must form the basis for any interpretation of the P-T regimes of crystallization. Clearly this requires knowledge of the phase equilibria in appropriate systems at a variety of pressures and temperatures, but only limited experimental information is available for the quinary granite system Ab-Or-Q-An-H₂O which is the least complicated system that might adequately represent the natural magmas here considered. The textural data will be considered first.

The Cerro Alto Metadacite is generally fine grained and apparently crystallized under conditions of considerable undercooling, which probably is typical of volcanic or subvolcanic rocks. This is because a relatively great degree of undercooling is required in order to produce the high nucleation rates that must have given rise to the fine grain size (Fenn, 1973; Swanson, 1974). In fact, portions of this rock may have been glassy initially and since been devitrified, but in any case the small phenocrysts of quartz and plagioclase indicate that these minerals probably coexisted with the melt at the time of intrusion or shortly thereafter. Their small size would suggest that the magma may have been nearly all liquid at depth and that crystallization did not begin until the magma was intruded. It is not known if biotite coexisted with the melt at that time or if it crystallized later.

The Puntiaquedo Granite Porphyry, in contrast to the Cerro Alto Metadacite, has coarse crystals of microcline and quartz set in a

fine-grained groundmass, and it also has polygonated masses of plagioclase which are interpreted as relict phenocrysts. Thus it seems evident that K-feldspar, quartz, and plagioclase coexisted with a melt at the time of intrusion. Furthermore, both the barium zoning patterns and the textural relationships suggest that either plagioclase and/or quartz already had begun to crystallize when microcline began to nucleate. The timing of quartz crystallization is uncertain from the textures but there is a slight suggestion that it crystallized fairly early. For example, in formation of some Punttiagudo border-zone rocks, quartz and plagioclase or quartz and biotite apparently coexisted with liquid. Biotite probably also coexisted with the melt at the time of quenching, but this is difficult to positively ascertain in most Punttiagudo rocks. Only a few samples of the border zone contain glomeroporphyrritic clotlets of biotite.

The order of crystallization in the Rana Quartz Monzonite is in some ways the most difficult to interpret, owing in part to deformation and in part to conflicting relationships in the border-zone rocks. Within the unfoliated parts of the Rana body the subequigranular texture of the rock indicates that there may have been no "quenching" per se but rather a moderate nucleation rate relative to growth rate at the early and middle stages of crystallization. The interstitial distribution of the microcline, however, does indicate that it was the last major phase to appear. Biotite, quartz, and plagioclase all preceded K-feldspar, but the order of their appearance is not clear from examination of the unfoliated samples. Quartz and biotite may have been early phases, or at least the large, blocky character and the zoning of the quartz suggests a low nucleation rate during its initial crystallization.

The association of biotite with the quartz is taken to mean that they crystallized together, the biotite perhaps nucleating on the quartz. The plagioclase in general is less aggregated and occurs as grains smaller than those of the quartz, suggesting a slightly higher nucleation rate for plagioclase. It is not clear whether this is because plagioclase nucleated under slightly different conditions or whether its nucleation rate is inherently different from that of the quartz. The border zone of the Rana Quartz Monzonite has a distinctly porphyritic texture, which illustrates compositional effects on the crystallization sequence. Parts of the border zone contain rounded and zoned phenocrysts of quartz that are in places accompanied by less abundant biotite or plagioclase. The groundmass is normally very fine grained, but it is suggested that the quartz phenocrysts continued to crystallize after quenching because of the late rim of clear quartz on the clouded interiors of the phenocrysts. Other more potassium-rich parts of the border zone, however, show phenocrysts of K-feldspar and quartz \pm plagioclase in a fine- to medium-grained groundmass.

The aplites of the Rana Quartz Monzonite have a typical sugary allotriomorphic texture which ordinarily cannot be interpreted in terms of a crystallization sequence. Some, however, do contain small- to medium-sized phenocrysts, and these show that plagioclase, K-feldspar, and quartz \pm biotite coexisted with a liquid at the time of quenching.

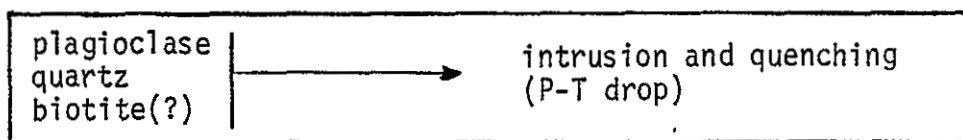
The Peñasco Quartz Monzonite and Rana Quartz Monzonite present similar difficulties of textural interpretation. In some of the samples K-feldspar appears interstitial and thus probably was the last phase to crystallize, whereas in the megacrystic samples the barium zoning suggests that K-feldspar was earlier and crystallized concomitantly with

quartz and/or plagioclase, probably while the magma was still largely melt. In either case it appears that, during much of the crystallization of the Peñasco rocks, plagioclase, K-feldspar, quartz, and probably biotite crystallized together.

This basic information on the crystallization behavior of the granitic rock units is summarized in figure 147. The other fundamental information required is the bulk compositions which have been given previously, and averages of the data are plotted in figure 148. Also plotted are bulk compositions used by Whitney (1975) in his experimental investigation of the quinary granite system $\text{Ab-Or-Q-An-H}_2\text{O}$. When his data are combined with the detailed information for the system $\text{Ab-Or-Q-H}_2\text{O}$ (Steiner and others, 1975) and Presnall and Bateman's (1973) interpretation of the phase equilibria of the vapor-saturated quinary system, then it is possible at least to consider the variables that might give rise to the different crystallization sequences.

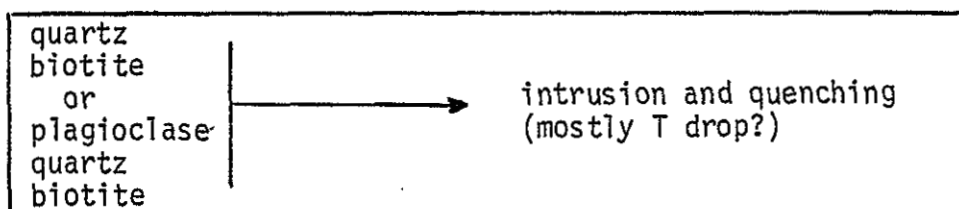
Summarization of the phase relations in the vapor-saturated system $\text{Ab-Or-Q-An-H}_2\text{O}$ at 5.kbar (Presnall and Bateman, 1973) is reproduced in figure 149 showing the trend for the Sierran rocks and the projections of compositions plotted in figure 148. Presnall and Bateman give fairly cogent reasons for assuming that the system $\text{Ab-Or-Q-An-H}_2\text{O}$ adequately describes the natural rocks even though mafic components are missing. However, their supposition that vapor-undersaturated conditions need not be considered explicitly is less than correct, especially when we are attempting to assign some significance to crystallization sequence. Notice, for example, that on figure 149 almost all of the rocks considered here plot in the primary phase field of plagioclase, and yet quartz may have been the primary phase in some of the Rana border-zone rocks. As

CERRO ALTO METADACITE

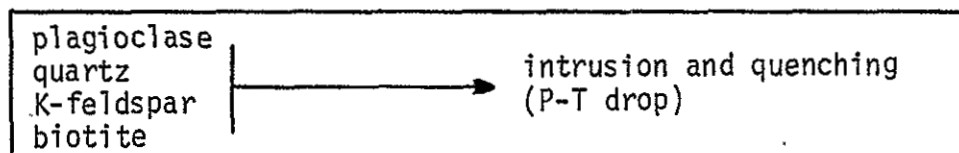


PUNTIAGUDO GRANITE PORPHYRY

Border zone



Main mass



RANA QUARTZ MONZONITE

Border zone

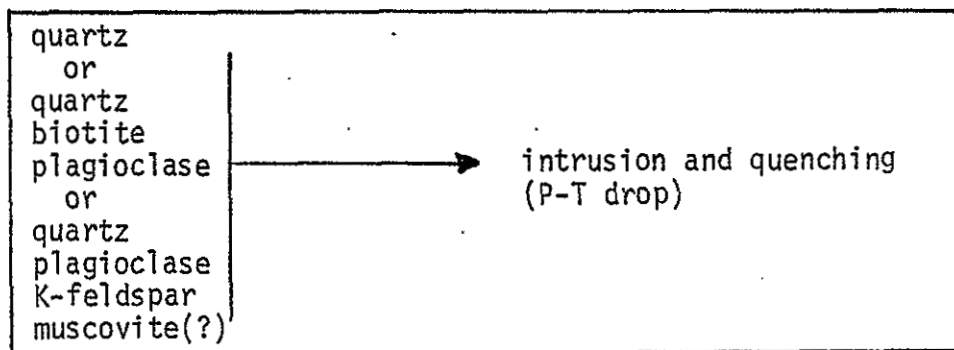


Figure 147. Summary of crystallization behavior of the principal granitic rocks. Mineral phases listed are assumed to have coexisted with a silicate liquid.

RANA QUARTZ MONZONITE

Main mass

plagioclase quartz biotite		+ K-feldspar → simultaneous crystallization (mostly T drop?)
----------------------------------	--	---

Aplites

plagioclase K-feldspar quartz + biotite		→ quenching (P drop?)
--	--	--------------------------

PEÑASCO QUARTZ MONZONITE

plagioclase quartz biotite		+ K-feldspar → simultaneous crystallization (mostly T drop?)
or plagioclase quartz K-feldspar biotite		simultaneous crystallization (mostly T drop?)

Figure 147.

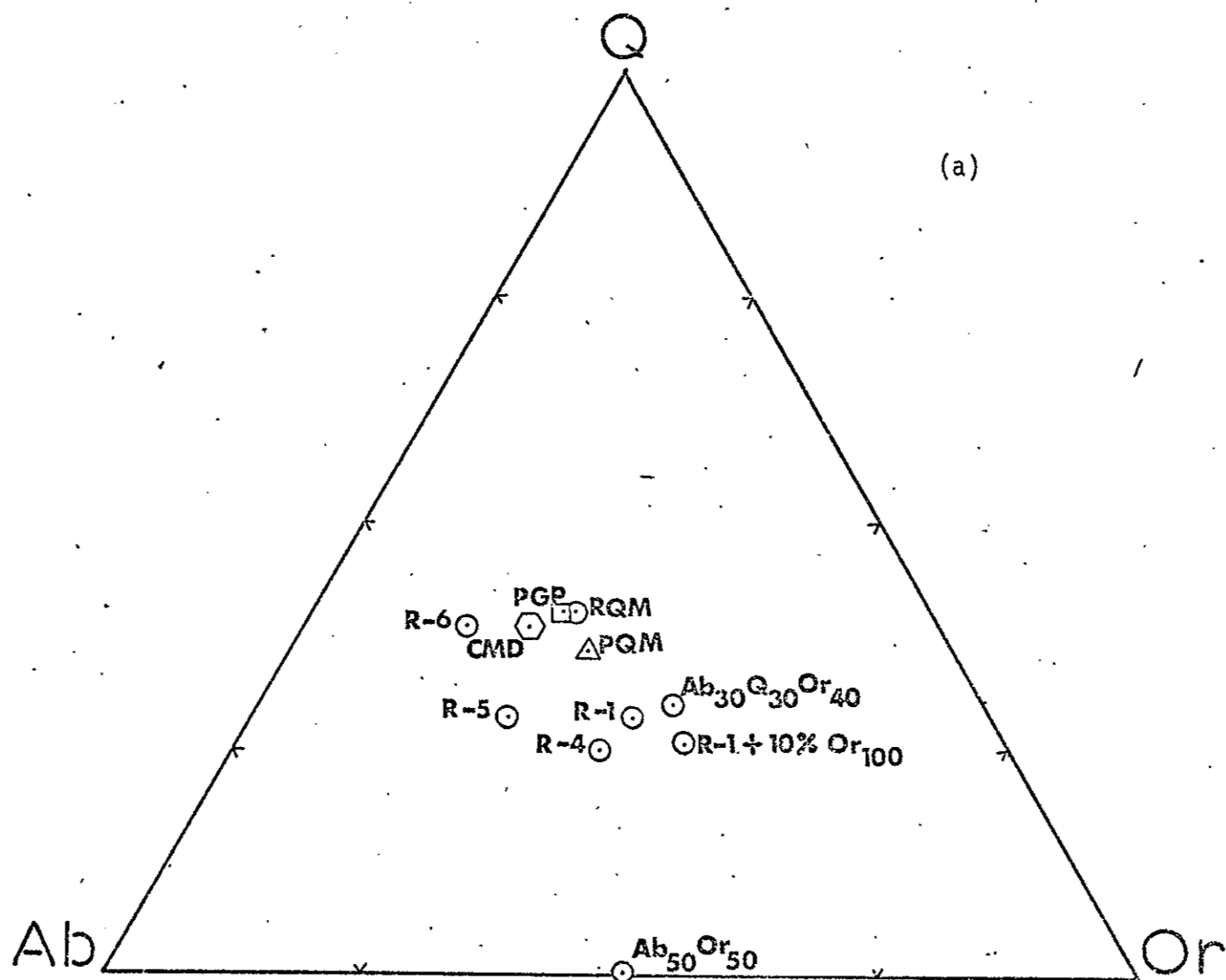


Figure 148. Averages of the chemical data for the granitic rocks of the Dixon-Peñasco area plotted on (a) Ab-Or-Q and (b) Ab-Or-An triangular diagrams.

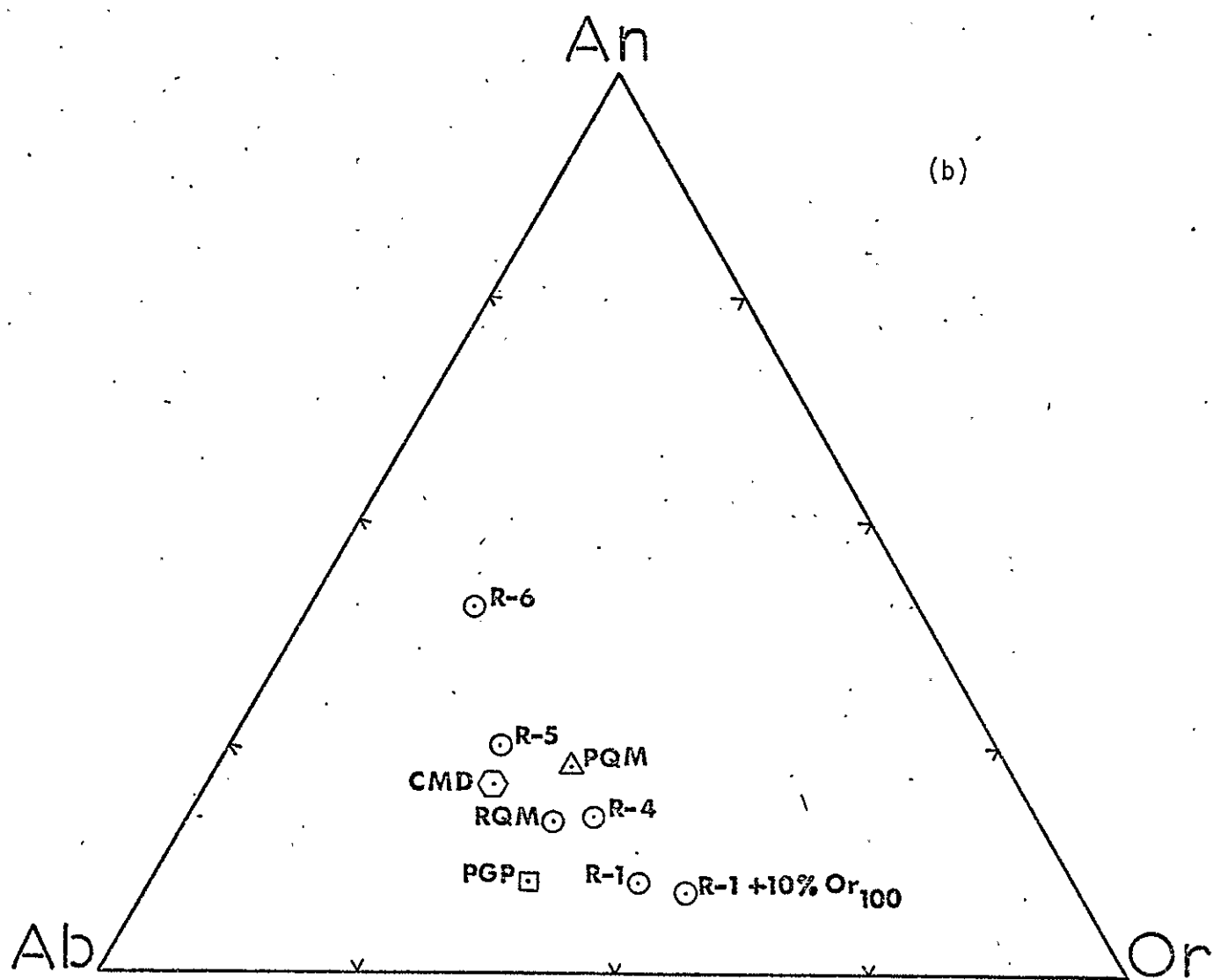


Figure 148.

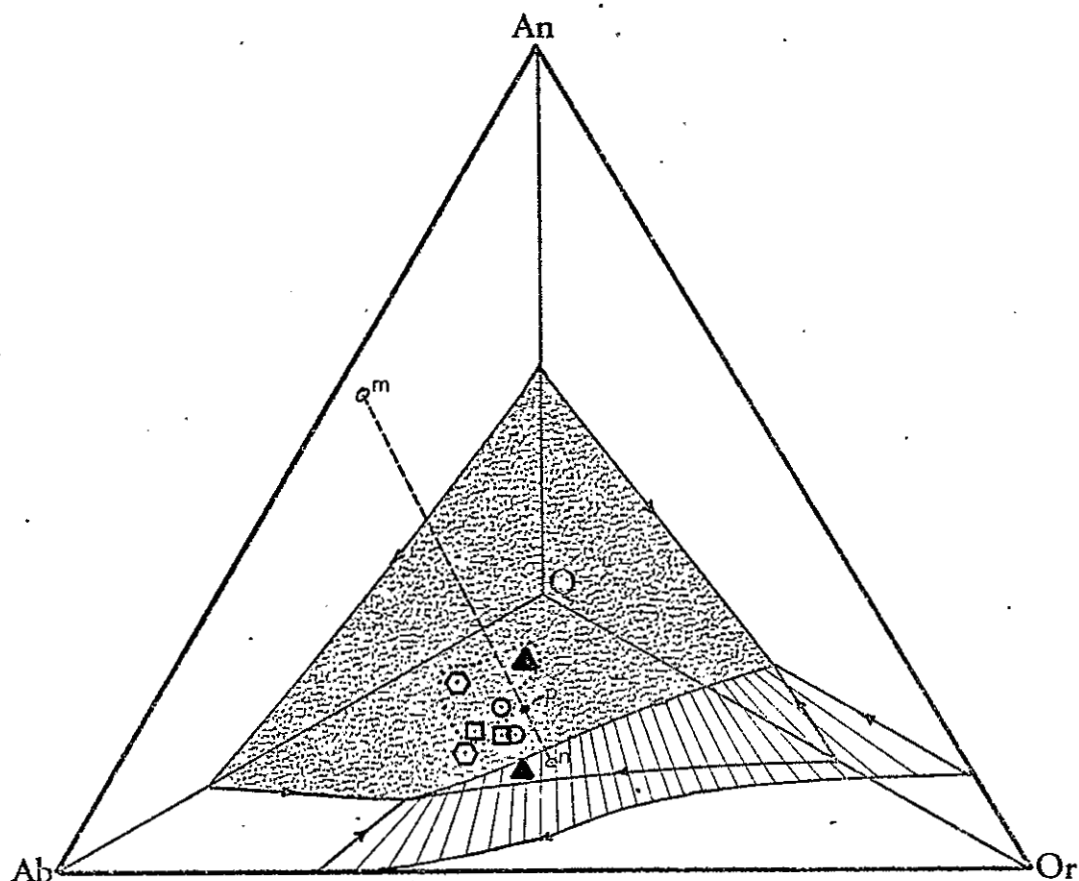


Figure 149. Interpretation of the vapor-saturated phase relations in the quinary system Ab-Or-An-Q-H₂O at 5 kbar according to Presnall and Bateman (1973). Ruled surface separates the primary phase field of plagioclase from that of K-feldspar. Stippled surface separates plagioclase primary phase field from that of quartz. Dashed line is the Sierran trend. P is the point at which it pierces the stippled surface. Symbols within the dotted line are plotted on the Ab-An-Or surface, the others are on the Ab-Q-Or surface. Hexagon = average Cerro Alto Metadacite; square = Puntiagudo Granite Porphyry; circle = average Rana Quartz Monzonite; triangle = average Peñasco Quartz Monzonite.

Presnall and Bateman (1973) note, the size of the primary phase field of quartz increases with pressure, a fact confirmed by Whitney (1972, 1975). Whitney also recognized and experimentally confirmed the importance of H_2O content in the undersaturated region. Figure 150 shows the effect of H_2O on his sample R-1 at 8 kbar. Notice that at high water contents K-feldspar instead of plagioclase is a liquidus phase, thus reversing the order of appearance of the feldspars. This means that some combination of pressure change and change in H_2O content and/or anhydrous bulk composition could readily account for the variation in crystallization behavior in these rocks. However, in all the granitic rocks considered here the three major minerals coexisted for much of the crystallization interval and plagioclase + quartz were commonly the two earliest phases. Thus only the broadest limits can be placed on the pressure and temperature of crystallization. For example, consider the Puntagudo Granite Porphyry. If we used Whitney's R-1 as a model, although the Puntagudo Granite Porphyry is considerably more quartz-rich than R-1, then the fact that $Q + Pl$ or $Q + Pl + Or$ coexisted with a liquid restricts pressure, temperature, and H_2O content to the shaded regions in figures 150 and 151. If locally in the border zone of the Puntagudo Granite Porphyry, however, quartz coexisted with a liquid then the phase relations suggest that the quartz must have grown at considerable depth, i.e. prior to the intrusion of the magma. A similar argument can be made for the quartz phenocrysts in the Rana Quartz Monzonite border zone, in which quartz may have been an early phase. Here, however, there is no evidence for corrosion of the phenocrysts as predicted by Whitney, but instead there is an overgrowth of clear quartz on the early, cloudy cores. If the overgrowth is a magmatic

RI SYN. GRANITE

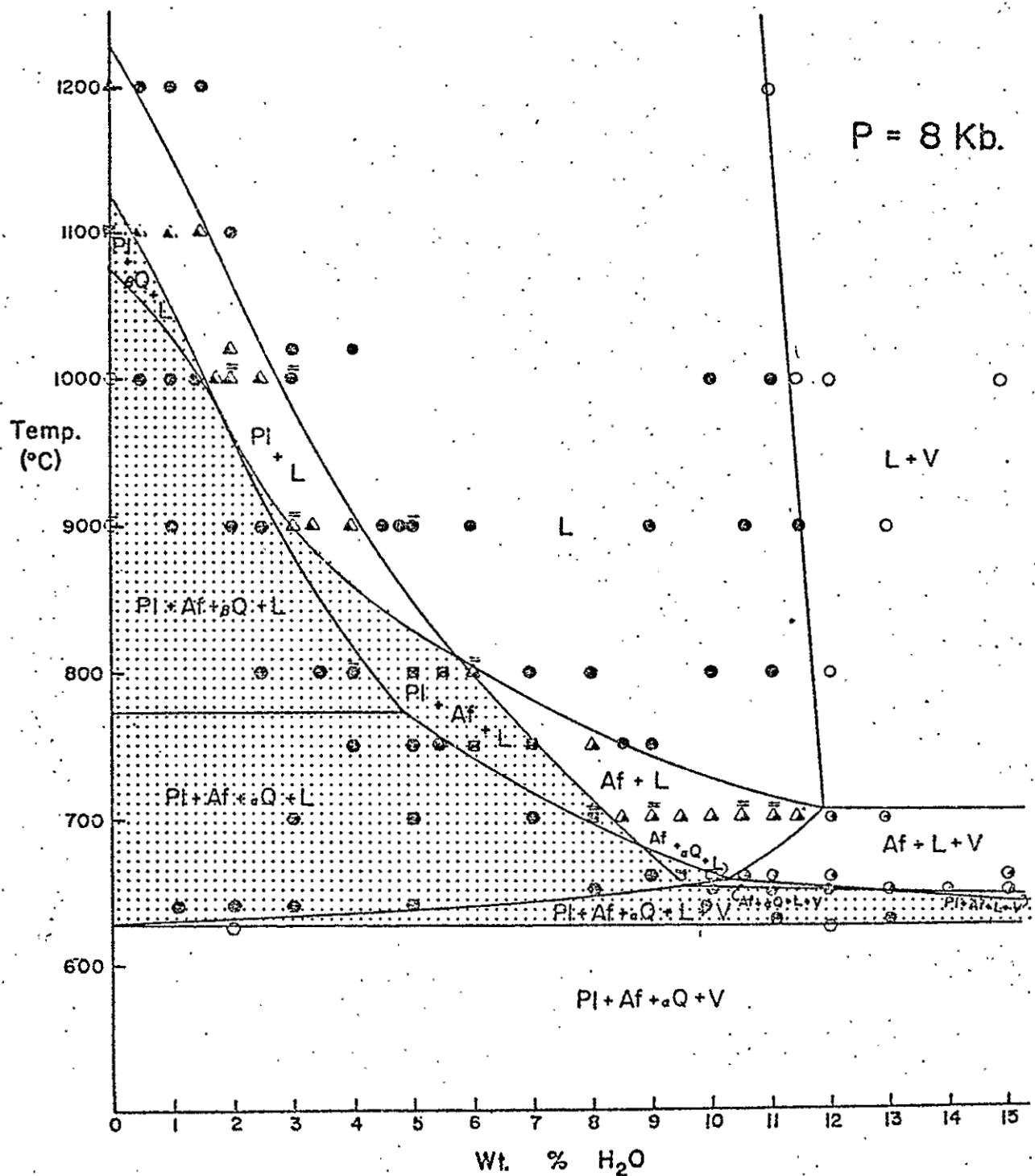


Figure 150. Temperature vs. weight percent H₂O at 8 kbar for sample R-1 of Whitney (1975). See text for explanation.

RI SYN. GRANITE

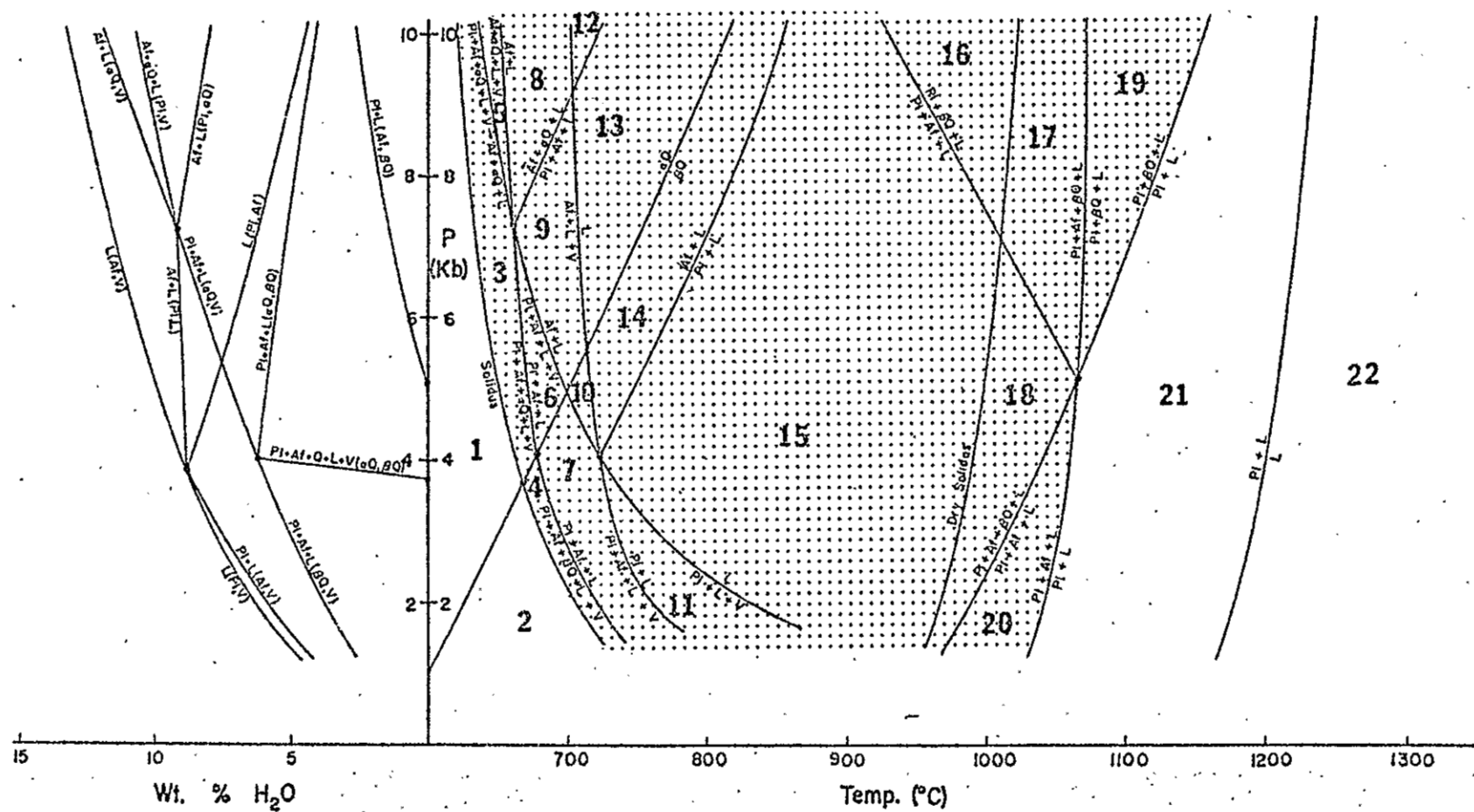


Figure 151. P-T and P-X projections for synthetic granite R-1 of Whitney (1975).
See text for explanation.

feature it suggests that quartz may have continued to precipitate after intrusion. This could be accounted for by loss of H_2O via a vapor phase, thus causing quartz to remain stable even though total pressure had been dropped.

The Peñasco Quartz Monzonite lacks a border zone with phenocrysts and this makes it more difficult to interpret its crystallization sequence. Nonetheless, fairly early local appearance of K-feldspar may indicate high pressure and a combination of moderately high water content and relatively high K_2O . This is because these factors apparently favor the early appearance of K-feldspar. However, the data on barium zoning show that the microcline was not homogenized with respect to barium, which can be interpreted to mean that H_2O contents were generally low. Assuming this to be correct and considering that the Peñasco Quartz Monzonite was probably largely liquid at the time of intrusion, i.e. it crystallized mostly in place, it must have been intruded at a greater depth than either the Puntigudo Granite Porphyry or the Rana Quartz Monzonite in order for K-feldspar to have formed early in its crystallization sequence.

In summary, the phase equilibria data and the crystallization sequences of these rocks do not provide sharply quantitative limits on physical conditions, but they do indicate consistency with the basic idea that the granites crystallized from melts. Furthermore, the general interpretation of the Peñasco Quartz Monzonite as the most deep-seated granitic pluton in the area is not inconsistent with these data.

Another possible constraint on the P-T regime of primary crystallization is the intersection of the granite minimum melting curve with the upper stability limit of epidote plus quartz. This relationship is

shown in figure 152. The upper stability limit of epidote plus quartz used is that of Holdaway (1972), with the hematite-magnetite buffer as the control on oxygen fugacity. This fugacity value was selected because hematite and magnetite coexisted in all these granitic rocks at least at some stage.* The other condition for the epidote stability curve is that it is for epidotes with 10 mole percent pistacite (Ps_{10}). The iron content of the epidotes in these rocks is not positively known, but it is assumed here that it is close to Ps_{10} as is suggested by optical properties. This is confirmed semiquantitatively by spectral scans with the electron probe on epidote from the Peñasco Quartz Monzonite.

The difficulty in applying the stability of epidote comes in interpreting whether or not the epidote grew as a magmatic phase. The epidote overgrowths on allanite from the Peñasco Quartz Monzonite are here interpreted as late-magmatic, i.e. they formed above the minimum melting curve for granite. This means that the Peñasco Quartz Monzonite must have crystallized at pressures in excess of 5 kbar, corresponding to a depth of 12 km or more. Epidote rims on similar cigar-shaped allanite in the Puntiaquedo Granite Porphyry are generally lacking, and it is here suggested that the epidote in that unit formed as a postmagmatic reaction product. Epidote, some of which is euhedral, does rim tiny allanite grains in the Cerro Alto Metadacite and the Rana Quartz Monzonite, but this probably represents preintrusion crystallization at a depth greater than 12 km. Thus it is possible to interpret the stability of

*Whitney and others (1976) have used this intersection to infer an approximate oxygen fugacity for the Stone Mountain Granite. Here the fugacity is interpreted from the oxide assemblage in the rocks themselves whereas the intersection is used to put constraints on P-T conditions.

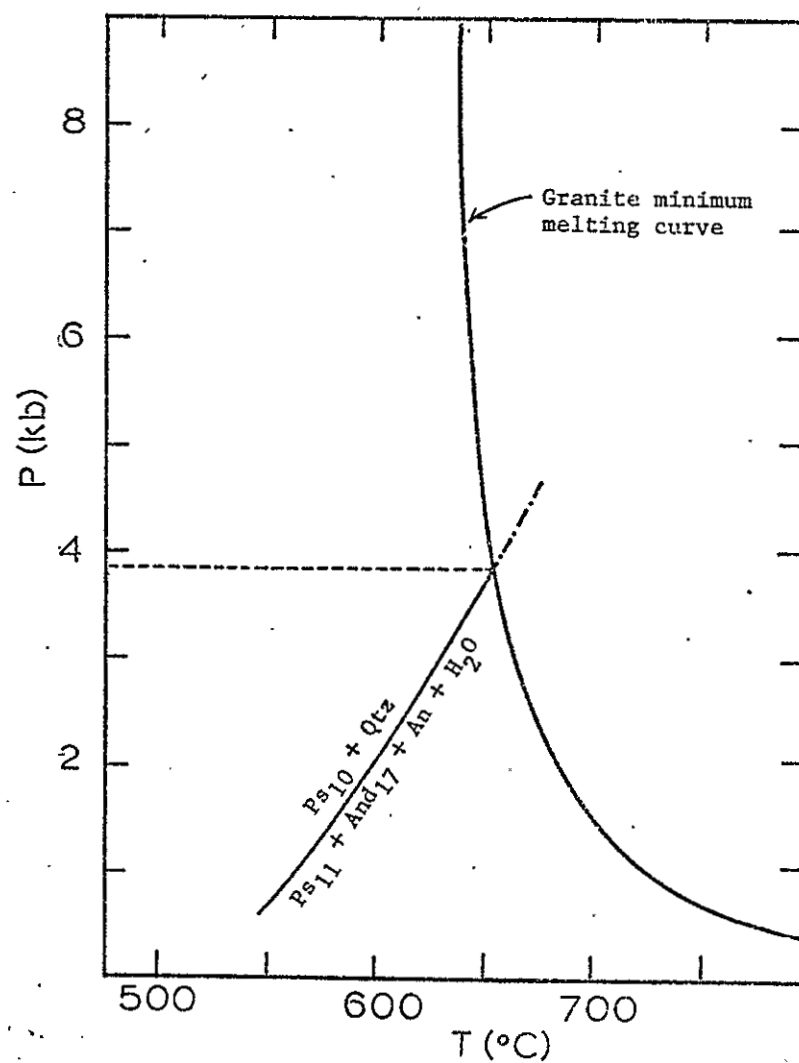


Figure 152. Intersection of stability curve for epidote (H-M buffer, Ps_{10}) (Holdaway, 1972) and minimum melting for granite (Bowen and Tuttle, 1958; Luth and others, 1964).

epidote relative to the granite minimum melting curve in a manner that corroborates the interpretation of depth of intrusion based on Buddington's classification.

Late-Stage Crystallization Versus Metamorphism and Alteration

One of the fundamental goals of this investigation was to develop criteria for distinguishing petrographic features due to deuteritic alteration from those that could be attributed to later metamorphism and/or alteration. In retrospect it was partly naive to expect such a goal would be realized in an area where the general complexity of the history of magmatism opens many possibilities for later thermal events and contact metamorphism of older granites by younger ones. On the other hand, the Dixon-Peñasco area has provided an unusual opportunity to examine the interaction of polyphase deformation, regional metamorphism, and late-stage magmatic processes, and despite the complex history of the area it is possible to draw some general conclusions regarding these processes.

Before considering possible criteria, it will be useful to recapitulate the interpretations of specific petrologic features starting with those related to the initial magmatic crystallization of these rocks. First, most of the granitic rocks retain bulk- and trace-element compositions that bespeak a magmatic origin. The principal exceptions are severely altered parts of the Rana Quartz Monzonite border zone and many of the felsites. Second, the general mineralogy of most of the granitic rocks reflects their igneous origin. Possible exceptions are some of the muscovite, some of the epidote, and some of the albite. The original igneous textures, however, are less well preserved and it

is less certain what exactly they were. This is particularly true in the severely deformed rocks of the Rana Quartz Monzonite and older units. Still, wherever deformation has been less severe, e.g. the unfoliated phase of the Rana Quartz Monzonite, it appears that the gross mesoscopic texture of the rock is primarily due to its igneous history. In less altered parts of the border zone of the Rana Quartz Monzonite the bimodal texture is an igneous feature, as is the bimodal texture of the Punttiagudo Granite Porphyry. The microcline megacrysts of the Peñasco Quartz Monzonite evidently grew from a melt, as did the other major minerals in that unit. Except for minor granulation and muscovite-epidote alteration, the state of aggregation of that rock is largely as it was when the last melt was consumed by crystallization.

On a gross scale all of the granitic rocks retain much of their igneous character. The major megascopic exceptions are the presence of epidote alteration, the locally severe muscovite-quartz alteration, and the superimposed foliation. Field evidence demonstrates that neither the epidote alteration nor the foliation is strictly deuteric in nature. The quartz-muscovite alteration in the border zones of the Punttiagudo Granite Porphyry and the Rana Quartz Monzonite may have been in part generated by the vapors given off during cooling of their respective main bodies, but even this is in a sense superimposed in that it was probably not due to effects of vapor generated in situ.

If the granitic textures are considered in detail, however, the distinctions are much less clear cut. It is relatively easy to distinguish igneous features such as euhedral to subhedral plagioclase grains, but it is uncertain how much of the zoning has been affected by subsolidus diffusion. The basic problem, however, remains in positively

distinguishing the nondeformational metamorphic features from the deuteric ones. The features involved, as noted previously, are albitic rims on plagioclase, perthitic intergrowths, myrmekite, muscovite replacement of biotite, and muscovite and epidote replacement of plagioclase. These features are not incompatible with the conditions of metamorphism in the area, as they persist and even are more pronounced in the older, more metamorphosed granites. On the other hand, it is well known that similar features are sometimes observed in rocks where no metamorphic events have occurred subsequent to initial cooling. The formation of perthite, for example, almost certainly does not depend on a metamorphic event but rather on the nature of the cooling path, the composition of the original feldspar, and perhaps the composition and amount of interstitial fluid. The cooling path is probably very important, as the time during which a given granite resides in a given temperature-pressure regime doubtless is crucial to the size and spacing of perthitic lamellae and at least partly determines the thickness of albitic rims by controlling the amount of sodium diffusing out of the K-feldspar. After the temperature falls below a certain level or if a fluid phase escapes, kinetic barriers tend to prevent further redistribution of elements. If temperature is raised again, if a fluid phase permeates the rock from another source, or if deformation increases the surface area of some of the phases, reactions toward ultimately stable phases can continue or resume. Thus it may be very difficult to distinguish, from the rock textures, where one process left off and the other started, as in principle the composition of the two products may be identical. A metamorphic fabric such as that in the Rana Quartz Monzonite and older granitic rocks is an indicator of the importance

of metamorphism and deformation in those rocks, but it remains difficult to say how much of a given albitic rim was inherited from the state of the rock previous to deformation and how much might have been created by the deformation. Zoning of plagioclase in some of the most severely deformed rocks is reminiscent of that seen in some metamorphic rocks and probably is due to the metamorphism rather than the initial igneous history. This suggests that recrystallization may have been rather complete in these rocks, perhaps so complete that the late-stage features are a second generation. For example, the initial albitic rims may have been resorbed and then reformed as temperatures fell again. Unfortunately, there is no direct evidence for this, but in a terrane with a polymetamorphic history it stands as one of several possibilities.

Similar uncertainty plagues the interpretation of the muscovite-epidote alterations of plagioclase in these rocks. If, however, the alteration of plagioclase and the formation of myrmekite are in any way related, as is suggested by the possible nature of the reactions involved and if myrmekite formed after the perthite, as is indicated by one piece of textural evidence then the alteration might be later than the perthite. In addition, the sporadic distribution and preponderance of the alteration in the older units suggest that it is not related solely to an internally generated process. This intuitive approach, however, is of heuristic value only for the Dixon-Peñasco area in that there are examples of very extensive alteration (e.g. the Cornwall granites in England) that is due largely to deuteritic processes. Yet in the Rana and older granitic rocks, which are affected by megascopic epidote alteration, the microscopic alteration of plagioclase is generally most severe. Field relations show that the megascopic epidote alteration

is much younger than the Rana Quartz Monzonite itself, so if the megascopic alteration and microscopic plagioclase alteration have the same origin, then the plagioclase-epidote alteration reflects a subsequent metamorphic or alteration event rather than a deuteritic alteration associated with the Rana Quartz Monzonite itself.

In summary, the gross textures and appearance of the granitic rocks are largely results of either the initial igneous processes that formed them or of subsequent deformation, metamorphism, and alteration affecting them long after they initially cooled. Some of the details of their textures, in particular perthitic intergrowths and homogenization of barium in some microcline, probably arose from deuteritic alteration of the cooling bodies. Most such features, however, have been altered and modified by the subsequent metamorphism and alteration.

The complexity of the Dixon-Peñasco terrane has not lent itself to the development of general criteria for use in making a distinction between deuteritic and metamorphic features. There may be no theoretical reason to expect consistent mineralogical differences in products of the two processes, which creates difficulty in attempting to pin down any useful generalizations. Nevertheless, some possibilities are worth considering for indications of worthwhile directions future research might take. The soundest criteria, of course, are field relations such as those reported here. These suggested the wide separation in time of crystallization of the granitic rocks, and of the epidote alteration. If timing of the alteration is uncertain, then its spatial distribution can give clues as to its origin. For example the exo-deuteritic alteration of the border zone of the Rana Quartz Monzonite is restricted in distribution to the border zone, an indication of its

intimate relationship to the main Rana body. The epidote alteration, on the other hand, occurs sporadically in irregular domains that bear no consistent spatial relationship to a supposedly related igneous body. It is therefore suggested that, in general, a lack of correlation between spatial distribution of alteration and some feature or features related to primary crystallization and differentiation in the host body may be taken to indicate that the alteration is due to events subsequent to late-stage crystallization.

Textural criteria seem less trustworthy, but it appears that whenever a penetrative deformation is present in granitic rocks, some effects of metamorphic alteration and modification of deuteritic features must be suspected. One of the most useful indicators on a microscopic scale may be the distribution of barium in K-feldspar. It cannot be applied uncritically, however, as evidence from these rocks suggests that both deuteritic and metamorphic processes can destroy barium zoning under certain circumstances. Furthermore, homogenization conceivably could occur under magmatic conditions as well, so caution must be exercised in the interpretation of barium zoning or the lack thereof. It is suggested here that a significant amount of a confined vapor phase probably will generally result in homogenization of interstitial barium zoned K-feldspar. In the rocks examined here, such homogenization apparently took place during late-stage growth, by recrystallization or diffusion which was catalyzed by a ubiquitous exsolved vapor phase. In contrast, the microcline megacrysts that were homogenized are restricted to very localized domains of severe alteration in shear zones.

This study far from exhausts the possibilities for research on the basic question deuteritic versus metamorphic alteration. The use of

cathodeluminescence for examining albite lamellae and albite rims, for example, should provide additional information on the exsolution process and the degree of interaction between the internal parts of a K-feldspar crystal and its surroundings. The limited data presented in the section on barium zoning suggest that little interaction may have occurred, at least with respect to some activator element(s) that are responsible for the color difference between b lamellae and b rims. This kind of study should be extended. No quantitative data have been presented here on composition of epidote and muscovite as related to paragenesis, and this also is an area that deserves more attention. Additional experimental work is needed to determine controls of the compositions of these minerals, and to estimate P-T conditions of the formation of these minerals. Eventually, as consistent patterns of P-T regimes begin to emerge, we may be able to distinguish the products of late-stage deuteritic alteration from those of a later metamorphic event.

VII. SUMMARY AND CONCLUSIONS

The Dixon-Peñasco area was the locus of episodic magmatic activity for at least 300 m.y. during Precambrian time. This magmatic activity was preceded by deposition of a thick sequence of sedimentary rocks ranging from quartz sandstones to pelitic shales. The deposition of sediments was succeeded by initial magmatic activity that resulted in basaltic to andesitic flows and in development of volcanic conglomerates and volcanoclastic sediments. Simultaneously, mafic dikes were injected into the uppermost layers of the underlying strata.

After the basaltic magmatism ceased, some unknown amount of time elapsed before magmatism was again initiated, this resulting in emplacement of the Cerro Alto Metadacite at shallow levels and perhaps partly as flows on the surface. Subsequent episodes of magmatism resulted in emplacement of the Punttiagudo Granite Porphyry, the Rana Quartz Monzonite, and the Peñasco Quartz Monzonite at successively deeper levels in the crust. The final magmatic episodes gave rise to the multitude of pegmatites in the area. It is significant that these pegmatites apparently are not genetically related to any of the granitic rocks now exposed in the area.

After intrusion of the Rana Quartz Monzonite there were one or more major regional metamorphic events and at least three asynchronous deformation events. These events raised the country rocks to a middle amphibolite grade of metamorphism and imparted a regional foliation to the terrane, including the older granitic rocks. One or more of the

later metamorphic events gave rise to alteration, especially in, but not strictly limited to, the older granitic rocks. The timing of these events is best summarized in figure 143.

The conclusions of this work regarding the origin and development of late-stage features in these rocks are as follows: (1) The bulk of the gross textural features of these rocks formed while a silicate melt was still present. (2) The features, both microscopic and megascopic, that are not ascribable to igneous processes were formed mainly during subsequent metamorphic and alteration events. The most notable exceptions are the lack of barium zoning in interstitial K-feldspar in the Rana Quartz Monzonite and the formation of perthitic intergrowths, both of which are probably the result of deuteritic processes. Even so, most of the strictly deuteritic features have been largely modified by later events.

Some of these conclusions might be extrapolated to other granitic terranes, but it would seem wise to judge each occurrence according to its own evidence before attempting to draw broad conclusions about the general importance of metamorphic processes versus deuteritic ones in granitic rocks.

EPILOGUE

The broader interpretation of the rocks here studied may be as interesting and eventually as valuable as the results of the study of the details of these rocks. That is to say, speculation is irresistible. The possibly profound significance of the persistence of magmatism in the Dixon-Penasco area over such a large span of geologic time and its occurrence first as extrusions followed by intrusions at deeper and deeper levels cannot be ignored. It is as if the Precambrian crust here foundered, perhaps under the weight of accumulating but now largely eroded volcanic debris. If the nature and character of the metamorphosed sedimentary rocks are considered as well, interpretation of the area as a petrotectonic assemblage suggests a convergent plate boundary, perhaps the margin of a protocontinent. This immediately raises several questions: Why did episodic magmatism occur in one place for so long a time? What was the general spatial configuration of similar rocks in the North America shield, and was it consistent with a plate tectonic model? Clearly the "postage-stamp size" of this study area does not permit verification of the idea on a continental scale, and what is needed is a series of many such detailed studies. This in-depth comprehension of Precambrian terranes must be one of the most fruitful areas of geologic research over the next few decades.

REFERENCES

- Afonina, G. G., and Shmakin, B. M., 1970, Inhibition of lattice ordering of potassic feldspar by barium ions: *Doklady Akademii Nauk SSSR*, v. 195, p. 133-135.
- Albarede, J., and Bottinga, Y., 1972, Kinetic disequilibrium in trace element partitioning between phenocrysts and host lava: *Geochim. et Cosmochim. Acta*, v. 36, p. 141-156.
- Aldrich, L. T., Wetherill, G. W., Davis, G. L., and Tilton, G. R., 1958, Radioactive ages of micas from granitic rocks by Rb-Sr and K-Ar methods: *Am. Geophys. Union Trans.*, v. 39, p. 1124-1134.
- Augustithis, S. S., 1962, Non-eutectic, graphic, micrographic and graphic-like "myrmekitic" structures and textures: *Beitrage zur Miner. and Petrog.*, v. 8, p. 491-498.
- , 1964, Nonexsolution perthites from pegmatoids of Yavello/Borona, S. Ethiopia: *Chemie der Erde*, v. 23, p. 227-247.
- Baldwin, B., 1956, The Santa Fe group of north-central New Mexico: *New Mexico Geol. Soc. Guidebook*, 7th field conference, p. 115-121.
- Barker, D. S., 1970, Compositions of granophyre, myrmekite and graphic granite: *Geol. Soc. America Bull.*, v. 81, p. 3339-3350.
- Barker, F., 1958, Precambrian and Tertiary geology of the Las Tablas quadrangle, New Mexico: *New Mexico Bur. Mines Min. Res. Bull.* 45.
- Becke, R., 1908, Uber myrmekit: *Min. Pet. Mitt.*, v. 27, p. 337-390.
- Berlin, R., and Henderson, C. M. B., 1969, The distribution of Sr and Ba between the alkali feldspar, plagioclase and groundmass phase of porphyritic trachytes and phonolites: *Geochim. et Cosmochim. Acta*, v. 33, p. 247-255.
- Bethke, P. M., Barton, P. B., Jr., Lanphere, M. A., and Stevens, T. A., 1976, Environment of ore deposition in the Creed mining district, San Juan Mountains, Colorado, pt. II, Age of mineralization: *Econ. Geology*, in press.
- Brookins, D. G., 1974, Summary of recent Rb-Sr age determinations from Precambrian rocks of north-central New Mexico: *New Mexico Geol. Soc. Guidebook*, 25th field conference, Ghost Ranch (central-northern New Mexico), p. 119-121.

- Brookins, D. G., 1976, Rubidium-strontium geochronologic study of GT-1 and GT-2 whole rocks: *Am. Geophys. Union Trans.*, v. 57, no. 4, p. 352.
- Buddington, A. F., 1959, Granite emplacement with special reference to North America: *Geol. Soc. America Bull.*, v. 70, p. 671-747.
- Colony, R. J., 1923, The final consolidation phenomena in the crystallization of igneous rock: *Jour. Geology*, v. 31, p. 169-178.
- Dickson, F. W., 1968, Growth of K feldspars and plagioclases by replacement processes in rocks of the Papoose Flat pluton and in country rocks, Inyo Mountains, California abs.: *Geol. Soc. America Spec. Paper* 101, p. 53.
- Drake, M. J., and Weill, D. F., 1975, Partition of Sr, Ba, Ca, Y, Eu^{2+} , Eu^{3+} , and other REE between plagioclase feldspar and magmatic liquid: an experimental study: *Geochim. et Cosmochim. Acta*, v. 39, p. 689-712.
- Emmerrmann, Rolf, 1968, Differentiation and metasomatoses des albalganits (Sudschwarz-wald): *Neues Jahrb. Miner. Abh.*, v. 109, p. 94-130.
- 1969, Genetic relations between two generations of K-feldspar in a granite pluton: *Neues Jahrb. Miner. Abh.*, v. 3, no. 3, p. 289-313.
- Erd, R. C., 1977, Boron in metamorphic rocks, in *Mellor's Comprehensive treatise of inorganic chemistry, Boron volume supplement*: Essex, England, Longman Group Ltd., p. 96-105.
- Eskola, Pentti, 1956, Post magmatic potash metasomatism of granite: *Finland Comm. Geologique Bull.*, no. 172, p. 85-100.
- Evans, B. W., 1965, Application of a reaction-rate method to the breakdown equilibria of muscovite and muscovite plus quartz: *Am. Jour. Sci.*, v. 263, p. 647-667.
- Ewart, A., and Taylor, S. R., 1969, Trace element geochemistry of the rhyolitic volcanic rocks, central north island, New Zealand; phenocryst data: *Contr. Mineral. and Petrology*, v. 22, p. 127-146.
- Fenn, P. M., 1973, Nucleation and growth of alkali feldspars from melts in the system $\text{NaAlSi}_3\text{O}_8$ - KAlSi_3O_8 - H_2O : Stanford, Calif., Stanford University Ph.D. thesis.
- Foord, E. E., 1976, Mineralogy and petrogenesis of layered pegmatite-aplite dikes in the Mesa Grande district, San Diego County, California: Stanford, Calif., Stanford University Ph.D. thesis.
- Frick, C., 1937, Horned ruminants of North America: *Am. Mus. Nat. History Bull.*, v. 69.

- Fullager, P. D., and Shiver, W. S., 1973, Geochronology and petrochemistry of the Embudo Granite, New Mexico: *Geol. Soc. America Bull.*, v. 84, p. 2705-2712.
- Galusha, T., and Blick, J. C., 1971, Stratigraphy of the Santa Fe Group, New Mexico: *Am. Mus. Nat. History Bull.*, v. 144, art. 1, p. 6-13.
- Gates, R. M., 1953, Petrogenic significance of perthite, in Emmons, ed., *Selected petrogenic relationships of plagioclase*: *Geol. Soc. America Mem.* 52.
- Gay, P., and Roy, N. N., 1968, The mineralogy of the potassium-bearing feldspar series, III, Subsolidus relationships: *Mineral. Mag.*, v. 36, no. 283, p. 914-932.
- Gresens, R. L., 1971, Application of hydrolysis equilibria to the genesis of pegmatite and kyanite deposits in northern New Mexico: *Mtn. Geology*, v. 8, no. 1, p. 3-16.
- 1975, Geochronology of Precambrian metamorphic rocks, north-central New Mexico: *Geol. Soc. America Bull.*, v. 86, p. 1444-1448.
- Gresens, R. L., and Stensrud, H. L., 1974a, Recognition of more meta-rhyolite occurrences in northern New Mexico and a possible Precambrian stratigraphy: *Mtn. Geology*, v. 11, p. 109-124.
- 1974b, Geochemistry of muscovite from Precambrian metamorphic rocks of northern New Mexico: *Geol. Soc. America Bull.*, v. 85, p. 1581-1594.
- Hemley, J. J., and Jones, W. R., 1964, Chemical aspects of hydrothermal alteration with emphasis on hydrogen metasomatism: *Econ. Geology*, v. 59, no. 4, p. 538-567.
- Hibbard, M. J., 1965, Origin of some alkali feldspar phenocrysts and their bearing on petrogenesis: *Am. Jour. Sci.*, v. 263, p. 245-261.
- Holdaway, M. J., 1971, Stability of andalusite and the aluminum silicate phase diagram: *Am. Jour. Sci.*, v. 271, p. 97-131.
- 1972, Thermal stability of Al-Fe epidote as a function of f_{O_2} and Fe content: *Contr. Mineral. and Petrology*, v. 37, p. 302-340.
- 1975, Effect of rock and fluid composition on chloritoid-staurolite equilibria, Picuris Range, New Mexico: *Geol. Soc. America Abs. with Programs*, v. 7, no. 7, p. 1119.
- Iiyama, J. T., 1968, Etude experimentale de la distribution d'elements en traces entre deux feldspaths; feldspath potassique et plagioclase coexistants; I. Distribution de Rb, Cs, Sr et Ba a 600°C: *Soc. Fr. Mineral. Cristallogr. Bull.*, v. 91, no. 2, p. 130-140.

- Iiyama, J. T., 1972, Behaviour of trace elements in feldspars under hydrothermal conditions, in MacKenzie, W. S., and Zussman, J., eds., *The feldspars: Proc. of a NATO Adv. Study Inst., Manchester*, v. 11, no. 21, p. 553-573.
- 1973, Etude experimentale de la distributions d'elements en traces entre deux feldspaths coexistants, II. Influence de la temperature sur la distribution de Cs, Rb, Ba et Sr: *Reun. Amer. Sci., Terre. Prog. Resumes*, p. 224.
- Jahns, R. H., 1953, The genesis of pegmatites, I. Occurrence and origin of giant crystals: *Am. Mineralogist*, v. 36, p. 568-598.
- 1954, Pegmatites of southern California: *Calif. Div. Mines Bull.* 170, p. 37-50.
- 1955, The study of pegmatites: *Econ. Geology*, 50th Anniv. Vol., p. 1025-1130.
- 1956, Resurgent boiling and the formation of magmatic pegmatites [abs.]: *Geol. Soc. America Bull.*, v. 67, p. 1772.
- Jahns, R. H., and Burnham, C. W., 1969, Experimental studies of pegmatite genesis, I. A model for the derivation and crystallization of granitic pegmatites: *Econ. Geology*, v. 64, p. 843-864.
- Jahns, R. H., and Ewing, R. C., 1976, The Harding mines, Taos County, New Mexico: *New Mexico Geol. Soc. Guidebook*, Vermejo Park (northeastern New Mexico), in press.
- Just, E., 1937, Geology and economic features of the pegmatites of Taos and Rio Arriba Counties, New Mexico: *New Mexico State Bur. Mines and Miner. Res. Bull.* 13.
- Kerrick, D. M., 1969, K-feldspar megacrysts from porphyritic quartz monzonite, central Sierra Nevada, California: *Am. Mineralogist*, v. 54, p. 839-848.
- Kuryvial, R. J., 1976, Element partitioning in alkali feldspars from three intrusive bodies of the central Wasatch Range, Utah: *Geol. Soc. America Bull.*, v. 87, p. 657-660.
- Leggo, P. J., 1966, A study of potash feldspar gneisses of Connemara and feldspar comparison with the Galway Granite: *Geol. Mag.*, v. 103, no. 6, p. 522-533.
- Long, L. E., 1972, Rb-Sr geochronology of Precambrian schist and pegmatite, La Madera quadrangle, northern New Mexico: *Geol. Soc. America Bull.*, v. 83, no. 11, p. 3425-3431.

- Long, P. E., and Luth, W. C., 1975, Genetic implications of Ba zoning in microcline megacrysts from Precambrian granitic rocks of the Dixon-Penasco area, northern New Mexico: *Geol. Soc. America Abs. with Programs*, v. 7, no. 7, p. 1176.
- Luth, W. C., Jahns, R. H., and Tuttle, O. F., 1964, The granite system at pressures of 4 to 10 kilobars: *Jour. Geophys. Res.*, v. 69, p. 759-773.
- Mall, A. P., and Rudert, V., 1974, Studies in the system $\text{KAlSiO}_4\text{-BaAl}_2\text{Si}_2\text{O}_8\text{-SiO}_2\text{-H}_2\text{O}$: *Contr. Miner. Petrol.*, v. 48, p. 81-88.
- Manley, Kim, 1974, Late Cenozoic history of the Espanola Basin, New Mexico: *Geol. Soc. America Abs. with Programs*, v. 6, no. 3, p. 213.
- Maxon, J. R., 1976, Age and implications of the Tres Piedras Granite, north central New Mexico: *Geol. Soc. America Abs. with Programs*, v. 8, no. 5, p. 608.
- McIntire, W. L., 1963, Trace element partition coefficients--a review of theory and applications to geology: *Geochim. et Cosmochim. Acta*, v. 27, p. 1209-1264.
- Mehnert, K. R., 1969, Petrology of the Precambrian basement complex, in *The earth's crust and upper mantle*: *Am. Geophys. Union Mon. 13* (*Natl. Acad. Sci.-Natl. Res. Council Pub. 1708*), p. 513-518.
- Miller, J. P., Montgomery, A., and Sutherland, P. D., 1963, Geology of part of the Sangre de Cristo Mountains, New Mexico: *New Mexico State Bur. Mines and Miner. Res. Mem. 11*.
- Miyashiro, Akiho, 1973, *Metamorphism and metamorphic belts*: New York, John Wiley and Sons, Inc., 492 p.
- Montgomery, A., 1953, Precambrian geology of the Picuris Range, north-central New Mexico: *New Mexico State Bur. Mines Miner. Res. Bull. 30*.
- Muffler, L. J. P., and White, D. E., 1969, Active metamorphism of upper Cenozoic sediments in the Salton Sea geothermal field and the Salton Trough, southeastern California: *Geol. Soc. America Bull.*, v. 80, p. 157-182.
- Nagasawa, Hiroshi, and Schnetzler, C. C., 1971, Partitioning of rare earth alkali and alkaline earth elements between phenocrysts and acidic igneous magmas: *Geochim. et Cosmochim. Acta*, v. 35, p. 953-968.
- Nemec, D., 1967, Determination of the character of oriented potash feldspar overgrowth on plagioclase crystals in igneous rocks: *Contr. Mineral. Petrol.*, v. 16, p. 149-155.

- Nemec, D., 1975, Barium in K-feldspar megacrysts from granite and syenitic rocks of the Bohemian Massif: *TMPM Tschermarks Min. Petr. Mitt.* 22, p. 109-116.
- Nielsen, K. C., 1972, Structural evolution of the Picuris Mountains, New Mexico: Chapel Hill, N. C., University of North Carolina M.S. thesis.
- Nielsen, K. C., and Dunn, D. E., 1974, Structural evolution of the Picuris Mountains, New Mexico: *Geol. Soc. America Abs. with Programs*, v. 6, no. 5, p. 463.
- Perry, E. A., Jr., 1972, Diagenesis and the validity of the boron paleosalinity technique: *Am. Jour. Sci.*, v. 272, p. 150-160.
- Perry, E. A., Jr., and Hower, J., 1970, Burial diagenesis in Gulf Coast pelitic sediments: *Clays Clay Minerals*, v. 18, p. 165-177.
- Pfann, W. G., 1966, Zone melting: New York, John Wiley and Sons, Inc., 2nd ed., 310 p.
- Phillips, E. R., 1964, Myrmekite and albite in some granites of the New England batholith, New South Wales: *Jour. Geol. Soc. Aust.*, v. 11, p. 49-59.
- 1972, Compositions of granophyre, myrmekite, and graphic granite: discussion: *Geol. Soc. America Bull.*, v. 83, p. 249-250.
- Phillips, E. R., and Stone, I. J., 1974, Reverse zoning between myrmekite and albite in a quartzofeldspathic gneiss from Brsken Hill, New South Wales: *Mineralog. Mag.*, v. 39, p. 654-657.
- Phillips, E. R., Ransom, D. M., and Vernon, R. H., 1972, Myrmekite and muscovite developed by retrograde metamorphism at Broken Hill, New South Wales: *Mineralog. Mag.*, v. 38, no. 297, p. 570-578.
- Philpotts, J. A., and Schnetzler, C. C., 1970, Phenocryst-matrix partition coefficient for K, Rb, Sr and Ba with applications to anorthosite and basalt genesis: *Geochim. et Cosmochim. Acta*, v. 34, p. 307-322.
- Presnall, D. C., and Bateman, P. C., 1973, Fusion relationships in the system $\text{NaAlSi}_3\text{O}_8$ - $\text{CaAl}_2\text{Si}_2\text{O}_8$ - KAlSi_3O_8 - H_2O and generation of granitic magmas in the Sierra Nevada batholith: *Geol. Soc. America Bull.*, v. 84, p. 3181-3202.
- Ragland, P. C., and Butler, J. R., 1972, Crystallization of the West Farrington pluton, North Carolina, U.S.A.: *Jour. Petrology*, v. 13, p. 381-404.
- Ribbe, P. H., 1975, The chemistry, structure, and nomenclature of feldspars, in *Feldspar mineralogy*, v. 2, *Mineralog. Soc. America Short Course Notes*: Blacksburg, Va., Southern Printing Co.

- Robertson, Forbes, 1959, Perthite formed by reorganization of albite from plagioclase during potash feldspar metasomatism: *Am. Mineralogist*, v. 44, p. 603-619.
- Roy, D. M., 1967, Calcium silicate and hydrogarnet formation in the system $\text{CaO-Al}_2\text{O}_3\text{-SiO}_2\text{-H}_2\text{O}$ [abs.]: *Internatl. Mineralog. Assoc. 4th Gen. Mtg.*, New Delhi, 1964, *Papers and Proc.*, p. 234-235.
- Rudert, Volkhart, 1972, Das system $\text{NaAlSi}_3\text{O}_8\text{-BaAl}_2\text{Si}_2\text{O-H}_2\text{O}$ bei 1 Kbar: *Contr. Miner. Petrol.*, v. 35, p. 313-329.
- Schermerhorn, L. J. G., 1961, Orthoclase, microcline and albite in granites: *Schweiz. Mineral. Petrogr. Mitt.*, v. 41, p. 13-36.
- Schwantke, A., 1909, Die Beimischung von Ca im Kalifeldspat und die Myrmekitbildung: *Centralbl. Mineral.*, p. 311-316.
- Sederholm, J. J., 1916, On synatetic minerals and related phenomena (reaction rims, corona minerals, kelyphite, myrmekite, etc.): *Bull. de la Comm. Geolog. de Finlande*, no. 48.
- Shade, J. W., 1968, Hydrolysis equilibria in the system $\text{K}_2\text{O-Al}_2\text{O}_3\text{-SiO}_2\text{-H}_2\text{O}$: State College, Penna., Pennsylvania State University Ph.D. thesis.
- Shmakin, B. M., 1971, The role of pressure in geochemical differentiation of granites and pegmatites: *Trans. from Geokhimlya*, 1971, no. 12, p. 1494-1500, *in Geochem. Internatl.*, v. 8, p. 913-918.
- Simpson, G. G., 1933, Glossary and correlation charts of North American Tertiary mammal-bearing formations: *Am. Mus. Nat. History Bull.*, v. 57, p. 79-121.
- Smith, J. V., and Stenstrom, R. C., 1965, Electron-excited luminescence as a petrologic tool: *Jour. Geology*, v. 73, no. 4, p. 627-635.
- Smith, T. E., 1974, The geochemistry of the granitic rocks of Halifax County, Nova Scotia: *Canada Jour. Earth Sci.*, p. 650-657.
- Spiegel, Z., Baldwin, B., Kottowski, F. E., and Barrows, E. L., 1963, Geology and water resources of the Santa Fe area, New Mexico: *U. S. Geol. Survey Water-Supply Paper 1525*, 258 p.
- Steiner, J. C., Jahns, R. H., and Luth, W. C., 1975, Crystallization of alkali feldspar and quartz in the haplogranite system $\text{NaAlSi}_3\text{O}_8\text{-KAlSi}_3\text{O}_8\text{-SiO}_2\text{-H}_2\text{O}$ at 4 Kb: *Geol. Soc. America Bull.*, v. 86, p. 83-98.
- Storre, B., 1970, Stabilitäts beding ungen Grossular-führen der Paragenesen im System $\text{CaO-Al}_2\text{O}_3\text{-SiO}_2\text{-CO}_2\text{-H}_2\text{O}$ (Stability relations of grossular-bearing paragenesis in the system $\text{CaO-Al}_2\text{O}_3\text{-SiO}_2\text{-CO}_2\text{-H}_2\text{O}$) [abs.]: *Fortschr. Mineral.*, v. 47 (1969), Beiheft 1, p. 68-69.

- Swanson, S. E., 1974, Phase equilibria and crystal growth in granodioritic and related systems with H_2O and $H_2O + CO_2$: Stanford, Calif., Stanford University Ph.D. thesis.
- Tiller, W. A., 1970, The use of phase diagrams in solidification, in Alper, A. M., ed., Phase diagrams in materials science and technology, v. 1: New York, Academic Press, p. 199-244.
- Tiller, W. A., Jackson, K. A., Rutter, J. W., and Chalmers, B., 1953, The redistribution of solute atoms during the solidification of metals: *Acta Metall.*, v. 1, p. 428-437.
- Trzcinski, W. E., Jr., and Kulick, C. G., 1972, Plagioclase and Ba-K phases from Apollo samples 12063 and 14310, in *Lunar Science Conf., 3rd Proc.*: *Geochim. et Cosmochim. Acta Suppl.*, no. 3, v. 1, p. 591-602.
- Turner, F. J., 1968, Metamorphic petrology; mineralogical and field aspects: New York, McGraw-Hill Book Co., 403 p.
- Turner, F. J., and Weiss, L. F., 1963, Structural analysis of metamorphic tectonites: New York, McGraw-Hill Book Co.
- Tuttle, O. F., and Bowen, N. L., 1958, Origin of granite in the light of experimental studies in the system $NaAlSi_3O_8$ - $KAlSi_3O_8$ - SiO_2 - H_2O : *Geol. Soc. America Mem.* 74, 142 p.
- Weaver, C. E., Beck, K. C., and Pollard, C. O., Jr., 1971, Clay water diagenesis during burial: how mud becomes gneiss: *Geol. Soc. America Spec. Paper* 134, 96 p.
- Wedepohl, K. H., 1969, Handbook of geochemistry: New York, Springer-Verlag, 2 v.
- Whitney, J. A., 1972, History of granodioritic and related magma systems: an experimental study: Stanford, Calif., Stanford University Ph.D. thesis.
- 1975, The effects of pressure, temperature and XH_2O on phase assemblage in four synthetic rock compositions: *Jour. Geology*, v. 83, no. 1, p. 1-31.
- Whitney, J. A., Jones, L. M., and Walker, R. L., 1976, Age and origin of the Stone Mountain Granite, Lithonia district, Georgia: *Geol. Soc. America Bull.*, v. 87, p. 1067-1077.
- Winkler, H. G. F., 1974, Petrogenesis of metamorphic rocks: New York, Springer-Verlag, 3rd ed.
- Wright, T. L., 1968, X-ray and optical study of alkali feldspars: II. An X-ray method for determining the composition and structural state from measurement of 2 theta values for three reflections: *Am. Mineralogist*, v. 53, p. 88-104.

APPENDICES

APPENDIX I

Petrographic Descriptions of Selected Samples of Granitic Rocks from the Dixon-Peñasco Area

The following brief petrographic descriptions provide a framework for conceptualizing differences and similarities among the granitic rocks in the Dixon-Peñasco area. Here described are representative samples that reflect the major variations within each of the granitic rock units. Not all samples for which chemical or modal data are available are described here, but all rock types which have been so analyzed are covered in this appendix. Color designations are from the Geological Society of America rock-color chart.

A. Cerro Alto Metadacite

General Comments

The Cerro Alto Metadacite has not been recognized previously as a distinct lithologic unit. Its dark-gray color and fine grain size make it difficult to distinguish from some of the metasedimentary and meta-volcanic rocks that it intrudes. Its contacts with these rocks are sharp, but its occurrence as sills, and possibly as flows, further complicates its positive identification. However, its grain structure is compact relative to that of the metasediments, and it contains small phenocrysts of quartz and/or plagioclase. Thus it can be identified by careful observation in the field.

PL71-53 Metadacite; T. 23 N., R. 11 E., NW¼ sec. 33

Occurs as an intrusive, stocklike body of relatively uniform lithology. It is a light-olive-gray (5 Y 6/1) to greenish-gray (5 GY 6/1), fine- to medium-grained semiporphyrific rock composed of quartz, plagioclase, microcline, biotite, magnetite, muscovite, and accessory minerals epidote and sphene. Relict oblate phenocrysts of quartz up to 4 mm long are set in a groundmass (0.15 mm average grain size) of quartz, plagioclase, microcline, biotite, and magnetite. The quartz phenocrysts consist of 1 mm subgrains. Less obvious are 3 mm relict plagioclase phenocrysts consisting of 0.5 mm subgrains. The groundmass in particular has a very granular aspect in thin section, and 120° triple junctions are common. Muscovite occurs as 0.6 mm poikilitic plates seemingly superimposed on the groundmass, and the biotite occurs as irregular flakes that appear to be interstitial in the groundmass fabric.

PL71-57 Metadacite; T. 23 N., R. 11 E., NE¼ sec. 34

This rock occurs as sill-like bodies in amphibolites and amphibolite schists of the Vadito Group. Marked textural variations, both from one rock body to another and within bodies, characterize this lithology. The rock is medium dark gray (N 4) to dark brownish gray (5 YR 3/1), fine to medium grained, and consists of quartz, plagioclase, microcline, biotite, muscovite, magnetite, and accessory minerals epidote and idocrase(?). The texture is allotriomorphic interlocking granular, with anhedral relict phenocrysts of quartz and large interconnected patchy aggregates of muscovite.

Average grain size is 0.15 mm. The quartz phenocrysts are about 3.5 mm and consist of about six subgrains. The muscovite patches are 1.0 to 0.5 mm, and muscovite also occurs as small anhedral intergranular flakes. Biotite occurs as thin, shabby plates about 0.5 mm long. Microcline can be concentrated in 2 mm or larger patches of smaller subgrains, suggesting the possibility of K-feldspar phenocrysts having been present. Some of the muscovite shows a symplectic intergrowth with quartz and/or feldspar. The orientation of the oblate phenocrysts and the biotite flakes produces a distinct foliation in the rock.

PL72-130 Metadacite; T. 23 N., R. 11 E., NE $\frac{1}{4}$ NE $\frac{1}{4}$ sec. 32

This sample is most typical of the metadacite lithology as a whole. It represents a sill that is satellitic to the main stocklike body of metadacite. The color is a typical medium dark gray (N 4), and weathered surfaces are brownish gray (5 YR 4/1).

The rock consists of quartz, plagioclase, microcline, biotite, muscovite, and epidote, with magnetite and sphene as accessory minerals. The texture is allotriomorphic granular to porphyritic. Subgrained, oblate quartz phenocrysts (2 to 3 mm with 0.5 to 0.1 mm subgrains) and granulose clots of microcline and plagioclase are set in a fine-grained groundmass (0.03 to 0.05 mm) of quartz, plagioclase, microcline, muscovite, and biotite. The groundmass constitutes roughly 75 percent of the rock. The quartz phenocrysts are distinct from the groundmass, but the subgrains of the relict microcline and plagioclase phenocrysts are similar in size to the grains of the groundmass. Rare plagioclase grains are nearly intact; these are subhedral and about 1 to 2 mm in length. Most of the plagioclase shows alteration to muscovite and

epidote, and associated with the plagioclase are randomly oriented subpoikilitic flakes of muscovite that show areas of optical continuity up to 2 mm in diameter. Platelets of muscovite and biotite are scattered throughout the groundmass, but there are crude aggregations of magnetite, biotite, epidote, and muscovite which may be the relicts of glomeroporphyrific clots of mafic minerals in the original magma. Orientation of the oblate phenocrysts and of biotite grains impart a strong foliation to the rock. The interlocking nature of the major minerals, however, means that the rock rarely fractures along the foliation plane.

B. Puntiaquedo Granite Porphyry

General Comments

The Puntiaquedo Granite Porphyry is a high-level granitic (quartz monzonite) intrusive body consisting largely of a single facies that has undergone differing degrees of deformation. In addition, there is a narrow and ill-defined border zone of more leucocratic and finer grained porphyritic rock, and fine-grained, slightly porphyritic dikes commonly are associated with this zone. These three major types of Puntiaquedo Granite Porphyry are included in the following descriptions.

PL71-44 Porphyritic biotite quartz monzonite; T. 23 N., R. 11 E., SE $\frac{1}{4}$ NW $\frac{1}{4}$ sec. 32

This rock consists of subequant, nearly euhedral, 1 cm microcline grains (grayish orange pink, 5 YR 7/2; stained moderate red, 5 R 5/4) and oblate 4 to 6 mm quartz grains (light gray, N 7) in a fine-grained matrix of 0.07 mm quartz, plagioclase, and microcline. The groundmass is a light olive gray (5 Y 6/1) and makes up about 60 percent of the

rock. The large quartz grains are composed of 1.0 to 1.5 mm subgrains. The microcline megacrysts show Carlsbad twinning as well as crosshatch or M-twinning. Some of them are partially granulated, especially near their margins, and they commonly include or partially include large grains of plagioclase (5 to 8 mm). Biotite occurs as large clots (1 to 2 mm) or partly shredded and bent grains (0.5 mm) and as scattered flakes in the matrix. Muscovite is associated with biotite as fresh, randomly oriented plates (≤ 1 mm), and it also appears to have replaced deformed and polygonized grains of plagioclase (5 x 2 mm) in the ground-mass. These polygonized patches are coarser (0.15 mm) than the ground-mass proper and apparently represent plagioclase phenocrysts. Accessory minerals are epidote as granules and stubby crystals replacing plagioclase, allanite as elongate, zoned 0.1 mm crystals, sphene as granules associated with biotite, zircon commonly included in biotite, magnetite as octahedra partly altered to hematite, and chlorite formed from biotite. The rock has a strong but compact foliation.

PL71-41b Leucocratic porphyritic quartz monzonite (border zone);
T. 23 N., R. 11 E., SE $\frac{1}{4}$ SW $\frac{1}{4}$ sec. 30

This sample was collected within 30 cm of the contact with vadito schist. This rock has a semisugary texture, and is grayish orange pink in color (5 YR 7/2). It consists of 2 to 4 mm polygonized quartz grains set in a matrix of quartz (≤ 1 mm) as irregular and semi-interlocking grains, microcline as generally smaller, subequant grains, and plagioclase as interlobate grains (≤ 0.5 mm) that appear to hold the matrix together. Rare clots (1 to 2 mm) of biotite and muscovite are enclosed in the matrix and in corroded and partially replaced relict phenocrysts of plagioclase (≤ 6 mm). Very rarely 3 to 6 mm phenocrysts

of microcline are present. Randomly oriented flakes of muscovite (≤ 0.5 mm) are scattered throughout the matrix. The common accessory minerals are sphene, magnetite-hematite, and epidote. A slight foliation is present, but it is not readily noticed. The outstanding feature of the texture is the odd, interlobate, serrated character of the feldspars.

PL72-127f Porphyritic marginal aplite; T. 23 N., R. 10 E., NW $\frac{1}{4}$ NW $\frac{1}{4}$ sec. 26

This rock occurs as a small dike cutting rocks similar to PL72-44. It is generally very fine grained (≤ 0.1 mm) and pale yellowish brown (10 YR 6/2), with phenocrysts of quartz (1 to 3 mm), microcline (0.5 to 1 mm), plagioclase (0.5 to 2 mm), and rare clots of biotite. The quartz phenocrysts consist of 0.5 mm subgrains and are crudely aligned. The microcline microphenocrysts are tabular and nearly euhedral, whereas the plagioclase microphenocrysts are commonly polygonized and invariably are partially replaced by muscovite, especially in their cores. Their margins appear to have a lower An content (albite-oligoclase) and show little or no alteration to muscovite. The matrix consists of interlobate grains of quartz, microcline, and plagioclase, and scattered through it are irregular flakes of muscovite (≤ 0.3 mm). Some larger grains of muscovite are associated with the grains of altered plagioclase. A definite foliation is present in the rock, but the fine grain size and the scarcity of phenocrysts make it difficult to see.

C. Rana Quartz Monzonite

General Comments

The Rana Quartz Monzonite is divided into three subunits: (1) an unfoliated facies, (2) a foliated facies, and (3) a leucocratic border

zone. Samples from each of these subunits are described here, along with two samples of felsite dikes and three aplite samples from the unfoliated facies. The main mass of the Rana Quartz Monzonite is foliated facies, and the degree of deformation in it tends to increase from northwest to southeast. The samples described here cover most of the range of textures seen in this subunit.

1. Unfoliated Facies

The unfoliated facies is in gradational contact with the foliated facies of the biotite quartz monzonite, but otherwise is fairly uniform. The only exception to this uniformity is in sporadic occurrences of pink to reddish-colored feldspars. In places this reddening is accompanied by epidote veining, but generally its only readily observable mineralogic manifestation is an increased alteration of plagioclase to muscovite and epidote in the reddened feldspars.

PL71-14 Biotite quartz monzonite; T. 22 N., R. 10 E., NW $\frac{1}{4}$ sec. 1

This rock is typically granitic in texture, with subequigranular, interlocking grains of medium-light-gray (N 6) to light-gray (N 7) quartz (≤ 10 mm), tabular to rounded grains of white to very-light-gray (N 9 to N 8) plagioclase (≤ 6 mm), and mostly interstitial anhedral grains of very-light-gray to light-gray (N 8 to N 7) microcline (≤ 9 mm). Scattered throughout the rock are 1 to 7 mm aggregates of black (N 1) to grayish-black (N 2) biotite and magnetite (+ hematite). There are minor spots of dusky-red (5 R 3/4) hematite staining of the feldspars. Under the microscope the quartz-grain aggregates are composed of 1 to 2 mm quartz grains that show some undulatory extinction. Although they are

generally anhedral, the largest single grains are microcline (≤ 7 mm) occurring as Carlsbad-twinned individuals and showing typical crosshatch twining. They commonly are perthitic, contain round quartz blebs or rods and patchy masses of albite, as well as rounded inclusions of albite. Blebs of intergranular albite between adjacent grains of microcline are very common. The subhedral grains of plagioclase (≤ 4 mm) are altered, especially in their calcic cores, to muscovite and fine-grained epidote. They show undulatory normal zoning from An_{22} to An_{15} and in many places, particularly adjacent to microcline, the plagioclase has discrete unaltered rims of albite-oligoclase (An_9 to An_0). Large plates of green-brown biotite (≤ 2 mm) and biotite with magnetite and hematite appear to be interstitial in the fabric of the rock and commonly lie adjacent to or are included by quartz grains. Sphene, allanite, zircon, muscovite, apatite, and epidote are associated with the magnetite and biotite. Muscovite occurs either as fine-grained stubby flakes (≤ 0.5 mm) in plagioclase or as large (2 mm) fresh flakes transecting or infiltrating biotite. The grains of magnetite + hematite (≤ 3 mm) are subhedral to anhedral and nearly equant. They are mostly magnetite, with hematite along grain margins or cleavage fractures as spindly branches extending into the magnetite interiors of the grains. It also occurs as irregular trails of discrete blebs within the interiors of the magnetite grains. Sphene commonly rims the magnetite grains and also forms tiny granules throughout the rock. Epidote occurs as individual grains associated with biotite, as thick rims (≤ 0.4 mm) around tiny allanite grains, or as small granules (0.05 mm) in altered plagioclase. The allanite, rimmed by epidote or otherwise associated with it, occurs as zoned, equant to slightly elongate crystals (≤ 0.3 mm).

Apatite is usually found with biotite, either as inclusions or sandwiched between it and another mineral. The crystals of apatite are sausage-shaped single grains (≤ 0.5 mm). Zircon grains have a similar habit, but they tend to be more elongate and more idiomorphic, characteristically containing one or more tubelike inclusions. A minor amount of chlorite occurs as an alteration product of biotite. Myrmekite commonly forms a cauliflower or wartlike projection into microcline where a plagioclase grain is in contact with the microcline grain. In one place myrmekite appeared to transect an albite lamella in microcline.

In thin section the rock appears as a framework of fresh quartz and microcline that is partly collapsed around the altered plagioclase grains. There is only the slightest hint of foliation. The mutually perpendicular sets of closely spaced fractures seen in sawn slabs and the slight granulation seen in thin section indicate that the rock has undergone some deformation.

2. Foliated Phase

Three samples representing degrees of foliation are described here. PL73-193 is the least foliated and PL72-74 is the most strongly foliated, the foliation increasing from roughly northwest to southeast within the study area. The foliation is best developed near the contact with Peñasco Quartz Monzonite about 1.25 mi north-northwest of Trampas.

PL72-193 Foliated biotite quartz monzonite; T. 22 N., R. 11 E., NW $\frac{1}{4}$ NW $\frac{1}{4}$ sec. 5

This rock is similar in many ways to PL71-1 except for its much greater degree of foliation and granulation. This is evidenced by

a crude by distinctly planar alignment of biotite clots, and by the granulation of feldspars, especially plagioclase. Some orientation of oblate quartz-grain aggregates yields a slight lineation as well as a flattening. Thus the rock fabric is an inequigranular network of translucent light-gray (N 6) quartz aggregates (≤ 12 mm), granulose masses of white (N 9) to very-light-gray (N 8) plagioclase (≤ 5 to 9 mm), and anhedral, broken-appearing grains of pale-red (5 R 6/2) to moderate-red (5 R 4/6) microcline (≤ 7 mm). The black (N 1) clots of biotite and magnetite (+ hematite) show a slight tendency to be grouped in 3 to 4 cm patches. The subparallel orientation of the clots is apparent, as is the orientation of individual biotite grains within each clot. Microscopically, the quartz aggregates consist of 0.3 to 0.5 mm grains with strong undulatory extinction giving each grain a shattered appearance as the stage is rotated. The microcline occurs as fairly large (> 5 mm) grains and as 0.4 mm grains generally in aggregates associated with the larger grains. Most of the larger grains do show some granulation around grain margins but rarely the granular polygonized portions are entirely surrounded by intact microcline. Flame and film microperthite are common, as are patchy areas of albite, rounded inclusions of albite, and blebs of quartz. Crosshatch twinning is ubiquitous in the microcline, but only a few of the larger grains show Carlsbad twinning. Nearly all of the plagioclase has the form of altered aggregates of 0.5 to 0.1 mm grains with composition An_{11} to An_4 . No primary zoning is apparent in thin section, and all of the grains are dusted with epidote and muscovite. The only unaltered plagioclase occurs as perthite, and as rims on the altered grains adjacent to microcline. Biotite, muscovite, magnetite + hematite, and the accessory minerals sphene,

allanite, epidote, zircon, and apatite occur as in PL71-14 except that the mafic clots appear to be less intact. The biotite has an especially shredded appearance. Sphene is less commonly associated with the magnetite grains. The plagioclase of myrmekite is typically altered, and its wartlike projections into microcline stem from adjacent plagioclase grains.

PL73-227 Foliated biotite quartz monzonite; 0.5 mi northwest of Vallecitos on Rio de las Trampas

This rock is thoroughly deformed but it has no distinct foliation plane. Instead it is actually lineated, with the constituent minerals strung out primarily in one dimension. It is mineralogically similar to PL71-14, consisting of semitransparent grains (<5 mm) of light-gray (N 6) quartz, granulated aggregates of white (N 9) to very-light-gray (N 8) plagioclase (<10 mm), and fractured grains (4 mm) of pinkish-gray (5 YR 8/1) microcline. Clots of black (N 1) biotite (1 to 3 mm) appear to be intertwined throughout the fabric of the rock on surfaces perpendicular to the direction of lineation, but they resemble streaks or pods of pepper on surfaces subparallel to the lineation. In thin section the rock has a hypidiomorphic granular texture that is interrupted only by stubby laths of green-brown biotite and crisp, crosscutting flakes of muscovite. The texture is moderately inequigranular with the microcline and quartz having slightly larger grain size than the more polygonized plagioclase. The quartz grains show moderate undulatory extinction and consist of three or four subgrains (0.5 to 2.0 mm). Microcline occurs as 0.3 to 3.0 mm grains exhibiting crosshatch twinning and rarely Carlsbad twinning. They are typically perthitic and contain rounded inclusions of plagioclase. The plagioclase occurs as disoriented

groups of anhedral grains (≤ 1.5 mm) that show polysynthetic twinning and a sporadic alteration to epidote and muscovite. Some of the grains are zoned in continuous normal fashion from An_{25} to An_{20} . The biotite flakes (1 mm) are arranged in discontinuous trains and are associated with minerals such as muscovite, epidote, magnetite (+ hematite), allanite, zircon, and apatite. The muscovite grains generally crosscut biotite or appear to have replaced that mineral. In some places the muscovite shows symplectic intergrowths (≤ 2 mm) with quartz. The opaque grains are mostly magnetite with hematite associated in a manner identical to that of PL71-14. The epidote that is part of the biotite trains is generally found rimming small (≤ 0.3 mm) allanite grains. Commonly both the allanite grain and its epidote rim are included between two biotite grains. Both apatite and zircon are commonly included in biotite or muscovite, and occur as stubby rounded prisms ≤ 0.5 mm in maximum dimension, with the zircon tending to be more elongate and idiomorphic. In one instance a zircon grain appeared to be zoned.

PL72-74 Gneissic biotite quartz monzonite; about 1.3 mi north-northwest of Trampas, New Mexico

This rock has a well-foliated gneissic texture expressed by an alternation of crude, undulatory biotite layers with irregular lenses and layers of granulose quartz and feldspar. In addition to its concentration in pods and layers, the biotite is scattered throughout the rock. The biotite flakes are black (N 1) and about 1 mm in size. Translucent granules (≤ 1 mm) of medium-gray (N 5) quartz are found in pods up to 6 mm thick and no longer than about 1.5 cm. Plagioclase (very light gray, N 8) and microcline (pinkish gray, 5 YR 8/1) occur in pods and layers that are more flattened and elongate than the quartz

pods. The foliation is crude because of the discontinuous nature of the pods and the general admixture of the minerals between the more monominerallic pods. In thin section the rock has a foliated and seriate allotriomorphic granular texture. Microcline has the largest grain size followed closely in size by quartz. Plagioclase is distinctly smaller and more granulose. The microcline occurs as anhedral grains (≤ 5 mm) showing crosshatch twinning and rarely a crude Carlsbad twinning. Some of the crosshatch twinning is deformed, and the larger grains tend to have their c-axis lying close to the trace of the foliation plane. The quartz occurs as allotriomorphic odd-shaped grains that are crackled and commonly have their longest apparent dimension (1 mm maximum) parallel to the foliation plane. Undulatory extinction is present but it is not particularly strong. The plagioclase grains (≤ 0.5 mm) are anhedral, commonly altered, and showing uniform continuous normal zoning from An_{20} to An_{25} . Some of the grains show polysynthetic twinning. Biotite occurs as pods and trains of anastomatizing strongly oriented flakes most of which have the appearance of being well recrystallized (fresh looking) while others appear shredded. An assortment of minerals is associated with biotite: muscovite as crisp, clear flakes replacing biotite; magnetite-hematite grains as irregular octahedra; sphene as anhedral 0.5 mm granules associated with the magnetite; epidote as thick rims to tiny allanite grains; apatite as clear anhedral stubby grains; and zircon as euhedral to anhedral prisms with tube-shaped fluid(?) inclusions. Muscovite and epidote also occur as fine-grained alteration products of plagioclase.

3. Border Zone

The border zone of the Rana Quartz Monzonite consists of leucocratic, porphyritic rocks which grade into the foliated phase. It is thus difficult in describing a small number of samples, to cover the large degree of variability that occurs from one outcrop to another. The samples described here, however, will give the reader some idea of the main differences among the border zone rocks.

PL72-206 Leucocratic foliated porphyritic quartz monzonite; T. 23 N., R. 11 E., SE $\frac{1}{4}$ sec. 33

This rock has an overall grayish-orange-pink color (5 YR 7/2) that is punctuated by medium translucent gray (N 5) quartz phenocrysts. The rock also contains phenocrysts of microcline but these are barely distinguished from the groundmass in that they have very nearly the same color. Flakes and groups of flakes of muscovite are visible as are rare biotite flakes. In thin section the rock consists of 2 to 5 mm subhedra of crosshatched microcline, irregular-shaped quartz grains (1 to 3 mm) set in finer grained plagioclase, quartz, muscovite, and microcline (≤ 1 mm). Accessory minerals are magnetite, hematite, and garnet. The quartz shows undulatory extinction. The microcline is partly Carlsbad twinned whereas the plagioclase shows polysynthetic albite twinning and is in some places partially replaced by microcline as shows continuous normal zoning. It also shows a moderate degree of alteration by very fine-grained muscovite, and possibly epidote and/or kaolinite. Muscovite mainly occurs as remarkably clear plates that form strings and patches in the groundmass. They show a moderate degree of alignment that reflects the foliation that is only weakly expressed in hand specimen.

PL73-267 Foliated, porphyritic muscovite quartz monzonite; T. 23 N., R. 11 E., NW $\frac{1}{4}$ sec. 32

A foliated leucocratic rock with oblate rounded quartz grains (2 to 10 mm) and flattened muscovite masses (≤ 4 mm) in a fine-grained matrix of feldspar, muscovite, and quartz (average grain size 0.2 mm or less). The muscovite is brownish gray to light olive gray (5 YR 4/1 to 5 Y 6/1) and the oblate quartz grains are light bluish gray (5 B 7/1) with narrow rims of transparent granular quartz. The matrix is pinkish to yellowish gray (5 YR 8/1 to 5 Y 8/1). In thin section the oblate quartz grains are seen to consist of numerous subgrains (≤ 1.5 mm) which are themselves oblate and which commonly show very serrated contacts with each other. High magnification reveals that the bluish portion of the grains contains minute rutile needles which are absent in the granular, clear grains rimming the bluish portion. Muscovite flakes (≤ 0.5 mm) show a strong preferential orientation and occur in discontinuous patches and stringers that make up the main fabric of the rock. Irregular grains (≤ 1 mm) of plagioclase in the matrix show preferential alteration by the muscovite and some of them have albitic rims. Microcline occurs as very small grains (≤ 0.25 mm) in the matrix. Accessory minerals are epidote, allanite, schorl, and magnetite (+ hematite?), and biotite. Epidote forms thick overgrowths on very tiny reddish allanite grains, schorl occurs as small prisms in the plane of foliation, and magnetite as oxidized octahedra. Biotite is extremely rare and has very weak pleochroism. The rock has an especially strong and well-defined foliation.

PL72-131 Foliated quartz muscovite porphyry; T. 23 N., R. 11 E.,
NE $\frac{1}{4}$ NE $\frac{1}{4}$ sec. 32

This rock consists largely (90 to 95 percent) of a fine-grained (≤ 0.5 mm) grayish-orange-pink (10 R 8/2) matrix of quartz, muscovite, plagioclase, and microcline. This matrix contains typical ovoid light-gray (N 7) quartz phenocrysts (≤ 8 mm) as well as clots of greenish-gray (5 GY 6/1) muscovite (≤ 3 mm), rare oxidized octahedra of magnetite (1 mm), and occasional grains of schorl (1 mm, black N 1). In thin section the matrix has an interlocking allotriomorphic granular texture with the quartz grains appearing much like pieces of a jigsaw puzzle. The microcline in the groundmass appears not to be microperthitic and occurs as 0.25 mm anhedral grains. Plagioclase occurs in the matrix as altered anhedral grains (≤ 0.3 mm) and as larger (0.8 mm) grains or grain aggregates showing alteration by muscovite and epidote. Muscovite occurs as 1 mm flakes scattered throughout the matrix, as minute flakes altering plagioclase and as aggregates or pods of muscovite grains. No preferential alignment of the pods or individual flakes is obvious in thin section, but such an alignment occurs locally in hand specimen and in outcrop. The quartz phenocrysts are composed of subgrains (≤ 1.5 mm) which show undulatory extinction and which have a tendency to have serrated edges where they are in contact with a neighboring quartz grain. The accessory minerals are allanite, epidote, zircon, and hematite (after magnetite). Allanite grains are dark brown, ≤ 0.1 mm and usually rimmed with epidote. The occurrence is similar to other Rana rocks except that the allanite grains are less well formed and somewhat darker colored. Epidote grains typically rim allanite but also are associated with plagioclase as an alteration product and form

single grains or aggregates of grains in association with muscovite. Zircon occurs as single, euhedral prismatic grains about 0.15 mm in maximum dimension and typically contains tubelike inclusions. The hematite is at least in part a weathering product of magnetite.

PL73-241 Muscovite-biotite quartz porphyry; T. 23 N., R. 11 E., SW $\frac{1}{4}$ NE $\frac{1}{4}$ sec. 32

Light- to medium-gray (N 7, N 6) oblate fractured quartz grains are set in a matrix of microcline, plagioclase, and quartz with clots of muscovite + biotite. The matrix is very light-gray (N 8) to pinkish gray (5 YR 8/1) and shows considerable differences in concentration of microcline and quartz. In thin section the rock is seen to have a very fuzzy texture. The groundmass is partly replaced with both fine-grained muscovite and semicontinuous poikilitic plates of muscovite (≤ 2 mm). The relict quartz phenocrysts (≤ 8 mm) consist of subgrains (≤ 0.5 mm) which show undulatory extinction but which have fairly regular (i.e. not serrated) margins with neighboring grains. Some of the phenocrysts show clear or iron-stained granules of quartz as margins to light-gray cores. Rarely, plagioclase occurs as 5 mm altered phenocrysts. Aside from its much greater degree of alteration by muscovite, the matrix is similar to that of PL72-131. Epidote also is much more abundant and typically occurs as tiny granules in patches associated with biotite. The biotite occurs as ragged 0.5 mm brown flakes which are commonly grouped in stringers or pods. Accessory minerals are allanite, zircon, and magnetite (+ hematite?). Allanite and zircon are especially rare but occur as in PL72-131.

D. Aplites

General Comments

Aplites in the Rana Quartz Monzonite are reasonably common and occur as irregular dikes ranging in thickness from about 3 cm to nearly 50 cm. They are usually either white or pink in color and sometimes contain small amounts of biotite and are somewhat porphyritic. The aplite dikes are older than pegmatites in the Rana Quartz Monzonite, a fact that is demonstrated by consistent crosscutting relationships. The following sample descriptions give the range of textures and mineralogy seen in the Rana aplites. Aplites associated with the Rana Quartz Monzonite seem to occur only within Rana Quartz Monzonite itself and not in any surrounding rocks.

PL73-233 Pink aplite; T. 22 N., R. 10 E., SW $\frac{1}{4}$ NE $\frac{1}{4}$ sec. 1

This rock has a typical aplite texture, i.e. fine grained, sugary, and a pale-red color (5 R 6/2) that is offset by local cone-shaped splays of dendritic schorl (grayish black, N 2). These schorl masses typically measure 20 x 40 mm and are composed of 1 mm and smaller sized schorl grains that are interspersed with quartz grains of a similar size. In thin section the grain size of the nontourmaline-bearing portion of the rock averages about 0.5 to 0.6 mm and has fairly regular sub-equigranular texture with microcline tending to be slightly larger in grain size than the other minerals and quartz showing undulatory extinction and tending to be inequigranular and irregularly shaped. The microcline shows crosshatch twinning but is not strongly microperthitic. Plagioclase is primarily intergranular and is altered by dusty appearing

muscovite and possibly epidote and kaolinite(?). Muscovite occurs throughout the rock as anhedral flakes generally smaller in size than the other minerals and, like the plagioclase, appears to occupy interstitial areas in the fabric of the rock. Where schorl occurs it is optically continuous over regions of about 10 x 5 mm or more and forms granular anhedral fractured grains. Microcline and plagioclase occur interstitially to the schorl but quartz is more abundant than in the surrounding untourmalinized aplite. Accessory minerals are very rare magnetite and euhedral to subhedral epidote.

PL73-232crs Subporphyritic biotite aplite; T. 22 N., R. 10 E., SW $\frac{1}{4}$ SW $\frac{1}{4}$ sec. 6

PL73-232crs and PL73-232fn are rock types from the same dike. They occur in a subparallel configuration each occupying about half of the dike thickness at the point the sample was taken but the fine-grained type generally is most abundant.

Pale-yellowish-brown (10 YR 6/4) to light-brownish-gray (5 YR 6/1) perthitic equant microcline phenocrysts (3 to 10 mm) and sparse medium-gray rounded quartz phenocrysts (3 to 5 mm) are set in a sheared, medium-grained (1.5 to 0.2 mm), aplitic textured groundmass that also contains scattered and somewhat aligned clots of biotite (3 to 6 mm), muscovite, and magnetite. Plagioclase (white, N 9) occurs in the groundmass and as irregular aggregates of granules (3 to 6 mm) distinct from the groundmass. There are also rare intact phenocrysts of plagioclase (≤ 2 mm). In thin section the microcline phenocrysts show crosshatch twinning and have irregular Carlsbad twins as well. They contain numerous inclusions of plagioclase which commonly have fairly thick rims of generally lower An content which are themselves zoned from

An₂ to An₁. The cores of most of the inclusions (An₁₆) show muscovite-epidote alteration. Perthite stringers are common in the large microclines and in some places altered plagioclase phenocrysts are partially included. Quartz shows undulatory extinction and the larger quartz phenocrysts are typically composed of three or four subgrains. Quartz grains are rounded to lobate and their grain size ranges continuously from 4 mm to less than 0.1 mm. Some of the quartz is slightly smokey and it definitely lacks abundant rutile needles seen in quartz from the Rana Quartz Monzonite itself. Plagioclase occurs mainly as polygonized crystal aggregates (0.5 mm) of roughly rectangular outlines that are typically altered by muscovite and epidote. The size, shape, and lack of quartz or microcline between the grains suggests that they are relict phenocrysts. Plagioclase also occurs as altered irregular, intergranular grains in the groundmass, and these grains commonly show clear albitic rims against microcline. Muscovite occurs as 1 mm scattered anhedral flakes and as a fine-grained alteration product of plagioclase, which generally is more abundant in the more An-rich cores. Biotite occurs as shabby green-brown flakes that are found in clots with associated muscovite. Accessory minerals are oxidized magnetite octahedra and epidote, and a very minor amount of zircon, allanite, and schorl. Much of the epidote is an alteration product of plagioclase but it also occurs associated with biotite clots.

PL73-232fn

The finer grained portion of this two-part dike is light yellowish gray in overall color (5 Y 8/2) and has a more uniformly fine grain size (0.8 mm) than PL73-232crs. Phenocrysts are present but they are much

less abundant and fairly small (≤ 3 mm) relative to the coarse portion of the dike. The quartz phenocrysts are composed of several disoriented and irregular subgrains, while the plagioclase phenocrysts are either intact (but altered by epidote and muscovite) or severely polygonized. The smaller plagioclase phenocrysts appear to have more commonly escaped deformation. The microcline phenocrysts occur as in the coarse sample except for smaller size. Biotite occurs as large flakes (3 mm) that are associated with the quartz phenocrysts--usually in contact with or partially included in them. The biotite contains numerous inclusions of apatite, magnetite, and has some allanite and epidote associated with it. The groundmass is virtually the same as the coarser portion of the dike except of course for the finer grain size. In terms of texture and occurrence of the minerals, the finer grained facies is a scaled-down version of the coarser grained facies. The proportions of minerals, however, are different as can be seen by comparing modes (Appendix II).

E. Felsite Dikes

General Comments

The felsite dikes are apparently discrete tabular bodies that are most common in the amphibolite country rocks but they also occur in the schists of the Vadito Group. They consist of leucocratic, fine-grained rocks making it difficult to ascertain their relationship to the Rana Quartz Monzonite, but they are either older or the same age as that unit. It is also possible that they may be of more than one age, but for the most part they probably represent the initial phase

of Rana magmatism. They are difficult to characterize in that in detail they show large contrasts in texture. It is thus impossible even in describing several samples to fully cover the lithologic differences observed in the field.

PL72-140 Felsite; T. 23 N., R. 11 E., NE $\frac{1}{4}$ NE $\frac{1}{4}$ sec. 32

This sample is from a dike which appears to be a direct extension of the Rana border zone. It is a light-pinkish-gray (5 YR 9/1), fine-grained rock which typically shows veinlets of quartz (5.0 to 0.5 mm) crosscutting each other. Tiny schorl crystals occur in stringers and in hand specimen quartz phenocrysts are barely visible. In thin section phenocrysts are sheared and altered making their positive identification difficult. Texturally the rock is fine grained (≤ 0.25 mm) and consists of anhedral partially flattened grains of quartz and plagioclase. The quartz grains commonly have polygonal outlines whereas the plagioclase seems to occupy the interstices of the rock. Both quartz and plagioclase are slightly concentrated in certain parts of the rock, creating a slightly banded texture. The parts where plagioclase is most concentrated possibly are relict phenocrysts in that they have subrectangular outlines. The granular texture of the rock is offset by the presence of scattered semipoikilitic muscovite grains (≤ 2 mm). Muscovite also occurs as smaller interstitial grains and as tiny flakes altering plagioclase and makes up 5 to 15 percent of the rock. Epidote and biotite are common; the epidote occurring as tiny granules generally in plagioclase and rarely as 2 mm anhedral grains. Biotite is a reddish-brown color and forms 0.1 mm sized irregular flakes. There are minor amounts of sphene and magnetite (+ hematite?).

PL73-216 Biotite felsite; T. 23 N., R. 11 E. NE $\frac{1}{4}$ sec. 28

This sample is a foliated yellowish-gray (5 Y 3/1) rock that contains thin, discontinuous stringers of biotite (0.5 mm x 1 cm), and rounded, iron-stained quartz phenocrysts (≤ 2 mm), as well as similar sized aggregates of fine-grained plagioclase that are relict phenocrysts. In thin section the quartz grains are seen to consist of 0.3 mm polygonized subgrains. They are generally oblate and are aligned subparallel to stringers of biotite and muscovite which are responsible for the marked foliation in the rock. The groundmass of the rock is finer grained quartz and plagioclase (≤ 0.05 mm) which have a very granular and polygonized appearance. The biotite stringers are typically composed of 0.3 mm flakes of brown biotite which have a strong orientation parallel to the plane of foliation but a number of the biotite grains violate this preferred orientation. Muscovite occurs in stringers similar to the biotite but it also occurs in association with biotite as larger flakes and as scattered anhedral grains commonly associated with plagioclase. Plagioclase is found in the groundmass as anhedral interstitial grains and as rare, altered subhedral phenocrysts (≤ 1 mm) showing polysynthetic albite twinning and moderate continuous normal zoning. Accessory minerals, all associated with biotite, are magnetite (+ hematite), sphene, epidote, and zircon.

PL72-157 Porphyritic felsite; T. 23 N., R. 11 E., NE $\frac{1}{4}$ SE $\frac{1}{4}$ sec. 31

This rock is grayish pink (5 R 8/2) and very fine grained except for 4 mm phenocrysts of quartz and plagioclase. It contains very fine veinlets of quartz and/or muscovite that cross through the rock at odd angles and tiny, flat, dark-yellowish-brown (10 YR 6/2) to olive-gray

(5 Y 3/2) flecks scattered throughout the groundmass. In thin section the porphyritic nature of the rock is even more pronounced. The large quartz grains are seen to consist of 0.2 to 2 mm sized irregular shaped subgrains which show strong undulatory extinction and serrated boundaries with neighboring subgrains. The quartz phenocrysts tend to be of two sizes (2 to 4 mm or 0.5 mm) and the groundmass grains are about 0.05 mm or smaller. Plagioclase on the other hand, occurs as phenocrysts which tend to have a more seriate grain size distribution from about 4 mm down to about 0.5 mm. They are nearly euhedral and have irregular polysynthetic albite twinning and show normal continuous zoning. Relatively rare subhedral to anhedral phenocrysts of microcline are generally less than 0.5 mm and exhibit very fine crosshatch twinning. Muscovite occurs both as 2 mm flakes that are thinly scattered through the rock, and as the main constituent of the crosscutting veinlets. Chlorite, apparently after biotite, is commonly associated with the larger muscovite flakes. Rare biotite (brownish colored), magnetite (+ hematite), epidote, and zircon are associated with muscovite and chlorite as part of relict glomeroporphyritic clots. Allanite occurs with some of the epidote, and in one instance, as a core to an epidote crystal. The zircons typically show tubelike fluid(?) inclusions. The groundmass of the rock is an intimate mixture of polygonal grains of quartz, plagioclase, and minor microcline.

F. Peñasco Quartz Monzonite

General Comments

The Penasco Quartz Monzonite is the youngest major granitic rock unit in the Dixon-Penasco area. Unlike the Puntiaquedo Granite Porphyry

and the Rana Quartz Monzonite it lacks a distinctive border zone, but it does show differences in modal mineralogy that can be attributed to some form of differentiation. However, these differences are continuous for the most part and the exposures of the unit are not always good, hence it was impractical to map separate subunits. The most distinctive subtype is a medium- to coarse-grained biotite quartz monzonite which contains microcline megacrysts, and it generally has a gradational relationship with surrounding quartz monzonite and occurs in sporadic, rather small localized areas. This mode of occurrence created further difficulties in mapping internal contacts in the unit. In general, though, the less mafic rocks with more megacrysts tend to occur in the most southerly and easterly outcrops of the unit while the more mafic rocks with less megacrysts are found along the northwesterly margin of the body where it is in contact with amphibolite. Four examples of the unit itself and one example of an aplite from the unit are described here.

PL72-92 Biotite granodiorite; about 1.25 mi north-northwest of Trampas on the upper reaches of Cañada del Agua

This sample was collected adjacent to a large inclusion of Rana Quartz Monzonite. It has an overall equigranular granitic texture with a slight hint of foliation of the 1 to 2 mm sized biotite grains. Rounded to tabular light-gray (N 7) plagioclase grains (≤ 0.5 mm) are irregularly distributed in a very slightly finer grained matrix of medium-gray (N 5) quartz, microcline, light-gray (N 7) and black (N 1) biotite, as well as finer plagioclase grains. The microcline crystals are generally blocky, although not euhedral, and are less than 4 mm in size. The quartz occurs as irregular shaped aggregates of grains,

slightly elongate and up to 6 mm long. The biotite occurs both as subequant aggregates of grains and as apparently interstitial flakes. Wedges of accessory sphene (0.5 mm) are visible in hand specimen. In thin section, the subhedral blocky plagioclases show fine polysynthetic albite twinning and continuous normal zoning from An_{26} to An_{19} . The crosshatch twinned microcline grains are distinctly anhedral as are the quartz grain aggregates. Albite ($\approx An_{2-3}$) rims and myrmekite are common where microcline and plagioclase are in contact, but this sample lacks the pervasive alteration of the plagioclase that is typical of the Puntigudo Granite Porphyry and the Rana Quartz Monzonite. Rarely, twin lamellae in the plagioclases are bent. The microcline typically contains altered inclusions of plagioclase with clear, unaltered rims. The biotite occurs as aggregates of tapered flakes that are pleochroic in shades of green to light yellow green and have associated sphene, magnetite (+ hematite), allanite, epidote, zircon, and apatite. The magnetite occurs as generally subrounded to angular, subequant grains that commonly are in groups associated with biotite. Hematite occurs as branching, dendritelike forms which appear to be invading the magnetite crystal from the outside margins. The hematite is much less common in the interior of the crystals than along the margins, and the exterior portions of the magnetite crystals are in many places completely replaced by hematite. The sphene occurs as wedges which are typically altered to anatase. Epidote is usually found as irregularly shaped, 0.5 mm crystals that commonly include allanite, or apatite, or both, and are very closely associated with biotite. Allanite occurs as cores or inclusions in epidote and as individual elongate crystals up to 1 mm long. These individual allanite grains generally have some

epidote associated with them though not consistently as epitaxial overgrowths. Apatite forms elongate but rounded prisms (≤ 0.3 mm) which are commonly included in biotite. Zircon is typically found as 0.1 mm stubby prisms associated with sphene and/or biotite.

PL72-231 Biotite quartz monzonite; T. 23 N., R. 11 E., S $\frac{1}{2}$ sec. 27

This is a medium- to coarse-grained granitic textured rock with a slight foliation and a granular character, and a marked contrast in grain size even within a single hand specimen. Large (≤ 9 mm), subhedral tabular, but fractured grains of microcline, light brownish gray (5 YR 6/1) are scattered among clots of black (N 1) biotite, large (12 mm) fractured anhedral grains of plagioclase medium light gray (N 6), clots of granulated plagioclase, light gray (N 7), and 2 to 6 mm sized grains of medium-dark-gray (N 4) transparent quartz. Millimeter sized wedges of sphene partially altered to anatase are clearly visible in hand specimen (grayish red, 5 R 4/2, to very dusky red, 10 R 2/2). In thin section the quartz occurs as aggregates of subgrains (≤ 1 mm) that show strong undulatory extinction. The microcline is crosshatch twinned and shows considerable granulation especially around the margins of the subhedral grains. Warts of myrmekite project into the edges of some of the grains and there is commonly a relict Carlsbad twin plane in some of the larger grains. Plagioclase shows fine polysynthetic albite twinning and slightly undulatory normal continuous zoning. Much of the plagioclase, however, consists of irregular anhedral grains that appear to be the product of granulation. In such areas, microcline is granulated as well and commonly one mineral appears to be replacing the other. There is a minor amount of replacement of plagioclase by

very fine muscovite and/or epidote. Biotite occurs as large (≤ 3 mm) flakes that are commonly bent and in many places they have a shredded appearance. The mafic assemblage is generally similar to that of PL72-92. The biotite has associated with it magnetite + hematite in 0.5 mm sized granules. Sphene has a typical wedge shape and some wedges show polysynthetic twinning. Epidote occurs as tabular euhedral crystals commonly enclosed in biotite and rarely as rims to tiny allanite crystals. Apatite occurs as typical sausage-shaped rounded prisms.

PL71-5 Porphyritic biotite quartz monzonite; T. 23 N., R. 12 E., NE $\frac{1}{4}$ SW $\frac{1}{4}$ sec. 31

In this sample large tabular megacrysts of microcline are set in a matrix of plagioclase, quartz, and biotite. Accessory altered sphene is visible in hand specimen. The microcline megacrysts are grayish orange pink (10 R 8/2) to light brownish gray (5 YR 6/1), and are up to 2.5 x 9 cm. They are perthitic and contain inclusions (≤ 1 mm) of plagioclase, some of which are oriented subparallel to ghost crystal faces. The megacrysts themselves show a strong subparallel orientation. The matrix in contrast, shows only a moderate amount of foliation primarily expressed as a very crude orientation of the biotite flakes and as subparallel fractures in the quartz grains. Plagioclase occurs as large (5 to 10 mm) aggregates of anhedral grains (very light gray, N 8) interspersed with nearly transparent fractured grains of quartz (blocky, 2 to 8 mm) with sporadic brownish stain. Very slightly oriented, black (N 1) biotite occurs as irregular 3 mm sized grain aggregates with associated grayish black magnetite octahedra and wedges of sphene (altered to anatase, yellowish gray 5 Y 8/1) both about 0.5 to 1.0 mm in size. In thin section the microcline shows typical crosshatch

twinning, commonly includes rather large plagioclase grains (2 to 4 mm), and commonly shows granulation near the margins of some of the grains, and in some places in the interior of the larger grains. Irregular perthitic lamellae are common. Plagioclase is usually anhedral to subhedral except where it is included in microcline, and it typically shows a moderate amount of alteration by muscovite and epidote. The quartz has strongly undulatory extinction that appears unrelated to any obvious fractures but the differences in extinction angles are so great that it appears as though the grains are in the incipient stages of being broken into subgrains. Biotite is pleochroic in shades of green, brown, and straw yellow and commonly shows bent cleavage planes. Associated opaque grains are similar in occurrence to those in the Rana Quartz Monzonite, the bulk of the grain consisting of magnetite with oxidation to hematite occurring at grain rims and branching out from cleavage planes. The less altered sphene wedges show polysynthetic twinning and zoning. Allanite occurs as large (2 mm) honey-brown prisms commonly with narrow rims of epidote. Epidote also occurs as separate grains associated with biotite, as does apatite which ordinarily occurs as rounded grains included in biotite. There are also minor amounts of muscovite (apparently replacing biotite), and rare subhedral prisms of zircon.

PL72-96 Porphyritic biotite quartz monzonite; approximately 0.25 mi west of Trampas, just north of Highway 76 at east end of large roadcut

This sample was taken from a 1 to 2 m thick dike of Peñasco Quartz Monzonite in foliated Puntagudo Granite Porphyry. Of all the Peñasco Quartz Monzonite, it has the greatest difference in grain size between

megacrysts and matrix. The megacrysts are up to and occasionally in excess of 8 cm in maximum dimension. Typical aspect ratios are 1:0.8:0.3. The concentration of megacrysts is not constant even in a single outcrop. They very commonly show subparallel alignment. In the case of this sample the alignment is subparallel to the walls of the dike. These megacrysts are very similar internally to those in PL71-5, being perthitic and showing well-developed alignment of plagioclase inclusions that define ghost crystal faces. Biotite and rarely hematite also occur as inclusions. The megacrysts are pale red (10 R 6/2) to grayish orange pink (5 YR 7/2) to light brownish gray (5 YR 6/1), and are set in a matrix that is a granodiorite consisting of 2 to 5 mm subhedral plagioclase grains (yellowish gray, 5 Y 8/1), medium-gray (N 5) 2 to 4 mm subtransparent anhedral quartz, and 2 to 5 mm subhedral to euhedral microcline grains (same color as megacrysts). The mafic mineral is grayish-black biotite (N 2) that occurs as 2 to 10 mm clots of 1 mm sized grains that show a crude orientation roughly orthogonal to the orientation of the megacrysts. In thin section the plagioclase shows polysynthetic twinning on both the albite and pericline(?) laws, and is zoned from An_{26} to An_{18} . The zoning is continuous and generally normal although some undulatory reverse zoning is observed. Some of the apparent reversed zoning is due to synusis between two plagioclase cores. Quartz shows undulatory extinction and the microcline has crosshatch twinning. Alteration of plagioclase, while not ubiquitous, is fairly common and is in places concentrated in the more calcic cores of the plagioclase grains. The alteration is for the most part very fine grained, finer than that found in the plagioclase of the Rana Quartz Monzonite, making positive identification of the minerals

difficult. However, epidote and muscovite can be identified in some of the more coarse-grained alteration areas. The biotite is a green-brown color in thin section, shows bent cleavage, and in general has a shraty appearance--commonly showing ragged edges and in places being crosscut by muscovite. Associated with the biotite are the typical assemblage of mafic minerals: magnetite (+ hematite), sphene, epidote, apatite, and zircon. The bulk of the opaque grains are magnetite with the hematite occurring as oblate blebs within the magnetite and as dendritelike incursions into the magnetite from the rim of the grains and from cracks within the interiors of the grains. Typically there will be in a thin section grains which show different stages of what is apparently an oxidation process; i.e. grains will have contrasting proportions of hematite and magnetite. Sphene is abundant and occurs in its usual wedge-shaped form and is commonly altered to anatase. Epidote occurs as subhedral grains sandwiched between biotite grains and as narrow rims on elongate reddish allanites. Apatite occurs as tiny inclusions in biotite and as larger oblate grains between or adjacent to biotites. Zircon occurs as rounded prisms commonly showing large tubular fluid inclusions.

Myrmekite and plagioclase rims on albite are commonly associated with microcline. The myrmekite is cauliform or wartlike and consistently projects into microcline whereas the albite rims are typically on plagioclase grains where they abut against microcline.

PL72-86 Biotite aplite; approximately 1.5 mi north-northwest of Trampas along Cañada de la Madera

This rock occurs as a narrow dike approximately 2 ft thick in Peñasco Quartz Monzonite. The aplite dike in turn is cut by a typical

pegmatite dike. It is a medium-grained biotite-bearing aplite with some very local coarser portions and narrow (2 mm) veinlets of more leucocratic material. An overall equigranular texture of quartz, microcline, and plagioclase is set off by a slight subparallel orientation of biotite (black, N 1), and by the presence of 1.5 mm sized subhedral magnetite octahedra. The overall color is a pinkish gray (5 YR 8/1) and the average grain size is about 0.75 to 1.2 mm. Microcline has the largest grain size (≤ 2.5 mm). The rock appears to be an intimate mixture of two facies, one being a finer grained biotite-bearing facies which appears to have been completely invaded by the more leucocratic microcline-rich phase. This latter facies occurs as veinlets and irregular masses in the finer grained facies. The masses are about 5 mm across and make up from 30 percent to less than 10 percent of the rock. In thin section the two facies are difficult to distinguish because the entire rock, regardless of biotite content, has an allotriomorphic granular texture. The microcline is perthitic and is crosshatch twinned. Myrmekite is common and occurs in its usual form of wartlike projections into the microcline. Plagioclase occurs as nondescript grains, which may or may not show polysynthetic twinning and which are slightly altered in some places. The quartz grains are rounded and show very little undulatory extinction. Biotite, for the most part, forms single grains that are about 0.4 x 0.25 mm in cross sectional size and are pleochroic in shades of brown and straw yellow. Magnetite grains lack any association with biotite and show alteration to hematite at grain margins and along cleavage fractures. Rarely the hematite occurs as blebs within the magnetite grains. Apatite and muscovite are common accessory minerals as is anatase(?),

which occurs as odd-shaped interstitial blebs that take on the shape of surrounding grains, suggesting that the constituents of the mineral(s) were once a residual immiscible liquid. Associated with the blebs are small grains of magnetite. The anatase may also be in part an alteration product of sphene. Sphene also occurs as very narrow rims on margins of the larger magnetite grains. Muscovite is found as an alteration product of plagioclase and as flakes crosscutting biotite. Apatite is associated with biotite and usually occurs as oblate, rounded grains.

APPENDIX II

Modal Analyses

Most of the following modal analyses were obtained by a modified point count method whereby stained slabs were counted for major constituents (quartz, microcline, plagioclase, and biotite) and then thin or polished sections were counted in order to correct for accessory constituents. One thousand points each were usually counted on the slabs and thin sections. Given the grain size, area of slabs, and the number of points counted the precision of the analyses is thought to be within a two sigma analytical error of about 2.8 (Chayes, 1956, p. 81). That is, 95 percent of the time the stated modal percentage of a major constituent will be within 2.8 percent of the true value. Another approach has been used by Van Der Plas and Tobi (1965a), whereby they assume that if the grid spacing is larger than the largest grain fraction then the analytical error is approximated by the binomial counting error (Chayes, 1965; Van Der Plas and Tobi, 1965b). Applying their chart of counting error as a function of count length gives the following result for an average analysis of Rana Quartz Monzonite:

Quartz	34.4% \pm 3.0% (two sigma)
Plagioclase	31.2 \pm 2.9
Microcline	20.8 \pm 2.5
Biotite	5.6 \pm 1.4
Muscovite	4.7 \pm 1.3
Epidote	0.7 \pm 0.5
Clinozoisite	2.1 \pm 0.8
Hematite + magnetite	0.4 \pm 0.5

In some instances thin sections only were counted and the results of these analyses are less precise than stated above except in the case of fine-grained rocks such as aplites and felsites. The results in the following tables are reported to the tenth of a percent regardless of the actual precision. The advisability of this has been succinctly argued by Chayes in his 1953 paper, "In Defense of the Second Decimal."

References

- Chayes, F., 1953, In defense of the second decimal: *Am. Mineralogist*, v. 38, p. 784-793.
- 1956, *Petrographic modal analysis*: New York, John Wiley and Sons.
- 1965, Reliability of point counting results (discussion): *Am. Jour. Sci.*, v. 263, p. 719-721.
- Van Der Plas, L., and Tobi, A. C., 1965a, A chart for judging the reliability of point counting results: *Am. Jour. Sci.*, v. 263, p. 87-90.
- 1965b, Reply to Dr. Chayes' discussion: *Am. Jour. Sci.*, v. 263, p. 722-724.

AVERAGE MODES

	Rana Quartz Monzonite (border zone) (17)		Rana Quartz Monzonite (foliated phase) (24)		Rana Quartz Monzonite (unfoliated phase) (4)	
	%	S.D.	%	S.D.	%	S.D.
Quartz	38.8	11.0	32.0	2.6	37.6	2.4
Plagioclase	26.5	7.4	35.8	4.2	34.7	2.5
K-feldspar	19.7	11.4	19.7	3.3	17.8	2.1
Biotite	0.5	0.7	6.9	2.1	7.4	2.1
Muscovite	13.2	5.8	5.7	3.3	4.7	-
Epidote	1.7	1.6	1.6	0.9	0.7	-
Clinozoisite	-	-	-	-	2.1	-
Tourmaline	0.1	0.2	-	-	-	-
Hematite + magnetite	0.3	0.2	0.7	0.5	0.6	0.3

	Rana Quartz Monzonite aplites (4)		Metadacite (3)		Felsites (6)	
	%	S.D.	%	S.D.	%	S.D.
Quartz	35.2	4.0	44.5	5.6	56.1	7.6
Plagioclase	26.6	6.8	23.9	12.2	22.8	2.8
K-feldspar	33.8	6.5	14.5	2.6	8.4	5.9
Biotite	0.4	0.4	5.8	4.9	2.9	2.2
Muscovite	1.8	1.5	8.7	9.4	9.0	5.9
Epidote	0.4	0.3	1.6	0.5	0.4	0.4
Clinozoisite	-	-	-	-	-	-
Sphene	-	-	0.3	0.3	-	-
Allanite	-	-	-	-	-	-
Tourmaline	1.9	3.8	-	-	-	-
Hematite + magnetite	0.1	0.1	0.7	0.2	0.5	0.4

	Puntiagudo Granite Porphyry (9)		Peñasco Quartz Monzonite (11)		Peñasco Quartz Monzonite aprites (2)	
	%	S.D.	%	S.D.	%	S.D.
Quartz	34.7	4.7	25.1	3.4	28.7	3.0
Plagioclase	36.7	6.9	39.6	6.1	27.8	1.6
K-feldspar	20.2	8.6	15.9	6.0	40.9	2.0
Biotite	3.1	2.1	13.9	2.7	2.3	3.3
Muscovite	4.8	2.4	2.4	1.8	0.1	0.1
Epidote	0.9	0.4	1.5	0.6	-	-
Sphene	0.1	0.1	0.6	0.3	-	-
Allanite	0.0	0.1	0.2	0.1	-	-
Tourmaline	-	-				
Hornblende			0.1	0.4	-	-
Hematite + magnetite	0.4	0.2	0.8	0.5	0.3	0.4

Rana Quartz Monzonite (border zone)

Sample number	PL72- 138	PL73- 267	PL72- 131	PL72- 206	PL72- 197	PL72- 146**
Quartz (total)	28.7	32.3	34.7	33.4	40.4	61.3
Quartz (phenocrysts)	(9.5)	(10.4)	(8.3)	-	-	-
Plagioclase	32.7	33.8	33.7	24.3	23.7	26.0
Microcline	17.8	17.2	19.5	32.6	29.6	1.7
Biotite	-	-	-	-	0.5	-
Muscovite	14.7	14.1	10.6	9.2	5.6	30.8
Epidote	5.0	2.4	1.0	-	0.1	0.1
Tourmaline	0.7	0.1	-	-	-	-
Allanite	0.2	-	-	-	-	-
Garnet	-	-	-	0.2	-	-
Hematite	0.2	0.1	0.6	0.2@	0.1@	0.1

Sample number	PL72- 130**	PL73- 268**	PL73- 251**	PL73- 265*	PL72- 195*	PL72- 139*
Quartz (total)	46.5	42.7	54.6	30.2	38.1	35.8
Quartz (phenocrysts)	-	-	-	(6.0)	-	(6.7)
Plagioclase	34.4	27.4	15.1	31.4	20.8	31.7
Microcline	5.3	14.1	17.3	23.0	35.9	32.5
Biotite	1.8	0.2	0.1	1.5	-	-
Muscovite	9.1	14.2	12.5	13.6	4.9	8.1
Epidote	2.1	1.0	0.2	-	-	-
Tourmaline	-	-	-	-	-	-
Allanite	-	-	-	-	-	-
Garnet	-	0.3	-	-	-	-
Hematite	0.8	0.1	0.1	0.3	0.3	-

*Slabs only counted.

**Thin sections only counted.

@Opaque mineral is hematite + magnetite.

Rana Quartz Monzonite (border zone traverse)

Sample number	PL73- 237	PL73- 238	PL73- 240	PL73- 239	PL73- 241	PL73- 242	PL73- 243
Quartz (total)	53.5	27.8	22.2	49.0	28.2	24.3	32.1
Quartz (phenocrysts)	-	(4.6)	(3.3)	(10.0)	(5.3)	(9.4)	(13.3)
Plagioclase	26.1	27.7	26.0	25.0	30.0	33.6	35.1
Microcline	1.6	23.8	35.1	5.7	22.4	25.9	18.3
Biotite	-	0.8	1.2	1.6	1.3	5.5	2.2
Muscovite	18.0	16.4	13.0	14.5	14.6	6.9	8.8
Epidote	0.3	3.1	2.2	3.8	2.8	3.0	3.2
Sphene	-	-	-	-	0.3	-	-
Tourmaline	-	-	-	-	-	0.1	-
Hematite + magnetite	0.5	0.3	0.3	0.3	0.4	0.7	0.3

Sample number	PL73- 244	PL73- 245	PL73- 246	PL73- 247	PL73- 248	PL73- 249
Quartz (total)	33.4	30.9	28.2	32.8	34.3	33.9
Quartz (phenocrysts)	(11.3)	-	36.8	33.2	33.3	35.7
Plagioclase	34.9	33.0	19.7	14.6	21.6	19.6
Microcline	18.9	19.8				
Biotite	5.2	4.8	4.7	6.7	3.3	6.3
Muscovite	5.1	9.0	8.1	8.7	5.9	3.1
Epidote	2.2	2.0	1.9	2.3	1.0	0.8
Sphene	-	0.4	-	0.1	0.1	-
Tourmaline	-	-				
Hematite + magnetite	0.3	0.1	0.6	1.5	0.5	0.5

Rana Quartz Monzonite (foliated phase)

Sample number	PL72- 228	PL72- 229	PL72- 259	PL72- 193	PL72- 227	PL72- 154*	PL72- 168*	PL72- 174*	PL72- 167*
Quartz	34.3	31.1	28.1	32.4	31.9	33.9	32.6	34.8	32.5
Plagioclase	25.5	27.3	32.6	36.6	39.7	40.7	38.5	36.1	38.8
Microcline	23.9	21.1	25.1	14.7	14.5	15.5	18.1	20.1	23.2
Biotite	5.5	7.3	8.3	9.4	6.4	9.7	9.8	8.4	5.1
Muscovite	10.0	11.6	4.3	4.6	2.4	-	-	-	-
Epidote	0.3	0.3	1.1	1.7	0.6	-	-	-	-
Clinozoisite	0.3	0.3	-	-	0.3	-	-	-	-
Sphene	0.1	-	-	-	-	-	-	-	-
Tourmaline	-	-	-	0.2	-	-	-	-	-
Hematite + magnetite	0.8	0.9	0.5	0.4	0.8	0.1	1.0	0.7	0.5

Sample number	PL72- 172*	PL72- 181*	PL72- 163*	PL72- 175*	PL72- 170*	PL72- 224*	PL72- 226*
Quartz	35.9	33.6	33.5	29.2	30.3	29.6	34.2
Plagioclase	30.6	37.9	37.3	42.6	38.4	40.5	41.6
Microcline	21.8	20.1	18.0	16.6	20.9	21.3	20.3
Biotite	9.9	7.1	6.6	8.8	9.0	7.5	8.0
Muscovite	-	-	4.2	2.4	-	0.4	1.1
Hematite + magnetite	1.9	1.3	0.3	0.3	1.4	0.4	0.9

*Slabs only counted.

Rana Quartz Monzonite
(unfoliated phase)

Rana Quartz Monzonite
(aplites)

Sample number	PL71- 14	PL72- 186*	PL72- 187*	PL72- 183*	PL72- 188**	PL73- 233**	PL73- 232c**	PL73- 232f**
Quartz	34.4	38.5	37.3	40.0	39.7	36.9	30.3	33.8
Plagioclase	31.2	35.0	35.6	37.1	33.8	18.8	30.5	23.4
Microcline	20.8	16.1	17.9	16.4	24.9	36.2	34.0	40.2
Biotite	5.6	10.1	8.2	5.8	-	-	0.8	0.6
Muscovite	4.7	-	-	-	1.5	0.4	3.9	1.2
Epidote	0.7	-	-	-	-	0.3	0.6	0.7
Clinozoisite	2.1	-	-	-	-	-	-	-
Tourmaline	-	-	-	-	-	7.5	-	-
Hematite + magnetite	0.4	0.4	1.0	0.7	0.1	-	-	0.1

*Slabs only counted.

**Thin sections only counted.

Felsite DikesCerro Alto Metadacite

Sample number	PL72- 108	PL73- 260	PL72- 216	PL72- 149	PL72- 157	PL72- 106	PL71- 53	PL72- 133	PL72- 214
Quartz	63.7	65.7	47.9	51.4	58.2	49.4	41.7	40.9	51.0
Plagioclase	23.6	18.6	25.4	21.0	26.2	22.2	31.8	30.1	9.9
Microcline	2.0	2.6	7.8	8.4	11.8	17.8	11.9	14.5	17.1
Biotite	2.3	5.6	4.7	-	0.7	3.8	10.5	6.1	0.7
Muscovite	7.6	6.8	13.3	18.8	3.0	4.6	1.6	5.2	19.3
Epidote	0.1	0.2	0.4	0.2	0.1	1.2	1.6	2.0	1.1
Sphene	-	-	-	-	-	-	0.3	0.5	-
Hematite + magnetite	0.7	0.6	0.6	0.1	-	1.1	0.6@	0.6@	0.9@

Puntiagudo Granite Porphyry

Sample number	PL71- 44	PL72- 179	PL72- 126	PL72- 100	PL72- 127mc	PL72- 127f	PL72- 177*	PL72- 97	PL72- 80
Quartz	28.4	32.3	34.4	31.7	44.7	38.8	33.2	33.0	35.9
Plagioclase	36.2	42.0	28.9	27.8	41.0	48.6	29.8	36.4	39.3
Microcline	23.6	17.8	28.2	28.5	5.7	8.5	29.4	22.6	17.6
Biotite	3.3	5.6	1.5	3.8	0.3	-	2.8	4.5	5.9
Muscovite	6.8	6.9	6.1	6.0	7.0	3.5	4.5	1.7	0.4
Epidote	1.3	0.8	0.8	1.5	0.9	0.6	-	0.7	0.3
Sphene	-	-	-	-	-	-	-	0.2	0.2
Allanite	-	-	-	-	-	-	-	0.2	-
Hematite + magnetite	0.4	0.6	0.2	0.6	0.4	-	0.4	0.7	0.5

*Slab only counted.

@Magnetite only.

Peñasco Quartz Monzonite

Sample number	PL72-96	PL72-96grdm	PL71-5	PL71-56	PL73-263	PL73-264	PL72-92	PL71-35a**
Quartz	17.5	23.2	26.8	26.3	25.0	22.1	21.7	27.9
Plagioclase	32.0	42.4	36.8	36.3	32.9	44.5	48.3	33.1
Microcline	23.0	11.8	24.6	17.8	17.9	11.4	10.3	19.3
Biotite	16.4	16.4	7.8	12.9	13.8	17.4	13.9	13.4
Muscovite	3.5	3.5	1.5	3.1	6.9	1.7	2.4	3.0
Epidote	0.9	0.9	1.2	2.1	2.2	0.5	1.3	1.0
Clinozoisite	-	-	-	-	-	-	0.1	0.5
Sphene	0.6	0.6	0.4	1.1	0.4	0.3	0.5	1.0
Allanite	0.2	0.2	0.1	-	0.3	0.1	0.3	0.2
Hematite + magnetite	1.0	1.0	0.3	0.5	0.7	2.0	1.1	0.7

Peñasco Quartz Monzonite (aprites)

Sample number	PL71-35b**	PL72-85**	PL72-83**	PL72-231*	PL72-8b*	PL73-5ap*
Quartz	26.4	27.9	29.1	25.5	26.5	30.8
Plagioclase	38.0	48.9	41.3	43.6	28.9	26.7
K-feldspar	19.1	4.5	10.9	16.6	39.5	42.3
Biotite	13.1	14.1	12.7	17.3	4.6	-
Muscovite	1.2	2.0	0.8	0.1	-	0.2
Epidote	1.2	0.8	2.2	-	-	-
Clinozoisite	-	0.3	0.3	-	-	-
Sphene	0.1	0.7	0.7	1.0	-	-
Allanite	0.3	0.1	0.1	-	-	-
Hornblende	-	-	1.4	-	-	-
Hematite + magnetite	0.7	0.7	0.5	0.7	0.6	-

*Slabs only counted.

**Thin sections only counted.

APPENDIX III

Whole-Rock Analyses for Major and Minor Elements plus Barium, Rubidium, Strontium, and Zirconium by Energy Dispersive X-ray Fluorescence

The whole-rock analyses that follow were done with a Kevex (TM) 0810 excitation subsystem and a Kevex (TM) 5100 X-ray energy spectrometer. Special thanks is due the Kevex Corporation, Burlingame, California, for the use of their equipment and to Drs. R. Woldseth and T. C. Yao for help with the analyses.

The samples were prepared by trimming and slabbing appropriate-sized hand samples with a diamond saw. After thorough washing in tap water the slabs were fractured into pieces with maximum dimension 3 cm using an hydraulic rock splitter. These chunks were then fed into a small ceramic-faced jaw crusher. The minimum sample weight at this stage was generally 1.5 to 2.0 kg although in some instances lower weights were allowed especially for very fine-grained samples. For the very coarse-grained pegmatite samples larger sample weights were used--up to about 4 kg.

After the preliminary cr-shing, the samples were split to a weight of 100 g which was then ground in a tungsten carbide shatterbox (TM). After 5 to 10 min of grinding the sample was removed, split to half its weight and ground for an additional 20 to 25 min for a total grinding time of 30 min. Sieving of typical test samples demonstrated that this grinding procedure produced grain sizes that were 99.6 percent -200 mesh and 99 percent -400 mesh. Microscopic examination showed that the bulk

of the grains were uniformly less than 3 μm in size with only scattered quartz grains being 10 to 15 μm .

In order to reduce the total sample preparation time, an attempt was made to perform the analyses on whole-rock, undiluted pressed powder pellets. This technique has been successfully used by Fabbi (1971) for barium and strontium and is discussed as a technique for analyzing major elements by Welday and others (1964). Three types of problems arise in using this technique: (1) the "grain size" problem which results in different counting rates generally for major elements from different grain-sized samples, (2) preferred orientation of platy minerals on the surface of the pressed pellets which to X-rays, changes the apparent composition of such samples, and (3) matrix corrections are more severe than in diluted samples due to greater variation in absorption and enhancement of characteristic radiation from one sample to the next. One or more of these problems have been discussed by the following authors: Welday and others (1964), Volborth (1964), Berry and others (1964), and Claisse and Samson (1962). On problem (1) there is little agreement in the literature as to the appropriate mathematical treatment but it does appear that for a wide range of wavelengths, the problem can be overcome by grinding below a 5 μm grain size. Since these samples have largely fulfilled that criterion it is assumed that the grain size problem is not a significant source of error. Preferred orientation may be a problem, especially for the Peñasco Quartz Monzonite samples which are biotite-rich relative to the others. Still, the fine grain size has definitely helped to reduce the problem and no specific attempt was made to correct for it. The third problem, matrix effect,

was apparently significant only for Al, Si, Na, and Mg. Al and Si were corrected for using empirical techniques similar to those discussed by Fabbi (1971) combined with the use of a wide range of standard compositions. Na and Mg were corrected using an absorption correction of the type

$$I_{\text{corr}}^a = I_{\text{init}}^a \frac{k W_a \mu_a^0}{\sum W_i \mu_i}$$

where I_{corr}^a is the corrected intensity for element a, I_{init}^a is the uncorrected intensity for element a, k is an empirical constant, W is the weight fraction, μ_a^0 is the mass absorption coefficient for element a by element a in the sample and μ_i is the mass absorption coefficient of the element a by the i-th element in the sample. The results gave good R-factors (0.95) for least-squares fits of the standard data as long as the composition did not extend into the basaltic or more mafic range. R-factors for the other elements were excellent over wide composition ranges (0.99) except for Mn which was less precise due to difficulties in determining backgrounds. Rb, Sr, and Zr were corrected empirically using the methods of Fabbi (1971).

The analyses were actually performed in four passes. Na and Mg were analyzed using an aluminum secondary target, no secondary filter, with a chromium tube at 20 kV and 50 mA. Al, Si, K, Ca, Ti, and Mn were analyzed using an iron secondary target, no secondary filter, with a tungsten tube at 20 kV and 25 mA. Ti, Fe, Rb, Sr, and Zr, were analyzed using a silver tube at 35 kV and 35 mA with a silver secondary target and a silver filter. Ba was analyzed in a unique manner using a New England nuclear XRF exciter system (TM) in which a 900 MCi ^{241}Am radioactive source excited a dysprosium secondary target which in turn

excited the barium $K\alpha$ line giving very high sensitivity for Ba. The theoretical detection limit was about 1 ppm but both precision and accuracy for barium turned out to be less favorable than was anticipated from the counting statistics. The reasons for this are not clear but further work with this technique should make it one of the best for analyzing Ba in a wide variety of rocks.

Overall, the analyses are of high quality with the exception of Si and Al which apparently need additional matrix and/or peak overlap corrections. The precision (based on replicate analyses) for each element is given below beside each value obtained analyzing G-2 against the other standards used (USGS AGV-1, USGS GSP-1, USGS BCR-1, JGS JB-1, and JGS JG-1). The accuracy of the analyses can be estimated by noting the differences between Flanagan's (1973) values and those obtained by this method. The combination of not measuring H_2O content and the relatively poor analyses for Al and Si gives low totals in some cases, but the analyses still provide relative trends in Al and Si and reasonable accuracy for the other elements.

The CIPW norms given for each analysis were calculated using the standard NORMCOMP Fortran program.

<u>USGS G-2</u>	<u>Flanagan (1973)</u>	<u>This study</u>	<u>Estimated precision at 2 sigma</u>
SiO ₂	69.11	67.91	±1.30
TiO ₂	0.50	0.35	±0.05
Al ₂ O ₃	15.40	15.30	±0.15
Fe as Fe ₂ O ₃	2.65	2.61	±0.09
MnO	0.034	0.04	±0.02
MgO	0.76	0.81	±0.12
CaO	1.94	2.01	±0.09
Na ₂ O	4.07	4.05	±0.10
K ₂ O	4.51	4.45	±0.10
Total	99.25	98.06	
Ba	1870 ppm	1871 ppm	±100 ppm
Sr	479	475	±20
Rb	168	170	±20
Zr	300	331	±40

References

- Berry, P. F., Furula, T., and Rhodes, J. R., 1964, Particle size effects in radioisotope X-ray spectrometry: advances in X-ray analysis: New York, Plenum Press, v. 7, p. 612-632.
- Claisse, F., and Samson, P., 1962, Heterogeneity effects in X-ray analysis: advances in X-ray analysis: New York, Plenum Press, v. 5, p. 335-364.
- Fabbi, B. P., 1971, X-ray fluorescence determination of barium and strontium in geologic samples: Applied Spectroscopy, v. 25, no. 3, p. 316-318.
- Flanagan, F. J., 1973, 1972 values for international geochemical reference samples: Geochim. et Cosmochim. Acta, v. 37, p. 1189-1200.
- Weldday, E. E., Baird, A. K., McIntyre, D. B., and Madlem, K. W., 1964, Silicate sample preparation for light-element analyses by x-ray spectrography: Am. Mineralogist, v. 49, p. 889-903.
- Volborth, A., 1964, Biotite mica effect in x-ray spectrographic analysis of pressed-rock powders: Am. Mineralogist, v. 49, p. 634-643.

Cerro Alto Metadacite

SAMPLE NUMBER 36
00 PL71-36 CMD

OXIDE	WT PCT	MOLE PCT
SiO2	65.80	74.67
TiO2	0.65	0.55
Al2O3	14.97	10.01
Fe2O3	4.88	2.08
FeO	0.00	0.00
HNO	0.06	0.06
MGO	1.47	2.49
CAO	4.02	4.89
NA2O	3.11	3.42
K2O	2.42	1.75
P2O5	0.00	0.00
BAO	0.08	0.04
SRO	0.03	0.02
CR2O3	0.00	0.00
F	0.00	0.00
CL	0.00	0.00
SO3	0.00	0.00
S	0.00	0.30
CO2	0.00	0.00
ZRO2	0.03	0.02

BA 750 PPM
SR 289 PPM
RB 86 PPM
ZR 195 PPM
RE/SR 0.298
RE/BA 0.115

97.52

NORMATIVE MINERALS	WT PCT	MOLE PCT
KS	0.00	0.00
KP	0.00	0.00
LC	0.00	0.00
NS	0.00	0.00
OR	14.30	3.77
AB	26.32	7.36
AN	19.74	10.41
NE	0.00	0.00
Q	27.62	67.41
OL	0.00	0.00
FO	0.00	0.00
FA	0.00	0.00
LN	0.00	0.00
HY	3.66	5.35
EN	3.66	5.35
FS	0.00	0.00
DI	0.00	0.00
WO	0.00	0.00
EN	0.00	0.00
FS	0.00	0.00
WO	0.00	0.00
AC	0.00	0.00
AP	0.00	0.00
IL	0.13	0.12
SP	0.30	0.23
RU	0.46	0.84
PV	0.00	0.00
C	0.00	0.00
MT	0.00	0.00
HEM	4.88	4.48
CH	0.00	0.00
HL	0.00	0.00
FR	0.00	0.00
TH	0.00	0.00
PR	0.00	0.00
NC	0.00	0.00
CC	0.00	0.00
Z	0.04	0.04

97.46

SAMPLE NUMBER 133
00 PL72-133 CMD

OXIDE	WT PCT	MOLE PCT
SiO2	68.62	77.75
TiO2	0.38	0.32
Al2O3	14.29	9.54
Fe2O3	3.54	1.51
FeO	0.00	0.00
MNO	0.04	0.04
MGO	0.72	1.22
CAO	2.03	2.46
NA2O	4.39	4.82
K2O	3.11	2.25
P2O5	0.00	0.00
BAO	0.13	0.06
SRO	0.02	0.01
CR2O3	0.00	0.00
F	0.00	0.00
CL	0.00	0.00
SO3	0.00	0.00
S	0.00	0.00
CO2	0.00	0.00
ZRO2	0.02	0.01

BA 1191 PPM
SR 193 PPM
RB 99 PPM
ZR 182 PPM
RB/SR 0.513
RB/BA 0.083

97.29

NORMATIVE MINERALS	WT PCT	MOLE PCT
KS	0.00	0.00
KP	0.00	0.00
LC	0.00	0.00
NS	0.00	0.00
OR	18.38	5.39
AB	37.15	11.56
AN	10.10	5.93
NE	0.00	0.00
Q	25.68	69.78
OL	0.00	0.00
FO	0.00	0.00
FA	0.00	0.00
LN	0.00	0.00
HY	1.79	2.92
EN	1.79	2.92
FS	0.00	0.00
DI	0.00	0.00
WO	0.00	0.00
EN	0.00	0.00
FS	0.00	0.00
WO	0.00	0.00
AC	0.00	0.00
AP	0.00	0.00
IL	0.09	0.09
SP	0.18	0.15
RU	0.26	0.53
PV	0.00	0.00
C	0.00	0.00
NT	0.00	0.00
HEM	3.54	3.62
CH	0.00	0.00
HL	0.00	0.00
FR	0.00	0.00
TH	0.00	0.00
PR	0.00	0.00
NC	0.00	0.00
CC	0.00	0.00
Z	0.03	0.03

97.20

SAMPLE NUMBER 198
00 PL72-198 CMD

OXIDE	WT PCT	MOLE PCT	NORMATIVE MINERALS	WT PCT	MOLE PCT
SiO2	72.70	80.23	KS	0.00	0.00
TiO2	0.42	0.35	KP	0.00	0.00
AL2O3	14.71	9.57	LC	0.00	0.00
FE2O3	2.52	1.05	NS	0.00	0.00
FeO	0.00	0.00	OR	10.40	2.32
MNO	0.05	0.05	AB	33.85	8.00
MGO	0.56	0.92	AN	9.66	4.30
CAO	1.91	2.26	NE	0.00	0.00
NA2O	4.00	4.28	Q	37.67	77.74
K2O	1.76	1.24	OL	0.00	0.00
P2O5	0.00	0.00	FO	0.00	0.00
BAO	0.07	0.03	FA	0.00	0.00
SE0	0.02	0.01	LN	0.00	0.00
CR2O3	0.00	0.00	HY	1.39	1.72
F	0.00	0.00	EN	1.39	1.72
CL	0.00	0.00	FS	0.00	0.00
SO3	0.00	0.00	DI	0.00	0.00
S	0.00	0.00	WO	0.00	0.00
CO2	0.00	0.00	EN	0.00	0.00
ZRO2	0.04	0.02	FS	0.00	0.00

BA 622 PPM
SR 170 PPM
RB 53 PPM
ZR 273 PPM
RB/SR 0.312
RB/BA 0.085

98.76

SAMPLE NUMBER 209
00 PL72-209 CMD

OXIDE	WT PCT	MOLE PCT	NORMATIVE MINERALS	WT PCT	MOLE PCT
SiO2	69.32	78.22	KS	0.00	0.00
TiO2	0.40	0.34	KP	0.00	0.00
AL2O3	14.52	9.66	LC	0.00	0.00
FE2O3	3.71	1.58	NS	0.00	0.00
FeO	0.00	0.00	OR	20.27	5.35
MNO	0.05	0.05	AB	29.95	8.40
MGO	0.59	0.99	AN	11.56	6.11
CAO	2.29	2.77	NE	0.00	0.00
NA2O	3.54	3.87	Q	29.72	72.73
K2O	3.43	2.47	OL	0.00	0.00
P2O5	0.00	0.00	FO	0.00	0.00
BAO	0.08	0.04	FA	0.00	0.00
SRO	0.02	0.01	LN	0.00	0.00
CR2O3	0.00	0.00	HY	1.47	2.15
F	0.00	0.00	EN	1.47	2.15
CL	0.00	0.00	FS	0.00	0.00
SO3	0.00	0.00	DI	0.00	0.00
S	0.00	0.00	WO	0.00	0.00
CO2	0.00	0.00	EN	0.00	0.00
ZRO2	0.02	0.01	FS	0.00	0.00

BA 728 PPM
SR 156 PPM
RB 95 PPM
ZR 160 PPM
RB/SR 0.609
RB/BA 0.130

97.97

97.91

SAMPLE NUMBER 213
00 PL72-213 CMD

OXIDE	WT PCT	MOLE PCT	NORMATIVE MINERALS	WT PCT	MOLE PCT
SiO2	70.75	79.09	KS	0.00	0.00
TiO2	0.39	0.33	KP	0.00	0.00
Al2O3	14.60	9.62	LC	0.00	0.00
Fe2O3	3.13	1.32	NS	0.00	0.00
FeO	0.00	0.00	OR	24.05	6.35
MnO	0.04	0.04	AB	29.36	8.23
NGO	0.35	0.58	AN	9.74	5.15
CaO	1.92	2.30	NE	0.00	0.00
Na2O	3.47	3.76	Q	30.25	74.04
K2O	4.07	2.90	OL	0.00	0.00
P2O5	0.00	0.00	FO	0.00	0.00
BaO	0.09	0.04	FA	0.00	0.00
SrO	0.02	0.01	LN	0.00	0.00
CR2O3	0.00	0.00	HY	0.87	1.28
F	0.00	0.00	EN	0.87	1.28
CL	0.00	0.00	FS	0.00	0.00
SO3	0.00	0.00	DI	0.00	0.00
S	0.00	0.00	WO	0.00	0.00
CO2	0.00	0.00	EN	0.00	0.00
ZrO2	0.02	0.01	FS	0.00	0.00

BA 809 PPM
SR 167 PPM
RB 96 PPM
ZR 162 PPM
RB/SR 0.575
RB/BA 0.119

98.85

SAMPLE NUMBER 261
00 PL73-261 CMD

OXIDE	WT PCT	MOLE PCT	NORMATIVE MINERALS	WT PCT	MOLE PCT
SiO2	68.97	77.63	KS	0.00	0.00
TiO2	0.24	0.20	KP	0.00	0.00
Al2O3	14.25	9.45	LC	0.00	0.00
Fe2O3	5.05	2.14	NS	0.00	0.00
FeO	0.00	0.00	OR	5.67	1.54
MnO	0.07	0.07	AB	44.00	12.72
NGO	0.35	0.59	AN	12.71	6.92
CaO	2.91	3.51	NE	0.00	0.00
Na2O	5.20	5.67	Q	28.62	72.21
K2O	0.96	0.69	OL	0.00	0.00
P2O5	0.00	0.00	FO	0.00	0.00
BaO	0.04	0.02	FA	0.00	0.00
SrO	0.02	0.01	LN	0.00	0.00
CR2O3	0.00	0.00	HY	0.40	0.61
F	0.00	0.00	EN	0.40	0.61
CL	0.00	0.00	FS	0.00	0.00
SO3	0.00	0.00	DI	1.01	0.71
S	0.00	0.00	WO	0.54	0.35
CO2	0.00	0.00	EN	0.47	0.35
ZrO2	0.03	0.02	FS	0.00	0.00

BA 331 PPM
SR 164 PPM
RB 46 PPM
ZR 238 PPM
RB/SR 0.280
RB/BA 0.139

98.09

WO	0.00	0.00
AC	0.00	0.00
AP	0.00	0.00
IL	0.15	0.15
SP	0.40	0.31
RU	0.00	0.00
PV	0.00	0.00
C	0.00	0.00
MT	0.00	0.00
HEM	5.05	4.79
CH	0.00	0.00
HL	0.00	0.00
FR	0.00	0.00
TH	0.00	0.00
PR	0.00	0.00
NC	0.00	0.00
CC	0.00	0.00
Z	0.04	0.04

98.06

1

SAMPLE NUMBER 129
00 PL72-129 FEL

OXIDE	WT PCT	MOLE PCT	NORMATIVE MINERALS	WT PCT	MOLE PCT
SiO2	79.37	85.90	KS	0.00	0.00
TiO2	0.37	0.30	KP	0.00	0.00
Al2O3	10.86	6.93	LC	0.00	0.00
Fe2O3	3.40	1.38	NS	0.00	0.00
FeO	0.00	0.00	OR	20.03	3.22
MnO	0.03	0.03	AB	8.63	1.47
MgO	0.83	1.34	LN	2.97	0.95
CaO	0.56	0.65	NE	0.00	0.00
Na2O	1.02	1.07	Q	57.92	86.28
K2O	3.39	2.34	OL	0.00	0.00
P2O5	0.00	0.00	FO	0.00	0.00
BaO	0.09	0.04	FA	0.00	0.00
SR0	0.01	0.01	LN	0.00	0.00
CR2O3	0.00	0.00	HY	2.07	1.84
F	0.00	0.00	EN	2.07	1.84
CL	0.00	0.00	FS	0.00	0.00
SO3	0.00	0.00	DI	0.00	0.00
S	0.00	0.00	WO	0.00	0.00
CO2	0.00	0.00	EN	0.00	0.00
ZrO2	0.04	0.02	FS	0.00	0.00
			WO	0.00	0.00
			AC	0.00	0.00
			AP	0.00	0.00
			IL	0.06	0.04
			SP	0.00	0.00
			RU	0.34	0.38
			PV	0.00	0.00
			C	4.43	3.88
			NT	0.00	0.00
			HEM	3.40	1.91
			CH	0.00	0.00
			HL	0.00	0.00
			FR	0.00	0.00
			TH	0.00	0.00
			PR	0.00	0.00
			NC	0.00	0.00
			CC	0.00	0.00
			Z	0.06	0.03
				99.91	
	99.97				

SAMPLE NUMBER 140
00 PL72-140 FEL

OXIDE	WT PCT	MOLE PCT	NORMATIVE MINERALS	WT PCT	MOLE PCT
SiO2	74.18	81.74	KS	0.00	0.00
TiO2	0.28	0.23	KF	0.00	0.00
Al2O3	13.96	9.07	LC	0.00	0.00
Fe2O3	0.46	0.19	NS	0.00	0.00
FeO	0.00	0.00	OR	8.51	2.03
MnO	0.04	0.04	AB	40.96	10.37
MgO	0.24	0.39	AN	8.95	4.27
CaO	1.75	2.07	NE	0.00	0.00
Na2O	4.84	5.17	Q	36.27	80.14
K2O	1.44	1.01	OL	0.00	0.00
P2O5	0.00	0.00	PO	0.00	0.00
BAO	0.12	0.05	FA	0.00	0.00
SRO	0.02	0.01	LN	0.00	0.00
CR2O3	0.00	0.00	HY	0.60	0.79
F	0.00	0.00	EN	0.60	0.79
CL	0.00	0.00	FS	0.00	0.00
SO3	0.00	0.00	DI	0.00	0.00
S	0.00	0.00	WO	0.00	0.00
CO2	0.00	0.00	EN	0.00	0.00
ZRO2	0.04	0.02	FS	0.00	0.00
			WO	0.00	0.00
			AC	0.00	0.00
			AP	0.00	0.00
			IL	0.09	0.07
BA	1079	PPM	SP	0.00	0.00
SR	210	PPM	RU	0.23	0.39
R2	36	PPM	PV	0.00	0.00
IR	333	PPM	C	1.16	1.51
RB/SR		0.171	MT	0.00	0.00
RB/BA		0.033	HEM	0.46	0.38
			CH	0.00	0.00
			HL	0.00	0.00
			FR	0.00	0.00
			TH	0.00	0.00
			PR	0.00	0.00
			NC	0.00	0.00
			CC	0.00	0.00
			Z	0.06	0.04
				97.29	
	97.37				

SAMPLE NUMBER 157
00 PL72-157 FEL

OXIDE	WT PCT	MOLE PCT
SiO2	77.01	84.29
TiO2	0.10	0.08
Al2O3	11.50	7.42
Fe2O3	0.63	0.26
FeO	0.00	0.00
MnO	0.05	0.05
MgO	0.18	0.29
CaO	0.62	0.73
Na2O	6.23	6.61
K2O	0.35	0.24
P2O5	0.00	0.00
BaO	0.02	0.01
SrO	0.01	0.01
Cr2O3	0.00	0.00
P	0.00	0.00
CL	0.00	0.00
SO3	0.00	0.00
S	0.00	0.00
CO2	0.00	0.00
ZrO2	0.02	0.01

BA	151 PPM
SR	61 PPM
RB	6 PPM
ZR	127 PPM
RB/SR	0.098
RB/BA	0.040

96.72

NORMATIVE MINERALS	WT PCT	MOLE PCT
KS	0.00	0.00
KP	0.00	0.00
LC	0.00	0.00
NS	0.00	0.00
OR	2.07	0.49
AB	52.72	13.32
AN	2.38	1.13
NE	0.00	0.00
Q	37.96	83.75
OL	0.00	0.00
FO	0.00	0.00
FA	0.00	0.00
LN	0.00	0.00
HY	0.23	0.30
EN	0.23	0.30
FS	0.00	0.00
DI	0.47	0.29
WO	0.25	0.14
EN	0.22	0.14
FS	0.00	0.00
WO	0.00	0.00
AC	0.00	0.00
AP	0.00	0.00
IL	0.11	0.09
SP	0.11	0.07
RU	0.00	0.00
PV	0.00	0.00
C	0.00	0.00
MT	0.00	0.00
HEM	0.63	0.52
CH	0.00	0.00
HL	0.00	0.00
FR	0.00	0.00
TH	0.00	0.00
PR	0.00	0.00
NC	0.00	0.00
CC	0.00	0.00
Z	0.03	0.02
	96.70	

SAMPLE NUMBER 199
00 PL72-199 FEL

OXIDE	WT PCT	MOLE PCT
SiO2	75.31	82.39
TiO2	0.27	0.22
Al2O3	13.12	8.46
Fe2O3	1.30	0.54
FeO	0.00	0.00
MnO	0.04	0.04
MgO	0.36	0.59
CaO	1.19	1.39
Na2O	3.41	3.62
K2O	3.82	2.67
P2O5	0.00	0.00
BaO	0.15	0.06
SrO	0.01	0.01
Cr2O3	0.00	0.00
P	0.00	0.00
CL	0.00	0.00
SO3	0.00	0.00
S	0.00	0.00
CO2	0.00	0.00
ZrO2	0.04	0.02

BA	1354 PPM
SR	121 PPM
RB	108 PPM
ZR	279 PPM
RB/SR	0.893
RB/BA	0.080

99.02

NORMATIVE MINERALS	WT PCT	MOLE PCT
KS	0.00	0.00
KP	0.00	0.00
LC	0.00	0.00
NS	0.00	0.00
OR	22.58	5.23
AB	28.85	7.09
AN	6.20	2.87
NE	0.00	0.00
Q	37.62	80.73
OL	0.00	0.00
FO	0.00	0.00
FA	0.00	0.00
LN	0.00	0.00
HY	0.90	1.15
EN	0.90	1.15
FS	0.00	0.00
DI	0.00	0.00
WO	0.00	0.00
EN	0.00	0.00
FS	0.00	0.00
WO	0.00	0.00
AC	0.00	0.00
AP	0.00	0.00
IL	0.09	0.07
SP	0.00	0.00
RU	0.22	0.36
PV	0.00	0.00
C	1.10	1.39
MT	0.00	0.00
HEM	1.30	1.05
CH	0.00	0.00
HL	0.00	0.00
FR	0.00	0.00
TH	0.00	0.00
PR	0.00	0.00
NC	0.00	0.00
CC	0.00	0.00
Z	0.06	0.04
	98.92	

SAMPLE NUMBER 217
00 PL72-217 FEL

OXIDE	WT PCT	MOLE PCT	NORMATIVE MINERALS	WT PCT	MOLE PCT
SiO2	72.90	81.73	KS	0.00	0.00
TiO2	0.24	0.20	KP	0.00	0.00
Al2O3	15.62	10.32	LC	0.00	0.00
Fe2O3	2.56	1.08	NS	0.00	0.00
FeO	0.00	0.00	GR	21.16	4.19
MnO	0.03	0.03	AB	18.87	3.96
MgO	0.30	0.50	AN	4.69	1.86
CaO	0.90	1.08	NE	0.00	0.00
Na2O	2.23	2.42	Q	43.73	80.17
K2O	3.58	2.56	OL	0.00	0.00
P2O5	0.00	0.00	PO	0.00	0.00
BaO	0.11	0.05	FA	0.00	0.00
SR0	0.01	0.01	LN	0.00	0.00
CR2O3	0.00	0.00	HY	0.75	0.82
F	0.00	0.00	EN	0.75	0.82
CL	0.00	0.00	FS	0.00	0.00
SO3	0.00	0.00	DI	0.00	0.00
S	0.00	0.00	WO	0.00	0.00
CO2	0.00	0.00	EN	0.00	0.00
ZRO2	0.04	0.02	FS	0.00	0.00
			WO	0.00	0.00
			AC	0.00	0.00
			AP	0.00	0.00
BA	1013 PPM		IL	0.06	0.05
SR	69 PPM		SP	0.00	0.00
RB	79 PPM		RU	0.21	0.28
ZR	275 PPM		PV	0.00	0.00
RB/SR	1.145		C	6.36	6.87
RB/BA	0.078		HT	0.00	0.00
			HEM	2.56	1.77
			CH	0.00	0.00
			HL	0.00	0.00
			FR	0.00	0.00
			TH	0.00	0.00
			PR	0.00	0.00
			NC	0.00	0.00
			CC	0.00	0.00
			Z	0.06	0.04
98.52				98.45	

SAMPLE NUMBER 254
00 PL73-254 PEL

OXIDE	WT PCT	MOLE PCT	NORMATIVE MINERALS	WT PCT	MOLE PCT
SiO2	77.78	83.56	KS	0.00	0.00
TiO2	0.23	0.19	KP	0.00	0.00
Al2O3	12.46	7.89	LC	0.00	0.00
Fe2O3	1.47	0.59	NS	0.00	0.00
FeO	0.00	0.00	OR	7.45	1.54
MnO	0.04	0.04	AB	36.72	8.06
MgO	0.27	0.43	AN	8.21	3.40
CaO	1.63	1.88	NE	0.00	0.00
Na2O	4.34	4.52	Q	43.75	83.75
K2O	1.26	0.86	OL	0.00	0.00
P2O5	0.00	0.00	FO	0.00	0.00
BaO	0.04	0.02	FA	0.00	0.00
SrO	0.02	0.01	LN	0.00	0.00
Cr2O3	0.00	0.00	HY	0.67	0.77
F	0.00	0.00	EN	0.67	0.77
CL	0.00	0.00	FS	0.00	0.00
SO3	0.00	0.00	DI	0.00	0.00
S	0.00	0.00	WO	0.00	0.00
CO2	0.00	0.00	EH	0.00	0.00
ZrO2	0.03	0.02	FS	0.00	0.00
			WO	0.00	0.00
			AC	0.00	0.00
			AP	0.00	0.00
BA	381	PPM	IL	0.09	0.06
SR	123	PPM	SP	0.00	0.00
RB	36	PPM	RU	0.18	0.27
ZR	232	PPM	PV	0.00	0.00
RB/SR	0.271		C	0.95	1.07
RB/BA	0.094		MT	0.00	0.00
			HEM	1.47	1.06
			CH	0.00	0.00
			HL	0.00	0.00
			FR	0.00	0.00
			TH	0.00	0.00
			PR	0.00	0.00
			NC	0.00	0.00
			CC	0.00	0.00
			Z	0.04	0.03
99.57			99.54		

Puntiagudo Granite Porphyry

SAMPLE NUMBER 176
00 PL72-176 PGP-BZ

OXIDE	WT PCT	MOLE PCT	NORMATIVE MINERALS	WT PCT	MOLE PCT
SiO2	77.71	83.31	KS	0.00	0.00
TiO2	0.19	0.15	KP	0.00	0.00
Al2O3	13.04	8.24	LC	0.00	0.00
Fe2O3	0.95	0.38	NS	0.00	0.00
FeO	0.00	0.00	OR	26.06	5.91
MnO	0.03	0.03	AB	28.77	6.92
MgO	0.29	0.46	AN	3.74	1.70
CaO	0.73	0.84	NE	0.00	0.00
Na2O	3.40	3.53	Q	39.00	81.88
K2O	4.41	3.02	OL	0.00	0.00
P2O5	0.00	0.00	FO	0.00	0.00
BAO	0.05	0.02	FA	0.00	0.00
SP0	0.01	0.01	LN	0.00	0.00
CR2O3	0.00	0.00	HY	0.72	0.91
F	0.00	0.00	EN	0.72	0.91
CL	0.00	0.00	FS	0.00	0.00
SO3	0.00	0.00	DI	0.00	0.00
S	0.00	0.00	WO	0.00	0.00
CO2	0.00	0.00	EN	0.00	0.00
ZrO2	0.02	0.01	FS	0.00	0.00
			WO	0.00	0.00
			AC	0.00	0.00
BA	486 PPM		AP	0.00	0.00
SR	104 PPM		IL	0.06	0.05
RB	178 PPM		SP	0.00	0.00
ZR	132 PPM		RU	0.16	0.25
RB/SR	1.712		PV	0.00	0.00
RE/BA	0.366		C	1.30	1.61
			MT	0.00	0.00
			HEM	0.95	0.75
			CH	0.00	0.00
			HL	0.00	0.00
			FR	0.00	0.00
			TH	0.00	0.00
			PR	0.00	0.00
			NC	0.00	0.00
			CC	0.00	0.00
			Z	0.03	0.02
100.83			100.79		

SAMPLE NUMBER 66
00 PL71-66 PGP-BZ

OXIDE	WT PCT	MOLE PCT	NORMATIVE MINERALS	WT PCT	MOLE PCT
SiO2	76.52	84.43	KS	0.00	0.00
TiO2	0.17	0.14	KP	0.00	0.00
Al2O3	11.64	7.57	LC	0.00	0.00
Fe2O3	1.22	0.51	NS	0.00	0.00
FeO	0.00	0.00	OR	24.05	5.32
MnO	0.03	0.03	AB	26.82	6.30
MgO	0.25	0.41	AN	2.70	1.19
CaO	0.52	0.61	NE	0.00	0.00
Na2O	3.17	3.39	Q	40.96	83.95
K2O	4.07	2.86	OL	0.00	0.00
P2O5	0.00	0.00	FO	0.00	0.00
BaO	0.05	0.02	FA	0.00	0.00
SrO	0.01	0.01	LN	0.00	0.00
Cr2O3	0.00	0.00	HY	0.62	0.76
F	0.00	0.00	EN	0.62	0.76
Cl	0.00	0.00	FS	0.00	0.00
SO3	0.00	0.00	DI	0.00	0.00
S	0.00	0.00	WO	0.00	0.00
CO2	0.00	0.00	EN	0.00	0.00
ZrO2	0.02	0.01	FS	0.00	0.00
			WO	0.00	0.00
			AC	0.00	0.00
BA	443	PPM	AP	0.00	0.00
SR	55	PPM	IL	0.06	0.05
RB	137	PPM	SP	0.00	0.00
ZR	131	PPM	RU	0.14	0.21
RB/SR	2.491		PV	0.00	0.00
RB/BA	0.309		C	1.03	1.25
			HT	0.00	0.00
			HEM	1.22	0.94
			CH	0.00	0.00
			HL	0.00	0.00
			FR	0.00	0.00
			TH	0.00	0.00
			PR	0.00	0.00
			NC	0.00	0.00
			CC	0.00	0.00
			Z	0.03	0.02
97.67				97.63	

SAMPLE NUMBER 127F
00 PL72-127FN PGP-RHY

OXIDE	WT PCT	MOLE PCT	NORMATIVE MINERALS	WT PCT	MOLE PCT
SiO2	77.43	83.80	KS	0.00	0.00
TiO2	0.08	0.07	KP	0.00	0.00
AL2O3	12.93	8.25	LC	0.00	0.00
FE2O3	0.45	0.18	NS	0.00	0.00
FeO	0.00	0.00	OR	21.28	5.04
MNO	0.03	0.03	AB	36.39	9.15
MGO	0.11	0.18	AN	2.10	0.99
CAO	0.41	0.48	NE	0.00	0.00
NA2O	4.30	4.51	Q	37.56	82.40
K2O	3.60	2.49	OL	0.00	0.00
P2O5	0.00	0.00	FO	0.00	0.00
BAO	0.02	0.01	FA	0.00	0.00
SRO	0.01	0.01	LN	0.00	0.00
CR2O3	0.00	0.00	HY	0.27	0.36
F	0.00	0.00	EN	0.27	0.36
CL	0.00	0.00	FS	0.00	0.00
SO3	0.00	0.00	DI	0.00	0.00
S	0.00	0.00	WO	0.00	0.00
CO2	0.00	0.00	EN	0.00	0.00
ZRO2	0.02	0.01	FS	0.00	0.00
			WO	0.00	0.00
			AC	0.00	0.00
			AP	0.00	0.00
EA	150 PPM		IL	0.06	0.06
SR	63 PPM		SP	0.00	0.00
RB	124 PPM		RU	0.05	0.08
ZR	135 PPM		PV	0.00	0.00
RB/SR	1.963		C	1.19	1.54
RE/EA	0.827		MT	0.00	0.00
			HEM	0.45	0.37
			CH	0.00	0.00
			HL	0.00	0.00
			FR	0.00	0.00
			TH	0.00	0.00
			PR	0.00	0.00
			NC	0.00	0.00
			CC	0.00	0.00
			Z	0.03	0.02
				99.37	

99.39

SAMPLE NUMBER 235
00 PL73-235 PGP-RHY

OXIDE	WT PCT	MOLE PCT	NORMATIVE MINERALS	WT PCT	MOLE PCT
SiO2	76.86	82.18	KS	0.00	0.00
TiO2	0.32	0.26	KP	0.00	0.00
AL2O3	12.88	8.12	LC	0.00	0.00
FE2O3	1.70	0.68	NS	0.00	0.00
FeO	0.00	0.00	OR	22.10	5.14
MNO	0.04	0.04	AB	31.05	7.66
MGO	0.40	0.64	AN	7.45	3.46
CAO	1.37	1.57	NE	0.00	0.00
NA2O	3.67	3.80	Q	37.36	80.46
K2O	3.74	2.55	OL	0.00	0.00
P2O5	0.00	0.00	FO	0.00	0.00
BAO	0.18	0.08	FA	0.00	0.00
SRO	0.12	0.07	LN	0.00	0.00
CR2O3	0.00	0.00	HY	1.00	1.28
F	0.00	0.00	EN	1.00	1.28
CL	0.00	0.00	FS	0.00	0.00
SO3	0.00	0.00	DI	0.00	0.00
S	0.00	0.00	WO	0.00	0.00
CO2	0.00	0.00	EN	0.00	0.00
ZRO2	0.02	0.01	FS	0.00	0.00
			WO	0.00	0.00
			AC	0.00	0.00
			AP	0.00	0.00
BA	1575 PPM		IL	0.09	0.07
SR	990 PPM		SP	0.00	0.00
RB	86 PPM		RU	0.27	0.45
ZR	143 PPM		PV	0.00	0.00
RB/SR	0.087		C	0.07	0.08
RB/BA	0.055		MT	0.00	0.00
			HEM	1.70	1.38
			CH	0.00	0.00
			HL	0.00	0.00
			FR	0.00	0.00
			TH	0.00	0.00
			PR	0.00	0.00
			NC	0.00	0.00
			CC	0.00	0.00
			Z	0.03	0.02
				101.13	

101.30

SAMPLE NUMBER 234
00 PL73-234 PGP-RHY

OXIDE	WT PCT	MOLE PCT	NORMATIVE MINERALS	WT PCT	MOLE PCT
SiO2	80.18	86.69	KS	0.00	0.00
TiO2	0.09	0.07	KP	0.00	0.00
Al2O3	12.42	7.91	LC	0.00	0.00
Fe2O3	0.43	0.17	NS	0.00	0.00
FeO	0.00	0.00	OR	28.60	4.98
MnO	0.03	0.03	AB	9.22	1.70
HgO	0.10	0.16	AN	2.02	0.70
CaO	0.39	0.45	NE	0.00	0.00
Na2O	1.09	1.14	Q	54.29	87.57
K2O	4.84	3.34	OL	0.00	0.00
P2O5	0.00	0.00	FO	0.00	0.00
BaO	0.03	0.01	FA	0.00	0.00
SrO	0.01	0.01	LN	0.00	0.00
Cr2O3	0.00	0.00	HY	0.25	0.24
F	0.00	0.00	EN	0.25	0.24
CL	0.00	0.00	FS	0.00	0.00
SO3	0.00	0.00	DI	0.00	0.00
S	0.00	0.00	WO	0.00	0.00
CO2	0.00	0.00	EN	0.00	0.00
ZrO2	0.02	0.01	FS	0.00	0.00
			WO	0.00	0.00
			AC	0.00	0.00
			AP	0.00	0.00
			IL	0.06	0.04
			SP	0.00	0.00
			RU	0.06	0.07
			PV	0.00	0.00
			C	4.65	4.42
			MT	0.00	0.00
			HEM	0.43	0.26
			CH	0.00	0.00
			HL	0.00	0.00
			FR	0.00	0.00
			TH	0.00	0.00
			PR	0.00	0.00
			NC	0.00	0.00
			CC	0.00	0.00
			Z	0.03	0.02

B4 283 PPM
SR 44 PPM
RB 196 PPM
ZR 130 PPM
RB/SR 4.455
RB/BA 0.693

99.63

SAMPLE NUMBER 68
00 PL71-68LS PGP

OXIDE	WT PCT	MOLE PCT	NORMATIVE MINERALS	WT PCT	MOLE PCT
SiO2	75.41	82.25	KS	0.00	0.00
TiO2	0.25	0.21	KP	0.00	0.00
Al2O3	12.97	8.34	LC	0.00	0.00
Fe2O3	1.65	0.68	NS	0.00	0.00
FeO	0.00	0.00	OR	24.47	5.78
MnO	0.05	0.05	AB	29.11	7.30
MgO	0.41	0.67	AN	5.45	2.58
CaO	1.06	1.24	NE	0.00	0.00
Na2O	3.44	3.64	Q	36.58	80.11
K2O	4.14	2.88	OL	0.00	0.00
P2O5	0.00	0.00	FO	0.00	0.00
BaO	0.09	0.04	FA	0.00	0.00
SrO	0.01	0.01	LN	0.00	0.00
Cr2O3	0.00	0.00	HY	1.02	1.34
F	0.00	0.00	EN	1.02	1.34
CL	0.00	0.00	FS	0.00	0.00
SO3	0.00	0.00	DI	0.00	0.00
S	0.00	0.00	WO	0.00	0.00
CO2	0.00	0.00	EN	0.00	0.00
ZrO2	0.03	0.02	FS	0.00	0.00
			WO	0.00	0.00
			AC	0.00	0.00
			AP	0.00	0.00
			IL	0.11	0.09
			SP	0.00	0.00
			RU	0.19	0.32
			PV	0.00	0.00
			C	0.83	1.08
			MT	0.00	0.00
			HEM	1.65	1.36
			CH	0.00	0.00
			HL	0.00	0.00
			FR	0.00	0.00
			TH	0.00	0.00
			PR	0.00	0.00
			NC	0.00	0.00
			CC	0.00	0.00
			Z	0.04	0.03

BA 776 PPM
SR 63 PPM
RB 154 PPM
ZR 186 PPM
RB/SR 2.444
RB/BA 0.198

99.51

99.45

SAMPLE NUMBER 122
00 PL72-122 PGP

OXIDE	WT PCT	MOLE PCT	NORMATIVE MINERALS	WT PCT	MOLE PCT
SiO2	76.68	82.93	KS	0.00	0.00
TiO2	0.22	0.18	KP	0.00	0.00
AL2O3	12.75	8.13	LC	0.00	0.00
FE2O3	1.21	0.49	NS	0.00	0.00
FeO	0.00	0.00	OR	23.82	5.59
MNO	0.05	0.05	AB	31.14	7.76
MGO	0.30	0.48	AN	4.70	2.21
CAO	0.91	1.05	NE	0.00	0.00
NA2O	3.68	3.86	Q	37.36	81.30
K2O	4.03	2.78	OL	0.00	0.00
P2O5	0.00	0.00	FO	0.00	0.00
BAO	0.09	0.04	FA	0.00	0.00
SRO	0.01	0.01	LN	0.00	0.00
CR2O3	0.00	0.00	HY	0.75	0.97
F	0.00	0.00	EN	0.75	0.97
CL	0.00	0.00	FS	0.00	0.00
SO3	0.00	0.00	DI	0.00	0.00
S	0.00	0.00	WO	0.00	0.00
CO2	0.00	0.00	EN	0.00	0.00
ZRO2	0.02	0.01	FS	0.00	0.00
			WO	0.00	0.00
			AC	0.00	0.00
			AP	0.00	0.00
			IL	0.11	0.09
			SP	0.00	0.00
			RU	0.16	0.27
			PV	0.00	0.00
			C	0.61	0.78
			MT	0.00	0.00
			HEM	1.21	0.99
			CH	0.00	0.00
			HL	0.00	0.00
			FR	0.00	0.00
			TH	0.00	0.00
			PR	0.00	0.00
			NC	0.00	0.00
			CC	0.00	0.00
			Z	0.03	0.02

BA 851 PPM
SR 72 PPM
RB 117 PPM
ZR 147 PPM
RB/SR 1.625
RB/BA 0.138

99.95

SAMPLE NUMBER 124
00 PL72-124 PGP

OXIDE	WT PCT	MOLE PCT	NORMATIVE MINERALS	WT PCT	MOLE PCT
SiO2	74.01	81.30	KS	0.00	0.00
TiO2	0.32	0.26	KP	0.00	0.00
AL2O3	13.68	8.86	LC	0.00	0.00
FE2O3	1.91	0.79	NS	0.00	0.00
FeO	0.00	0.00	OR	22.63	5.48
MNO	0.05	0.05	AB	30.80	7.92
MGO	0.44	0.72	AN	6.11	2.96
CAO	1.20	1.41	NE	0.00	0.00
NA2O	3.64	3.88	Q	34.87	78.26
K2O	3.83	2.68	OL	0.00	0.00
P2O5	0.00	0.00	FO	0.00	0.00
BAO	0.07	0.03	FA	0.00	0.00
SRO	0.01	0.01	LN	0.00	0.00
CR2O3	0.00	0.00	HY	1.10	1.47
F	0.00	0.00	EN	1.10	1.47
CL	0.00	0.00	FS	0.00	0.00
SO3	0.00	0.00	DI	0.00	0.00
S	0.00	0.00	WO	0.00	0.00
CO2	0.00	0.00	EN	0.00	0.00
ZRO2	0.02	0.01	FS	0.00	0.00
			WO	0.00	0.00
			AC	0.00	0.00
			AP	0.00	0.00
			IL	0.11	0.10
			SP	0.00	0.00
			RU	0.26	0.45
			PV	0.00	0.00
			C	1.31	1.73
			MT	0.00	0.00
			HEM	1.91	1.61
			CH	0.00	0.00
			HL	0.00	0.00
			FR	0.00	0.00
			TH	0.00	0.00
			PR	0.00	0.00
			NC	0.00	0.00
			CC	0.00	0.00
			Z	0.03	0.02

BA 613 PPM
SR 77 PPM
RB 129 PPM
ZR 176 PPM
RB/SR 1.675
RB/BA 0.210

99.18

99.13

SAMPLE NUMBER 126
00 PL72-126 PGP

OXIDE	WT PCT	MOLE PCT	NORMATIVE MINERALS	WT PCT	MOLE PCT
SiO2	73.20	82.55	KS	0.00	0.00
TiO2	0.26	0.22	KP	0.00	0.00
Al2O3	12.71	8.45	LC	0.00	0.00
Fe2O3	1.43	0.61	NS	0.00	0.00
FeO	0.00	0.00	OR	21.10	5.14
MnO	0.03	0.03	AB	31.99	8.27
MgO	0.36	0.61	AN	3.37	1.64
CaO	0.65	0.79	NE	0.00	0.00
Na2O	3.78	4.13	Q	35.54	80.20
K2O	3.57	2.57	OL	0.00	0.00
P2O5	0.00	0.00	FO	0.00	0.00
BAO	0.08	0.04	FA	0.00	0.00
SrO	0.00	0.00	LN	0.00	0.00
CR2O3	0.00	0.00	HY	0.90	1.21
F	0.00	0.00	EN	0.90	1.21
CL	0.00	0.00	FS	0.00	0.00
SO3	0.00	0.00	DI	0.00	0.00
S	0.00	0.00	WO	0.00	0.00
CO2	0.00	0.00	EN	0.00	0.00
ZHO2	0.03	0.02	FS	0.00	0.00
			WO	0.00	0.00
			AC	0.00	0.00
			AP	0.00	0.00
			IL	0.06	0.06
			SP	0.00	0.00
			RU	0.23	0.38
			PV	0.00	0.00
			C	1.39	1.85
			MT	0.00	0.00
			HEM	1.43	1.21
			CH	0.00	0.00
			HL	0.00	0.00
			FR	0.00	0.00
			TH	0.00	0.00
			PR	0.00	0.00
			NC	0.00	0.00
			CC	0.00	0.00
			Z	0.04	0.03

96.10

96.05

SAMPLE NUMBER 127C
00 PL72-127CRS PGP

OXIDE	WT PCT	MOLE PCT	NORMATIVE MINERALS	WT PCT	MOLE PCT
SiO2	76.19	83.76	KS	0.00	0.00
TiO2	0.22	0.18	KP	0.00	0.00
Al2O3	12.42	8.05	LC	0.00	0.00
Fe2O3	1.30	0.54	NS	0.00	0.00
FeO	0.00	0.00	OR	9.57	2.18
MnO	0.03	0.03	AB	43.75	10.60
MgO	0.28	0.46	AN	1.37	0.63
CaO	0.26	0.31	NE	0.00	0.00
Na2O	5.17	5.51	Q	38.89	82.23
K2O	1.62	1.14	OL	0.00	0.00
P2O5	0.00	0.00	FO	0.00	0.00
BAO	0.03	0.01	FA	0.00	0.00
SrO	0.01	0.01	LN	0.00	0.00
CR2O3	0.00	0.00	HY	0.70	0.88
F	0.00	0.00	EN	0.70	0.88
CL	0.00	0.00	FS	0.00	0.00
SO3	0.00	0.00	DI	0.00	0.00
S	0.00	0.00	WO	0.00	0.00
CO2	0.00	0.00	EN	0.00	0.00
ZRO2	0.03	0.02	FS	0.00	0.00
			WO	0.00	0.00
			AC	0.00	0.00
			AP	0.00	0.00
			IL	0.06	0.05
			SP	0.00	0.00
			RU	0.19	0.30
			PV	0.00	0.00
			C	1.66	2.07
			MT	0.00	0.00
			HEM	1.30	1.03
			CH	0.00	0.00
			HL	0.00	0.00
			FR	0.00	0.00
			TH	0.00	0.00
			PR	0.00	0.00
			NC	0.00	0.00
			CC	0.00	0.00
			Z	0.04	0.03

97.56

97.54

SAMPLE NUMBER 178
00 PL72-178 PGP

OXIDE	WT PCT	MOLE PCT	NORMATIVE MINERALS	WT PCT	MOLE PCT
SiO2	71.03	80.16	KS	0.00	0.00
TiO2	0.36	0.31	KP	0.00	0.00
Al2O3	13.12	8.73	LC	0.00	0.00
Fe2O3	2.32	0.99	NS	0.00	0.00
FFO	0.00	0.00	OR	20.98	5.64
MNO	0.06	0.06	AB	33.26	9.49
MGO	0.60	1.01	AN	7.68	4.13
CAO	1.52	1.84	NE	0.00	0.00
NA2O	3.93	4.30	Q	30.35	75.62
K2O	3.55	2.56	OL	0.00	0.00
P2O5	0.00	0.00	FO	0.00	0.00
BAO	0.08	0.04	FA	0.00	0.00
SRO	0.01	0.01	LN	0.00	0.00
CR2O3	0.00	0.00	HY	1.49	2.23
F	0.00	0.00	EN	1.49	2.23
CL	0.00	0.00	FS	0.00	0.00
SO3	0.00	0.00	DI	0.00	0.00
S	0.00	0.00	WO	0.00	0.00
CO2	0.00	0.00	EN	0.00	0.00
ZRO2	0.03	0.02	FS	0.00	0.00
			WO	0.00	0.00
			AC	0.00	0.00
			AP	0.00	0.00
BA	683 PPM		IL	0.13	0.13
SR	117 PPM		SP	0.03	0.02
RB	133 PPM		RU	0.28	0.53
ZR	209 PPM		PV	0.00	0.00
RB/SR	1.137		C	0.00	0.00
RB/BA	0.195		MT	0.00	0.00
			HEM	2.32	2.18
			CH	0.00	0.00
			HL	0.00	0.00
			FR	0.00	0.00
			TH	0.00	0.00
			PR	0.00	0.00
			NC	0.00	0.00
			CC	0.00	0.00
			Z	0.04	0.04
				96.56	
96.61					

SAMPLE NUMBER 125
00 PL72-125 PGP-ALT

OXIDE	WT PCT	MOLE PCT	NORMATIVE MINERALS	WT PCT	MOLE PCT
SiO2	72.74	81.38	KS	0.00	0.00
TiO2	0.37	0.31	KP	0.00	0.00
Al2O3	13.83	9.12	LC	0.00	0.00
Fe2O3	2.09	0.88	NS	0.00	0.00
PEO	0.00	0.00	OR	16.72	3.78
MNO	0.05	0.05	AB	30.04	7.21
MGO	0.50	0.83	AN	6.40	2.90
CAO	1.26	1.51	NE	0.00	0.00
NA2O	3.55	3.85	Q	37.73	79.09
K2O	2.83	2.02	OL	0.00	0.00
P2O5	0.00	0.00	FO	0.00	0.00
BAO	0.07	0.03	FA	0.00	0.00
SRO	0.01	0.01	LN	0.00	0.00
CR2O3	0.00	0.00	HY	1.25	1.56
F	0.00	0.00	EN	1.25	1.56
CL	0.00	0.00	FS	0.00	0.00
SO3	0.00	0.00	DI	0.00	0.00
S	0.00	0.00	WO	0.00	0.00
CO2	0.00	0.00	EN	0.00	0.00
ZRO2	0.03	0.02	FS	0.00	0.00
			WO	0.00	0.00
			AC	0.00	0.00
			AP	0.00	0.00
BA	612 PPM		IL	0.11	0.09
SR	94 PPM		SP	0.00	0.00
RB	119 PPM		RU	0.31	0.49
ZR	207 PPM		PV	0.00	0.00
RB/SR	1.266		C	2.58	3.19
RB/BA	0.194		MT	0.00	0.00
			HEM	2.09	1.65
			CH	0.00	0.00
			HL	0.00	0.00
			FR	0.00	0.00
			TH	0.00	0.00
			PR	0.00	0.00
			NC	0.00	0.00
			CC	0.00	0.00
			Z	0.04	0.03
				97.28	
97.33					

98.82

96.43

466

Rana Quartz Monzonite

SAMPLE NUMBER 58-A
00 PL71-58A RQM-BZ

OXIDE	WT PCT	MOLE PCT
SiO2	74.32	81.32
TiO2	0.24	0.20
Al2O3	14.33	9.24
Fe2O3	1.32	0.54
FeO	0.00	0.00
MnO	0.04	0.04
MgO	0.32	0.52
CaO	1.39	1.63
Na2O	3.13	3.32
K2O	4.47	3.12
P2O5	0.00	0.00
BaO	0.11	0.05
SrO	0.01	0.01
Cr2O3	0.00	0.00
F	0.00	0.00
CL	0.00	0.00
SO3	0.00	0.00
S	0.00	0.00
CO2	0.00	0.00
ZrO2	0.02	0.01

BA 970 PPM
SR 89 PPM
RB 169 PPM
ZR 147 PPM
RB/SR 1.899
RB/BA 0.174

99.70

NORMATIVE MINERALS	WT PCT	MOLE PCT
KS	0.00	0.00
KP	0.00	0.00
LC	0.00	0.00
NS	0.00	0.00
OR	26.42	6.33
AB	26.49	6.74
AN	7.12	3.41
NE	0.00	0.00
Q	35.44	78.67
OL	0.00	0.00
FO	0.00	0.00
FA	0.00	0.00
LN	0.00	0.00
HY	0.80	1.06
EN	0.80	1.06
FS	0.00	0.00
DI	0.00	0.00
WO	0.00	0.00
EN	0.00	0.00
FS	0.00	0.00
WO	0.00	0.00
AC	0.00	0.00
AP	0.00	0.00
IL	0.09	0.08
SP	0.00	0.00
RU	0.19	0.33
PV	0.00	0.00
C	1.73	2.27
MT	0.00	0.00
HEM	1.32	1.10
CH	0.00	0.00
HL	0.00	0.00
FR	0.00	0.00
TH	0.00	0.00
PR	0.00	0.00
NC	0.00	0.00
CC	0.00	0.00
Z	0.03	0.02

99.63

SAMPLE NUMBER 58-B
00 PL71-58B RQM-BZ

OXIDE	WT PCT	MOLE PCT
SiO2	75.21	83.12
TiO2	0.28	0.23
Al2O3	14.14	9.21
Fe2O3	1.51	0.63
FeO	0.00	0.00
MnO	0.03	0.03
MgO	0.25	0.41
CaO	0.89	1.05
Na2O	3.18	3.41
K2O	2.57	1.81
P2O5	0.00	0.00
BaO	0.16	0.07
SrO	0.01	0.01
Cr2O3	0.00	0.00
F	0.00	0.00
CL	0.00	0.00
SO3	0.00	0.00
S	0.00	0.00
CO2	0.00	0.00
ZrO2	0.04	0.02

BA 1408 PPM
SR 112 PPM
RB 91 PPM
ZR 272 PPM
RB/SR 0.813
RB/BA 0.065

98.27

NORMATIVE MINERALS	WT PCT	MOLE PCT
KS	0.00	0.00
KP	0.00	0.00
LC	0.00	0.00
NS	0.00	0.00
OR	15.19	3.64
AB	26.91	5.72
AN	4.73	1.89
NE	0.00	0.00
Q	44.44	82.38
OL	0.00	0.00
FO	0.00	0.00
FA	0.00	0.00
LN	0.00	0.00
HY	0.62	0.69
EN	0.62	0.69
FS	0.00	0.00
DI	0.00	0.00
WO	0.00	0.00
EN	0.00	0.00
FS	0.00	0.00
WO	0.00	0.00
AC	0.00	0.00
AP	0.00	0.00
IL	0.06	0.05
SP	0.00	0.00
RU	0.25	0.34
PV	0.00	0.00
C	4.39	4.80
MT	0.00	0.00
HEM	1.51	1.05
CH	0.00	0.00
HL	0.00	0.00
FR	0.00	0.00
TH	0.00	0.00
PR	0.00	0.00
NC	0.00	0.00
CC	0.00	0.00
Z	0.06	0.04

98.16

SAMPLE NUMBER 138
00 PL72-138 RQM-BZ

OXIDE	WT PCT	MOLE PCT	NORMATIVE MINERALS	WT PCT	MOLE PCT
SiO2	73.02	81.82	KS	0.00	0.00
TiO2	0.30	0.25	KP	0.00	0.00
Al2O3	14.06	9.29	LC	0.00	0.00
Fe2O3	1.48	0.62	NS	0.00	0.00
FeO	0.00	0.00	OR	21.28	4.75
MNO	0.04	0.04	AB	25.30	6.00
MGO	0.41	0.68	AN	6.03	2.69
CAO	1.18	1.42	NE	0.00	0.00
NA2O	2.99	3.25	Q	38.63	79.94
K2O	3.60	2.57	OL	0.00	0.00
P2O5	0.00	0.00	FO	0.00	0.00
BAO	0.08	0.04	PA	0.00	0.00
SRO	0.01	0.01	LN	0.00	0.00
CR2O3	0.00	0.00	HY	1.02	1.26
F	0.00	0.00	EN	1.02	1.26
CL	0.00	0.00	FS	0.00	0.00
SO3	0.00	0.00	DI	0.00	0.00
S	0.00	0.00	WO	0.00	0.00
CO2	0.00	0.00	EN	0.00	0.00
ZRO2	0.02	0.01	FS	0.00	0.00
			WO	0.00	0.00
			AC	0.00	0.00
			AP	0.00	0.00
			IL	0.09	0.07
			SP	0.00	0.00
			RU	0.25	0.40
			PV	0.00	0.00
			C	3.04	3.70
			MT	0.00	0.00
			HEM	1.48	1.15
			CH	0.00	0.00
			HL	0.00	0.00
			FR	0.00	0.00
			TH	0.00	0.00
			PR	0.00	0.00
			NC	0.00	0.00
			CC	0.00	0.00
			Z	0.03	0.02
				97.14	
	97.19				

SAMPLE NUMBER 145
00 PL72-145 RQM-BZ

OXIDE	WT PCT	MOLE PCT	NORMATIVE MINERALS	WT PCT.	MOLE PCT
SiO2	76.94	85.42	KS	0.00	0.00
TiO2	0.20	0.17	KP	0.00	0.00
Al2O3	13.18	8.62	LC	0.00	0.00
Fe2O3	0.73	0.30	NS	0.00	0.00
FeO	0.00	0.00	OR	15.78	2.79
MNO	0.04	0.04	AB	18.36	3.45
MGO	0.28	0.46	AN	3.09	1.10
CAO	0.60	0.71	NE	0.00	0.00
NA2O	2.17	2.34	Q	52.33	85.86
K2O	2.67	1.89	OL	0.00	0.00
P2O5	0.00	0.00	FO	0.00	0.00
BAO	0.05	0.02	FA	0.00	0.00
SRO	0.01	0.01	LN	0.00	0.00
CR2O3	0.00	0.00	HY	0.70	0.68
F	0.00	0.00	EN	0.70	0.68
CL	0.00	0.00	FS	0.00	0.00
SO3	0.00	0.00	DI	0.00	0.00
S	0.00	0.00	WO	0.00	0.00
CO2	0.00	0.00	EN	0.00	0.00
ZRO2	0.02	0.01	FS	0.00	0.00
			WO	0.00	0.00
			AC	0.00	0.00
			AP	0.00	0.00
			IL	0.09	0.06
			SP	0.00	0.00
			RU	0.15	0.19
			PV	0.00	0.00
			C	5.59	5.40
			MT	0.00	0.00
			HEM	0.73	0.45
			CH	0.00	0.00
			HL	0.00	0.00
			FR	0.00	0.00
			TH	0.00	0.00
			PR	0.00	0.00
			NC	0.00	0.00
			CC	0.00	0.00
			Z	0.03	0.02
				96.85	
	96.89				

SAMPLE NUMBER 197
00 PL72-197 RQM-BZ

OXIDE	WT PCT	MOLE PCT	NORMATIVE MINERALS	WT PCT	MOLE PCT
SiO2	78.47	84.17	KS	0.00	0.00
TiO2	0.14	0.11	KP	0.00	0.00
AL2O3	13.18	8.33	LC	0.00	0.00
FE2O3	0.63	0.25	NS	0.00	0.00
FeO	0.00	0.00	OR	29.79	6.36
MNO	0.03	0.03	AB	22.85	5.18
MGO	0.18	0.29	AN	2.40	1.02
CAO	0.45	0.52	NE	0.00	0.00
NA2O	2.70	2.81	Q	42.17	83.42
K2O	5.04	3.45	OL	0.00	0.00
P2O5	0.00	0.00	FO	0.00	0.00
BAO	0.09	0.04	FA	0.00	0.00
SRO	0.00	0.00	LN	0.00	0.00
CR2O3	0.00	0.00	HY	0.45	0.53
F	0.00	0.00	EN	0.45	0.53
CL	0.00	0.00	FS	0.00	0.00
SO3	0.00	0.00	DI	0.00	0.00
S	0.00	0.00	WO	0.00	0.00
CO2	0.00	0.00	EN	0.00	0.00
ZRO2	0.01	0.01	FS	0.00	0.00
			WO	0.00	0.00
			AC	0.00	0.00
			AP	0.00	0.00
BA	833 PPM		IL	0.06	0.05
SR	29 PPM		SP	0.00	0.00
RB	194 PPM		RU	0.11	0.16
ZR	100 PPM		PV	0.00	0.00
RB/SR	6.690		C	2.41	2.80
RB/BA	0.233		MT	0.00	0.00
			HEM	0.63	0.47
			CH	0.00	0.00
			HL	0.00	0.00
			FR	0.00	0.00
			TH	0.00	0.00
			PR	0.00	0.00
			NC	0.00	0.00
			CC	0.00	0.00
			Z	0.01	0.01
100.92			100.86		

SAMPLE NUMBER 267
00 PL73-267 RQM-BZ

OXIDE	WT PCT	MOLE PCT	NORMATIVE MINERALS	WT PCT	MOLE PCT
SiO2	71.97	81.71	KS	0.00	0.00
TiO2	0.32	0.27	KP	0.00	0.00
AL2O3	13.93	9.32	LC	0.00	0.00
FE2O3	1.18	0.50	NS	0.00	0.00
FeO	0.00	0.00	OR	18.97	4.31
MNO	0.03	0.03	AB	26.32	6.34
MGO	0.44	0.74	AN	6.77	3.07
CAO	1.33	1.62	NE	0.00	0.00
NA2O	3.11	3.42	Q	38.00	79.90
K2O	3.21	2.32	OL	0.00	0.00
P2O5	0.00	0.00	FO	0.00	0.00
BAO	0.08	0.04	FA	0.00	0.00
SRO	0.01	0.01	LN	0.00	0.00
CR2O3	0.00	0.00	HY	1.10	1.38
F	0.00	0.00	EN	1.10	1.38
CL	0.00	0.00	FS	0.00	0.00
SO3	0.00	0.00	DI	0.00	0.00
S	0.00	0.00	WO	0.00	0.00
CO2	0.00	0.00	EN	0.00	0.00
ZRO2	0.02	0.01	FS	0.00	0.00
			WO	0.00	0.00
			AC	0.00	0.00
			AP	0.00	0.00
BA	703 PPM		IL	0.06	0.05
SR	124 PPM		SP	0.00	0.00
RB	119 PPM		RU	0.29	0.45
ZR	164 PPM		PV	0.00	0.00
RB/SR	0.960		C	2.86	3.54
RB/BA	0.169		MT	0.00	0.00
			HEM	1.18	0.93
			CH	0.00	0.00
			HL	0.00	0.00
			FR	0.00	0.00
			TH	0.00	0.00
			PR	0.00	0.00
			NC	0.00	0.00
			CC	0.00	0.00
			Z	0.03	0.02
95.63			95.57		

SAMPLE NUMBER 148
00 PL72-148 ROM-F

OXIDE	WT PCT	MOLE PCT	NORMATIVE MINERALS	WT PCT	MOLE PCT
SiO2	69.86	80.49	KS	0.00	0.00
TiO2	0.41	0.36	KP	0.00	0.00
Al2O3	13.10	8.89	LC	0.00	0.00
Fe2O3	1.51	0.65	NS	0.00	0.00
FeO	0.00	0.00	OR	19.32	4.85
MnO	0.06	0.06	AB	26.40	7.03
MgO	0.53	0.91	AN	11.00	5.52
CaO	2.18	2.69	NE	0.00	0.00
Na2O	3.12	3.48	Q	33.64	78.16
K2O	3.27	2.40	OL	0.00	0.00
P2O5	0.00	0.00	PO	0.00	0.00
BAO	0.07	0.03	FA	0.00	0.00
SrO	0.02	0.01	LN	0.00	0.00
Cr2O3	0.00	0.00	HY	1.32	1.84
F	0.00	0.00	EN	1.32	1.84
CL	0.00	0.00	FS	0.00	0.00
SO3	0.00	0.00	DI	0.00	0.00
S	0.00	0.00	WO	0.00	0.00
CO2	0.00	0.00	EN	0.00	0.00
ZrO2	0.03	0.02	FS	0.00	0.00
			WO	0.00	0.00
			AC	0.00	0.00
BA	629 PPM		AP	0.00	0.00
SR	150 PPM		IL	0.13	0.12
RS	128 PPM		SP	0.00	0.00
ZR	213 PPM		RU	0.34	0.60
RB/SR	0.853		PV	0.00	0.00
RE/SA	0.203		C	0.40	0.55
			HT	0.00	0.00
			HEM	1.51	1.32
			CH	0.00	0.00
			HL	0.00	0.00
			FR	0.00	0.00
			TH	0.00	0.00
			PR	0.00	0.00
			NC	0.00	0.00
			CC	0.00	0.00
			Z	0.04	0.03
94.16				94.11	

SAMPLE NUMBER 148A
00 PL72-148A ROM-P

OXIDE	WT PCT	MOLE PCT	NORMATIVE MINERALS	WT PCT	MOLE PCT
SiO2	69.69	79.76	KS	0.00	0.00
TiO2	0.35	0.30	KP	0.00	0.00
Al2O3	13.43	9.06	LC	0.00	0.00
Fe2O3	2.93	1.26	NS	0.00	0.00
FeO	0.00	0.00	OR	20.63	5.15
MnO	0.07	0.07	AB	26.82	7.11
MgO	0.70	1.19	AN	9.21	4.61
CaO	1.82	2.23	NE	0.00	0.00
Na2O	3.17	3.52	Q	32.86	76.08
K2O	3.49	2.55	OL	0.00	0.00
P2O5	0.00	0.00	FO	0.00	0.00
BaO	0.07	0.03	FA	0.00	0.00
SrO	0.02	0.01	LN	0.00	0.00
Cr2O3	0.00	0.00	HY	1.74	2.42
F	0.00	0.00	EN	1.74	2.42
CL	0.00	0.00	FS	0.00	0.00
SO3	0.00	0.00	DI	0.00	0.00
S	0.00	0.00	WO	0.00	0.00
CO2	0.00	0.00	EN	0.00	0.00
ZrO2	0.02	0.01	FS	0.00	0.00
			WO	0.00	0.00
			AC	0.00	0.00
			AP	0.00	0.00
BA	670	PPM	IL	0.15	0.14
SR	137	PPM	SP	0.00	0.00
RB	129	PPM	RU	0.27	0.47
ZR	173	PPM	PV	0.00	0.00
RB/SR	0.942		C	1.06	1.45
RB/BA	0.192		MT	0.00	0.00
			HEM	2.93	2.55
			CH	0.00	0.00
			HL	0.00	0.00
			FR	0.00	0.00
			TH	0.00	0.00
			PR	0.00	0.00
			NC	0.00	0.00
			CC	0.00	0.00
			Z	0.03	0.02
95.76				95.71	

SAMPLE NUMBER 154
00 PL72-154 RQM-F

OXIDE	WT PCT	MOLE PCT	NORMATIVE MINERALS	WT PCT	MOLE PCT
SiO2	71.15	79.61	KS	0.00	0.00
TiO2	0.43	0.36	KP	0.00	0.00
Al2O3	13.90	9.17	LC	0.00	0.00
Fe2O3	3.19	1.34	NS	0.00	0.00
FeO	0.00	0.00	OR	19.21	4.70
MNO	0.06	0.06	AB	29.36	7.62
NGO	0.64	1.07	AN	9.51	4.65
CAO	1.88	2.25	NE	0.00	0.00
NA2O	3.47	3.76	Q	33.45	75.79
K2O	3.25	2.32	OL	0.00	0.00
P2O5	0.00	0.00	FO	0.00	0.00
BAO	0.07	0.03	FA	0.00	0.00
SRO	0.02	0.01	LN	0.00	0.00
CR2O3	0.00	0.00	HY	1.59	2.16
F	0.00	0.00	EN	1.59	2.16
CL	0.00	0.00	FS	0.00	0.00
SO3	0.00	0.00	DI	0.00	0.00
S	0.00	0.00	WO	0.00	0.00
CO2	0.00	0.00	EN	0.00	0.00
ZRO2	0.03	0.02	FS	0.00	0.00
			WO	0.00	0.00
			AC	0.00	0.00
			AP	0.00	0.00
BA	658 PPM		IL	0.13	0.12
SR	159 PPM		SP	0.00	0.00
RB	118 PPM		RU	0.36	0.62
ZR	202 PPM		PV	0.00	0.00
RB/SR	0.742		C	1.19	1.59
RB/BA	0.179		MT	0.00	0.00
			HEM	3.19	2.72
			CH	0.00	0.00
			HL	0.00	0.00
			FR	0.00	0.00
			TH	0.00	0.00
			PR	0.00	0.00
			NC	0.00	0.00
			CC	0.00	0.00
			Z	0.04	0.03
				98.04	

98.09

SAMPLE NUMBER 168
00 PL72-168 RQM-F

OXIDE	WT PCT	MOLE PCT	NORMATIVE MINERALS	WT PCT	MOLE PCT
SiO2	70.28	78.95	KS	0.00	0.00
TiO2	0.44	0.37	KP	0.00	0.00
Al2O3	14.48	9.59	LC	0.00	0.00
Fe2O3	2.78	1.18	NS	0.00	0.00
FeO	0.00	0.00	OR	22.52	5.83
MNO	0.06	0.06	AB	28.85	7.93
NGO	0.66	1.11	AN	9.43	4.88
CAO	1.85	2.23	NE	0.00	0.00
NA2O	3.41	3.71	Q	30.79	73.84
K2O	3.81	2.73	OL	0.00	0.00
P2O5	0.00	0.00	FO	0.00	0.00
BAO	0.11	0.05	FA	0.00	0.00
SRO	0.02	0.01	LN	0.00	0.00
CR2O3	0.00	0.00	HY	1.64	2.36
F	0.00	0.00	EN	1.64	2.36
CL	0.00	0.00	FS	0.00	0.00
SO3	0.00	0.00	DI	0.00	0.00
S	0.00	0.00	WO	0.00	0.00
CO2	0.00	0.00	EN	0.00	0.00
ZRO2	0.03	0.02	FS	0.00	0.00
			WO	0.00	0.00
			AC	0.00	0.00
			AP	0.00	0.00
BA	956 PPM		IL	0.13	0.12
SR	156 PPM		SP	0.00	0.00
RB	146 PPM		RU	0.37	0.67
ZR	226 PPM		PV	0.00	0.00
RB/SR	0.936		C	1.29	1.82
RB/BA	0.153		MT	0.00	0.00
			HEM	2.78	2.51
			CH	0.00	0.00
			HL	0.00	0.00
			FR	0.00	0.00
			TH	0.00	0.00
			PR	0.00	0.00
			NC	0.00	0.00
			CC	0.00	0.00
			Z	0.04	0.04
				97.85	

97.93

SAMPLE NUMBER 174
00 PL72-174 RQM-F

OXIDE	WT PCT	MOLE PCT	NORMATIVE MINERALS	WT PCT	MOLE PCT
SiO2	70.03	79.01	KS	0.00	0.00
TiO2	0.42	0.36	KP	0.00	0.00
Al2O3	14.09	9.37	LC	0.00	0.00
Fe2O3	2.93	1.24	NS	0.00	0.00
FeO	0.00	0.00	OR	20.39	5.22
MNO	0.06	0.06	AB	28.43	7.73
MGO	0.62	1.04	AN	11.29	5.79
CAO	2.24	2.71	NE	0.00	0.00
NA2O	3.36	3.67	Q	31.46	74.69
K2O	3.45	2.48	OL	0.00	0.00
P2O5	0.00	0.00	FO	0.00	0.00
BAO	0.07	0.03	FA	0.00	0.00
SRO	0.02	0.01	LN	0.00	0.00
CR2O3	0.00	0.00	HY	1.54	2.19
F	0.00	0.00	EN	1.54	2.19
CL	0.00	0.00	FS	0.00	0.00
SO3	0.00	0.00	DI	0.00	0.00
S	0.00	0.00	WO	0.00	0.00
CO2	0.00	0.00	EN	0.00	0.00
ZRO2	0.03	0.02	FS	0.00	0.00
			WO	0.00	0.00
			AC	0.00	0.00
			AP	0.00	0.00
BA	611 PPM		IL	0.13	0.12
SR	134 PPM		SP	0.00	0.00
RB	136 PPM		RU	0.35	0.63
ZR	196 PPM		PV	0.00	0.00
RB/SR	1.015		C	0.69	0.97
RB/BA	0.223		MT	0.00	0.00
			HEM	2.93	2.62
			CH	0.00	0.00
			HL	0.00	0.00
			FR	0.00	0.00
			TH	0.00	0.00
			PR	0.00	0.00
			NC	0.00	0.00
			CC	0.00	0.00
			Z	0.04	0.03
				97.27	

97.32

SAMPLE NUMBER 175
00 PL72-175 RQM-F

OXIDE	WT PCT	MOLE PCT	NORMATIVE MINERALS	WT PCT	MOLE PCT
SiO2	69.30	78.60	KS	0.00	0.00
TiO2	0.40	0.34	KP	0.00	0.00
Al2O3	14.42	9.64	LC	0.00	0.00
Fe2O3	2.59	1.11	NS	0.00	0.00
FeO	0.00	0.00	OR	21.98	6.05
MNO	0.06	0.06	AB	31.48	9.19
MGO	0.72	1.22	AN	9.15	5.04
CAO	1.79	2.18	NE	0.00	0.00
NA2O	3.72	4.09	Q	28.38	72.32
K2O	3.72	2.69	OL	0.00	0.00
P2O5	0.00	0.00	FO	0.00	0.00
BAO	0.12	0.05	FA	0.00	0.00
SRO	0.02	0.01	LN	0.00	0.00
CR2O3	0.00	0.00	HY	1.79	2.73
F	0.00	0.00	EN	1.79	2.73
CL	0.00	0.00	FS	0.00	0.00
SO3	0.00	0.00	DI	0.00	0.00
S	0.00	0.00	WO	0.00	0.00
CO2	0.00	0.00	EN	0.00	0.00
ZRO2	0.03	0.02	FS	0.00	0.00
			WO	0.00	0.00
			AC	0.00	0.00
			AP	0.00	0.00
BA	1059 PPM		IL	0.13	0.13
SR	166 PPM		SP	0.00	0.00
RB	142 PPM		RU	0.33	0.64
ZR	217 PPM		PV	0.00	0.00
RB/SR	0.855		C	0.92	1.38
RB/BA	0.134		MT	0.00	0.00
			HEM	2.59	2.48
			CH	0.00	0.00
			HL	0.00	0.00
			FR	0.00	0.00
			TH	0.00	0.00
			PR	0.00	0.00
			NC	0.00	0.00
			CC	0.00	0.00
			Z	0.04	0.04
				96.81	

96.89

SAMPLE NUMBER 181
00 PL72-181 RQM-F

OXIDE	WT PCT	MOLE PCT
SiO2	72.43	80.10
TiO2	0.38	0.32
Al2O3	13.95	9.09
Fe2O3	2.68	1.12
FeO	0.00	0.00
MnO	0.06	0.06
MgO	0.59	0.97
CaO	1.90	2.25
Na2O	3.33	3.57
K2O	3.52	2.48
P2O5	0.00	0.00
BAO	0.66	0.03
SrO	0.02	0.01
CR2O3	0.00	0.00
F	0.00	0.00
CL	0.00	0.00
SO3	0.00	0.00
S	0.00	0.00
CO2	0.00	0.00
ZRO2	0.02	0.01

BA 572 PPM
SR 148 PPM
RB 161 PPM
ZR 182 PPM
RB/SR 1.088
RB/BA 0.282

98.94

NORMATIVE MINERALS	WT PCT	MOLE PCT
KS	0.00	0.00
KP	0.00	0.00
LC	0.00	0.00
NS	0.00	0.00
OR	20.80	4.99
AB	28.18	7.18
AN	9.59	4.61
NE	0.00	0.00
Q	34.56	76.86
OL	0.00	0.00
FO	0.00	0.00
FA	0.00	0.00
LN	0.00	0.00
HY	1.47	1.96
EN	1.47	1.96
FS	0.00	0.00
DI	0.00	0.00
WO	0.00	0.00
EN	0.00	0.00
FS	0.00	0.00
WO	0.00	0.00
AC	0.00	0.00
AP	0.00	0.00
IL	0.13	0.11
SP	0.00	0.00
RU	0.31	0.52
PV	0.00	0.00
C	1.15	1.51
MT	0.00	0.00
HEM	2.68	2.24
CH	0.00	0.00
HL	0.00	0.00
FR	0.00	0.00
TH	0.00	0.00
PR	0.00	0.00
NC	0.00	0.00
CC	0.00	0.00
Z	0.03	0.02

98.89

SAMPLE NUMBER 193
00 PL72-193 RQM-F

OXIDE	WT PCT	MOLE PCT
SiO2	69.91	79.05
TiO2	0.42	0.36
Al2O3	13.99	9.32
Fe2O3	2.97	1.26
FeO	0.00	0.00
MnO	0.06	0.06
MgO	0.68	1.15
CaO	2.11	2.56
Na2O	3.30	3.62
K2O	3.56	2.57
P2O5	0.00	0.00
BAO	0.07	0.03
SrO	0.02	0.01
CR2O3	0.00	0.00
F	0.00	0.00
CL	0.00	0.00
SO3	0.00	0.00
S	0.00	0.00
CO2	0.00	0.00
ZRO2	0.03	0.02

BA 624 PPM
SR 176 PPM
RB 123 PPM
ZR 201 PPM
RB/SR 0.756
RB/BA 0.213

97.12

NORMATIVE MINERALS	WT PCT	MOLE PCT
KS	0.00	0.00
KP	0.00	0.00
LC	0.00	0.00
NS	0.00	0.00
OR	21.04	5.39
AB	27.92	7.59
AN	10.65	5.45
NE	0.00	0.00
Q	31.46	74.61
OL	0.00	0.00
FO	0.00	0.00
FA	0.00	0.00
LN	0.00	0.00
HY	1.69	2.40
EN	1.69	2.40
FS	0.00	0.00
DI	0.00	0.00
WO	0.00	0.00
EN	0.00	0.00
FS	0.00	0.00
WO	0.00	0.00
AC	0.00	0.00
AP	0.00	0.00
IL	0.13	0.12
SP	0.00	0.00
RU	0.35	0.63
PV	0.00	0.00
C	0.81	1.13
MT	0.00	0.00
HEM	2.97	2.65
CH	0.00	0.00
HL	0.00	0.00
FR	0.00	0.00
TH	0.00	0.00
PR	0.00	0.00
NC	0.00	0.00
CC	0.00	0.00
Z	0.04	0.03

97.07

SAMPLE NUMBER
00 TA16 (MONTGOMERY, 1953) RQM-F

SAMPLE NUMBER 14
00 PL71-14 RQM

OXIDE	WT. PCT	MOLE PCT	NORMATIVE MINERALS	WT PCT	MOLE PCT
SiO2	73.70	81.16	KS	0.00	0.00
TiO2	0.29	0.24	KF	0.00	0.00
Al2O3	14.42	9.36	LC	0.00	0.00
Fe2O3	1.73	0.72	NS	0.00	0.00
FeO	0.42	0.39	OR	20.80	4.63
MnO	0.13	0.12	AB	27.25	6.44
MgO	0.29	0.48	AN	5.67	2.53
CaO	1.30	1.53	NE	0.00	0.00
Na2O	3.22	3.44	Q	38.62	79.66
K2O	3.52	2.47	OL	0.00	0.00
P2O5	0.14	0.07	FO	0.00	0.00
BaO	0.07	0.03	FA	0.00	0.00
SrO	0.00	0.00	LN	0.00	0.00
Cr2O3	0.00	0.00	HY	0.72	0.89
F	0.00	0.00	EN	0.72	0.89
CL	0.00	0.00	FS	0.00	0.00
SO3	0.00	0.00	DI	0.00	0.00
S	0.00	0.00	WO	0.00	0.00
CO2	0.00	0.00	EN	0.00	0.00
ZrO2	0.00	0.00	FS	0.00	0.00
			WO	0.00	0.00
			AC	0.00	0.00
			AP	0.33	0.12
			IL	0.55	0.45
			SP	0.00	0.00
			RU	0.00	0.00
			PV	0.00	0.00
			C	3.23	3.93
			MT	0.94	0.50
			HEM	1.08	0.84
			CH	0.00	0.00
			HL	0.00	0.00
			FR	0.00	0.00
			TH	0.00	0.00
			PR	0.00	0.00
			NC	0.00	0.00
			CC	0.00	0.00
			Z	0.00	0.00
	99.23			99.19	

OXIDE	WT PCT	MOLE PCT	NORMATIVE MINERALS	WT PCT	MOLE PCT
SiO2	71.33	79.57	KS	0.00	0.00
TiO2	0.43	0.36	KF	0.00	0.00
Al2O3	13.58	8.93	LC	0.00	0.00
Fe2O3	2.86	1.20	NS	0.00	0.00
FeO	0.00	0.00	OR	20.51	5.15
MnO	0.06	0.06	AB	28.43	7.57
MgO	0.62	1.03	AN	11.35	5.70
CaO	2.24	2.68	NE	0.00	0.00
Na2O	3.36	3.63	Q	32.66	75.94
K2O	3.47	2.47	OL	0.00	0.00
P2O5	0.00	0.00	FO	0.00	0.00
BaO	0.10	0.04	FA	0.00	0.00
SrO	0.02	0.01	LN	0.00	0.00
Cr2O3	0.00	0.00	HY	1.54	2.15
F	0.00	0.00	EN	1.54	2.15
CL	0.00	0.00	FS	0.00	0.00
SO3	0.00	0.00	DI	0.00	0.00
S	0.00	0.00	WO	0.00	0.00
CO2	0.00	0.00	EN	0.00	0.00
ZrO2	0.04	0.02	FS	0.00	0.00
			WO	0.00	0.00
			AC	0.00	0.00
			AP	0.00	0.00
			IL	0.13	0.12
			SP	0.00	0.00
			RU	0.36	0.63
			PV	0.00	0.00
			C	0.14	0.19
			MT	0.00	0.00
			HEM	2.86	2.50
			CH	0.00	0.00
			HL	0.00	0.00
			FR	0.00	0.00
			TH	0.00	0.00
			PR	0.00	0.00
			NC	0.00	0.00
			CC	0.00	0.00
			Z	0.06	0.05
	98.11			98.04	

OXIDE	WT PCT	MOLE PCT	NORMATIVE MINERALS	WT PCT	MOLE PCT
SiO2	70.74	78.85	KS	0.00	0.00
TiO2	0.43	0.36	KP	0.00	0.00
Al2O3	14.34	9.42	LC	0.00	0.00
Fe2O3	2.98	1.25	NS	0.00	0.00
FeO	0.00	0.00	OR	21.75	5.58
MnO	0.06	0.06	AB	29.62	8.07
MgO	0.81	1.35	AN	9.58	4.92
CaO	1.88	2.25	NE	0.00	0.00
Na2O	3.50	3.78	Q	30.94	73.56
K2O	3.68	2.62	OL	0.00	0.00
P2O5	0.00	0.00	FO	0.00	0.00
BaO	0.11	0.05	FA	0.00	0.00
SrO	0.02	0.01	LN	0.00	0.00
Cr2O3	0.00	0.00	HY	2.02	2.87
F	0.00	0.00	EN	2.02	2.87
Cl	0.00	0.00	FS	0.00	0.00
SO3	0.00	0.00	DI	0.00	0.00
S	0.00	0.00	WO	0.00	0.00
CO2	0.00	0.00	EW	0.00	0.00
ZrO2	0.03	0.02	FS	0.00	0.00
			WO	0.00	0.00
			AC	0.00	0.00
			AP	0.00	0.00
Ba	1604	PPM	IL	0.13	0.12
Sr	154	PPM	SP	0.00	0.00
Rb	152	PPM	RU	0.36	0.65
Zr	237	PPM	PV	0.00	0.00
RE/SR	0.987		C	1.09	1.53
RE/Ba	0.151		MT	0.00	0.00
			HEM	2.98	2.67
			CH	0.00	0.00
			HL	0.00	0.00
			FR	0.00	0.00
			TH	0.00	0.00
			PR	0.00	0.00
			NC	0.00	0.00
			CC	0.00	0.00
			Z	0.04	0.03
	98.58			98.50	

OXIDE	WT PCT	MOLE PCT	NORMATIVE MINERALS	WT PCT	MOLE PCT
SiO2	72.06	79.63	KS	0.00	0.00
TiO2	0.55	0.46	KP	0.00	0.00
Al2O3	14.16	9.22	LC	0.00	0.00
Fe2O3	1.48	0.62	NS	0.00	0.00
FeO	1.27	1.17	OR	20.33	4.90
MnO	0.09	0.08	AB	28.77	7.36
MgO	0.37	0.61	AN	8.49	4.09
CaO	1.76	2.08	NE	0.00	0.00
Na2O	3.40	3.64	Q	34.73	77.54
K2O	3.44	2.42	GL	0.00	0.00
P2O5	0.06	0.03	FO	0.00	0.00
BAO	0.08	0.03	FA	0.00	0.00
SrO	0.00	0.00	LN	0.00	0.00
CR2O3	0.00	0.00	HY	1.29	1.61
F	0.00	0.00	EN	0.92	1.23
CL	0.00	0.00	FS	0.37	0.37
SO3	0.00	0.00	DI	0.00	0.00
S	0.00	0.00	WO	0.00	0.00
CO2	0.00	0.00	EN	0.00	0.00
ZrO2	0.00	0.00	FS	0.00	0.00
			WO	0.00	0.00
			AC	0.00	0.00
			AP	0.14	0.06
			IL	1.04	0.92
			SP	0.00	0.00
			RU	0.00	0.00
			PV	0.00	0.00
			C	1.73	2.28
			MT	2.15	1.24
			HEM	0.00	0.00
			CH	0.00	0.00
			HL	0.00	0.00
			FR	0.00	0.00
			TH	0.00	0.00
			PR	0.00	0.00
			NC	0.00	0.00
			CC	0.00	0.00
			Z	0.00	0.00
	98.72			98.67	

SAMPLE NUMBER 184
00 PL72-184 RQM

OXIDE	WT PCT	MOLE PCT	NORMATIVE MINERALS	WT PCT	MOLE PCT
SiO2	72.28	79.57	KS	0.00	0.00
TiO2	0.39	0.32	KP	0.00	0.00
AL2O3	14.45	9.38	LC	0.00	0.00
FE2O3	2.68	1.11	NS	0.00	0.00
FE0	0.00	0.00	OR	19.44	4.71
MNO	0.05	0.05	AB	30.12	7.75
MGO	0.67	1.10	AN	9.90	4.81
CAO	1.96	2.31	NE	0.00	0.00
NA2O	3.56	3.80	Q	33.69	75.68
K2O	3.29	2.31	OL	0.00	0.00
P2O5	0.00	0.00	FO	0.00	0.00
BAO	0.07	0.03	FA	0.00	0.00
SRO	0.02	0.01	LN	0.00	0.00
CR2O3	0.00	0.00	HY	1.67	2.24
F	0.00	0.00	EN	1.67	2.24
CL	0.00	0.00	FS	0.00	0.00
SO3	0.00	0.00	DI	0.00	0.00
S	0.00	0.00	WO	0.00	0.00
CO2	0.09	0.00	EN	0.00	0.00
ZRO2	0.02	0.01	FS	0.00	0.00
			WO	0.00	0.00
			AC	0.00	0.00
BA	595 PPM		AP	0.00	0.00
SR	148 PPM		IL	0.11	0.10
RB	120 PPM		SP	0.00	0.00
ZR	177 PPM		RU	0.33	0.56
RB/SR	0.811		PV	0.00	0.00
RE/BA	0.202		C	1.40	1.86
			MT	0.00	0.00
			HEM	2.68	2.27
			CH	0.00	0.00
			HL	0.00	0.00
			FR	0.00	0.00
			TH	0.00	0.00
			PR	0.00	0.00
			NC	0.00	0.00
			CC	0.00	0.00
			Z	0.03	0.02
99.44				99.39	

SAMPLE NUMBER 186
00 PL72-186 RQM

OXIDE	WT PCT	MOLE PCT	NORMATIVE MINERALS	WT PCT	MOLE PCT
SiO2	71.98	79.24	KS	0.00	0.00
TiO2	0.45	0.37	KP	0.00	0.00
AL2O3	14.26	9.25	LC	0.00	0.00
FE2O3	3.19	1.32	NS	0.00	0.00
FE0	0.00	0.00	OR	22.34	5.63
MNO	0.06	0.06	AB	30.80	8.24
MGO	0.79	1.30	AN	8.02	4.05
CAO	1.58	1.86	NE	0.00	0.00
NA2O	3.64	3.88	Q	31.68	73.99
K2O	3.78	2.65	OL	0.00	0.00
P2O5	0.00	0.00	FO	0.00	0.00
BAO	0.07	0.03	FA	0.00	0.00
SRO	0.02	0.01	LN	0.00	0.00
CR2O3	0.00	0.00	HY	1.97	2.75
F	0.00	0.00	EN	1.97	2.75
CL	0.00	0.00	FS	0.00	0.00
SO3	0.00	0.00	DI	0.00	0.00
S	0.00	0.00	WO	0.00	0.00
CO2	0.00	0.00	EN	0.00	0.00
ZRO2	0.03	0.02	FS	0.00	0.00
			WO	0.00	0.00
			AC	0.00	0.00
BA	613 PPM		AP	0.00	0.00
SR	137 PPM		IL	0.13	0.12
RB	176 PPM		SP	0.00	0.00
ZR	208 PPM		RU	0.38	0.67
RB/SR	1.285		PV	0.00	0.00
RB/BA	0.287		C	1.24	1.71
			MT	0.00	0.00
			HEM	3.19	2.80
			CH	0.00	0.00
			HL	0.00	0.00
			FR	0.00	0.00
			TH	0.00	0.00
			PR	0.00	0.00
			NC	0.00	0.00
			CC	0.00	0.00
			Z	0.04	0.03
99.85				99.80	

SAMPLE NUMBER
00 FMRUCO 48 (FULLAGAR AND SHIVER, 1973) PL71-14 RQM

OXIDE	WT PCT	MOLE PCT	NORMATIVE MINERALS	WT PCT	MOLE PCT
SiO2	72.54	78.09	KS	0.00	0.00
TiO2	0.43	0.35	KP	0.00	0.00
AL2O3	15.70	9.96	LC	0.00	0.00
FE2O3	2.98	1.21	NS	0.00	0.00
FE0	0.00	0.00	OR	23.58	6.17
MNO	0.00	0.00	AB	32.66	9.08
MGO	0.82	1.32	AN	9.92	5.20
CAO	2.00	2.31	NE	0.00	0.00
NA2O	3.86	4.03	Q	29.31	71.09
K2O	3.99	2.74	OL	0.00	0.00
P2O5	0.00	0.00	FC	0.00	0.00
BAO	0.00	0.00	FA	0.00	0.00
SPN	0.00	0.00	LN	0.00	0.00
CR2O3	0.00	0.00	HY	2.04	2.96
F	0.00	0.00	FN	2.04	2.96
CL	0.00	0.00	FS	0.00	0.00
SO3	0.00	0.00	DT	0.00	0.00
S	0.00	0.00	WC	0.00	0.00
CO2	0.00	0.00	EN	0.00	0.00
ZRC2	0.00	0.00	FS	0.00	0.00
			WO	0.00	0.00
			AC	0.00	0.00
			AP	0.00	0.00
			IL	0.00	0.00
RB	153 PPM		SP	0.00	0.00
SR	155 PPM		RU	0.43	0.78
			PV	0.00	0.00
			C	1.40	1.99
			MT	0.00	0.00
			HEM	2.98	2.72
			CH	0.00	0.00
			HL	0.00	0.00
			FR	0.00	0.00
			TH	0.00	0.00
			PR	0.00	0.00
			NC	0.00	0.00
			CC	0.00	0.00
			Z	0.00	0.00
	102.32			102.32	

SAMPLE NUMBER 31
00 PL71-31 RQM

OXIDE	WT PCT	MOLE PCT	NORMATIVE MINERALS	WT PCT	MOLE PCT
SiO2	72.04	79.32	KS	0.00	0.00
TiO2	0.42	0.35	KP	0.00	0.00
AL2O3	14.34	9.31	LC	0.00	0.00
FE2O3	2.83	1.17	NS	0.00	0.00
FE0	0.00	0.00	OR	22.10	5.51
MNO	0.05	0.05	AB	28.18	7.46
MGO	0.56	0.92	AN	11.31	5.64
CAO	2.24	2.64	NE	0.00	0.00
NA2O	3.33	3.55	Q	32.62	75.33
K2O	3.74	2.63	OL	0.00	0.00
P2O5	0.00	0.00	FO	0.00	0.00
BAO	0.08	0.03	FA	0.00	0.00
SRO	0.02	0.01	LN	0.00	0.00
CR2O3	0.00	0.00	HY	1.39	1.93
F	0.00	0.00	EN	1.39	1.93
CL	0.00	0.00	FS	0.00	0.00
SO3	0.00	0.00	DI	0.00	0.00
S	0.00	0.00	WO	0.00	0.00
CO2	0.00	0.00	EN	0.00	0.00
ZRO2	0.03	0.02	FS	0.00	0.00
			WO	0.00	0.00
			AC	0.00	0.00
			AP	0.00	0.00
BA	688 PPM		IL	0.11	0.10
SR	153 PPM		SP	0.00	0.00
RB	134 PPM		RU	0.36	0.63
ZR	203 PPM		PV	0.00	0.00
RB/SR	0.876		C	0.67	0.91
RB/BA	0.195		MT	0.00	0.00
			HEM	2.83	2.46
			CH	0.00	0.00
			HL	0.00	0.00
			FR	0.00	0.00
			TH	0.00	0.00
			PR	0.00	0.00
			NC	0.00	0.00
			CC	0.00	0.00
			Z	0.04	0.03
	99.68			99.62	

SAMPLE NUMBER 187
00 PL72-187 RQM

OXIDE	WT PCT	MOLE PCT
SiO2	72.66	80.04
TiO2	0.42	0.35
AL2O3	13.96	9.06
FE2O3	2.86	1.19
FeO	0.00	0.00
MNO	0.06	0.06
MGO	0.59	0.97
CAO	2.04	2.41
NA2O	3.10	3.31
K2O	3.62	2.54
P2O5	0.00	0.00
BAO	0.10	0.04
SRO	0.02	0.01
CR2O3	0.00	0.00
F	0.00	0.00
CL	0.00	0.00
SO3	0.00	0.00
S	0.00	0.00
CO2	0.00	0.00
ZRO2	0.03	0.02

BA	887 PPM
SR	155 PPM
RU	171 PPM
ZR	224 PPM
RB/SR	1.103
RE/BA	0.193

99.46

NORMATIVE MINERALS	WT PCT	MOLE PCT
KS	0.00	0.00
KP	0.00	0.00
LC	0.00	0.00
NS	0.00	0.00
OR	21.39	5.03
AB	26.23	6.55
AN	10.36	4.87
NE	0.00	0.00
Q	35.41	77.10
OL	0.00	0.00
FO	0.00	0.00
FA	0.00	0.00
LN	0.00	0.00
HY	1.47	1.91
EN	1.47	1.91
FS	0.00	0.00
DI	0.00	0.00
WO	0.00	0.00
EN	0.00	0.00
FS	0.00	0.00
WO	0.00	0.00
AC	0.00	0.00
AP	0.00	0.00
IL	0.13	0.11
SP	0.00	0.00
RU	0.35	0.58
PV	0.00	0.00
C	1.15	1.47
MT	0.00	0.00
HEM	2.86	2.34
CH	0.00	0.00
HL	0.00	0.00
FR	0.00	0.00
TH	0.00	0.00
PR	0.00	0.00
NC	0.00	0.00
CC	0.00	0.00
Z	0.04	0.03
	99.39	

SAMPLE NUMBER 255
00 PL73-255 RQM-BZ

OXIDE	WT PCT	MOLE PCT
SiO2	75.26	83.25
TiO2	0.21	0.17
AL2O3	13.65	8.90
FE2O3	0.59	0.25
FeO	0.00	0.00
MNO	0.02	0.02
MGO	0.26	0.43
CAO	0.52	0.62
NA2O	3.52	3.77
K2O	3.59	2.53
P2O5	0.00	0.00
BAO	0.09	0.04
SRO	0.01	0.01
CR2O3	0.00	0.00
F	0.00	0.00
CL	0.00	0.00
SO3	0.00	0.00
S	0.00	0.00
CO2	0.00	0.00
ZRO2	0.02	0.01

BA	781 PPM
SR	85 PPM
RU	118 PPM
ZR	149 PPM
RB/SR	1.388
RE/BA	0.151

97.74

NORMATIVE MINERALS	WT PCT	MOLE PCT
KS	0.00	0.00
KP	0.00	0.00
LC	0.00	0.00
NS	0.00	0.00
OR	21.22	4.74
AB	29.79	7.07
AN	2.77	1.24
NE	0.00	0.00
Q	39.45	81.73
OL	0.00	0.00
FO	0.00	0.00
FA	0.00	0.00
LN	0.00	0.00
HY	0.65	0.80
EN	0.65	0.80
FS	0.00	0.00
DI	0.00	0.00
WO	0.00	0.00
EN	0.00	0.00
FS	0.00	0.00
WO	0.00	0.00
AC	0.00	0.00
AP	0.00	0.00
IL	0.04	0.04
SP	0.00	0.00
RU	0.19	0.29
PV	0.00	0.00
C	2.96	3.61
MT	0.00	0.00
HEM	0.59	0.46
CH	0.00	0.00
HL	0.00	0.00
FR	0.00	0.00
TH	0.00	0.00
PR	0.00	0.00
NC	0.00	0.00
CC	0.00	0.00
Z	0.03	0.02
	97.68	

OXIDE	WT PCT	MOLE PCT	NORMATIVE MINERALS	WT PCT	MOLE PCT
SiO2	69.61	79.02	KS	0.00	0.00
TiO2	0.45	0.38	KF	0.00	0.00
Al2O3	14.10	9.43	LC	0.00	0.00
Fe2O3	3.22	1.38	NS	0.00	0.00
FeO	0.00	0.00	OR	22.34	5.69
MnO	0.06	0.06	AB	27.59	7.46
MgO	0.78	1.32	AN	8.46	4.31
CaO	1.67	2.03	NE	0.00	0.00
Na2O	3.26	3.59	Q	31.35	73.96
K2O	3.78	2.74	OL	0.00	0.00
P2O5	0.00	0.00	PO	0.00	0.00
BaO	0.08	0.04	FA	0.00	0.00
SR0	0.01	0.01	LN	0.00	0.00
CR2O3	0.00	0.00	HY	1.94	2.74
F	0.00	0.00	EN	1.94	2.74
CL	0.00	0.00	FS	0.00	0.00
SO3	0.00	0.00	DI	0.00	0.00
S	0.00	0.00	WO	0.00	0.00
CO2	0.00	0.00	EN	0.00	0.00
ZRO2	0.03	0.02	FS	0.00	0.00
			WO	0.00	0.00
			AC	0.00	0.00
BA	701 PPM		AP	0.00	0.00
SR	117 PPM		IL	0.13	0.12
RB	156 PPM		SP	0.00	0.00
ZR	193 PPM		RU	0.38	0.68
RB/SR	1.333		PV	0.00	0.00
RB/BA	0.223		C	1.55	2.15
			MT	0.00	0.00
			HEM	3.22	2.86
			CH	0.00	0.00
			HL	0.00	0.00
			FR	0.00	0.00
			TH	0.00	0.00
			PR	0.00	0.00
			NC	0.00	0.00
			CC	0.00	0.00
			Z	0.04	0.03
97.05				97.00	

OXIDE	WT PCT	MOLE PCT	NORMATIVE MINERALS	WT PCT	MOLE PCT
SiO2	71.17	79.07	KS	0.00	0.00
TiO2	0.43	0.36	KP	0.00	0.00
Al2O3	14.39	9.42	LC	0.00	0.00
Fe2O3	2.96	1.24	NS	0.00	0.00
FeO	0.00	0.00	OR	20.51	5.18
MnO	0.06	0.06	AB	30.72	8.24
MgO	0.75	1.24	AN	9.26	4.68
CaO	1.83	2.18	NE	0.00	0.00
Na2O	3.63	3.91	Q	31.64	74.12
K2O	3.47	2.46	OL	0.00	0.00
P2O5	0.00	0.00	FO	0.00	0.00
BaO	0.07	0.03	FA	0.00	0.00
SrO	0.02	0.01	LN	0.00	0.00
Cr2O3	0.00	0.00	HY	1.87	2.62
F	0.00	0.00	EN	1.87	2.62
CL	0.00	0.00	FS	0.00	0.00
SO3	0.00	0.00	DI	0.00	0.00
S	0.00	0.00	WO	0.00	0.00
CO2	0.00	0.00	EN	0.00	0.00
ZrO2	0.03	0.02	FS	0.00	0.00
			WO	0.00	0.00
			AC	0.00	0.00
			AP	0.00	0.00
			IL	0.13	0.12
			SP	0.00	0.00
			RU	0.36	0.64
			PV	0.00	0.00
			C	1.27	1.75
			MT	0.00	0.00
			HEM	2.96	2.61
			CH	0.00	0.00
			HL	0.00	0.00
			FR	0.00	0.00
			TH	0.00	0.00
			PR	0.00	0.00
			NC	0.00	0.00
			CC	0.00	0.00
			Z	0.04	0.03
				98.76	
	98.81				

OXIDE	WT PCT	MOLE PCT
SiO2	70.31	79.40
TiO2	0.42	0.36
Al2O3	14.06	9.36
Fe2O3	2.71	1.15
P2O5	0.00	0.00
MnO	0.04	0.04
CaO	0.76	1.28
Na2O	1.56	1.89
K2O	3.38	3.70
Cr2O3	3.84	2.77
B2O3	0.00	0.00
BaO	0.08	0.04
Gd2O3	0.03	0.02
Cr2O3	0.00	0.00
P2O5	0.00	0.00
CaO	0.00	0.00
Na2O	0.00	0.00
K2O	0.00	0.00
Cr2O3	0.00	0.00
B2O3	0.02	0.01

97.21

OXIDE	WT PCT	MOLE PCT	NORMATIVE MINERALS	WT PCT	MOLE PCT
SiO2	72.32	79.50	KS	0.00	0.00
TiO2	0.47	0.39	KF	0.00	0.00
Al2O3	13.69	8.87	LC	0.00	0.00
Fe2O3	3.04	1.26	NS	0.00	0.00
FeO	0.00	0.00	OR	18.91	5.13
MnO	0.06	0.06	AB	39.01	11.24
MgO	0.66	1.08	AN	7.06	3.83
CaO	1.39	1.64	NE	0.00	0.00
Na2O	4.61	4.91	Q	29.21	73.44
K2O	3.20	2.24	OL	0.00	0.00
P2O5	0.00	0.00	FO	0.00	0.00
BaO	0.06	0.03	FA	0.00	0.00
SrO	0.02	0.01	LN	0.00	0.00
Cr2O3	0.00	0.00	HY	1.64	2.47
F	0.00	0.00	EN	1.64	2.47
CL	0.00	0.00	FS	0.00	0.00
SO3	0.00	0.00	DI	0.00	0.00
S	0.00	0.00	WO	0.00	0.00
CO2	0.00	0.00	EN	0.00	0.00
ZrO2	0.03	0.02	FS	0.00	0.00
			WO	0.00	0.00
			AC	0.00	0.00
			AP	0.00	0.00
BA	568 PPM		IL	0.13	0.13
SR	148 PPM		SP	0.00	0.00
RB	121 PPM		RU	0.40	0.76
ZR	214 PPM		PV	0.00	0.00
RB/SR	0.613		C	0.06	0.08
RB/BA	0.213		MT	0.00	0.00
			HEM	3.04	2.88
			CH	0.00	0.00
			HL	0.00	0.00
			FR	0.00	0.00
			TH	0.00	0.00
			FR	0.00	0.00
			NC	0.00	0.00
			CC	0.00	0.00
			Z	0.04	0.04
99.55				99.50	

99.55

SAMPLE NUMBER 188
00 PL72-188 RQM-AP

OXIDE	WT PCT	MOLE PCT	NORMATIVE MINERALS	WT PCT	MOLE PCT
SiO2	78.55	83.84	KS	0.00	0.00
TiO2	0.04	0.03	KP	0.00	0.00
Al2O3	13.35	8.40	LC	0.00	0.00
Fe2O3	0.48	0.19	NS	0.00	0.00
FeO	0.00	0.00	OR	29.79	6.76
MnO	0.03	0.03	AB	27.16	6.54
MgO	0.11	0.17	AN	2.50	1.13
CaO	0.50	0.57	NE	0.00	0.00
Na2O	3.21	3.32	Q	39.34	82.67
K2O	5.04	3.43	CL	0.00	0.00
P2O5	0.00	0.00	FO	0.00	0.00
BaO	0.01	0.00	FA	0.00	0.00
SrO	0.00	0.00	LN	0.00	0.00
CR2O3	0.00	0.00	HY	0.27	0.34
F	0.00	0.00	EN	0.27	0.34
CL	0.00	0.00	FS	0.00	0.00
SO3	0.00	0.00	DI	0.00	0.00
S	0.00	0.00	WO	0.00	0.00
CO2	0.00	0.00	EN	0.00	0.00
ZrO2	0.01	0.01	FS	0.00	0.00

BA 59 PPM
SR 1 PPM
RB 283 PPM
ZR 66 PPM
RB/SR 283.000
RB/BA 4.772

101.33

SAMPLE NUMBER 232C
00 PL73-232CRS RQM-AP

OXIDE	WT PCT	MOLE PCT	NORMATIVE MINERALS	WT PCT	MOLE PCT
SiO2	76.40	82.88	KS	0.00	0.00
TiO2	0.14	0.11	KP	0.00	0.00
Al2O3	13.40	8.57	LC	0.00	0.00
Fe2O3	0.81	0.33	NS	0.00	0.00
FeO	0.00	0.00	OR	25.29	5.87
MnO	0.04	0.04	AB	28.52	7.02
MgO	0.23	0.37	AN	5.07	2.35
CaO	1.01	1.17	NE	0.00	0.00
Na2O	3.37	3.54	Q	37.88	81.40
K2O	4.28	2.96	OL	0.00	0.00
P2O5	0.00	0.00	FO	0.00	0.00
BaO	0.03	0.01	FA	0.00	0.00
SrO	0.00	0.00	LN	0.00	0.00
CR2O3	0.00	0.00	HY	0.57	0.74
F	0.00	0.00	EN	0.57	0.74
CL	0.00	0.00	FS	0.00	0.00
SO3	0.00	0.00	DI	0.00	0.00
S	0.00	0.00	WO	0.00	0.00
CO2	0.00	0.00	EN	0.00	0.00
ZrO2	0.01	0.01	FS	0.00	0.00

BA 224 PPM
SR 41 PPM
RB 169 PPM
ZR 96 PPM
RB/SR 4.122
RB/BA 0.755

99.72

SAMPLE NUMBER 232F
00 PL73-232FN RQM-AP

OXIDE	WT PCT	MOLE PCT	NORMATIVE MINERALS	WT PCT	MOLE PCT
SiO2	78.48	83.98	KS	0.00	0.00
TiO2	0.05	0.04	KP	0.00	0.00
Al2O3	12.76	8.05	LC	0.00	0.00
Fe2O3	0.47	0.19	NS	0.00	0.00
FeO	0.00	0.00	OR	35.81	8.13
MNO	0.03	0.03	AB	19.80	4.77
MGO	0.10	0.16	AN	4.28	1.95
CAO	0.86	0.99	NE	0.00	0.00
NA2O	2.34	2.43	Q	39.67	83.42
K2O	6.06	4.14	OL	0.00	0.00
P2O5	0.00	0.00	FO	0.00	0.00
BAO	0.01	0.00	FA	0.00	0.00
SRO	0.00	0.00	LN	0.00	0.00
CR2O3	0.00	0.00	HY	0.25	0.31
F	0.00	0.00	EN	0.25	0.31
CL	0.00	0.00	FS	0.00	0.00
SO3	0.00	0.00	DI	0.00	0.00
S	0.00	0.00	WO	0.00	0.00
CO2	0.00	0.00	EN	0.00	0.00
ZRO2	0.00	0.00	FS	0.00	0.00

BA 120 PPM
SR 35 PPM
RB 190 PPM
ZR 36 PPM
RB/SR 5.429
RB/BA 1.589

101.16

SAMPLE NUMBER 233
00 PL73-233 RQM-AP

OXIDE	WT PCT	MOLE PCT	NORMATIVE MINERALS	WT PCT	MOLE PCT
SiO2	76.78	82.22	KS	0.00	0.00
TiO2	0.04	0.03	KP	0.00	0.00
Al2O3	14.84	9.37	LC	0.00	0.00
Fe2O3	0.27	0.11	NS	0.00	0.00
FeO	0.00	0.00	OR	46.21	11.53
MNO	0.03	0.03	AB	15.82	4.19
MGO	0.07	0.11	AN	3.64	1.82
CAO	0.73	0.84	NE	0.00	0.00
NA2O	1.87	1.94	Q	34.29	79.23
K2O	7.82	5.34	OL	0.00	0.00
P2O5	0.00	0.00	FO	0.00	0.00
BAO	0.01	0.00	FA	0.00	0.00
SRO	0.00	0.00	LN	0.00	0.00
CR2O3	0.00	0.00	HY	0.17	0.24
F	0.00	0.00	FN	0.17	0.24
CL	0.00	0.00	FS	0.00	0.00
SO3	0.00	0.00	DI	0.00	0.00
S	0.00	0.00	WO	0.00	0.00
CO2	0.00	0.00	EN	0.00	0.00
ZRO2	0.01	0.01	FS	0.00	0.00

BA 95 PPM
SR 35 PPM
RB 242 PPM
ZR 43 PPM
RB/SR 6.914
RB/BA 2.560

102.47

WT PCT	MOLE PCT
WO	0.00
AC	0.00
AP	0.00
IL	0.06
SP	0.00
RU	0.01
PV	0.00
C	1.97
MT	0.00
HEM	0.27
CH	0.00
HL	0.00
FR	0.00
TH	0.00
PR	0.00
NC	0.00
CC	0.00
Z	0.01

102.46

SAMPLE NUMBER
00 EMBUDO 6 (FULLAGAR AND SHIVER, 1973) RQM-AP

OXIDE	WT PCT	MOLE PCT	NORMATIVE MINERALS	WT PCT	MOLE PCT
SiO2	77.96	83.73	KS	0.00	0.00
TiO2	0.10	0.08	KP	0.00	0.00
Al2O3	13.79	8.73	LC	0.00	0.00
Fe2O3	0.56	0.23	NS	0.00	0.00
FeO	0.00	0.00	OR	31.68	7.05
MnO	0.00	0.00	AB	23.95	5.66
MgO	0.08	0.13	AN	2.08	0.93
CaO	0.42	0.48	NE	0.00	0.00
Na2O	2.83	2.95	Q	39.96	82.41
K2O	5.36	3.67	OL	0.00	0.00
P2O5	0.00	0.00	FO	0.00	0.00
BAO	0.00	0.00	FA	0.00	0.00
SrO	0.00	0.00	LN	0.00	0.00
CR2O3	0.00	0.00	HY	0.20	0.25
P	0.00	0.00	EN	0.20	0.25
CL	0.00	0.00	FS	0.00	0.00
SO3	0.00	0.00	DI	0.00	0.00
S	0.00	0.00	WO	0.00	0.00
CO2	0.00	0.00	EN	0.00	0.00
ZRO2	0.00	0.00	FS	0.00	0.00
			WO	0.00	0.00
			AC	0.00	0.00
			AP	0.00	0.00
			IL	0.00	0.00
			SP	0.00	0.00
			RU	0.10	0.16
			PV	0.00	0.00
			C	2.57	3.12
			HT	0.00	0.00
			HEM	0.56	0.43
			CH	0.00	0.00
			HL	0.00	0.00
			FR	0.00	0.00
			TH	0.00	0.00
			PR	0.00	0.00
			NC	0.00	0.00
			CC	0.00	0.00
			Z	0.00	0.00
				101.10	
					101.10

SAMPLE NUMBER
00 RMBUDO 7 (PULLAGAR AND SHIVER, 1973) RQH-AP

[illegible]

Peñasco Quartz Monzonite

SAMPLE NUMBER 5
00 PL71-5 PQM

OXIDE	WT PCT	MOLE PCT
SiO2	69.52	78.37
TiO2	0.38	0.32
Al2O3	14.11	9.37
Fe2O3	2.68	1.14
FeO	0.00	0.00
MNO	0.04	0.04
MGO	1.05	1.76
CAO	1.71	2.07
NA2O	3.76	4.11
K2O	3.82	2.75
P2O5	0.00	0.00
BAO	0.08	0.04
SRO	0.04	0.03
CR2O3	0.00	0.00
F	0.00	0.00
CL	0.03	0.00
SO3	0.00	0.00
S	0.00	0.00
CO2	0.00	0.00
ZRO2	0.03	0.02

BA 727 PPM
SR 372 PPM
RB 179 PPM
ZR 194 PPM
RB/SR 0.481
RB/BA 0.246

97.22

NORMATIVE MINERALS	WT PCT	MOLE PCT
KS	0.00	0.00
KP	0.00	0.00
LC	0.00	0.00
NS	0.00	0.00
OR	22.58	6.27
AB	31.82	9.38
AN	8.74	4.85
NE	0.00	0.00
Q	27.67	71.21
OL	0.00	0.00
FO	0.00	0.00
FA	0.00	0.00
LN	0.00	0.00
HY	2.61	4.03
EN	2.61	4.03
FS	0.00	0.00
DI	0.00	0.00
WO	0.00	0.00
EN	0.00	0.00
FS	0.00	0.00
WO	0.00	0.00
AC	0.00	0.00
AP	0.00	0.00
IL	0.09	0.09
SP	0.00	0.00
RU	0.33	0.65
PV	0.00	0.00
C	0.59	0.89
MT	0.00	0.00
HEM	2.68	2.59
CH	0.00	0.00
HL	0.00	0.00
FR	0.00	0.00
TH	0.00	0.00
PR	0.00	0.00
NC	0.00	0.00
CC	0.00	0.00
Z	0.04	0.04

97.15

SAMPLE NUMBER
00 EMBUDO 1 (FULLAGAR AND SHIVER, 1973) PL71-5 PQM

OXIDE	WT PCT	MOLE PCT
SiO2	70.84	78.07
TiO2	0.40	0.33
Al2O3	14.73	9.57
Fe2O3	2.81	1.17
FeO	0.00	0.00
MNO	0.00	0.00
MGO	1.03	1.69
CAO	1.79	2.11
NA2O	3.81	4.07
K2O	4.26	2.99
P2O5	0.00	0.00
BAO	0.00	0.00
SRO	0.00	0.00
CR2O3	0.00	0.00
F	0.00	0.00
CL	0.00	0.00
SO3	0.00	0.00
S	0.00	0.00
CO2	0.00	0.00
ZRO2	0.00	0.00

RB 184 PPM
SR 402 PPM

99.67

NORMATIVE MINERALS	WT PCT	MOLE PCT
KS	0.00	0.00
KP	0.00	0.00
LC	0.00	0.00
NS	0.00	0.00
OR	25.18	7.04
AB	32.24	9.58
AN	8.88	4.97
NE	0.00	0.00
Q	27.00	76.00
OL	0.00	0.00
FO	0.00	0.00
FA	0.00	0.00
LN	0.00	0.00
HY	2.57	3.98
EN	2.57	3.98
FS	0.00	0.00
DI	0.00	0.00
WO	0.00	0.00
EN	0.00	0.00
FS	0.00	0.00
WO	0.00	0.00
AC	0.00	0.00
AP	0.00	0.00
IL	0.00	0.00
SP	0.00	0.00
RU	0.40	0.78
PV	0.00	0.00
C	0.60	0.91
MT	0.00	0.00
HEM	2.81	2.74
CH	0.00	0.00
HL	0.00	0.00
FR	0.00	0.00
TH	0.00	0.00
PR	0.00	0.00
NC	0.00	0.00
CC	0.00	0.00
Z	0.00	0.00

99.67

SAMPLE NUMBER 35A
00 PL71-35A PQM

OXIDE	WT PCT	MOLE PCT	NORMATIVE MINERALS	WT PCT	MOLE PCT
SiO2	62.79	73.25	KS	0.00	0.00
TiO2	0.83	0.73	KP	0.00	0.00
AL2O3	15.92	10.95	LC	0.00	0.00
FE2O3	5.78	2.54	NS	0.00	0.00
PFO	0.00	0.00	OR	22.34	6.12
HNO	0.07	0.07	AB	21.24	6.18
MGO	1.72	2.99	AN	15.09	8.27
CAO	2.97	3.71	NE	0.00	0.00
NA2O	2.51	2.84	Q	24.62	62.51
K2O	3.78	2.81	OL	0.00	0.00
P2O5	0.00	0.00	FO	0.00	0.00
BAO	0.12	0.05	FA	0.00	0.00
SRO	0.05	0.03	LN	0.00	0.00
CR2O3	0.00	0.00	HY	4.28	6.51
F	0.00	0.00	EN	4.28	6.51
CL	0.00	0.00	FS	0.00	0.00
SO3	0.00	0.00	DI	0.00	0.00
S	0.00	0.00	WO	0.00	0.00
CO2	0.00	0.00	EN	0.00	0.00
ZRO2	0.04	0.02	FS	0.00	0.00
			WO	0.00	0.00
			AC	0.00	0.00
BA	1074 PPM		AP	0.00	0.00
SR	397 PPM		IL	0.15	0.15
RB	132 PPM		SP	0.00	0.00
ZR	264 PPM		RU	0.75	1.43
RB/SR	0.332		PV	0.00	0.00
RB/BA	0.123		C	2.17	3.25
			MT	0.00	0.00
			HEM	5.78	5.52
			CH	0.00	0.00
			HL	0.00	0.00
			FR	0.00	0.00
			TH	0.00	0.00
			PR	0.00	0.00
			NC	0.00	0.00
			CC	0.00	0.00
			Z	0.06	0.05
96.58			96.48		

SAMPLE NUMBER 35B
00 PL71-35B PQM

OXIDE	WT PCT	MOLE PCT	NORMATIVE MINERALS	WT PCT	MOLE PCT
SiO2	63.29	73.25	KS	0.00	0.00
TiO2	0.83	0.72	KP	0.00	0.00
AL2O3	15.24	10.39	LC	0.00	0.00
FE2O3	6.02	2.62	NS	0.00	0.00
FEO	0.00	0.00	OR	21.39	6.02
HNO	0.08	0.08	AB	23.35	6.98
MGO	1.82	3.14	AN	16.03	9.03
CAO	3.16	3.92	NE	0.00	0.00
NA2O	2.76	3.10	Q	23.72	61.90
K2O	3.62	2.67	OL	0.00	0.00
P2O5	0.00	0.00	FO	0.00	0.00
BAO	0.12	0.05	FA	0.00	0.00
SRO	0.05	0.03	LN	0.00	0.00
CR2O3	0.00	0.00	HY	4.53	7.08
F	0.00	0.00	EN	4.53	7.08
CL	0.00	0.00	FS	0.00	0.00
SO3	0.00	0.00	DI	0.00	0.00
S	0.00	0.00	WO	0.00	0.00
CO2	0.00	0.00	EN	0.00	0.00
ZRO2	0.04	0.02	FS	0.00	0.00
			WO	0.00	0.00
			AC	0.00	0.00
BA	1055 PPM		AP	0.00	0.00
SR	397 PPM		IL	0.17	0.18
RB	150 PPM		SP	0.00	0.00
ZR	277 PPM		BU	0.74	1.45
RB/SR	0.378		PV	0.00	0.00
RB/BA	0.142		C	0.91	1.40
			MT	0.00	0.00
			HEM	6.02	5.91
			CH	0.00	0.00
			HL	0.00	0.00
			FR	0.00	0.00
			TH	0.00	0.00
			PR	0.00	0.00
			NC	0.00	0.00
			CC	0.00	0.00
			Z	0.06	0.05
97.03			96.93		

OXIDE	WT PCT	MOLE PCT	NORMATIVE MINERALS	WT PCT	MOLE PCT
SiO2	68.32	75.43	KS	0.00	0.00
TiO2	0.74	0.61	KP	0.00	0.00
Al2O3	15.09	9.82	LC	0.00	0.00
Fe2O3	5.54	2.30	NS	0.00	0.00
FeO	0.00	0.00	OR	21.69	5.30
MnO	0.06	0.06	AB	22.42	5.82
MgO	1.76	2.90	AN	14.43	7.06
CaO	2.80	3.31	NE	0.00	0.00
Na2O	2.65	2.84	Q	29.98	67.90
K2O	3.67	2.58	OL	0.00	0.00
P2O5	0.00	0.00	FO	0.00	0.00
BaO	0.21	0.09	FA	0.00	0.00
SrO	0.06	0.04	LN	0.00	0.00
Cr2O3	0.00	0.00	HY	4.38	5.94
F	0.00	0.00	EN	4.38	5.94
Cl	0.00	0.00	FS	0.00	0.00
SO3	0.00	0.00	DI	0.00	0.00
S	0.00	0.00	WO	0.00	0.00
CO2	0.00	0.00	EN	0.00	0.00
ZrO2	0.04	0.02	FS	0.00	0.00
			WO	0.00	0.00
			AC	0.00	0.00
			AP	0.00	0.00
BA	1266	PPH	IL	0.13	0.12
SR	473	PPH	SP	0.00	0.00
RB	137	PPH	RU	0.67	1.15
ZR	302	PPH	PV	0.00	0.00
RB/SR		0.290	C	1.47	1.96
RB/BA		0.073	MT	0.00	0.00
			HEM	5.54	4.72
			CH	0.00	0.00
			HL	0.00	0.00
			FR	0.00	0.00
			TH	0.00	0.00
			FR	0.00	0.00
			KC	0.00	0.00
			CC	0.00	0.00
			Z	0.06	0.04
100.94				100.78	

100.94

OXIDE	WT PCT	MOLE PCT	NORMATIVE MINERALS	WT PCT	MOLE PCT
SiO ₂	64.05	73.68	KS	0.00	0.00
TiO ₂	0.73	0.63	KP	0.00	0.00
Al ₂ O ₃	15.87	10.76	LC	0.00	0.00
Fe ₂ O ₃	5.46	2.36	NS	0.00	0.00
FEO	0.00	0.00	OR	18.73	4.90
MNO	0.07	0.07	AB	21.66	6.02
MGO	1.66	2.85	AN	17.90	9.37
CAO	3.50	4.31	NE	0.00	0.00
NA ₂ O	2.56	2.86	Q	26.80	64.97
K ₂ O	3.17	2.33	OL	0.00	0.00
P ₂ O ₅	0.00	0.00	FO	0.00	0.00
BAO	0.22	0.10	FA	0.00	0.00
SRO	0.05	0.03	LN	0.00	0.00
CR ₂ O ₃	0.00	0.00	HY	4.13	6.00
F	0.00	0.00	EN	4.13	6.00
CL	0.00	0.00	FS	0.00	0.00
SO ₃	0.00	0.00	DI	0.00	0.00
S	0.00	0.00	WO	0.00	0.00
CO ₂	0.00	0.00	EN	0.00	0.00
ZR ₂ O	0.04	0.02	FS	0.00	0.00
			WO	0.00	0.00
			AC	0.00	0.00
			AP	0.00	0.00
BA	1997	PPM	IL	0.15	0.14
SR	435	PPM	SP	0.00	0.00
RH	148	PPM	RU	0.65	1.19
ZR	262	PPM	PV	0.00	0.00
RB/SR	0.340		C	1.67	2.38
RH/BA	0.074		MT	0.00	0.00
			HEM	5.46	4.98
			CH	0.00	0.00
			HL	0.00	0.00
			FR	0.00	0.00
			TH	0.00	0.00
			PR	0.00	0.00
			NC	0.00	0.00
			CC	0.00	0.00
			Z	0.06	0.05
97.38				97.22	

97.38

SAMPLE NUMBER 231
00 PL72-231 PQM

OXIDE	WT PCT	MOLE PCT	NORMATIVE MINERALS	WT PCT	MOLE PCT
SiO2	62.89	72.87	KS	0.00	0.00
TiO2	0.83	0.72	KP	0.00	0.00
Al2O3	15.59	10.65	LC	0.00	0.00
Fe2O3	6.03	2.63	NS	0.00	0.00
FeO	0.00	0.00	OR	22.22	6.18
MnO	0.07	0.07	AB	21.41	6.32
MgO	1.93	3.33	AN	16.34	9.10
CaO	3.22	4.00	NE	0.00	0.00
Na2O	2.53	2.84	Q	23.83	61.42
K2O	3.76	2.78	OL	0.00	0.00
P2O5	0.00	0.00	PO	0.00	0.00
BaO	0.13	0.06	FA	0.00	0.00
SrO	0.05	0.03	LN	0.00	0.00
Cr2O3	0.00	0.00	HY	4.81	7.41
F	0.00	0.00	EN	4.81	7.41
CL	0.00	0.00	FS	0.00	0.00
SO3	0.00	0.00	DI	0.00	0.00
S	0.00	0.00	WO	0.00	0.00
CO2	0.00	0.00	EN	0.00	0.00
ZrO2	0.03	0.02	FS	0.00	0.00

BA 1141 PPM
SR 431 PPM
RB 124 PPM
ZR 254 PPM
RB/SR 0.288
RB/BA 0.109

97.06

SAMPLE NUMBER 263
00 PL73-263 PQM

OXIDE	WT PCT	MOLE PCT	NORMATIVE MINERALS	WT PCT	MOLE PCT
SiO2	63.92	73.90	KS	0.00	0.00
TiO2	0.74	0.64	KP	0.00	0.00
Al2O3	15.61	10.64	LC	0.00	0.00
Fe2O3	5.13	2.23	NS	0.00	0.00
FeO	0.00	0.00	OR	23.52	6.61
MnO	0.06	0.06	AB	22.25	6.64
MgO	1.61	2.77	AN	15.44	8.69
CaO	3.02	3.74	NE	0.00	0.00
Na2O	2.63	2.95	Q	24.30	63.27
K2O	3.98	2.94	OL	0.00	0.00
P2O5	0.00	0.00	FO	0.00	0.00
BaO	0.18	0.08	FA	0.00	0.00
SrO	0.05	0.03	LN	0.00	0.00
Cr2O3	0.00	0.00	HY	4.01	6.25
F	0.00	0.00	EN	4.01	6.25
CL	0.00	0.00	FS	0.00	0.00
SO3	0.00	0.00	DI	0.00	0.00
S	0.00	0.00	WO	0.00	0.00
CO2	0.00	0.00	EN	0.00	0.00
ZrO2	0.04	0.02	FS	0.00	0.00

BA 1598 PPM
SR 435 PPM
RB 133 PPM
ZR 283 PPM
RB/SR 0.306
RB/BA 0.083

96.97

SAMPLE NUMBER 96GM
00 PL72-96GM PQM-GM

OXIDE	WT PCT	MOLE PCT	NORMATIVE MINERALS	WT PCT	MOLE PCT
SiO2	65.05	74.88	KS	0.00	0.00
TiO2	0.65	0.56	KP	0.00	0.00
Al2O3	15.39	10.44	LC	0.00	0.00
Fe2O3	4.90	2.12	NS	0.00	0.00
FeO	0.00	0.00	OR	17.79	4.58
MNO	0.06	0.06	AB	24.71	6.75
HGO	1.75	3.00	AN	13.88	7.14
CAO	2.73	3.37	NE	0.00	0.00
NA2O	2.92	3.26	Q	27.93	66.56
K2O	3.01	2.21	OL	0.00	0.00
P2O5	0.00	0.00	FO	0.00	0.00
BAO	0.08	0.04	FA	0.00	0.00
SRO	0.07	0.05	LN	0.00	0.00
CR2O3	0.01	0.00	HY	4.36	6.22
F	0.00	0.00	EN	4.36	6.22
CL	0.00	0.00	FS	0.00	0.00
SO3	0.00	0.00	DI	0.00	0.00
S	0.00	0.00	WO	0.00	0.00
CO2	0.00	0.00	EN	0.00	0.00
ZRO2	0.03	0.02	FS	0.00	0.00
			WO	0.00	0.00
			AC	0.00	0.00
			AP	0.00	0.00
			IL	0.12	0.11
			SP	0.00	0.00
			RU	0.59	1.05
			PV	0.00	0.00
			C	2.24	3.15
			MT	0.00	0.00
			HEM	4.90	4.39
			CH	0.01	0.01
			HL	0.00	0.00
			FR	0.00	0.00
			TH	0.00	0.00
			PR	0.00	0.00
			NC	0.00	0.00
			CC	0.00	0.00
			Z	0.04	0.03

BA 718 PPM
SR 569 PPM
RD 165 PPM
ZA 257 PPM
RB/SR 0.290
RD/BA 0.230

96.65

SAMPLE NUMBER 86
00 PL72-86 PQM-AP

OXIDE	WT PCT	MOLE PCT	NORMATIVE MINERALS	WT PCT	MOLE PCT
SiO2	70.34	78.36	KS	0.00	0.00
TiO2	0.32	0.27	KP	0.00	0.00
Al2O3	15.51	10.18	LC	0.00	0.00
Fe2O3	1.58	0.66	NS	0.00	0.00
FeO	0.00	0.00	OR	35.75	10.88
MNO	0.04	0.04	AB	25.98	8.39
HGO	0.44	0.73	AN	8.85	5.38
CAO	1.67	1.99	NE	0.00	0.00
NA2O	3.07	3.32	Q	24.84	69.99
K2O	6.05	4.30	OL	0.00	0.00
P2O5	0.00	0.00	FO	0.00	0.00
BAO	0.25	0.11	FA	0.00	0.00
SRO	0.04	0.03	LN	0.00	0.00
CR2O3	0.00	0.00	HY	1.10	1.85
F	0.00	0.00	EN	1.10	1.85
CL	0.00	0.00	FS	0.00	0.00
SO3	0.00	0.00	DI	0.00	0.00
S	0.00	0.00	WO	0.00	0.00
CO2	0.00	0.00	EN	0.00	0.00
ZRO2	0.03	0.02	FS	0.00	0.00
			WO	0.00	0.00
			AC	0.00	0.00
			AP	0.00	0.00
			IL	0.09	0.10
			SP	0.00	0.00
			RU	0.27	0.58
			PV	0.00	0.00
			C	0.67	1.11
			MT	0.00	0.00
			HEM	1.58	1.68
			CH	0.00	0.00
			HL	0.00	0.00
			FR	0.00	0.00
			TH	0.00	0.00
			PR	0.00	0.00
			NC	0.00	0.00
			CC	0.00	0.00
			Z	0.04	0.04

BA 2226 PPM
SR 311 PPM
RD 268 PPM
ZH 205 PPM
RH/SR 0.862
RD/BA 0.120

99.34

SAMPLE NUMBER
00 TAI2A (MONTGOMERY, 1953) PQM

OXIDE	WT PCT	MOLE PCT	NORMATIVE MINERALS	WT PCT	MOLE PCT
SiO2	71.11	78.52	KS	0.00	0.00
TiO2	0.41	0.34	KP	0.00	0.00
AL2O3	14.14	9.20	LC	0.00	0.00
FE2O3	1.23	0.51	NS	0.00	0.00
FeO	1.28	1.18	OR	30.26	8.02
MNO	0.05	0.05	AB	24.45	6.88
MGO	0.89	1.46	AN	7.24	3.84
CAO	1.63	1.93	NE	0.00	0.00
NA2O	2.89	3.09	Q	29.90	73.39
K2O	5.12	3.61	OL	0.00	0.00
P2O5	0.15	0.07	FO	0.00	0.00
BAO	0.07	0.03	FA	0.00	0.00
SRO	0.00	0.00	LN	0.00	0.00
CR2O3	0.00	0.00	HY	2.97	4.09
F	0.00	0.00	EN	2.22	3.26
CL	0.00	0.00	FS	0.75	0.84
SO3	0.00	0.00	DI	0.00	0.00
S	0.00	0.00	WO	0.00	0.00
CO2	0.00	0.00	EN	0.00	0.00
ZRO2	0.01	0.01	FS	0.00	0.00
			WO	0.00	0.00
			AC	0.00	0.00
			AP	0.35	0.16
			IL	0.78	0.76
			SP	0.00	0.00
			RU	0.00	0.00
			PV	0.00	0.00
			C	1.19	1.72
			MT	1.78	1.14
			HEM	0.00	0.00
			CH	0.00	0.00
			HL	0.00	0.00
			FR	0.00	0.00
			TH	0.00	0.00
			PR	0.00	0.00
			NC	0.00	0.00
			CC	0.00	0.00
			Z	0.01	0.01
	98.98			98.94	

SAMPLE NUMBER
00 EMBUDO 2 (FULLAGAR AND SHIVER, 1973) PQM

OXIDE	WT PCT	MOLE PCT	NORMATIVE MINERALS	WT PCT	MOLE PCT
SiO2	66.13	72.40	KS	0.00	0.00
TiO2	0.81	0.67	KP	0.00	0.00
AL2O3	15.09	9.74	LC	0.00	0.00
FE2O3	5.95	2.45	NS	0.00	0.00
FeO	0.00	0.00	OR	21.10	6.79
MNO	0.00	0.00	AB	35.62	12.18
MGO	2.31	3.77	AN	11.73	7.56
CAO	3.42	4.01	NE	0.00	0.00
NA2O	4.21	4.47	Q	18.34	54.70
K2O	3.57	2.49	OL	0.00	0.00
P2O5	0.00	0.00	FO	0.00	0.00
BAO	0.00	0.00	FA	0.00	0.00
SRO	0.00	0.00	LN	0.00	0.00
CR2O3	0.00	0.00	HY	4.89	8.72
F	0.00	0.00	EN	4.88	8.72
CL	0.00	0.00	FS	0.00	0.00
SO3	0.00	0.00	DI	1.88	1.55
S	0.00	0.00	WO	1.01	0.78
CO2	0.00	0.00	EN	0.87	0.78
ZRO2	0.00	0.00	FS	0.00	0.00
			WO	0.00	0.00
			AC	0.00	0.00
			AP	0.00	0.00
			IL	0.00	0.00
			SP	1.99	1.82
			RU	0.00	0.00
			PV	0.00	0.00
			C	0.00	0.00
			MT	0.00	0.00
			HEM	5.95	6.68
			CH	0.00	0.00
			HL	0.00	0.00
			FR	0.00	0.00
			TH	0.00	0.00
			PR	0.00	0.00
			NC	0.00	0.00
			CC	0.00	0.00
			Z	0.00	0.00
				101.49	
	101.49				

SAMPLE NUMBER 5AP1
00 PL73-5AP1 PQM AP

OXIDE	WT PCT	MOLE PCT
SiO2	74.44	81.10
TiO2	0.21	0.17
Al2O3	14.25	9.15
Fe2O3	0.95	0.39
FeO	0.00	0.00
MnO	0.03	0.03
MgO	0.39	0.63
CaO	1.08	1.26
Na2O	3.44	3.63
K2O	5.11	3.55
P2O5	0.00	0.00
BaO	0.14	0.06
SrO	0.02	0.01
Cr2O3	0.00	0.00
F	0.00	0.00
Cl	0.00	0.00
SO3	0.00	0.00
S	0.00	0.00
CO2	0.00	0.00
ZrO2	0.01	0.01

BA 1270 PPM
SR 163 PPM
RB 189 PPM
ZR 97 PPM
RB/SR 1.160
RB/BA 0.149

100.07

NORMATIVE MINERALS	WT PCT	MOLE PCT
KS	0.00	0.00
KP	0.00	0.00
LC	0.00	0.00
NS	0.00	0.00
OR	30.20	7.89
AB	29.11	8.07
AN	5.67	2.96
NE	0.00	0.00
Q	31.84	77.02
OL	0.00	0.00
FO	0.00	0.00
FA	0.00	0.00
LN	0.00	0.00
HY	0.97	1.41
EN	0.97	1.41
FS	0.00	0.00
DI	0.00	0.00
WO	0.00	0.00
EN	0.00	0.00
FS	0.00	0.00
WO	0.00	0.00
AC	0.00	0.00
AP	0.00	0.00
IL	0.06	0.06
SP	0.00	0.00
RU	0.18	0.32
PV	0.00	0.00
C	0.98	1.40
MT	0.00	0.00
HEM	0.95	0.86
CH	0.00	0.00
HL	0.00	0.00
FR	0.00	0.00
TH	0.00	0.00
PR	0.00	0.00
NC	0.00	0.00
CC	0.00	0.00
Z	0.01	0.01
	99.97	

Pegmatites

SAMPLE NUMBER 45-B
00 PL71-45B PEG

OXIDE	WT PCT	MOLE PCT
SiO2	73.90	80.62
TiO2	0.00	0.00
Al2O3	16.23	10.44
Fe2O3	0.31	0.13
FeO	0.00	0.00
MNO	0.07	0.06
MGO	0.07	0.11
CAO	0.38	0.44
NA2O	4.37	4.62
K2O	5.12	3.56
P2O5	0.00	0.00
BAO	0.01	0.00
SRO	0.00	0.00
CR2O3	0.00	0.00
F	0.00	0.00
CL	0.00	0.00
SO3	0.00	0.00
S	0.00	0.00
CO2	0.00	0.00
ZRO2	0.01	0.01

BA 59 PPM
SR 19 PPM
RE 1102 PPM
ZR 54 PPM
RB/SR 58.000
RB/BA 18.581

100.47

NORMATIVE MINERALS	WT PCT	MOLE PCT
KS	0.00	0.00
KP	0.00	0.00
LC	0.00	0.00
NS	0.00	0.00
OR	30.26	8.65
AB	36.98	11.22
AN	1.90	1.09
NE	0.00	0.00
Q	27.95	74.06
OL	0.00	0.00
PO	0.00	0.00
FA	0.00	0.00
LN	0.00	0.00
HY	0.17	0.28
EN	0.17	0.28
FS	0.00	0.00
DI	0.00	0.00
WO	0.00	0.00
EN	0.00	0.00
FS	0.00	0.00
WO	0.00	0.00
AC	0.00	0.00
AP	0.00	0.00
IL	0.00	0.00
SP	0.00	0.00
RU	0.00	0.00
PV	0.00	0.00
C	2.80	4.38
MT	0.23	0.16
HEM	0.15	0.15
CH	0.00	0.00
HL	0.00	0.00
FR	0.00	0.00
TH	0.00	0.00
PR	0.00	0.00
NC	0.00	0.00
CC	0.00	0.00
Z	0.01	0.01

100.46

SAMPLE NUMBER 5AP2
00 PL73-5AP2 PEG-AP

OXIDE	WT PCT	MOLE PCT
SiO2	75.40	81.15
TiO2	0.02	0.02
Al2O3	15.24	9.67
Fe2O3	0.48	0.19
FeO	0.00	0.00
MNO	0.02	0.02
MGO	0.08	0.13
CAO	1.02	1.18
NA2O	3.15	3.29
K2O	6.22	4.27
P2O5	0.00	0.00
BAO	0.02	0.01
SRO	0.12	0.07
CR2O3	0.00	0.00
F	0.00	0.00
CL	0.00	0.00
SO3	0.00	0.00
S	0.00	0.00
CO2	0.00	0.00
ZRO2	0.03	0.02

BA 140 PPM
SR 1015 PPM
RB 125 PPM
ZR 200 PPM
RB/SR 0.123
RB/BA 0.893

101.80

NORMATIVE MINERALS	WT PCT	MOLE PCT
KS	0.00	0.00
KP	0.00	0.00
LC	0.00	0.00
NS	0.00	0.00
OR	36.76	9.89
AB	26.65	7.61
AN	5.42	2.92
NE	0.00	0.00
Q	30.80	76.78
OL	0.00	0.00
PO	0.00	0.00
FA	0.00	0.00
LN	0.00	0.00
HY	0.20	0.30
EN	0.20	0.30
FS	0.00	0.00
DI	0.00	0.00
WO	0.00	0.00
EN	0.00	0.00
FS	0.00	0.00
WO	0.00	0.00
AC	0.00	0.00
AP	0.00	0.00
IL	0.04	0.04
SP	0.00	0.00
RU	0.00	0.00
PV	0.00	0.00
C	1.34	1.97
MT	0.01	0.00
HEM	0.47	0.45
CH	0.00	0.00
HL	0.00	0.00
FR	0.00	0.00
TH	0.00	0.00
PR	0.00	0.00
NC	0.00	0.00
CC	0.00	0.00
Z	0.04	0.04

101.73

SAMPLE NUMBER 223
00 PL72-223 PEG (AB-Q)

OXIDE	WT PCT	MOLE PCT
SiO2		
TiO2		
Al2O3		
Fe2O3	0.30	0.12
FeO	0.00	0.00
MnO		
HgO	0.07	0.11
CaO		
Na2O	7.60	8.06
K2O		
P2O5	0.00	0.00
BaO	0.00	0.00
SrO	0.01	0.01
Cr2O3	0.00	0.00
F	0.00	0.00
CL	0.00	0.00
SO3	0.00	0.00
S	0.00	0.00
CO2	0.00	0.00
ZrO2	0.01	0.01

BA	33 PPM
SR	47 PPM
RB	107 PPM
ZR	92 PPM
RB/SR	2.277
RB/BA	3.238

APPENDIX IV

Quantitative Electron Microprobe Analyses of Feldspars from the Dixon-Peñasco Area and of Synthetic Glasses and Feldspars from Experimental Runs

The electron microprobe analyses presented here were done on the School of Earth Sciences' ARL EMX three-channel microprobe using an acceleration potential of 20 kV. Sample current was between 0.01 and 0.05 μA depending on susceptibility of sample to damage by electron bombardment. Beam size was generally 2 to 3 μm . Counting time was 300 sec for quantitative analyses of barium and correspondingly less for more abundant elements. Care was taken to avoid sodium loss in the analyses of the crystalline materials but the hydrous synthetic glasses are very susceptible to degradation by the electron beam and as a result some such analyses have low sodium. Considerable damage can be done to the glasses, however, before significant changes in the counting rate for barium result. Since the barium analyses were of primary concern, accuracy of sodium analyses was sometimes sacrificed in order to gain precision in the barium analyses at low counting rates. All of the glass analyses show low totals, this being due to both high water contents (up to 12 weight percent) and in some instances sodium loss.

Drift corrected raw intensity data were corrected for deadtime, background, absorption, characteristic fluorescence, backscatter, and ionization-penetration losses, using a modified version of Colby's

(1968) MAGIC IV program. Typical analyses with estimates of precision based on replicate analyses are given below.

Reference

Colby, J. W., 1968, Quantitative microprobe analysis of thin insulating films, in Newkirk, J., Mallett, G., and Pfeiffer, H., eds., *Advances in X-ray analysis*, v. II: New York, Plenum Press, p. 287.

<u>Oxide</u>	<u>Wt. percent</u>	<u>2 sigma limits</u>	<u>Estimated detection limit</u>
Na ₂ O	0.46	±0.04	300 ppm
K ₂ O	16.02	±0.30	200
CaO	0.00	±0.01	100
Al ₂ O ₃	18.26	±0.90	500
SiO ₂	<u>64.70</u>	±1.30	200
Total	99.47		
Ba	240 ppm	±100 ppm	100 ppm
Na ₂ O	11.15	±0.25	300 ppm
K ₂ O	0.12	±0.06	200
CaO	0.46	±0.04	100
Al ₂ O ₃	20.03	±0.90	500
SiO ₂	<u>68.59</u>	±1.40	200
Total	100.37		
Ba	160 ppm	±100 ppm	100 ppm

IVa. Vadito Group Amphibolite (Metabasalt)

Amph Plg3		Amp Plg2		Amph Plg1	
<u>Oxide</u>	<u>Wt. %</u>	<u>Oxide</u>	<u>Wt. %</u>	<u>Oxide</u>	<u>Wt. %</u>
Na ₂ O	8.12	Na ₂ O	9.02	Na ₂ O	7.18
K ₂ O	0.19	K ₂ O	0.14	K ₂ O	0.14
CaO	5.25	CaO	4.41	CaO	6.08
BaO	0.04	BaO	0.02	BaO	0.00
Al ₂ O ₃	23.37	Al ₂ O ₃	22.98	Al ₂ O ₃	23.98
SiO ₂	62.93	SiO ₂	64.15	SiO ₂	61.77
Total	99.89	Total	100.72	Total	99.15
Ba	340 ppm	Ba	140 ppm	Ba	30 ppm
	Mo1 %		Mo1 %		Mo1 %
Ab	72.81	Ab	78.09	Ab	67.52
Or	1.12	Or	0.78	Or	0.89
An	26.00	An	21.10	An	31.58
Cn	0.07	Cn	0.03	Cn	0.01

IVb. Puntigudo Granite Porphyry

68 Plg1		68 Plg2		68 Plg2.1	
<u>Oxide</u>	<u>Wt. %</u>	<u>Oxide</u>	<u>Wt. %</u>	<u>Oxide</u>	<u>Wt.%</u>
Na ₂ O	11.83	Na ₂ O	11.43	Na ₂ O	11.45
K ₂ O	0.03	K ₂ O	0.12	K ₂ O	0.12
CaO	0.17	CaO	0.81	CaO	0.81
BaO	0.00	BaO	0.01	BaO	0.01
Al ₂ O ₃	19.41	Al ₂ O ₃	20.48	Al ₂ O ₃	19.53
SiO ₂	68.54	SiO ₂	67.65	SiO ₂	68.42
Total	99.98	Total	100.50	Total	100.33
Ba	30 ppm	Ba	80 ppm	Ba	80 ppm
	Mo1 %		Mo1 %		Mo1 %
Ab	99.01	Ab	95.62	Ab	95.62
Or	0.19	Or	0.63	Or	0.63
An	0.79	An	3.73	An	3.73
Cn	0.01	Cn	0.02	Cn	0.02

68 Ksp1		68 Ksp2		68 Ksp3		68 Ksp4	
<u>Oxide</u>	<u>Wt. %</u>	<u>Oxide</u>	<u>Wt. %</u>	<u>Oxide</u>	<u>Wt. %</u>	<u>Oxide</u>	<u>Wt. %</u>
Na ₂ O	0.44	Na ₂ O	0.37	Na ₂ O	0.23	Na ₂ O	0.28
K ₂ O	15.95	K ₂ O	15.91	K ₂ O	16.43	K ₂ O	16.43
CaO	0.00	CaO	0.00	CaO	0.00	CaO	0.00
BaO	0.67	BaO	1.09	BaO	0.25	BaO	0.18
Al ₂ O ₃	18.52	Al ₂ O ₃	18.57	Al ₂ O ₃	18.34	Al ₂ O ₃	18.09
SiO ₂	63.62	SiO ₂	63.65	SiO ₂	64.25	SiO ₂	64.17
Total	99.20	Total	99.59	Total	99.51	Total	99.15
Ba	6030 ppm	Ba	9720 ppm	Ba	2230 ppm	Ba	1640 ppm
	Mol %		Mol %		Mol %		Mol %
Ab	3.94	Ab	3.33	Ab	2.11	Ab	2.50
Or	94.83	Or	94.69	Or	97.44	Or	97.17
An	0.00	An	0.00	An	0.00	An	0.00
Cn	1.23	Cn	1.98	Cn	0.45	Cn	0.33

127FN Ksp1

Oxide	Wt. %
Na ₂ O	0.62
K ₂ O	15.92
CaO	0.01
BaO	0.02
Al ₂ O ₃	18.13
SiO ₂	65.15
Total	99.85
Ba	160 ppm
	Mol %
Ab	5.55
Or	94.38
An	0.04
Cn	0.03

127FN Ksp2

Oxide	Wt. %
Na ₂ O	1.34
K ₂ O	15.42
CaO	0.01
BaO	0.01
Al ₂ O ₃	18.31
SiO ₂	64.83
Total	99.92
Ba	120 ppm
	Mol %
Ab	11.67
Or	88.24
An	0.07
Cn	0.02

127F Plg2

Oxide	Wt. %
Na ₂ O	5.92
K ₂ O	2.38
CaO	0.88
BaO	0.01
Al ₂ O ₃	19.97
SiO ₂	66.89
Total	96.05
Ba	80 ppm
	Mol %
Ab	74.21
Or	19.68
An	6.08
Cn	0.02

127F Plg1

Oxide	Wt. %
Na ₂ O	10.76
K ₂ O	0.11
CaO	0.72
BaO	0.00
Al ₂ O ₃	20.52
SiO ₂	68.22
Total	100.33
Ba	30 ppm
	Mol %
Ab	95.81
Or	0.66
An	3.52
Cn	0.01

IVc. Rana Quartz Monzonite

74 Plg1		74 Plg2		74 Plg3		74 Plg4	
Oxide	Wt. %	Oxide	Wt. %	Oxide	Wt. %	Oxide	Wt. %
Na ₂ O	10.85	Na ₂ O	8.32	Na ₂ O	8.42	Na ₂ O	7.96
K ₂ O	0.19	K ₂ O	0.14	K ₂ O	0.16	K ₂ O	0.13
CaO	1.89	CaO	5.51	CaO	5.31	CaO	6.12
BaO	0.03	BaO	0.02	BaO	0.02	BaO	0.00
Al ₂ O ₃	21.04	Al ₂ O ₃	22.79	Al ₂ O ₃	23.81	Al ₂ O ₃	24.74
SiO ₂	67.26	SiO ₂	62.81	SiO ₂	61.74	SiO ₂	61.06
Total	101.26	Total	99.59	Total	99.46	Total	100.02
Ba	250 ppm	Ba	140 ppm	Ba	200 ppm	Ba	30 ppm
Mol %		Mol %		Mol %		Mol %	
Ab	90.23	Ab	72.58	Ab	73.45	Ab	69.67
Or	1.04	Or	0.82	Or	0.93	Or	0.77
An	8.68	An	26.57	An	25.58	An	29.56
Cn	0.05	Cn	0.03	Cn	0.04	Cn	0.01

74 Plg5	
<u>Oxide</u>	<u>Wt. %</u>
Na ₂ O	9.19
K ₂ O	1.06
CaO	1.11
BaO	0.01
Al ₂ O ₃	21.44
SiO ₂	65.54
Total	98.34
Ba	80 ppm
	<u>Mol %</u>
Ab	87.49
Or	6.65
An	5.83
Cn	0.02

74 Ksp1	
<u>Oxide</u>	<u>Wt. %</u>
Na ₂ O	0.55
K ₂ O	15.76
CaO	0.01
BaO	0.59
Al ₂ O ₃	18.46
SiO ₂	64.60
Total	99.96
Ba	5280 ppm
	<u>Mol %</u>
Ab	4.99
Or	93.90
An	0.03
Cn	1.08

74 Ksp2	
<u>Oxide</u>	<u>Wt. %</u>
Na ₂ O	0.56
K ₂ O	15.73
CaO	0.01
BaO	0.54
Al ₂ O ₃	18.47
SiO ₂	64.39
Total	99.69
Ba	4830 ppm
	<u>Mol %</u>
Ab	5.07
Or	93.90
An	0.04
Cn	0.99

14A Plg1	
<u>Oxide</u>	<u>Wt. %</u>
Na ₂ O	9.68
K ₂ O	0.11
CaO	3.14
BaO	0.00
Al ₂ O ₃	22.42
SiO ₂	65.23
Total	100.59
Ba	30 ppm
	<u>Mol %</u>
Ab	84.24
Or	0.65
An	15.10
Cn	0.01

14C Plg1	
<u>Oxide</u>	<u>Wt. %</u>
Na ₂ O	10.77
K ₂ O	0.10
CaO	1.52
BaO	0.04
Al ₂ O ₃	21.60
SiO ₂	67.08
Total	101.12
Ba	390 ppm
	Mol %
Ab	92.14
Or	0.59
An	7.20
Cn	0.08

14E Plg1	
<u>Oxide</u>	<u>Wt. %</u>
Na ₂ O	0.90
K ₂ O	2.09
CaO	4.83
BaO	0.00
Al ₂ O ₃	22.29
SiO ₂	61.35
Total	91.45
Ba	30 ppm
	Mol %
Ab	18.18
Or	27.85
An	53.96
Cn	0.01

14E Plg2	
<u>Oxide</u>	<u>Wt. %</u>
Na ₂ O	7.90
K ₂ O	0.14
CaO	6.95
BaO	0.00
Al ₂ O ₃	25.63
SiO ₂	60.86
Total	101.49
Ba	30 ppm
	Mol %
Ab	66.76
Or	0.79
An	32.44
Cn	0.01

14B Ksp1	
<u>Oxide</u>	<u>Wt. %</u>
Na ₂ O	0.61
K ₂ O	15.82
CaO	0.01
BaO	0.54
Al ₂ O ₃	18.50
SiO ₂	64.33
Total	99.81
Ba	4830 ppm
	Mol %
Ab	5.44
Or	93.52
An	0.06
Cn	0.98

14B Ksp2		228 Plg1		228 Plg2		228 Plg3	
<u>Oxide</u>	<u>Wt. %</u>	<u>Oxide</u>	<u>Wt. %</u>	<u>Oxide</u>	<u>Wt. %</u>	<u>Oxide</u>	<u>Wt. %</u>
Na ₂ O	0.53	Na ₂ O	1.16	Na ₂ O	8.59	Na ₂ O	8.23
K ₂ O	15.98	K ₂ O	2.07	K ₂ O	0.12	K ₂ O	0.73
CaO	0.02	CaO	5.71	CaO	5.33	CaO	4.56
BaO	0.39	BaO	0.04	BaO	0.02	BaO	0.02
Al ₂ O ₃	18.55	Al ₂ O ₃	23.22	Al ₂ O ₃	23.86	Al ₂ O ₃	24.01
SiO ₂	64.49	SiO ₂	60.84	SiO ₂	62.37	SiO ₂	62.43
Total	99.96	Total	93.05	Total	100.29	Total	99.98
Ba	3460 ppm	Ba	370 ppm	Ba	140 ppm	Ba	170 ppm
	<u>Mol %</u>		<u>Mol %</u>		<u>Mol %</u>		<u>Mol %</u>
Ab	4.77	Ab	20.46	Ab	73.93	Ab	73.26
Or	94.44	Or	23.90	Or	0.68	Or	4.28
An	0.09	An	55.49	An	25.36	An	22.42
Cn	0.70	Cn	0.15	Cn	0.03	Cn	0.03

228 Plg4

Oxide	Wt. %
Na ₂ O	11.63
K ₂ O	0.11
CaO	0.26
BaO	0.00
Al ₂ O ₃	19.86
SiO ₂	69.33
Total	101.20
Ba	30 ppm
	Mol %
Ab	98.14
Or	0.64
An	1.21
Cn	0.01

228 Ksp1

Oxide	Wt. %
Na ₂ O	0.46
K ₂ O	16.05
CaO	0.01
BaO	0.50
Al ₂ O ₃	18.29
SiO ₂	64.47
Total	99.79
Ba	4510 ppm
	Mol %
Ab	4.13
Or	94.92
An	0.04
Cn	0.91

228 Ksp2

Oxide	Wt. %
Na ₂ O	0.44
K ₂ O	16.04
CaO	0.00
BaO	0.45
Al ₂ O ₃	18.30
SiO ₂	64.53
Total	99.77
Ba	4020 ppm
	Mol %
Ab	3.98
Or	95.21
An	0.00
Cn	0.82

193 Plg1

Oxide	Wt. %
Na ₂ O	10.79
K ₂ O	0.19
CaO	0.76
BaO	0.04
Al ₂ O ₃	20.45
SiO ₂	66.98
Total	99.22
Ba	390 ppm
	Mol %
Ab	95.08
Or	1.13
An	3.71
Cn	0.08

193 Plg2

<u>Oxide</u>	<u>Wt. %</u>
Na ₂ O	8.83
K ₂ O	1.09
CaO	2.20
BaO	0.02
Al ₂ O ₃	21.16
SiO ₂	65.84
Total	99.14

Ba 140 ppm

Mol %

Ab	82.00
Or	6.68
An	11.29
Cn	0.03

193 Ksp1

<u>Oxide</u>	<u>Wt. %</u>
Na ₂ O	0.56
K ₂ O	15.93
CaO	0.01
BaO	0.43
Al ₂ O ₃	18.21
SiO ₂	63.86
Total	98.99

Ba 3860 ppm

Mol %

Ab	4.99
Or	94.18
An	0.05
Cn	0.78

193 Ksp2

<u>Oxide</u>	<u>Wt. %</u>
Na ₂ O	0.59
K ₂ O	15.93
CaO	0.01
BaO	0.42
Al ₂ O ₃	18.43
SiO ₂	64.00
Total	99.37

Ba 3730 ppm

Mol %

Ab	5.31
Or	93.88
An	0.06
Cn	0.75

232CRS Plg1

<u>Oxide</u>	<u>Wt. %</u>
Na ₂ O	9.69
K ₂ O	0.13
CaO	3.55
BaO	0.02
Al ₂ O ₃	22.44
SiO ₂	64.84
Total	100.68

Ba 200 ppm

Mol %

Ab	82.52
Or	0.72
An	16.72
Cn	0.04

232CRS Plg2		232CRS Plg3		232CRS Plg4		232CRS Plg5	
<u>Oxide</u>	<u>Wt. %</u>	<u>Oxide</u>	<u>Wt. %</u>	<u>Oxide</u>	<u>Wt. %</u>	<u>Oxide</u>	<u>Wt. %</u>
Na ₂ O	11.66	Na ₂ O	9.98	Na ₂ O	11.70	Na ₂ O	11.11
K ₂ O	0.16	K ₂ O	0.14	K ₂ O	0.15	K ₂ O	0.14
CaO	0.39	CaO	3.46	CaO	0.28	CaO	0.41
BaO	0.01	BaO	0.04	BaO	0.01	BaO	0.02
Al ₂ O ₃	19.60	Al ₂ O ₃	22.27	Al ₂ O ₃	19.83	Al ₂ O ₃	20.15
SiO ₂	69.08	SiO ₂	65.21	SiO ₂	68.47	SiO ₂	70.08
Total	101.09	Total	100.44	Total	101.92	Total	101.92
Ba	80 ppm	Ba	370 ppm	Ba	80 ppm	Ba	170 ppm
	<u>Mol %</u>		<u>Mol %</u>		<u>Mol %</u>		<u>Mol %</u>
Ab	97.34	Ab	83.21	Ab	97.88	Ab	97.16
Or	0.86	Or	0.76	Or	0.82	Or	0.80
An	1.79	An	15.96	An	1.28	An	2.00
Cn	0.02	Cn	0.07	Cn	0.02	Cn	0.03

232CRS Ksp1

<u>Oxide</u>	<u>Wt. %</u>
--------------	--------------

Na ₂ O	0.55
-------------------	------

K ₂ O	15.84
------------------	-------

CaO	0.00
-----	------

BaO	0.60
-----	------

Al ₂ O ₃	18.51
--------------------------------	-------

SiO ₂	64.45
------------------	-------

Total	99.95
-------	-------

Ba	5360 ppm
----	----------

Mol %

Ab	4.95
----	------

Or	93.96
----	-------

An	0.00
----	------

Cn	1.09
----	------

232CRS Ksp2

<u>Oxide</u>	<u>Wt. %</u>
--------------	--------------

Na ₂ O	0.50
-------------------	------

K ₂ O	16.09
------------------	-------

CaO	0.01
-----	------

BaO	0.16
-----	------

Al ₂ O ₃	18.31
--------------------------------	-------

SiO ₂	64.82
------------------	-------

Total	99.88
-------	-------

Ba	1460 ppm
----	----------

Mol %

Ab	4.48
----	------

Or	95.19
----	-------

An	0.03
----	------

Cn	0.30
----	------

232FN Plg1

<u>Oxide</u>	<u>Wt. %</u>
--------------	--------------

Na ₂ O	9.71
-------------------	------

K ₂ O	0.30
------------------	------

CaO	3.71
-----	------

BaO	0.02
-----	------

Al ₂ O ₃	22.69
--------------------------------	-------

SiO ₂	64.37
------------------	-------

Total	100.79
-------	--------

Ba	140 ppm
----	---------

Mol %

Ab	81.19
----	-------

Or	1.65
----	------

An	17.13
----	-------

Cn	0.03
----	------

232FN P1g2

<u>Oxide</u>	<u>Wt. %</u>
Na ₂ O	11.52
K ₂ O	0.14
CaO	0.78
BaO	0.00
Al ₂ O ₃	20.83
SiO ₂	67.84
Total	100.75

Ba 30 ppm

Mol %

Ab	95.64
Or	0.79
An	3.57
Cn	0.01

232FN Ksp1

<u>Oxide</u>	<u>Wt. %</u>
Na ₂ O	0.38
K ₂ O	16.23
CaO	0.00
BaO	0.04
Al ₂ O ₃	18.18
SiO ₂	64.68
Total	99.50

Ba 360 ppm

Mol %

Ab	3.46
Or	96.47
An	0.00
Cn	0.07

232FN Ksp2

<u>Oxide</u>	<u>Wt. %</u>
Na ₂ O	0.46
K ₂ O	16.02
CaO	0.00
BaO	0.03
Al ₂ O ₃	18.26
SiO ₂	64.70
Total	99.47

Ba 240 ppm

Mol %

Ab	4.15
Or	95.79
An	0.01
Cn	0.05

IVd. Peñasco Quartz Monzonite

92 Ksp1		92 Ksp2		92 Plg1		92 Plg2	
<u>Oxide</u>	<u>Wt. %</u>	<u>Oxide</u>	<u>Wt. %</u>	<u>Oxide</u>	<u>Wt. %</u>	<u>Oxide</u>	<u>Wt. %</u>
Na ₂ O	0.61	Na ₂ O	0.54	Na ₂ O	7.75	Na ₂ O	7.88
K ₂ O	15.43	K ₂ O	15.67	K ₂ O	0.15	K ₂ O	1.11
CaO	0.00	CaO	0.01	CaO	7.29	CaO	4.83
BaO	1.16	BaO	0.90	BaO	0.03	BaO	0.02
Al ₂ O ₃	18.59	Al ₂ O ₃	18.59	Al ₂ O ₃	25.90	Al ₂ O ₃	24.44
SiO ₂	64.18	SiO ₂	64.29	SiO ₂	60.68	SiO ₂	61.77
Total	99.98	Total	99.99	Total	101.79	Total	100.06
Ba	10430 ppm	Ba	8080 ppm	Ba	230 ppm	Ba	200 ppm
	Mol %		Mol %		Mol %		Mol %
Ab	5.53	Ab	4.86	Ab	65.26	Ab	69.81
Or	92.32	Or	93.45	Or	0.81	Or	6.48
An	0.01	An	0.03	An	33.89	An	23.67
Cn	2.14	Cn	1.65	Cn	0.04	Cn	0.04

92 Plg2.1	
<u>Oxide</u>	<u>Wt. %</u>
Na ₂ O	7.89
K ₂ O	0.12
CaO	4.82
BaO	0.02
Al ₂ O ₃	24.46
SiO ₂	61.84
Total	99.16
Ba	200 ppm
	Mol %
Ab	74.18
Or	0.73
An	25.05
Cn	0.04

92 Plg3	
<u>Oxide</u>	<u>Wt. %</u>
Na ₂ O	11.28
K ₂ O	0.13
CaO	0.59
BaO	0.05
Al ₂ O ₃	20.21
SiO ₂	68.56
Total	100.81
Ba	420 ppm
	Mol %
Ab	96.40
Or	0.71
An	2.80
Cn	0.08

96C Ksp1-01	
<u>Oxide</u>	<u>Wt. %</u>
Na ₂ O	5.54
K ₂ O	10.30
CaO	1.77
BaO	0.66
Al ₂ O ₃	21.41
SiO ₂	64.52
Total	104.20
Ba	5900 ppm
	Mol %
Ab	41.28
Or	50.46
An	7.27
Cn	0.99

96C Ksp1-02	
<u>Oxide</u>	<u>Wt. %</u>
Na ₂ O	5.53
K ₂ O	10.79
CaO	0.11
BaO	0.28
Al ₂ O ₃	21.55
SiO ₂	67.27
Total	105.54
Ba	2540 ppm
	Mol %
Ab	43.39
Or	55.67
An	0.48
Cn	0.45

96C Ksp1-03		96C Ksp1-04		96C Ksp1-05		96C Ksp1-06	
<u>Oxide</u>	<u>Wt. %</u>	<u>Oxide</u>	<u>Wt. %</u>	<u>Oxide</u>	<u>Wt. %</u>	<u>Oxide</u>	<u>Wt. %</u>
Na ₂ O	0.48	Na ₂ O	3.80	Na ₂ O	0.58	Na ₂ O	1.04
K ₂ O	16.07	K ₂ O	8.35	K ₂ O	15.51	K ₂ O	15.16
CaO	0.00	CaO	0.09	CaO	0.00	CaO	0.00
BaO	0.35	BaO	0.45	BaO	0.86	BaO	0.55
Al ₂ O ₃	21.08	Al ₂ O ₃	22.01	Al ₂ O ₃	19.64	Al ₂ O ₃	20.09
SiO ₂	65.93	SiO ₂	67.47	SiO ₂	65.75	SiO ₂	66.55
Total	103.91	Total	102.16	Total	102.34	Total	103.38
Ba	3130 ppm	Ba	4000 ppm	Ba	7740 ppm	Ba	4940 ppm
	<u>Mol %</u>		<u>Mol %</u>		<u>Mol %</u>		<u>Mol %</u>
Ab	4.29	Ab	40.29	Ab	5.29	Ab	9.32
Or	95.06	Or	58.21	Or	93.12	Or	89.67
An	0.01	An	0.55	An	0.00	An	0.00
Cn	0.64	Cn	0.96	Cn	1.59	Cn	1.00

96C Ksp1-07

<u>Oxide</u>	<u>Wt. %</u>
Na ₂ O	0.54
K ₂ O	15.97
CaO	0.00
BaO	0.44
Al ₂ O ₃	18.15
SiO ₂	65.38
Total	100.48

Ba 3960 ppm

Mol %

Ab	4.86
Or	94.34
An	0.00
Cn	0.80

96C Ksp1-08

<u>Oxide</u>	<u>Wt. %</u>
Na ₂ O	0.49
K ₂ O	16.11
CaO	0.00
BaO	0.51
Al ₂ O ₃	19.19
SiO ₂	65.62
Total	101.92

Ba 4530 ppm

Mol %

Ab	4.40
Or	94.69
An	0.00
Cn	0.91

96C Ksp1-09

<u>Oxide</u>	<u>Wt. %</u>
Na ₂ O	0.84
K ₂ O	15.30
CaO	0.00
BaO	0.45
Al ₂ O ₃	18.15
SiO ₂	65.35
Total	100.10

Ba 4030 ppm

Mol %

Ab	7.68
Or	91.49
An	0.00
Cn	0.83

96C Ksp1-10

<u>Oxide</u>	<u>Wt. %</u>
Na ₂ O	0.54
K ₂ O	15.87
CaO	0.00
BaO	0.60
Al ₂ O ₃	18.90
SiO ₂	64.76
Total	100.68

Ba 5350 ppm

Mol %

Ab	4.87
Or	94.04
An	0.00
Cn	1.09

96C Ksp2-01		96C Ksp2-02		96C Ksp2-03		96C Ksp2-04	
<u>Oxide</u>	<u>Wt. %</u>	<u>Oxide</u>	<u>Wt. %</u>	<u>Oxide</u>	<u>Wt. %</u>	<u>Oxide</u>	<u>Wt. %</u>
Na ₂ O	0.5	Na ₂ O	0.90	Na ₂ O	0.61	Na ₂ O	0.55
K ₂ O	15.6	K ₂ O	15.18	K ₂ O	15.46	K ₂ O	15.64
CaO	0.0	CaO	0.02	CaO	0.00	CaO	0.10
BaO	0.7	BaO	0.91	BaO	0.90	BaO	0.60
Al ₂ O ₃	17.7	Al ₂ O ₃	21.56	Al ₂ O ₃	19.45	Al ₂ O ₃	20.01
SiO ₂	62.3	SiO ₂	64.25	SiO ₂	65.70	SiO ₂	65.57
Total	97.1	Total	102.82	Total	102.12	Total	102.47
Ba	6500 ppm	Ba	8140 ppm	Ba	8070 ppm	Ba	5350 ppm
	<u>Mol %</u>		<u>Mol %</u>		<u>Mol %</u>		<u>Mol %</u>
Ab	5.1	Ab	8.12	Ab	5.54	Ab	5.01
Or	93.5	Or	90.12	Or	92.78	Or	93.41
An	0.0	An	0.11	An	0.02	An	0.48
Cn	1.3	Cn	1.66	Cn	1.66	Cn	1.10

96C Ksp2-05

<u>Oxide</u>	<u>Wt. %</u>
Na ₂ O	0.57
K ₂ O	15.89
CaO	0.00
BaO	0.40
Al ₂ O ₃	18.82
SiO ₂	64.78
Total	100.44

Ba 3540 ppm

	<u>Mol %</u>
Ab	5.15
Or	94.13
An	0.00
Cn	0.72

96C Ksp2-06

<u>Oxide</u>	<u>Wt. %</u>
Na ₂ O	0.64
K ₂ O	15.85
CaO	0.00
BaO	0.35
Al ₂ O ₃	19.39
SiO ₂	65.20
Total	101.42

Ba 3130 ppm

	<u>Mol %</u>
Ab	5.72
Or	93.64
An	0.00
Cn	0.63

96C Ksp2-07

<u>Oxide</u>	<u>Wt. %</u>
Na ₂ O	0.53
K ₂ O	15.75
CaO	0.00
BaO	0.45
Al ₂ O ₃	20.77
SiO ₂	65.52
Total	103.02

Ba 4040 ppm

	<u>Mol %</u>
Ab	4.87
Or	94.30
An	0.00
Cn	0.83

96C Ksp2-08

<u>Oxide</u>	<u>Wt. %</u>
Na ₂ O	0.74
K ₂ O	14.93
CaO	0.01
BaO	0.46
Al ₂ O ₃	19.19
SiO ₂	64.45
Total	99.78

Ba 4110 ppm

	<u>Mol %</u>
Ab	6.94
Or	92.15
An	0.04
Cn	0.87

96C Ksp2-09

<u>Oxide</u>	<u>Wt. %</u>
Na ₂ O	0.44
K ₂ O	16.48
CaO	0.00
BaO	0.22
Al ₂ O ₃	19.71
SiO ₂	65.19
Total	102.05

Ba 1980 ppm

	<u>Mol %</u>
Ab	3.86
Or	95.72
An	0.02
Cn	0.39

96C Ksp2-10

<u>Oxide</u>	<u>Wt. %</u>
Na ₂ O	1.93
K ₂ O	13.41
CaO	0.01
BaO	0.46
Al ₂ O ₃	19.10
SiO ₂	65.46
Total	100.36

Ba 4110 ppm

	<u>Mol %</u>
Ab	17.79
Or	81.31
An	0.04
Cn	0.85

96C Ksp2-11

<u>Oxide</u>	<u>Wt. %</u>
Na ₂ O	1.50
K ₂ O	15.94
CaO	0.02
BaO	0.63
Al ₂ O ₃	19.28
SiO ₂	65.43
Total	102.78

Ba 5600 ppm

	<u>Mol %</u>
Ab	12.35
Or	86.53
An	0.08
Cn	1.04

96C Ksp3-02

<u>Oxide</u>	<u>Wt. %</u>
Na ₂ O	0.30
K ₂ O	16.37
CaO	0.00
BaO	0.55
Al ₂ O ₃	18.83
SiO ₂	65.02
Total	101.07

Ba 4910 ppm

	<u>Mol %</u>
Ab	2.67
Or	96.34
An	0.00
Cn	0.99

96C Ksp3-01		96C Ba1		96I Ba1		96I Ba2	
<u>Oxide</u>	<u>Wt. %</u>	<u>Oxide</u>	<u>Wt. %</u>	<u>Oxide</u>	<u>Wt. %</u>	<u>Oxide</u>	<u>Wt. %</u>
Na ₂ O	0.23	Na ₂ O	0.47	Na ₂ O	0.63	Na ₂ O	0.63
K ₂ O	16.50	K ₂ O	14.36	K ₂ O	12.45	K ₂ O	12.40
CaO	0.00	CaO	0.01	CaO	0.02	CaO	0.01
BaO	0.74	BaO	4.45	BaO	6.41	BaO	4.76
Al ₂ O ₃	19.43	Al ₂ O ₃	19.98	Al ₂ O ₃	20.87	Al ₂ O ₃	19.18
SiO ₂	66.63	SiO ₂	61.76	SiO ₂	61.55	SiO ₂	60.68
Total	103.54	Total	101.03	Total	101.94	Total	97.66
Ba	6620 ppm	Ba	39820 ppm	Ba	57440 ppm	Ba	42620 ppm
	<u>Mol %</u>		<u>Mol %</u>		<u>Mol %</u>		<u>Mol %</u>
Ab	2.02	Ab	4.39	Ab	6.26	Ab	6.48
Or	96.64	Or	87.27	Or	80.85	Or	83.61
An	0.02	An	0.05	An	0.11	An	0.05
Cn	1.33	Cn	8.30	Cn	12.79	Cn	9.86

96B Plg1

Oxide	Wt. %
Na ₂ O	9.47
K ₂ O	0.13
CaO	3.49
BaO	0.01
Al ₂ O ₃	22.83
SiO ₂	64.95
Total	100.87
Ba	80 ppm
	Mol %
Ab	82.47
Or	0.73
An	16.78
Cn	0.02

96B Plg2

Oxide	Wt. %
Na ₂ O	8.68
K ₂ O	0.27
CaO	4.71
BaO	0.04
Al ₂ O ₃	23.23
SiO ₂	64.00
Total	100.93
Ba	370 ppm
	Mol %
Ab	75.65
Or	1.56
An	22.71
Cn	0.07

96C Plg1

Oxide	Wt. %
Na ₂ O	10.13
K ₂ O	0.12
CaO	1.29
BaO	0.01
Al ₂ O ₃	21.45
SiO ₂	67.93
Total	100.92
Ba	70 ppm
	Mol %
Ab	92.73
Or	0.75
An	6.50
Cn	0.01

96C Plg2

Oxide	Wt. %
Na ₂ O	11.15
K ₂ O	0.12
CaO	0.46
BaO	0.02
Al ₂ O ₃	20.03
SiO ₂	68.59
Total	100.37
Ba	160 ppm
	Mol %
Ab	97.07
Or	0.68
An	2.22
Cn	0.03

96C Plg3

<u>Oxide</u>	<u>Wt. %</u>
Na ₂ O	11.17
K ₂ O	0.11
CaO	0.91
BaO	0.00
Al ₂ O ₃	20.30
SiO ₂	67.67
Total	100.17

Ba 30 ppm

	<u>Mol %</u>
Ab	95.10
Or	0.61
An	4.28
Cn	0.01

96I Plg1

<u>Oxide</u>	<u>Wt. %</u>
Na ₂ O	10.14
K ₂ O	0.16
CaO	2.50
BaO	0.04
Al ₂ O ₃	22.19
SiO ₂	63.95
Total	98.98

Ba 330 ppm

	<u>Mol %</u>
Ab	87.16
Or	0.89
An	11.88
Cn	0.06

96I Plg2

<u>Oxide</u>	<u>Wt. %</u>
Na ₂ O	10.22
K ₂ O	0.17
CaO	2.54
BaO	0.03
Al ₂ O ₃	22.05
SiO ₂	64.35
Total	99.36

Ba 290 ppm

	<u>Mol %</u>
Ab	87.05
Or	0.92
An	11.96
Cn	0.06

96I Plg3

<u>Oxide</u>	<u>Wt. %</u>
Na ₂ O	11.33
K ₂ O	0.16
CaO	0.52
BaO	0.01
Al ₂ O ₃	22.04
SiO ₂	65.28
Total	99.35

Ba 130 ppm

	<u>Mol %</u>
Ab	96.63
Or	0.88
An	2.47
Cn	0.03

86 Plg1		86 Plg2		86 Plg3		86 Ksp1	
<u>Oxide</u>	<u>Wt. %</u>	<u>Oxide</u>	<u>Wt. %</u>	<u>Oxide</u>	<u>Wt. %</u>	<u>Oxide</u>	<u>Wt. %</u>
Na ₂ O	8.91	Na ₂ O	9.29	Na ₂ O	11.42	Na ₂ O	0.54
K ₂ O	0.23	K ₂ O	0.17	K ₂ O	0.14	K ₂ O	15.66
CaO	4.42	CaO	3.95	CaO	0.37	CaO	0.00
BaO	0.04	BaO	0.02	BaO	0.00	BaO	0.40
Al ₂ O ₃	23.29	Al ₂ O ₃	22.90	Al ₂ O ₃	19.88	Al ₂ O ₃	18.34
SiO ₂	63.53	SiO ₂	63.49	SiO ₂	68.97	SiO ₂	64.77
Total	100.42	Total	99.82	Total	100.78	Total	99.71
Ba	390 ppm	Ba	200 ppm	Ba	30 ppm	Ba	3580 ppm
	<u>Mol %</u>		<u>Mol %</u>		<u>Mol %</u>		<u>Mol %</u>
Ab	77.41	Ab	80.17	Ab	97.46	Ab	4.91
Or	1.29	Or	0.96	Or	0.80	Or	94.35
An	21.22	An	18.83	An	1.73	An	0.00
Cn	0.08	Cn	0.04	Cn	0.01	Cn	0.74

IVe. Experimental Charges

CHG1 Ksp1.1		CHG1 Ksp1.12		CHG1 G1 1.2		CHG1 G1 1.22	
<u>Oxide</u>	<u>Wt. %</u>	<u>Oxide</u>	<u>Wt. %</u>	<u>Oxide</u>	<u>Wt. %</u>	<u>Oxide</u>	<u>Wt. %</u>
Na ₂ O	1.96	Na ₂ O	1.90	Na ₂ O	1.52	Na ₂ O	1.46
K ₂ O	7.90	K ₂ O	7.65	K ₂ O	4.71	K ₂ O	4.47
CaO	0.00	CaO	0.00	CaO	0.01	CaO	0.01
BaO	13.69	BaO	14.26	BaO	1.76	BaO	1.67
Al ₂ O ₃	20.99	Al ₂ O ₃	22.07	Al ₂ O ₃	12.38	Al ₂ O ₃	11.31
SiO ₂	56.84	SiO ₂	55.92	SiO ₂	70.51	SiO ₂	69.25
Total	101.38	Total	101.80	Total	90.89	Total	88.17
Ba	122590 ppm	Ba	127700 ppm	Ba	15740 ppm	Ba	14970 ppm
	Mo1 %		Mo1 %		Mo1 %		Mo1 %
Ab	19.75	Ab	19.37	Ab	15.10	Ab	14.81
Or	52.36	Or	51.26	Or	30.79	Or	29.84
An	0.02	An	0.00	Q	54.11	Q	55.35
Cn	27.87	Cn	29.37				

CHG3 Ksp3.1		CHG3 G1 3.2		CHG22 G1 1		CHG22 Ksp2	
<u>Oxide</u>	<u>Wt. %</u>	<u>Oxide</u>	<u>Wt. %</u>	<u>Oxide</u>	<u>Wt. %</u>	<u>Oxide</u>	<u>Wt. %</u>
Na ₂ O	2.40	Na ₂ O	1.99	Na ₂ O	0.71	Na ₂ O	2.29
K ₂ O	8.60	K ₂ O	5.48	K ₂ O	2.75	K ₂ O	11.59
CaO	0.00	CaO	0.00	CaO	1.64	CaO	0.39
BaO	9.18	BaO	0.10	BaO	0.14	BaO	1.84
Al ₂ O ₃	20.48	Al ₂ O ₃	16.51	Al ₂ O ₃	10.79	Al ₂ O ₃	16.24
SiO ₂	61.80	SiO ₂	57.32	SiO ₂	64.98	SiO ₂	63.96
Total	102.47	Total	81.40	Total	81.00	Total	96.31
Ba	82260 ppm	Ba	870 ppm	Ba	1250 ppm	Ba	16460 ppm
	Mol %		Mol %				Mol %
Ab	24.21	Ab	35.43			Ab	21.82
Or	57.06	Or	64.21			Or	72.61
An	0.00					An	2.04
Cn	18.73					Cn	3.53

CHG22 Plg3

<u>Oxide</u>	<u>Wt. %</u>
Na ₂ O	8.90
K ₂ O	0.92
CaO	2.40
BaO	0.11
Al ₂ O ₃	18.92
SiO ₂	68.25
Total	99.50

Ba 990 ppm

Mol %

Ab	82.01
Or	5.58
An	12.21
Cn	0.21

CHG22 Ksp4

<u>Oxide</u>	<u>Wt. %</u>
Na ₂ O	2.32
K ₂ O	9.57
CaO	0.25
BaO	2.01
Al ₂ O ₃	15.25
SiO ₂	70.06
Total	99.46

Ba 17980 ppm

Mol %

Ab	25.34
Or	68.74
An	1.49
Cn	4.43

CHG22 Gl 5

<u>Oxide</u>	<u>Wt. %</u>
Na ₂ O	0.56
K ₂ O	2.08
CaO	1.85
BaO	0.16
Al ₂ O ₃	10.60
SiO ₂	62.25
Total	77.50

Ba 1460 ppm

Mol %

Ab	21.92
Or	64.58
An	0.99
Cn	12.51

CHG22 Ksp6

<u>Oxide</u>	<u>Wt. %</u>
Na ₂ O	2.06
K ₂ O	9.21
CaO	0.17
BaO	5.81
Al ₂ O ₃	19.87
SiO ₂	62.06
Total	99.17

Ba 52040 ppm

CHG22 Ksp7	
<u>Oxide</u>	<u>Wt. %</u>
Na ₂ O	2.09
K ₂ O	10.69
CaO	0.30
BaO	2.35
Al ₂ O ₃	18.48
SiO ₂	63.66
Total	97.57
Ba	21040 ppm

	<u>Mol %</u>
Ab	21.37
Or	72.05
An	1.72
Cn	4.86

CHG22 G1 8	
<u>Oxide</u>	<u>Wt. %</u>
Na ₂ O	0.62
K ₂ O	2.17
CaO	1.70
BaO	0.11
Al ₂ O ₃	12.02
SiO ₂	66.23
Total	82.85
Ba	990 ppm

CHG22 Ksp9	
<u>Oxide</u>	<u>Wt. %</u>
Na ₂ O	2.05
K ₂ O	9.12
CaO	0.24
BaO	1.51
Al ₂ O ₃	19.10
SiO ₂	62.54
Total	94.54
Ba	13530 ppm

	<u>Mol %</u>
Ab	24.12
Or	70.72
An	1.56
Cn	3.60

CHG22 G1 10	
<u>Oxide</u>	<u>Wt. %</u>
Na ₂ O	1.26
K ₂ O	3.16
CaO	1.76
BaO	0.46
Al ₂ O ₃	10.51
SiO ₂	65.10
Total	82.26
Ba	4130 ppm

CHG23 Ksp1	
Oxide	Wt. %
Na ₂ O	2.82
K ₂ O	10.74
CaO	0.18
BaO	2.42
Al ₂ O ₃	14.29
SiO ₂	72.31
Total	102.77

Ba 21660 ppm

	Mol %
Ab	26.95
Or	67.42
An	0.97
Cn	4.66

CHG23 G1 2	
Oxide	Wt. %
Na ₂ O	3.22
K ₂ O	3.32
CaO	2.10
BaO	0.25
Al ₂ O ₃	12.60
SiO ₂	64.97
Total	86.45

Ba 2220 ppm

CHG27 G1 1	
Oxide	Wt. %
Na ₂ O	2.93
K ₂ O	5.59
CaO	1.16
BaO	1.12
Al ₂ O ₃	14.08
SiO ₂	63.60
Total	88.47

Ba 10020 ppm

CHG25 Ksp1	
Oxide	Wt. %
Na ₂ O	1.27
K ₂ O	11.43
CaO	0.04
BaO	4.90
Al ₂ O ₃	12.80
SiO ₂	66.91
Total	97.36

Ba 43930 ppm

	Mol %
Ab	12.99
Or	76.70
An	0.21
Cn	10.11

CHG25 G1 2	
<u>Oxide</u>	<u>Wt. %</u>
Na ₂ O	1.54
K ₂ O	4.28
CaO	1.01
BaO	0.43
Al ₂ O ₃	7.30
SiO ₂	62.26
Total	76.82
Ba	3860 ppm

CHG24 G1 1	
<u>Oxide</u>	<u>Wt. %</u>
Na ₂ O	2.22
K ₂ O	3.66
CaO	1.49
BaO	0.25
Al ₂ O ₃	12.90
SiO ₂	66.70
Total	87.21
Ba	2250 ppm

CHG24 Ksp2	
<u>Oxide</u>	<u>Wt. %</u>
Na ₂ O	2.20
K ₂ O	12.43
CaO	0.22
BaO	3.42
Al ₂ O ₃	18.16
SiO ₂	62.21
Total	98.64
Ba	30610 ppm

CHG16 Ksp1	
<u>Oxide</u>	<u>Wt. %</u>
Na ₂ O	1.68
K ₂ O	11.82
CaO	0.05
BaO	0.00
Al ₂ O ₃	9.41
SiO ₂	81.46
Total	104.41
Ba	10 ppm

	<u>Mol %</u>
Ab	19.63
Or	73.11
An	1.08
Cn	6.17

	<u>Mol %</u>
Ab	17.69
Or	82.04
An	0.26
Cn	0.00

CHG16 G1 2.1

<u>Oxide</u>	<u>Wt. %</u>
Na ₂ O	3.02
K ₂ O	3.88
CaO	1.56
BaO	0.00
Al ₂ O ₃	12.68
SiO ₂	61.35
Total	82.50

Ba 10 ppm

CHG16 G1 2.2

<u>Oxide</u>	<u>Wt. %</u>
Na ₂ O	3.30
K ₂ O	3.49
CaO	1.55
BaO	0.00
Al ₂ O ₃	12.70
SiO ₂	61.43
Total	82.48

Ba 10 ppm

CHG25 Ksp Z1

<u>Oxide</u>	<u>Wt. %</u>
Na ₂ O	1.28
K ₂ O	12.32
CaO	0.03
BaO	4.13
Al ₂ O ₃	19.39
SiO ₂	62.53
Total	99.67

Ba 36960 ppm

Mol %

Ab	12.49
Or	79.19
An	0.17
Cn	8.15

CHG25 Ksp Z2

<u>Oxide</u>	<u>Wt. %</u>
Na ₂ O	1.25
K ₂ O	11.84
CaO	0.05
BaO	5.55
Al ₂ O ₃	19.81
SiO ₂	61.42
Total	99.92

Ba 49700 ppm

Mol %

Ab	12.28
Or	76.47
An	0.25
Cn	11.01

CHG25 Ksp Z3	
<u>Oxide</u>	<u>Wt. %</u>
Na ₂ O	1.27
K ₂ O	11.94
CaO	0.03
BaO	5.35
Al ₂ O ₃	19.89
SiO ₂	61.39
Total	99.88

Ba 47940 ppm

	<u>Mol %</u>
Ab	12.40
Or	76.84
An	0.19
Cn	10.58

CHG25 Ksp Z4	
<u>Oxide</u>	<u>Wt. %</u>
Na ₂ O	1.26
K ₂ O	12.44
CaO	0.03
BaO	4.42
Al ₂ O ₃	19.54
SiO ₂	62.14
Total	99.82

Ba 39560 ppm

	<u>Mol %</u>
Ab	12.15
Or	79.05
An	0.18
Cn	8.62

CHG25 Ksp Z5	
<u>Oxide</u>	<u>Wt. %</u>
Na ₂ O	1.44
K ₂ O	12.51
CaO	0.04
BaO	3.60
Al ₂ O ₃	19.40
SiO ₂	62.80
Total	99.79

Ba 32270 ppm

	<u>Mol %</u>
Ab	13.83
Or	78.97
An	0.21
Cn	6.99

CHG25 Ksp Z6

<u>Oxide</u>	<u>Wt. %</u>
Na ₂ O	1.42
K ₂ O	12.30
CaO	0.08
BaO	4.23
Al ₂ O ₃	19.56
SiO ₂	61.79
Total	99.37

Ba 37920 ppm

Mol %

Ab	13.61
Or	77.76
An	0.41
Cn	8.22

CHG25 Ksp Z7

<u>Oxide</u>	<u>Wt. %</u>
Na ₂ O	1.20
K ₂ O	11.16
CaO	0.05
BaO	7.91
Al ₂ O ₃	20.18
SiO ₂	62.17
Total	102.66

Ba 70800 ppm

Mol %

Ab	11.77
Or	72.26
An	0.25
Cn	15.72

CHG25 G1 Z8

<u>Oxide</u>	<u>Wt. %</u>
Na ₂ O	0.68
K ₂ O	3.54
CaO	1.04
BaO	0.35
Al ₂ O ₃	12.48
SiO ₂	69.97
Total	88.05

Ba 3090 ppm

CHG25 G1 Z8.1	
<u>Oxide</u>	<u>Wt. %</u>
Na ₂ O	1.10
K ₂ O	3.95
CaO	1.04
BaO	0.35
Al ₂ O ₃	12.50
SiO ₂	70.02
Total	88.96
Ba	3100 ppm

CHG25 G1 Z9	
<u>Oxide</u>	<u>Wt. %</u>
Na ₂ O	2.13
K ₂ O	4.72
CaO	1.15
BaO	0.36
Al ₂ O ₃	12.62
SiO ₂	68.37
Total	89.34
Ba	3220 ppm

CHG25 G1 Z10	
<u>Oxide</u>	<u>Wt. %</u>
Na ₂ O	1.40
K ₂ O	4.43
CaO	1.10
BaO	0.32
Al ₂ O ₃	12.39
SiO ₂	69.93
Total	89.56
Ba	2860 ppm

APPENDIX V

Estimates of the Structural State of Feldspars from the Granitic Rocks of the Dixon-Peñasco Area

The structural state of selected, hand-picked samples of feldspar--mostly K-feldspar--was determined by the three-peak method of Wright (1968). The techniques used were almost identical to those recommended by Wright except that only one 2θ scan was taken instead of the average of three and a smaller 2θ range was scanned ($2\theta = 52^\circ$ to 20°). The scatter in the data around theoretical maximum microcline suggests that it is not as precise as the data obtained by Wright (1968). However, since no systematic trends were noticed, attempts to improve the quality of the data did not seem to be warranted. The table below gives the 2θ values for $\bar{2}04$, 060 , and $\bar{2}01$ corrected to 2θ $\text{CuK}_{\alpha 1}$ radiation.

Reference

- Wright, T. L., 1968, X-ray and optical study of alkali feldspar:
II. An X-ray method for determining the composition and structural
state from measurement of 2θ values for three reflections: *Am.
Mineralogist*, v. 53, p. 88-104.

<u>Sample number</u>	<u>204</u>	<u>060</u>	<u>201</u>
PL72-174	50.574	41.832	21.05
PL71-5 mega	50.529	41.800	21.061
PL71-45b	50.522	41.856	21.158
PL72-96 mega	50.567	41.822	21.043
PL71-40	50.590	41.838	21.104
PL71-31	50.260	41.773	20.892
PL71-14 pink	50.547	41.820	20.903
PL72-80	50.573	41.832	20.927
PL71-56	50.508	41.810	20.931
PL72-84 (peg)	50.560	41.854	21.083
Pen-Peg Kf top	50.612	41.851	21.096
Pen-Peg Ab bottom	51.097	42.364	22.251
PL73-223 Ab	51.153	42.494	22.064
PL72-84 Ab	51.260	42.376	22.446
PL72-125	51.190	42.514	22.096

APPENDIX VI

Derivation of Equations 2, 5, and 6

In order to maintain mass balance for a single component across a moving crystal-liquid interface in a closed system the flux across the interface must equal the mass that is exchanged due to movement of the interface and partitioning between the two phases. From Fick's first law (one dimensional) the total flux across the interface must be

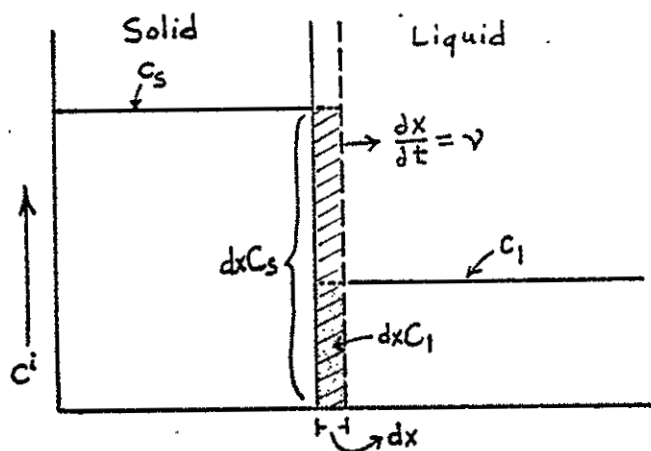
$$D_l^i \frac{\partial C_l^i}{\partial X} - D_s^i \frac{\partial C_s^i}{\partial X} \quad (I)$$

where $D_l^i(C_l^i/X)$ is the flux due to mass transport by diffusion in the liquid phase to or from the solid phase, and $D_s^i(\partial C_s^i/\partial X)$ is the flux due to mass transport by diffusion in the solid phase to or from the liquid phase. The flux in the solid is subtracted from the flux in the liquid because the coordinate system is chosen so that the interface is always at the origin and the solid always lies to the left of the origin. Furthermore, flux from the liquid to the solid or from right to left is considered positive.

The mass exchanged due to movement of the interface and partitioning behavior is

$$\frac{\partial X_I}{\partial t} C_s^i - \frac{\partial X_I}{\partial t} C_l^i \quad (II)$$

as is demonstrated by the following diagram:



$$\frac{\partial X_I}{\partial t} C_s^i - \frac{\partial X_I}{\partial t} C_l^i$$

clearly is the rate at which material is exchanged across the interface as it moves at a rate $\partial X_I / \partial t$ and this must equal the flux due to diffusion. Thus

$$D_l^i \frac{\partial C_l^i}{\partial X} - D_s^i \frac{\partial C_s^i}{\partial X} = \frac{\partial X_I}{\partial t} C_s - \frac{\partial X_I}{\partial t} C_l \quad (\text{III})$$

or

$$D_l^i \frac{\partial C_l^i}{\partial X} - D_s^i \frac{\partial C_s^i}{\partial X} = \frac{\partial X_I}{\partial t} (C_s - C_l) \quad (\text{IV})$$

which is equation (5). Note that $K_D = C_s^i / C_l^i$ or $K_D C_l^i = C_s^i$ and $\partial X_I / \partial t = v$.

$$D_l^i \frac{\partial C_l^i}{\partial X} - D_s^i \frac{\partial C_s^i}{\partial X} = v C_l (K_D - 1) \quad (\text{V})$$

If $D_s^i = 0$, then

$$D \frac{\partial C_l^i}{\partial X} + v C_l (1 - K) = 0 \quad (\text{VI})$$

which is equation (2) or equation 4 of Albarede and Bottinga (1972).

Equation (6) in the text is the same as (V) above except that a temperature dependence for K_D has been substituted such that

$$K_D = \exp (10^4/T)a + b \quad (\text{VII})$$

where a and b are appropriate coefficients derived from an Arrhenius plot such as figure 138 in the text, and T is the absolute temperature in degrees Kelvin. For barium in R-1 + 10% Or₁₀₀ and at 8 weight percent H₂O and 8 kbar, $a = 0.67$ and $b = 1.3$.

Solving equation (5) for the gradient in the solid, $\partial C_s^i / \partial X$, allows the determination of conditions under which the gradient is positive or negative:

$$\frac{\partial C_s^i}{\partial X} = \frac{\frac{\partial X_I}{\partial t} (C_l - C_s) + D_l^i \frac{\partial C_l^i}{\partial X}}{D_s^i}$$

Clearly if $C_l - C_s$ is negative (true for all $K_D > 1$) and $\partial X_I / \partial t > 0$ as well as $D_l^i > 0$, $D_s^i > 0$, and $\partial C_l^i / \partial X > 0$ (true for most cases where $K_D > 1$), then $\partial C_s^i / \partial X$ will always have a negative absolute slope if

$$D_l^i \frac{\partial C_l^i}{\partial X} > \frac{\partial X_I}{\partial t} (C_l - C_s) .$$

Employing values for these parameters that are typical of silicate systems gives results indicating that this inequality holds.

**GEOLOGIC MAP OF THE
DIXON-PENASCO AREA
NEW MEXICO**

SCALE 1:24,000

0 1 mile
0 2 kilometers

Contour intervals 20 and 40 feet.

geology by
Philip E. Long
1971-1973

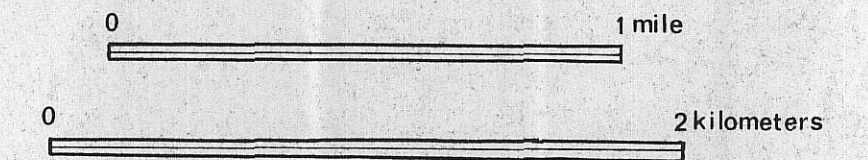
N
↑

Topographic base from U.S. Geological Survey
Trampas and Penasco 7½' quadrangles.

(See Plate Ia for explanation)

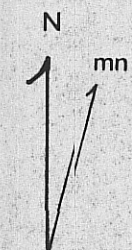
GEOLOGIC MAP OF THE DIXON-PENASCO AREA NEW MEXICO

SCALE 1 : 24 000



Contour intervals 20 and 40 feet.

geology by
Philip E. Long
1971 - 1973

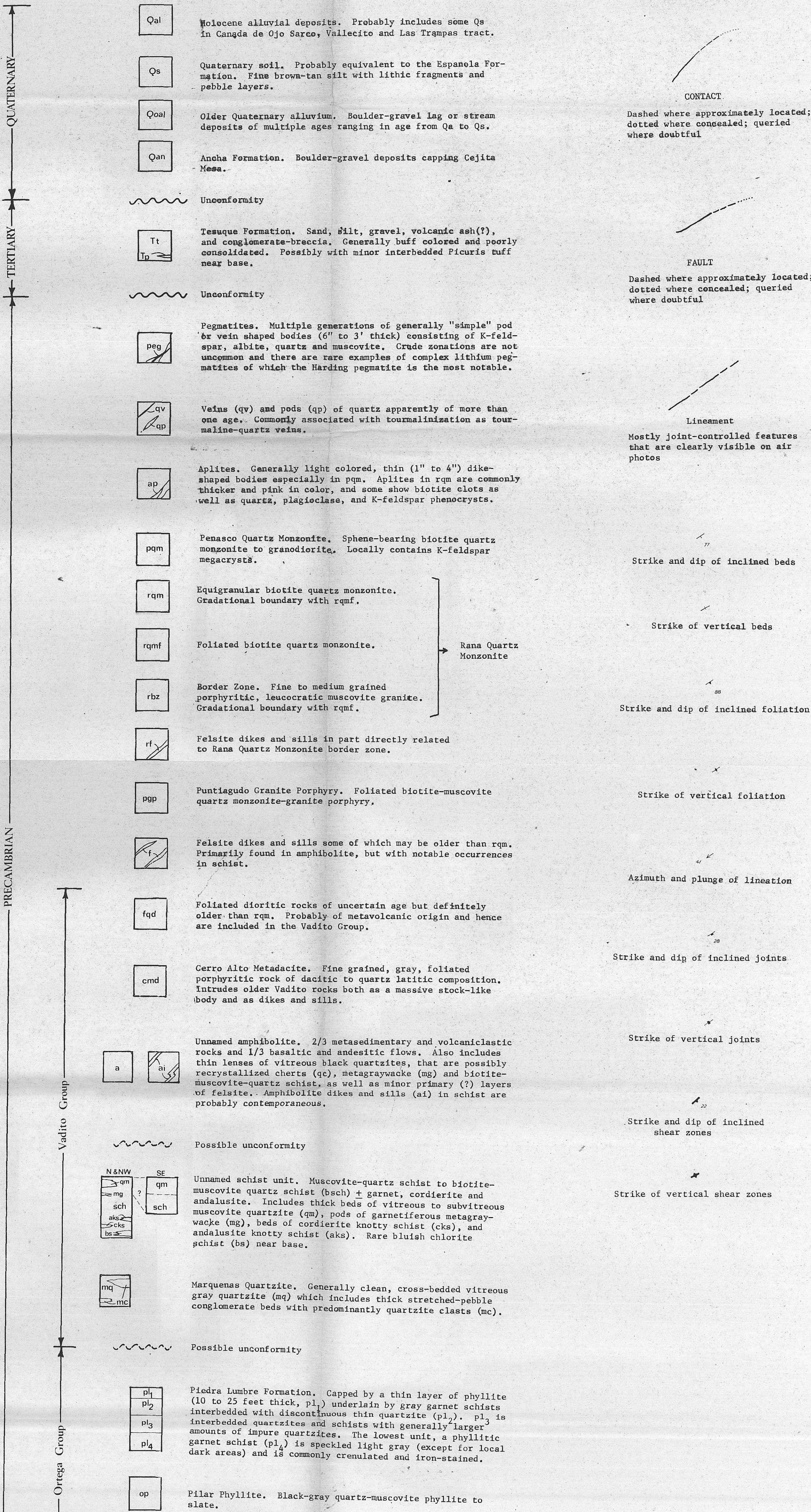


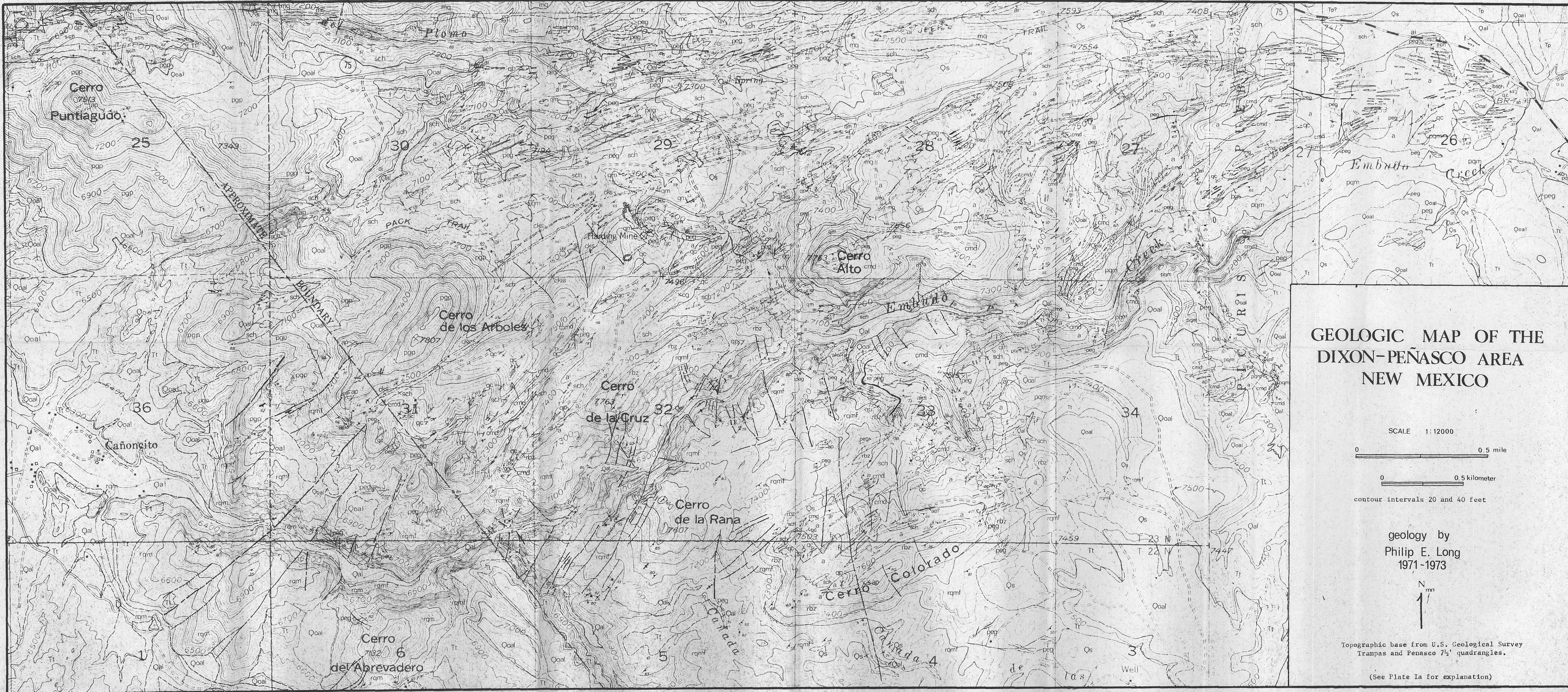
Topographic base from U.S. Geological Survey
Trampas and Penasco 7½' quadrangles.

(See Plate Ia for explanation)

PLATE Ia

EXPLANATION





GEOLOGIC MAP OF THE DIXON-PENASCO AREA NEW MEXICO

SCALE 1:12000

0 0.5 mile

0 0.5 kilometer

contour intervals 20 and 40 feet

geology by
Philip E. Long
1971-1973



Topographic base from U.S. Geological Survey
Trampas and Penasco 7 1/2' quadrangles.

(See Plate Ia for explanation)

PLATE III Cross Section

